

See discussions, stats, and author profiles for this publication at: <https://www.researchgate.net/publication/369893347>

# Animal Environment and Welfare — Proceedings of International Symposium 2019

Book · October 2019

---

CITATIONS

0

READS

518

3 authors:



Lingjuan Wang-Li  
North Carolina State University  
108 PUBLICATIONS 1,048 CITATIONS

[SEE PROFILE](#)



Chaoyuan Wang  
China Agricultural University  
87 PUBLICATIONS 1,001 CITATIONS

[SEE PROFILE](#)



Ji-Qin Ni  
Purdue University  
195 PUBLICATIONS 4,352 CITATIONS

[SEE PROFILE](#)



# Animal Environment and Welfare

— Proceedings of International Symposium 2019



Edited by  
**Lingjuan Wang-Li, Chaoyuan Wang, Ji-Qin Ni**



CHINA AGRICULTURE PRESS



# **Animal Environment and Welfare**

## **— Proceedings of International Symposium**

**October 21–24, 2019**  
**Rongchang, Chongqing, China**

**动物环境和福利化养殖  
国际研讨会论文集**

**2019 年 10 月 21–24 日**

**中国 · 重庆 · 荣昌**



**International Research Center for  
Animal Environment and Welfare**

**Edited by**

**Lingjuan Wang-Li, Chaoyuan Wang, Ji-Qin Ni**

**China Agriculture Press**

**Beijing, China**



***Sponsored by***

International Research Center for Animal Environment and Welfare  
Chongqing Commission of Science and Technology  
Chinese Society of Agricultural Engineering  
China Agricultural University (CAU)

***Hosted by***

Chongqing Academy of Animal Sciences (CAAS)  
Key Lab of Agricultural Engineering in Structure and Environment,  
Ministry of Agriculture (MOA), China

***Symposium Co-Chairs***

Dr. Baoming Li, Professor, China Agricultural University, China  
Dr. Hongwei Xin, Dean of AgResearch and Professor, The University of Tennessee, USA

***Program Co-Chairs***

Dr. Lingying Zhao Professor, The Ohio State University, USA  
Dr. Ruqian Zhao Professor, Nanjing Agricultural University, China

***Proceedings Co-Chairs***

Dr. Lingjuan Wang Li, Professor, North Carolina State University, USA  
Dr. Chaoyuan Wang, Professor, China Agricultural University, China  
Dr. Ji-Qin Ni, Associate Professor, Purdue University, USA

**Proceedings Committee:** Dr. Andre Aarnink, Dr. Hao Li, Dr. Teng Lim, Dr. Guoqiang Zhang,  
Dr. Qiang Zhang, Dr. Weicaho Zheng

***Organizing Committee***

Dr. Zuohua Liu, Professor and President, CAAS, China (Chair)  
Dr. Yong Huang, Professor, Vice President, CAAS, China  
Dr. Chaoyuan Wang, Professor, CAU, China  
Dr. Feiyun Yang, Professor, CAAS, China  
Ms. Wen Liu, Associate Professor, CAAS, China  
Dr. Weichao Zheng, Associate Professor, CAU, China  
Dr. Hao Li, Associate Professor CAU, China  
Dr. Qin Tong, Assistant Professor, CAU, China  
Dr. Chao Zong, Assistant Professor, CAU, China

## Acknowledgements

We would like to thank those who helped to ensure the quality and scientific merits of the papers. In particular, our gratitude goes to the following individuals who reviewed the abstracts and/or full length of the papers:

Andre Aarnink	Wageningen University and Research	The Netherlands
Lilong Chai	University of Georgia	USA
Peter Groot Koerkamp	Wageningen University and Research	The Netherlands
Suzanne Leonard:	Iowa State University	USA
Hao Li	China Agricultural University	China
Rong Li	Aarhus University	Denmark
Teng T. Lim	University of Missouri	USA
Ray Massey	University of Missouri	USA
Daniella Jorge de Moura	State University of Campinas	Brazil
Jofran Oliveira	Iowa State University	USA
Brett Ramirez	Iowa State University	USA
Günther Schauberger	University of Veterinary Medicine	Austria
Guoqiang Zhang	Aarhus University	Denmark
Qiang Zhang	University of Manitoba	Canada
Yang Zhao	Mississippi State University	USA

The Editors

**Disclaimer:** It is authors' responsibility to obtain written permissions to use copyrighted materials (e.g., figure, photo, table) when writing their papers.

© 2019 of individual papers by the authors of the papers

## **A Message from the Symposium Co-Chairs**

Greetings!

International Symposium on Animal Environment and Welfare (ISAEW) is a flagship event of the International Research Center for Animal Environment and Welfare (IRCAEW). It has been held every two years since 2011 in the City of Rongchang, Chongqing, China. The biennial symposia aim to address current and emerging issues facing the global animal production industry by bringing together some of the best minds and future professionals in the fields to exchange latest research findings, technological innovation, farm-level applications/adoptions, regulations, and outlook. At each symposium, specially invited internationally renowned experts share state of the science, the industry, global situations, and visions on the thematic topics.

Since its inaugural holding in 2011, ISAEW has received increasing attention. For instance, attendance jumped from under 100 in 2011 to over 350 in 2017. The impacts of ISAEW have been equally commendable, from identifying mission-oriented research directions, discussing lessons learned from various parts of the world, enhancing collaborations among multidisciplinary scientists and animal production entrepreneurs with a shared vision, fostering networking and collaborations among global researchers and future leaders, stimulating investment of resources into animal environment and welfare research, to providing valuable training and development opportunities for graduate students and other young professionals.

Established in 2011, IRCAEW (<http://www.ircaew.org/>) is headquartered at the Chongqing Academy of Animal Sciences, China. The purposes of this international center are two-fold: 1) to fully utilize research capabilities and resources of global scientists and institutions in synthesizing successful experiences, proven management practices and technologies to advance the field of animal environment and welfare worldwide; and 2) to provide a platform for global networking and information exchange among those who, through research, development and/or adoption of new technologies, strive to improve farm animal health and well-being, production efficiency and product quality, and ultimately to improve the quality of life for the mankind. At the present time, membership of the Center consists of 20 institutions from 10 countries representing Asia, Europe, North America, South America, and Oceania.

For those of you who are attending this ISAEW2019, welcome and enjoy the symposium and the beautiful fall season in the City of Rongchang! For those who were unable to join us this time, we hope that the proceedings will give you a good perspective of the technical contents.

On behalf of the IRCAEW board of directors, we would like to extend our heartfelt gratitude to all the individuals and organizations who contributed their valuable time and resources to the various aspects of the symposium. ISAEW2019 would not have been possible without your dedication and support.

Look forward to your engagement at future symposia or other IRCAEW-related events.



Baoming Li, Professor  
China Agricultural University  
Co-chair, ISAEW2019  
Co-chair, IRCAEW Board of Directors



Hongwei Xin, Dean and Professor  
UT AgResearch  
The University of Tennessee  
Co-chair, ISAEW2019  
Co-chair, IRCAEW Board of Directors

## Preface

The 2019 International Symposium on Animal Environment and Welfare (ISAEW2019) continued to bring in diversified experts and participants to share the latest research and development in animal environment and welfare. The ISAEW2019 is the fifth of a series of biennial symposia that were organized by the International Research Center for Animal Environment and Welfare (IRCAEW <http://www.ircaew.org/>) and began in 2011 in Rongchang, Chongqing, China. The previous symposia include the International Symposium on Health Environment and Animal Welfare (ISHEAW2011), October 19–22, 2011; the ISAEW2013, October 19–22, 2013; the ISAEW2015, October 23–26, 2015; and the ISAEW2017, October 23–26, 2017.

The ISAEW2019 attracted the worldwide interest with 97 symposium abstract submission. A total of 51 research and review papers were accepted and included in this proceedings book. These papers cover various interesting subject matters with cutting-edge research findings and improved understanding of the issues associated with animal production environment and animal welfare in Asia, Europe, and North and South Americas. The papers were prepared by the authors (and co-authors) from research institutions in various areas, state academies and key laboratories, animal production companies, animal research and monitoring centers, and universities in 13 countries (i.e., Austria, Belgium, Brazil, Canada, China, Denmark, Germany, Italy, Poland, Republic of Korea, The Netherlands, Turkey, and USA). It is very encouraging to observe that ISAEW has gained worldwide interests and has become an attractive platform to address issues to make the global animal production industry sustainable.

ISAEW2019 had an overarching theme of “Green Development and New Industrialization of Animal Husbandry”, with six supporting subject areas (I) Biosecurity and Animal Management; (II) Environmental Monitoring, Assessment and Control; (III) Impacts of Production Systems and Management Practices; (IV) Manure Management and Utilization; (V) Precision Livestock Farming; and (VI) Innovative Production Systems and Equipment. In this proceedings book, each paper is assigned to one of the six subject areas accordingly. However, because the topics of many papers cover more than one subject area, the topic areas in this book do not mean a clear-cut division of the papers.

We sincerely hope that this book is informative and will be a valuable reference source for those who are interested in animal production systems, animal environment, and animal welfare.

We also hope that the formal and informal information exchanges and networking at ISAEW2019 will enable a sustainable discussion and/or collaboration in the future research and development of animal environment and welfare.

We would like to thank all the authors and paper reviewers, presenters, speakers, moderators, the symposium co-chairs and the organizing committee. We are also very much thankful for the support from the International Research Center for Animal Environment and Welfare (IRCAEW). Last, but not least, we would like to thank Responsible Editor Wei Liu of China Agriculture Press. The publication of the book could not be possible without the support from all the above individuals and agencies.

The Editors  
October 8, 2019

## Table of Contents

Acknowledgements .....	iv
A Message from the Symposium Co-Chairs .....	v
Preface .....	vi
Table of Contents.....	vii
<b>Theme I: Biosecurity and Animal Management.....</b>	<b>1</b>
Disinfecting Egg Pallets and Flats with Heat Treatment at the Poultry Farm Gate of the USA	
<i>Lilong Chai, Yang Zhao, Hongwei Xin, Brad Richardson .....</i>	<i>3</i>
A Tracing Method of Airborne Bacteria Transmission across Built Environments: Establishment and Field Evaluation	
<i>Zonggang Li, Hongning Wang, Weichao Zheng, Baoming Li, Yongxiang         Wei, Jinxin Zeng, Changwei Lei.....</i>	<i>11</i>
Effect of Concentration of SAEW on Pathogenic Bacteria Viability in a Broiler House	
<i>Zhifang Shi, Weichao Zheng, Lei Xi, Tongshuai Liu, Xue Hui.....</i>	<i>19</i>
Environment-Friendly Management of Livestock and Poultry Mortalities	
<i>Tom Tabler.....</i>	<i>26</i>
Recommendations for Effective Biosecurity Management	
<i>Teng-Teeh Lim, Corinne Bromfield, Craig Payne, Lauren Delaney,         Raymond Massey, Joseph Zulovich.....</i>	<i>39</i>
<b>Theme II: Environmental Monitoring, Assessment, and Control.....</b>	<b>47</b>
Numerical Study Using CFD on the Efficiency of a Partial Pit Ventilation to Remove Ammonia from Different Emission Sources	
<i>Li Rong.....</i>	<i>49</i>
Effect of Cage Size and Nutrition on Performance and Health of Pullets	
<i>Yi Wan, Ruiyu Ma, Yan Li, Wei Liu, Junying Li, Kai Zhan.....</i>	<i>57</i>
Heat Stress for Fattening Pigs in Confined Livestock Buildings: Simulation of the Impact of Global Warming for 1981–2017 for the Mid-latitudes	
<i>Günther Schauberger, Christian Mikovits, Werner Zollitsch, Stefan J.         Hörtenhuber, Johannes Baumgartner, Knut Niebuhr, Martin Piringer,         Werner Knauder, Ivonne Anders, Konrad Andre, Isabel Hennig-Pauka,         Martin Schönhart .....</i>	<i>65</i>
Efficacy of Adaptation Measures to Reduce Heat Stress due to the Impact of Global Warming on Confined Livestock Buildings for Fattening Pigs	
<i>Günther Schauberger, Christian Mikovits, Werner Zollitsch, Stefan J.         Hörtenhuber, Johannes Baumgartner, Knut Niebuhr, Martin Piringer,         Werner Knauder, Ivonne Anders, Konrad Andre, Isabel Hennig-Pauka,         Martin Schönhart .....</i>	<i>72</i>

Bioenergetics of Laying Hens in Aviary Systems <i>Jofran L. Oliveira, Brett C. Ramirez, Hongwei Xin, Yu Wang, Steven J. Hoff....</i>	79
Effect of Calcium Sulphate Dihydrate on GHG and Ammonia Emissions from Cattle Slurry during Storage <i>Borgonovo Federica, Conti Cecilia, Lovarelli Daniela, Bacenetti Jacopo, Ferrante Valentina, Guarino Marcella .....</i>	85
Effect of the Installation Location of Weather Station on Sampled Wind Speed <i>Li Rong, Guoqiang Zhang.....</i>	92
Water Footprint Assessment of Eggs in a Parent-Stock Layer Breeder Farm <i>Haohan Xing, Baoming Li, Weichao Zheng, Zhidan Liu, Yuanhui Zhang.....</i>	100
Simultaneous Removal of Low Concentration H <sub>2</sub> S and NH <sub>3</sub> by a Biotrickling Filter: Interaction between the Two Pollutants and Microbial Community Changes <i>Shihao Ying, Xianwang Kong, Zhen Cai, Zun Man, Yicong Xin, Dezhao Liu... </i>	107
Calculation Method for Chicken-Perceived Light Intensity <i>Zhichao Li, Xiaocui Wang, Baoming Li, Weichao Zheng, Zhengxiang Shi, Ziyue Cao, Qin Tong.....</i>	113
Isotopomer Analyses of N <sub>2</sub> O Produced from NH <sub>3</sub> -loaded Biofilter: Microbial Production Pathways <i>Xianwang Kong, Shihao Ying, Yicong Xin, Zhen Cai, Liangcheng Yang, Dezhao Liu .....</i>	119
A Preliminary Study on Dispersion Modeling of Hydrogen Sulfide from a Six-story Pig House in China <i>Dejia Liu , Li Rong, Günther Schauberger, Chuandong Wu, Yicong Xin, Xiusong Li, Bin Chen, Dezhao Liu.....</i>	127
Effects of Different Color LED lights on Layer Chickens During Brooding and Rearing Periods <i>Yongxiang Wei, Weichao Zheng, Baoming Li, Qin Tong.....</i>	134
Development of a Farm Scale, Quasi Mechanistic Model for Estimation of NH <sub>3</sub> Emission from Commercial Manure-Belt Layer Facilities <i>Xinjie Tong, Lingying Zhao, Albert Heber, Ji-Qin Ni.....</i>	143
Effects of Electrode Materials and Dimensions on Water Droplet Charging for Dust Removal <i>Xiaochuan Li, Reyna Knight, Lingying Zhao, Jeb Hocter.....</i>	151
Modeling a Wire-Plate Electrostatic Precipitator for Poultry PM Collection Using COMSOL <i>Reyna M. Knight, Lingying Zhao .....</i>	159
Ammonia Transport from Multi-Floor Pig Houses Based on CFD Simulations <i>Yicong Xin, Li Rong, Dejia Liu, Xiusong Li, Bin Chen, Xianwang Kong, Shihao Ying, Dezhao Liu.....</i>	167

The Dose-effect Relationships between Green Light and Metabolism Rate in Chick Embryos <i>Tao Wang, Zhentao Zhong, Qiong Liu, Yue Yu, Jinming Pan</i>	174
Modelling the Reduction of Ammonia Emission of a Naturally Ventilated Cow House Using an Acidified Water Curtain <i>Bert van 't Ooster, Roland W. Melse, Sjoerd Bokma, Marjolein Derkx, Yeb P. Andela, Jeroen A. A. Verstegen, Peter W. G. Groot Koerkamp</i>	180
Evaluation of Indoor Environment of A Six-Story Swine Barn and Associated Impact on the Surrounding Environment <i>Kaiying Wang, Xiaoshuai Wang, Xiaorong Dai, Leiping Wang, Jiegang Wu, Ailun Wang, Xiusong Li, Zhihua Yang, Bin Chen, Kangning Huan</i>	188
<b>Theme III: Impacts of Production Systems and Management Practices.....</b>	<b>189</b>
Design and Experimental Study of Clam Automatic Cleaning Equipment <i>Hanbing Zhang, Jialin Tian, Jian Zhang, Xiuchen Li, Guochen Zhang, Yanfei Ren, Gang Mua</i>	191
Best Available Techniques (BAT) for Emission Reduction of Livestock Farming Industry in Denmark <i>Peter Kai, Guoqiang Zhang</i>	197
Outcome-Based Measures of Animal Welfare: the Challenges and the Opportunities <i>Janice C. Swanson</i>	207
Impacts of Exercise or Pasture Access on the Welfare of Transition Dairy Cows <i>Peter D. Krawczel, Ramdi A. Black</i>	215
Optimisation of Environment-Animal-Welfare Interactions in High-Performance Dairy Cows Housed in Naturally Ventilated Barns <i>Thomas Amon, Qianying Yi, Julia Heinicke, Severino Pinto, Gundula Hoffmann, Sabrina Hempel, Theresa Müschner Siemens, David Janke, Christian Ammon, Barbara Amon</i>	223
Image Analysis of Heavy Broiler Behavior under Summer Heat Stress Condition <i>Yingying Liu, Bin Cheng, Derek West, Suraiya Akter, Lingjuan Wang-Li, Alejandro H. Cordova-Noboa, Edgar Oviedo-Rondon</i>	232
<b>Theme IV: Manure Management and Utilization .....</b>	<b>233</b>
Impact of Fieldwork Day Constraints on Manure Application Regulations <i>Raymond E. Massey, Haluk Gedikoglu</i>	235
Isolation, Identification and Optimization of Heat-tolerant Bacteria in Composting of Pig manure <i>Yifan Zhang, Zengli Ouyang, Xuehua Mei, Jianan Tang, Maixun Zhu, Yong Huang, Weichao Zheng, Zonggang Li</i>	242

A Dispersion-Based Model for Assessing the Impact of Odor from Swine Operations <i>Amy La, Qiang Zhang</i> .....	250
Economic Conditions for Implementing Solid-Liquid Separation Barn <i>Ryamond E. Massey, Teng-Teeh Lim, Joe Zulovich</i> .....	256
Preparation of UIO-66 (Zr) Series MOFs and Their Adsorption of Heavy Metals in Animal Wastewater <i>Leiping Wang, Yifeng Jiang, Jianrong Li, Dezhao Liu, Zun Man, Xiaorong Dai</i> .....	264
<b>Theme V: Precision Livestock Farming</b> .....	<b>271</b>
A Novel Quantification Method for Keel Bone Fracture and Deformation of Laying Hens <i>Kailao Wang, Brett C. Ramirez, Hongwei Xin, Rebecca Parsons, Jinming Pan, Yibin Ying</i> .....	273
Sequential Patterns of Broilers Behavior under Comfort and Stress Conditions <i>Daniella Jorge de Moura, Tatiane Branco Irenilza de Alencar Naas, Stanley Robson de Oliveira Medeiros</i> .....	279
Preliminary Study on a Data-driven Prediction Method for the Early Detection of Coccidiosis in Intensive Livestock Systems <i>Ferrante Valentina, Grilli Guido, Borgonovo Federica, Pascuzzo Riccardo, Guarino Marcella</i> .....	286
Evaluation of Convolutional Neural Networks for Detecting Floor Eggs of Cage-Free Hen Housing Systems <i>Guoming Li, Yang Zhao, Yan Xu, Qian Du</i> .....	293
A Rapid Test for Avian Influenza Detection of Chicken Based on Sound Analysis <i>Tiemin Zhang, Junduan Huang, Kaixuan Cuan</i> .....	301
Recognition and Classification of Abnormal Droppings of Broilers Based on Deep Convolution Neural Network <i>Jintao Wang, Longshen Liu, Yi Xu, Mingxia Shen, Hongxiang Xue, Meng Tai</i> .....	309
Classification of Broiler Behaviors Using Triaxial Accelerometer and Machine Learning <i>Xiao Yang, Yang Zhao, Garrett M. Street, Yanbo Huang</i> .....	317
Implication of Modern Sow's Static and Dynamic Space Usage on Gestation Stall Design <i>Suzanne Leonard, Hongwei Xin, Tami M. Brown-Brandl, Brett C. Ramirez, John P. Stinn, Anna K. Johnson</i> .....	324
ROS-based Autonomous Navigation Control System for Animal Farm Inspection Robots <i>Tiemin Zhang, Zhong Peng, Jinfeng Lu</i> .....	329

Is Continuous Heart Rate Monitoring of Livestock a Dream or Is It Realistic? <i>Luwei Nie, Daniel Berckmans, Chaoyuan Wang, Baoming Li</i> .....	337
Animal Welfare Monitoring by Real-time Physiological Signals <i>Pieter Joosen, Tomas Norton, Jeremy Marchant-Ford, Daniel Berckmans</i> ....	347
<b>Theme VI: Animal Production Systems and Equipment .....</b>	<b>355</b>
Poultry Farming Information Management System Based on Cloud Database <i>Tiemin Zhang, Haikun Zhen</i> .....	357
Effects of Different Claw Shortening Devices on Claw Condition, Fear, Stress and Feather Coverage of Layer Breeders <i>Haipeng Shi, Baoming Li, Qin Tong, Weichao Zheng</i> .....	364
Effects of Stocking Density and Toy Provision on Production Performance, Behaviour and Physiology of Growing Pigs <i>Yongzhen Li, Chaoyuan Wang, Shiwei Huang, Zuohua Liu, Hao Wang</i> .....	373
Optimal Indoor Climate by Partial Recirculation of Air in a Fattening Pig House <i>André J.A. Aarnink, In-Bok Lee</i> .....	381
<b>Indexes .....</b>	<b>389</b>
Author Name Index .....	391
Author Affiliation Index .....	395



**Theme I:**

**Biosecurity and Animal Management**



# Disinfecting Egg Pallets and Flats with Heat Treatment at the Poultry Farm Gate of the USA

Lilong Chai <sup>a</sup>, Yang Zhao <sup>b#</sup>, Hongwei Xin <sup>c\*</sup>, Brad Richardson <sup>d</sup>

<sup>a</sup> Department of Poultry Science, University of Georgia, Athens, GA 30602, USA

<sup>b</sup> Department of Agricultural and Biological Engineering, Mississippi State University, Hood Road, MS 39762, USA

<sup>c</sup> University of Tennessee Institute of Agriculture, Knoxville, TN 37996, USA

<sup>c</sup> Department of Agricultural and Biological Engineering, Iowa State University, Ames, IA 50011, USA

# Authors contributed equally to this work. \* Corresponding author. Email: [hxin2@utk.edu](mailto:hxin2@utk.edu)

## Abstract

Disinfecting shell egg transport pallets and flats before their reuse has become an integral biosecurity step after the 2015 highly pathogenic avian influenza (AI) outbreaks in the United States of America (USA). The lab-scale test and field verification were conducted to investigate dynamic temperature changes and distributions inside stacks of egg pallet and flat at a surrounding air temperature of 54–60 °C (130–140 °F) in this study. The heat treatment test was conducted in the lab first, and then verified in a newly built heat treatment room (dimension is 12 m L × 4 m W × 3 m H) at a commercial laying hen farm in Iowa, the largest egg production state in the USA. Iowa lost more than 30 million hens during 2015 outbreak of AI. According to the lab test, air circulation with fans could accelerate the heat exchange between air and stacks. Blowing air from top and bottom at the same time plus arranging a 2.5 cm (1 inch) space between stacks could reduce the heat treatment time for the target temperature zone (54–60 °C) from 26–60 h (without air circulation) to 7–9 h. Heat treatment tests results show that the room air and pallet stacks temperature reached the target zone (54–60 °C) 30 min and 4 h after starting the heater, respectively. However, the temperature of flat stacks failed to reach the targeted zone after 5–6 h heating, because it had larger volume and heat transfer resistance as compared to pallet stacks. Further studies such as extending heating period and installing mixing fans to accelerate heat exchange between the room air and the stacks are guaranteed.

**Keywords:** Avian influenza, egg pallet and flat, heat treatment, disinfection

## 1. Introduction

The outbreak of highly pathogenic avian influenza (HPAI) between December 2014 and June 2015 led to losses of more than 50 million chickens and turkeys in the United States (accounted for about 12% table-egg layer population and 8% of grow-out turkeys) (Ramos et al., 2017). Avian influenza viruses could be passed through many ways such as direct contact and airborne transmission (Lu et al., 2003; Capua and Marangon, 2006; Baron and Jan, 2011; Zhao et al., 2018). Farm gate biosecurity measures include vehicle disinfection by spraying liquid agent, UV disinfection on smaller stuff, shower-in and shower-out, etc. (Böhm, 1998; Kelly et al., 2008; Jeong et al., 2010; Gangadharan et al., 2013).

Reusable plastic egg flats are used by some producers to transport eggs from off-line hen farms to processing plants. After the 2015 AI outbreaks, disinfecting egg flats before their reuse has become an integral biosecurity step. AI viruses are heat labile viruses, so sanitation of egg flat stacks may be done by heating them up above 54–60 °C (130–140 °F) and maintaining the high temperatures for a period of time. Shahid et al. (2009) and Zou et al. (2013) reported that the sterilization on AI virus of H7N9 will occur after 30 min at 56 °C, after 1 day at 28°C but remained viable for more than 100 days at 4°C. However, it remains unclear how the temperature of flat and pallet stacks responds to different heating strategies. In addition, the temperature distribution inside the stacks of egg flats, pallets (for transporting the flat stacks), and boards (separating flat stacks) need to be examined for improving the system design. Therefore, the lab-scale test and

field verification were conducted to investigate dynamic temperature changes and distributions inside egg flat stacks at a surrounding air temperature of 56 °C.

The objectives of this field study were 1) to assess the time required for the flat/pallet stacks in the heat treatment room to reach an effective disinfection temperature range 55–60 °C; 2) to verify the lab findings at a commercial egg farm; and 3) to provide recommendations to expedite the heating process for egg farms.

## 2. Materials and Methods

### 2.1. Lab test experimental setup

This lab-scale study was conducted in a heat treatment chamber (Figure 1) at the Iowa State University. In each experiment, polypropylene flats (30 cm × 30 cm, 30-egg capacity each) were arranged in two tiers for an overall stack dimensions of 1.2 m L × 0.9 m W × 1.8 m H. The entire flat stacks were wrapped with plastic film prior to heat treatment and moved to an insulated enclosure containing three 1.5 kWh heaters. Three heat treatments were tested in the lab-scale study: no air circulation, air circulation without space between stacks, and air circulation with 2.5 cm spacing between flat stacks (Figure 1). About 32 thermocouples were connected to NI Fieldpoint data acquisition system (using LabVIEW program) to assess the temperature distribution in the heating chamber. Thermocouples recorded temperatures at three levels: near top (3/4 stack height), middle (1/2 stack height) and near bottom (1/4 stack height) (Figure 2 and Figure 3). Each level had nine measurement points to assess the horizontal temperature distribution. An infrared thermography camera was used to monitor the immediate temperature change before and after heat treatment for stacks.



Figure 1. The stacks with 2.5 cm space while blowing air upward from bottom and down with box fans.

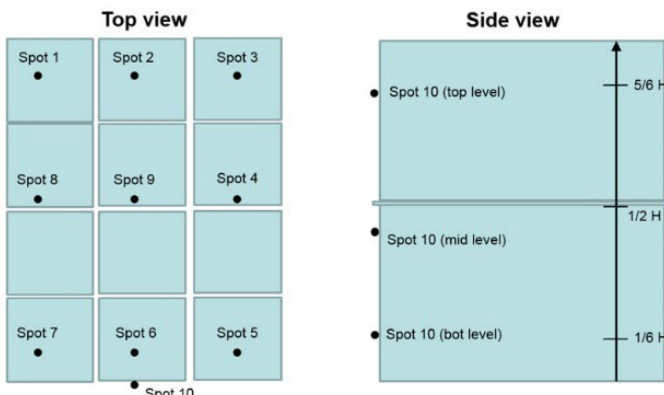


Figure 2. Temperature monitoring spots.



Figure 3. Thermocouple placement in the flat stacks.

## 2.2. Field test experimental setup

The field test and verification were conducted in a newly built heat treatment room (dimension is 12 m L × 4 m W × 3 m H) at a commercial laying hen farm in Iowa. Iowa is the largest egg production state in the USA. Iowa lost more than 30 million hens during 2015 outbreak of AI. The heat treatment room (the capacity of heater is 73 kW or 250,000 btu hr<sup>-1</sup>) was built in 2016 (Figure 4). To monitor indoor air temperature and the temperature distribution in stacked pallet and flats at different height, 24 thermal couples were used together with a LabVIEW program (Figure 5). The room temperature was set at 68 °C. The pallets and flats were heated gradually by indoor air (Figures 6 and 7). Seven locations were monitored for the room air temperature during the heat treatment (Figure 8).

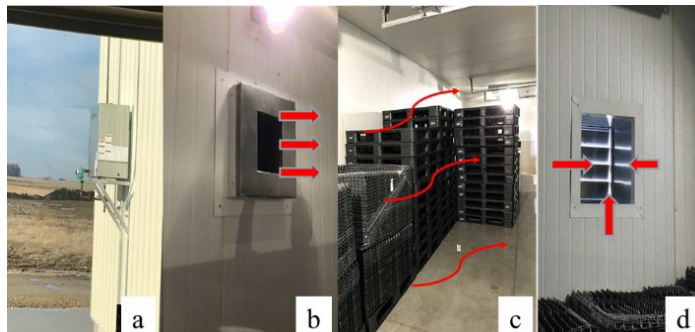


Figure 4. Heat treatment room (room dimension is 11.6 L × 3.9 W × 3 H m; a- heater, b- air outlet of heater, c- stacked pallets/flats, d- air outlet of the room).

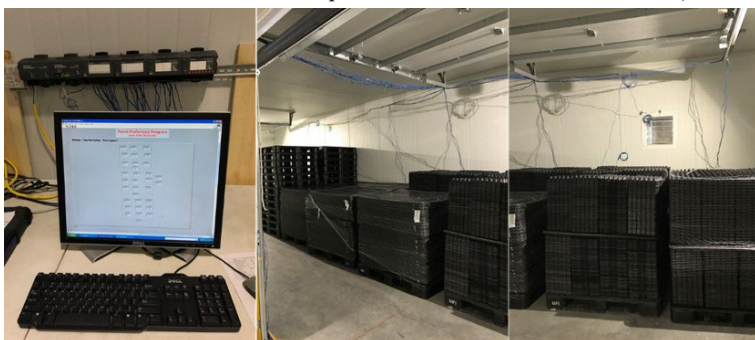


Figure 5. LabVIEW program and stacked egg flats and pallets.

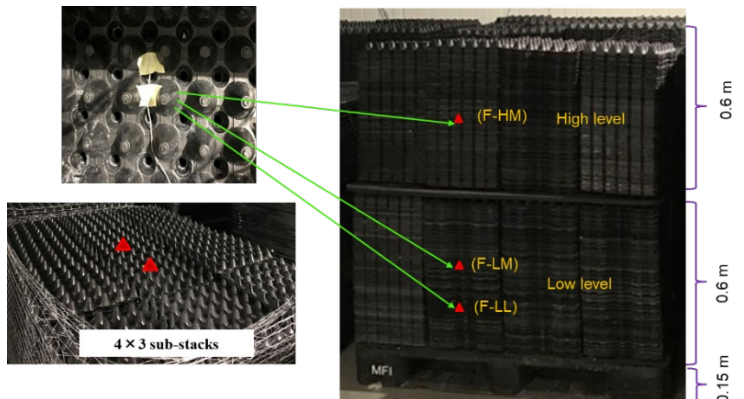


Figure 6. Temperature monitoring of egg flat stacks (F-HM: flat stack at mid-location of high level; F-LM: flat stack at mid-location of low level; F-LL: flat stack at low-location of low level).



Figure 7. Temperature monitoring for stacks of board and pallets (B-H: board stack of high level; B-L: board stack of low level; P-H: pallet stack of high level; P-L: pallet stack of low level).

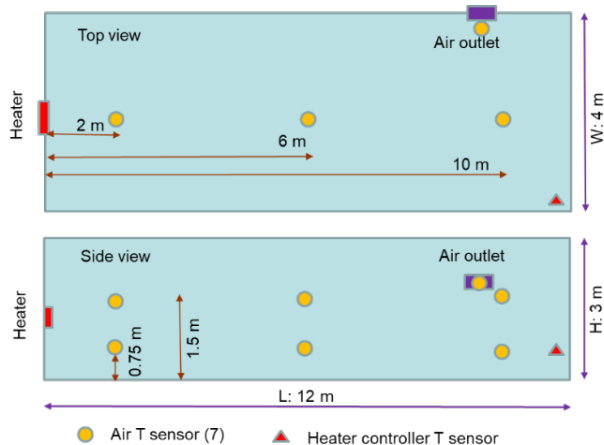


Figure 8. Layout of air temperature monitoring in the heat treatment room.

Air flow pattern from the heater outlet was found to affect the heating effect on the room air temperature and egg flats/pallets during the first test on Dec. 6, 2016. Therefore, four metal discharge deflectors were added to direct the air toward the floor to improve the heating efficiency (Figure 9).

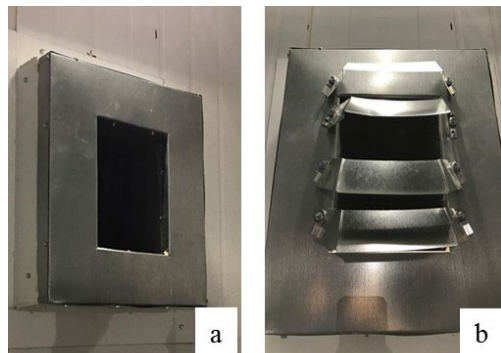


Figure 9. Heater air outlet (a- without deflector, b- with deflector).

### 3. Results and Discussion

#### 3.1. Lab test results

For treatment without air circulation, the top level in-stack temperature reached the target temperature zone ( $54\text{--}60^{\circ}\text{C}$ ) after 26 h heating, middle level in-stack temperature reached target temperature zone after 32 h heating, and the bottom level in-stack temperature reached target temperature zone after 60 h heating. For treatment without air circulation, the top level in-stack temperature reached temperature zone after 8-h heating, the middle level in-stack temperature reached target temperature after 9.5 h heating, and the bottom level in-stack temperature reached target temperature after 9.5 h heating. For treatment without air circulation, the top level in-stack temperature reached target zone after 7.5 h heating, the middle level in-stack temperature reached target zone after 7 h heating, and the bottom level in-stack temperature reached that after 9 h heating. The start and end in-stack temperature and temperature increase during first 12-h heating is shown in Table 1. The treatment of air circulation with fans has higher heating efficiency than the treatment without air circulation. Adding a 2.5 cm (1 inch) space between stacks could accelerate the heat exchange between air and in-stacks. The general surface temperature change on pallet/flat stacks expressed in thermal imaging method is shown in Figure 10.

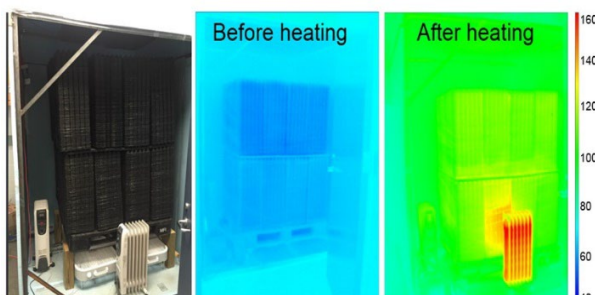


Figure 10. Thermographs of heat treatment on stacks/palate before and after heat treatment (circulation with space) (color bar represents temperature in Fahrenheit ( $^{\circ}\text{F}$ ): 40–160  $^{\circ}\text{F}$  = 4.4–71  $^{\circ}\text{C}$ ).

Table 1. In-stack temperature and change during first 12-h heating.

Treatment (replicate #)	Start/End temperature (°C)			Temperature increase (°C hr <sup>-1</sup> )		
	Top	Mid	Bot	Top	Mid	Bot
No circulation (1)	-11/30	0/33	-13/66	3.4	2.8	2.7
No circulation (2)	-13/36	2/43	-10/26	4.1	3.4	2.9
Circulation (1)	-17/62	-3/59	-17/61	6.6	5.2	6.5
Circulation (r2)	-16/65	-1/62	-16/59	6.8	5.2	6.3
Circulation (r3)	-18/66	0/57	-18/61	6.9	4.8	6.6
Circulation + Space (1)	-4/61	6/60	-6/59	5.4	4.5	5.4
Circulation + Space (2)	7/63	10/64	-5/61	4.6	4.5	5.5
Circulation + Space (3)	-2/60	7/60	-3/57	5.2	4.4	5.0

### 3.2. Field test results

Air temperature of the heat treatment room before and after adding the deflectors to the heater outlet are shown in Figure 11. Before adding the deflectors, most of the hot air was thrown directly from the heater outlet to the farthest end of the treatment room; as a result, air temperature at 10 m (see Figure 9 for sensors location) from the heater was warmer than at 2 m and 6 m. Because air outlet of the heat treatment room was near the 10 m location, the hot air was quickly lost to the outside. With installation of the deflectors, air temperature at 2 m was higher than 6 m and 10 m. In addition, the room was heated to the target zone temperature faster.

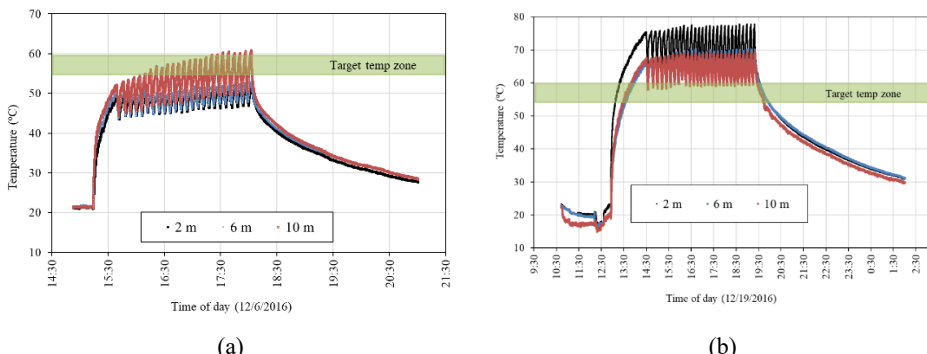


Figure 11. Room air temperature: (a) before installation of discharge deflectors to the heater; (b) after installation of discharge deflectors to the heater.

On Dec. 19<sup>th</sup>, 2016, the heater was turned on around 12:30. Temperature of the room at 2 m, 6 m, and 10 m and stacks of boards, pallets and flats are shown in Figure 12. The room air and pallets temperature reached the target zone of 54–60 °C 30 min and 4 h after starting the heater, respectively. However, the temperature of flat and board stacks failed to reach the targeted zone before the heating was stopped at 19:00, because the stacks of flats and boards had larger volumes and heat resistance than the pallet stacks. Further studies such as extending heating period and installing mixing fans to accelerate heat exchange between the room air and the flat and board stacks are guaranteed.

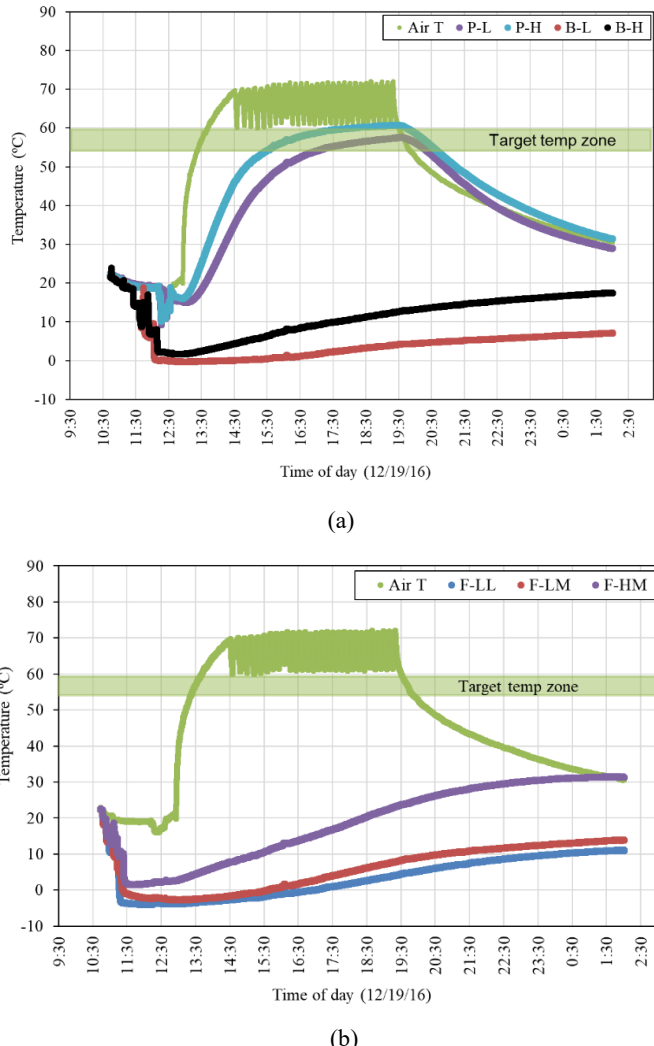


Figure 12. Temperature of room air: (a) stacks of boards and pallets: B-H: board stack of high level; B-L: board stack of low level; P-H: pallet stack of high level; P-L: pallet stack of low level); (b) flat stacks (F-HM: flat stack at middle place of high level; F-LM: flat stack at middle place of low level; F-LL: flat stack at low place of low level).

#### 4. Conclusions

In the lab-scale test, the target temperature zone of 54–60 °C (130–140 °F) in the enclosure was achieved by using three 1.5 kW oil-filled heaters (a total nominal heating capacity of 4.5 kW). Target flat temperature of 54–60 °C was reached after 60 h for no air mixing, 9.5 h for treatment of air circulation with fans only, and 9.0 h for treatment of air circulation with fans and the 2.5 cm space between stacks. It is critical to apply air mixing during stack heating in order to achieve overnight disinfection. Providing spacing between stacks (e.g., 2.5 cm) could accelerate the heat exchange. In field test, the installation of deflector improved the heat distribution and room

temperature. The room air and pallet stacks temperature reached the target zone (54–60 °C) about 30 min and 4 h after starting the heater, respectively. The temperature of flat stacks did not reach the target temperature zone due to higher heat resistance in the flat stacks than pallet stacks. Findings of this study provide basis to improve the design of the heat treatment system for disinfecting the egg flats and pallets for commercial laying hen farms.

### Acknowledgments

Financial support of the study was provided by USDA-NIFA, American Egg Board, and Egg Industry Center.

### References

- Baron, F., S. Jan. 2011. Egg and egg product microbiology. Improving the safety and quality of eggs and egg products (pp. 330–350). Woodhead Publishing.
- Böhm, R. 1998. Disinfection and hygiene in the veterinary field and disinfection of animal houses and transport vehicles. International biodeterioration & biodegradation, 41(3–4), 217–224.
- Capua, I., S. Marangon. 2006. Control of avian influenza in poultry. Emerging Infectious Diseases, 12(9), 1319.
- De Benedictis, P., M.S. Beato, and I. Capua., 2007. Inactivation of avian influenza viruses by chemical agents and physical conditions: a review. Zoonoses and Public Health, 54(2), 51–68.
- De Reu, K., K. Grijsspeerd, L. Herman, M. Heyndrickx, M. Uyttendaele, J. Debevere, and N.M. Bolder. 2006. The effect of a commercial UV disinfection system on the bacterial load of shell eggs. Letters in Applied Microbiology, 42(2), 144–148.
- Gangadharan, D., J. Smith, and, R. Weyant. 2013. Biosafety recommendations for work with influenza viruses containing a hemagglutinin from the A/goose/Guangdong/1/96 lineage. Morbidity and Mortality Weekly Report: Recommendations and Reports, 62(6), 1–7.
- Jeong, E.K., J.E. Bae, and I.S. Kim. 2010. Inactivation of influenza A virus H1N1 by disinfection process. American Journal of Infection Control, 38(5), 354–360.
- Kelly, T. R., M.G. Hawkins, C. E. Sandrock, and W. M. Boyce. 2008. A review of highly pathogenic avian influenza in birds, with an emphasis on Asian H5N1 and recommendations for prevention and control. Journal of Avian Medicine and Surgery, 22(1), 1–17.
- Lu, H., A.E. Castro, K. Pennick, J. Liu, Q. Yang, P. Dunn, D. Weinstock, and D. Henzler. 2003. Survival of avian influenza virus H7N2 in SPF chickens and their environments. Avian Diseases, 47(s3), 1015–1021.
- Ramos, S., M. MacLachlan, and A. Melton. 2017. Impacts of the 2014–2015 Highly Pathogenic Avian Influenza Outbreak on the Poultry, U. S Sector, LDPM–282–02. USDA, Economic Research Service.
- Shahid, M. A., M. Abubakar, S. Hameed, and S. Hassan. 2009. Avian influenza virus (H5N1): effects of physico-chemical factors on its survival. Virology Journal, 6(1), 38.
- Wanaratana, S., R. Tantilertcharoen, J. Sasipreeyajan, and S. Pakpinyo. 2010. The inactivation of avian influenza virus subtype H5N1 isolated from chickens in Thailand by chemical and physical treatments. Veterinary Microbiology, 140(1–2), 43–48.
- Zhao, Y., L. Chai, B. Richardson, and H. Xin. 2018. Field evaluation of an electrostatic air filtration system for reducing incoming particulate matter of a hen house. Transactions of the ASABE. 61(1): 295–304.
- Zou, S., J. Guo, R. Gao, L. Dong, J. Zhou, Y. Zhang, and Y. Shu. 2013. Inactivation of the novel avian influenza A (H7N9) virus under physical conditions or chemical agents treatment. Virology Journal, 10(1), 289.

# A Tracing Method of Airborne Bacteria Transmission across Built Environments: Establishment and Field Evaluation

Zonggang Li<sup>a,b</sup>, Hongning Wang<sup>c,d</sup>, Weichao Zheng<sup>a,b,\*</sup>, Baoming Li<sup>a,b</sup>,  
Yongxiang Wei<sup>a,b</sup>, Jinxin Zeng<sup>c,d</sup>, Changwei Lei<sup>c,d</sup>

<sup>a</sup> College of Water Resources and Civil Engineering, China Agricultural University,  
Beijing 100083, P.R. China

<sup>b</sup> Key Laboratory of Agricultural Engineering in Structure and Environment,  
Ministry of Agriculture and Rural Affairs, Beijing 100083, P.R. China

<sup>c</sup> College of Life Sciences, Sichuan University, Chengdu, Sichuan 610065, P.R. China

<sup>d</sup> Key Laboratory of Bio-Resource and Eco-Environment, Ministry of Education, Chengdu,  
Sichuan 610065, P.R. China

\* Corresponding author. Email: [weichaozheng@cau.edu.cn](mailto:weichaozheng@cau.edu.cn)

## Abstract

Airborne transmission is a vital route of disease infection caused by bacteria and virus. Homology detection, tracer gas and fluorescent particles used for airborne transmission of microorganisms in both lab and field research failed to veritably express the transporting process of the microorganisms in the air. We sought to establish a tracing method of airborne bacteria transmission across built environments and demonstrated its feasibility by conducting a field evaluation. High-voltage electroporation was used to introduce a specific gene fragment (pFPV-mCherry fluorescent protein plasmid) into nonpathogenic *E. coli* DH5α as tracer bacteria. In field experiment, tracer *E. coli* was aerosolized into the air from a source point while air was sampled at different target points for *E. coli* detection. Tracer *E. coli* was synthesized successfully with the guarantee of gel electrophoresis testing and correct genetic sequencing. The stable rates of introduced plasmid were both above 95% before and after aerosolization. The survival rates of tracer bacteria through aerosolization by an air atomizer operated at air pressure of 207, 310, and 414 kPa were 97.5%, 70.8%, and 61.3%, respectively. In the field experiment, the airborne transmission of *E. coli* between poultry houses was proved and emitted *E. coli* was more easily transmitted into the original house than adjacent houses (48 vs 21 CFU m<sup>-3</sup> at source intensity of 828 CFU m<sup>-3</sup>) due to the ventilation design and weather condition. The tracing method using *E. coli* with a specific gene fragment was available for the investigation of airborne microbial transmission across built environments. Field experiment proved the existence of airborne transmission between layer hen houses, which indicated that exhaust or inlet air filtration was essential to reduce the risk of airborne microorganisms transmission.

**Keywords:** Airborne bacteria tracing, airborne transmission, biological decay, building environment, field evaluation

## 1. Introduction

Airborne transmission which can occur between individuals, buildings and regions has been known as a vital route of disease infection caused by aerosol or respiratory with bacteria and virus. Severe acute respiratory syndrome (SARS) caused worldwide severe epidemic outbreak in 2003 (Lee et al., 2003). Air was verified as one of the SARS transmission pathways across built environments by the epidemiological proof and numerical simulation(Yu et al., 2004). Airborne transmission was also proved as an important mode of influenza A virus spread (Cowling et al., 2013). For animal production, more than 50 million chickens and turkeys in USA died of highly pathogenic avian influenza (HPAI) or were destroyed to prevent the disease spread between December 2014 and June 2015, involving Iowa and Minnesota and other adjacent states (Ramos et al., 2017). Evidences obtained from both laboratory-simulated process and field investigation supported the existence of airborne transmission of HPAI virus (Bertran et al., 2017).

Laboratory-scale manual controlled experiments had proved that short distance airborne

transmission of several infectious pathogens could occur from animal to animal (Bertran et al., 2017). Field studies, mostly focused on human case study and presented as evidences of airborne transmission between individuals, rooms or residential buildings, had also demonstrated the existence of airborne transmission of virus and bacteria (Xiao et al., 2018). Homology detection using ERIC-PCR and REP-PCR was applied in animal farm to conduct the source identification of airborne *E. coli* surrounded swine house (Duan et al., 2009). The airborne transmission of porcine reproductive and respiratory syndrome virus (PRRS) between buildings and via long spatial distance were supported based on virus homology between sampling points (Pitkin et al., 2009). It was challenged to directly certify the air transmission of microorganisms by homology detection due to its inability to suppress the interference of surrounding microorganisms. Results-orientated research of airborne transmission neglected the transporting process of the microorganisms in the air and was lack of quantitative description of airborne pathogens concentration. Tracer was required to express the movement and decay of airborne microorganism in both experiment and numerical simulation.

To comprehend the route of airborne transmission, tracer had been applied into both lab and field experiment. Tracer gas, such as nitrous oxide ( $N_2O$ ), sulfur hexafluoride ( $SF_6$ ), 1,1,1,2-tetrafluoroethane (R134a) and helium (He), was widely used to investigate the spread of airborne microorganisms in indoor and outdoor environment by means of computational fluid dynamics (CFD) for its quantitative evaluation of the cross-infection risks and economy (Wei et al., 2018). However, airborne microorganisms transporting process across built environments was unable to be interpreted thoroughly by tracer gas for its distinct absence of physical and biological characteristics of airborne microorganisms. Particles (e.g., fluorescent particles) and some microbial surrogate were also considered as tracers to investigate the airborne transmission of microorganisms (Zhou et al., 2016). Airborne microorganisms tracing was still a big challenge for its reliability on environment factor, complicated detection, and species-dependence. The decay of airborne microorganisms was indispensable factor in both empirical and theoretical models of airborne transmission, which was difficult to be quantified. Whereas, the lack of biological characteristic for particles or narrow application of microbial surrogate in clean or isolated room prevented it to be an ideal substitution of airborne microorganisms. Current tracer of airborne microorganisms failed to veritably express the airborne transporting process in atmosphere. Both physical and biological characteristics of bacterial tracer made it a more reasonable substitution of current tracer of airborne microorganisms.

Gene modification of bacteria could make it a unique existence in particular environment. Specific gene strain tracing had already been applied in many food safety-related studies to monitor their fate in complex environment or in laboratory animal medicine to explore the distribution of target bacteria in internal organs (Ma et al., 2011; Zeng et al., 2018). However, there was still a knowledge gap of gene-modified bacteria in the trace of airborne microorganisms. Aerosolization of bacteria, which was susceptible to the suspending medium and shear stress, was widely performed in lab-experiment such as air sterilization and air infection (Kim and Kang, 2018; Zhou et al., 2018). Aerosolization and gene modification of bacteria could be jointly used for tracing airborne microorganisms. The new method which could fulfill the following three conditions was essential to set up for airborne bacteria tracing across built environments.

- i) The modified gene should be specific to make it distinguished in surrounding environment.
- ii) Selected bacteria could be genetic-modified into a bacterial tracer.
- iii) Aerosolization should have little impact on the survival of the bacteria and the stability of the modified gene.

*E. coli* was selected in this method due to its universality, culturability and non-pathogenicity of certain category. pFPV-mCherry fluorescent protein plasmid was the selected gene, which was introduced into the *E. coli* by high-voltage electroporation. The objective of this article is to establish a tracing method of airborne bacteria transmission and demonstrate its feasibility by

conducting a field evaluation across built environments.

## 2. Materials and Methods

### 2.1. Establishment of airborne bacteria tracing method

The tracing method of airborne bacteria transmission was summarized in Figure 1. Selected gene fragment should be specific so that it could not be found in the air environment of the place where the research was conducted. Besides, the selected gene fragment should be compatible so that it could be introduced into the selected nonpathogenic bacteria without affecting its reproduction. The tracer bacteria were synthesized successfully when both of the two above conditions were accomplished, or new gene fragment needed to be selected and tested again. The finished tracer bacteria could be aerosolized into the air environment at a source point using a nebulizer, and airborne bacteria sampling was conducted at the target points. Taking the activity of the airborne bacteria into consideration, the bacteria sampled at the target points should be incubated on solid selective medium, followed by PCR and Gel electrophoresis which were used for the detection of the tracer bacteria. Finally, the concentration of the tracer bacteria and the ratios of the tracer bacteria to the total selected bacteria at the source and different target points could be used for analyzing the transporting process of the microorganisms in the air.

Several considerations needed to be taken for the application of this bacteria tracing method. Firstly, a specificity testing to confirm the absence of the elected gene fragment in the air environment needed to be performed. Liquid collision sampling technology of airborne bacteria could be used for the air sampling, followed by PCR and Gel electrophoresis analysis to determine whether the selected gene fragment existed. Secondly, a successful introducing of the selected gene fragment should satisfy three simultaneous conditions, natural reproduction capacity, positive reaction of PCR and Gel electrophoresis testing, correct genetic sequencing. Thirdly, the airborne bacteria sampled after the aerosolization needed to be incubated on the solid medium since only the active bacteria which could be cultured on the solid medium was considered.

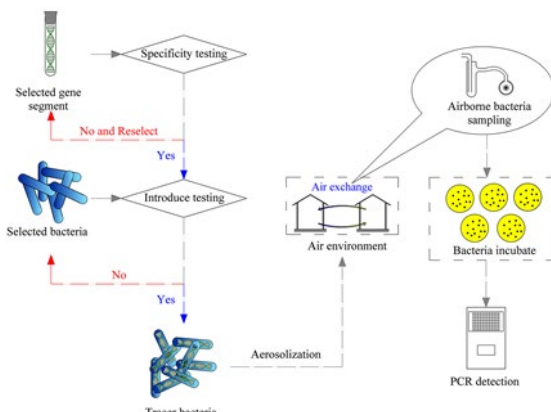


Figure 1. Flowchart of bacteria tracing method for airborne transmission.

### 2.2. Synthesis of the tracer bacteria

Non-pathogenic *E. coli* DH5 $\alpha$  and pFPV-mCherry fluorescent protein plasmid was chosen as selected bacteria species and the selected gene fragment in this experiment, respectively. High-voltage electroporation was used to introduce the pFPV-mCherry fluorescent protein plasmid into the *E. coli* DH5 $\alpha$ . The isolated and identified tracer bacteria was kept in -48 °C for backup. A primer was designed to amplify the 550bp region of pFPV-mCherry fluorescent protein plasmid.

Forward primer: CACGAGTTCGAGATCGAGGG;

Reverse primer: GGTGTAGTCCTCGTTGTGGG

### 2.3. DNA extraction and PCR amplification

Single bacteria colony was randomly isolated and cultured in liquid media at 37 °C for 6 h. Afterwards, the liquid media with the bacteria were centrifuge at 4 °C and 8000 rmp for 2 min. Supernatant was discarded and 2 mL sterilized deionized water was poured into the centrifuge tube and resuspended, which was repeated for 3 times. Water bath at 100 °C for 5 min was used to extract the bacteria gene. The extracted gene were amplified by PCR (95 °C for 5 min, followed by 35 cycles at 95 °C for 30 s, 55 °C for 30 s, and 72 °C for 30 s and a final extension at 72 °C for 10 min) using primers described above. PCR reactions were performed in triplicate 25 μL mixture containing 22 μL Mix, 1 μL of each primer and 1 μL sample.

### 2.4. Tracer bacteria aerosolization and sampling

Frozen beads containing tracer bacteria were rolled on a sterilized tryptic soy agar before being incubated at 37 °C for 24 h. The colonies of tracer bacteria were scraped off and transferred into sterilized liquid nutrient broth (Qingdao Hope Bio-Technology Co., Ltd, Qingdao, China) before the incubation at 37 °C for 24 h.

An air-atomize spraying nozzle or nebulizer was used to aerosolize the liquid nutrient broth with tracer bacteria. Airborne bacteria sampler (e.g. liquid collision sampler or Anderson sampler) could be used to sample airborne bacteria.

### 2.5. Genetic stability of plasmid

The genetic stability of tracer bacteria (Gene-modified *E. coli* DH5α in this experiment) was accessed by continuous passage method. The conjugant (pFPV-mCherry fluorescent protein plasmid + *E. coli* DH5α) was cultured in liquid culture-medium and 100 μL of the bacteria solution was removed to new liquid culture-medium every 12 h for 5 days. Duplicate 0.1 mL aliquots of the diluted sample were transferred on four Petri dishes with sterilized tryptic soy agar every 24 h. Ninety-six colonies on the Petri dishes (twenty-four colonies from each Petri dish) were randomly selected to conduct DNA extraction, PCR amplification and gel electrophoresis analysis. Stability rate of the plasmid is ratio of the quantity of the positive reacted bacteria to ninety-six.

### 2.6. Effect of aerosolization on the tracer bacteria

Both the survival and genetic stability of plasmid after aerosolization were measured and quantified by survival rate and stability rate. The bacteria solutions before and after aerosolization were diluted and transferred on five Petri dishes with selective medium of *E. coli*, respectively. The survival rate of aerosolization is the ratio of the average bacterial colony count on the Petri dishes with *E. coli* selective medium of the bacteria solutions before aerosolization to that of the bacteria solutions after aerosolization. Stability rate of the plasmid was definition above.

### 2.7. Field invalidation of the tracing method in layer hen farm

Field experimental site: The field experiment of airborne bacteria transmission was carried out between two side-by-side layer hen houses with the approval of a farm located in Sichuan Province of China from December, 2017 to January, 2018 (Figure 2. a and b). Each experimental house (12.0 m W × 96.0 mL) had a capacity of 65,000 Roman hens (28 week of hen age at the starting of experiment) and were equipped with manure belts to remove manure out of the house every 3 d. Both layer hen housing facilities and the environment control system were supplied by Big Dutchman (Vechta, Germany). The distance between the two experimental houses was 11 m and the height of the side-wall inlet (0.8 m × 0.5 m) was 6.1 m. The 28 inlets and 3 exhaust fans evenly distributed in each side-wall were used for the air exchange in winter. The room and ambient temperature & relative humidity were monitored using HOBO data loggers (Onset Computer Corp., Bourne, MA, USA) with a 5-min interval. Wind speed and direction was recorded by the weather station (BX-5, Jingge Co., Ltd, Beijing, China) installed in the farm.

The specificity testing before the experiment indicated that pFPV-mCherry fluorescent protein plasmid was not found in the surrounding environment of the two houses. An air-atomize

spraying nozzle was used to aerosolize the liquid nutrient broth with tracer bacteria, at a flow rate of 100 mL min<sup>-1</sup> and 207 kPa air pressure. As shown in Figure 2, the nozzle was installed at the height of the fan axis and 70 cm away from the fan inside the layer hen house. All-glass airborne bacteria impingers (AGI-30, Ace Glass, Inc., Vineland, N.J., USA) were used to collect the airborne bacteria between the two houses (points 1–5). The impingers were sterilized in an autoclave at 121 °C and 100 kPa for 15 min before each sampling and each airborne bacteria sampling lasted 15 min.

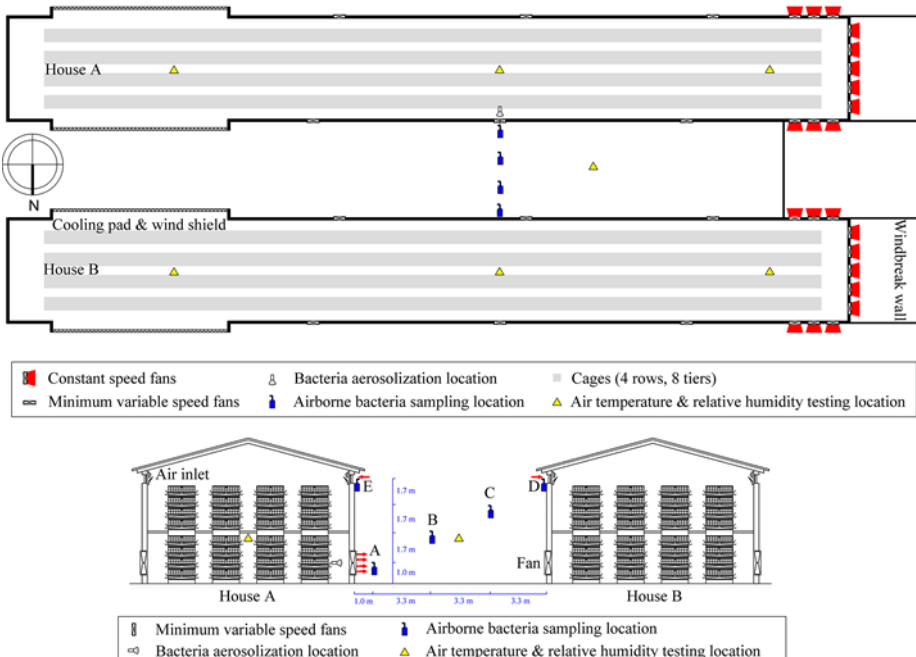


Figure 2. Layer hen houses at the field experiment site (a: Top view of the experimental layer hen houses; b: Cross-sectional view of the experimental layer hen houses).

The airborne bacteria were collected in 15 mL of sterilized 0.9% physiological saline solution in the impinger at a stable flow rate of 12.5 L min<sup>-1</sup>. Duplicate 0.1 mL aliquots of the concentrated sample were transferred on five Petri dishes with sterilized tryptic soy agar. Then the Petri dishes were incubated at 37 °C for 24 to 48 h. The total colonies on the Petri dishes were considered to be the total bacterial number in the original sample. 90 colonies of all the bacteria colonies (or total bacteria colonies if the total bacteria colonies were less than 90) were randomly isolated and cultured in liquid media at 37 °C for 6 h for DNA extraction and PCR amplification. The proportion of tracer bacteria account for the total detected bacteria could be used for calculate the tracer bacteria concentration.

## 2.8. Experimental operation

Tracer bacteria aerosolization and air sampling at the points 1–5 were carried out from 16:00 to 17:00 as an experimental trial. In total 5 experimental trials were carried out (each trial once a week). Air sampling was carried out at the point 1–5 between the two houses using liquid collision samplers (AGI-30, Ace Glass, Inc., Vineland, N.J., USA). The pFPV-mCherry fluorescent protein plasmid was not found by PCR and Gel electrophoresis analysis before each experiment trial.

### 3. Results and Discussion

#### 3.1. Synthesis and genetic stability of tracer bacteria

Results of gel electrophoresis indicated that the pFPV-mCherry fluorescent protein plasmid was successfully introduced into *E. coli* DH5 $\alpha$  (Figure 3). Gene sequencing analysis (Conducted by Tsingke Biological Technology Ltd., Beijing, China) also proved the successful introduction of the pFPV-mCherry fluorescent protein plasmid accurately in molecular level. Stable rate of the introduced pFPV-mCherry fluorescent protein plasmid was tested in five days to cater for application duration of the tracer bacteria. Results showed that stable rate of introduced plasmid was above 95% in all five testing days with little fluctuation (Figure 4). Feasibility of *E. coli* DH5 $\alpha$  gene-modified and high stable rate of pFPV-mCherry fluorescent protein plasmid in the passage of *E. coli* DH5 $\alpha$  made it practicable for bacteria tracing.

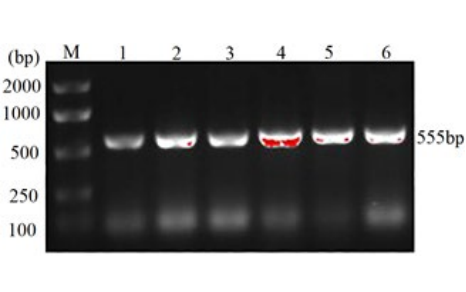


Figure 3. Gel electrophoresis map of the pFPV-mCherry fluorescent protein plasmid.

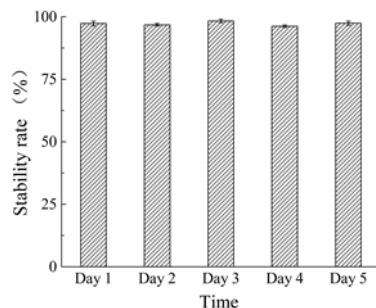


Figure 4. Stable rate of introduced plasmid before aerosolization.

#### 3.2. Assessment of the effect of aerosolization on the tracer bacteria

The survival rate of tracer bacteria through aerosolization decreased with the increase of operated pressure of the air-atomize spraying nozzle. The survival rate of tracer bacteria was 97.5%, 70.8%, and 61.3% at operated pressure of 207, 310, and 414 kPa, respectively (Figure 5). 207 kPa was determined as the optimal operated pressure of the selected air-atomize spraying nozzle used in field experiment. However, there was no difference in stable rate of the pFPV-mCherry fluorescent protein plasmid among different operated pressure of the air-atomize spraying nozzle (Figure 6). Results showed that stable rate of introduced plasmid was above 95% in all five testing days with little fluctuation. Assessment result of the effect of aerosolization on the survival and stable rate of introduced plasmid supported its application of airborne bacteria.

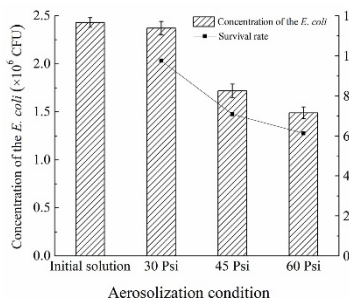


Figure 5. Survival rate of tracer bacteria after aerosolization.

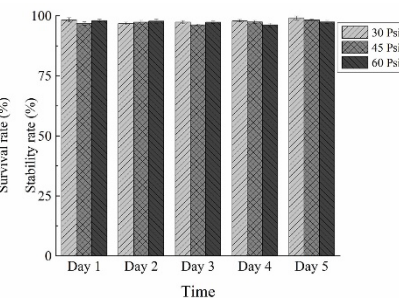


Figure 6. Stable rate of introduced plasmid after aerosolization.

### 3.3. Airborne bacteria transmission between layer hen houses based on tracer bacteria

The room temperature of the experimental house ranged 20.1–23.0 °C, which was higher than ambient temperature 0.2–8.7 °C. Room relative humidity (58.3–92.5%) was more fluctuant than the ambient relative humidity. The wind speed between the two houses was  $< 0.8 \text{ m s}^{-1}$  with an astatic direction for the windbreak of the houses.

The tracer bacteria concentrations measured at the 5 sampling points were shown in Figure 7. Small *E. coli* population originally existed in the air environment of the field site (averaged  $18 \pm 6 \text{ CFU m}^{-3}$ ) and the ratios of the tracer *E. coli* to total *E. coli* were all larger than 98% for the 5 sampling points. The concentrations of tracer *E. coli* decreased from sampling point 1 to 4 (namely with the increase of the distance from the source point). The concentrations of tracer *E. coli* at sampling point 5 was higher than sampling point 4, which indicated emitted *E. coli* was more easily transmitted into the original house than adjacent houses ( $48 \pm 7$  vs.  $21 \pm 5 \text{ CFU m}^{-3}$  at source intensity of  $828 \pm 173 \text{ CFU m}^{-3}$ ). The field application directly demonstrated the existence of airborne transmission between animal houses and current mode of ventilation system design.

In field invalidation of the method, the results proved that the airborne transmission of *E. coli* happened between the two layer hen houses and more tracer *E. coli* went back to the original house than to the adjacent house in condition of present ventilation mode of the house and the weather in winter. Exhausted air would rise and easily reach to the inlets of original house due to the temperature difference of exhausted air and ambient air.

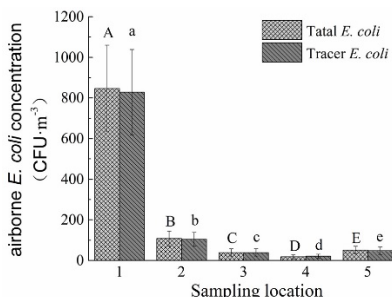


Figure 7. Concentration of total airborne *E. coli* and tracer *E. coli* at different sampling locations. Different capital letters mean the concentrations of total airborne *E. coli* at different sampling locations are different ( $P < 0.05$ ); Different lowercase letters mean the concentrations of tracer airborne *E. coli* at different sampling locations are different ( $P < 0.05$ ).

The present tracing method has several limitations. First, wet aerosolization used in this method does imitate the fate of microbials expelled from respiratory tracts in wet aerosols. However, the other way of microbials aerosolization (e.g. dry aerosolization) needs further study when airborne microorganisms originated from different source were considered. Second, bioaerosol particles with single diameter is hard to generated, which results in blend with multiple factors. In this field invalidation experiment, particle size was not taken into consideration. Third, although precise identification is achieved by this airborne bacteria tracing method, the operation procedure was complicate for essential bacteria culture and large amount of PCR amplifications. Fourth, risk of experimental site infection by tracer bacteria was one potential obstacle for duplicate test. This airborne bacteria tracing method depends largely on the improvement of bioaerosol technology. Applicable complexity of this airborne bacteria tracing method will reduce in the future.

### 4. Summary

In summary, this tracing method of airborne bacteria transmission across built environments provides a novel and integrated way to conduct disease airborne transmission research. To our

knowledge, this is the first bacteria tracing method that physical and biological characteristics of airborne bacteria could be expressed veritably. This method warrants further investigation and needs to be improved with the development of bioaerosol technology.

Both the introduced plasmid stability rates of tracer *E. coli* before and after aerosolization were above 95% in 5 days. Tracer *E. coli* survival rates of  $97.5\% \pm 1.2\%$  through aerosolization was obtained by an air atomizer operated at air pressure of 207 kPa. In the field experiment, the airborne transmission of *E. coli* between poultry houses was proved and emitted *E. coli* was more easily transmitted into the original house than adjacent houses due to the ventilation design and weather condition. Our results suggested that the tracing method of airborne bacteria was available for the investigation of airborne microbial transmission across built environments.

### Acknowledgements

This study was funded by the National Key R&D Program of China (2018YFD0500701), Agricultural Research System of China (CARS-40), and Fundamental Research Funds for the Central Universities (2018QC137).

### References

- Bertran, K., C. Balzli, Y.K. Kwon, T.M. Tumpey, A. Clark, D.E. Swayne, 2017. Airborne Transmission of Highly Pathogenic Influenza Virus during Processing of Infected Poultry. *Emerging Infectious Diseases*. 23 (11), 1806–1814.
- Cowling, B.J., D.K.M. Ip, V.J. Fang, P. Suntarattiwong, S.J. Olsen, J. Levy, T.M. Uyeki, G.M. Leung, J.S.M. Peiris, T. Chotpitayasunondh, H. Nishiura, J.M. Simmerman, 2013. Aerosol transmission is an important mode of influenza A virus spread. *Nature Communications*. 4 (1), 1935.
- Duan, H., T. Chai, J. Liu, X. Zhang, C. Qi, J. Gao, Y. Wang, Y. Cai, Z. Miao, M. Yao, G. Schlenker, 2009. Source identification of airborne Escherichia coli of swine house surroundings using ERIC-PCR and REP-PCR. *Environmental Research*. 109 (5), 511–517.
- Kim, D.K., D.H. Kang, 2018. UVC LED Irradiation Effectively Inactivates Aerosolized Viruses, Bacteria, and Fungi in a Chamber-Type Air Disinfection System. *Applied and Environmental Microbiology*. 84 (17), e00944–00918.
- Lee, N., D. Hui, A. Wu, P. Chan, P. Cameron, G.M. Joynt, A. Ahuja, M.Y. Yung, C.B. Leung, K.F. To, S.F. Lui, C.C. Szeto, S. Chung, J.J.Y. Sung, 2003. A Major Outbreak of Severe Acute Respiratory Syndrome in Hong Kong. *New England Journal of Medicine*. 348 (20), 1986–1994.
- Ma, L., G. Zhang, M.P. Doyle, 2011. Green fluorescent protein labeling of Listeria, Salmonella, and Escherichia coli O157:H7 for safety-related studies. *PloS One*. 6 (4), e18083–e18083.
- Pitkin, A., J. Deen, S. Dee, 2009. Use of a production region model to assess the airborne spread of porcine reproductive and respiratory syndrome virus. *Veterinary Microbiology*. 136 (1–2), 1–7.
- Ramos, S., M. MacLachlan, A. Melton, 2017. Impacts of the 2014–2015 Highly Pathogenic Avian Influenza Outbreak on the U.S. Poultry Sector. In: USDA Ed.
- Wei, J., J. Zhou, K. Cheng, J. Wu, Z. Zhong, Y. Song, C. Ke, H.-L. Yen, Y. Li, 2018. Assessing the risk of downwind spread of avian influenza virus via airborne particles from an urban wholesale poultry market. *Building and Environment*. 127, 120–126.
- Xiao, S., Y. Li, M. Sung, J. Wei, Z. Yang, 2018. A study of the probable transmission routes of MERS-CoV during the first hospital outbreak in the Republic of Korea. *Indoor Air*. 28 (1), 51–63.
- Yu, I.T.S., Y. Li, T.W. Wong, W. Tam, A.T. Chan, J.H.W. Lee, D.Y.C. Leung, T. Ho, 2004. Evidence of Airborne Transmission of the Severe Acute Respiratory Syndrome Virus. *New England Journal of Medicine*. 350 (17), 1731–1739.
- Zeng, J., C. Lei, Y. Wang, Y. Chen, X. Zhang, Z. Kang, X. Zhai, X. Ye, H. Wang, 2018. Distribution of *Salmonella Enteritidis* in internal organs and variation of cecum microbiota in chicken after oral challenge. *Microbial Pathogenesis*. 122, 174–179.
- Zhou, J., J. Wei, K.T. Choy, S.F. Sia, D.K. Rowlands, D. Yu, C.Y. Wu, W.G. Lindsley, B.J. Cowling, J. McDevitt, M. Peiris, Y. Li, H.L. Yen, 2018. Defining the sizes of airborne particles that mediate influenza transmission in ferrets. *Proceedings of the National Academy of Sciences of the United States of America*. 115 (10), E2386–e2392.
- Zhou, P., Y. Yang, A.C.K. Lai, G. Huang, 2016. Inactivation of airborne bacteria by cold plasma in air duct flow. *Building and Environment*. 106, 120–130.

# Effect of Concentration of SAEW on Pathogenic Bacteria Viability in a Broiler House

Zhifang Shi <sup>a,b</sup>, Weichao Zheng <sup>d</sup>, Lei Xi <sup>a,b\*</sup>, Tongshuai Liu <sup>b,c</sup>, Xue Hui <sup>b,c</sup>

<sup>a</sup> College of Animal Science and Technology, Henan University of Animal Husbandry and Economy, Zhengzhou, Henan 450011, P.R. China

<sup>b</sup> Henan Engineering Research Center on Animal Healthy Environment and Intelligent Equipment, Zhengzhou, Henan 450011, P.R. China

<sup>c</sup> College of Intelligent Manufacturing and Automation, Henan University of Animal Husbandry and Economy, Zhengzhou, Henan 450011, P.R. China

<sup>d</sup> College of Water Resources & Civil Engineering, China Agricultural University, Beijing 100083, P.R. China

\* Corresponding author. Email: [xilei@hnuah.edu.cn](mailto:xilei@hnuah.edu.cn)

## Abstract

Spraying slightly acidic electrolyzed water (SAEW) has been considered as a novel approach to reduce microbes in poultry houses. The objective of this study was to determine the minimum inhibitory concentrations (MICs) of SAEW for the microbes isolated from broiler houses, and to evaluate the effectiveness of SAEW in reducing pathogenic microorganisms on internal surfaces of broiler houses. SAEW with available chlorine concentrations (ACCs) at 10, 20, 30, 40, 50 and 60 mg L<sup>-1</sup> was applied to suspension of *Escherichia coli*, *Salmonella*, *Staphylococcus aureus*, and fungi bacteria isolated form the surfaces of broiler houses, and also directly to the internal surfaces of broiler houses by wiping or spraying. The results showed that SAEW had strong antimicrobial effect on *Escherichia coli*, *Salmonella*, *Staphylococcus aureus* and fungi isolated from broiler barns, and the bactericidal effectiveness increased with the increasing ACC. The measured MIC of SAEW for *Salmonella* and *Staphylococcus aureus* isolated form broiler barns was 20 mg L<sup>-1</sup> of ACC, while it was 30 mg L<sup>-1</sup> for *Escherichia coli* and fungi. SAEW with ACC at 50 mg L<sup>-1</sup> and 60 mg L<sup>-1</sup> could completely inactivate the total suspended bacteria and fungi isolated from feathers and feed, respectively. It has a sterilization rate of 87.87%–100% by SAEW for bacteria which was used in the broiler house. The wiping method is better than spray with the same concentration of.

**Keywords:** Slightly acidic electrolyzed water (SAEW), microbes, minimum inhibitory concentration (MIC), disinfection

## 1. Introduction

Regular disinfection of the breeding environment is an important measure to prevent the diseases occurrence of breeding animals and to improve the economic efficiency of breeding farms. At present, the farm environment is mainly disinfected with large amounts of chemical disinfectants, because the chemical disinfectants are cheap, easy to use, and effective. But they are chemical toxic, corrosive and instable. The resistance problems of pathogenic microorganisms, caused by chemical disinfectants, may reduce the effectiveness of disinfection, which may trigger larger-scale outbreaks of the epidemic, restricting the healthy development of modern animal husbandry. The use of chemical disinfectants have caused great concerns for breeding environment and product safety (Böhm, 1998; Gräslund et al., 2001). Developing an alternative disinfectant that is not a biohazard to animal and human health is crucial for environmental decontamination. Slightly acidic electrolyzed water (SAEW) has been considered as an effective and environment-friendly disinfectant for reducing microbes in farms. SAEW is an anti-microbial agent produced by electrolyzing a dilute solution of sodium chloride (NaCl) or hydrochloric acid (HCl), generating the major germicidal component-free chlorine (including ClO<sup>-</sup>, HClO and Cl<sub>2</sub>). Compared to the traditional membrane acidic electrolyzed water (pH < 3.0, oxidation reduction potential ‘ORP’ > 1,000 mV), the SAEW has a similar anti-microbial ability, but is less corrosive and easier and cheaper to produce due to its near neutral pH value (5.5–6.5)

and lower ORP. The available chlorine is mainly in the form of  $\text{HClO}$ , and the sterilization effect of  $\text{HClO}$  is about 80 times that of  $\text{ClO}^-$  (Anonymous, 1997). In the past decade, SAEW has been increasingly gaining interest as a disinfectant in agriculture, dentistry, medicine and food industry (Zheng et al., 2012; Zheng et al., 2016; Sakurai et al., 2003; Huang et al., 2008). It has been shown that SAEW can effectively inactivate *E.coli*, *Salmonella*, *Staphylococcus aureus*, molds and viruses in the air and on the surfaces, which could be highly hazardous for feed safety and human health (Quan et al., 2010; Nan et al., 2010; Zhang et al., 2011; Hao et al., 2013). SAEW with an available chlorine concentration (ACC) of  $20 \text{ mg L}^{-1}$  has a 79% bactericidal effect against microorganisms in 30 s to 60 s of exposure time (Okamoto, 2006). Yang et al. (2011) reported that the level of total airborne bacteria was reduced by 70% by spraying SAEW in a cage hen house. Zhao et al. (2014), Hao et al. (2013) and Ji et al. (2017) also found that SAEW had antimicrobial effect on airborne bacteria from flat raise broiler house. Wu et al. (2010) and Hao et al. (2013) found a reduction of 98% in total viable bacteria and 68% in airborne fungi after spraying SAEW in a swine house. SAEW can also be added into drinking water for animals to promote the intestinal health and improve the production performance of animals (Bodas et al., 2013; Bügener et al., 2014). It has been reported that SAEW can effectively sterilize microorganisms such as *Escherichia coli*, *Salmonella*, *Staphylococcus aureus*, yeasts, molds and viruses that exist on the surfaces and in the air (Quan et al., 2010; Nan et al., 2010; Zhang et al., 2011; Hao et al., 2013). However, there is little published information regarding the minimum inhibitory concentrations (MICs) of SAEW for the microbes present in broiler houses, and the effectiveness of SAEW to reduce pathogenic microorganisms of broiler houses.

The objective of this study was to 1) determine the MICs of SAEW for the *Escherichia coli*, *Salmonella*, *Staphylococcus aureus*, and fungi isolated from broiler houses, and 2) to evaluate the effectiveness of SAEW in reducing the microorganisms on internal surfaces of broiler houses.

## 2. Materials and Methods

### 2.1 SAEW preparation

SAEW containing different available chlorine concentrations (ACC) were generated by electrolyzing 9% HCl solution using a continuous SAEW generator (Beijing Zhouji Ziyuan Huanbao Technology Co. Ltd., Beijing, China). SAEW with a pH of 5.0 to 6.5, an oxidation-reduction potential (ORP) of 800 to 1150 mV, and an ACC of 0 to  $250 \text{ mg L}^{-1}$  was produced in the SAEW generator with different electrolyzing time. SAEW with  $100 \text{ mg L}^{-1}$  of available chlorine was diluted in sterile deionized water to obtain different available chlorine concentrations of 10, 20, 30, 40, 50 and  $60 \text{ mg L}^{-1}$ . The pH and oxidation-reduction potential values of SAEW were measured using a dual scale pH/ORP meter (Shanghai Kangyi Technology Co. Ltd., Shanghai, China) bearing pH and ORP electrodes. The ACC of SAEW was determined by a colorimetric method with a digital chlorine test kit (RC-3F, Kasahara Chemical Instruments Corp., Saitama, Japan). Sterilized distilled water (ACC 0  $\text{mg L}^{-1}$ ) was used as the control. The properties of SAEW are shown in Table 1.

Table 1. Main characteristics of the slightly acidic electrolyzed water (Mean $\pm$ SD, n=5).

ACC $\text{mg L}^{-1}$	pH	ORP, mV
0	5.67 $\pm$ 0.13	1012.6 $\pm$ 12.4
10	6.01 $\pm$ 0.11	1008.3 $\pm$ 21.5
20	5.89 $\pm$ 0.08	1003.7 $\pm$ 29.4
30	5.83 $\pm$ 0.09	1007.1 $\pm$ 47.7
40	5.88 $\pm$ 0.11	999.3 $\pm$ 40.1
50	6.07 $\pm$ 0.14	998.4 $\pm$ 29.0
60	6.07 $\pm$ 0.07	1002.5 $\pm$ 13.9

### 2.2 Collection and preparation of bacterial cultures

The types of microorganisms and its collection media used in this study are shown in Table

2. Samples were collected by wiping the surfaces of floor, walls, window glass, feed troughs, drinking water sinks and iron wires net in a flat bedding broilers house, with 15 to 35 days old white feather broilers, using sterilized cotton swabs soaked in sterilized saline. Each sampling area was 2 cm<sup>2</sup> which was wiped 20 times repeatedly. The cotton swab head was removed and dropped into 10 mL sterilized saline. The supernatant was collected after intensive mixing.

Manure, feed, and dust, 1g for each, and 10 pieces of chicken feathers were collected in the broiler barn. These 4 samples were placed into a tube with 100 mL of sterile saline to make a bacterial suspension. A 1 mL aliquot of the suspension was used to determine the sterilization rate for fungi.

After routine cleaning of the broiler barn, SAEW with ACC at 0 (the control), 10, 20, 30, 40, 50 and 60 mg L<sup>-1</sup> were used for wiping or spraying on the internal surfaces of the broiler house, respectively, including ground, walls, troughs, metal wires. Microbial samples were collected 5 min before and after disinfection, respectively, using the same method of wiping the surfaces.

The collected suspensions were spread on the plates with the corresponding sterilized medium described in Table 2. All the plates were cultured at 37 °C for 48–72 h, except that the fungi plates were cultured at 28 °C (Hao et al., 2013). A single colony of each of the typically grown strains was then picked and streaked to new plates. These selection steps were repeated until pure colonies of each strain were confirmed. The pure colonies were stored at 4 °C before use.

Table 2. Microbial groups isolated form the broiler house and the selective media used in this research for culturing.

Microbe	Media
<i>Escherichia coli</i>	Mc Conkey
<i>Salmonella</i>	SS agar
<i>Staphylococcus aureus</i>	BCP Medium
Fungi	Sabaurauds agar

### 2.3. Minimum inhibitory concentration determination of SAEW

Each isolated bacterial strain was suspended in sterile physiological saline and inoculated to a plate count agar (PCA) with the gradient method. The plates were cultured at 37 °C for 48–72 h, except that the fungi plates were cultured at 28 °C. Then the number of colonies was counted. The concentration of microorganisms for each bacterial suspension was calculated using Eq.(1).

$$P = 50 \cdot N \cdot 10^x / L \quad (1)$$

where,  $P$  is the colony count for each bacterial suspension, CFU mL<sup>-1</sup>;  $N$  is the average number of colonies per plate, CFU;  $x$  is the dilution ratio;  $L$  is the inoculation volume, mL.

A 0.1 mL aliquot of each bacterial suspension with the determined concentration was mixed with 0.9 mL SAEW at ACC of 10, 20, 30, 40, 50 and 60 mg L<sup>-1</sup>, respectively. Another 0.1 mL liquid was mixed with sterile distilled water as the control. After mixing for 5 min, 1 mL mixture was added to 9 mL 0.1% sodium thiosulfate solution for another 5-min mixing. Then 0.1 mL of each mixture was inoculated on PCA. The number of microbes in each bacterial suspension after sterilization was also calculated using Eq. (1). The sterilization rate was calculated using Eq. (2).

$$\text{Sterilization rate}(\%) = 100(P_c - P_T)/P_c \quad (2)$$

where,  $P_c$  is the total number of microbial colonies before disinfection, CFU mL<sup>-1</sup>;  $P_T$  is the total number of microbial colonies after disinfection, CFU mL<sup>-1</sup>.

## 3. Results and Discussion

### 3.1. Microbicidal effect on microorganism isolated from broiler barns

The effect of SAEW on pure microbes isolated from broiler barns is shown in Table 3. SAEW with an ACC of  $\geq 30$  mg L<sup>-1</sup> inhibited the growth of *Escherichia coli* and fungi isolated from broiler barns. For *Salmonella* and *Staphylococcus aureus*, SAEW with an ACC  $\geq 20$  mg L<sup>-1</sup> inhibited their growth completely. After a treatment with SAEW at ACC 20 mg L<sup>-1</sup>, the survival

of *Escherichia coli* and fungi was reduced by 88.5%, and was completely inhibited by SAEW with an ACC at 30 mg L<sup>-1</sup>. SAEW with an ACC of 30 mg L<sup>-1</sup> could completely inhibit the growth of *Escherichia coli*, *Salmonella*, *Staphylococcus aureus* and fungi isolated from broiler houses, which is consistent with the results of previous studies (Nan et al., 2010; Cao et al., 2009; Guentzel et al., 2010).

The results of this study confirmed that SAEW has a great germicidal effect for disinfection in broiler barns. A treatment for 5 min with SAEW at ACC of 20 mg L<sup>-1</sup> could completely inhibit the growth of *Salmonella* and *Staphylococcus aureus* isolated from broiler barns. At an ACC of 30 mg L<sup>-1</sup>, SAEW could completely sterilize *Escherichia coli* and fungi. A minimum of 20 mg L<sup>-1</sup> ACC was required for sterilization of *Salmonella* and *Staphylococcus aureus* with a 5-min treatment time for a separated strain of microbes suspended in saline, while the ACC was 30 mg L<sup>-1</sup> for *Escherichia coli* and fungi isolated from broiler barns. This result is slightly different from previous reports in which SAEW with ACC at 10 mg L<sup>-1</sup> for 5 min could completely suppress the growth of *Escherichia coli*, *Salmonella* and *Staphylococcus aureus* (Nan et al., 2010; Cao et al., 2009) and SAEW with ACC at 25 mg L<sup>-1</sup> could inhibit fungal growth after 10 min treatment (Guentzel et al., 2010). The reason for the difference may be due to individual differences of the microorganisms from different regions or the difference of the organic content in the germ suspension extracted from the sample. Because the ACC in SAEW decreases with the increase of organic matter in the solution, this will weaken its germicidal ability (Park et al., 2009).

Table 3. Efficacy of slightly acidic electrolyzed water for inactivation of microbes isolated from chicken barns

Microbes	colonies (log <sub>10</sub> CFU mL <sup>-1</sup> )	SAEW concentration (mg L <sup>-1</sup> )					
		0	10	20	30	40	50
<i>Escherichia coli</i>	5.12±0.11	+++	+++	+--	---	---	---
<i>Salmonella</i>	4.79±0.17	+++	+++	---	---	---	---
<i>Staphylococcus aureus</i>	5.77±0.21	+++	+++	---	---	---	---
Fungi	6.23±0.10	+++	+++	+--	---	---	---

Note: The processing time for all treatments was 5 min. + means there was still microbial growth after plating. - no microorganisms growth after plating and after re-plating. +++, ---, and +-- represent the results of three consecutive operations.

The effect of SAEW treatment on the microbial survival of total bacteria and fungi isolated from faces, feathers and feed is shown in Table 4. The results showed an increasing trend of sterilization rate along with the increasing of ACC. The treatment with SAEW at 20 mg L<sup>-1</sup> ACC for 5 min inactivated 50.51% microorganisms in the fecal suspension. The sterilization rate increased to 83.64% and 99.99%, when using SAEW with an ACC of 30 mg L<sup>-1</sup> and 40 mg L<sup>-1</sup>, respectively. The sterilizing effect of SAEW for microorganisms in feed also increased with increasing ACC. SAEW with an ACC of 10 mg L<sup>-1</sup> inactivated 55.36% microorganisms in the feed suspension. With the ACC at 30 mg L<sup>-1</sup> and 40 mg L<sup>-1</sup>, the SAEW sterilization rate could reach to about 94.87% and 99.99%, respectively. SAEW with an ACC of 60 mg L<sup>-1</sup> could completely sterilize all the microorganisms in the feed suspension. Great antimicrobial effect on microbes by SAEW on broiler chicken feathers could also be proved. The sterilization rate reached 94.96% at the ACC of 20 mg L<sup>-1</sup>, and the microorganisms in the feather suspension was completely eliminated at the ACC of 50 mg L<sup>-1</sup>.

A slight difference in the minimum inhibitory concentration of SAEW required for inactivation was also observed for the same microbial strain from different sources in broiler barns. For example, SAEW with an ACC of 30 mg L<sup>-1</sup> inactivated 83.64% of the microorganisms in the feces suspension, 94.87% in the suspension of the feed, and 99.87% in the suspension of feathers. When the ACC reached 50 mg L<sup>-1</sup>, SAEW killed all the microbes in the suspension of feathers. At ACC 60 mg L<sup>-1</sup>, SAEW killed all microorganisms in the feed suspension. These observations indicate that there is a difference in the tolerance of microorganisms from different

sources to SAEW. To reach a same inactivation rate, a higher ACC was required to treat the germs in feces suspension, which might be related to the different microbial species and concentrations in different samples.

Table 4. The number of colonies in suspension of dust, faces, feathers and feed before and after SAEW treatment with concentrations varying from 10–60 mg L<sup>-1</sup>, and the calculated sterilization rate per treatment (n=5).

Sources	ACC (mg L <sup>-1</sup> )	Colonies (CFU L <sup>-1</sup> )		Sterilization rate Mean± SE (%)
		Before	After	
Faces	10		1.56×10 <sup>7</sup>	21.21±9.89
	20		9.80×10 <sup>6</sup>	50.51±23.00
	30	1.98×10 <sup>7</sup>	3.24×10 <sup>6</sup>	83.64±31.97
	40		2.08×10 <sup>4</sup>	99.89±11.03
	50		<1	99.99
	60		<1	99.99
Feed	10		1.00×10 <sup>3</sup>	55.36±29.09
	20		8.71×10 <sup>2</sup>	61.12±18.88
	30	2.24×10 <sup>3</sup>	115	94.87±6.68
	40		6.88	99.99±22.04
	50		<1	99.99
	60		Not detectable	100.00
Feather	10		4.73×10 <sup>5</sup>	30.75±12.12
	20		3.44×10 <sup>4</sup>	94.96±4.99
	30	6.83×10 <sup>5</sup>	8.81×10 <sup>2</sup>	99.87±26.72
	40		<1	99.99
	50		Not detectable	100.00
	60		Not detectable	100.00

Note: treatment time was 5 min. for all samples and concentrations.

### 3.2. Disinfection efficiency on the surfaces

Table 5 shows the sterilization effects of SAEW on the internal surfaces of the broiler house. As shown in Table 5, the sterilization effect on the internal surfaces of the broiler barn increased with the increasing ACC. However, the sterilization effect differed between the two disinfection methods. The disinfection effect of each method varied with the different conditions of the surface. Wiping using SAEW at an ACC of 30 mg L<sup>-1</sup> inactivated 93.01% microbes on average on the surfaces of various facilities. The average inactivation rate for all surfaces was only 78.99% when spraying SAEW with ACC of 30 mg L<sup>-1</sup>. The average sterilization rate reached to 92.92% for SAEW with ACC of 50 mg L<sup>-1</sup>. The inactivation rate of SAEW was affected by the method application of wiping and spraying when used for sanitizing the surfaces in broiler barns. The results showed that using SAEW with ACC at 30 mg L<sup>-1</sup>, the wipe method could inactivate 93.01% of microbes on average for various surfaces in broiler barns, while the spray method could only inactivate 78.99% of the germs ( $P<0.05$ ). The materials in facilities also has an impact on the sterilization rate. The reason for the difference in sterilization rates between the two methods was that the spray disinfection operation itself leads to the loss of available chlorine in SAEW (Hsu et al., 2004), thereby reduces the effectiveness of disinfection and sterilization on the surfaces in the facility.

### 4. Conclusions

Spraying slightly acidic electrolyzed water has strong germicidal activity against Escherichia coli, Salmonella, Staphylococcus aureus and fungi isolated from broiler houses. The germicidal effect of SAEW increases with increasing ACC. After a treatment for 5 min, SAEW with ACC at 20 mg L<sup>-1</sup> could completely inhibit the growth of Salmonella and Staphylococcus aureus isolated

from a broiler house. With ACC at 30 mg L<sup>-1</sup>, SAEW completely inhibited the growth of Escherichia coli and fungi. For mixed microbes of different sources from broiler barns, SAEW with an ACC of 50 mg L<sup>-1</sup> could kill all the microorganisms in the suspension of feathers. SAEW with an ACC at 60 mg L<sup>-1</sup> could sterilize all microorganisms in the feed suspension. To completely kill microorganism in feces, a higher ACC is required. SAEW could significantly reduce the microbial content on the surface of facilities in broiler houses. Wiping using SAEW with the ACC at 30 mg L<sup>-1</sup> could sterilize 93.01% of germs, while spraying SAEW could averagely sterilize only 78.99% of the germs, vindicating that the wiping method is more effective than the spraying method in surface disinfection.

Table 5. Sterilization effect of SAEW for surface disinfection in a broiler barn.

Surface	ACC(mg L <sup>-1</sup> )	Wipe		Spray	
		Mean (%)	S.E.M. (±)	Mean (%)	S.E.M. (±)
Floor	30	89.87a	9.27	76.44b	20.05
	40	95.77a	13.02	85.13b	14.02
	50	98.00a	21.45	90.18b	6.67
	60	100.00a	11.53	97.03a	10.31
Wall	30	95.23a	8.98	93.00a	6.96
	40	94.12a	10.17	94.42a	6.11
	50	100.00a	8.66	94.92a	8.33
	60	100.00a	20.05	99.00a	9.95
Glass	30	98.76a	13.02	86.88b	7.92
	40	99.77a	11.45	90.69b	13.58
	50	100.00a	11.53	97.00a	15.22
	60	100.00a	8.98	100.00a	8.87
Feed trough	30	92.23a	10.17	77.00b	9.65
	40	94.12a	8.66	79.12b	8.19
	50	98.55a	12.80	90.92b	15.52
	60	100.00a	13.02	96.07a	11.71
drinking water Sink	30	91.99a	21.45	69.67b	8.40
	40	95.77a	11.53	75.58b	13.11
	50	98.00a	8.98	90.16b	10.45
	60	100.00a	10.17	92.70b	11.43
Iron wire net	30	90.00a	8.66	73.03b	8.98
	40	94.12a	18.05	85.49b	10.04
	50	97.92a	6.26	94.34a	8.76
	60	99.00a	8.13	98.10a	9.05

Note: All samples were collected 5 min after disinfection. In the same line, values with different small letters mean significant difference at P<0.05.

## References

- Anonymous, 1997. Principle of formation of electrolytic water. Hoshizaki Electric Co. Ltd., Sakae, Aichi, Japan.
- Bodas R., D. J. Bartolomé, M. J. Tabernero De Paz, R. Posado, J. J. García, L. Rodríguez, S. Olmedo, A. B. Martín-Diana, 2013. Electrolyzed water as novel technology to improve hygiene of drinking water for dairy ewes. Research in Veterinary Science, 95:1169–1170.
- Bügener E., A. W. S. Kump, M. Casteel, G. Klein, 2014. Benefits of neutral electrolyzed oxidizing water as a drinking water additive for broiler chickens. Poultry Science, 93:2320–2326.
- Böhm R., 1998. Disinfection and hygiene in the veterinary field and disinfection of animal houses and transport vehicles. International Biodeterioration and Biodegradation, 41:217–224.
- Cao W, Z. W. Zhu, Z. X. Shi, C.Y. Wang, B. M. Li, 2009. Efficiency of slightly acidic electrolyzed water for inactivation of *Salmonella enteritidis* and its contaminated shell eggs. International Journal of Food Microbiology 130:88–93.

- Guentzel J. L., K. L. Lam, M. A. Callan, S. A. Emmons, V. L. Dunham, 2010. Postharvest management of gray mold and brown rot on surfaces of peaches and grapes using electrolyzed oxidizing water. International Journal of Food Microbiology, 143:54–60.
- Gräslund S. and B. E. Bengtsson, 2001. Chemicals and biological products used in south-east Asian shrimp farming, and their potential impact on the environment--a review. Science of Total Environment, 280:93–131.
- Hao X. X., Z. Q. Shen, J. L. Wang, Q. Zhang, B. M. Li, C.Y. Wang, W. Cao, 2013. In vitro inactivation of porcine reproductive and respiratory syndrome virus and pseudorabies virus by slightly acidic electrolyzed water. The Veterinary Journal 197:297–301.
- Hao X. X., B. M. Li, C.Y. Wang, Q. Zhang, W. Cao, 2013. Application of slightly acidic electrolyzed water for inactivating microbes in a layer breeding house. Poultry Science, 92:2560–2566.
- Hao X. X., B. M. Li, Q. Zhang, B. Z. Lin, P. Ge, C.Y. Wang, W. Cao, 2013. Disinfection effectiveness of slightly acidic electrolyzed water in swine barns. Journal of Applied Microbiology, 115:703–710.
- Hsu S. Y. and H. Y. Kao, 2004. Effect of stronger conditions on chemical and physical properties of electrolyzed oxidizing water. Journal of Food Engineering, 65:465–471.
- Huang Y R, Y. C. Hung, S. Y. Hsu, Y. W. Huang, 2008. Application of electrolyzed water in the food industry. Food Control, 19:329–345.
- Ji Z. Z., Z. F. Shi, J. Y. Fan, F. R. Zhao, W. T. Li, L. Xi, 2017. Effect of Slightly Acidic Electrolyzed Water on the Disinfection of Particulate and Microbial in Broiler House. China J. Anim. Sci., 53:96–99.
- Nan S. J., Y. Y. Li, B. M. Li, C.Y. Wang, X. D. Cui, W. Cao, 2010. Effect of slightly acidic electrolyzed water for inactivating *Escherichia coli* O157:H7 and *Staphylococcus aureus* analyzed by transmission electron microscopy. Journal of Food Protection, 73:2211–2216.
- Okamoto M., 2006. Microbicidal effect of slightly acidic electrolyzed water. Journal of Antibact Antifung Agents, 34:31–36.
- Park E. J., E. Alexander, G. A. Taylor, R. Costa, D. H. Kang, 2009. The decontaminative effects of acidic electrolyzed water for *Escherichia coli*, O157:H7, *Salmonella typhimurium*, and *Listeria monocytogenes*, on green onions and tomatoes with differing organic demands. Food Microbiology, 26:386–390.
- Quan Y., K. D. Choi, D. H. Chung, I. S. Shin, 2010. Evaluation of bactericidal activity of weakly acidic electrolyzed water (WAEW) against *Vibrio vulnificus* and *Vibrio parahaemolyticus*. International Journal of Food Microbiology, 136:255–260.
- Sakurai Y., M. Nakatsu, Y. Sato, K. Sato, 2003. Endoscope contamination from HBV– and HCV–positive patients and evaluation of a cleaning/ disinfecting method using strongly acidic electrolyzed water. Digestiv Endoscopy, 15: 19–24.
- Wu P, 2010. Applying electrolyzed water as disinfectant in animal house. Master Thesis. National Ilan University, Ilan, Yilan City.
- Yang S, M. Y. Chang and P. C. Hung, 2011. A Study of Membrane-less Electrolyzed Water fogging-spread for Airborne Bacteria and Fungus Decontamination in Hen House. Advances in Biomedical Engineering Proceedings of 2011 International Conference on Agricultural and Biosystems Engineering.
- Zhao Y, H. W. Xin, D. L. Zhao, W. C. Zheng, W. Tian, H. Ma, K. Liu, H. Hu, T. Wang, M. L. Soupir, 2014. Free chlorine loss during spraying of membraneless acidic electrolyzed water and its antimicrobial effect on airborne bacteria from poultry house. Annals of Agricultural and Environmental Medicine, 21:249–255.
- Zhang C. L., Z. H. Lu, Y. Y. Li, Y. C. Shang, G. Zhang, W. Cao, 2011. Reduction of *Escherichia coli* O157:H7 and *Salmonella enteritidis* on mung bean seeds and sprouts by slightly acidic electrolyzed water. Food Control, 22:792–796.
- Zheng W. C., W. Cao, B. M. Li, 2012. Bactericidal activity of slightly acidic electrolyzed water produced by different methods analyzed with ultraviolet spectrophotometric characteristics. International Journal of Food Engineering, 8: 41–52.
- Zheng W. C., L. Ni, X. Hui, 2016. Optimization of slightly acidic electrolyzed water spray for airborne culturable bacteria reduction in animal housing. International Journal of Agricultural and Biological Engineering, 9: 185–191.

# **Environment-Friendly Management of Livestock and Poultry Mortalities**

**Tom Tabler**

Mississippi State University Extension Service, Poultry Science Department,  
Mississippi State University, Hood Road, MS 39762, USA

Email: [t.tabler@msstate.edu](mailto:t.tabler@msstate.edu)

## **Abstract**

Mortality disposal associated with routine and occasional catastrophic death losses at livestock, poultry, and egg operations is a daily management challenge made more complicated by the need to address this disposal in an environmentally safe and sustainable manner. While overall percentage of animals lost is small, the massive size of global livestock and poultry industries means billions of pounds of mortalities are generated annually. Common methods for routine and catastrophic mortality management include burial, landfills, incineration, rendering, and composting. Each method has its own unique advantages and disadvantages, as well as its own associated costs and benefits. Choosing the best method(s) should be based on individual farm circumstances at the time and any restrictions that may apply. When available and managed properly, any of the previously mentioned options can be used successfully for daily routine disposal without adverse environmental impacts. However, determining the proper method(s) to use during a catastrophic event will likely prove more challenging. In event of a catastrophic loss situation, it is vital to have an emergency response plan in place well ahead of time that addresses individual farm situation(s), cause of death (reportable disease or otherwise), state/local regulations, environmental implications, and operational/cleanup costs; as these will affect applicability and feasibility of selected carcass disposal options. Time is critical during an emergency or catastrophic event and first responders should consider all possible options that allow for rapid, environmentally safe disposal of carcasses, because no single option can adequately address all issues in every situation.

**Keywords:** Environmental impact, waste stream, composting, catastrophic, carcass disposal

## **1. Introduction**

At the forefront of critical issues facing today's technically advanced livestock and poultry industries are those age old problems of dealing with waste management streams and the associated environmental issues that these waste streams present. The high level of concentration associated with livestock and poultry production involves large volumes of byproducts such as mortalities, manure, and hatching/processing wastes that require regular and prompt disposal (CAST, 2008). Carcass disposal is a daily challenge facing livestock, poultry, and egg production operations.

Routine (and occasional catastrophic) loss of animals is an inevitable consequence on livestock farming operations. Disposing of mortalities is a natural part of animal agriculture; although it is not limited to on-farm applications (Bonhotal et al., 2014). Whether resulting from typical animal production mortality, natural disasters (storms, fires, floods, power failures, etc.), disease entry, or an act of terrorism, livestock mortality losses pose a daunting carcass disposal challenge to producers. Many livestock producers are, with good reason, concerned about proper mortality management and disposal. Proper management of animal losses on livestock operations has several important implications for environmental protection, nutrient management, herd/flock health, as well as public health. The goal of proper mortality management and disposal is to protect the environment (soil, air, and water quality) and to prevent the spread of infectious, contagious, and communicable diseases. Laws related to proper disposal and processing of animal mortalities vary from state-to-state within the United States (U.S.) and it is the producer's responsibility to be aware of these laws. Most animal feeding operations operate under a state-issued permit, and

disposal of routine operational mortalities and catastrophic mortalities must be addressed in a farm-specific comprehensive nutrient management plan (CNMP) associated with that permit for each individual operation.

In cases where animal mortalities are suspected of, or confirmed with, prion diseases, working closely with state and federal officials and veterinarians is required. A prion is a protein chain that has become misfolded and can infect and replace normal protein chains in the brain of an animal. Bovine Spongiform Encephalopathy (BSE or Mad Cow Disease), Chronic Wasting Disease (CWD) in deer and elk, and Scrapie in sheep and goats are all diseases called Transmissible Spongiform Encephalopathies (TSEs) caused by prions. The transmission of disease among same and different species with prion diseases is not well understood. However, we do understand that disabling this misfolded protein is extremely difficult: it takes exposure to heat of 1800–2000°F or alkaline digestion to accomplish the task. Neither of these will occur in a simple composting process (Bonhotal et al., 2014). However, composting might be used to reduce the volume and moisture of the affected carcasses. Then the remaining materials (wood chips, bones, etc.) could be burned in a high temperature incinerator to destroy the prions.

The market for U.S. meat and meat products in 2017 required the slaughter of 156 million heads of cattle, calves, sheep and hogs (USDA, 2018a), as well as 9.3 billion heads of poultry (USDA, 2018b). Rising incomes worldwide and continued and evolving preferences for animal-based protein is increasing the pressure on the U.S. livestock industry to increase meat production even further, resulting in more intensive production of meat animals on U.S. livestock operations. Along with the increased production in animal protein destined for the human food supply comes an increase (despite the best efforts of farm managers, veterinarians, and drug companies) in animal mortalities that cannot be used for human consumption. How to safely manage that mortality while also protecting the environment is the topic of this presentation.

## 2. Livestock Mortalities in the United States

The United States is one of the largest and most highly developed livestock production areas in the world. In 2017, the U.S. produced 26.3 billion pounds of beef, 25.6 billion pounds of pork, 56.1 billion pounds of chicken, along with hundreds of millions of pounds of meat from various other livestock species, including lamb, sheep, goats, turkeys, and ducks (USDA, 2018a,b). The greatest majority of livestock raised on farms and ranches are eventually slaughtered for human consumption. However, a small proportion of the total either die naturally or accidentally prior to slaughter, or are condemned upon inspection at the time of slaughter and declared unfit for human consumption.

These animals must be disposed of in an environmentally safe and friendly manner by alternative means. Even though the percentage of animals that die prematurely or are condemned at slaughter is very small, the massive size of the U.S. livestock industry results in the generation of several billion pounds of livestock mortalities annually. This creates a disposal challenge for livestock operations and meatpackers that is made more complicated because of the need to avoid adverse environmental consequences such as the spread of disease or pollution of ground and surface waters.

### 2.1. Cattle

Over 32 million head of cattle were slaughtered in the U.S. in 2017 (USDA, 2018a). However, a much larger number of cattle (parent stock and young calves) remain on farms and ranches across the country than are, annually slaughtered for human consumption. As of July 1, 2018, USDA estimated there were 103 million cattle and calves in the U.S. In addition, a continuous inventory of approximately 9.4 million dairy cattle is needed to supply the 216 billion pounds of milk annually consumed in the U.S. The USDA (2017) estimated that almost 3.9 million cattle and calves were lost to all causes (predator and non-predator) in 2015.

## 2.2. Other livestock

A small proportion of the population of all species of commercial livestock dies on the farm/ranch/feedlot before being slaughtered. Much like cattle, disposal of dead swine, sheep, goat, and poultry carcasses creates challenges for producers that are not only similar to those faced by beef and dairy producers, but also different as well. For example, death losses from commercial swine and poultry operations occur at a younger age than cattle. In addition, swine and poultry are much smaller and lighter in weight than cattle and, individually, may be easier to handle. However, the large populations of animals on commercial swine and poultry operations may mean more individual deaths per year than in the cattle industry.

In addition, consolidation in the swine, and, particularly the poultry, industries in recent years has resulted in fewer, but much larger, operations. Many commercial hog farms now produce tens of thousands of hogs each year. Consolidation in the poultry industry is even greater than in the swine industry with many farms housing 250,000 or more broiler chickens per flock and perhaps averaging 5 to 8 flocks per year. Numbers of this magnitude will naturally produce large volumes of mortalities, even if the death rate remains extremely low. What this means is that, with a global livestock population of approximately  $1.9 \times 10^{10}$  birds and  $2.31 \times 10^8$  mammals (FAO, 2007), farming systems generate a significant volume of mortalities that must be disposed of safely, practically, economically, and environmentally friendly.

## 2.3. Methods of animal mortality disposal

Throughout history, the most widely used methods for disposal of on-farm mortalities has likely been burial and, to a lesser extent, burning (Gwyther et al., 2011). However, despite potential logistical and perhaps economic advantages, and because of recent advances in science and technology, growing concerns about the environment, and increased awareness of public health, these methods now have a somewhat less favorable standing than before. A variety of common animal mortality disposal options exist including: 1) burial, 2) landfills, 3) incineration, 4) rendering, and 5) composting. Producers and researchers recognize that mortality disposal is a continuous and growing challenge; and that economics and available resources all come into play in determining which method(s) works best for each individual situation, whether routine or catastrophic. Therefore, it is important to consider all options that allow for the biologically and environmentally safe disposal of animal carcasses, because no single method will work in every situation. These options will be reviewed below.

### 2.3.1. Burial

Mortality disposal by trench burial involves excavating a trough in the earth, placing carcasses in the trench, and backfilling or covering with the excavated material. It is likely the most common method of catastrophic dead animal disposal in the U.S., although some states have outlawed it in recent years. Most states that still allow burial have regulatory burial guidelines outlining site location, distance from waterways, depth to groundwater, etc. Characteristics to consider in determining the suitability of a site as a burial location include: soil properties, slope or topography, hydrological properties, accessibility, future intended use of the site, and proximity of the site to public areas, roadways, bodies of water, wells, dwellings and residences, municipalities, and property lines (National Agricultural Biosecurity Center Consortium (NABCC, 2004).

Poor site selection, sandy soils, areas with high water tables and karst topography may pose a threat to groundwater contamination. In addition, carcasses may not fully degrade when buried. Parts of carcasses may persist for years in an anaerobic (low oxygen) environment and pathogen reduction or elimination cannot be assured in such an environment. Burial pits are essentially mass graves and may pose additional threats through the spread of disease or other means of environmental contamination. On July 1, 1994, Arkansas became the first U.S. state to enact legislation prohibiting the use of burial pits as an option for routine poultry carcass disposal. Since then, other states have passed regulations that restrict or limit the use of burial as a carcass disposal

option. However, in certain emergency situations, burial may be permitted where there is a catastrophic loss of birds and prompt action is required.

Compared to other disposal options, burial is often considered a relatively economical method of carcass disposal. In a catastrophic or emergency situation, with an acceptable land mass or site assessment, it is quick, simple, and relatively convenient because the process is straightforward and the equipment required is widely available. Burial prevents the need to haul potentially infectious material on public roadways, which could increase the risk of spreading disease. On-farm burial, if done away from public roadways, also attracts less attention from the general public.

However, there are disadvantages associated with burial that include the potential for serious environmental effects, particularly in the area of water quality, and the fact that burial does not eliminate disease agents that may be present. In addition, residue at the burial site can last for decades, affecting the use of the site for years into the future. Also, some states may not allow burial, regulations may limit the number of sites that are acceptable, public perception of burial as a disposal option is becoming less popular, and burial may be difficult or impossible if the ground is wet or frozen.

### 2.3.2. Landfill

Landfill disposal may be another option under certain conditions. Modern U.S. landfills are highly regulated operations specifically designed to protect the environment. However, many older landfills do not have this capability or level of protection. In addition, in many states, the disposal of animal carcasses at landfills is an allowed, but not necessarily available, option. Often times, the individual landfill owner/operator has decision making power over whether or not to accept animal carcasses. Arrangements should be made with the landfill operators ahead of time as to whether or not the landfill will accept animal carcasses in event of an emergency. If the landfill will accept carcasses, terms of use in case of an emergency should also be worked out ahead of time (fees, amount of material to accept, etc.).

Depending on the age and environmental protection capabilities, landfills may represent an option that poses little threat to the environment. In addition, the quantity of material that can be disposed of in an approved landfill(s) may be quite large. This can be important in an emergency or catastrophic situation when time is critical and death losses are high. However, in some cases, a suitable landfill site may not be near the site of the emergency or a landfill near the emergency location may refuse to accept animal carcasses. It is vital to assess these issues and have a plan in place well ahead of an emergency. In addition, landfilling is considered more a containment practice and not actually elimination/disposal. This means that the waste will have to be managed long-term; in addition, carcasses must be transported from the emergency site to the landfill, which increases the potential for disease spread when infected material is moved off-site.

### 2.3.3. Incineration

Incineration is the thermal destruction of carcasses by auxiliary fuel such as propane, diesel, or natural gas. Modern incinerators are capable of reducing carcasses to ash and generally are biosecure. Unfortunately, incinerators require a great deal of energy compared with other disposal methods, and are not considered a viable economic disposal option because of the cost and labor involved. In addition, regular cleaning and maintenance are required to keep the incinerator functioning properly. Also, incinerators must be loaded and operated according to the manufacturer's recommendations (Rahman and Berg, 2017). Odor nuisance complaints generated by poorly functioning incinerators are a common occurrence in the U.S.

However, incineration can be a safe and effective means of carcass disposal, especially from the standpoint of biosecurity. The carcass is completely consumed by fire and heat within a self-contained incinerator. Although, an air quality permit may be required by the Department of Environmental Quality where you live based on the size and quantity of the carcasses to be burned. Throughout history, incineration has played an important role in carcass disposal. Today,

however, increased awareness of public health, recent advances in science and technology, concerns about environmental protection, and economic considerations have all affected the use of incineration for carcass disposal. Currently, it is generally accepted that open-air burning and other poorly-managed incineration options pose legitimate pollution concerns. Therefore, incineration should be considered only after other more environmentally-friendly options have been ruled out.

#### 2.3.4. *Rendering*

Where available, rendering is one of the best means for recycling poultry carcasses from the farm, and converting carcasses into a valuable byproduct in an environmentally acceptable manner. The rendering of animal mortalities converts carcasses into protein meal, fat, and water through the use of various mechanical (grinding, mixing, pressing, and separating), thermal (cooking, evaporating, and drying), and possibly chemical processes. End products of rendering have economic value and are capable of being stored for long periods of time. Depending on the amount of mortality, livestock carcasses can be a huge source of organic matter. Typically, a fresh carcass contains approximately 32 percent dry matter that includes 52 percent protein, 41 percent fat and 6 percent ash (Malone et al., 1987). Rendering can provide a source of protein for animal feed, and results in a safe, hygienic means of disposing of lost animals. Proper heat treatment during the rendering process should eliminate most bacterial pathogens in the finished product and remove the moisture needed for further bacterial growth. However, recontamination after processing is possible so care must be taken when handling the processed product.

In many situations, rendering is also the best available disposal option for large ruminant mortalities. In fact, USDA reported that the majority of cattle carcasses (80.2 percent) from feedlots in the U.S. were disposed of by rendering while only 8.8 percent were disposed of by composting, the second most favored method (USDA, 2013). The rendering industry has infrastructure and capabilities in place to accomplish volume control reduction and heat treatment while also managing environmental regulations. In most areas of concentrated ruminant livestock production, rendering plants are available and have capabilities for collection, transportation, and processing of ruminant mortalities. The cost of rendering in these areas is generally reasonable when compared with other mortality management options.

#### 2.3.5. *Composting*

Carcass composting is a natural, aerobic (requires oxygen), biological decomposition process. While it occurs naturally under a wide range of conditions, to achieve rapid decomposition specific conditions are required (VanDevender and Pennington, 2004). These specific conditions are often thought of as the compost “recipe.” When these conditions are met, the microbial populations will increase rapidly, resulting in elevated temperatures in the composting mix. If conditions are favorable, during the first phase of composting, the temperature of the compost material increases, organic materials break down into smaller compounds, soft tissue gradually decomposes, and bones partially soften. In the second phase, bones and any remaining carcass material fully breaks down and the compost material eventually becomes dark brown in color and more humus-like. Numerous factors affect the composting process including:

- Moisture level
- Carbon to nitrogen (C:N) ratio
- Temperature
- Oxygen
- Particle size
- Surface area
- Size and activity level of the microbial populations
- Physical properties of the waste

Bin or alleyway composters are quite popular on U.S. poultry farms today. These structures

typically have concrete floors to prevent leachate from contaminating soil or reaching surface or groundwater supplies, sidewalls to contain compost materials, and roofs to prevent rainfall from entering the material. The composter is sized to the size of the farm based on factors such as the type of operation, animal species raised, regularity and amount of mortalities, weather, and available funding (including cost share funds) (Bonhotal et al., 2014). Assistance from state and federal officials is available on properly sizing composters.

Moisture level is likely the most critical factor in successful composting. A moisture content of 50 to 60 percent seems to work best. The composting process slows considerably if moisture content drops to 40 percent or less and it goes anaerobic (without oxygen) if moisture content remains at 70 percent or greater for any length of time. Fortunately, however, composting is a fairly forgiving process. In other words, if it gets messed up, it can be fixed. It may take a little time but compost will allow mistake(s) to be corrected. If the material gets too wet or too dry and the process stops working, the moisture level can be corrected and it will start working again. Typically, too wet is a bigger problem than too dry. I've known numerous individuals that have gotten their compost material too wet and almost no one that ever managed to get the material too dry. Theoretically, getting compost material too dry is possible but, in actuality, it is very difficult to do. Several factors that make up the ideal compost recipe are listed in Table 1.

Table 1. Range of conditions for rapid composting<sup>1</sup>.

Condition	Reasonable Range	Preferred range
Carbon to nitrogen (C:N) ratio	20:1 – 40:1	25:1 – 30:1
Moisture content	40–65%	50–60%
Oxygen concentration	>5%	Much greater than 5%
Particle size (diameter in inches)	1/8 – 1/2	Varies <sup>2</sup>
pH	5.5 – 9.0	6.5–8.0
Temperature (°F)	110–150	130–140

<sup>1</sup>Adapted from VanDevender and Pennington, 2004.

<sup>2</sup>Will depend on specific materials, management, and weather conditions.

Maintaining the correct compost moisture level over the life of a flock of broiler chickens sounds simple. However, it is much more difficult than it sounds because birds increase in size each day and this requires that constant adjustments be made to the amount bulking material that is mixed with the mortality. While a 1:1 ratio of bulking material to mortality may be fine for small birds, it may require a 4:1 ratio or more by the time those birds reach market age, depending on bird size and type of bulking material used.

The C:N ratio of the material is also important for proper composting. A C:N ratio in the range of 25:1 to 35:1 tends to work well and produces little odor. If the ratio is less than 25:1, nitrogen will be lost and unpleasant odors become a possibility. Therefore, it is important to know the C:N ratio of your bulking agent/carbon source. Common bulking agents and their C:N ratios are listed in Table 2.

Oxygen level is also important because composting is an aerobic process and the bacteria that do the work require oxygen. Oxygen level in the material should be at least 5 percent. As mentioned previously, proper composting requires following a fairly specific "recipe." That recipe includes:

- Moisture content of 50–60%
- C:N ratio of 25–35:1
- Oxygen level of at least 5 percent
- Correct level of bulking agent/carbon source (enough to soak up fluids)
- Correct level of mortality (too much can overwhelm the process)

Particle size of the bulking agent is also critical because too fine a particle size will allow too much compaction and limit the oxygen supply and, as a result, limit microbial growth and heat

level. Slower microbial growth will mean lower composting temperatures and increased composting time. The ratio of bulking material to carcasses should result in a bulk density of the final compost that is around  $600 \text{ mg m}^{-3}$  ( $37.5 \text{ lb ft}^{-3}$ ). A good rule of thumb is that the weight of compost in a 19 liter (5 gal) bucket should be around 11.4 kg (25 lbs). If issues arise, common troubleshooting tips are listed in Table 3.

Table 2. Common bulking agents and their C:N ratios.

Source	C:N ratios
Softwood shavings	641:1
Hardwood chips	560:1
Sawdust	442:1
Wheat straw	127:1
Rice hulls	121:1
Straw (general)	80:1
Corn stalks	67:1
Finished compost	40:1
Horse manure	35:1
Hay (general)	24:1
Cattle manure	19:1
Turkey litter	16:1
Broiler litter	12:1
Cottonseed meal	7:1
Soybean meal	5:1
Animal carcasses	5:1

Table 3. Troubleshooting common composter problems.

Problem/Symptom	Probable cause	Suggestions
Improper temperature	Too dry (<40% moisture)	Add water
	Too wet (>60% moisture)	Add bulking material; turn pile
	Improper C:N ratio	Evaluate & adjust bulking material
	Improper ingredient mixing	Layer ingredients appropriately
Failure to decompose	Adverse environment	Ensure adequate cover
	Improper C:N ratio	Evaluate & adjust bulking material
	Carcasses layered too thickly	Single layer the carcasses
	Carcasses at outside edges	Keep 15.24–25.40 cm (6–10") between carcasses & edges
Flies	Too wet	Add bulking material & turn
	Too low C:N ratio	Evaluate & adjust bulking material
	Inadequate carcass cover	Cover with 25.40–30.48 cm (10–12") of bulking material
	Inadequate carcass cover	Cover with 25.40–30.48 cm (10–12") of bulking material
Scavenging animals	Poor sanitation conditions	Avoid leaching from pile
	Too wet	Add bulking material; turn pile
	Failure to reach proper temp	Assess C:N ratio and layering
	Inadequate cover over top	25.40–30.48 cm (10–12") cover; fences, barriers, or covers

DeRouche et al. (2005) indicated that composting of animal mortalities has increased in popularity, in part because of the decreased availability of renderers in some areas. In addition, with the increased threat of foreign animal disease transmission, composting has received considerably more attention as a potential method for mass mortality disposal. For many years, burial or burning of carcasses have traditionally been the methods of choice for disposal of mass mortalities. However, burning raises concerns with airborne infectious agents. While burial is still the main option for many state agencies as the preferred disposal method in catastrophic mortality events, other disposal options must be available when limitations to carcass burial exist such as in areas of shallow groundwater or in winter months when the ground may be frozen.

The composting methodology and procedures previously discussed for routine mortalities can be easily adapted for catastrophic mortality loss. On-farm mass mortality composting will avoid many of the water and air quality issues that may be associated with burial and incineration, respectively. Composting will also eliminate costs associated with transportation (rendering, incineration, and landfilling) and tipping fees often charged by landfills. In recent years, the poultry industry has discovered the value of windrow composting catastrophic mortality losses inside the poultry house. In a disease outbreak situation such as with avian influenza, in-house or outside windrow composting of meat-type birds may be one of the most biosecure options available, because, when done correctly, heat generated by the composting process 56 to 60 °C (133 to 140 °F) is sufficient to inactivate the avian influenza virus in the carcass and the litter (Lu et al., 2003). However, it is critical to have proper knowledge of the procedure, and that the process be implemented correctly. When managed properly, composting may likely be the best option for both routine and catastrophic mortality losses.

#### 2.4. Importance of composting

Composting works by surrounding the carcasses with carbonaceous material and using the available microbial population to break down the carcasses. The carbon provides energy for microorganisms while the carcasses and fluids supply nitrogen for microbial protein synthesis (Payne, 2018). The process converts carcasses into a stable, humus-like product that has added value. In addition, composting uses thermophilic temperatures associated with the process to destroy most pathogens in the material. However, proper construction and management are key to an effective composting process, particularly where windrow composting is concerned.

If dealing with an emergency or catastrophic mortality situation, all options should be kept open and planning ahead is key. Each method has its own set of advantages and disadvantages that must be weighed against other options. If multiple farms are involved, as may be the case in a disease outbreak situation, a disposal plan should be in place for each farm. Individual site assessments, an understanding of the size and severity of the situation, and available resources will all be key components to meeting the challenges ahead. In a catastrophic disease situation, there must be coordination between depopulation crews and disposal crews. Planning ahead includes having crews and equipment ready and on standby should they be needed. If composting, having a large, readily available source of carbon material located and the ability to transport this material on short notice is also critical. Similar to other mortality disposal options, composting has both pros and cons that include the following:

- Pros
  - Can be done on-site
  - Serves as a pathogen inactivation procedure when managed correctly
  - Environmentally sustainable process
  - End-product is a valuable fertilizer/soil amendment
- Cons
  - Time-consuming process (minimum of 28 days)
  - Must have enough space in-house or outside to create windrows

- Proper windrow construction, maintenance, and monitoring are vital to success

Also, in a catastrophic mortality situation where windrow composting is used, the importance of monitoring and turning the windrow(s) at the appropriate time should not be underestimated. The windrows should be monitored, and record temperatures measured daily using a 91.44 cm (36-inch) compost thermometer. In the initial composting phase, the windrow is built and left intact for 14 days, hopefully reaching a target temperature of at least 55 °C (131 °F) for 3 days. In the second composting phase, the windrow is turned and left for another 14 days, again hopefully reaching at least 55 °C (131 °F) for 3 days. A subject matter expert should be available to troubleshoot any issues as well as approve windrow turning and release of the finished product. Other supplies, equipment, and labor include the following:

- Skilled equipment operators
- General laborers
- Skid-steer loaders
- Pay loaders
- Portable pressure washers
- Pump up sprayers
- Disinfectant
- 91.44 cm (36") compost thermometers
- Personal protection equipment (disposable suits, boots, hairnets, dust masks/respirators, etc.)

### 3. Rotary Drum (or In-Vessel) Composting

Rotary drum or in-vessel composters are the latest addition to the composting family. In-vessel composting is usually done in an enclosed vessel, such as a large-diameter drum. The material is typically agitated, turned, and force-aerated on a daily basis or perhaps multiple times each day, depending on the size of the unit and how it is operated. Because of this daily turning and aeration, the composting process starts quicker and progresses faster in a rotary drum than with static-bin, alleyway, or windrow composting; and the highly degradable, oxygen-demanding materials are decomposed in a shorter time frame than with other composting alternatives. There are several rotary drum composters available on the market today, including Biovator™, Ecodrum™, and Rotoposter™, among others. Rotary drum composters, in general, all operate in a similar fashion to one another and offer additional advantages to traditional composting methods by being totally enclosed with less chance of escaping leachate, are quicker and more efficient at material breakdown because of daily turning and aeration, and use less added carbon source material, such as shavings or poultry litter.

Rotary drum composters have their origin in the swine industry; however, in recent years, the poultry industry has discovered the value of in-vessel composting for commercial poultry operations. Rotary composters are designed for large-scale animal/poultry production facilities and offer the following benefits:

- Reduce odor and disease-causing organisms
- Eliminate the leaching threat and potential for soil and water contamination
- Remove animal decomposition from the public eye
- Enhance biosecurity by enclosing material and removing the scavenger threat
- Produce finished compost material that has value as a soil amendment

Carcass composting materials typically have mesophilic (grows best in moderate temperatures) and thermophilic (grows best at high temperatures) species of three groups of microorganisms, including bacteria (present in the largest numbers), fungi, and actinomycetes (gram positive bacteria that produce bioactive agents such as enzymes and vitamins) (Kalbasi et al., 2005). Bacteria are faster decomposers than other microbes and usually do well in the early stages of the composting process. Fungi do not do well in low-oxygen environments compared

to bacteria, but are better decaying agents on woody substrates such as shavings and are better able to withstand low moisture and low pH conditions. Critical to success is temperature, because nearly all microorganisms in compost material will die if the temperature rises above 70 °C (158 °F), leaving only a few heat-resistant spores. Therefore, it is important that the compost material gets hot enough for the process to work efficiently, but not too hot.

Another useful feature of rotary drum composters is that they do their work out of the public eye. Public acceptance of agricultural practices is an important issue today that every farming operation must be aware of and take seriously. Public acceptance of a rotary drum composter may be better simply because a drum composter may be more aesthetically pleasing than a bin or alleyway composter. In addition, scavengers are not a problem with a rotary drum composter because all the material is contained inside the drum, preventing scavenger access. With increased awareness of the threat of avian influenza, infectious laryngotracheitis, and other diseases, this can enhance a poultry farm's biosecurity program.

The Poultry Science Department at Mississippi State University has an Ecodrum™ rotary drum composter (Figure 1) on the poultry research farm to handle daily flock mortalities. The composter has a built in thermometer that allows temperature monitoring on a daily basis. The composter does a good job of holding 38 °C to 60° C (100 °F to 140 °F) if we keep enough material in the unit to maintain an adequate critical mass and keep the moisture level in the correct range. Five years' worth of temperature data from the unit is presented in Figure 2. Periods when the temperature dropped below 38 °C (100 °F) are associated with times when we had the material too wet or when we were out of chickens and we let the unit discharge too much material without adding mortality and it lost its critical mass.



Figure 1. Ecodrum rotary drum composter.

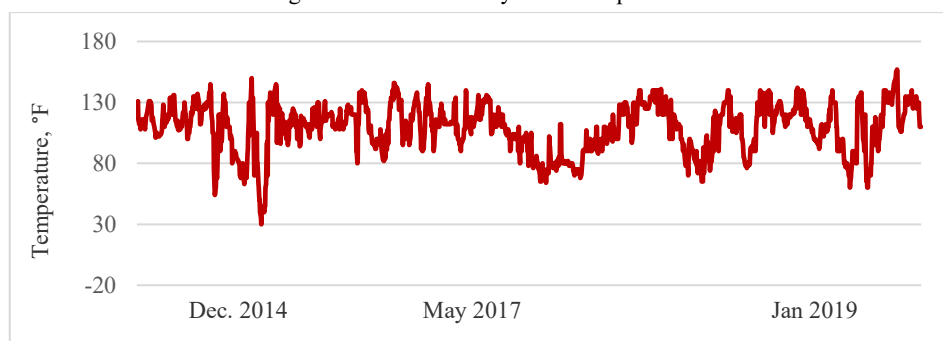


Figure 2. Mississippi State University Ecodrum temperature data (May 2014–May 2019).

We use pine shavings/sawdust as a carbon source. Initially we tried using chicken litter but our two commercial broiler houses have not been totally cleaned out in several years and the carbon content of our litter is too low to act as a good carbon source. Therefore, we could not achieve the results we wanted. We do re-use a portion of the discharged compost back through the unit and that seems to work fine if the moisture content is adequate. Manufacturer literature indicates that up to 50 percent of the compost exiting the unit can be re-used. We have a small unit, which consists of two 11-foot drums, 5 feet in diameter, connected to each other. Our unit turns either once or twice each day (starting at 6 am), depending on the size of chickens we have on the farm. Start times and number of turns are programmed into the control box on the side of the unit by the grower and can be changed at any time as conditions warrant. The unit turns very slowly and one complete revolution takes approximately 15 minutes and will discharge about half of a 30-gal trash barrel of material. Two revolutions will take about 30 minutes and produces a full 30-gal trash barrel of material.

Larger farms may turn their units 3 or 4 times per day instead of once or twice and will also need longer units than ours. Units are sized based on the number of poultry houses on the farm, with additional 11-foot drum sections added to meet the capacity requirements. There are paddles inside the drum (similar to the paddles inside of a cement truck) to help break down the material during rotation and move the material from the front loading door to the far end of the drum and the discharge chute. The unit also has a blower that pulls air through it on a routine schedule to ensure that there is oxygen available for the aerobic (oxygen requiring) microorganisms that break down the material. The drum turns on long rollers, and the unit does have grease fittings that should be greased once a quarter. Fluid levels in the gear box should be checked regularly. Technical support is available to help determine the initial recipe that works best for a particular situation and to troubleshoot any issues that may occur later.

In most cases, issues incurred with rotary drum composters are similar to problems seen with static bin, alleyway, or windrow composting. Again, most growers use too much mortality and not enough dry carbon source to account for all the water in the birds. Once the material gets too wet, it becomes dense and heavy and loses its porosity. When that happens, the material converts from an aerobic to anaerobic state. Anaerobic conditions yield more odors, flies and lower temperatures. The lower temperatures slow the decomposition of mortalities and this may be evident in the product being discharged from a rotary composter or the product remaining in a bin, alleyway, or windrow situation when the material is turned if the problem is serious enough. Again, composting requires following a recipe. If the recipe isn't followed, bad things can happen.

#### 4. Choosing a Disposal Method

The increasing volume and concentration of on-farm-generated wastes and increased environmental awareness now requires that producers, researchers, and regulation/enforcement officials work together to examine and determine acceptable carcass disposal methods. The best disposal strategies for routine and mass mortality events will take into consideration and make use of all available disposal options that are suitable for the task. It is, therefore, vital and beneficial that everyone understand the wide array of disposal options and the advantages and disadvantages of each. Mortality disposal is a continuous and growing challenge on every livestock operation. Numerous factors go into deciding which disposal method is best suited for an individual producer in routine and catastrophic situations. These include environmental and disease agent considerations, advantages and disadvantages of each method, equipment and personnel requirements, principals and logistics of operation, and lessons learned from the past. In assessing and choosing an appropriate catastrophic poultry carcass disposal method, CAST (2008) recommends the following questions be asked:

- What caused the catastrophic event?
- How many and what size birds are involved?

- Is it a partial, whole-house, or entire farm loss, and is it a widespread or isolated incident?
- What resources and disposal options are available on the farm and from the poultry company overseeing the situation?
- What is the state of carcass decomposition?
- What is proximity of the affected farm to other farms and to potential options for disposal?
- What local, state, and federal regulations apply to the situation?
- Will site conditions and weather restrict the chosen disposal method?
- How will the public perceive the recommended disposal option?
- What are the disposal costs, and who will pay for such costs?
- Is the method used for mass depopulation compatible and complementary to the disposal option?
- Will farms be accessible during or immediately after the mortality-causing event?

Should a catastrophic loss occur, a rapid coordinated response involving animal health, public health, sanitation, and environmental agencies, along with segments of the private sector, is critical to recovery efforts. Having an emergency response plan in place before a catastrophic loss event occurs and a plan of action to follow during a catastrophic event are important steps when working through any emergency situation. Advanced planning for mass mortality disposal should be implemented as part of an emergency preparedness plan.

## 5. Summary

Dealing with waste management streams and their associated environmental issues are some of the greatest challenges facing today's livestock and poultry industries. Several common methods for routine and catastrophic mortality management include burial, landfills, incineration, rendering, and composting. Choosing the best method means recognizing that each method has its own advantages and disadvantages and should be based on unique farm circumstances at the time and any restrictions that may apply. Any of the above methods can be successful for routine mortality disposal without any adverse environmental impacts when managed properly. However, a catastrophic or emergency event will likely make choosing the proper method(s) more difficult. Time will be critical during a catastrophic event and all possible options that allow for rapid, environmentally safe disposal of carcasses should be considered because no single option can adequately address all issues in every situation. Furthermore, while not currently as common, future research efforts should address alternative technologies such as acid/base and lactic acid fermentation, alkaline hydrolysis, and anaerobic digestion that may, down the road, offer a more cost-effective and biosecure method for carcass disposal and produce a smaller carbon footprint with less environmental impact.

## Acknowledgement

The information given here is for educational purposes only. References to commercial products, trade names, or suppliers are made with the understanding that no endorsement is implied and that no discrimination against other products or suppliers is intended.

## References

- Bonhotal, J., M. Schwarz, and R. Runk. 2014. Composting animal mortalities. Cornell Waste Management Institute. Crop and Soil Sciences Department. Cornell University. Ithaca, NY.
- Council for Agricultural Science and Technology (CAST). 2008. Poultry carcass disposal options for routine and catastrophic mortality. Issue Paper 40. CAST, Ames, Iowa.
- FAO. 2007. FAOSTAT, Food and Agriculture Organization of the United Nations, vol. 2009.
- Gwyther, C. L., A. Pryor Williams, P. N. Golayshin, G. Edwards-Jones, and D. L. Jones. 2011. The environmental and biosecurity characteristics of livestock carcass disposal methods: A review. Waste Management. <http://dx.doi.org/10.1016/j.wasman.2010.12.005>.
- Kalbasi, A., S. Mukhtar, S. E. Hawkins, and B. W. Auvermann. 2005. Carcass composting for management of farm mortalities: A review. Compost Science and Utilization. 13(3):180–193.

- Lu, H., A. E. Castro, K. Pennick, K. Liu, Q. Yang, P. Dunn, D. Weinstock, and D. Henzler. 2003. Survival of avian influenza virus H7N2 in SPF chickens and their environments. *Avian Dis.* 47:1015–1021.
- Malone, G. W., W. W. Saylor, M. G. Ariza, K. M. Lomax, and C. R. Kaifer. 1987. Acid preservation and utilization of poultry carcasses resulting from mortality losses. Pp 13–16. In: *Progress through Research and Extension 1987. Report 11.* University of Delaware, College of Agricultural Sciences, Newark.
- National Agricultural Biosecurity Center Consortium. 2004. Carcass disposal: A comprehensive review. Carcass Disposal Working Group for USDA-APHIS. March.
- Payne, J. 2018. Avian influenza mortality management options, composting procedures and lessons learned. Presented at: *6<sup>th</sup> International Symposium on Animal Mortality Management.* Amarillo, TX.
- Rahman, S., and M. Berg. 2017 Animal carcass disposal options. *Rendering • Incineration • Burial • Composting.* NM1422. North Dakota State University Extension Service. Fargo.
- USDA. 2013. *Feedlot 2011. Part 1: Management practices on U.S. feedlots with a capacity of 1,000 or more head.* USDA-APHIS-VS-CEAH-NAHMS. Fort Collins, CO. #626.0313
- USDA. 2017. Death loss in U.S. cattle and calves due to predator and nonpredator causes, 2015. USDA, APHIS, Veterinary Services and National Animal Health Monitoring System. December.
- USDA. 2018a. Livestock slaughter: 2017 summary. United States Department of Agriculture. National Agriculture Statistics Service. April.
- USDA. 2018b. Poultry slaughter: 2017 summary. United States Department of Agriculture. National Agriculture Statistics Service. February.
- VanDevender, K. and J. Pennington. 2004. Organic burial composting of cattle mortality. University of Arkansas, Division of Agriculture, Cooperative Extension Service. FSA1044.

## Recommendations for Effective Biosecurity Management

Teng-Teeh Lim <sup>a,\*</sup>, Corinne Bromfield <sup>b</sup>, Craig Payne <sup>b</sup>, Lauren Delaney <sup>c</sup>,  
Raymond Massey <sup>d</sup>, Joseph Zulovich <sup>a</sup>

<sup>a</sup> Food Systems and Bioengineering, University of Missouri, Columbia, MO 65211, USA

<sup>b</sup> Veterinary Medical Extension and Continuing Education, University of Missouri,  
Columbia, MO 65211, USA

<sup>c</sup> Veterinary Medical Diagnostic Laboratory, University of Missouri, Columbia, MO 65211, USA

<sup>d</sup> Agricultural and Applied Economics, University of Missouri, Columbia, MO 65211, USA

\* Corresponding author. Email: [limt@missouri.edu](mailto:limt@missouri.edu)

### Abstract

A series of biosecurity workshops were conducted in Missouri, USA, to improve on-farm biosecurity management. Stakeholders were also encouraged to take steps in preparing for mass mortality management, especially to be acquainted with the local and federal levels of authority personnel. Should a major disease outbreak happen, movement restrictions will be put in place for the control area(s) to limit disease spread by animals, animal products, vehicles, and other equipment. Farm operations need to recognize the shortages and risks of their operations, and prepare for several days to weeks before the officials have sufficient knowledge of the extent of the outbreak to have confidence that animals can be safely moved without contributing to disease spread. Agencies involved would typically include federal disease inspection, state veterinarian, disease diagnostic laboratory, and environmental protection. Secure Food Supply Plans have been developed for different animal species farm operations. All operations, including small farms, should request a National Premises Identification Number (PIN), and develop an Enhanced Biosecurity Plan prior to an outbreak. Farm operations need to closely monitor animals for symptoms of potential foreign animal diseases and highly pathogenic diseases. Methods to sample and test for different diseases, or where to obtain information and help needed in short time frame are critical for containment of diseases. Indemnity and economics should be considered to ensure farm operations can manage cash flow for several months. This paper summarizes some of the important lessons learned from previous mass mortality management, details needed to ensure disease containment and disinfecting efforts, and provides recommendations to improve effective biosecurity management.

**Keywords:** Major disease; disease prevention; outbreak management; authority; training; workshop.

### 1. Introduction

Animal agriculture is important for providing protein sources for consumption. Additionally, within the state of Missouri, many people make their living within these fields. Within the United States, Missouri ranks 3<sup>rd</sup> in beef cows (2.06M heads), 6<sup>th</sup> in turkey (17.3M heads), and 7<sup>th</sup> in hog (3.5M heads) production (MDA, 2019); animal industry plays an important role in the Missouri economy. When disease outbreaks have the potential to be costly affairs, as well as effectors of poor animal welfare, it is prudent to take steps to minimize the spread of disease.

Missouri animal agriculture has seen outbreaks of domestic animal diseases, from the 2013 Porcine Epidemic Diarrhea virus (PEDv) introduction to the United States (US) in hog farms to the 2014 Avian Influenza outbreak in local poultry flocks. Both of these diseases illustrate the need for producers to evaluate biosecurity protocols and institute plans to prepare themselves. Along with domestic disease concerns, foreign animal diseases, (FAD) have been gaining traction in other countries, leading Missouri producers to become more aware and concerned about their potential impact.

Producers following the news will be aware of FAD such as African Swine Fever, Foot and Mouth Disease, and Virulent Newcastle Disease. While these diseases may be limited in which

production animal species they affect, producers can observe how other operations respond to a disease outbreak and utilize lessons learned across species. The 2018 Virulent Newcastle Disease (VND) outbreak in southern California proved difficult to control and is continuing to cause economic hardship for affected flocks. However, biosecurity protocols designed to mitigate spread of this disease appear to be useful, of 448 reported infected premises, only one was a commercial flock. Four hundred forty seven (447) have been retail feed stores selling chickens and backyard birds with minimal, if any, biosecurity protocols in place (USDA, 2019).

As potential outbreaks continue to threaten US animal production, the USDA APHIS funded the preparation of the Secure Food Supply Plans (SFSP). These plans are voluntary programs, which producers of poultry and egg products, pigs, beef cattle, and dairy cattle can participate in to evaluate the current biosecurity on farm, as well as prepare for enhanced biosecurity, which can be employed in the face of a major disease introduction to the US. The secure food supply plans are species and product specific (for example, <http://www.securepork.org/>, <http://securebeef.org/>, and <http://securemilksupply.org/>). Each plan includes a biosecurity checklist, steps necessary for producers to obtain a Premise Identification Number (PIN) to allow for animal and disease traceability, enhanced biosecurity plans, and a list of records that should be accessible in the face of an outbreak. These plans are intended to help a farm prepare for business continuity in the face of a FAD introduction. By evaluating biosecurity and having a plan in place, each producer has a greater chance of keeping the disease out of their farm. (CFSPH Secure Food Supply Plan, 2019).

An effective farm biosecurity plan is one that takes into account characteristics of the disease of interest, specifics of farm itself including animal housing, manure handling, transportation, personnel movement, feed, and the animals themselves. Each plan needs to be tailored to the farm of interest, but there are many similarities that need to be evaluated. Producers need to know how local, state, and federal agencies will respond in the face of an outbreak. Pork producers are uniquely aware of biosecurity protocols related to the industry's attempt to control and eradicate Porcine Respiratory and Reproductive Syndrome virus (PRRSv). PRRSv was identified in 1987 and recently has been estimated to cost the pork industry \$664 million annually (Holtkamp et al., 2013). Producers routinely design biosecurity plans to minimize or mitigate PRRSv entry and establishment in a herd. Aerosol, fomite, and direct contact transmission of PRRSv mean that individual producer protocols may be ineffective in controlling the disease. Mitigation strategies that include vaccination with modified live viruses have the potential to circulate within a herd and cause clinical disease, and can be spread via aerosol to neighboring farms. If control of PRRSv in an area is desired, all farms need to consider working together. To that end, the US pork industry formed the Area Regional Control (ARC) groups or Area Regional Control and Eradication (ARC&E) groups targeting PRRSv.

The University of Missouri Extension has collaborated with stakeholders to improve the combined biosecurity efforts and offered a series of workshops (Lim et al., 2017). Many of the stakeholders quickly came together after the highly pathogenic H5N2 strain of avian influenza confirmed in states included Washington, Oregon, Idaho and Minnesota, while two cases were confirmed in Missouri's turkey operations (MDA, 2015). The Missouri Department of Agriculture (MDA) and USDA Animal and Plant Health Inspection Service (APHIS) acted quickly to put together a team and quarantined the affected facilities. In 2017, five workshops were offered at various locations in the state, and speakers from University of Missouri Extension, Department of Natural Resources (DNR), MDA, and other land grant universities put together the materials and training (Lim et al., 2017). The University Extension personnel have since then identified a need to continue enhancing biosecurity training in the region, and secured grants to conduct another series of workshops in 2019.

The objectives of this paper are to document the key and new information delivered in the 2019 biosecurity workshops, critical discussion, and findings and recommendations to improve

future biosecurity plans and education.

## 2. Materials and Methods

### 2.1. Identify emerging needs and objectives

Surveys were conducted to gauge the workshop effectiveness and collect feedbacks from the attendees. The survey results indicated a need to cater to regional livestock producers (less focused on Avian Influenza, and expand more on the latest information of biosecurity, disease diagnosis, carcass disposal methods and regional regulations, and quarantine and eradication. Additional discussion time and case studies (experience learned) regarding major disease outbreak were requested. The workshops targeted producers, veterinarians, regulators, and Extension personnel.

### 2.2. Identify and working with collaborators

A team of faculty first met to draft the curriculum of the workshops. Collaborators were also identified and contacted to discuss and put together the training materials. The team decided to have presenters to include:

- 1) University of Missouri faculty from Agricultural Engineering, Agricultural Economics, and Veterinary Medicine;
- 2) MDA Animal Health Division, and Missouri DNR;
- 3) USDA Animal and Plant Health Inspection Service (APHIS), and Natural Resources Conservation Service;
- 4) Industry collaborators, including FCS Financial, Missouri Pork Association and Cattlemen's Association, Egg Council, and The Poultry Federation.

### 2.3. Obtain funding to execute programs

The team was awarded a grant from the North Central Extension Risk Management Education Center, to help support most of the workshop expenses and offered free registrations and materials to the attendees.

### 2.4. Design framework to compile and deliver curriculum

Similar to the 2017 workshops, the team met to identify a curriculum with specific topics and speakers, workshop locations and dates. The team also worked closely to identify biosecurity related materials (extension publication, USDA brochures, reports, checklists, and Secure Food Supply Plans) to be used in the workshops, and provided to the attendees.

### 2.5. Promote workshops and pre-registration

The team recognized the importance of offering continuing education credit certification to encourage attendance. The team applied to the Missouri State Veterinary Association and was approved for four continuous education units. Promotion of the workshop started at least five months before the workshop. In order to better estimate seating and meals, pre-registration (no fee) was required and was managed by the University of Missouri Extension.

### 2.6. Organize and collect workshop evaluations and complete final report

As with the 2017 workshops, surveys were collected at the end of each of the workshop. The survey consisted of a two-page survey questions, including scales to gauge level of understanding of different topics before and after the workshops. A follow-up survey was sent to the attendees via emails during the month of July, to conduct a follow-up survey.

## 3. Results and Discussion

### 3.1. Workshop promotion, registration, and continuous education unit certification

A single-page flyer was first made available in early January to start the pre-registration. All collaborators helped promote the workshops by informing their contacts, via electronic mails, newsletters, webpages, and announcements at various functions. University of Missouri Extension also published news releases with short stories and webpages (that contained the flyer). The flyer

and news releases were then reprinted with permission in various local channels, including regional radio stations and commodity newsletters.

There was no cost to attend the workshops, although pre-registration was required. A sponsorship was provided by a regional lender (FCS Financial), which helped to ensure the free registration. All expenses (venue, meals and refreshments, travel expenses, etc.) were covered by the grant and sponsorship funds obtained. The workshops was approved for four hours of Veterinary Continuing Education, which attracted many veterinarians to attend the workshops.

### 3.2. Workshops conducted and materials offered

The collaborative team conducted a series of “Preventing and Responding to Disease Outbreak” workshops. Five workshops were offered March 6<sup>th</sup> to 18<sup>th</sup> of 2019, at Versailles, Springfield, Jackson, Kirksville, and St. Joseph, Missouri, US.

The same program was offered at each of the locations, which started at 10:15 AM and concluded at 3:30 PM. The attendees averaged about 40 per workshop, total attendees (including speakers) were 201, and were 148 excluding speakers.

Materials developed and distributed at the workshops included:

- A booklet that contained all the presentation files, consisted of topics on “Detection, Quarantine, and Lessons Learned” (MDA Animal Health Division); “Mortality Management and Preparation in Advance” (DNR); USDA’s Role and Resources (USDA APHIS); “Disease Identification and Turnaround Time” (MU Veterinary Medical Diagnostic Laboratory); “Economic Reasons to Improve and Maintain Biosecurity” (Agricultural Economist), secure food supply plans for beef, pork, dairy, and poultry (Veterinarian); and “Overview of Secure Supply Plans” (Veterinarian).
- An interactive table top exercise was designed for attendees to apply for a premise identification number (PIN) for animal traceability, evaluate a farm site, and create a line of separation (LOS) and perimeter buffer area (PBA) as a foundation for implementing the secure food supply plans.
- A laminated, one-page critical biosecurity checklist, along with important contacts of Extension, laboratory, and agencies.
- USB flash drive (Swivel and wrist-band types) that contains all the electronic presentation files, check list, and related documents.
- A webpage was dedicated to contain all the presentations files (downloadable files):
- <http://faculty.missouri.edu/lmt/Biosecurity.shtml>

### 3.3. Pre- and post-workshop evaluations

Data were collected from 137 attendees:

- 96.2% of attendees felt that the workshop was applicable to their job (strongly agree or agree).
- 92.4% of the respondents rated the overall program was either “Excellent” or “Very good”, while another 6.8% of respondents rated the overall program as “Good”.
- 97.7% of attendees would recommend this workshop to others (strongly agree or agree), Figure 1.
- Nearly 58% of the respondents have shown a gain in level of understanding regarding practical carcass disposal methods. In addition, 73% of the respondents have gained more understanding about regional regulations during major disease outbreak.
- 78% of the respondents indicated they gained knowledge and training to reevaluate and improve biosecurity protocols, and plans for quarantine and eradication.

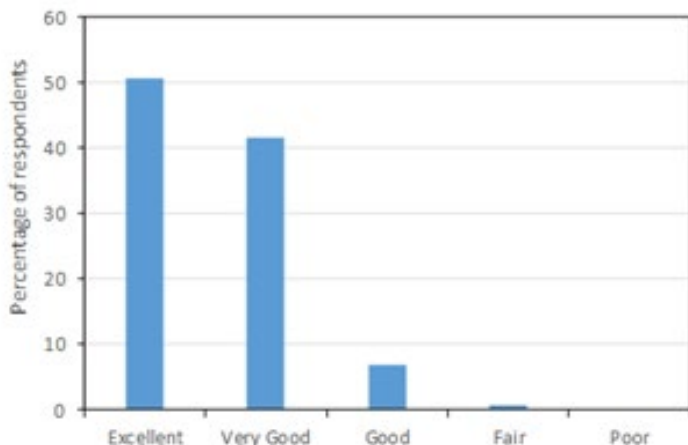


Figure 1. Percentage of respondents rating the overall workshop program.

Attendees were asked what they appreciated about the workshop as well as for response about what could be improved upon. Table 1 lists the comments arranged in two categories: either appreciated or complained.

Table 1. Comments/Feedback collected from the survey.

Appreciated	<ul style="list-style-type: none"> <li>The discussion with producers were really lively &amp; informative. There was a good awareness of how devastating a foreign animal disease outbreak would be for some producers.</li> <li>Creating awareness of the need for emergency plans.</li> <li>Learned not to be overconfident about the plan &amp; knowledge. Always ways to improve &amp; don't forget about the basics</li> <li>Enjoyed the multiple speakers. Hearing from many different people of different areas of expertise. I liked that there was info on many different species.</li> </ul>
Suggestions	<ul style="list-style-type: none"> <li>More (real world) examples of outbreaks.</li> <li>Would make material more oriented for producers (disease ID, plans of action, specific sources of weaknesses, etc.)</li> <li>The producers in livestock production are the ones who need to be here. More producers need to have better ID of animals, premise ID, BETTER handling of dead animals.</li> <li>Example of a secure biosecurity plan. What does a complete plan entail?</li> </ul>

Throughout the workshops, questions asked were recorded and answered when possible. Table 2 contains a list of commonly asked questions and the agency to which the questions were commonly directed. Not all questions were able to be answered at this time. These unanswered questions will be the scaffold of the next round of biosecurity workshops.

### 3.4. Area Regional Control and Eradication of PRRSv

University of Missouri Extension has been working with the US pork industry contributing to the PRRSv ARC&E effort. These groups bring all producers within a defined region together to share current PRRSv disease status and mitigation strategies, including vaccination and live virus inoculation. The PRRSv ARCs include sharing of pig flow information, transportation, and

locations of barns. This information is shared so that regional control groups can implement decisions on farm that may be impacted by neighboring farms actions. The University of Missouri Extension Swine Veterinarian serves as a coordinator of information within three Missouri ARCs. One Missouri ARC&E has been successful at eradicating PRRSv from within its borders three separate times through the use of traffic pattern controls, changing pig flows to allow PRRSv positive pigs to move to buildings further away from naïve herds, and quick sharing of information to allow personnel restrictions to be implemented when needed. Area Regional Control efforts create a framework that further biosecurity projects can build upon. In the face of a foreign animal disease threat, this framework can be employed to trace disease, animal movement, and potential contamination.

Table 2. Commonly asked questions at the workshop.

USDA APHIS	<ul style="list-style-type: none"> <li>• When does depopulation apply to affected animals? Unaffected animals?</li> <li>• Who makes decisions on depopulation of a farm?</li> <li>• Who pays for testing?</li> <li>• What about quarantine of species not affected by the disease in an outbreak situation?</li> </ul>
Missouri DNR	<ul style="list-style-type: none"> <li>• When is burial/compost/incineration the appropriate method of carcass disposal?</li> <li>• Does composting require oversight? Is it possible for composted animals to contaminate the ground water?</li> </ul>
University of Missouri Extension	<ul style="list-style-type: none"> <li>• Using a Secure Food Supply Plan, how do you determine what disinfectants to use?</li> <li>• Is there concern about runoff from cleaning and disinfection?</li> <li>• Are there recommendations for dealing with media in an outbreak and depopulation situation?</li> <li>• How do you tailor a Secure Food Supply Plan to a farm?</li> <li>• Creeks, rivers, ponds, and other natural resources that cross farm boundaries, are these potential sources of infection and what can be done about them?</li> </ul>

#### 4. Summary and Conclusions

An Extension grant was secured to help offer five Biosecurity workshops in Missouri. The collaborative team included University of Missouri Extension, University of Missouri Veterinary Medical Diagnostic Laboratory, Missouri Department of Natural Resources, Missouri Department of Agriculture Animal Health Division, and USDA Animal and Plant Health Inspection Service (APHIS) and Natural Resource Services (NRCS). A few important experiences learned during the workshop execution were:

- 1) It was most critical to engage a collaborative team to provide the training. Each member plays a different role and can cover the different topics more effectively.
- 2) It is important to stay informed of the new disease and biosecurity recommendations, and actively reevaluate the existing biosecurity plan to address areas that need improvement. As different diseases threaten farms, different plans may need to be employed.
- 3) Promotion and continuous education units encourage workshop participation.
- 4) Financial support was essential to provide free registration and other expenses.
- 5) Economic factors are also critical to the biosecurity, producers need to develop financial plans specific to major disease outbreak, and be aware that biosecurity plans can be

costly, but should not be more costly than disease.

- 6) Preventative actions are the best strategy of controlling disease proactively: have good biosecurity protocols, and routinely review and execute the protocols.
- 7) The tabletop exercise was helpful in understanding the logistics of a farm biosecurity plan, encourage attendees to apply for a premise identification number (PIN) for animal traceability, and visualize the importance of a line of separation (LOS) and perimeter buffer area (PBA), as a foundation for implementing the secure food supply plans.

### Acknowledgements

North Central Extension Risk Management Education Center, USDA-APHIS, MDA, DNR,

This material is based upon work supported by USDA/NIFA under Award Number 2015-49200-24226.

### References

- MDA, 2015. MDA implementing response to contain, eliminate virus following detection of avian influenza in Missouri. Missouri Department of Agriculture. March 08, 2015. <http://agriculture.mo.gov/news/newsitem/uuid/a7b9529c-9050-4a1d-ada5-c1aa94ed9593>. Accessed June 28, 2019.
- MDA, 2019. Missouri agriculture at a glance. Missouri Department of Agriculture. <https://agriculture.mo.gov/abd/intmkt/pdf/missouriag.pdf>. Accessed June 29, 2019.
- Holtkamp D.J., J.B. Kliebenstein, E.J. Neumann, J.J. Zimmerman, H.F. Rotto, T.K. Yoder, C. Wang, P.E. Yeske, C.L. Mowrer, and C.A. Haley. 2013. Assessment of the economic impact of porcine reproductive and respiratory syndrome virus on United States pork producers. Journal Swine Health and Production. 2013;21(2):72–84.
- NPB, 2002. Biosecurity Guide for Producers. National Pork Board. <http://porkcdn.s3.amazonaws.com/sites/all/files/documents/Biosecurity/BiosecurityBook.pdf>. Accessed June 28, 2019.
- NPB, 2013a. Biosecure Manure Pumping Protocols for PED Control: Recommendations for Pork Producers. National Pork Board. <https://extensiondata.missouri.edu/Pro/Swine/Docs/PEDproducer.pdf?ga=2.45937060.1610304562.1561652946-1964391761.1557862015>. Accessed June 28, 2019.
- NPB, 2013b. Biosecure Manure Pumping Protocols for PED Control: Recommendations for Commercial Manure Haulers. National Pork Board. <https://extensiondata.missouri.edu/Pro/Swine/Docs/PEDhauler.pdf?ga=2.188552104.1610304562.1561652946-1964391761.1557862015>. Accessed June 28, 2019.
- Payne, J., 2016. Mortality management options during an avian influenza outbreak. Oklahoma Cooperative Extension Service. <http://factsheets.okstate.edu/documents/ansi-8218-mortality-management-options-during-an-avian-influenza-outbreak/>. Accessed June 28, 2019
- Pork Checkoff, 2017. PEDV Reourrces. <https://www.pork.org/?s=PEDV>. Accessed June 28, 2019.
- USDA-NASS, 2019. 2018 State Agriculture Overview for Missouri. United States Department of Agriculture, National Agricultural Statistics Service. [https://www.nass.usda.gov/Quick\\_Stats/Ag\\_Overview/?php?state=MISSOURI](https://www.nass.usda.gov/Quick_Stats/Ag_Overview/?php?state=MISSOURI). Accessed June 28, 2019.
- USDA 2017. HPAI Biosecurity Checklist. United States Department of Agriculture, Animal and Plant Health Inspection Service. [https://www.aphis.usda.gov/animal\\_health/downloads/animal\\_diseases/ai/.pdf](https://www.aphis.usda.gov/animal_health/downloads/animal_diseases/ai/.pdf). Accessed June 26, 2010.
- USDA 2019. APHIS June 2019 Animal disease information Avian Virulent Newcastle Disease. <https://www.aphis.usda.gov/aphis/ourfocus/animalhealth/animal-disease-information/avian/virulent-newcastle/vnd>. Accessed June 28, 2019.



**Theme II:**  
**Environmental Monitoring, Assessment,**  
**and Control**



# Numerical Study Using CFD on the Efficiency of a Partial Pit Ventilation to Remove Ammonia from Different Emission Sources

Li Rong \*

Department of Engineering, Aarhus University, Aarhus 8000, Denmark

\* Corresponding author. Email: [li.rong@eng.au.dk](mailto:li.rong@eng.au.dk)

## Abstract

A partial pit ventilation (PPV) system installed below the slatted floor has been widely used in fattening pig barns in Denmark. Experimental tests showed that annually around 50% of ammonia emissions can be collected by PPV system. However, the percent of emissions collected by PPV system from different emission sources including slurry floor, top surface, bottom surface and side surface of the slatted floor has not been investigated as well as the mass transfer coefficients. This study applied CFD simulation to investigate the removal ratio of ammonia emissions from the four emission surfaces. The CFD model was validated by experimental air speeds and the validated CFD model was further used for simulations under conditions of five ventilation rates ( $2000\text{--}4000\text{ m}^3\text{ h}^{-1}$ ), four emission sources and two locations of PPV system exhaust. The results showed that the removal ratios of ammonia emissions from the four emission sources were generally higher for the cases that the PPV exhaust was installed opposite to the air supplier than the values of those cases that the PPV exhaust was located at the same side of side wall air supplier. The removal ratios of ammonia emissions were the highest with the emission source of slurry floor and generally 30% higher than the values of other cases. The mass transfer coefficients with the slat side emission sources were the largest. The results indicated that the airflow patterns and locations of emission sources greatly influenced the removal ratios of ammonia emissions and ammonia mass transfer coefficients.

**Keywords:** Ammonia emission, pig barn, partial pit ventilation, CFD.

## 1. Introduction

Food Agriculture Organization (FAO) predicted that the world food production must increase by 50% within the next 20 years and 80% of that increase must come from the intensification of agricultural production. The global livestock sector is growing faster than any other agricultural sub-sectors. However, intensive livestock production can contribute largely to gaseous emissions such as ammonia, greenhouse and odor. Ammonia has been recognized as one of the important pollutant gases to accelerate fine particulate formation in the atmosphere and significantly contribute to the acidification and eutrophication of ecosystems and indirect emissions of nitrous oxide (IPCC, 2006). In order to abate ammonia emissions, a partial pit ventilation (PPV) system has been developed in Denmark and widely implemented into the pig production houses now.

The partial pit ventilation was installed below the slatted floor and the ventilation rate exhausted by PPV was 10% of maximum ventilation rate ( $100\text{ m}^3\text{ h}^{-1}\text{ pig}^{-1}$ ). A few studies conducted by Saha et al. (2010) and Zong et al. (2014; 2015) can be found in literature to investigate the effects of PPV system on indoor air quality and ammonia ratio collected by PPV system. In their studies, the PPV was installed at the end of the wall near resting area. The results found that PPV system could significantly reduce the indoor ammonia concentration by 42.6% and around 47–63% of ammonia emissions collected by PPV systems.

It was noticed that the airflow pattern had an important effect on mass transfer process (Rong and Aarnink, 2019). Wu et al. (2012a; 2012b) assessed the effects of PPV system and PPV exhaust locations on ammonia emissions in a scaled wind channel as well as in Computational Fluid Dynamics (CFD) simulations. It was found that the ammonia removal ratio by PPV was independent of the airflow rate with PPV exhaust located upwind while the ammonia removal ratio reduced from 80% to 50% with decreased airflow rate with PPV exhaust downwind. Van Huffel et al. (2016) performed experimental tests in the same sections as Zong et al. (2014) used

and compared the emissions of odors and ammonia under three cases: only room ventilation, room ventilation with PPV exhaust close to corridor and room ventilation with PPV exhaust close to the end wall of resting area. They found that the removal ratio of ammonia was higher with the PPV exhaust close to the corridor. Bjerg and Zhang (2013) studied the effects of three ventilation systems and locations of PPV exhaust on ammonia removal ratio by using CFD. They concluded that the ammonia removal ratio was higher when PPV exhaust was installed close to the end wall of the resting area.

The early studies showed the potential of PPV system to abate the ammonia emissions and were aware that the PPV exhaust locations could affect the ammonia removal ratio. Some of the results conflicted with each other. The objectives of this study are: (1) to investigate the effects of PPV exhaust locations on ammonia removal ratio by using validated CFD models; (2) to study the mass transfer coefficients of ammonia from four emission source surfaces.

## 2. Materials and Methods

The study was conducted by using CFD modeling of one section at climate labs of Foulum in Aarhus University. To validate the CFD simulations, the experimental data obtained from the same section of the climate lab were thus used for validation of the CFD modeling. In this section, a brief description of the experimental measurement was presented and then followed by the CFD modeling.

### 2.1. Experimental measurement

The dimensions of the section where experimental measurement was conducted and measuring locations were shown in Figure 1. The section contains one corridor and two full scale pig pens with length in 5.68 m (X), width of 4.8 m (Z) and height of 2.68 m (Y). The floor of the pig pen consists of one-third of a drained floor (opening ratio of 8.5% and length in 1.6 m) and two-third of a slatted floor (opening ratio of 16.5% and length in 3.2 m). The air was supplied by a side-wall inlet for each pen and exhausted by a fan installed on the ceiling. The experimental measurement was conducted under isothermal situations with ventilation rate of  $2996 \pm 75 \text{ m}^3 \text{ h}^{-1}$ . The airflow rate was measured by a measuring fan and recorded by a climate control system (Vensys, Denmark) with sampling interval of one minute. Air speed at the measuring points of three lines (see Figure 1) was measured by omnidirectional Air Velocity Transducer (TSI, model 8475) with repeatability in 2% of the readings. The sampling time is 0.2 s and logged the average value of one minute. The measuring period was 90 minutes at each point and recorded by CR1000 data logger (Campbell Scientific Ltd.). The room temperature and humidity were also continuously measured and recorded by Vensys with  $19.3 \pm 0.5 \text{ }^\circ\text{C}$  and  $43.6 \pm 1.4\%$ .

### 2.2. CFD modeling

#### 2.2.1. Geometry models and mesh resolution

The geometry models used for CFD validation and simulations with PPV system were presented in Figure 1. Figure 1(a) was the geometry model used for validation of CFD simulation, Figure 1(b) was the geometry model with PPV system installed opposite to the side-wall air supplier (PPV position 1) and Figure 1(c) was the geometry model with PPV system installed at the same side of the side-wall air supplier (PPV position 2). The geometry model was built in a Cartesian coordinate system and the spatial domain was discretized into finite control volume using polyhedral mesh and prism layers near the solid surfaces. The mesh resolution was determined based on the  $y^+$  value, guidance of CFD validation and the authors' experience. The prism layers were added to the region near all the solid surfaces with 2–4 layers except for the region near the emission surface where normally 10 layers were added. The mesh number was around 5.8 million for both validation case and simulations with PPV systems. The mesh distribution was shown in Figure 1(d).

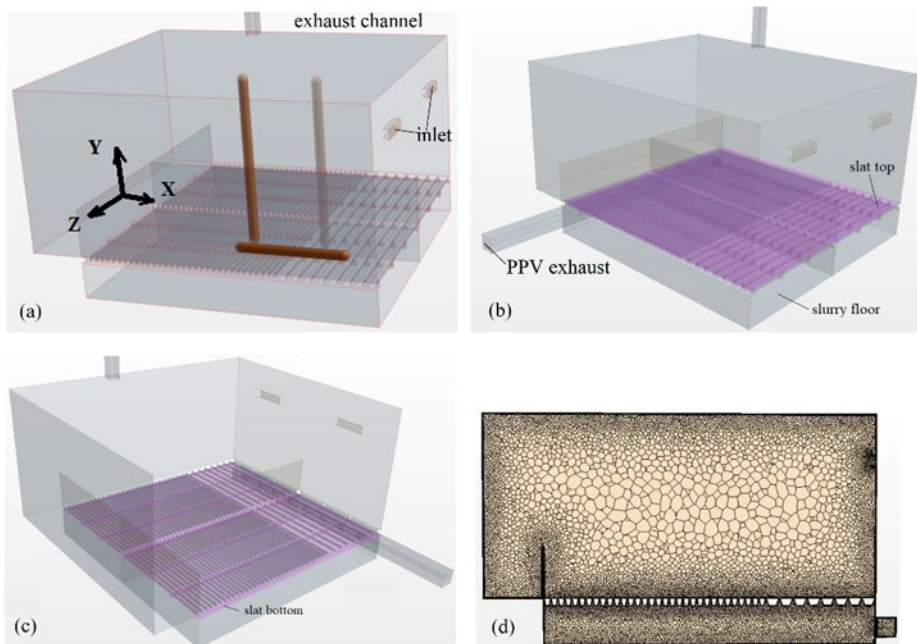


Figure 1. Schematic configurations and mesh distribution for CFD simulations. (a) Geometry model and positions of three lines measured for validation of CFD modelling, (b) geometry model for PPV exhaust position 1, (c) geometry model for PPV exhaust position 2, and (d) mesh distribution for PPV exhaust position 2.

### 2.2.2. Governing equations and numerical discretization

The simulations were conducted in a commercial software of Star CCM+. The governing equations included momentum, turbulence model, species transport and energy conservation. Due to the activation of species equation, the energy conservation equation had to be solved even though it was an isothermal case. Two-layer  $y^+$  treatment was selected to the modeling of near wall regions, which could be applied for variable  $y^+$  situation with  $y^+ \sim 1$  near the emission surface and  $y^+ < 150$  in the regions near the other solid surfaces. Realizable  $k - \varepsilon$  model was used. The second order upwind scheme was used for discretizing the convection term of each governing equation. The residual was set as  $10^{-4}$  and the convergence was not assumed to be reached until both the monitored air speed of points and the residual have stabilized. After the simulation was completed, the mass balance was also checked.

### 2.2.3. Boundary conditions

A non-slip condition was imposed at solid surfaces. The temperature of the inlet and on the solid surfaces was set the same value of  $19.3\text{ }^\circ\text{C}$ . Ammonia concentration was set at the emission surface as a constant value with mass fraction of  $1.28\text{E-}04$ . The ammonia mass fraction was set on the whole slurry floor surface ( $4.8\text{ m} \times 4.8\text{ m}$ ), while the ammonia mass fraction was only set on the specific solid surface associated with slatted floor because the drained floor was assumed as the resting area of pigs. The fan exhaust was set as velocity inlet with a minus value which indicated that it was functioned as an outlet. The same setting was imposed on the PPV exhaust, that is, velocity inlet with a minus value  $-0.99\text{ m s}^{-1}$ , which was equivalent to 10% of maximum ventilation  $100\text{ m}^3\text{ pig}^{-1}\text{ h}^{-1}$  in Denmark. The side-wall air supplier was set as pressure outlet with  $0.0\text{ Pa}$  of pressure and  $0.0$  mass fraction of ammonia. The boundary conditions are summarized

in Table 1.

Table 1. Boundary conditions for CFD simulations

Boundaries	Boundary types	Boundary conditions
Air supply inlet	Pressure outlet	0 Pa , mass fraction of 0.0
Air outlet	Velocity inlet	Air speed: -23.18, 20.03, -16.88, -13.73, -10.58 m s <sup>-1</sup> (accordingly airflow rate of 4000, 3500, 2996, 2500, 2000 m <sup>3</sup> h <sup>-1</sup> ) Ammonia mass fraction: 0.0 Turbulence intensity:10% Turbulent length scale: 0.0147 m
PPV exhaust	Velocity inlet	-0.99 m s <sup>-1</sup>
Emission surface	Wall	Ammonia mass fraction of 1.28E-04 Adiabatic Non-slip
Other solid surfaces	Wall	Ammonia mass fraction of 0.0 Adiabatic Non-slip

### 2.3. Data analysis

The ammonia emission was calculated by the Equation (1):

$$E = Q \cdot (C_o - C_{in}) \quad (1)$$

where  $E$  was the ammonia emission rate, mg s<sup>-1</sup>;  $Q$  was the ventilation rate through the fan exhaust and PPV system exhaust, m<sup>3</sup> h<sup>-1</sup>;  $C_o$  was the ammonia concentration at the fan exhaust or PPV system exhaust, mg m<sup>-3</sup> and  $C_{in}$  was the ammonia concentration at the air supplier, mg m<sup>-3</sup>, which was set as 0.0.

The results were presented with the removal ratio of ammonia by PPV system, which was denoted as:

$$R_{PPV} = \frac{E_{PPV}}{E_{PPV} + E_{fan}} \quad (2)$$

where  $R_{PPV}$  was the removal ratio of ammonia emission by PPV system;  $E_{PPV}$  was the ammonia emission through the PPV exhaust, mg s<sup>-1</sup> and  $E_{fan}$  was the ammonia emission through the fan exhaust, mg s<sup>-1</sup>.

The mass transfer coefficients for each emission surface were also calculated by:

$$h_c = E/C_s \quad (3)$$

where  $h_c$  was the mass transfer coefficient, m s<sup>-1</sup>;  $C_s$  was the ammonia concentration on the emission surface, which was corresponding to the ammonia mass fraction of 1.28E-04.

## 3. Results and Discussion

This section started with the CFD validation and the effects of PPV system locations, emission sources and ventilation rate on removal of ammonia emissions by PPV system were then presented and discussed.

### 3.1. Validation of CFD modeling

The comparison between measured and simulated air speeds was presented in Figure 2. The error bars were standard deviation of the measured air speeds. The vector distribution showed that the jet supplied by the side-wall air inlet hit the opposite wall and turned down to the corridor. Part of them flowed into the pen and part of them joined in the large vortex formulated below the jet. Reasonable agreement was found between the measured and simulated air speeds at the three lines (two vertical lines and one horizontal line). Discrepancies were also observed at the points close to the slatted floor. Based on the reasonable prediction of the air velocity magnitude and airflow pattern, the realizable k-e model and two-layer  $y^+$  treatment was used for further

simulations.

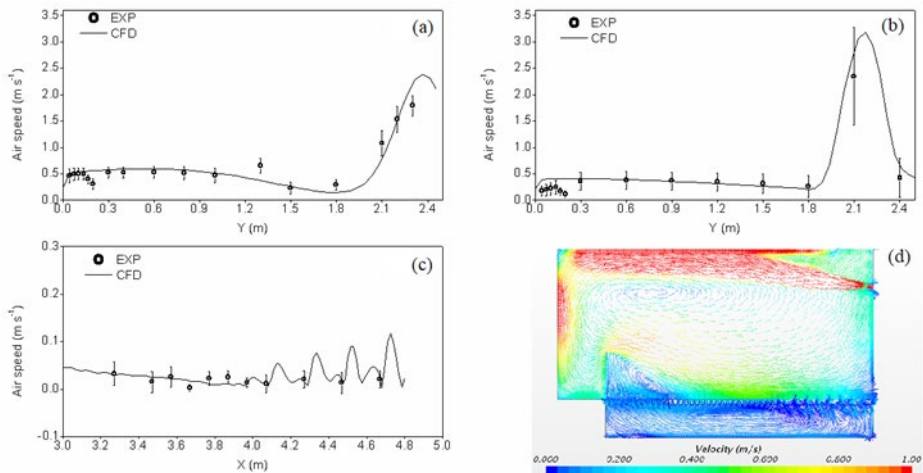


Figure 2. Comparison of measured and simulated air speed at three lines in the plane of  $Z=1.2$  m and vector distribution at plane of  $Z=1.2$  m. (a) was the comparison at line of  $X=3.27$  m; (b) was the comparison at line of  $X=4.4$  y m and (c) was the comparison at line of  $Y=-0.15$  m.

### 3.2. Effects of ventilation rates and locations of PPV exhaust on removal ratios

The effects of ventilation rates and locations of PPV exhaust on ammonia removal ratios of PPV system were shown in Figure 3. With PPV exhaust located on the opposite to the air supplier, the ammonia removal ratios are generally higher than those with PPV exhaust located on the same side to the air supplier, especially for the case with emission source defined on the slurry floor. To explain this, airflow pattern and ammonia concentration distribution were shown in Figure 4.

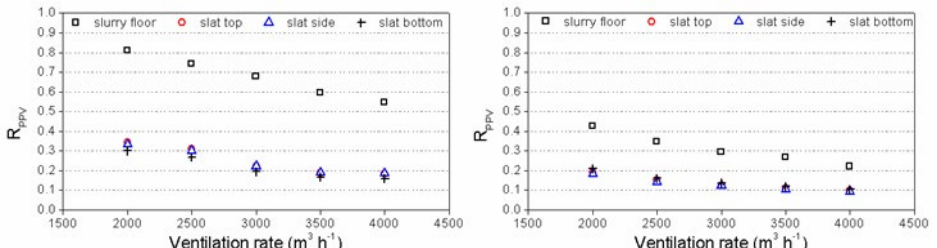


Figure 3. Ammonia removal ratio with different emission surfaces and ventilation rates, (a) PPV exhaust position1 and (b) PPV exhaust position 2.

The ammonia concentrations with PPV exhaust position 2 through the slots between the slats was generally larger than those with PPV exhaust position 1. It indicated that higher ammonia emission was exhausted by the room fan with PPV exhaust position 2 while the ammonia emission collected by PPV was actually lower than that with PPV exhaust position 1. This led to lower ammonia removal ratio with PPV exhaust position 2. That the ammonia emission collected by PPV with PPV exhaust position 2 was lower could be easily explained by the airflow pattern below the slatted floor. In Figure 4, the airflow above the slatted and drained floor entered into the slurry container through all the slots of drained floor and around one-third slots of the slatted floor on the right and then it entered into the room via the rest of the slots of the slatted floor on the left. With the PPV exhaust position 1, the air with accumulated ammonia was collected while with position 2 only ammonia emissions from a small emission surface was collected by the PPV

exhaust. This also applied for explaining why the ammonia removal ratio was higher with PPV exhaust at position 1 when the ammonia emission sources were defined on other emission surfaces of the slats. The PPV exhaust at position 2 could collect more airflow coming from the room directly comparing to the PPV exhaust at position 1 so that less ammonia emission was collected.

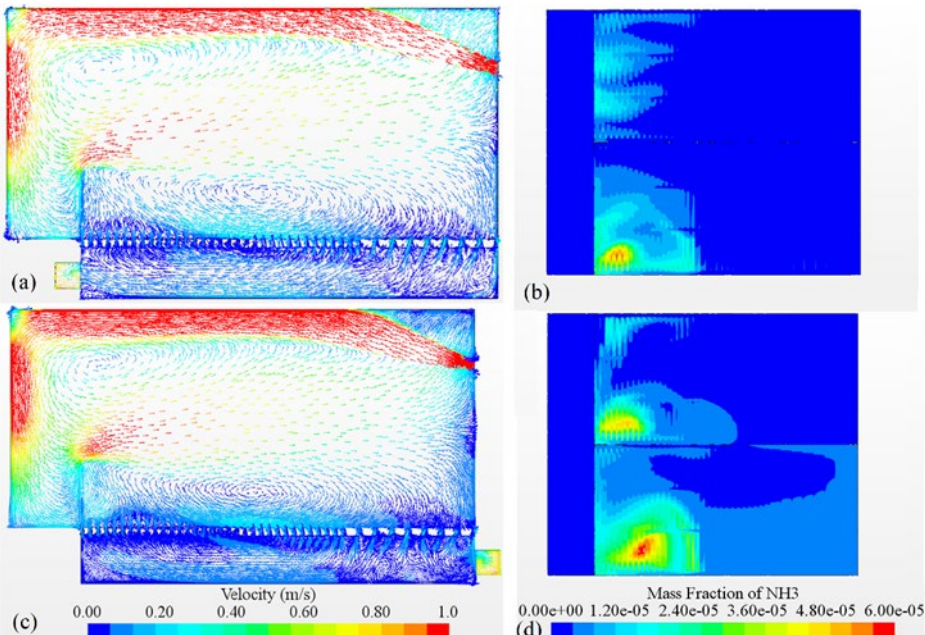


Figure 4. Vector distribution at plane of  $Z=1.2$  m and ammonia mass fraction distribution at plane of  $Y=0$  for cases with emission source defined on the slurry floor and ventilation rate of  $3500 \text{ m}^3 \text{ h}^{-1}$ . (a) and (b) is vector and ammonia mass fraction distribution with PPV exhaust position 1; (c) and (d) is vector and ammonia mass fraction distribution with PPV exhaust position 2.

### 3.3. Ammonia mass transfer coefficients

The ammonia mass transfer coefficients were presented in Figure 5, which were calculated by using Eq. (3) and the emission rate was the sum of ammonia emissions through the room fan and PPV exhaust. As expected, the overall ammonia mass transfer coefficients increased with higher ventilation rate. The highest mass transfer coefficient occurred with emission source on the slat side surfaces. The ammonia mass transfer coefficients with PPV exhaust position 1 were around 5–17% higher than those with PPV exhaust position 2. This indicated the sum of ammonia emissions via room fan and PPV exhaust was around 5–17% higher with PPV exhaust position 1 than the values with PPV exhaust position 2. In order to illustrate the effect of PPV exhaust positions on ammonia mass transfer process, the mass transfer coefficients were calculated by using ammonia emissions via room and PPV exhausts respectively and denoted as  $h_{c,R}$  and  $h_{c,PPV}$  shown in Figure 6.

In Figure 6, the ammonia mass transfer coefficients calculated by using ammonia emissions via room exhaust,  $h_{c,R}$ , increased with larger ventilation rates for all cases while with different slopes. The ammonia mass transfer coefficients calculated by ammonia emission via PPV exhaust,  $h_{c,PPV}$ , decreased slightly with higher room ventilation rate when PPV exhaust was at position 1. The reasons to cause this trend was not clear yet. The  $h_{c,PPV}$  hardly changed with ventilation rates

when PPV exhaust was located at position 2, which was not difficult to understand. When the PPV exhaust was at position 2, the airflow direction was opposite to the mainstream in the slurry so the PPV exhaust has limited effect on the airflow pattern, which constrained the collection of ammonia emissions. Higher  $h_{c,R}$  occurred for cases with emission sources defined at the slat top and slat side surfaces and highest  $h_{c,R}$  was obtained with emission sources defined at the slat side surfaces (seen in Figure 6 c). Larger air speed above the slatted floor led to larger mass transfer coefficients with emission source defined at the slat side and top surface. When the emission source was defined at the slat side surfaces, not only the mean flow influenced the mass transfer of ammonia but also the turbulent fluctuation could contribute to the ammonia mass transfer through the slots. This could be the reasons why the  $h_{c,R}$  was the highest among all the cases.

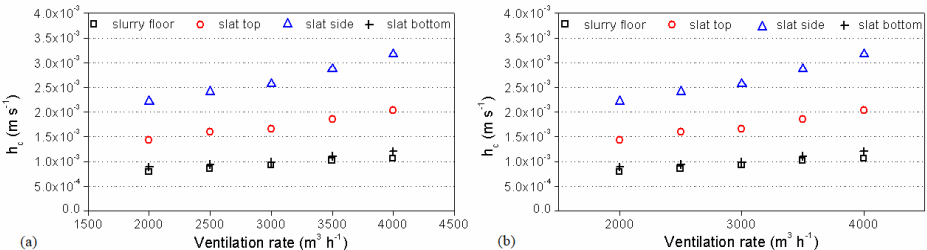


Figure 5. Ammonia mass transfer coefficients along with ventilation rates with ammonia emission sources defined on different surfaces. (a) PPV exhaust position 1 and (b) PPV exhaust position 2.

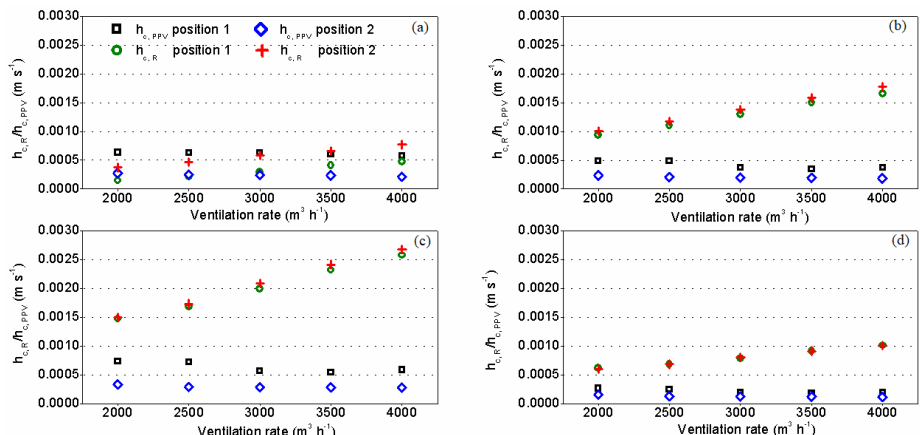


Figure 6. Ammonia mass transfer coefficient calculated by ammonia emissions via room exhaust and PPV exhaust respectively with two PPV exhaust positions and ammonia emission sources defined on different emission surfaces: (a) slurry floor, (b) slat top, (c) slat side and (d) slat bottom.

#### 4. Conclusions

The partial pit ventilation (PPV) system is widely used in fattening pig houses in Denmark. This study investigated the position of PPV exhaust and ammonia emission source's locations on ammonia removal ratio by PPV. The two locations of PPV exhaust could hardly change the airflow patterns but affects the ammonia removal ratio because the PPV exhaust could collect more ammonia emissions when the PPV exhaust location aligned with the airflow pattern but not against the airflow pattern. When the emission source was located on surfaces of slatted floor, the

ammonia removal ratio was relatively low especially with higher ventilation rate. This indicates that it is important to remove the emission source on the surfaces of slatted floor in time to abate the ammonia emissions. The high mass transfer coefficient on the side surfaces of slatted floor indicated that it is important to optimize the design of the slatted floor so the manure/urine could be least stick on the side surfaces.

### References

- Berg, B., G.Q. Zhang, 2013. CFD analyses of the influence of ventilation system on the effectiveness of a partial pit exhaust. *Acta Horticulturae*, 143–150 p. <http://dx.doi.org/10.17660/ActaHortic.2013.1008.18>.
- IPCC, 2006. 2006 IPCC (Intergovernmental Panel on Climate Change) Guidelines for National Greenhouse Gas Inventories, Prepared by the National Greenhouse Gas inventories Programme. Hayama, Japan: Institute for Global Environmental Strategies.
- Rong, L., A.J.A. Aarnink, 2019. Development of ammonia mass transfer coefficient models for the atmosphere above two types of the slatted floors in a pig house using computational fluid dynamics. *Biosystems Engineering*, 183, 13–25. <http://dx.doi.org/10.1016/j.biosystemseng.2019.04.011>.
- Saha, C.K., G. Zhang, P. Kai, B. Bjerg, 2010. Effects of a partial pit ventilation system on indoor air quality and ammonia emission from a fattening pig room. *Biosystems Engineering*, 105 (3), 279–287. <http://dx.doi.org/10.1016/j.biosystemseng.2009.11.006>.
- Van Huffel, K., M.J. Hansen, A. Feilberg, D. Liu, H. Van Langenhove, 2016. Level and distribution of odorous compounds in pig exhaust air from combined room and pit ventilation. *Agriculture, Ecosystems and Environment*. 218, 209–219. <http://dx.doi.org/10.1016/j.agee.2015.11.020>.
- Wu, W., P. Kai, G. Zhang, 2012a. An assessment of a partial pit ventilation system to reduce emission under slatted floor – Part 1: Scale model study. *Computers and Electronics in Agriculture*. 83, 127–133. <http://dx.doi.org/10.1016/j.compag.2012.01.008>.
- Wu, W., G. Zhang, B. Bjerg, P.V. Nielsen, 2012b. An assessment of a partial pit ventilation system to reduce emission under slatted floor – Part 2: Feasibility of CFD prediction using RANS turbulence models. *Computers and Electronics in Agriculture*. 83, 134–142. <http://dx.doi.org/10.1016/j.compag.2012.01.011>.
- Zong, C., Y. Feng, G. Zhang, M.J. Hansen, 2014. Effects of different air inlets on indoor air quality and ammonia emission from two experimental fattening pig rooms with partial pit ventilation system – summer condition. *Biosystems Engineering*, 122, 163–173. <http://dx.doi.org/10.1016/j.biosystemseng.2014.04.005>.
- Zong, C., H. Li, G. Zhang, 2015. Ammonia and greenhouse gas emissions from fattening pig house with two types of partial pit ventilation systems. *Agriculture, Ecosystems and Environment*. 208, 94–105. <http://dx.doi.org/10.1016/j.agee.2015.04.031>.

## Effect of Cage Size and Nutrition on Performance and Health of Pullets

Yi Wan, Ruiyu Ma, Yan Li, Wei Liu, Junying Li, Kai Zhan \*

Anhui Key Laboratory of Livestock and Poultry Product Safety Engineering,  
Institute of Animal Husbandry and Veterinary Medicine, Anhui Academy of Agriculture Science,  
Hefei, Anhui 230031, P.R. China

\* Corresponding author. Email: [Zhankai633@126.com](mailto:Zhankai633@126.com)

### Abstract

In this study, we evaluated the effects of different-sized cages with a low metabolizable energy (LME) and low crude protein (LCP) diet on pullets. A total of 668 one-day-old female Gushi chicks were randomly allocated into three different cages, namely, large ( $1.60\text{ m} \times 1.60\text{ m} \times 0.42\text{ m}$ ), medium ( $1.20\text{ m} \times 1.20\text{ m} \times 0.42\text{ m}$ ) and small ( $0.8\text{ m} \times 0.7\text{ m} \times 0.37\text{ m}$ ) cages, and fed with LME-LCP diet, referred to as Group A, Group B and Group C, respectively. An additional group in a small cage and fed with standard diet (STD) were designated as Group D for control. Equal stocking densities were maintained among the four groups throughout the experiment. Body weight, shank length and shank girth were measured biweekly from day 1 to day 98, and blood serum parameters were determined biweekly from day 56 to day 98. The results showed that in large cages with LME-LCP diets (Group A) increased the shank length and shank girth during the period and increased the level of CK in the blood serum and reduced the level of TG, T-CH and GSH. The total cost (RMB bird<sup>-1</sup>) of feed consumption was 6.70% lower in Group A than in Group D, which indicated the cost-effectiveness of large cages. Overall, the current findings provide support for the role of large cages with LME-LCP diets in improving poultry performance and welfare during rearing.

**Keywords:** Large cage, growth performance, blood parameter, immune response

### 1. Introduction

With an increased interest on animal welfare, the space in cage for layers has been concerned in recent decades. Cage design is one component of the environment of a hen that plays a critical role for the well-being of the birds in cage. Decreased cage space decreases biological function, egg production, egg weight, body weight and feed intake and increases mortality (Sohail et al., 2004). For caged hens, enough freedom of movement could enable the performance of most normal patterns of behaviour (Dawkins and Hardie, 1989). Chickens grow more slowly at higher stocking densities and jostle each other more, and fewer of them show the best gaits (Stamp et al., 2004). Wing stretching, leg stretching and tail wagging all increase in frequency when birds housed with less space are released into larger cages (Baxter, 1994), and larger spaces for chickens improve bone mass and bone quality (Eric et al., 2015). Therefore, increasing the space in cages could be advantageous for poultry production.

In addition to the various reported effects of cage size on the performance of chickens, differing diets have also been implicated as having an effect on the growth, carcass traits and blood serum parameters of hens. Low metabolizable energy and low crude protein diets reportedly enhance immune functions and the feed conversion ratio (Nahashon et al., 2007; Sigolo et al., 2017). Moreover, Kidd et al. (2001) reported that LCP diets improved protein efficiency and increased feed intake. However, few studies concerning the effect of an interaction between cage size and diet on the performance of chickens have been conducted. Madrid et al. (1981) reported that maintenance energy requirements increased as cage space decreased, while Jalal et al. (2006) found that energy intake increased as cage space increased.

Based on the abovementioned findings, cage size plays an important role in enhancing the well-being of chickens and affects their energy needs, and larger cages are expected to improve chicken growth. Thus, we carried out this study to evaluate the effects of a large-sized cage with

LME-LCP diets on the growth performance, blood parameters, and immune responses of pullets.

## 2. Materials and Methods

The study protocol was approved by the Committee for the Care and Use of Experimental Animals at Anhui Academy of Agricultural Science under permit no. A11-CS06.

### 2.1. Birds, cages and grouping

Gushi chickens originated in central China, are used as dual-purpose breeds. A total of 668 female 1-day-old Gushi chicks were obtained from Anhui Wanxi Poultry Development Co., Ltd. (Luan, China) and were assigned to two dietary treatments (Table 1): a standard diet (STD) and an LME-LCP diet. The STD contained 12.38 MJ of metabolizable energy (ME) kg<sup>-1</sup> and 20.13% crude protein (CP) from 1 to 28 days of age, 12.68 MJ of ME kg<sup>-1</sup> and 18.20% CP from 29 to 56 days of age, and 12.72 MJ of ME kg<sup>-1</sup> and 16.03% CP from 57 to 98 days of age, while the LME-LCP diet contained 2% less CP than the STD at each growth stage and 6.7%, 6.0% and 5.9% less ME than the STD at the three growth stages, respectively. The diets were provided in mash form, and feed and water were provided for ad libitum consumption. Feeds were prepared once per week to avoid mildew.

Table 1. Ingredient composition and nutrient levels of diets fed from 1 to 98 days of age.

Age (d) Level of diet	1–28		29–56		57–98	
	STD	LME-LCP	STD	LME-LCP	STD	LME-LCP
Ingredients, %						
Corn	50.3	61.8	54.9	66.0	61.7	72.8
Soybean meal	36.7	30.1	31.5	25.0	25.4	18.9
Soybean oil	5.5	0.6	6.1	1.5	5.4	0.8
Limestone	2.5	2.5	2.5	2.5	2.5	2.5
Salt	0.3	0.3	0.3	0.3	0.3	0.3
Premix	4.7	4.7	4.7	4.7	4.7	4.7
Calculated level						
ME, MJ kg <sup>-1</sup>	12.38	11.55	12.68	11.92	12.72	11.97
CP, %	20.13	18.13	18.20	16.20	16.03	14.03
Lysine, %	1.10	1.00	1.00	0.83	0.83	0.68
Methionine, %	0.45	0.42	0.42	0.40	0.38	0.36
Methionine + cystine, %	0.82	0.75	0.74	0.71	0.68	0.62
Calcium, %	1.00	1.00	1.00	1.00	1.00	1.00
Available phosphorus, %	0.47	0.43	0.42	0.42	0.40	0.38

This study was performed using three different-sized cages for birds: a large cage (1.6 m × 1.6 m × 0.42 m), medium cage (1.2 m × 1.2 m × 0.42 m) and small cage (0.8 m × 0.7 m × 0.37 m). Experimental birds raised in large, medium, and small cages and fed the LME-LCP diet were assigned to Group A, Group B and Group C, respectively. Birds raised in small cages and fed the STD were assigned to Group D as a control. The stocking densities of different groups from 1 to 98 days of age are shown in Table 2. The four groups were maintained at equal stocking densities of 50 birds m<sup>-2</sup> (from the 1st to 14th day), 40 birds m<sup>-2</sup> (from the 15th to 28th day), 30 birds m<sup>-2</sup> (from the 29th to 42nd day), 25 birds m<sup>-2</sup> (from the 43rd to 56th day), 22 birds m<sup>-2</sup> (from the 57th to 70th day), and 20 birds m<sup>-2</sup> (from the 71st to 98th day).

The stocking density was reduced and cages were added every two weeks as chickens grew to provide enough space for the birds due to animal welfare concerns. When birds in the experimental cages died or were separated to change stocking densities, extra chickens were selected to add as supplements.

Table 2. Stocking density of different groups of Gushi chickens during different growth periods.

Group	Age (d)	1 <sup>st</sup>	14 <sup>th</sup>	28 <sup>th</sup>	42 <sup>nd</sup>	56 <sup>th</sup>	70 <sup>th</sup> –98 <sup>th</sup>
Group A, large cages, 1.6 m×1.6 m	Number of cages	2	2	3	3	3	3
	Birds cage <sup>-1</sup>	128	102	76	64	56	51
	Total number of birds	256	204	228	192	168	153
	Base area of cage (m <sup>2</sup> )				2.56		
Group B, medium cages, 1.2 m×1.2 m	Number of cages	3	3	5	5	5	5
	Birds cage <sup>-1</sup>	72	58	43	36	32	29
	Total number	216	174	215	180	160	145
	Base area of cage (m <sup>2</sup> )				1.44		
Groups C and D, small cages, 0.8 m×0.7 m	Number of cages	7	8	11	13	12	13
	Birds cage <sup>-1</sup>	28	22	17	14	12	11
	Total number	196	176	187	182	144	143
	Base area of cage (m <sup>2</sup> )				0.56		
	Stocking density (birds m <sup>-2</sup> )	50	40	30	25	22	20

## 2.2. Measurements and sampling

On day 1, the chicks were individually weighed, wing-tagged and separated into different groups. Body weight, shank length, and shank girth were measured every 2 weeks (from 1 to 14 weeks). Body weight was measured using an electronic scale. Shank length was measured using a digital Vernier caliper, while shank girth was measured using a tape measurer. Feed intake and mortality were recorded on a pen basis daily.

For each group, 30 birds were randomly selected for blood sampling on the 56th, 70th, 84th, and 98th days of age. A 4-mL blood sample was collected into 2 heparinized tubes (2 mL in each tube) from the chickens by wing vein. The time between catching the bird and obtaining the blood sample did not exceed 45 s. Samples were placed in an ice bath immediately after collection and then transported to the laboratory for processing. Blood serum was separated by centrifugation at 3000 rpm for 10 min and stored at -20°C until analysis.

Collected serum was assayed for levels of cortisol, creatine kinase (CK), triglyceride (TG), total cholesterol (T-CH), blood urea nitrogen (BUN), and glutathione (GSH). The concentrations of these parameters were determined by using commercial laboratory kits (Xinqidi Biotech Co., Wuhan, China) as described by Swennen et al. (2005).

## 2.3. Statistical analysis

Data were subjected to analysis of variance (ANOVA) using the General Linear Model (GLM) command in SAS version 9.3 statistical software (SAS Institute Inc., Cary, NC, USA). The statistical model used for the analysis of dependent variables was as follows:

$$Y_{jkl} = \mu + C_i + D_j + (CD)ij + B_k + e_{jkl} \quad (1)$$

where  $Y_{jkl}$  is the individual observation,  $\mu$  is the overall mean,  $C_i$  is the cage size effect,  $D_j$  is the dietary effect,  $(CD)ij$  is the interaction of cage size with diet,  $B_k$  is the block effect and  $e_{jkl}$  is the random error. Statistical analyses were performed by Student's t-test. Duncan's multiple range test at a 5% probability was used to compare means. All data are presented as means and standard error of the mean.

## 3. Results

### 3.1. Growth performance

The effects of large cages fed with LME-LCP diet on body weight, shank length and shank girth of chickens over the 14-week study period are presented in Table 3. The body weight of Group D (fed the STD) was significantly higher ( $P < 0.05$ ) than that of Groups A, B and C, which were fed an LME and LCP diet during the early period (from 14 to 56 days). As the hens aged,

the body weights of Groups A, B and D were similar from 70 to 98 days of age, while birds from Group C were significantly ( $P < 0.05$ ) lighter in weight than those raised in the other groups. No significant differences were found in shank length between Groups A and D from 14 to 70 days of age except on the 42nd day. There was some suggestion that large cages (Group A) increased shank length from 84 to 98 days of age as chickens grew, with lengths of 8.08 cm and 8.47 cm, which were significantly ( $P < 0.05$ ) longer than those observed for Groups C and D. A similar trend was found in the values of shank girth in which chickens from Group A had a greater shank girth than those in the other three groups from 42 to 98 days of age, while the shank girth of Group C was significantly shorter than that of the other three groups.

Table 3. The body weight, shank length and shank girth of different groups of Gushi chickens during different growth periods.

Age (d)	LME-LCP <sup>1</sup>			STD <sup>2</sup> Group D	SEM <sup>3</sup>	<i>P</i> -value
	Group A	Group B	Group C			
Mean body weight, g						
14 <sup>th</sup>	91.56 <sup>a</sup>	89.08 <sup>a</sup>	91.94 <sup>a</sup>	97.80 <sup>b</sup>	0.597	<0.001
28 <sup>th</sup>	189.36 <sup>a</sup>	184.31 <sup>a</sup>	197.36 <sup>b</sup>	210.73 <sup>c</sup>	1.428	<0.001
42 <sup>nd</sup>	340.92 <sup>a</sup>	331.06 <sup>ab</sup>	322.36 <sup>b</sup>	356.94 <sup>c</sup>	2.518	<0.001
56 <sup>th</sup>	524.17 <sup>a</sup>	520.85 <sup>a</sup>	507.62 <sup>a</sup>	553.04 <sup>b</sup>	3.757	<0.001
70 <sup>th</sup>	727.95 <sup>a</sup>	706.77 <sup>a</sup>	675.62 <sup>b</sup>	728.59 <sup>a</sup>	4.968	<0.001
84 <sup>th</sup>	870.77 <sup>a</sup>	887.15 <sup>a</sup>	824.59 <sup>b</sup>	866.19 <sup>a</sup>	5.750	<0.001
98 <sup>th</sup>	1006.30 <sup>a</sup>	1009.99 <sup>a</sup>	945.29 <sup>b</sup>	1006.95 <sup>a</sup>	6.477	<0.001
Shank length, cm						
14 <sup>th</sup>	3.25 <sup>a</sup>	3.06 <sup>b</sup>	3.10 <sup>b</sup>	3.21 <sup>a</sup>	0.010	<0.001
28 <sup>th</sup>	4.33 <sup>ab</sup>	4.26 <sup>a</sup>	4.37 <sup>b</sup>	4.26 <sup>a</sup>	0.014	0.012
42 <sup>nd</sup>	5.18 <sup>a</sup>	5.12 <sup>a</sup>	5.13 <sup>a</sup>	5.31 <sup>b</sup>	0.019	0.002
56 <sup>th</sup>	6.47 <sup>ac</sup>	6.37 <sup>ad</sup>	6.31 <sup>bd</sup>	6.57 <sup>c</sup>	0.023	<0.001
70 <sup>th</sup>	6.95 <sup>a</sup>	6.93 <sup>a</sup>	6.80 <sup>b</sup>	7.02 <sup>a</sup>	0.023	0.005
84 <sup>th</sup>	8.08 <sup>a</sup>	8.05 <sup>a</sup>	7.75 <sup>b</sup>	7.54 <sup>c</sup>	0.026	<0.001
98 <sup>th</sup>	8.47 <sup>a</sup>	8.26 <sup>b</sup>	8.16 <sup>b</sup>	8.26 <sup>b</sup>	0.024	<0.001
Shank girth, cm						
14 <sup>th</sup>	1.71 <sup>a</sup>	1.73 <sup>ab</sup>	1.75 <sup>b</sup>	1.75 <sup>b</sup>	0.006	0.008
28 <sup>th</sup>	2.20 <sup>ac</sup>	2.17 <sup>bc</sup>	2.23 <sup>ad</sup>	2.27 <sup>d</sup>	0.007	<0.001
42 <sup>nd</sup>	2.70 <sup>a</sup>	2.66 <sup>ab</sup>	2.61 <sup>b</sup>	2.66 <sup>a</sup>	0.009	0.005
56 <sup>th</sup>	2.97 <sup>a</sup>	2.94 <sup>a</sup>	2.93 <sup>a</sup>	2.95 <sup>a</sup>	0.008	0.400
70 <sup>th</sup>	3.24 <sup>a</sup>	3.22 <sup>a</sup>	3.09 <sup>b</sup>	3.20 <sup>a</sup>	0.010	<0.001
84 <sup>th</sup>	3.42 <sup>a</sup>	3.41 <sup>a</sup>	3.34 <sup>b</sup>	3.41 <sup>a</sup>	0.009	<0.001
98 <sup>th</sup>	3.58 <sup>a</sup>	3.55 <sup>a</sup>	3.49 <sup>b</sup>	3.53 <sup>ab</sup>	0.009	<0.001

<sup>a–d</sup>Means with different superscripts are significantly different ( $P < 0.05$ ).

<sup>1</sup>LME-LCP: low metabolizable energy and low crude protein diet.

<sup>2</sup>STD: Standard diet.

<sup>3</sup>SEM: Pooled standard error of the means for traits analyzed with linear mixed models.

### 3.2. Blood parameters

The effects of cage type on blood serum parameters are given in Table 4. Birds in large cages that received an LME-LCP diet (Group A) had higher ( $P < 0.05$ ) blood serum concentrations of CK than those in the other groups throughout the experiment but lower concentrations of TG and T-CH as well as a lower concentration of BUN from 56 to 84 days of age. Similar levels of BUN were found between Groups C and D throughout the experiment. Birds in small cages that received an STD (Group D) had lower ( $P < 0.05$ ) blood serum concentrations of CK and GSH than those in the other groups throughout the experiment. There were no significant differences

in cortisol among the four groups from 70 to 98 days of age. The concentrations of TG and T-CH were higher in Groups B and C than in Groups A and D ( $P < 0.05$ ) throughout the experiment

Table 4. Blood serum concentrations of CK, cortisol, TG, T-CH, BUN, and GSH in Gushi chickens from the four groups during different growth periods.

Items	Age (d)	LME-LCP <sup>1</sup>			STD <sup>2</sup>		<i>P</i> -value
		Group A	Group B	Group C	Group D	SEM <sup>3</sup>	
CK (ng mL <sup>-1</sup> )	56	234.49 <sup>a</sup>	185.28 <sup>c</sup>	213.87 <sup>b</sup>	163.66 <sup>d</sup>	1.655	<0.001
	70	274.28 <sup>a</sup>	175.51 <sup>c</sup>	212.32 <sup>b</sup>	150.37 <sup>d</sup>	1.756	<0.001
	84	264.87 <sup>a</sup>	195.39 <sup>c</sup>	228.19 <sup>b</sup>	175.55 <sup>d</sup>	1.712	<0.001
	98	222.77 <sup>a</sup>	164.55 <sup>c</sup>	195.13 <sup>b</sup>	153.40 <sup>d</sup>	1.610	<0.001
Cortisol (ng mL <sup>-1</sup> )	Mean	253.40	186.21	217.69	167.17		
	56	156.59 <sup>ab</sup>	149.12 <sup>ab</sup>	142.44 <sup>b</sup>	157.15 <sup>a</sup>	1.221	<0.001
	70	172.13	179.36	179.24	182.92	1.389	0.546
	84	158.94	158.82	165.79	167.48	1.301	0.633
TG (ng mL <sup>-1</sup> )	98	165.16	164.39	161.04	158.30	1.332	0.689
	Mean	161.83	163.61	163.04	164.74		
	56	15.30 <sup>b</sup>	17.49 <sup>a</sup>	18.49 <sup>a</sup>	14.72 <sup>b</sup>	0.095	0.006
	70	14.77 <sup>c</sup>	15.87 <sup>b</sup>	18.11 <sup>a</sup>	12.65 <sup>d</sup>	0.097	<0.001
T-CH (ng mL <sup>-1</sup> )	84	15.97 <sup>b</sup>	20.07 <sup>a</sup>	20.25 <sup>a</sup>	17.17 <sup>b</sup>	0.090	0.011
	98	13.76 <sup>c</sup>	16.59 <sup>a</sup>	17.56 <sup>a</sup>	15.32 <sup>b</sup>	0.085	<0.001
	Mean	14.63	16.96	18.12	14.27		
	56	2.45 <sup>c</sup>	3.34 <sup>b</sup>	4.06 <sup>a</sup>	3.11 <sup>b</sup>	0.011	<0.001
BUN (ng mL <sup>-1</sup> )	70	3.10 <sup>c</sup>	4.14 <sup>a</sup>	3.72 <sup>b</sup>	3.23 <sup>c</sup>	0.013	<0.001
	84	2.84 <sup>c</sup>	3.60 <sup>b</sup>	4.42 <sup>a</sup>	3.40 <sup>b</sup>	0.012	<0.001
	98	3.35 <sup>c</sup>	4.33 <sup>b</sup>	4.93 <sup>a</sup>	4.57 <sup>ab</sup>	0.017	<0.001
	Mean	2.95	3.80	4.11	3.52		
GSH (ng mL <sup>-1</sup> )	56	3.76 <sup>c</sup>	6.36 <sup>a</sup>	5.05 <sup>b</sup>	5.47 <sup>b</sup>	0.020	<0.001
	70	4.72 <sup>c</sup>	6.65 <sup>a</sup>	5.41 <sup>b</sup>	5.09 <sup>bc</sup>	0.022	<0.001
	84	4.22 <sup>c</sup>	6.35 <sup>a</sup>	5.40 <sup>b</sup>	6.03 <sup>ab</sup>	0.025	<0.001
	98	6.75 <sup>a</sup>	6.38 <sup>b</sup>	5.66 <sup>c</sup>	6.72 <sup>a</sup>	0.033	<0.001
Mean	4.85	6.44	5.34	5.56			
	56	42.68 <sup>c</sup>	51.78 <sup>a</sup>	47.33 <sup>b</sup>	36.90 <sup>d</sup>	0.211	<0.001
	70	43.20 <sup>b</sup>	48.57 <sup>a</sup>	44.90 <sup>b</sup>	37.62 <sup>c</sup>	0.198	<0.001
	84	36.07 <sup>b</sup>	37.70 <sup>b</sup>	44.94 <sup>a</sup>	32.94 <sup>c</sup>	0.190	<0.001
98	31.06 <sup>b</sup>	32.06 <sup>b</sup>	38.88 <sup>a</sup>	27.21 <sup>c</sup>	0.162	<0.001	
	Mean	38.16	42.51	56.01	51.47		

<sup>a-d</sup>Means with different superscripts are significantly different ( $P < 0.05$ ).

<sup>1</sup>LME-LCP: low metabolizable energy and low crude protein diet.

<sup>2</sup>STD: Standard diet.

<sup>3</sup>SEM: Pooled standard error of the means for traits analyzed with linear mixed models.

### 3.3. Feed cost

The consumption and cost of feed of different groups are shown in Table 5. The total feed intake per bird of Group A was 3775.76 g bird<sup>-1</sup>, which was higher than that observed for the other groups at every stage, while Group C (small cages with an LME-LCP diet) had the lowest total feed intake of 3392.04 g bird<sup>-1</sup>. The total feed costs per bird throughout the experiment (from birth to 98 days) among the four groups ranked as follows: Group D > Group A > Group B > Group C, with values of 10.60, 9.89, 9.47 and 8.87 RMB, respectively.

Table 5. The consumption and cost of feed per bird among the four groups of Gushi chickens during different growth periods.

Age (d)	Item	LME-LCP <sup>1</sup>				SEM <sup>3</sup>	<i>P</i> -value
		Group A	Group B	Group C	Group D		
1–14	Mean feed intake (g bird <sup>-1</sup> d <sup>-1</sup> )	10.01 <sup>a</sup>	9.22 <sup>a</sup>	9.52 <sup>a</sup>	9.97 <sup>a</sup>	0.481	0.993
15–28	Total feed intake (g bird <sup>-1</sup> )	17.81 <sup>a</sup>	18.39 <sup>a</sup>	16.41 <sup>a</sup>	17.21 <sup>a</sup>	0.504	0.556
	Feed prices (RMB kg <sup>-1</sup> )		2.7		3.10		
29–42	Cost (RMB bird <sup>-1</sup> )	1.05	1.04	0.98	1.18		
43–56	Mean feed intake (g bird <sup>-1</sup> d <sup>-1</sup> )	29.35 <sup>a</sup>	24.51 <sup>bc</sup>	23.55 <sup>b</sup>	26.82 <sup>ac</sup>	0.556	<0.001
	Total feed intake (g bird <sup>-1</sup> )	46.58 <sup>a</sup>	42.25 <sup>b</sup>	33.69 <sup>c</sup>	32.92 <sup>c</sup>	0.995	<0.001
	Feed prices (RMB bird <sup>-1</sup> )		2.7		3.07		
57–70	Cost (RMB bird <sup>-1</sup> )	2.87	2.52	2.16	2.57		
71–84	Mean feed intake (g bird <sup>-1</sup> d <sup>-1</sup> )	53.15 <sup>ab</sup>	50.75 <sup>a</sup>	51.93 <sup>ab</sup>	53.61 <sup>b</sup>	0.486	0.153
85–98	Cost (RMB bird <sup>-1</sup> )	56.30 <sup>a</sup>	56.31 <sup>a</sup>	53.55 <sup>a</sup>	54.78 <sup>a</sup>	0.535	0.200
	Total feed intake (g bird <sup>-1</sup> )	56.48 <sup>a</sup>	57.19 <sup>a</sup>	53.63 <sup>a</sup>	57.42 <sup>a</sup>	0.754	0.264
	Feed prices (RMB bird <sup>-1</sup> )		2.57		2.95		
1–98	Cost (RMB bird <sup>-1</sup> )	5.97	5.91	5.73	6.85		
	Total feed intake (g bird <sup>-1</sup> )	3775.76	3620.61	3392.04	3538.12		
	Total Cost (RMB bird <sup>-1</sup> )	9.89	9.47	8.87	10.60		

#### 4. Discussion

The difference in various indicators between groups showed the adaptability of birds to different-sized cages. In the present study, Groups A, B and C were grown in large cages but fed a relatively LME and LCP diet, and Group D was grown in small cages and fed an STD. Different dietary energy and protein contents were used to evaluate the effect of different-sized cages on birds.

Theoretically, birds raised in larger cages should have larger relative space allowances, which could contribute to growth, than those in small cages at an equal stocking density, which have less activity space (Widowski et al., 2017a). However, the body weight of birds in Group D was greater than that of birds in the other groups from 14 to 56 days. When the chickens were young, enough energy and protein seemed to be more important for growth, while large space allowances did not seem to work because of the small body size of chicks. As chickens grew, similar body weights were found between Groups A, B and D from 70 to 98 days, which reflected the advantages of large cages as Group A was given an LME-LCP diet. A previous report (Widowski et al., 2017b) in agreement with this result indicated that there was a significant effect of the interaction between age and space allowance on overall body weight as birds matured. Similarly, the shank length and shank girth of birds in Group A were greater than those of birds in the other groups during the late stages of the experiment (from 84 to 98 days). Birds in Group C, which were grown in small cages and fed an LME-LCP diet, had a lower body weight, shank length and shank girth than those in

the other groups (from 56 to 98 days), as expected.

Birds on lower-calorie diets tend to consume more feed to meet their energy needs than those fed higher-calorie diets (Nahashon et al., 2007). Similar results were found in the present study: the total feed intake (14 weeks) of Groups A and B was 6.72% and 2.33% higher than that of Group D, respectively. However, the total feed intake of Group C was lower than that of the other groups throughout the period. Therefore, the feed intake of chickens appears to have been influenced not only by dietary ME and CP levels but also by cage size. Numerically, the stocking density (bird m<sup>-2</sup>) was the same among the four groups at each growth stage, but large cages presumably offered a larger feeding space (Widowski et al., 2016). In addition, birds from Group A had a higher feed intake, which resulted in a lower total cost of feed consumption than that observed for Group D (6.70% reduction per bird). This finding is similar to that in a previous study (Morris, 1968), in which a low-calorie diet reduced the cost of feeding.

The release of CK is thought to be proportional to the intensity and duration of exercise (Apple, 1981), while exercise can briefly lower serum TG (Oscai et al., 1972) and cholesterol (Johnson et al., 1959) levels. As hens are social animals and sometimes gather together in natural conditions (Xiang et al., 2016), larger spaces appear in larger cages, which motivates the activities of birds. In this study, we observed a higher level of CK and lower levels of TG and T-CH in birds from larger cages (Group A). However, the levels of TG and T-CH were higher in Group C than in Group D, which may be attributed to the reduced dietary CP (Kamran et al., 2010; Jariyahathakij et al., 2017). GSH, an important intracellular antioxidant (Schulz et al., 2010), was higher in Groups A and B than in Group C (from 70 to 90 days) and Group D, while the levels of GSH were higher in Group C than in Group D. This result implied that GSH in the blood serum of birds can be influenced by cage size and nutritional level. Serum cortisol concentrations, indicating the level of stress response, increase as space allowances decrease (Kim et al., 2016). However, similar levels of serum cortisol were found among the four groups in the present study.

## 5. Summary

In summary, large cages with LME-LCP diets increased the shank length and shank girth as chicks grew and optimized the blood serum indices of CK, TG, T-CH and GSH. The reduction in feed cost by 6.70% per bird compared with the small-sized cages with STD diets indicated the cost-effectiveness of the former conditions. Overall, the current findings provide support for the role of large-sized cages with LME-LCP diets in improving poultry welfare during rearing.

## Acknowledgements

The authors are grateful to Dr. Cheng Zhang at Anhui Agricultural University for valuable comments on the manuscript. This work was supported in part by grants from the China Agriculture Research System (CARS-40-K21) and the Major Science and Technology Project of Anhui Province (18030701172).

## References

- Apple, F.S., 1981. Presence of creatine kinase MB isoenzyme during marathon training. *New England Journal of Medicine*. 305, 764–765.
- Baxter, M.R., 1994. The welfare problem of laying hens in battery cages. *Veterinary Record*. 134, 614–619.
- Dawkins, M.S., S. Hardie, 1989. Space needs of laying hens. *British Poultry Science*. 30, 413–416.
- Eric, A., P.G. Florence, G. Eric, A. Maurice, and C. Daniel, 2015. Bone mass and bone quality are altered by hypoactivity in the chicken. *PLoS One*. 10, e0116763.
- Jalal, M.A., S.E. Scheideler, and D. Marx, 2006. Effect of bird cage space and dietary metabolizable energy level on production parameters in laying hens. *Poultry Science*. 85, 306–311.
- Jariyahathakij, P., B. Chomtee, T. Poeikhampha, W. Loongyai, and C. Bunchasak, 2017. Methionine supplementation of low-protein diet and subsequent feeding of low-energy diet on the performance and blood chemical profile of broiler chickens. *Animal Production Science*. 58, 878–885.
- Johnson, D., A.L. Mehring, and H.W. Titus, 1959. Variability of the blood plasma cholesterol of laying chickens. *Poultry Science*. 38, 1109–1113.

- Kamran, Z., M. Sarwar, M.U. Nisa, M.A. Nadeem, and S. Mahmood, 2010. Effect of low levels of dietary crude protein with constant metabolizable energy on nitrogen excretion, litter composition and blood parameters of broilers. International Journal of agriculture and biology. 12, 401–405.
- Kidd, M.T., P.D. Gerard, J. Heger, B.J. Kerr, D. Rowe, K. Sistani, and D.J. Burnham, 2001. Threonine and crude protein responses in broiler chicks. Animal Feed Science and Technology. 94, 57–64.
- Kim, K.H., K.S. Kim, J.E. Kim, D.W. Kim, K.H. Seol, S.H. Lee, Y.H. Kim, 2016. The effect of optimal space allowance on growth performance and physiological responses of pigs at different stages of growth. Animal. 11, 478–485.
- Madrid, A., P.M. Maiorino, and B.N. Reid, 1981. Cage space and energy utilization. Nutrition reports international. 23, 89–93.
- Morris, T.R., 1968. The effect of dietary energy level on the voluntary calorie intake of laying birds. British Poultry Science. 9, 285–295.
- Nahashon, S.N., N. Adefope, A. Amenyenu, and D. Wright, 2007. Effect of varying metabolizable energy and crude protein concentrations in diets of pearl gray Guinea fowl pullets. 2. Egg production performance. Poultry Science. 86, 973–982.
- Oscai, L.B., J.A. Patterson, D.L. Bogard, R.J. Beck, and B.L. Rothermel, 1972. Normalization of serum triglycerides and lipoprotein electrophoretic patterns by exercise. American Journal of Cardiology. 30, 775–780.
- Schulz, J.B., J. Lindenau, J. Seyfried, and J. Dichgans, 2010. Glutathione, oxidative stress and neurodegeneration. European Journal of Biochemistry. 267, 4904–4911.
- Sigolo, S., Z. Zohrabi, A. Gallo, A. Seidavi, and A. Prandini, 2017. Effect of a low crude protein diet supplemented with different levels of threonine on growth performance, carcass traits, blood parameters, and immune responses of growing broilers. Poultry Science. 96, 2751–2760.
- Sohail, S.S., M.M. Bryant, and D.A. Roland, 2004. Effect of reducing cage density on performance and economics of second-cycle (Force Rested) commercial leghorns. Journal of Applied Poultry Research. 13, 401–405.
- Stamp, D.M., C.A. Donnelly, and T.A. Jones, 2004. Chicken welfare is influenced more by housing conditions than by stocking density. Nature. 427, 342–344.
- Swennen, Q., G. Janssens, S. Millet, G. Vansant, E. Decuyper, J. Buyse, 2005. Effects of substitution between fat and protein on feed intake and its regulatory mechanisms in broiler chickens: endocrine functioning and intermediary metabolism. Poultry Science. 84, 1051–1057.
- Widowski, T.M., L.J. Caston, T.M. Caseyrott, and M.E. Hunniford, 2017a. The effect of space allowance and cage size on laying hens housed in furnished cages, Part II: Behavior at the feeder. Poultry Science. 96, 3816–3823.
- Widowski, T.M., L.J. Caston, M.E. Hunniford, L. Cooley, and S. Torrey, 2017b. Effect of space allowance and cage size on laying hens housed in furnished cages, Part I: Performance and well-being. Poultry Science. 96, 3805–3815.
- Widowski, T.M., P.H. Hemsworth, J.L. Barnett, and J.L. Rault, 2016. Laying hen welfare I. Social environment and space. Worlds Poultry Science Journal. 72, 333–342.
- Xiang, L., D. Chen, J. Li, and J. Bao, 2016. Effects of furnished cage type on behavior and welfare of laying hens. Asian-Australasian Journal of Animal Sciences. 29, 887–894.

# Heat Stress of Fattening Pigs in Confined Livestock Buildings: Simulation of the Impact of Global Warming for 1981–2017 for the Mid-latitudes

Günther Schauberger <sup>a\*</sup>, Christian Mikovits <sup>a</sup>, Werner Zollitsch <sup>b</sup>,  
**Stefan J. Hörtenhuber** <sup>b</sup>, Johannes Baumgartner <sup>c</sup>, Knut Niebuhr <sup>c</sup>, Martin Piringer <sup>d</sup>,  
 Werner Knauder <sup>d</sup>, Ivonne Anders <sup>e</sup>, Konrad Andre <sup>e</sup>, Isabel Hennig-Pauka <sup>f</sup>,  
 Martin Schönhart <sup>g</sup>

<sup>a</sup> WG Environmental Health, Unit for Physiology and Biophysics, University of Veterinary Medicine,  
Vienna 20133, Austria

<sup>b</sup> Division of Livestock Sciences, Department of Sustainable Agricultural Systems, University of Natural  
Resources and Life Sciences, Vienna 20133, Austria

<sup>c</sup> Institute of Animal Husbandry and Animal Welfare, University of Veterinary Medicine, Vienna 20133,  
Austria

<sup>d</sup> Department of Environmental Meteorology, Central Institute of Meteorology and Geodynamics, Vienna,  
Austria

<sup>e</sup> Department for Climate Research, Central Institute of Meteorology and Geodynamics, Vienna 20133,  
Austria

<sup>f</sup> University Clinics for Swine, Department for Farm Animals and Veterinary Public Health, University of  
Veterinary Medicine, Vienna 20133, Austria

<sup>g</sup> Institute for Sustainable Economic Development, Department of Economics and Social Sciences,  
University of Natural Resources and Life Sciences, Vienna 20133, Austria

\* Corresponding author. Email: [gunther.schauberger@vetmeduni.ac.at](mailto:gunther.schauberger@vetmeduni.ac.at)

## Abstract

Global warming is a challenge which causes heat stress for farm animals as well. In the mid-latitudes, pigs and poultry are kept predominantly in confined livestock buildings with a mechanical ventilation system to provide an indoor climate close to the thermoneutral zone. A simulation model was used, driven by the meteorological time series from 1981 to 2017, to calculate heat stress parameters inside a reference building typical for livestock farming. By this model calculations, the time trend of several heat stress parameters over 37 years were analyzed. In addition to the meteorological conditions outside, the thermal environment inside the building depends also on the sensible and latent energy release of the animals, the thermal properties of the building, and the ventilation system and its control unit. The calculations were performed for a site in Austria in the North of the Alpine Ridge, which is representative for confined livestock buildings for growing-fattening pigs in Central Europe. The simulation for a reference building (1800 pigs, between 30 and 120 kg, all-in-all-out) resulted in an increase of the mean relative annual heat stress parameters in the range between 0.9% and 6.4% per year since 1981. To reduce the negative economic impacts as a consequence of this positive trend of heat stress, adaptation measures are needed. The model calculations for fattening pigs show that a simulation model for the indoor climate is an appropriate tool to predict heat stress of animals inside confined livestock buildings. By the use of hourly meteorological data and the adaptation of the system parameters of the building (livestock, ventilation system, and building), the model can be applied to animal farms in other geographical regions as well.

**Keywords:** Livestock, pig, heat stress, global warming, climate change, confined buildings

## 1. Introduction

Global warming is identified as a major threat for livestock keeping as well. The majority of pigs and poultry in mid-latitudes are kept in confined livestock buildings (Robinson et al., 2011); at the global level, it is more than half (Niamir-Fuller, 2016). Confined livestock buildings are predominantly mechanically ventilated. During summertime, the mechanical ventilation system

has a major goal: to remove the sensible heat of the animals with as high ventilation rates as possible to avoid high indoor air temperatures. As the ventilation rate is nevertheless limited, the indoor temperature lays about 3–5 K above the outdoor temperature. This means that the expected heat stress outside will be strengthened inside.

With a simulation model driven by the meteorological data on an hourly basis, the thermal conditions inside confined livestock buildings for growing-fattening pigs were investigated. We selected a steady state simulation model (Schauberger et al., 2000; Mikovits et al., 2019). The model calculations were performed for a typical livestock building for growing-fattening pigs in Central Europe for 1800 heads, divided into 9 sections with 200 animals each. This reference building enables the transferability of the model calculation to other countries. The calculations were performed for the period between 1981 and 2017. The meteorological dataset is representative for the Northeast of the Alpine Ridge in Austria which lies in the climate zone Cfb of Köppen and Geiger (temperate oceanic climate (warm temperature, fully humid, warm summers)) (Beck et al., 2005). The highest animal density (Robinson et al., 2011; Robinson et al., 2014) and farm density (Marquer, 2010) are found in Europe and as well in North America and Asia (predominantly China) in this Cfb zone.

The goal of the paper is to estimate the impact of global warming on the thermal conditions inside confined livestock buildings for growing-fattening pigs. Using several heat stress measures for pigs, the temporal trend over 37 years were investigated in comparison to the outdoor situation. The results will give an orientation whether adaptation measures should be applied to reduce heat stress for growing-fattening pigs in the future.

## 2. Materials and Methods

### 2.1. Meteorological data

For the calculation of the indoor air conditions, air temperature and relative humidity, meteorological data are needed on an hourly basis. A compiled climatic reference scenario was used on the basis of representative observational sites around the city of Wels in Austria (48.16°N, 14.07°E) for the time period 1981 to 2017, located within the climate zone Cfb. The number of hot days (daily maximum temperature  $\geq 30$  °C) is expected to increase in this region from a mean value of 3.3 days year<sup>-1</sup> in the reference period 1971-2000 to between 4.7 and 5.0 days year<sup>-1</sup> in the middle of the 21<sup>st</sup> century (Chimani et al., 2016).

### 2.2. Simulation of the indoor climate of a pig building

The indoor climate was simulated by a steady state model, which calculates the thermal indoor parameters (air temperature, humidity) and the ventilation flow rate. The thermal environment inside the building depends on the livestock, the thermal properties of the building, and the ventilation system and its control unit. The core of the model can be reduced to the sensible heat balance of a livestock building (Schauberger et al., 1999, 2000, 2001).

The simulations were performed for a typical livestock building for fattening pigs in Central Europe for 1800 heads, divided into 9 sections with 200 animals each. The system parameters, which describe the reference building, are summarised in Table 1.

The time course of the body mass of growing-fattening pigs behaves like a saw tooth wave over one fattening period (about 1/3 of a year). To avoid the superposition between animal growth and meteorological data a Monte-Carlo approach was used, called inverse transform sampling, a useful method for environmental sciences (e.g. Wilks, 2011; Schauberg et al., 2013). This method was applied to the simulation model for the indoor climate (Mikovits et al., 2017; Mikovits et al., 2019).

Heat stress for pigs can be quantified by the following parameters and related threshold values (Vitt et al., 2017): (1) air temperature  $T$ , (2) temperature-humidity index  $THI$ , and (3) specific enthalpy  $H$  with the related thresholds  $X_T = 25$  °C,  $X_{THI} = 75$ , and  $X_H = 55$  kJ kg<sup>-1</sup> mild heat stress. To adapt the heat stress measure to the growth of the pigs between 30 kg and 120 kg, the

exceedance of the controllable temperature range (indoor temperature range, were the ventilation flow is adapted by the control unit of the ventilation system) was used with the lower limit  $X_{TL} = T_C$  between 16 and 20 °C as a linear function of the body mass  $m$  and the upper limit with  $X_{TU} = T_C + \Delta T_C$  (Mikovits et al., 2019).

For a time series with the length  $t$  and  $n$  equidistant observations of a selected parameter  $x$ , the exceedance frequency of the selected threshold  $X$   $P_x = \text{prob}\{x | x > X\}$  can be given in hours per year ( $\text{h a}^{-1}$ ) (Turnpenny et al., 2001; Haskell et al., 2011). The second one describes the exceedance area (area under the curve)  $A_X$  of the selected threshold  $X$  calculated according to Thiers and Peuportier (2008) by

$$A_X = \sum_i \begin{cases} x_i - X & \text{for } x_i > X \\ 0 & \text{for } x_i \leq X \end{cases} \quad (1)$$

The trend was calculated for the exceedance frequency  $P_X$  and for the exceedance area  $A_X$  as a slope for the linear trend and as a relative trend, which was related to the reference year 1981.

Table 1. System parameters for livestock, building, and ventilation system related to one animal place for the indoor climate simulation

	Parameter	Value
Animal	Body mass $m$	30–120 kg
	Service period (building emptied for cleaning and disinfection)	10 days
Building	Area of the building orientated to the outside (ceiling, walls, windows)	1.41 m <sup>2</sup>
	Mean thermal transmission coefficient $U$ weighted by the area of the construction elements (wall, ceiling, door, windows) which are orientated to the outside	0.41 W m <sup>-2</sup> K <sup>-1</sup>
Ventilation system	Set point temperature of the ventilation control unit, $T_C$	16 – 20 °C
	Proportional range (band width) of the control unit, $\Delta T_P$	4 K
	Minimum volume flow rate of the ventilation system, $V_{min}$ , for maximum CO <sub>2</sub> concentration 3000 ppm and a body mass $m = 30$ kg	8.62 m <sup>3</sup> h <sup>-1</sup>
	Maximum volume flow rate, $V_{max}$ , by maximum temperature difference between indoor and outdoor of 3 K	107 m <sup>3</sup> h <sup>-1</sup>

### 3. Results and Discussion

The time course of the calculated parameters is shown in Figure 1A for the exceedance frequency  $P_X$  and in Figure 1B for the exceedance area  $A_X$ . The exceedance frequency  $P_X$  (Turnpenny et al., 2001; Haskell et al., 2011) and the exceedance area  $A_X$  (St-Pierre et al., 2003; Thiers and Peuportier, 2008; Gosling et al., 2013) are used widely as measures for heat stress.

The mean linear trend of the exceedance parameters  $P_X$  and  $A_X$  is positive for all heat stress measures (exceedance of the threshold values  $X_T$ ,  $X_H$ ,  $X_{THI}$ , and  $X_{TU}$ ), showing a mean relative annual change for the indoor climate of about 0.9% ( $P_{TU}$ ) to 3.0% ( $P_{THI}$ ) per year and 1.5% ( $A_{TU}$ ) to 6.4% ( $A_{THI}$ ). The lowest values are found for the temperature threshold  $X_{TU}$ , the highest values for the temperature-humidity index  $X_{THI}$  with more than a tripled relative trend. This shows that the heat stress is not only caused by the temperature increase but is also due to the increase of the humidity inside the livestock building. The investigation shows that stationarity of these parameters cannot be assumed under global warming (Hendry and Pretis, 2016). The trend displayed in Figs. 1A and 1B can be used as an educated guess for the near future (Table 2).

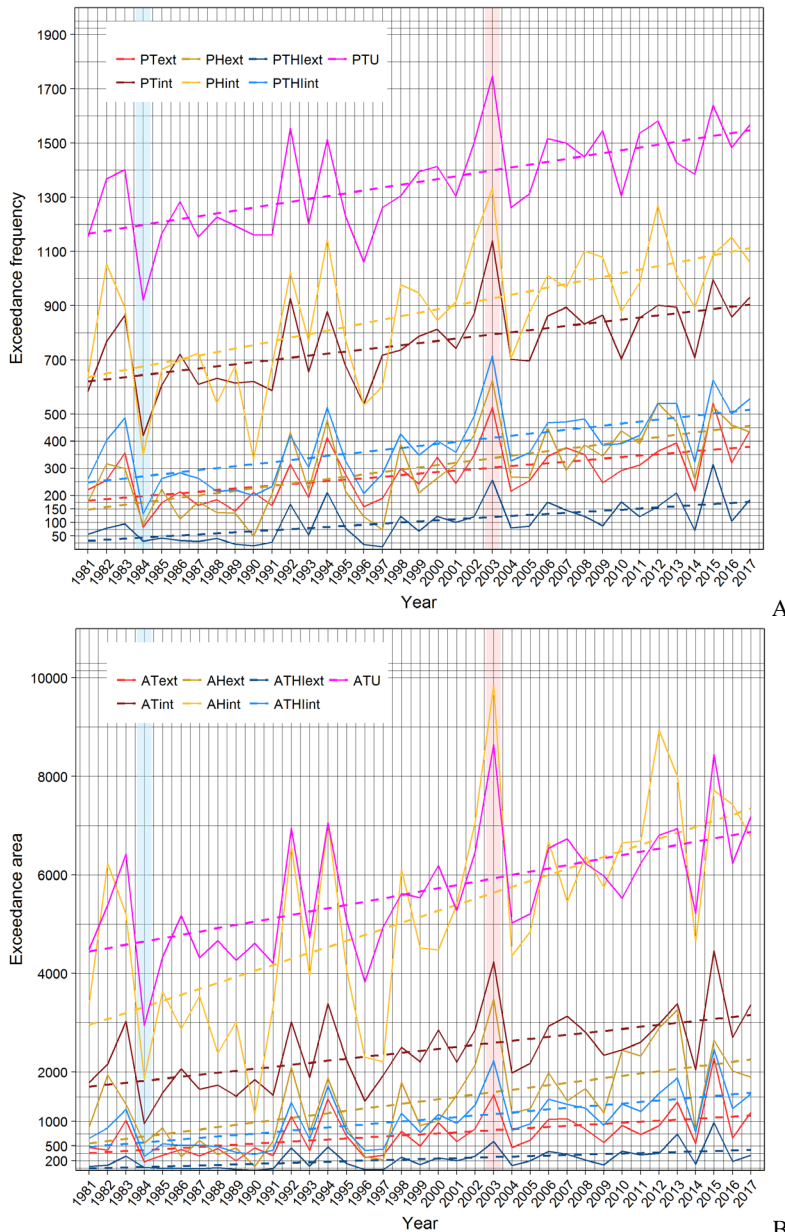


Figure 1. Time course of the exceedance frequency  $P_X$  (A) and the exceedance area  $A_X$  (B) of the thresholds for air temperature  $X_T = 25^\circ\text{C}$  (PText, AText, PTint, ATint), specific enthalpy  $X_H = 55 \text{ kJ kg}^{-1}$  (PHext, AHext, PHint, AHint), temperature humidity index  $X_{THI} = 75$  (PTHlext, ATHlext, PTHlint, ATHlint), and the controllable range  $X_{TU} = T_C + \Delta T_C$  (PTU, ATU) for indoor (int) and outdoor (ext) parameters (Mikovits et al., 2019).

The exceedance frequency of the upper limit of the controllable range  $P_{TU}$  was calculated

between  $P_{TU} = 921 \text{ h a}^{-1}$  (minimum in 1984) and  $P_{TU} = 1747 \text{ h a}^{-1}$  (maximum in 2003). Turnpenny et al. (2001) found for 1997 a value of  $P_{TU} = 1018 \text{ h a}^{-1}$ , calculated for Southeast England.

Table 2. Statistics of the heat stress parameters using the mean annual linear trend (slope), the relative trend, related to the reference year 1981, minimum (Min) and maximum (Max) between 1981 and 2017 of the exceedance frequency  $P_X$  and the exceedance area  $A_X$  for the threshold of air temperature  $X_T = 25^\circ\text{C}$ , specific enthalpy  $X_H = 55 \text{ kJ kg}^{-1}$ , temperature humidity index  $X_{THI} = 75$ , and the controllable range  $X_{TU} = T_C + \Delta T_C$ .

	Trend (unit $\text{a}^{-1}$ )	Relative Trend (% $\text{a}^{-1}$ )	Min (year)	Max (year)
Exceedance frequency $P$ ( $\text{h a}^{-1}$ )				
$P_T$	$7.8 \pm 1.8$	$1.26 \pm 0.30$	420 (1984)	1139 (2003)
$P_H$	$13.2 \pm 3.0$	$2.08 \pm 0.47$	335 (1990)	1333 (2003)
$P_{THI}$	$7.5 \pm 1.6$	$3.01 \pm 0.65$	132 (1984)	715 (2003)
$P_{TU}$	$10.6 \pm 2.1$	$0.91 \pm 0.18$	921 (1984)	1747 (2003)
$P_{TL}$	$-7.7 \pm 2.4$	$-0.73 \pm 0.23$	560 (2014)	1320 (1985)
Exceedance area $A$				
$A_T (\text{Kh a}^{-1})$	$40.5 \pm 9.8$	$2.38 \pm 0.58$	952 (1984)	4461 (2015)
$A_H (\text{kJ kg}^{-1} \text{ h a}^{-1})$	$121.9 \pm 25.2$	$4.12 \pm 0.85$	1151 (1990)	9846 (2003)
$A_{THI} (\text{h a}^{-1})$	$30.4 \pm 6.6$	$6.35 \pm 1.37$	294 (1984)	2463 (2015)
$A_{TU} (\text{Kh a}^{-1})$	$67.5 \pm 15.5$	$1.52 \pm 0.35$	2950 (1984)	8642 (2003)
$A_{TL} (\text{Kh a}^{-1})$	$-44.2 \pm 15.8$	$-1.16 \pm 0.41$	1307 (2014)	6236 (1985)

The slope of the linear annual temporal trend is distinctly steeper for the indoor values as compared to the outside situation (Figs. 1A and 1B). The increase lies in the range of 28% to 70% for  $P_X$  and 75% to 162% for  $A_X$ . Therefore, the indoor climate is more vulnerable to global warming than the outdoor situation. This means that the direct use of meteorological data - i.e. without the use of a simulation model for the indoor climate – will underestimate the likelihood of the occurrence of heat stress in animals inside confined livestock buildings (Table 2).

The impact of global warming on the air quality, expressed by the  $\text{CO}_2$  concentration, was discussed in Mikovits et al. (2019). Using a  $\text{CO}_2$  concentration of 3000 ppm as a threshold for poor air quality, the exceedance frequency of this threshold will decrease by about -1.4% per year. The mean indoor air quality will improve over the years due to the increase of the ventilation flow rate. In contrast, (Schauberger et al., 2018) could show that the ammonia and the odour emission will increase due to global warming. This has to be taken into account for the determination of the separation distance to avoid odour annoyance and to the impact on air quality. The odour and ammonia emissions will increase by 0.16% per year.

Long-term (seasonal) climate forecasts are essential for decision-makers aiming at the mitigation of heat stress for livestock inside confined buildings. Such seasonal climate forecasts for agricultural producers are well established (Klemm and McPherson, 2017), but the special needs of livestock keeping are not considered yet, particularly for confined livestock buildings.

#### 4. Conclusiones

Global warming shows a strong impact on livestock keeping inside confined buildings. The resilience against heat stress is distinctly lower than for outdoor keeping of animals. The mean relative annual trend for heat stress parameters between 1981 and 2017 lies in the range between 0.9 and 6.4% per year, relative to the year 1981. To reduce animal health and welfare problems as well as the economic impact of these changes, appropriate adaptation measures are needed.

#### Acknowledgements

The project PiPoCooL Climate change and future pig and poultry production: implications for animal health, welfare, performance, environment and economic consequences was funded by the

Austrian Climate and Energy Fund within the frame work of the Austrian Climate Research Program (ACRP8 – PiPoCooL – KR15AC8K12646).

## References

- Beck, C., J. Grieser, M. Kottek, F. Rubel, B. Rudolf, 2005. Characterizing global climate change by means of Köppen climate classification. *Klimastatusbericht*. 51, 139–149.
- Chimani, B., G. Heinrich, M. Hofstätter, M. Kerschbaumer, S. Kienberger, A. Leuprecht, A. Lexer, S. Peßenteiner, M.S. Poetsch, M. Salzmann, R. Spiekermann, M. Switanek, H. Truhetz, 2016. ÖKS15 - Klimaszenarien für Österreich. Daten, Methoden und Klimaanalyse. In: *Report*, Vienna.
- Gosling, S.N., E.K. Bryce, P.G. Dixon, K.M.A. Gabriel, E.Y. Gosling, J.M. Hanes, D.M. Hondula, L. Liang, P.A. Bustos Mac Lean, S. Mutters, S.T. Nascimento, M. Petralli, J.K. Vanos, E.R. Wanka, 2013. A glossary for biometeorology. *International Journal of Biometeorology*, 1–32. <http://dx.doi.org/10.1007/s00484-013-0729-9>.
- Haskell, M., P. Kettlewell, E. McCloskey, E. Wall, N. Fox, M. Mitchell, 2011. Animal Welfare and Climate Change: Impacts, Adaptations, Mitigation and Risks. Scottish Agricultural College (SAC), Edinburgh.
- Hendry, D.F., F. Pretis, 2016. All Change! The Implications of Non-Stationarity for Empirical Modelling, Forecasting and Policy. In: Oxford Martin School Policy Paper Series, Forthcoming. Available at SSRN: <https://ssrn.com/abstract=2898761>.
- Klemm, T., R.A. McPherson, 2017. The development of seasonal climate forecasting for agricultural producers. *Agricultural and Forest Meteorology*. 232, 384–399. <http://dx.doi.org/10.1016/j.agrformet.2016.09.005>.
- Marquer, P., 2010. Pig farming in the EU, a changing sector. *Statistics in focus*. Eurostat, 1–12.
- Mikovits, C., R. Vitt, G. Schauberger, 2017. Simulation of the indoor climate of livestock buildings to assess of adaptive measures to reduce heat stress due to climate change. In: Ni, J., L. Teng-Teeh, C. Wang, L. Zhao Eds. *Int. Symp. on Animal Environment & Welfare*. China Agriculture Press, Chongqing, China.
- Mikovits, C., W. Zollitsch, S.J. Hörtenhuber, J. Baumgartner, K. Niebuhr, M. Piringer, I. Anders, K. Andre, I. Hennig-Pauka, M. Schönhart, G. Schauberger, 2019. Impacts of global warming on confined livestock systems for growing-fattening pigs: simulation of heat stress for 1981 to 2017 in Central Europe. *International Journal of Biometeorology*. 63 (2), 221–230. <http://dx.doi.org/10.1007/s00484-018-01655-0>.
- Niamir-Fuller, M., 2016. Towards sustainability in the extensive and intensive livestock sectors. OIE Revue Scientifique et Technique. 35 (2), 371–387. <http://dx.doi.org/10.20506/rst.35.2.2531>.
- Robinson, T., P. Thornton, G. Franceschini, R. Kruska, F. Chiozza, A. Notenbaert, G. Cecchi, M. Herrero, M. Epprecht, S. Fritz, 2011. Global livestock production systems: Food and Agriculture Organization of the United Nations (FAO).
- Robinson, T.P., G.R.W. Wint, G. Conchedda, T.P. Van Boeckel, V. Ercoli, E. Palamara, G. Cinardi, L. D'Aietti, S.I. Hay, M. Gilbert, 2014. Mapping the Global Distribution of Livestock. *PLoS ONE*. 9 (5), e96084. <http://dx.doi.org/10.1371/journal.pone.0096084>.
- Schauberger, G., M. Piringer, E. Petz, 1999. Diurnal and annual variation of odour emission from animal houses: A model calculation for fattening pigs. *Journal of Agricultural and Engineering Research*. 74 (3), 251–259.
- Schauberger, G., M. Piringer, E. Petz, 2000. Steady-state balance model to calculate the indoor climate of livestock buildings, demonstrated for fattening pigs. *International Journal of Biometeorology*. 43 (4), 154–162.
- Schauberger, G., M. Piringer, E. Petz, 2001. Separation distance to avoid odour nuisance due to livestock calculated by the Austrian odour dispersion model (AODM). *Agriculture, Ecosystems and Environment*. 87 (1), 13–28.
- Schauberger, G., M. Piringer, K. Baumann-Stanzer, W. Knauder, E. Petz, 2013. Use of a Monte Carlo technique to complete a fragmented set of  $H_2S$  emission rates from a waste water treatment plant. *Journal of Hazardous Materials*. 263, 694–701.
- Schauberger, G., M. Piringer, C. Mikovits, W. Zollitsch, S.J. Hörtenhuber, J. Baumgartner, K. Niebuhr, I. Anders, K. Andre, I. Hennig-Pauka, M. Schönhart, 2018. Impact of global warming on the odour and ammonia emissions of livestock buildings used for fattening pigs. *Biosystems Engineering*. 175, 106–114. <http://dx.doi.org/10.1016/j.biosystemseng.2018.09.001>.
- St-Pierre, N.R., B. Cobanov, G. Schnitkey, 2003. Economic Losses from Heat Stress by US Livestock Industries. *Journal of Dairy Science*. 86, E52–E77. [http://dx.doi.org/10.3168/jds.S0022-0302\(03\)74040-5](http://dx.doi.org/10.3168/jds.S0022-0302(03)74040-5).

Thiers, S., B. Peuportier, 2008. Thermal and environmental assessment of a passive building equipped with an earth-to-air heat exchanger in France. *Solar Energy*. 82 (9), 820–831. <http://dx.doi.org/10.1016/j.solener.2008.02.014>.

Turnpenny, J.R., D.J. Parsons, A.C. Armstrong, J.A. Clark, K. Cooper, A.M. Matthews, 2001. Integrated models of livestock systems for climate change studies. 2. Intensive systems. *Global Change Biology*. 7 (2), 163–170.

Vitt, R., L. Weber, W. Zollitsch, S.J. Hörtenhuber, J. Baumgartner, K. Niebuhr, M. Piringer, I. Anders, K. Andre, I. Hennig-Pauka, M. Schönhart, G. Schuberger, 2017. Modelled performance of energy saving air treatment devices to mitigate heat stress for confined livestock buildings in Central Europe. *Biosystems Engineering*. 164, 85–97. <http://dx.doi.org/10.1016/j.biosystemseng.2017.09.013>.

Wilks, D.S., 2011. *Statistical Methods in the Atmospheric Sciences*. San Diego, CA: Academic press. XI, 467 S.

# Efficacy of Adaptation Measures to Reduce Heat Stress due to the Impact of Global Warming on Confined Livestock Buildings for Fattening Pigs

Günther Schauberger <sup>a\*</sup>, Christian Mikovits <sup>a</sup>, Werner Zollitsch <sup>b</sup>,  
 Stefan J. Hörtenhuber <sup>b</sup>, Johannes Baumgartner <sup>c</sup>, Knut Niebuhr <sup>c</sup>, Martin Piringer <sup>d</sup>,  
 Werner Knauder <sup>d</sup>, Ivonne Anders <sup>e</sup>, Konrad Andre <sup>e</sup>, Isabel Hennig-Pauka <sup>f</sup>,  
 Martin Schönhart <sup>g</sup>

<sup>a</sup> WG Environmental Health, Unit for Physiology and Biophysics, University of Veterinary Medicine,  
 Vienna 1210, Austria

<sup>b</sup> Division of Livestock Sciences, Department of Sustainable Agricultural Systems,  
 University of Natural Resources and Life Sciences, Vienna 1190, Austria

<sup>c</sup> Institute of Animal Husbandry and Animal Welfare, University of Veterinary Medicine,  
 Vienna 1210, Austria

<sup>d</sup> Department of Environmental Meteorology, Central Institute of Meteorology and Geodynamics,  
 Vienna 1190, Austria

<sup>e</sup> Department for Climate Research, Central Institute of Meteorology and Geodynamics,  
 Vienna 1190, Austria

<sup>f</sup> University Clinics for Swine, Department for Farm Animals and Veterinary Public Health,  
 University of Veterinary Medicine, Vienna 1210, Austria

<sup>g</sup> Institute for Sustainable Economic Development, Department of Economics and Social Sciences,  
 University of Natural Resources and Life Sciences, Vienna 1190, Austria

\* Corresponding author. Email: [gunther.schauberger@vetmeduni.ac.at](mailto:gunther.schauberger@vetmeduni.ac.at)

## Abstract

In the mid-latitudes, pigs and poultry are predominantly kept in confined insulated livestock buildings with a mechanical ventilation system and a high stocking density. Here, animals are more sensitive to heat stress than animals which are kept outside. Heat stress has increased in the last decades due to anthropogenic warming. To predict the effect of global warming on the indoor climate of farm animals in such confined livestock buildings, a dataset for 1981 – 2017 of hourly meteorological data was used to analyse the temporal variability and trends for Central Europe, selecting a site north of the Alpine Ridge (Austria). The meteorological data drive a simulation model for the indoor climate in a reference building (1800 pigs, between 30 and 120 kg, all-in-all-out). Beside the meteorological conditions, the thermal environment inside the building depends on the sensible and latent energy release of the animals, the thermal properties of the building, and the ventilation system and its control unit. Seven adaptation measures to reduce heat stress were selected including three energy saving air preparation systems, the increase of the maximum ventilation rate, the reduction of the stocking density, and the shift of the feeding and resting time patterns. The effect of these measures was quantified by the use of several heat stress metrics. The highest reduction of heat stress in comparison to the reference building was achieved by the three air preparation systems in the range of 74% to 92% for adiabatic systems and 90% and 100% for earth-air heat exchangers, followed by the increase of the ventilation rate, and the time shift. The reduction of the stocking density showed the lowest improvement. Beside the reduction of heat stress, also the temporal trend over three decades was used to quantify the resilience of livestock buildings.

**Keywords:** Climate change, simulation, indoor climate, farm animals

## 1. Introduction

Global warming and the related heat stress is a major threat not only for humans but also for farm animals. This is not only relevant from an animal welfare perspective (Huynh et al., 2005) but also from an economic point of view (St-Pierre et al., 2003). Mikovits et al. (2019) showed

for Central Europe that the indoor climate of confined livestock systems is more affected by heat stress than the outdoor situation with an increasing frequency of heat stress over the last three decades. This is predominantly caused by higher indoor than outdoor temperatures, even in summer, due to the sensible heat release of the animals. To reduce the impact of heat stress on animals several adaptation measures AMs are in use. The AMs can be divided into two groups (Schauberger et al., 2019a). The first group modifies the sensible and latent heat balance of the building by cooling the inlet air, reducing the sensible and latent heat release, and modifying the thermal properties of the building. The second group influences the immediate thermal vicinity of the animals. The effects of the first group are investigated here.

In our investigation, we selected a steady state simulation model of the indoor climate (Schauberger et al., 2000; Mikovits et al., 2019) and applied it to a typical livestock building for growing-fattening pigs in Central Europe. On the basis of such model calculations, the multi-decadal temporal trend of the thermal climate inside livestock buildings can be calculated. It is an indicator of future global warming impacts. The objectives of the paper are to estimate the temporal trend of the thermal conditions inside livestock buildings for growing-fattening pigs for a conventional reference system in relation to heat stress. This situation will be compared to various AMs and the related efficacy. The results for a time period over 37 years, and particularly on extreme years, should give an orientation, which of the AMs will be appropriate to reduce heat stress for growing-fattening pigs under future climate conditions.

## 2. Materials and Methods

### 2.1. Meteorological data

For the calculation of the indoor air conditions, air temperature and relative humidity, meteorological data are needed on an hourly basis. A compiled climatic reference scenario was used on the basis of representative observational sites around the city of Wels (48.16°N, 14.07°E) for the time period 1981 to 2017.

### 2.2. Simulation of the indoor climate of a pig building

The indoor climate of the pig building was simulated by a steady-state model which calculates the thermal indoor parameters (air temperature and humidity) and the ventilation flow rate. The thermal environment inside the building depends on the sensible and latent heat release of the animals, the thermal properties of the building, and the ventilation system and its control unit. The core of the model is the calculation of the sensible heat balance of a livestock building (Schauberger et al., 1999, 2000; Mikovits et al., 2019). The model calculation was performed for a typical livestock building for fattening pigs for Central Europe for 1800 head, divided into 9 sections, with 200 animals each. The system parameters, which describe the conventional reference system REF (properties of the livestock, building, and the mechanical ventilation system) can be found in Schauberger et al. (2019b) and Mikovits et al. (2019).

Heat stress for pigs is calculated using the indoor air temperature  $T$  with the related threshold  $X_T = 25^\circ\text{C}$ . Above this temperature, pigs are assumed to be prone to heat stress. For this parameter the annual sums of the exceedance frequency  $P_T$  (frequency above the threshold) and of the exceedance area  $A_T$  (defined as area under the heat stress curve and the related threshold) were calculated.

For a time series with the length  $t$  and  $n$  equidistant observations of a selected parameter  $x$ , the exceedance frequency of the selected threshold  $X_T$ ,  $P_T = \text{prob}\{x | x > X_T\}$  can be given in hours per year ( $\text{h a}^{-1}$ ) (Turnpenny et al., 2001; Haskell et al., 2011). The second one describes the exceedance area (area under the curve)  $A_T$  of the selected threshold  $X_T$  calculated according to Thiers and Peupotier (2008) by

$$A_x = \sum_i \begin{cases} x_i - X & \text{for } x_i > X \\ 0 & \text{for } x_i \leq X \end{cases} \quad (1)$$

The exceedance area  $A_T$  above the threshold  $X_T$  is defined analogously to the degree-days (Gosling et al., 2013) but with the selected parameter  $x$  being used on an hourly basis instead of daily mean values, with the results in ( $\text{Kh} \text{ a}^{-1}$ ).

The trend was calculated for the exceedance frequency  $P_T$  and for the exceedance area  $A_T$  as a slope for the linear trend.

For all seven AMs these two annual sums of  $P_T$  and  $A_T$  were used to calculate the mean relative reduction of heat stress  $R$  (in %) related to the REF system:

$$R_{P_T} = 1 - \sum_{i=1981}^{2017} \frac{P_{AM,i}}{P_{REF,i}} \quad \text{and} \quad R_{A_T} = 1 - \sum_{i=1981}^{2017} \frac{A_{AM,i}}{A_{REF,i}} \quad (2)$$

### 2.3. Investigated adaptation measures

The heat stress of the REF system was compared with seven adaptation measures AMs. Details on all seven AMs are presented below.

#### 2.3.1. Direct evaporative cooling: cooling pads CP

In livestock confinement buildings, direct evaporative cooling devices are in use to convert sensible heat (air temperature) via evaporation of water into latent heat (humidity) with the major goal to reduce the inlet air temperature. The efficacy of the CP  $\eta_{CP}$ , also called wet bulb depression efficacy (ASHRAE, 2009), is expressed by

$$\eta_{CP} = \frac{T_{out} - T_{CP}}{T_{out} - T_{out,WB}} 100\% \quad (3)$$

with the outside air temperature (dry bulb) entering the CP  $T_{out}$ , the air temperature leaving the CP entering the livestock building as inlet air  $T_{CP}$ , and the wet bulb temperature of the outside air  $T_{out,WB}$ . For the calculation, we assumed  $\eta_{CP} = 80\%$  according to Fehr et al. (1983). Details can be found in Vitt et al. (2017).

#### 2.3.2. Indirect evaporative cooling: cooling pads combined with a regenerative heat exchanger CPHE

Indirect evaporative cooling systems result in a reduction of the inlet air temperature by evaporation without humidification. The outside air is cooled using direct evaporative cooling. Then, this evaporatively cooled secondary air cools the outside air in a conventional air-to-air heat exchanger. We assumed CP and a downstream heat exchanger HE with a constant sensible efficiency of  $\eta_{CP} = 80\%$  and  $\eta_{HE} = 65\%$  (ASHRAE, 2008).

#### 2.3.3. Earth-air heat exchanger EAHE

EAHEs utilise the ground as heat storage. The performance, i.e., the air temperature and humidity at the ends of the tubes, depends on the soil temperature, the outside air temperature and humidity, the thermal features of the soil and the geometry of the tubes (Tzaferis et al., 1992; Ozgener, 2011; Bisoniya et al., 2014). The calculation of the model parameters for the sensible and latent heat transfer can be found in detail in Vitt et al. (2017).

#### 2.3.4. Reduction of stocking density SD during the summer season

To reduce the sensible heat load during the warm season, the stocking density was reduced by assuming a smaller number of pigs inside a section of the livestock building. Two scenarios were calculated with a reduction to 80% (SD80%) and 60% (SD60%) compared to REF.

#### 2.3.5. Doubling of the summer ventilation rate VENT

To reduce the difference between the inlet air temperature (outdoor temperature) and indoor air temperature due to the sensible heat release of the animals, the maximum ventilation rate was doubled from 107 to 214  $\text{m}^3 \text{ h}^{-1}$  according to the recommendations by the MWPS-32 (1990) for hot weather.

### 2.3.6. Inversion of the diurnal feeding and resting pattern SHIFT

Introducing a shift of the feeding and resting time pattern by approximately half a day, the maximum of the outdoor temperature coincides with the resting time. The time shift of 10 hours was determined by the diurnal temperature variation of heat days (daily maximum  $> 30^{\circ}\text{C}$ ).

## 3. Results and Discussion

The linear slope of the temporal trend  $k$  was used to evaluate the resilience against global warming for all AMs of the livestock system (Table 1). The resilience can be determined twofold, first in relation to the outdoor situation and second in comparison to REF. A lower resilience of the livestock system results in a steeper slope of the heat stress parameter. The slope of the REF system compared to the outdoor situation is higher for both heat stress parameters  $P_T$  and  $A_T$ , which means that the temporal trend caused by global warming (outdoor) will worsen the heat stress inside the livestock system (Mikovits et al., 2019). The slope of all AMs (except SHIFT) is lower compared to the REF system, which means that all AMs improve the indoor thermal situation due to lower heat stress.

Table 1. Heat stress parameters (exceedance frequency  $P_T$  in  $\text{h a}^{-1}$  and the exceedance area  $A_T$  in  $\text{Kh a}^{-1}$ ) for the conventional reference system REF, reduced stocking density SD80% and SD60%, diurnal shift of the activity pattern SHIFT, doubling of the summer ventilation rate VENT, cooling pads plus heat exchanger CPHE, cooling pads CP, and earth-air heat exchanger EAHE described by the mean annual linear trend  $k$  and the reduction factor  $R$  (%). The heat stress is determined by the exceedance of the threshold of the indoor air temperature  $X_T = 25^{\circ}\text{C}$ .

	Annual trend $k$	Reduction factor $R$ (%)
Exceedance frequency $P_T$ for $X_T = 25^{\circ}\text{C}$ ( $\text{h a}^{-1}$ )		
Outdoor	$6.110 \pm 1.460$	
Reference system REF	$7.849 \pm 1.847$	-
Stocking density 80% SD80%	$7.438 \pm 1.813$	4
Stocking density 60% SD60%	$7.255 \pm 1.783$	8
Diurnal shift SHIFT	$8.746 \pm 2.052$	23
Ventilation rate VENT	$6.599 \pm 1.644$	34
Cooling pads plus heat exchanger CPHE	$7.320 \pm 1.470$	61
Cooling pads CP	$6.235 \pm 1.300$	74
Earth air heat exchanger EAHE	$1.473 \pm 0.634$	93
Exceedance area $A_T$ for $X_T = 25^{\circ}\text{C}$ ( $\text{Kh a}^{-1}$ )		
Outdoor	$23.24 \pm 6.51$	
Reference system REF	$40.45 \pm 9.85$	-
Stocking density 80% SD80%	$39.09 \pm 9.66$	5
Stocking density 60% SD60%	$36.72 \pm 9.60$	10
Diurnal shift SHIFT	$36.45 \pm 9.45$	34
Ventilation rate VENT	$31.73 \pm 8.06$	40
Cooling pads plus heat exchanger CPHE	$16.02 \pm 3.48$	81
Cooling pads CP	$10.10 \pm 2.28$	90
Earth air heat exchanger EAHE	$1.54 \pm 0.77$	99

The performances of the seven AMs were analysed by the reduction factor  $R$ , which is related to the heat stress parameters of REF (Table 1). The AMs were ranked in ascending order according to the reduction factor  $R$  as a measure of the performance. The weakest performance was calculated for the reduction of the stocking densities SD80% and SD60% with  $R$  between 4 and 11%.  $R$  for SHIFT and VENT varies between 23% and 40%. The highest heat stress reduction of more than 50% for most of the heat stress parameters was found for the three air treatment devices (CP, CPHE, and EAHE) with  $R$  values between 61% and 99%. For other heat stress parameters, the reduction factors can be found in detail in (Schauberger et al., 2019a).

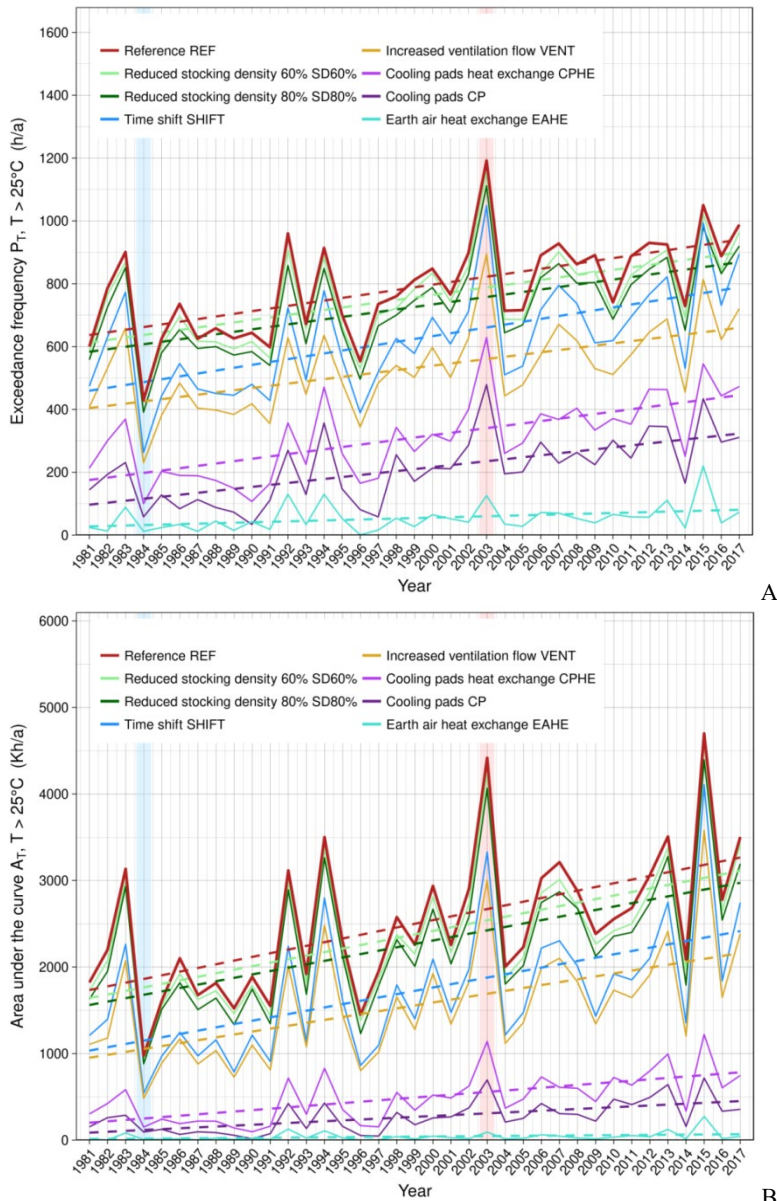


Figure 1. Annual exceedance frequency  $P_T$  (A) and exceedance area  $A_T$  (B) for the threshold of the indoor air temperature  $X_T = 25^\circ\text{C}$  determined for the conventional reference system REF and the seven adaptation measures AM: reduced stocking densities SD80% and SD60%, diurnal shift of the activity pattern SHIFT, doubling of the summer ventilation rate VENT, the cooling pads plus heat exchanger CPHE, cooling pads CP, and earth-air heat exchanger EAHE. The linear regressions are shown by dashed lines (Schauberger et al., 2019a).

The time course of the calculated parameters is shown in Figure 1A for the exceedance

frequency  $P_T$  (frequency above the temperature threshold  $X_T = 25^\circ\text{C}$ ) and in Figure 1B for the exceedance area  $A_T$ .  $P_T$  (Turnpenny et al., 2001; Haskell et al., 2011) and  $A_T$  (St-Pierre et al., 2003; Thiers and Peuportier, 2008; Gosling et al., 2013) are used widely as measures for heat stress. Other heat stress parameters, which include humidity (e.g., THI) or parameters which are adapted to the pig growth can be found in Schauberger et al. (2019a).

The resilience of REF and all AMs without air treatment (SD80%, SD60%, SHIFT, and VENT) shows a steeper slope (lower resilience) compared to the outside situation. The three AMs with air treatment (CPHE, CP, and EAHE) show lower slopes, which means that these systems increase the resilience for the livestock system in comparison to REF and are able to compensate the impact of global warming. The cooling efficacy of the three air treatment devices is high enough to keep the temperature inside the livestock system lower compared to outside, even though the animals are causing a high sensible heat release. All AMs improve the resilience of the livestock system against global warming. Nevertheless, the three air preparation AMs show a much better performance, compared to the other AMs.

The advantages of the presented model approach in comparison to measurements are manifold: (1) the model is driven by a meteorological dataset, which means that the calculation can be performed for other sites as well, (2) near future scenarios can be assessed by the extrapolation of the linear trend of long time series as robust predictions (Hendry and Pretis, 2016), (3) future climate scenarios can be calculated by datasets on an hourly basis (e.g., van Leuken et al., 2016), (4) case studies can be performed for combinations of AMs to optimize the indoor climate by the use of heat stress parameters as a cost function, (5) optimization of the design values (e.g., ventilation rate, AM) can help to improve the efficacy in relation to the climatic situation for a certain site, (6) future developments of system parameters can be considered (e.g., market demand of heavier pigs at slaughter), and (7) the advantage to quantify heat stress in comparison to qualitative assessments (e.g., Derner et al., 2017).

#### 4. Conclusions

Global warming has a strong impact on livestock keeping due to the increase of heat stress. During the last decades a distinct positive trend for many heat stress parameters could be shown. This results in a growing demand for cooling measures. By the use of model calculations of the indoor climate, seven adaptation measures were quantitatively evaluated to determine the performance.

#### Acknowledgements

The project *PiPoCooL Climate change and future pig and poultry production: implications for animal health, welfare, performance, environment and economic consequences* was funded by the Austrian Climate and Energy Fund within the frame work of the Austrian Climate Research Program (ACRP8 – PiPoCooL – KR15AC8K12646).

#### References

- ASHRAE, 2008. Air-to-Air Energy Recovery (Chapter 25). In: *ASHRAE Handbook—HVAC Systems and Equipment*. Atlanta, USA: American Society of Heating, Refrigerating and Air-Conditioning Engineers Inc.
- Bisoniya, T.S., A. Kumar, P. Baredar, 2014. Study on Calculation Models of Earth-Air Heat Exchanger Systems. *Journal of Energy*. Volume 2014, ID 859286, 1–15. <http://dx.doi.org/10.1155/2014/859286>.
- Derner, J., D. Briske, M. Reeves, T. Brown-Brandl, M. Meehan, D. Blumenthal, W. Travis, D. Augustine, H. Wilmer, D. Scasta, J. Hendrickson, J. Voilesky, L. Edwards, D. Peck, 2017. Vulnerability of grazing and confined livestock in the Northern Great Plains to projected mid- and late-twenty-first century climate. *Climatic Change*, 1–14. <http://dx.doi.org/10.1007/s10584-017-2029-6>.
- Gosling, S.N., E.K. Bryce, P.G. Dixon, K.M.A. Gabriel, E.Y. Gosling, J.M. Hanes, D.M. Hondula, L. Liang, P.A. Bustos Mac Lean, S. Muthers, S.T. Nascimento, M. Petralli, J.K. Vanos, E.R. Wanka, 2013. A glossary for biometeorology. *International Journal of Biometeorology*, 1–32. <http://dx.doi.org/10.1007/s00484-013-0729-9>.

Haskell, M., P. Kettlewell, E. McCloskey, E. Wall, N. Fox, M. Mitchell, 2011. Animal Welfare and Climate Change: Impacts, Adaptations, Mitigation and Risks. Scottish Agricultural College (SAC), Edinburgh.

Hendry, D.F., F. Pretis, 2016. All Change! The Implications of Non-Stationarity for Empirical Modelling, Forecasting and Policy. In: *Oxford Martin School Policy Paper Series, Forthcoming. Available at SSRN: https://ssrn.com/abstract=2898761*.

Huynh, T.T.T., A.J.A. Aarnink, W.J.J. Gerrits, M.J.H. Heetkamp, T.T. Canh, H.A.M. Spoolder, B. Kemp, M.W.A. Verstegen, 2005. Thermal behaviour of growing pigs in response to high temperature and humidity. *Applied Animal Behaviour Science*. 91 (1–2), 1–16. <http://dx.doi.org/10.1016/j.applanim.2004.10.020>.

Mikovits, C., W. Zollitsch, S.J. Hörtenhuber, J. Baumgartner, K. Niebuhr, M. Piringer, I. Anders, K. Andre, I. Hennig-Pauka, M. Schönhart, G. Schauberger, 2019. Impacts of global warming on confined livestock systems for growing-fattening pigs: simulation of heat stress for 1981 to 2017 in Central Europe. *International Journal of Biometeorology*. 63 (2), 221–230. <http://dx.doi.org/10.1007/s00484-018-01655-0>.

MWPS-32, 1990. Mechanical ventilating systems for livestock housing. Midwest Plan Service, Iowa State University, Ames 70 p.

Ozgener, L., 2011. A review on the experimental and analytical analysis of earth to air heat exchanger (EAHE) systems in Turkey. *Renewable and Sustainable Energy Reviews*. 15 (9), 4483–4490. <http://dx.doi.org/10.1016/j.rser.2011.07.103>.

Schauberger, G., M. Piringer, E. Petz, 1999. Diurnal and annual variation of odour emission from animal houses: A model calculation for fattening pigs. *Journal of Agricultural and Engineering Research*. 74 (3), 251–259.

Schauberger, G., M. Piringer, E. Petz, 2000. Steady-state balance model to calculate the indoor climate of livestock buildings, demonstrated for fattening pigs. *International Journal of Biometeorology*. 43 (4), 154–162.

Schauberger, G., C. Mikovits, W. Zollitsch, S.J. Hörtenhuber, J. Baumgartner, K. Niebuhr, M. Piringer, W. Knauder, I. Anders, K. Andre, I. Hennig-Pauka, M. Schönhart, 2019a. Global warming impact in confined livestock buildings: efficacy of adaptation measures to reduce heat stress for growing-fattening pigs. *Climatic Change*. <http://dx.doi.org/10.1007/s10584-019-02525-3>.

Schauberger, G., C. Mikovits, W. Zollitsch, S.J. Hörtenhuber, J. Baumgartner, K. Niebuhr, M. Piringer, W. Knauder, I. Anders, K. Andre, I. Hennig-Pauka, M. Schönhart, 2019b. Heat stress for fattening pigs in confined livestock buildings: Simulation of the impact of global warming for 1981–2017 for the mid-latitudes. In: *Animal Environment & Welfare*. Chongqing, China: China Agriculture Press. Eds., Ni, J., L. Teng-Teeh, C. Wang, L. Zhao.

St-Pierre, N.R., B. Cobanov, G. Schnitkey, 2003. Economic Losses from Heat Stress by US Livestock Industries. *Journal of Dairy Science*. 86, E52–E77. [http://dx.doi.org/10.3168/jds.S0022-0302\(03\)74040-5](http://dx.doi.org/10.3168/jds.S0022-0302(03)74040-5).

Thiers, S., B. Peuportier, 2008. Thermal and environmental assessment of a passive building equipped with an earth-to-air heat exchanger in France. *Solar Energy*. 82 (9), 820–831. <http://dx.doi.org/10.1016/j.solener.2008.02.014>.

Turnpenny, J.R., D.J. Parsons, A.C. Armstrong, J.A. Clark, K. Cooper, A.M. Matthews, 2001. Integrated models of livestock systems for climate change studies. 2. Intensive systems. *Global Change Biology*. 7 (2), 163–170.

Tzaferis, A., D. Liparakis, M. Santamouris, A. Argiriou, 1992. Analysis of the accuracy and sensitivity of eight models to predict the performance of earth-to-air heat exchangers. *Energy and Buildings*. 18 (1), 35–43. [http://dx.doi.org/10.1016/0378-7788\(92\)90049-M](http://dx.doi.org/10.1016/0378-7788(92)90049-M).

van Leuken, J.P.G., A.N. Swart, P. Droogers, A. van Pul, D. Heederik, A.H. Havelaar, 2016. Climate change effects on airborne pathogenic bioaerosol concentrations: a scenario analysis. *Aerobiologia*. 32 (4), 607–617. <http://dx.doi.org/10.1007/s10453-016-9435-5>.

Vitt, R., L. Weber, W. Zollitsch, S.J. Hörtenhuber, J. Baumgartner, K. Niebuhr, M. Piringer, I. Anders, K. Andre, I. Hennig-Pauka, M. Schönhart, G. Schauberger, 2017. Modelled performance of energy saving air treatment devices to mitigate heat stress for confined livestock buildings in Central Europe. *Biosystems Engineering*. 164, 85–97. <http://dx.doi.org/10.1016/j.biosystemseng.2017.09.013>.

## Bioenergetics of Laying Hens in Aviary Systems

Jofran L. Oliveira<sup>a</sup>, Brett C. Ramirez<sup>a,\*</sup>, Hongwei Xin<sup>b,\*</sup>, Yu Wang<sup>a</sup>, Steven J. Hoff<sup>a</sup>

<sup>a</sup> Department of Agricultural and Biosystems Engineering, Iowa State University, Ames, IA 50011, USA

<sup>b</sup> Institute of Agriculture, The University of Tennessee, Knoxville, TN 37996, USA

\* Corresponding authors. Email: [bramirez@iastate.edu](mailto:bramirez@iastate.edu), [hxin2@utk.edu](mailto:hxin2@utk.edu)

### Abstract

Aviaries are an alternative housing style that allows laying hens to freely move, increasing their diurnal activity and consequently impacting their heat and moisture production. Bioenergetics data measured from intensive livestock housings is important such that accurate design data can be used for modern animal production facilities, including proper ventilation and supplemental heating or cooling. However, there is limited information on house-level heat production of laying hens in such contemporary facilities. Therefore, the objectives of this study were to quantify bioenergetics by measuring and estimating the house-level heat production (total heat production, THP; sensible heat production, SHP; and latent heat production, LHP) of Dekalb White laying hens in a modern commercial laying hen aviary house, initially housing 140,000 hens. The values of THP, SHP and LHP were partitioned into light and dark period to evaluate the influence of hens' diurnal activity on bioenergetics. Overall, daily mean values were  $7.5 \pm 0.2$  W kg<sup>-1</sup> for THP,  $4.8 \pm 0.3$  W kg<sup>-1</sup> for SHP and  $2.7 \pm 0.2$  W kg<sup>-1</sup> for LHP, and THP was reduced by 40% in the dark period ( $5.1 \pm 0.3$  W kg<sup>-1</sup>) compared to the light period ( $8.5 \pm 0.3$  W kg<sup>-1</sup>). The house-level heat and moisture production data from this study will contribute to updating of the engineering standards or guidelines for efficient design of environmental control systems in modern cage-free layer production.

**Keywords:** House-level heat production, moisture production, environmental control, cage-free, diurnal activity

### 1. Introduction

Understanding the bioenergetics (heat and moisture production) associated with animal production systems and the interaction between animals and their environment are essential to provide data needed for an efficient design of modern animal production systems, including proper ventilation and supplemental heating and cooling (Albright, 1990; DeShazer, 2009). The design of a controlled environment with appropriate management of ventilation rates to control temperature, humidity, and noxious gases is typically based on heat and moisture production of the animals and their surroundings. The American Society of Agricultural and Biological Engineers (ASABE) and International Commission of Agricultural Engineering (CIGR) established values or guidelines on animal heat and moisture production rates (ASABE Standards, 2017; CIGR, 1999), based on studies conducted from 1950s to 1990s. Since then, many years of research has been committed to improving the understanding of animal and housing interaction. Considering that animal bioenergetics vary with genetics, nutrition, management practices (e.g., manure handling), housing equipment and design and thermal environment (Chepere et al., 2004), these guidelines or "standards" are likely outdated for application in modern production applications.

Indirect calorimetry is a method used to calculate animal metabolic rate or total heat production (THP) by quantifying CO<sub>2</sub> production and O<sub>2</sub> consumption rates of the animal. Gas production and consumption are assessed by calculating room ventilation rate (VR) and the difference in gas concentration between fresh inlet air and exhaust air. While the dry-bulb temperature is less than the temperature of the animal's skin, VR is the main environmental factor involved in thermoregulation, and with the increase of the air velocity, the convective heat loss will be increased. House VR is generally proportional to the outdoor temperature, with maximum occurring during the summer and minimum during the winter (DeShazer, 2009). The THP of

animals consists of sensible heat production (SHP) and latent heat production (LHP). Both SHP and LHP can be assessed for individual animals (used to delineate animal thermoregulation) or at the housing level, where part of the sensible heat is converted to latent heat by evaporating moisture in the surroundings. House-level SHP and LHP data are more useful when designing ventilation system for moisture control (minimum ventilation) and temperature control (maximum ventilation). Heat and moisture production of laying hens are influenced by the indoor thermal environment (e.g., air temperature and relative humidity), affecting the partition between latent and sensible heat.

Heat production changes with hen activity (Hayes et al., 2013) and in alternative housing systems (Zhao et al., 2015), hens have access to enrichment, litter area or outdoor area contributing to the increase in hen activities. Studies on the bioenergetics of laying hens have been performed using calorimetric chambers with conventional cage housing (Green and Xin, 2009a, 2009b), calorimetric chamber containing an aviary unit (Von Wachenfels et al., 2001), and whole-house commercial aviary (Hayes et al., 2013). However, housing systems and management practices change and vary among producers. Further, in current modern facilities, nominal hen capacities have increased from 50,000 (Hayes et al., 2013) to approximately 140,000 hens which in turn affect the ventilation design and consequently the bioenergetics.

Therefore, the objectives of this study were (i) to calculate the VR and the associated uncertainty, and (ii) to quantify THP and house-level SHP and LHP of Dekalb White laying hens in a modern commercial aviary laying-hen house. The values of THP, SHP and LHP were further partitioned into light and dark periods to evaluate the influence of hens' diurnal activities on the bioenergetics responses. Data from CIGR and recent literature quantifying heat and moisture production of laying hens were included for comparison purposes.

## 2. Materials and Methods

### 2.1. Animals and housing

This study was conducted in a newly constructed, two-story building ( $197.5\text{ m} \times 65.2\text{ m} \times 7.6\text{ m}$ ;  $L \times W \times H$ ) in the Midwest US, oriented north-south, and containing four aviary (cage-free) rooms ( $L \times W \times H$  of  $197.5\text{ m} \times 30.5\text{ m} \times 3.8\text{ m}$ ). Each room contained six rows of an aviary system (Bolegg Gallery, Vencomatic, Eersel, Netherlands) spanning the length of the room. The aviary system included three tiers of slatted floor (lower, middle, and upper tiers), two tiers of full-length curtained nests (lower and middle tiers, with average area of  $86.4\text{ cm}^2\text{ hen}^{-1}$ ), nipple drinkers with drip cups (lower and middle tiers, with average of  $10\text{ hens drinker}^{-1}$ ), and two full-length chain feeders in each tier (average feeder space of  $8\text{ cm hen}^{-1}$ ). It also contained full-length galvanized steel perches (average perch space of  $15.2\text{ cm hen}^{-1}$ ), ramps at  $45^\circ$  from lower tier to litter area, three manure belts located below the slatted floor of each tier, a perforated manure-drying air duct, two LED tube lights ( $4.6\text{ W light}^{-1}$ ) near the chain feeders and underneath the lower tier, and a scraper on the litter floor under the aviary system (Figure 1).

The upper-east room (the yellow-shaded rectangle in Figure 1) was used in this experiment and initially housed 140,707 DeKalb White pullets at 17 weeks of age (WoA). Pullets were beak trimmed at the hatchery and reared in an aviary style pullet house. Light traps (Munters Aerotech, Mason, MI, USA) were installed between the bird occupied space and the exhaust fans. Light stimulation began when the house was populated. An increasing photoperiod from 12-h light and 12-h dark to 16-h light and 8-h dark was scheduled over ten weeks, following the commercial management guidelines based on hens' body weight. Commercial feed was independently distributed to each room and was provided three times a day. The metabolizable energy (ME) and protein content of the feed were  $13.1 \pm 0.1\text{ MJ kg}^{-1}$  and 17.2%, respectively. Drinking water was provided *ad libitum*. Manure accumulated on the belts was removed from the house every three days (running one-third of the belt per day) and stored in a manure storage facility adjacent to the layer building. Litter accumulated on the floor was not removed until the end of the flock; however, a small portion was removed by the floor scraper.

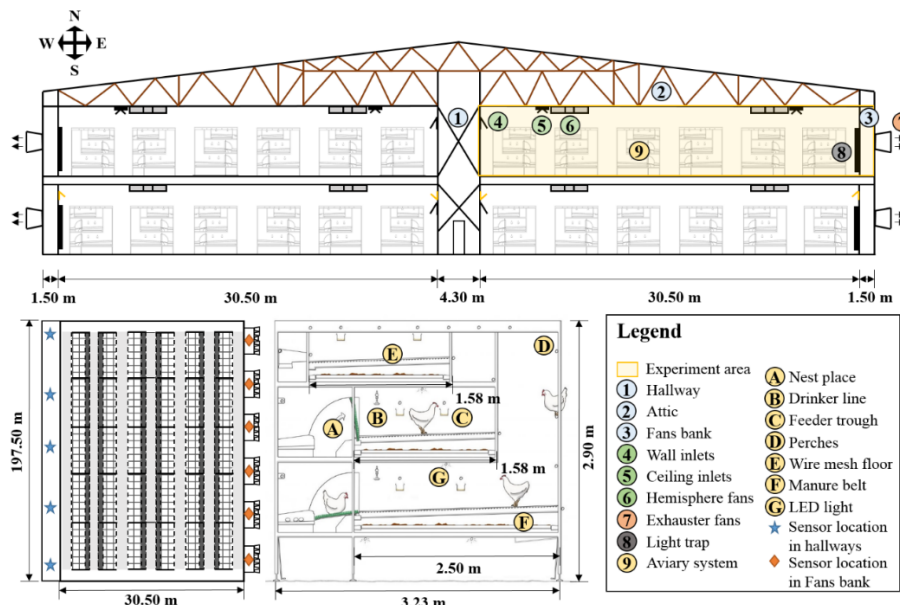


Figure 1. Schematic representation of the building and the aviary system used in the experiment.

Fresh air was distributed to the room by sidewall inlets located along the hallway, ceiling inlets and hemisphere fans connected to the attic. Exhaust fans provided air exchange and were located in six fans banks (Figure 1).

## 2.2. Ventilation system

The mechanical ventilation system featured 36 exhaust fans: 30 large fans (130 cm diameter; VX5115F3CP; Munters Aerotech) and 6 small fans (91 cm diameter; AT365ZC; Munters Aerotech). Fans were equally distributed among six banks. Fan airflow capacity was verified by BESS Labs (tests #11369 and #93239). Fans were grouped into 13 ventilation stages. An automated system controlled the opening of the baffled inlets and the fan duty cycle according to the indoor temperature (PMSI Command III module; Poultry Management Systems Inc., Lowell, MI, USA). Fans and light traps were cleaned weekly by the farm operators.

## 2.3. Measurements and data collection

Temperature (°C), RH (%), and CO<sub>2</sub> concentration (ppm<sub>v</sub>) were measured with 11 data loggers ( $\pm 0.21$  °C;  $\pm 2\%$  RH;  $\pm 50$  ppm or  $\pm 5\%$ ; MX1102A, Onset Computer Corp., Bourne, MA, USA) located in the fan banks (six data loggers, one in each fans bank) and in the hallway (five data loggers equally distributed along the hallway). Room differential static pressure (SP) was measured with a static pressure sensor ( $\pm 1.25$  Pa; model 265; Setra, Boxborough, MA, USA; see locations of the sensors in Figure 1).

A relay controlled each of the 36 fans with relay status (on or off) monitored by the room controller (PMSI Command III module, Poultry Management Systems Inc.). Two portable Fan Assessment Numeration Systems (FANS; Gates et al., 2004) were used to measure *in situ* airflow for ten fans (two small fans; eight large fans). Airflow curves for the small and large fans were generated and subsequently used to calculate VR.

Room setpoint air temperature was between 21.7 °C and 22.8 °C during cold weather, 22.8 °C and 24.4 °C during mild weather, 23.9 °C and 30.0 °C during the warm/hot weather.

## 2.4. Bioenergetics calculations

The indirect calorimetry method was used to calculate THP. Metabolic heat production of non-ruminants is related to their O<sub>2</sub> consumption and CO<sub>2</sub> production, of the following form (Brouwer, 1965; adopted by Hayes et al., 2013):

$$\text{THP} = 16.18 \text{O}_2 + 5.02 (\text{CO}_2 - \text{CO}_2\text{manure}) \quad (1)$$

where THP = total heat production rate of the hens in the room (W); O<sub>2</sub> = oxygen consumption rate (mL s<sup>-1</sup>); CO<sub>2</sub> = carbon dioxide production rate of the house (mL s<sup>-1</sup>); CO<sub>2</sub> manure = carbon dioxide production rate of the manure or litter (mL s<sup>-1</sup>); The ratio of CO<sub>2</sub> production and O<sub>2</sub> consumption is denoted as the respiratory quotient (RQ).

$$\text{RQ} = \frac{\text{CO}_2}{\text{O}_2} \quad (2)$$

The CO<sub>2</sub> production rate was determined from the CO<sub>2</sub> concentration data for the inlet and exhaust air:

$$\text{CO}_2 = \text{VR} [(\text{CO}_2)_{\text{exh}} - (\text{CO}_2)_{\text{in}}] 10^{-6} \quad (3)$$

where CO<sub>2</sub> = carbon dioxide production rate of the house (mL s<sup>-1</sup>); VR = building ventilation rate (m<sup>3</sup> s<sup>-1</sup>); (CO<sub>2</sub>)<sub>in</sub>, (CO<sub>2</sub>)<sub>exh</sub> = carbon dioxide concentration at inlet and exhaust (ppm<sub>v</sub>).

A prerequisite to calculating CO<sub>2</sub> production is that the CO<sub>2</sub> concentration in the exhaust air of the aviary house can be distinguished with sufficient accuracy from CO<sub>2</sub> concentration in inlet air. In practice, this means a difference in CO<sub>2</sub> concentration ( $\Delta\text{CO}_2$ ) of at least 200 ppm between the inlet and exhaust air (Van Ouwerkerk and Pedersen, 1994). Therefore, collected data where  $\Delta\text{CO}_2$  was lower than 200 ppm<sub>v</sub> were discarded.

The O<sub>2</sub> consumption rate was calculated as a function of RQ and rearranged into the expression:

$$\text{THP} = 16.18 \frac{\text{CO}_2}{\text{RQ}} + 5.02 (\text{CO}_2 - \text{CO}_2\text{manure}) \quad (4)$$

The house-level moisture production (MP), including the LHP of the hens and moisture evaporation from spilled water and manure, expressed as the amount of water produced in a period and was calculated from the mass-balance equation:

$$\text{MP} = \rho \text{VR} [(\text{W})_{\text{exh}} - (\text{W})_{\text{in}}] \quad (5)$$

where MP = moisture production rate of the house (kg<sub>water</sub> s<sup>-1</sup>); ρ = room moist air density (kg m<sup>-3</sup>); (W)<sub>in</sub>, (W)<sub>exh</sub> = humidity ratio of the inlet and exhaust air, respectively (g<sub>water</sub> g<sub>dry air</sub><sup>-1</sup>).

House-level LHP represents energy released from the environment as a result of the change in phase of water, in this case, vaporization, and was calculated as:

$$\text{LHP} = \text{MP} h_{fg} \quad (6)$$

where LHP = house-level heat production rate of the house (W); MP = moisture production rate of the house (kg<sub>water</sub> s<sup>-1</sup>); h<sub>fg</sub> = latent heat of vaporization of water, 2,427,000 J kg<sup>-1</sup>.

House-level SHP represents the energy released from the environment that involves a change in the temperature and is calculated by difference as:

$$\text{SHP} = \text{THP} - \text{LHP} \quad (7)$$

Heat and moisture production calculations considered the body mass and population based on weekly production reports provided by the farm. The indoor temperature during the experiment period was maintained without any supplemental heat.

## 3. Results and Discussion

Data from 50 days, with  $\Delta\text{CO}_2 > 200$  ppm<sub>v</sub>, were collected from 8 July 2018 to 19 October 2018. Outdoor temperature decreased during the experiment period; however, THP did not follow an obvious trend with days ( $P = 0.32$ ) or outdoor temperature ( $P = 0.59$ ), suggesting that the ventilation system and the lower stocking density were effective at maintaining the indoor thermal environment within the hen's thermoneutral zone. There is no evident trend between indoor

temperature and SHP ( $P = 0.74$ ). However, trends between indoor temperature and LHP ( $P = 0.03$ ) or THP ( $P = 0.03$ ) were observed.

Overall, daily mean values were  $7.5 \pm 0.2 \text{ W kg}^{-1}$  (THP),  $4.8 \pm 0.3 \text{ W kg}^{-1}$  (SHP) and  $2.7 \pm 0.2 \text{ W kg}^{-1}$  (LHP). In an experiment evaluating effect of stocking density and group size on heat and moisture production in conventional system inside calorimeter chambers, Green and Xin (2009a) reported that Hy-line W-36 hens (39 to 46 WOA, 1.5 to 1.6 kg) had THP of 6.4 to 6.6  $\text{W kg}^{-1}$  at 24 °C, 5.6 to 6.1  $\text{W kg}^{-1}$  at 32 °C and 5.9 to 6.5  $\text{W kg}^{-1}$  at 35°C. In a cage-free aviary system, THP of Lohmann Select Leghorn layers (59 to 68 WOA, 1.6 to 1.8 kg) was 22% higher at 20°C than the CIGR guideline value (Von Wachenfels et al., 2001). Hy-line Brown layers (17 to 83 WOA, 1.4–2.0 kg BW) produced 5.9  $\text{W kg}^{-1}$  THP with 1.8  $\text{W kg}^{-1}$  LHP in a cage-free aviary house (Hayes et al., 2013).

On average, the daily LHP was about 36% of THP. This value was somewhat different from those reported by Hayes et al. (2013) (31%) and Chepete et al. (2004) (~40%). Differences in the ventilation systems, housing styles, litter conditions, bird activity level, breeds, season, bird age, and management practices presumably contributed to the differences observed.

THP increased as the light came on at 06:30 h (5 min of onset period) and decreased when the light went off at 21:55 h (20 min dimming period). This pattern was previously observed by Hayes et al. (2013), suggesting the increase of HP was proportional to the activity level of laying hens in the aviary system. Overall, THP decreased by 40% in the dark period ( $5.1 \pm 0.3 \text{ W kg}^{-1}$ ) when compared with THP during the light period ( $8.5 \pm 0.3 \text{ W kg}^{-1}$ ) ( $P < 0.01$ ). The reduction in THP from light to dark has been reported to be ~30% (Hayes et al., 2013), 25% (Green and Xin, 2009a), 26% (Xin et al., 1996), and 35% (MacLeod and Jewitt, 1984). The reduction of THP during the dark period in this study was higher than the values found in the literature presumably due to the higher diurnal activity level experienced by the hens in the fully open aviary system. Both SHP and LHP during the light period ( $5.3 \pm 0.3 \text{ W kg}^{-1}$  and  $3.2 \pm 0.3 \text{ W kg}^{-1}$ , respectively) were also significantly different ( $P < 0.01$ ) when compared with the dark period ( $3.5 \pm 0.2 \text{ W kg}^{-1}$  and  $1.6 \pm 0.1 \text{ W kg}^{-1}$  for SHP and LHP, respectively).

#### 4. Summary and Conclusions

This study investigated bioenergetics of Dekalb White laying hens in a modern commercial fully-open aviary housing (~140,000 laying hens capacity). In doing so, *in situ* airflow curves of ventilation fans were established and fans runtime continuously monitored to calculate building ventilation rate (VR). Carbon dioxide (CO<sub>2</sub>) concentrations and thermal conditions of the inlet and exhaust air were continually recorded and used in quantifying the bioenergetics response. Total heat production (THP) of the hens were determined using indirect calorimetry method, and it was portioned into house-level sensible heat production (SHP) and latent heat production (LHP). The following observations and conclusions were made.

- Daily time-weighted average (TWA) THP, LHP and SHP were  $7.5 \pm 0.2 \text{ W kg}^{-1}$ ,  $4.8 \pm 0.3 \text{ W kg}^{-1}$  and  $2.7 \pm 0.2 \text{ W kg}^{-1}$ , respectively. THP decreased by 40% during the dark period ( $5.1 \pm 0.3 \text{ W kg}^{-1}$ ) as compared with THP during the light period ( $8.5 \pm 0.3 \text{ W kg}^{-1}$ ).
- The house-level heat and moisture production data from this study will contribute to updating of the engineering standards or guidelines for efficient design of environmental control systems in modern cage-free layer production.

#### References

- Albright, L. D., 1990. *Environment Control for Animals and Plants*. St. Joseph, Mich.: American Society of Agricultural Engineers.
- ASABE Standards, 2017. *Design of Ventilation Systems for Poultry and Livestock Shelters*. (ASAE EP270.5)
- Brouwer, E., 1965. Report of sub-committee on constant and factors. In K. L. Blaxter (Ed.), *3rd Symposium Energy Metabolism* (pp. 441–443). Troon, Scotland: European Association for Animal Production.

- Chepete, H. J., Xin, H., Puma, M. C., Gates, R. S., 2004. Heat and moisture production of poultry and their housing systems: Pullets and layers. *ASHRAE Journal*, 110(2), 286–299.
- CIGR, 1999. *CIGR Handbook of Agricultural Engineering Volume II: Animal Production and Aquacultural Engineering*.
- DeShazer, J. A., 2009. *Livestock Energetics and Thermal Environmental Management*. American Society of Agricultural and Biological Engineers.
- Gates, R. S., Casey, K. D., Xin, H., Wheeler, E. F., Simmons, J. D., 2004. Fan Assessment Numeration System (FANS) design and calibration specifications. *Transactions of the ASAE*, 47(5), 1709–1715.
- Green, A. R., Xin, H., 2009a. Effects of stocking density and group size on heat and moisture production of laying hens under thermoneutral and heat-challenging conditions. *Transactions of the ASABE*, 52(6), 2027–2032.
- Green, A. R., Xin, H. (2009b). Effects of stocking density and Group Size on Thermoregulatory Responses of Laying Hens under Heat-Challenging Conditions. *Transactions of the ASABE*, 52(6), 2033–2038.
- Hayes, M. D., Xin, H., Li, H., Shepherd, T. A., Zhao, Y., Stinn, J. P., 2013. Heat and moisture production of hy-line brown hens in aviary houses in the Midwestern U.S. *Transactions of the ASABE*, 56(2), 753–761.
- MacLeod, M. G., Jewitt, T. R., 1984. Circadian variation in the heat production rate of the domestic fowl, *Gallus domesticus*: Effects of limiting feeding to a single daily meal. *Comparative Biochemistry and Physiology – Part A: Physiology*, 78(4), 687–690. [https://doi.org/10.1016/0300-9629\(84\)90617-0](https://doi.org/10.1016/0300-9629(84)90617-0).
- Van Ouwerkerk, E. N. J., Pedersen, S., 1994. Application of the carbon dioxide mass balance method to evaluate ventilation rates in livestock buildings. In *XII World Congress on Agricultural Engineering* (pp. 516–529). CIGR.
- Von Wachenfelt, E., Pedersen, S., Gustafsson, G., 2001. Release of heat, moisture and carbon dioxide in an aviary system for laying hens. *British Poultry Science*, 42(2), 171–179. <https://doi.org/10.1080/00071660120048401>.
- Zhao, Y., Shepherd, T. A., Swanson, J. C., Mench, J. A., Karcher, D. M., Xin, H., 2015. Comparative evaluation of three egg production systems: Housing characteristics and management practices. *Poultry Science*, 94(3), 475–484. <https://doi.org/10.3382/ps/peu077>.

# Effect of Calcium Sulphate Dihydrate on GHG and Ammonia Emissions from Cattle Slurry during Storage

Borgonovo Federica <sup>a</sup>, Conti Cecilia <sup>a\*</sup>, Lovarelli Daniela <sup>b</sup>, Bacenetti Jacopo <sup>a</sup>, Ferrante Valentina <sup>a</sup>, Guarino Marcella <sup>a</sup>

<sup>a</sup> Department of Environmental Science and Policy, Università degli Studi di Milano, Milan 20133, Italy

<sup>b</sup> Department of Agricultural and Environmental Sciences. Università degli Studi di Milano, Milan 20133, Italy

\* Corresponding author. Email: [cecilia.conti@unimi.it](mailto:cecilia.conti@unimi.it)

## Abstract

A significant part of ammonia ( $\text{NH}_3$ ), methane ( $\text{CH}_4$ ), nitrous oxide ( $\text{N}_2\text{O}$ ), and carbon dioxide ( $\text{CO}_2$ ) are produced from the decomposition of slurry organic matter in livestock facilities during manure storage and treatment phases. Therefore, various strategies such as manure management practices, types of treatment and additives have been adopted in order to explore the nutrient losses from livestock manure and minimize the environmental impact due to  $\text{NH}_3$  and greenhouse gas (GHG) emissions. The aim of this study was to evaluate the effects of a commercial additive (calcium sulphate dihydrate) on slurry characteristics and N losses, and on  $\text{NH}_3$  and GHG emissions. Its environmental impact was assessed with a Life Cycle Assessment (LCA) methodology. Six barrels were filled with 65 litres of cattle slurry, among which three were used as the control, and three as the treatment. Gaseous emissions and slurry composition were studied over a 26-day storage period. The results indicated that the use of the additive led to a reduction of total nitrogen, nitrates as well as  $\text{NH}_3$  and GHG emissions. From the LCA results a higher environmental sustainability was achieved in the scenario with the additive compared to the scenario without it. In conclusion, the addition of calcium sulphate dihydrate has beneficial effects both on emission mitigations and on the environment. Moreover, the nitrogen present in the treated slurry makes it a valid substitute for a mineral fertilizer, which can be considered as an environmental credit.

**Keywords:** Ammonia, calcium sulphate dihydrate, greenhouse gases, environmental impact, slurry, storage

## 1. Introduction

Agriculture and livestock farming are known to emit relevant quantities of atmospheric pollutants, mainly occurring from faeces and urine in housing and manure storage systems, from excreta of grazing animals and from the application of manure and mineral N fertilizers (Velthof et al., 2014). In particular, manure management has a negative impact on the environment due to ammonia ( $\text{NH}_3$ ) volatilisation, and greenhouse gases (GHG) emissions, such as nitrous oxide ( $\text{N}_2\text{O}$ ), methane ( $\text{CH}_4$ ), and carbon dioxide ( $\text{CO}_2$ ) (Gerber et al., 2013) that occur during manure storage and the subsequent field spreading.

Ammonia can cause acidification, nutrient-N enrichment of ecosystems, and eutrophication of terrestrial and aquatic ecosystems. It is a precursor of secondary particulates matter and a secondary source of  $\text{N}_2\text{O}$  caused by denitrification process (Adviento-Borbe et al., 2010), and  $\text{CH}_4$  and  $\text{CO}_2$  are produced by the decomposition of organic matter in the manure.  $\text{N}_2\text{O}$  emissions are principally caused by the nitrification-denitrification process following manure application and are influenced by the nitrogen and carbon content of manure, storage duration, and treatment type (Adviento-Borbe et al., 2010; Baldini et al., 2016).

In this context, livestock farms and industries are developing mitigation strategies to reduce these emissions. Nevertheless, some of these management strategies (e.g. solid-liquid separation, anaerobic digestion, and manure storage covers) require large capital, high maintenance cost and necessitate specific knowledge for correct operation (Möller and Stinner, 2009; Sun et al., 2014). Therefore, an alternative approach is the use of additives during the slurry storage that are able to

modify both the chemical composition and the biological process of slurry, acting on the N content (Guarino et al., 2006) or stimulating microbiological processes (Sommer et al., 2013). Recent bibliographical documentation attests a growing interest in evaluating the potential of biochar, chemical additives, and gypsum to mitigate NH<sub>3</sub> and GHG emissions from the stored slurry. Among these, gypsum has a great ability to prevent N losses from manure and to reduce NH<sub>3</sub> volatilization during the composting process (Tubail et al., 2008). NH<sub>3</sub> volatilization reduction was also confirmed by Febrisantosa et al. (2018), Li et al. (2018) and Yang et al. (2015). The weak aspect of these studies' findings is related to the large amounts of material needed to achieve the desired results.

The purpose of this study is to test the effect of one commercial additive SOP LAGOON ([www.sopgroup.com](http://www.sopgroup.com)), made of agricultural gypsum (with chemical composition of calcium sulphate dihydrate) on: i) slurry properties and N losses; ii) reduction of NH<sub>3</sub> and GHG emissions; and iii) its environmental performance, through Life Cycle Assessment (LCA) methodology.

## 2. Materials and Methods

### 2.1. Experimental setup

The fresh slurry was collected from a dairy farm situated in Northern Italy. Six 220 litre barrels were filled with 65 l of fresh slurry. Three barrels were left as a control, and the other three as a treatment, for which 4 g m<sup>-3</sup> (0.260 g barrel<sup>-1</sup>) of additive was added. The product was added weekly during the first two weeks, at days 0 (T0), 7 (T7), and 14 (T14).

### 2.2. Chemical analyses

Slurry samples (treated and non-treated) were collected from each barrel and analysed for total solids (TS), volatile solids (VS), total nitrogen (TN), ammonium nitrogen (NH<sub>4</sub><sup>+</sup>-N), nitrites (NO<sub>2</sub>-N) and nitrates (NO<sub>3</sub>-N) in order to verify if they were affected by the additive applications. The samples were then stored at 4°C until the day of the analyses.

The pH was quantified using a pH meter at the beginning (T0) and at the end of the trial (T26).

### 2.3. Emission measurements

The concentrations of NH<sub>3</sub> and GHG (mg m<sup>-3</sup>) were measured by means of an Infrared Photoacoustic Detector (Brüel&Kjaer, multi-gas monitor type 1302). This method evaluates the increase in gas concentrations versus time within the internal volume of the closed chamber according to the “non-steady-state-chamber-method”. The concentration typically demonstrates a linear increasing trend followed by a saturation phase. The slope of the regression line, calculated within the linear part of the saturation curve, multiplied by the chamber volume to area ratio represents the emission potential of the surface, namely the emission flux in the tables below, expressed in mg m<sup>-2</sup> h<sup>-1</sup>. The emission fluxes (mg m<sup>-2</sup> h<sup>-1</sup>) were calculated according to Eq. (1):

$$\text{Emission flux}_{\text{gas}} \left[ \frac{\text{mg}}{\text{m}^2 \cdot \text{h}} \right] = \frac{\delta C \left[ \frac{\text{mg}}{\text{m}^3} \right]}{\delta t [\text{h}]} \cdot \frac{V_{\text{ch}} [\text{m}^3]}{A_{\text{ch}} [\text{m}^2]} \quad (1)$$

where  $\delta C$  - variation of the concentration of the monitored gas in the time interval;  $\delta t$  – time interval;  $V_{\text{ch}}$  – inner volume of the static chamber;  $A_{\text{ch}}$  – area of the chamber (emitting area).

The measurements were conducted on day 0, day 4, day 7, and day 26 (T0, T4, T7, and T26, respectively). Prior to the measurements, the slurry was mixed in order to prevent possible crusts that could affect the emission stream.

### 2.4. Statistical analysis

Data were subject to analysis of regression using the PROC REG statement of the SAS statistics program (SAS version 9.3; SAS Institute, Cary, NC, USA, 2012). The linear regression model was used to determine the specific emission fluxes of each gas, using as input data the concentrations measured in the chamber at regular time intervals (every 2 min). The calculated emission fluxes were then used to evaluate differences among emission fluxes originated from treated and control samples and also the environmental performance of the additive.

## 2.5. Life cycle assessment

Life Cycle Assessment (LCA) is a holistic approach, structured and recognized worldwide that consists of a systematic set of procedures to convert inputs and outputs of the studied system into its related environmental impact (ISO, 2006). In details, there are 4 steps in LCA: i) goal and scope definition, ii) Life Cycle Inventory, iii) Life Cycle Impact Assessment (LCIA), and iv) interpretation of the results and identification of the process hotspots.

### 2.5.1. Goal and scope definition

This LCA study aims to evaluate the environmental impact of the additive used. LCA was applied to the slurry storage without (Baseline Scenario, BS) and with additive (Alternative Scenario, AS) and, finally, the environmental impact of these two scenarios was compared to identify the most environmentally sustainable solution. Concerning the functional unit (FU), 1 ton of stored dairy cattle slurry was chosen. As described in the flow diagram (Figure 1), the analysis was conducted “from cradle to gate”, including in the system boundary all the processes, from the extraction of raw materials to slurry storage.

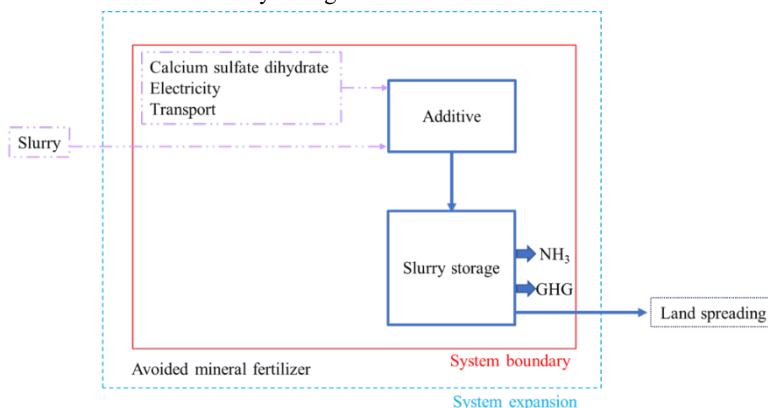


Figure 1. System boundaries.

In this study capital goods (e.g. slurry tank) were not taken into account due to their long life span (Frischknecht et al., 2007) and because their use was assumed to be the same in the two scenarios (BS and AS). A “zero burden” approach was considered for the slurry since it was considered a waste, as reported in previous LCA studies (Bacenetti et al., 2019). Moreover, the distribution of the stored dairy cattle slurry was excluded from the system boundary; instead, a system expansion was applied considering the substitution of the mineral fertilizer, as, at the end of the storage, the two slurries had a different N content. Specifically, a mineral fertilizer equivalence (MFE) equal to 100% was treated for the N-NH<sub>3</sub> in the slurry (Bacenetti et al., 2016) and the substitution of N from ammonium nitrate was taken into account. The (MFE) for nitrogen is a measure of the fertilizer ability to supply nitrogen to crops compared with mineral fertilizer)

### 2.5.2. Life cycle inventory

Inventory data related to NH<sub>3</sub>, N<sub>2</sub>O, and CH<sub>4</sub> emissions were collected during the trial. The storage capacity of 180 days is a common standard in Europe for slurries before land application. Thus, this time period was considered for the modeling of emissions in the LCA study. Consequently, emissions of NH<sub>3</sub>, N<sub>2</sub>O, and CH<sub>4</sub> from stored slurry were estimated after 180 days from the relative reduction that was achieved with the addition of the additive. Once quantified, these values were attributed also to slurry produced per cattle per year and referred to the FU.

Primary data about the additive were collected directly from the producer, in particular 0.899 kWh kg<sup>-1</sup> electricity, 1 kg gypsum, and 45 kg km<sup>-1</sup> transport distance. Secondary data about the

production of electricity, diesel fuel, and gypsum were obtained from Ecoinvent databases v 3.5 (Weidema et al., 2013).

### 2.5.3. Life cycle impact assessment (LCIA)

In the LCIA step, the inventory data are converted into few environmental indicators, by using specific characterization factors. The ILCD (International Reference Life Cycle Data System) midpoint characterization method was adopted, which is endorsed by the European Commission, Joint Research Centre in 2012 (EC-JRC - European Commission, 2012). The following impact categories were evaluated: climate change (CC), ozone depletion (OD), particulate matter formation (PM), human toxicity-no cancer effect (HTnoc), human toxicity with-cancer effect (HTc), photochemical ozone formation (POF), terrestrial acidification (TA), terrestrial eutrophication (TE), freshwater eutrophication (FE), marine eutrophication (ME), freshwater ecotoxicity (FEx) and mineral and fossil resource depletion (MFRD).

## 3. Results and Discussion

### 3.1. Changes in slurry composition after treatment and during storage

The results showed that the additive can actually modify slurry characteristics, as shown in Table 1. The TS increased until T7 and then decreased at T26 for both control and treatment. Regarding VS, its reduction occurred throughout the whole period of the study for both the treated slurry and the control, with more evident VS losses at the end. For NH<sub>4</sub><sup>+</sup>-N and NO<sub>2</sub>-N, subtle fluctuations were observed. Regarding TN and NO<sub>3</sub>-N contents, the slurry treated showed lower values of them at the end of the trial. In particular, the average TN content throughout the whole period of the study was 2.20 g kg<sup>-1</sup> for the control against 2.16 g kg<sup>-1</sup> for the treated.

The increase of TS and the reduction of NO<sub>3</sub>-N can improve the amendment features of the slurry avoiding excessive leaching of NO<sub>3</sub>-N into groundwater and providing the right quantity of nutrients to crops safeguarding the environment. Indeed, N is essential for the development of field crops, excesses of NO<sub>3</sub>-N deriving from slurry represent a serious threat to the environment. Hence, concerning slurry management, best practices are widely recommended and known to be essential (Sandars et al., 2003; Guarino et al., 2006).

Furthermore, acidification of slurry, obtained after the addition of calcium sulphate dihydrate, decreased the pH. Initial pH was 8.13 ± 0.20, whereas at the end of the experiment it was 8.53 ± 0.12, and 7.67 ± 0.10 for the control and the treated slurry, respectively.

Table 1. Slurry characteristics without additive (control) and with additive (treated) at T0, T4, T7, T26.

	T0		T4		T7		T26	
	Control	Treated	Control	Treated	Control	Treated	Control	Treated
TS (g kg <sup>-1</sup> DM)	78.41 ± 1.22	78.41 ± 1.37	97.48 ± 1.63	99.91 ± 2.11	99.36 ± 1.62	103.88 ± 1.11	91.37 ± 3.28	93.21 ± 2.81
VS (%TS DM)	83.86 ± 0.76	83.86 ± 0.41	84.45 ± 0.42	83.96 ± 0.93	83.85 ± 0.47	83.83 ± 0.59	81.76 ± 0.35	81.90 ± 0.86
TN (g kg <sup>-1</sup> WW)	1.86 ± 0.10	1.86 ± 0.11	1.88 ± 0.03	2.02 ± 0.04	2.75 ± 0.21	2.61 ± 0.24	2.30 ± 0.36	2.14 ± 0.02
NH <sub>4</sub> <sup>+</sup> -N (g kg <sup>-1</sup> WW)	0.88 ± 0.06	0.88 ± 0.03	0.99 ± 0.03	1.00 ± 0.03	1.00 ± 0.01	0.99 ± 0.01	1.03 ± 0.04	1.00 ± 0.09
NO <sub>2</sub> -N (mg kg <sup>-1</sup> WW)	12.80 ± 0.10	12.80 ± 0.20	14.29 ± 0.30	14.20 ± 0.80	16.77 ± 0.40	17.20 ± 0.60	17.07 ± 0.80	17.00 ± 0.30
NO <sub>3</sub> -N (mg kg <sup>-1</sup> WW)	89.60 ± 4.50	89.60 ± 2.80	158.40 ± 18.00	154.00 ± 3.5	152.88 ± 5.30	163.60 ± 4.60	736.12 ± 54.10	727.50 ± 38.40

DM: dry matter; WW: wet weight. Data represents mean ± Standard Error.

### 3.2. NH<sub>3</sub> and GHG emissions

The results showed that the additive had a strong effect on NH<sub>3</sub> emission in the first week (T4 and T7), with a reduction efficacy of 100% at T4. A mitigation effect was also observed at T26 (Table 2). The mitigation on the NH<sub>3</sub> emissions may be due to the formation of ammonium sulphate and calcium nitrate other than to the reduction of pH. Indeed, in an acidic environment, NH<sub>4</sub><sup>+</sup> and NO<sub>3</sub><sup>-</sup> ions, normally present in the slurry, react with SO<sub>4</sub><sup>2-</sup> and Ca<sup>2+</sup> deriving from the additive (CaSO<sub>4</sub> · 2H<sub>2</sub>O). These results were in line with Lim et al. (2017) and Febrisiantosa et al. (2018) that found a reduction of NH<sub>3</sub> volatilization of 56–69% and 26–59%, respectively, by using flue gas desulphurization gypsum. They attributed this reduction to a lower pH, and to NH<sub>3</sub> absorption affected by the addition of flue gas desulphurization gypsum. In fact, the NH<sub>3</sub> volatilization is favored by an alkaline pH and a high concentration of NH<sub>4</sub><sup>+</sup> in the slurry.

Regarding GHG emissions, the treated samples presented a strong reduction on T4, instead, the control samples had the highest peaks of emissions for all GHG (Table 2). During the trial, there was a fluctuation of the emission fluxes probably due to the increase of microbial activity in the slurry. The ability to reduce GHG emissions after 4 days and the rise of fluxes at the end of the trial period seem to indicate that more than three applications of the additive may be required to achieve maximum results. The CH<sub>4</sub> reduction could be attributed to the increasing SO<sub>4</sub><sup>2-</sup> content of slurry that has a toxic effect on methanogens, thus inhibiting CH<sub>4</sub> production.

The lowering of the pH of slurry obtained and the inhibition of denitrification process, arising from the lower accumulation of NO<sub>3</sub>-N, seems to have favored the reduction of CH<sub>4</sub> and N<sub>2</sub>O emissions in this study. Similar results were found by Hao et al. (2005) and Yang et al. (2015). Instead, regarding only the reduction of N<sub>2</sub>O emission, some authors have found opposite results, with a finding of a slight increment after treatment (Hao et al., 2005; Yang et al., 2015; Li et al., 2018).

Table 2. NH<sub>3</sub> and GHG emission fluxes (g m<sup>-2</sup>·h<sup>-1</sup>).

	T0		T4		T7		T26	
	Control	Treated	Control	Treated	Control	Treated	Control	Treated
NH <sub>3</sub>	1.109 (± 0.047)	1.109 (± 0.118)	0.091 (± 0.065)	0.000 (± 0.001)	0.408 (± 0.032)	0.136 (± 0.026)	1.654 (± 0.034)	0.646 (± 0.049)
N <sub>2</sub> O	0.003 (± 0.002)	0.003 (± 0.002)	0.018 (± 0.010)	0.000 (± 0.001)	0.000 (± 0.001)	0.001 (± 0.001)	0.015 (± 0.004)	0.018 (± 0.002)
CO <sub>2</sub>	28.078 (± 0.999)	28.078 (± 0.947)	603.730 (± 136.191)	465.615 (± 51.591)	74.723 (± 2.485)	69.526 (± 1.552)	92.968 (± 6.629)	104.323 (± 3.053)
CH <sub>4</sub>	0.632 (± 0.027)	0.632 (± 0.031)	109.827 (± 39.258)	86.184 (± 12.185)	8.943 (± 0.537)	9.318 (± 0.212)	10.389 (± 0.871)	12.699 (± 0.693)

### 3.2. Environmental impact

The LCA evaluation showed that the use of calcium sulphate dihydrate could be an interesting option to mitigate NH<sub>3</sub> emission. Since NH<sub>3</sub> emission is the main contributor to TA, TE, ME and PM impact categories, the AS turns out to be the best one. Moreover, environmental benefits can be achieved by avoiding the use and production of synthetic fertilizers resulting in considerable mitigation effects in terms of OD, HTnoc, HT-c, FEx, and MFRD impact categories.

The comparison between the environmental impact of the two scenarios, reported in Table 3, showed that the AS had a higher environmental sustainability than the BS, for CC, PM, POF, TA, TE, and ME impact categories.

Given that CC is deeply affected by CH<sub>4</sub> and N<sub>2</sub>O emissions and that the use of the additive presents a reduction of CH<sub>4</sub> and N<sub>2</sub>O emissions, the AS is the best one for CC impact category.

Considering the other impact categories (OD, HTnoc, HT-c, FE, FEx, MFRD), a worsening of the impact is shown due to the impact related to the production of the 12 g of additive (gypsum extraction, processing, and transport, as well as energy consumption) that are used per FU.

Table 3. Potential environmental impacts for BS and AS.

Impact category	Acronym	Baseline Scenario	Alternative Scenario
Climate change	CC	132.6 kg CO <sub>2</sub> eq	110.1 kg CO <sub>2</sub> eq
Ozone depletion	OD	-5·10 <sup>-10</sup> kg CFC-11 eq	-7.3·10 <sup>-12</sup> kg CFC-11 eq
Human toxicity, non-cancer effects	HTnoc	-1.6·10 <sup>-9</sup> CTUh	-8.3·10 <sup>-10</sup> CTUh
Human toxicity, cancer effects	HT-c	-1.8·10 <sup>-10</sup> CTUh	-1.7·10 <sup>-11</sup> CTUh
Particulate matter	PM	0.062 kg PM <sub>2.5</sub> eq	0.039 kg PM <sub>2.5</sub> eq
Photochemical ozone formation	POF	0.052 kg NMVOC eq	0.043 kg NMVOC eq
Terrestrial acidification	TA	2.785 molc H <sup>+</sup> eq	1.769 molc H <sup>+</sup> eq
Terrestrial eutrophication	TE	12.452 molc N eq	7.911 molc N eq
Freshwater eutrophication	FE	-1·10 <sup>-6</sup> kg P eq	4.95·10 <sup>-8</sup> kg P eq
Marine eutrophication	ME	0.085 kg N eq	0.054 kg N eq
Freshwater ecotoxicity	FEx	-0.039 CTUe	-0.014 CTUe
Mineral, fossil & ren resource depletion	MFRD	-3.3·10 <sup>-7</sup> kg Sb eq	-1.7·10 <sup>-7</sup> kg Sb eq

Figure 2 shows the contributions of the additive on the emissions and the avoided production of mineral fertilizer related to the environmental impact of AS, which is the scenario where the additive is introduced.

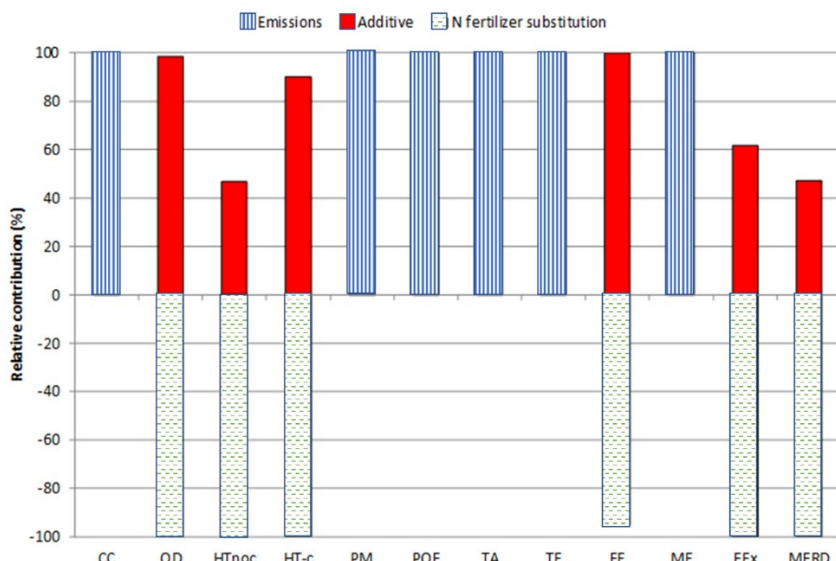


Figure 2. Relative environmental contribution for AS.

Spreading slurry on the field is identified as a credit in both the scenarios (BS and AS) because it involves valorizing the valuable content in N-NH<sub>3</sub> of slurry and avoiding the production of mineral fertilizer. Consequently, slurry spreading brings considerable environmental benefits. In particular, for OD, toxicity related impact categories and MFRD, this credit is much evident and makes even to achieve environmental benefits to the entire studied process. Instead, for the remaining six impact categories, the avoided production of ammonium nitrate is not a key driver of the environmental results.

#### 4. Conclusions

The application of the additive to slurry could be considered as an effective method to mitigate NH<sub>3</sub> and GHG emissions from slurry storage. The use of slurry treated as an organic fertilizer could be advantageous both economically and environmentally, because it avoids the use and the purchase of mineral fertilizer. It represents a beneficial solution for the environment since the NO<sub>3</sub>-N content appears to be lower. This result is also confirmed by LCA analyses since AS has a higher environmental sustainability than BS.

The results of this study are promising. Thus, pilot and large-scale tests are necessary to further investigate the effectiveness and economic feasibility, and this method might be also applicable in other types of slurry management systems.

#### References

- Adviento-Borbe, M.A.A., E.F. Wheeler, N.E. Brown, P.A. Topper, R.E. Graves, V.A. Ishler, G.A. Varga, 2010. Ammonia and Greenhouse Gas Flux from Manure in Freestall Barn with Dairy Cows on Precision Fed Rations. Transactions of the ASABE. 53 (4), 1251–1266. <http://dx.doi.org/10.13031/2013.32590>.
- Bacenetti, J., D. Lovarelli, M. Fiala, 2016. Mechanism of organic fertiliser spreading, choice of fertiliser and crop residue management as solutions for maize environmental impact mitigation. European Journal of Agronomy. 79, 107–118. <http://dx.doi.org/10.1016/j.eja.2016.05.015>.
- Bacenetti, J., A. Fusi, A. Azapagic, 2019. Environmental sustainability of integrating the organic Rankin cycle with anaerobic digestion and combined heat and power generation. Science of the Total Environment. 658, 684–696. <http://dx.doi.org/10.1016/j.scitotenv.2018.12.190>.
- Baldini, C., F. Borgonovo, D. Gardoni, M. Guarino, 2016. Comparison among NH<sub>3</sub> and GHGs emissive patterns from different housing solutions of dairy farms. Atmospheric Environment. 141, 60–66. <http://doi.org/10.1016/j.atmosenv.2016.06.047>.
- EC-JRC - European Commission, J.R.C., Institute for Environment and Sustainability, 2012. Characterisation factors of the ILCD Recommended Life Cycle Impact Assessment methods. Database and Supporting Information. Publications Office of the European Union. 1st edition., Brussels, Belgium.
- Febrisantosa, A., B. Ravindran, H.L. Choi, 2018. The Effect of Co-Additives (Biochar and FGD Gypsum) on Ammonia Volatilization during the Composting of Livestock Waste. Sustainability. 10 (3), 795. <http://doi.org/10.3390-su10030795>.
- Frischknecht, R., H.-J. Althaus, C. Bauer, G. Doka, T. Heck, N. Jungbluth, D. Kellenberger, T. Nemecek, 2007. The Environmental Relevance of Capital Goods in Life Cycle Assessments of Products and Services. International Journal of Life Cycle Assessment. 12. <http://dx.doi.org/10.1065/lca2007.02.309>.
- Gerber, P.J., H. Steinfeld, B. Henderson, A. Mottet, C. Opio, J. Dijkman, A. Falucci, G. Tempio, 2013. *Tackling climate change through livestock: a global assessment of emissions and mitigation opportunities*. Rome, Italy: Food and Agriculture Organization of the United Nations (FAO).
- Guarino, M., C. Fabbri, M. Brambilla, L. Valli, P. Navarotto, 2006. Evaluation of simplified covering systems to reduce gaseous emissions from livestock manure storage. Transactions of the ASABE. 49 (3), 737–747. <http://dx.doi.org/10.13031/2013.20481>.
- Hao, X., F.J. Larney, C. Chang, G.R. Travis, C.K. Nichol, E. Bremer, 2005. The effect of phosphogypsum on greenhouse gas emissions during cattle manure composting. Journal of Environmental Quality. 34 (3), 774–781. <http://dx.doi.org/10.2134/jeq2004.0388>.
- Li, Y., W. Luo, G. Li, K. Wang, X. Gong, 2018. Performance of phosphogypsum and calcium magnesium phosphate fertilizer for nitrogen conservation in pig manure composting. Bioresource Technology. 250, 53–59. <https://doi.org/10.1016/j.biortech.2017.07.172>.
- Lim, S.-S., H.-J. Park, X. Hao, S.-I. Lee, B.-J. Jeon, J.-H. Kwak, W.-J. Choi, 2017. Nitrogen, carbon, and dry matter losses during composting of livestock manure with two bulking agents as affected by co-amendments of phosphogypsum and zeolite. Ecological Engineering. 102, 280–290. <http://dx.doi.org/10.1016/j.ecoleng.2017.02.031>.
- Möller, K., W. Stinner, 2009. Effects of different manuring systems with and without biogas digestion on soil mineral nitrogen content and on gaseous nitrogen losses (ammonia, nitrous oxides). European Journal of Agronomy. 30 (1), 1–16. <http://dx.doi.org/10.1016/j.eja.2008.06.003>.
- Sandars, D., E. Audsley, C. Canete, T. Cumby, I. Scotford, A. Williams, 2003. Environmental benefits of livestock manure management practices and technology by life cycle assessment. Biosystems Engineering. 84 (3), 267–281. [http://dx.doi.org/10.1016/S1537-5110\(02\)00278-7](http://dx.doi.org/10.1016/S1537-5110(02)00278-7).

## Effect of the Installation Location of Weather Station on Sampled Wind Speed

Li Rong <sup>\*</sup>, Guoqiang Zhang

Department of Engineering, Aarhus University, Aarhus 8000, Denmark

\* Corresponding author. Email: [li.rong@eng.au.dk](mailto:li.rong@eng.au.dk)

### Abstract

A desire to decrease the energy consumption of fans, increase the daylighting and maintain the low odor emissions to the atmosphere, a newly developed hybrid ventilation system for confined fattening pig houses has been developed by AgriFarm A/S company in Denmark. The hybrid ventilation system combined the natural and mechanical partial pit ventilation has attracted more attention in Europe especially the countries with temperate climate. Due to the natural ventilation, one of the inputs to the control system was the wind speed and direction measured by a weather station installed on the roof. However, it is not known yet how the install location and surrounding buildings could affect the sampled wind speed and direction. This study used Computational Fluid Dynamics (CFD) to investigate what difference of air speed and direction between the weather station and the defined incoming wind conditions could be. Seven wind incidence angles were defined at the boundary conditions in CFD simulation and the data at three heights above the roof (1,2 and 3 meter) were drawn to be compared. Under the conditions that the openings were all open, the wind incidence angles at the three heights above the roof were in consistent with the incoming wind directions at most of the cases while the wind speed could be largely affected by the location of the weather station. The results could provide guidance for the company to adjust the weight coefficient of wind speed in the control strategy so that the performance of the hybrid ventilation system can be ensured.

**Keywords:** Natural ventilation, fattening pig, wind speed, CFD, control

### 1. Introduction

Natural ventilation combining mechanical ventilation, namely hybrid ventilation system, has been installed in a few large scale commercial pig production buildings, which was developed by AgriFarm A/S (Rong et al., 2015, 2017). Because natural ventilation is highly dependent on the outdoor climate, it is important to develop a sophisticated control strategy to provide proper indoor thermal environment as well as indoor air quality. To develop such a control strategy, it is imperative to investigate how outdoor climate influences the indoor thermal environment together with the opening regulations.

Before constructing a full-scale commercial building to test the performance of hybrid ventilation system, Computational Fluid Dynamics (CFD) has been used to simulate the air speed, temperature and contaminant distribution under various wind speeds, wind directions and opening regulations. The results obtained from CFD simulations are used as part of references to develop the control strategy. To conduct such simulations, wind profile at inlets is needed. Normally the wind profile developed by Richard and Hoxey (1993) is adopted, where reference wind speed at the reference height is required. In simulations, the wind profile is normally imposed at the inlet being five times of the building height away from the building. In reality, this is not practical to install a weather station so far away from the pig building to give inputs to the control system. It is normally installed above the ridge (one or two meters higher). If the wind speed and wind direction measured by the weather station installed on the ridge is very different from the defined wind profile at the same height while the system operate as it was defined based on the CFD simulations with the defined wind profile, then it brings the over- or under-regulations of the system. As to the authors' knowledge, the effect of the installation of the weather station on the sampled wind speed and direction has not been investigated by other researchers.

In addition, there are surrounding buildings on the site of pig production farms. The effects of

surrounding buildings on the performance of a ventilation system has been investigated by researchers. Wiren (1987) investigated the effects of surrounding buildings on wind pressure distribution and ventilation losses for single family house. Lopez et al. (2011) studied the effect of surrounding buildings on air flow patterns and turbulence in two greenhouses with natural ventilation. It is recognized that the surrounding buildings could influence the wind distribution around the naturally ventilated buildings. In this study, a surrounding building was added according to the site where a commercial pig building installed hybrid ventilation and the building configuration designed by AgriFarm was constructed in Lystrup Denmark.

Therefore the objectives of this paper are to: (1) investigate the effect of installation location of weather station on the wind speed and direction (three height levels were examined) and (2) study the impact of surrounding buildings on the wind speed at the location where the weather station could be installed.

## 2. Materials and Methods

Commercial software Star CCM+ was used for CFD modelling. Currently, validation of CFD modelling is imperative. In this study, a wind tunnel test conducted by Leibniz Institute for Agricultural Engineering and Bioeconomy (ATB) in Germany was used for the validation of CFD modelling. Dimensions of geometry model used in cases for investigations were scaled in 1:100 from a designed pig house installed with hybrid ventilation system provided by AgriFarm A/S in Denmark. These geometry models were introduced in sub-section 2.1.

### 2.1. Geometry models and wind tunnel test

The experimental test was conducted in the Atmospheric Boundary Layer wind tunnel with dimensions of length in 28.5 m, width in 3.0 m and height in 2.0 m at Leibniz Institute for Agricultural Engineering and Bioeconomy. A scaled model of a naturally ventilated dairy barn situated in Northeast Germany with ratio of 1:100 was used in the wind tunnel test. Figure 1 presents the scaled model located in the wind tunnel including a photo to present the physical model and a graph to illustrate the geometry model used in CFD simulation. The dimensions of the scaled model was 961 mm × 342 mm × 114 mm (L × W × H). The scaled model had pitched roof with the eave height in 44 mm. There was an opening with height in 4 mm on the ridge. Air velocities were measured at seven lines and named as X=-100, X=50, X=100, X=165, X=242, X=292 and X=392 mm seen in Figure 1 (c).

Figure 2 showed the geometry models for CFD simulations to investigate the locations of weather station and surrounding buildings on the sampled wind speed and direction. The dimensions of the pig barn model were scaled (1:100) from a commercial pig production house designed by AgriFarm A/S with the length in 50.0 m, width in 22.0 m and height in 10.2 m. Figure 2(a) presented the geometry model of a genetic building with wind angle of 0°. There were four rows of window openings on each side of the building, two rows were on the sidewall, one row was on the roof and one row was on the ridge. More detailed information of the building configuration and windows' arrangement can be found in Rong et al. (2015, 2017).

Figure 2(b) showed the geometry model of a genetic building with a surrounding building and wind angle of 15°. The dimensions of the surrounding building were 11.0 m in length, 20.0 m in width and 6.2 m in ridge height. The surrounding building was 11.0 m away in spanwise direction and 35.0 m away in streamwise direction from the pig barn. The dimensions and location of the surrounding building was based on a commercial pig production barn in Lystrup of Denmark. In CFD simulations, the wind directions changed from 0° and 90° with an interval of 15°. The dimensions of the computational domain varied with the wind incidence angles based on the suggestions of the Best practice guidelines by Franke et al. (2007). They suggested that the distance from inlet to the building was five times of the building height, the lateral distance to the building on both sides were also five times of the building height and the distance from the closest building surface to the outlet was 15 times of the building height.

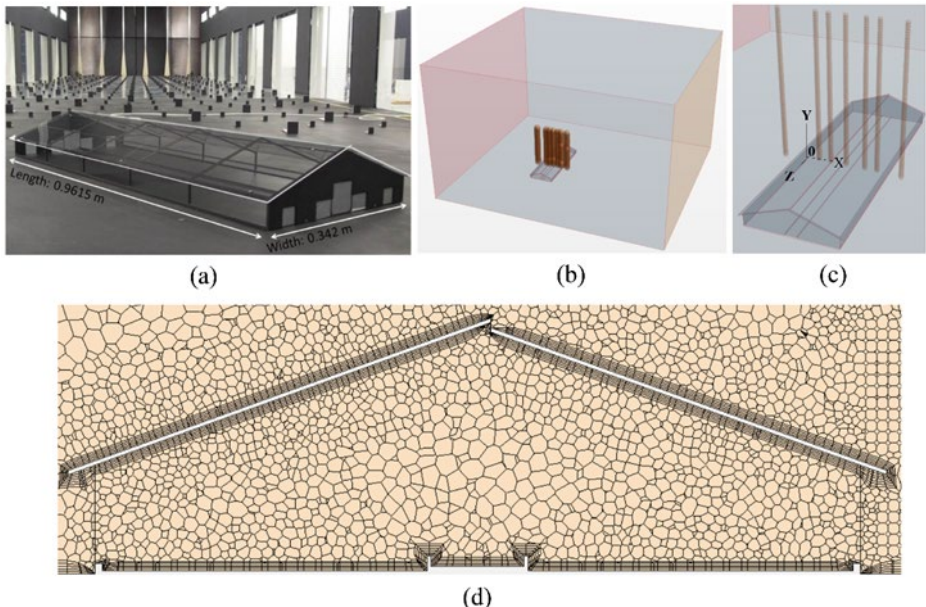


Figure 1. Graphs and schematic configuration of the scaled model (1:100) used in wind tunnel test and mesh resolution. (a) photo of scaled model situated in the wind tunnel (from Dr. David Janke at ATB), (b) computational domain, (c) measured lines with air speed associated with the scaled model and (d) mesh resolution for CFD simulation.

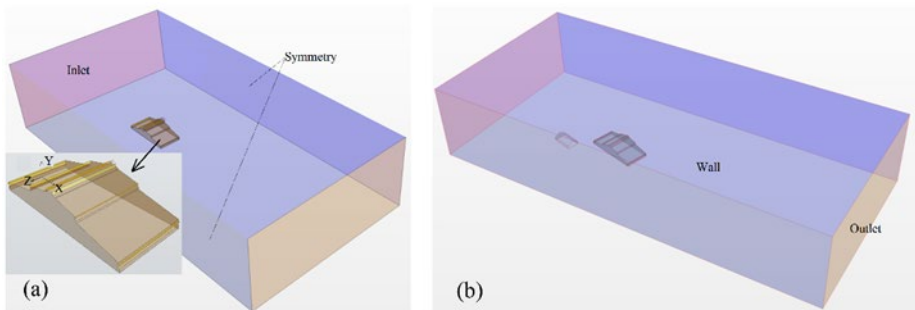


Figure 2. Geometry sketches of CFD modelling, (a) generic building with wind angle of 0° and (b) generic building with surrounding building and wind angle of 15°.

## 2.2. CFD modelling

### 2.2.1. Turbulence modelling method

In Star CCM+, realizable  $k - \varepsilon$  model was used and two-layer  $y^+$  wall function was adopted. Second order scheme was used to discretize the convection term of differential partial equations. The convergence criteria was set as  $10^{-4}$  for all residuals and a few points of velocity magnitude were monitors. The polyhedran and prism layer mesher was applied to generate the mesh. A few prism layers were added to the near wall area to catch the boundary layer and the total nodes of mesh was around 3.4 million. The mesh resolutions and modelling setting followed the Best guideline of CFD modeling outer flow by Franke et al. (2007).

### 2.2.2. Boundary conditions

The boundary conditions were shown in Figure 2. The walls of the building were defined as wall boundaries with no-slip conditions. The outlet was defined as pressure outlet with 0.0 Pa. The surfaces of sides and top of the computational domain were defined as Symmetry. At inlet, the profiles for wind speed and dissipation of turbulent kinetic energy were given as stated by Richards and Hoxey (1993):

$$U = \frac{u_*}{k} \ln \left( \frac{y+y_0}{y_0} \right) \quad (1)$$

$$K = \frac{u_*^2}{\sqrt{C_\mu}} \quad (2)$$

$$\varepsilon = \frac{u_*^3}{k(y+y_0)} \quad (3)$$

$$u_* = \frac{k U_{ref}}{\ln[(y_{ref}+y_0)/y_0]} \quad (4)$$

where  $u_*$  is the friction velocity,  $\text{m s}^{-1}$ ;  $U_{ref}$  is the reference velocity defined at a reference height (in simulations the reference height was 10.0 cm corresponding to 10.0 m in full scale modelling where the wind speed is  $5.0 \text{ m s}^{-1}$ . In wind tunnel, the profile in Figure 3 was adopted),  $\text{m s}^{-1}$ ;  $k$  is the von Karman Constant, 0.42;  $y$  is the height along the vertical coordinate in the computational domain,  $\text{m}$ ;  $y_0$  is the terrain roughness length, defined as 0.03m, a typical average value for a countryside area with grassland based on Wieringa (1998). The profiles of wind speed and turbulence intensity for CFD validation were defined based on the measured data in wind tunnel tests and shown in Figure 3.

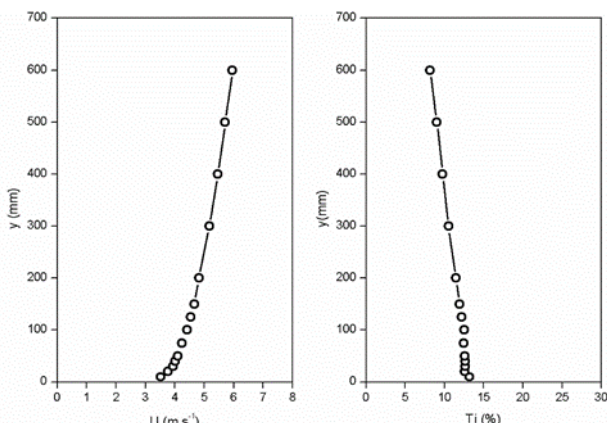


Figure 3. Streamwise wind speed and turbulence intensity profiles adopted in wind tunnel test.

## 3. Results and Discussion

### 3.1. Validation of CFD modelling

Figure 4 showed the distribution of velocity vectors and pressure at the central plane across the scaled barn. Due to the large openings on both sides, a cross flow was formed with air speed decayed from around  $4.0 \text{ m s}^{-1}$  to  $2.9 \text{ m s}^{-1}$ . A large recirculation zone was developed below the roof in the scaled barn. A recirculation region was observed in backward facing step flow with relatively lower pressure. Outside the scaled dairy barn, the wind was attached to the roof on the windward and separated from the ridge and a large vortex was produced along the leeward roof with lower pressure distribution. These phenomena seemed logical. In order to validate the CFD modelling, experimental data of air speeds were compared with the simulation results in Figure 5 with measured lines located at the wind upward, in the scaled barn and leeward.

Outside of the scaled model, a good agreement between simulated and measured results was achieved for all the measured points when the heights of the measured points were larger than 114 mm, the height of the scaled model. The good agreement was also obtained for the points below the barn height when the lines were situated either upwind or downwind. Inside the scaled model, a reasonable agreement was seen at line of  $X=50$  mm. Discrepancies were noticed at the points in the area where air speed changed from the maximum value to a smaller one at the lines of  $X=100$ ,  $X=165$ ,  $X=242$  and  $X=292$  mm. Based on the comparison, it was deemed that the present CFD modelling could provide reasonable predictions for this type of flow.

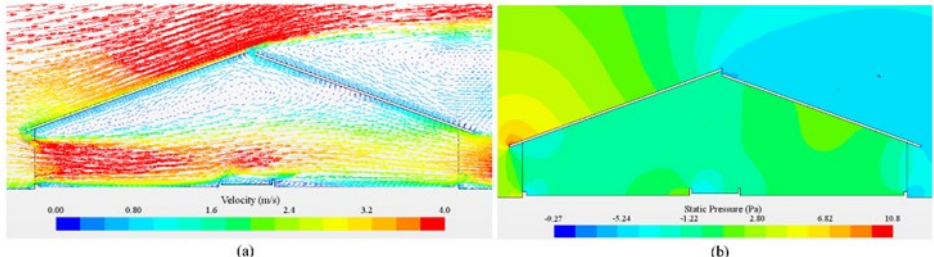


Figure 4. Vector and pressure distribution at the central plane across the scaled dairy barn tested in the wind tunnel, (a) vector and (b) pressure.

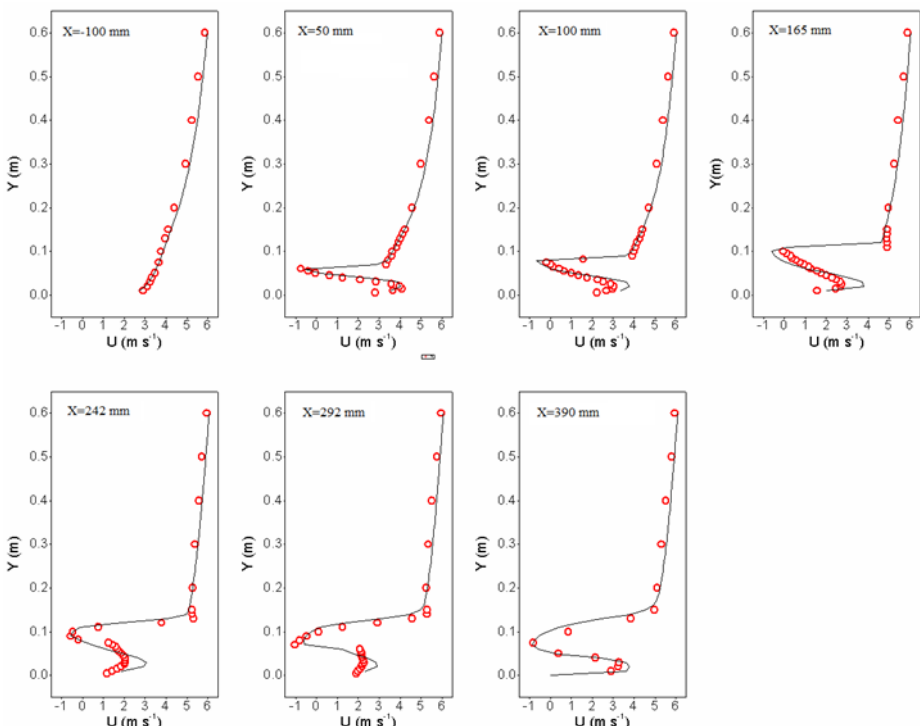


Figure 5. Comparison of streamwise velocity component  $U$  between simulated and measured results.

3.2. Wind speed and angle variations along the width of pig house for cases without surroundings  
Figure 6 and Figure 7 presented the wind speed and wind angle at three heights of 11.2, 12.2

and 13.2 cm (corresponding to 11.2, 12.2 and 13.2 m in full-scale pig house) under the condition of reference wind speed of  $5.0 \text{ m s}^{-1}$  at the reference height of 10.0 cm (10.0 m in full scale). When the wind angle was  $\leq 45.0^\circ$ , the wind speeds at the height of 12.2 and 13.2 cm obtained from simulations were comparable to the value of the same height defined by the wind profile. As the wind angle was  $75^\circ$  and  $90^\circ$ , the wind speeds at the locations of windward ( $Z > 0.0$ ) were still comparable to the reference wind speed while on the leeward they were noticeably lower than the wind speed at the same height of the defined wind profile. When the wind angle was  $> 30^\circ$ , the wind angles at height of 13.2 cm were representative of the incoming wind angle as shown in Figure 7.

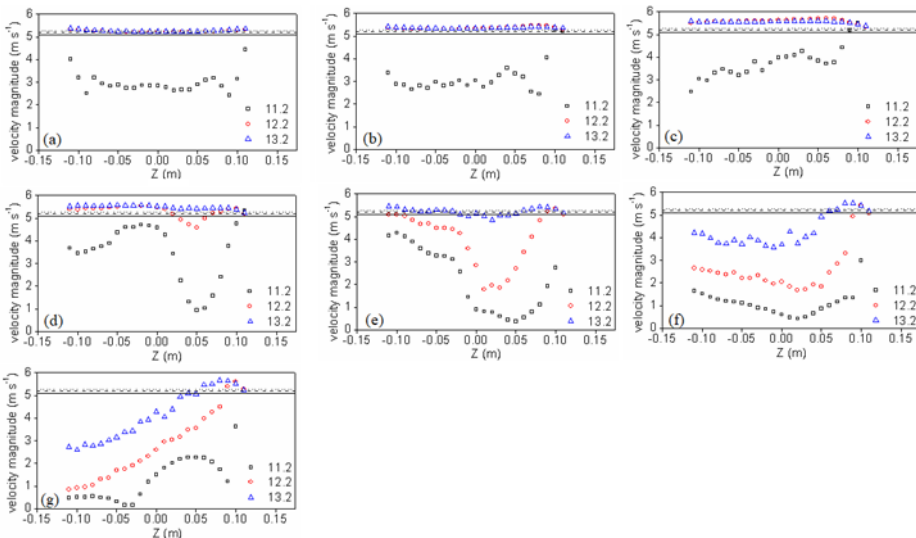


Figure 6. Wind speeds distribution along the width ( $Z$  direction shown in Figure 2a) of the pig house at three heights. Solid line, dash line and dotted line represents the wind speed at 11.2 cm, 12.2 cm and 13.2 cm in height of the defined wind profile. (a) wind angle of  $0.0^\circ$ , (b) wind angle of  $15.0^\circ$ , (c) wind angle of  $30.0^\circ$ , (d) wind angle of  $45^\circ$ , (e) wind angle of  $60^\circ$ , (f) wind angle of  $75^\circ$  and (g) wind angle of  $90^\circ$ .

### 3.3. Wind speed distribution along the width of pig house for cases with surrounding buildings

Figure 8 showed the wind speeds along the lines at heights of 11.2, 12.2 and 13.2 cm under wind angles between  $0^\circ$  and  $90^\circ$ . Comparing to Figure 6, slightly larger wind speeds were noticed at some points of 11.2 cm in height. Similarly, the wind speeds were comparable to the value at the same height of the defined wind profile with height of 12.2 and 13.2 cm when the wind angle was lower than  $60^\circ$ . Otherwise, the wind speeds at most of the places (especially at the leeward side) were lower than the value at the same height of the defined incoming wind profile. The height of the surrounding building in the windward was 6.2 m which was 4.0 m lower than the pig house at the ridge. The simulated results showed that the surrounding buildings hardly affected the wind speed if the weather station could be installed two meters above the ridge or higher. The results presented in Figure 6-8 showed that the weather station which is used to sample the wind speed as an input for the control system should be installed 3.0 m above the ridge at least and is suggested to be installed at the windward of the dominant wind direction to ensure the sampled wind speed can be comparable to the reference wind speed defined by the wind profile.

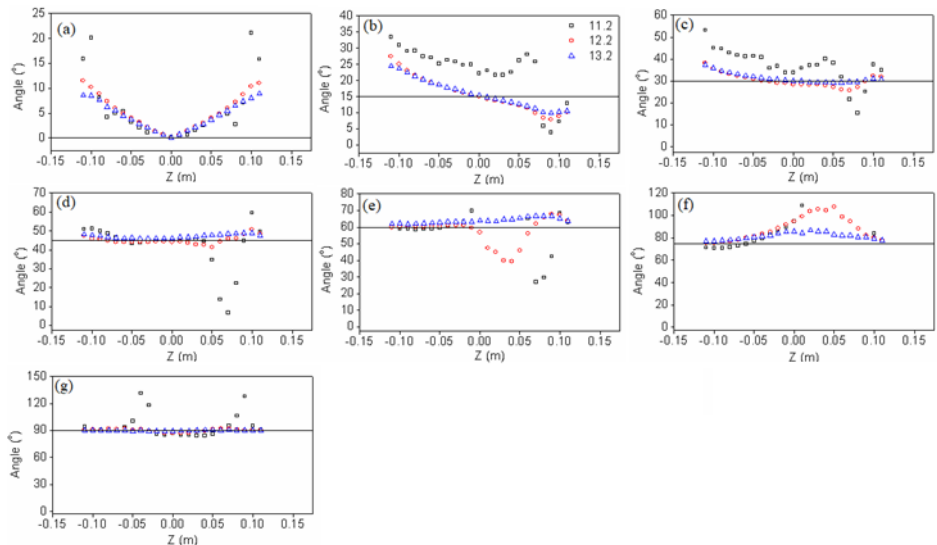


Figure 7. Variation of wind angles along the width (Z direction shown in Figure 2a) of the pig house at three heights. Solid line is the wind angle between the wind velocity and the normal direction of the openings. (a) wind angle of  $0.0^\circ$ , (b) wind angle of  $15.0^\circ$ , (c) wind angle of  $30.0^\circ$ , (d) wind angle of  $45.0^\circ$ , (e) wind angle of  $60.0^\circ$ , (f) wind angle of  $75.0^\circ$  and (g) wind angle of  $90.0^\circ$ .

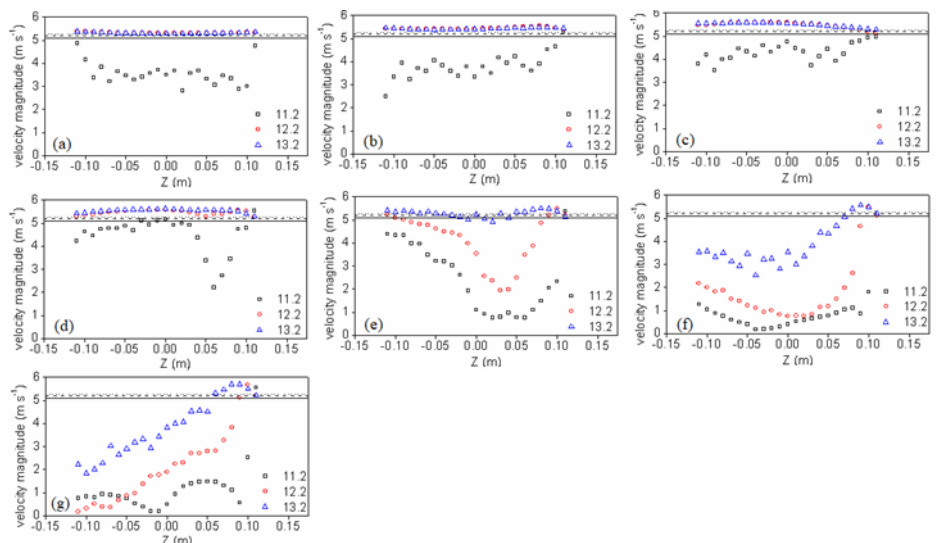


Figure 8. Wind speeds distribution along the width (Z direction shown in Figure 2a) of the pig house at three heights under cases with surrounding buildings shown in Figure 2b. Solid line is the wind speed at 11.2 cm in height, dash line is the wind speed at 12.2 cm in height and dotted line is the wind speed at 13.2 cm in height of the defined wind profile. (a) wind angle of  $0.0^\circ$ , (b) wind angle of  $15.0^\circ$ , (c) wind angle of  $30.0^\circ$ , (d) wind angle of  $45.0^\circ$ , (e) wind angle of  $60.0^\circ$ , (f) wind angle of  $75.0^\circ$  and (g) wind angle of  $90.0^\circ$ .

#### 4. Conclusions

The location of installing the weather station could affect the sampled wind speed in the studied geometry configuration of the pig building. The weather station to measure the wind speed should be installed at least three meters above the ridge so that the measured wind speed can be comparable to the one calculated by the defined wind profile. The effect of surrounding buildings could hardly affect the wind speed since the height of the surrounding buildings was normally lower than the height of the pig house with the current geometry configuration.

#### Acknowledgements

This work was supported by project ‘Green Precision Ventilation for Future Livestock Housing (GreenLiv)’ granted by GUDP in Denmark.

#### References

- Franke, J., A. Hellsten, H. Schlunzen, B. Carissimo, 2007. Best practice guideline for the CFD simulation of flows in the urban environment. Cost Action 732 Quality Assurance and Improvement of Microscale Meteorological Models. Hamburg University of Hamburg Meteorological Institute.
- López, A., D.L. Valera, F.D. Molina-Aiz, A. Peña, 2011. Effects of surrounding buildings on air patterns and turbulence in two naturally ventilated mediterranean greenhouses using tri-sonic anemometry. Transactions of the ASABE. 54 (5), 1941–1950.
- Richards, P.J., R.P. Hoxey, 1993. Appropriate boundary conditions for computational wind engineering models using the k- $\epsilon$  turbulence model. In: *Computational Wind Engineering I*. Oxford: Elsevier. Ed., Murakami, S. 145–153.
- Rong, L., E.F. Pedersen, G.Q. Zhang, 2015. Application of hybrid ventilation system in a pig house – study of winter case. 14th Conference of International Buildig Performance Simulation Association Hyderabad, India.
- Rong, L., E.F. Pedersen, G.Q. Zhang, 2017. Numerical Simulations on a Hybrid Ventilation System at a Confined Pig Building in Denmark – Summer Case Studies. In: Ni, J.Q., T. Lim, C.Y. Wang, L.Y. Zhao Eds. *2017 International Symposium on Animal Environment and Welfare*, China Agriculture Press, Tuoxin Ruier Hotel, Chongqing, China.
- Wieringa, J., 1998. How far can agrometeorological station observations be considered representative? In: *Prepr. 23rd Am. Meteor. Soc. Conf. on Agricultural and Forest Meteorology*, Albuquerque JI.5. 9–12.
- Wiren, B.G., 1987. Effects of surrounding buildings on wind pressure distributions and ventilation losses for single-family houses. Part 2. 2-storey terrace houses.

# Water Footprint Assessment of Eggs in a Parent-Stock Layer Breeder Farm

**Haohan Xing<sup>a</sup>, Baoming Li<sup>a,b,\*</sup>, Weichao Zheng<sup>a,b</sup>, Zhidan Liu<sup>a,b</sup>, Yuanhui Zhang<sup>a,b,c</sup>**

<sup>a</sup> Laboratory of Environment-Enhancing Energy (E2E) and Key Lab of Agricultural Engineering in Structure and Environment, Ministry of Agriculture and Rural Affairs, Beijing 100083, P.R. China

<sup>b</sup> Beijing Engineering Research Center for Livestock and Poultry Healthy Environment, Beijing 100083, P.R. China

<sup>c</sup> Department of Agricultural and Biological Engineering, University of Illinois at Urbana-Champaign, Urbana, IL 61801, USA

\* Corresponding author. Email: [libm@cau.edu.cn](mailto:libm@cau.edu.cn)

## Abstract

The egg production and consumption of egg in China account for about 40% of the global, which make significant demand for the water resource. The shortage of water resources in China make its egg production face great water challenges. However, there are little studies concerning the water use of egg production. In this study, water footprint network (WFN) methodology was applied to analyze the water footprint (WF) of intensive egg production using a typical parent-stock layer breeder farm in North China as a model, which raises 210,000 layer breeders and produces about 2653.27 t eggs per year. The feed and water consumption of 353 days was collected for analysis and the water footprint of chicken eggs was estimated at the farm level. The result shows that 1) the WF of eggs (water volume/egg weight) ranged from 3.123 to 3.461 m<sup>3</sup> t<sup>-1</sup> weight at the farm level, of which the green WF ranged from 2.003 to 2.220 m<sup>3</sup> t<sup>-1</sup>, and the blue WF was 0.610 to 0.676 m<sup>3</sup> t<sup>-1</sup> and the grey WF was 0.510 to 0.565 m<sup>3</sup> t<sup>-1</sup>; 2) the indirect WF generated by feed contributed over 99.8%; 3) the studied layer breeder farm in China had a high WF than the global average from the literature' results. In this paper, the variation of WF was also analyzed and some advice on the water management for the layer farms in China was provided.

**Keywords:** Water footprint; egg; laying hen; green water.

## 1. Introduction

The constant growth of the world's population has led to rising demand for food. The biggest challenge facing the world today is to ensure the sustainable use of natural resources while ensuring people's growing food needs. Food production has caused significant consumption and waste of limited freshwater (de Vries and de Boer, 2010; Notarnicola et al., 2012; Steinfeld et al., 2015), and this situation will continue in the future. Large amounts of freshwater are consumed to produce enough animal products for people every day. Given the great water scarcity in China, too much water is still wasted in animal production. Producing animal products with less water is one of the most important challenges for governments, producers and public.

The water footprint (WF) is a comprehensive indicator of freshwater resources appropriation, next to the traditional and restricted measure of water withdrawal. And the WF of a product is the volume of freshwater used to produce the product, measured over the full supply chain (Hoekstra et al., 2011). The WF of animal products has received much attention in recent years due to water assessment of the value chain of animal production, which concentrates on water saving. It has become clear that livestock and poultry products also significantly contributes to human's WF, water degradation and water scarcity (Hoekstra, 2014). The main way to decrease the WF of animal products is to reduce the fraction of animal products in our diet. Vanham (Vanham et al., 2016) analyses different diets of Mediterranean cities and the results show that the amount of water can be saved by shifting to a healthy diet which includes fewer animal products. However, it's difficult to persuade people to shift their eating habits. More progress should be made to save water at the farm level. The farm needs to increase on-farm water use efficiency because of limited water resources. And more reasonable and scientific ways for reducing the WF of the egg need to

be studied.

The laying hen sector in China is the largest contributor, accounting for 29.2%, to global egg production(FAO., 2013), which consumes a large amount of water. The information of how much water is consumed to produce per ton of egg in China which should be estimated and given to public and water resource managers is still limited. Although the production chain is water-intensive, as a result, it has practices and programs for improving water efficiency(Palhares and Pezzopane, 2015).

The aim of this study was to assess the WF of eggs which laid by Hy-line Brown and Hy-line Sonia in a typical parent-stock layer breeder farm in North China as a model, and identified the components that have the greatest water use in terms of green, blue and grey water. In addition, the differences in the WF on Hy-line Brown and Hy-line Sonia were analyzed. These were done following a WF method compliant with the Water Footprint Network.

## 2. Materials and Methods

### 2.1. The information of the farm

#### 2.1.1. Objectives and functional unit definition

In this study, WFN methodology was used as a tool with the objectives of accounting and assessing the WF of Chinese eggs in the parent generation. The functional unit was egg production from July 2nd, 2017 to June 19th, 2018 (44,221,169 eggs).

#### 2.1.2. System description and boundaries

The analysis was conducted from a life cycle perspective, including green, blue and grey WF of the most relevant processes in the production chain of eggs, from feed production to animal production (Figure 1). Some processes associated with egg production, such as constructing infrastructures and transportation of feed and chickens, contribute very little to the total WF, which justifies excluding them from the study.

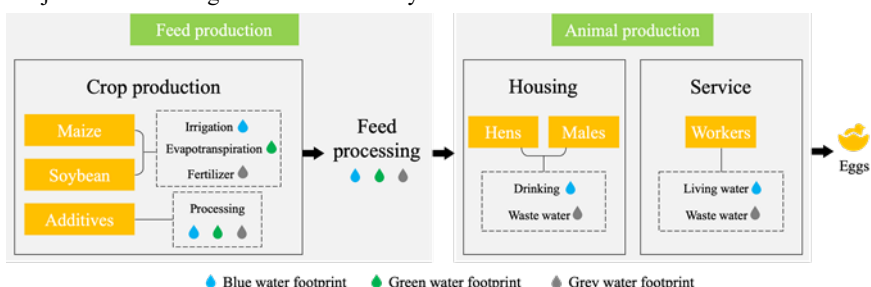


Figure 1. System boundaries and WF components of the egg production.

The laying hen farm involved in this research is located in Handan County, Hebei province, China. There are three areas on the farm which are living, production, and waste treatment areas. And 222,629 chickens were raised in 7 houses in the production area, includes 195,466 laying hens and 27,163 males. Because the volume of wastewater is not monitored in this farm and the data cannot be obtained.

Hy-line brown and Hy-line Sonia chickens are employed on this farm. Hy-line brown was employed in house A, house B and house C. Hy-line Sonia was employed in house D, house E, house F and house G. All the chickens are the same age and exploited at the same day. The laying period of chicken in seven houses is 110 to 461 day old, 108 to 459 day old, 106 to 457 day old, 103 to 454 day old, 98 to 449 day old, 91 to 442 day old, and 85 to 436 day old, respectively. After their productive life, all chicken is exhausted and sold for meat production. Automatic feed delivery systems are provided for commercial fodder for chicken. Drinking water is available form nipple drinker. Eggs are collected daily by automatic belts and moved to the egg-sorting

room where they are packaged in trays and boxes. Manure is moved to the end of each house via automatic manure belts under the cages.

## 2.2. The water footprint network methodology

The WF of the egg was estimated following the calculation framework developed by Mekonnen and Hoekstra (Mekonnen and Hoekstra, 2012). The WF of animal product is the total water use during the process of production, including WF of feed, drink and service, and is calculated as follows:

$$WF = WF_{feed} + WF_{drink} + WF_{serv} \quad (1)$$

where  $WF_{feed}$ ,  $WF_{drink}$  and  $WF_{serv}$  represent the WF of feed, drinking water and service water consumption of an animal, respectively. Service water includes water used to clean the chicken houses and sustain the living area.

The WF of feed consumed consists of the WF of all feed ingredients and the water used to mix the feed:

$$WF_{feed} = \frac{\sum_{p=1}^n (Feed_p \times WF_{prod}) + WF_{mixing}}{Pop} \quad (2)$$

where  $Feed_p$  represents the amount of feed ingredient p consumed by chickens during the period of egg production ( $ty^{-1}$ ),  $WF_{prod}$  the WF of ingredient p ( $m^3 t^{-1}$ ),  $WF_{mixing}$  the water use for mixing the feed for chickens ( $m^3 y^{-1} animal^{-1}$ ) and  $Pop$  the number of egg-producing chickens in a year. In this study, feed does not need to be mixed.

The calculation of  $WF_{drink}$  and  $WF_{serv}$  as follow:

$$WF_{prod}[o] = \frac{\sum_{s=1}^k WF_{proc}}{P} \quad (3)$$

where  $WF_{proc}$  is the process WF of drink or service ( $ty^{-1}$ ) and P the production weight of egg ( $ty^{-1}$ ).

## 2.3. Data collection

In this study, the data needed for analysis are as follows: basic data of the farm, feed intake, egg production, drink water and other water consumption.

### 2.3.1. Basic data of the farm

Basic data of the farm was based on process data from bookkeeping data and dialogue with property managers. Additionally, some information was obtained from published papers. Table 1 shows basic data for the farm.

Table 1. Basic data of the farm.

	Hen number	Male number	Beginning day old (day)	Egg production
A	Hy-line	27,900	3890	6,767,230
B	Brown	27,900	3811	6,459,150
C		20,705	3156	6,302,051
D		27,920	3957	6,141,363
E	Hy-line	27,907	3845	6,189,844
F	Sonia	22,875	3016	6,306,205
G		27,979	3802	6,055,326

### 2.3.2. Feed intake

WF coming from the feed is a major part of the total WF of animal products. Amount of water consumed by growing feed crops and the feed is a source of green water. Therefore, it is necessary

to estimate the WF of the feed. The data of feed intake was obtained from bookkeeping data. The components of feed are maize, soybean and some additives (Table 2). The major WF is from maize and soybean. Maize is produced in the east-northern region of China (Jilin province). The data of WF (blue, green and grey WF) of maize is obtained from a published paper (Duan et al., 2016), which assessed the WF of maize planted in Jilin province of China. And WF of soybean was taken from literature which estimated the green, blue and grey WF of crop products (Mekonnen and Hoekstra, 2011). The data of additives cannot be obtained, including some nutrients such as salt, sodium bicarbonate, etc., which is not considered.

Table 2. Composition of the commercial feed.

Component	% (w w <sup>-1</sup> )
Maize	62
Soybean	24.8
Additives	13.2

### 2.3.3. Egg production

Production quantity of animal product is the key part of estimate the WF of animal product. The egg production difference between Hy-line Brown and Hy-line Sonia is non-ignorable. Since the farm only could provide the quantity of egg production, the average weight of an egg laid by Hy-line Brown (Brown, 2016) was assumed 61.5 g and the Hy-line Sonia (Sonia, 2016) was 60.1 g in this paper.

### 2.3.4. Water consumption

Water consumption of the farm includes water use of production area and living area. Chicken drinking and cleaning processes are in the production area, and daily water use of workers is in the living area. Each house has only one water meter, drinking water, and cleaning water were put together into the data which counted into water use of the production area.

## 3. Results and Discussion

### 3.1. Water footprint of eggs from seven houses

As mentioned previously, the aim of the study was to assess the WF of eggs at farm level in China, and compare the WF of eggs laid by two chicken species. According to Mekonnen and Hoekstra (Mekonnen and Hoekstra, 2012), the WF of eggs is lower than other main animal products like pork, sheep meat and beef. In our study, the WF of eggs was estimated using the WF network method, a WF assessment modeling framework developed by Hoekstra (Hoekstra et al., 2011). Table 3 shows the results which are estimated using the WFN method.

Table 3. Water footprints of seven chicken houses (m<sup>3</sup> t<sup>-1</sup>).

		Green WF	Blue WF	Grey WF	Total WF
A	Hy-line	2.003	0.610	0.510	3.123
B	Brown	2.011	0.613	0.512	3.136
C		2.089	0.636	0.532	3.257
D		2.135	0.650	0.543	3.329
E	Hy-line	2.148	0.654	0.547	3.349
F	Sonia	2.156	0.657	0.549	3.362
G		2.220	0.676	0.565	3.461

The WF of eggs increases slightly from chicken house A (3.123 m<sup>3</sup> t<sup>-1</sup>) to chicken house G (3.461 m<sup>3</sup> t<sup>-1</sup>), which can be partly explained from the different consumption of the feed. Green WF accounts for the largest percentage of total WF which is consistent with other studies (de Miguel et al., 2015; Bai et al., 2018; Noya et al., 2018; Ibidhi and Ben Salem, 2019). Eggs laid by Hy-line Brown have lower WF than that from Hy-line Sonia on average. This is not the only factor that can explain the differences. The more important factor is the egg production of two species

of chickens. The egg production of Hy-line Brown is higher than Hy-line Sonia.

This study highlighted the water use of egg production of two species of chicken at the farm level in China identified based on WFN method. Results of this study can be compared with results from the previous study. The first estimates made by Chapagain and Hoekstra (Chapagain and Hoekstra, 2004) for the WF of the egg is very close to our results, but partly quite different. As its study did not estimate the grey WF component, the green and blue WF have been compared. They report a world average WF of eggs of  $3.340 \text{ m}^3 \text{ t}^{-1}$ , which is higher than our average estimate of  $2.751 \text{ m}^3 \text{ t}^{-1}$ . On the country level, they report a WF of  $3550 \text{ m}^3 \text{ t}^{-1}$  in China, which is also higher than our results. The data in this study comes from field research, while the former's research data comes from FAOSTAT, and the data varies greatly. In recent years, China has made progress in water conservation and reduced the WF. However, in the developed countries, such as the USA, Netherlands and Japan, the WF of eggs is  $1510 \text{ m}^3 \text{ t}^{-1}$ ,  $1404 \text{ m}^3 \text{ t}^{-1}$  and  $1884 \text{ m}^3 \text{ t}^{-1}$ , respectively. And the data is much lower than our estimate. Therefore, China made progress on saving water, but still had a big gap with developed countries.

When compared with previous study (Mekonnen and Hoekstra, 2012), more differences were found (Figure 2). The study of WF of animal products is a comprehensive publication with estimates of the WF of livestock and poultry products with specifications by some major countries in the world, such as China, India, USA, Netherlands and global average. Its major data source in the study is collected from FAOSTAT, and it's quite different from our data source. Different data sources make the composition of the water footprint different. It was found that green water footprint accounting for the largest percentage of total water footprint, and was higher than that of Netherlands and USA. It indicated that the ratio of feed used in the farm is unreasonable, there was waste of feed in the eating process of the chickens, and the feed conversion efficiency is lower than other countries. The percentage of blue WF is higher than in other countries, which indicates the irrational consumption of water is the main factor. In our research, blue water accounted for a large proportion, indicated that amount of water was consumed in irrigation in China, agricultural water use efficiency was low, and more water resources was wasted in the breeding process. In terms of grey WF, our estimates are higher than the Netherlands, USA and global average. It showed that too much fertilizer is used in the crop growing and make grey WF higher indirectly.

Chicken breeding is dependent on water resource and the selection of farm location is significant for minimizing the water scarcity. The WF of eggs is mostly determined by the feed distributed to the laying hens. In the north of China, under the context of climate change and water scarcity, growing feed crop is intense the stress of water resource. Laying hens eating concentrate feed in the industrial system. In general, concentrate feed has relatively large blue and grey WFs (Mekonnen and Hoekstra, 2012). Therefore, an increase in the consumption of eggs would put more pressure on the water resource of China.

There are differences in the water footprint of eggs produced by Hy-line Brown and Hy-line Sonia. Because of the lower egg production, the WF of eggs laid by Hy-line Sonia is higher than Hy-line brown. High dead rates and easy to get a stressed result in the low egg production of Hy-line Sonia. It's necessary to immune, and laying hens get stressed or even dead in this process that reduces the egg production. Different day old of entry results in a different time for laying eggs. Hy-line Sonia is younger than Hy-line Brown's day old, so Hy-line Sonia's laying time is later. Due to the same culling time of all chickens, Hy-line Sonia produced less egg production than Hy-line Brown during the same period of time, which made Hy-line Sonia's egg WF higher.

For future research related to the WF of poultry product in China, the following aspects should be considered. First, egg producers should pay more attention to the WF of eggs in China, and clarify and refine the other impact factors of it. Second, basic databases of the WF of livestock and poultry products in China need to be further estimated and assessed. Finally, more attention should be paid to the grey water of the farm, and dispose of wastewater properly is an efficient way to reduce the WF of livestock and poultry products.

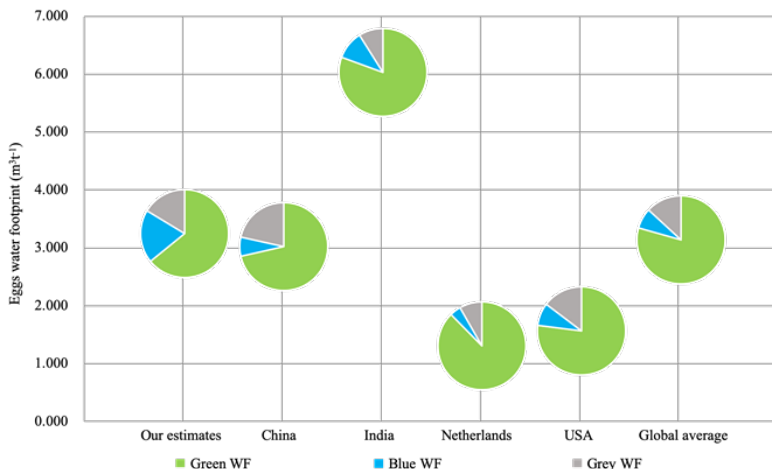


Figure 2. Comparison of our estimates of average WF of eggs at farm level and Mekonnen and Hoekstra (2012) at country level.

#### 4. Conclusions

In view of water scarcity is being exacerbated in China, and there is an increasing interest in WF in different agriculture sectors. The WF of animal products, like eggs, from different chicken varieties in parent generation, is not well documented at the farm level. This study firstly assessed the WF of Chinese egg production system using farm-specific data. It shows that an average of 3,326m<sup>3</sup> of water is required to produce one ton of eggs in a parent-stock. The vast majority of the WF of eggs came from an indirect WF, which was mainly caused by the cultivation of feed crops. The WF of feed represents 99.8% of the total volumetric WF of intensive egg production of the farm. In addition, the green WF accounts for over 64.1%. It illustrated that the value chain of feed could reduce water consumption in the full life cycle of egg production. The WF assessment of egg production varied across chicken varieties, which the eggs laid by Hy-line Sonia had the higher WF. And Hy-line Brown should be grown in some regions with water scarcity. The pressure on the Chinese freshwater resources will thus increase both because of the rising demand for animal products and the shift from traditional farming to industrial farming systems.

#### References

- Bai, X., X. Ren, N.Z. Khanna, G. Zhang, N. Zhou, Y. Bai, M. Hu, 2018. A comparative study of a full value-chain water footprint assessment using two international standards at a large-scale hog farm in China. Journal of Cleaner Production. 176, 557–565. <http://dx.doi.org/10.1016/j.jclepro.2017.11.248>.
- Brown, H.-L., 2016. Hy-Line Brown Parent Stock Management Guides. [https://www.hyline.com/userdocs/pages/BRN\\_PS\\_ENG.pdf](https://www.hyline.com/userdocs/pages/BRN_PS_ENG.pdf). Accessed 16th January, 2019.
- Chapagain, A.K., A.Y. Hoekstra, 2004. Water footprints of nations.
- de Miguel, Á., A.Y. Hoekstra, E. García-Calvo, 2015. Sustainability of the water footprint of the Spanish pork industry. Ecological Indicators. 57, 465–474. <http://dx.doi.org/10.1016/j.ecolind.2015.05.023>.
- de Vries, M., I.J.M. de Boer, 2010. Comparing environmental impacts for livestock products: A review of life cycle assessments. Livestock Science. 128 (1–3), 1–11. <http://dx.doi.org/10.1016/j.livsci.2009.11.007>.
- Duan, P.L., L.J. Qin, Y.Q. Wang, H.S. He, 2016. Spatial pattern characteristics of water footprint for maize production in Northeast China. Journal of the Science of Food and Agriculture. 96 (2), 561–568. <http://dx.doi.org/10.1002/jsfa.7124>.
- FAO., 2013. FAO Statistical Yearbook: World Food and Agriculture: FAO.
- Hoekstra, A.Y., A.K. Chapagain, M.M. Mekonnen, M.M. Aldaya, 2011. *The water footprint assessment manual: Setting the global standard*: Routledge.

- Hoekstra, A.Y., 2014. Water for animal products: a blind spot in water policy. *Environmental Research Letters*. 9 (9). <http://dx.doi.org/10.1088/1748-926/9/091003>.
- Ibidhi, R., H. Ben Salem, 2019. Water footprint assessment of sheep farming systems based on farm survey data. *Animal*. 13 (2), 407–416. <http://dx.doi.org/10.1017/S1751731118001593>.
- Mekonnen, M.M., A.Y. Hoekstra, 2011. The green, blue and grey water footprint of crops and derived crop products. *Hydrology and Earth System Sciences*. 15 (5), 1577–1600. <http://dx.doi.org/10.5194/hess-15-1577-2011>.
- Mekonnen, M.M., A.Y. Hoekstra, 2012. A Global Assessment of the Water Footprint of Farm Animal Products. *Ecosystems*. 15 (3), 401–415. <http://dx.doi.org/10.1007/s10021-011-9517-8>.
- Notarnicola, B., K. Hayashi, M.A. Curran, D.J.J.o.C.P. Huisingsh, 2012. Progress in working towards a more sustainable agri-food industry. 28 (3), 1–8.
- Noya, I., S. Gonzalez-Garcia, J. Berzosa, F. Baucells, G. Feijoo, M.T. Moreira, 2018. Environmental and water sustainability of milk production in Northeast Spain. *Science of the Total Environment*. 616–617, 1317–1329. <http://dx.doi.org/10.1016/j.scitotenv.2017.10.186>.
- Palhares, J.C.P., J.R.M. Pezzopane, 2015. Water footprint accounting and scarcity indicators of conventional and organic dairy production systems. *Journal of Cleaner Production*. 93, 299–307. <http://dx.doi.org/10.1016/j.jclepro.2015.01.035>.
- Sonia, H.-L., 2016. Hy-Line Sonia Parent Stock Management Guides. [https://www.hyline.com/userdocs/pages/SO\\_PS\\_ENG.pdf](https://www.hyline.com/userdocs/pages/SO_PS_ENG.pdf). Accessed 16th January, 2019.
- Steinfeld, H., P. Gerber, T. Wassenaar, V. Castel, M. Rosales, C. de Haan, 2015. Livestock's long shadow-Environmental issues and options. FAO Agriculture Technical paper, Rome.
- Vanham, D., S. del Pozo, A.G. Pekcan, L. Keinan-Boker, A. Trichopoulou, B.M. Gawlik, 2016. Water consumption related to different diets in Mediterranean cities. *Science of the Total Environment*. 573, 96–105. <http://dx.doi.org/10.1016/j.scitotenv.2016.08.111>.

# Simultaneous Removal of Low Concentration H<sub>2</sub>S and NH<sub>3</sub> by a Biotrickling Filter: Interaction between the Two Pollutants and Microbial Community Changes

Shihao Ying, Xianwang Kong, Zhen Cai, Zun Man, Yicong Xin, Dezhao Liu \*

College of Biosystems Engineering and Food Science, Zhejiang University,  
Hangzhou, Zhejiang 310058, P.R. China

\*Corresponding author. Email: [dezhao.liu@zju.edu.cn](mailto:dezhao.liu@zju.edu.cn)

## Abstract

A lab-scale biotrickling filter (BTF) packed with porcelain Rasching ring and ceramsite was tested for co-treatment of hydrogen sulfide (H<sub>2</sub>S) and ammonia (NH<sub>3</sub>) at low concentration as typically found in pig houses. The outlet concentrations of H<sub>2</sub>S and NH<sub>3</sub> were used as removal efficiency indicators. Overall, excellent removal efficiencies were obtained for both H<sub>2</sub>S and NH<sub>3</sub> in the BTF during Stage I (H<sub>2</sub>S alone) and Stage II (H<sub>2</sub>S and NH<sub>3</sub>). Specifically, the outlet H<sub>2</sub>S concentration was below the detection limit (~3.6 ppb) and the outlet NH<sub>3</sub> concentration was less than 0.4 ppm when the inlet concentration of H<sub>2</sub>S and NH<sub>3</sub> were 1.8 ppm and 35.3 ppm, respectively at a running empty bed residence time of 10.2 s. During Stage II, the outlet H<sub>2</sub>S concentration was decreased when the inlet NH<sub>3</sub> concentration was increased, likely due to the influence by pH. Meanwhile, the outlet nitrous oxide (N<sub>2</sub>O) concentration was kept low (< 1% NH<sub>3</sub>), indicating a proper operation of the BTFs. After the inlet gas shifted from H<sub>2</sub>S alone (Stage I) to H<sub>2</sub>S and NH<sub>3</sub> (Stage II), the main common sulfur bacteria species in the BTF changed from *Acidithiobacillus* to *Thiobacillus*.

**Keywords:** Biotrickling filter, hydrogen sulfide, ammonia, nitrous oxide, microbial community

## 1. Introduction

Ammonia (NH<sub>3</sub>) and hydrogen sulfide (H<sub>2</sub>S) are environmentally unfriendly and odorous air pollutants that are often released from livestock farming, wastewater treatment processes and composting (Filho et al., 2010; Bittman et al., 2015). Up to now, various odor treatment methods have been proposed for controlling odorous gases, involving physicochemical processes such as absorption, adsorption, and chemical oxidation. These methods are efficient but costly, and may have problems of possible generation of hazardous by-products and other pollutants. In comparison, biological processes, especially biotrickling filters (BTFs), have been widely accepted because of their cost-effective and eco-friendly route for the removal of low concentration gas streams (Jaber et al., 2014). The removal efficiency (RE) of BTFs is highly influenced by treated pollutants, inhibitory effect of metabolic products, and bacterial population (Tsang et al., 2015). Analyses of metabolites and microbial communities can help to understand the mechanism of degradation reaction and improve the removal efficiency of odor.

There are already some studies focusing on the simultaneous removal of H<sub>2</sub>S and NH<sub>3</sub> in BTFs, but most of their studies deal with high concentrations of H<sub>2</sub>S and NH<sub>3</sub> (Chung et al., 2005; Tsang et al., 2015). One study showed that NH<sub>3</sub> was oxidized to nitrite and nitrate by *Nitrosomonas* or *Nitrobacter*, and H<sub>2</sub>S was oxidized to elemental sulphur and sulfate by *Thiobacillus* (Luc et al., 2003). Another study reported that sulfide oxidation was significantly affected by NH<sub>3</sub> introduction, and high sulfate concentration further enhanced NH<sub>3</sub> removal through the chemical reaction (Tsang et al., 2015). Therefore, the BTF has a synergistic effect when simultaneously treating low concentrations of NH<sub>3</sub> and H<sub>2</sub>S.

The mixture of H<sub>2</sub>S at low concentrations and NH<sub>3</sub> at relatively high concentrations is usually emitted from livestock farms (Akdeniz and Janni, 2012). However, there are few studies on simultaneous treatment of low concentration H<sub>2</sub>S and NH<sub>3</sub> with BTF. A detailed study of the removal mechanisms is required for extensive application of the BTFs in the treatment of exhaust air from livestock farms. This study aimed to characterize the shifts of the bacterial community at

different heights under different operating conditions, identify the interaction among H<sub>2</sub>S, NH<sub>3</sub> and metabolic products, and evaluate the removal mechanisms of the BTF.

## 2. Materials and Methods

### 2.1. Experimental setup

A laboratory-scale BTF with a total effective volume of 6.8 L was designed and constructed in this study. Table 1 summarizes the basic characteristics and working parameters of the reactor. The inlet concentrations of H<sub>2</sub>S and NH<sub>3</sub> were separately supplied from gas cylinders (1% H<sub>2</sub>S and 10% NH<sub>3</sub> balanced in N<sub>2</sub>) and first diluted with nitrogen, then diluted with compressed air. The porcelain Rasching ring and ceramsite were packed at two different layers and a schematic diagram of the system is shown in Figure 1. The reactor adopted gas-liquid countercurrent operation in these experiments. Gas rates were controlled by mass flow meters (CS series, Beijing Sevenstar Flow Co., Ltd, China), and the odorous gases were fed into the BTF from the bottom.

Table 1. Biotrickling filter parameters and operating conditions.

Reactor parameter	Characteristics
Height and Internal diameter	133 × 12 cm
Bed height	30 cm (at lower level, the porcelain Rasching ring) + 30 cm (on the upper level, the ceramsite)
Characteristics of fillers	Height and diameter of the porcelain Rasching ring: ca. 5 × 5 mm Diameter of the ceramsite: ca. 5 mm
Recirculation liquid volume	10 L
Gas-liquid flow pattern	Counter flow
Gas flow rate	20 L min <sup>-1</sup> and 40 L min <sup>-1</sup>
Empty bed residence time (EBRT)	20.4 and 10.2 s
Stage I	Only H <sub>2</sub> S, 112 days in total
Stage II	Treatment of H <sub>2</sub> S and NH <sub>3</sub> , 116 days in total
H <sub>2</sub> S loading rates	250–2330 mg m <sup>-3</sup> h <sup>-1</sup>
NH <sub>3</sub> loading rates	2350–17900 mg m <sup>-3</sup> h <sup>-1</sup>
Medium sprayed rate	91.7 mL min <sup>-1</sup> (spray for 1 min, stop for 5 min)
Nutrient solution temperature	26 ± 2 °C

### 2.2. Inoculum and medium preparation

The packing media was mainly acclimatized by activated sludge obtained from a nitrifying tank of a wastewater treatment plant in Hangzhou, Zhejiang province, China. Firstly, the packing media was immersed into the activated sludge while aerated by air pump for 24 h. Then a 10 L of nutrient solution, containing 2 g L<sup>-1</sup> KH<sub>2</sub>PO<sub>4</sub>, 2 g L<sup>-1</sup> K<sub>2</sub>HPO<sub>4</sub>, 0.4 g L<sup>-1</sup> NH<sub>4</sub>Cl, 0.2 g L<sup>-1</sup> MgCl<sub>2</sub>·6H<sub>2</sub>O, 0.01 g L<sup>-1</sup> FeSO<sub>4</sub>·7H<sub>2</sub>O, 8 g L<sup>-1</sup> Na<sub>2</sub>SO<sub>3</sub>·5H<sub>2</sub>O and 2 L activated sludge (Jin et al., 2005), was sprayed into the reactor to keep an adequate supply of nutrients and moisture for bacterial growth. Compressed air is fed from the bottom of the reactor to provide oxygen. Four days later, the pH of the nutrient solution dropped from 7.0 to 4.0 (indication of oxidation of sulfide and ammonium), and a new nutrient solution was replaced with the same composition as before, but no activated sludge and Na<sub>2</sub>SO<sub>3</sub>·5H<sub>2</sub>O was added. Thereafter, H<sub>2</sub>S gas at concentration of about 1000 ppb was added.

### 2.3. Analytical methods

Inlet and outlet H<sub>2</sub>S concentrations were measured by a real-time H<sub>2</sub>S analyzer (Model 450i, Thermo Fisher, USA). Ammonia and N<sub>2</sub>O concentrations were determined using Photoacoustic Field Gas-Monitor (INNOVA 1412, LumaSense Technologies, USA). The concentrations of ammonia nitrogen, nitrite nitrogen and nitrate nitrogen in the liquid phase (tank) were measured according to standard methods for the examination of water and wastewater (APHA, 2005). The

pH and conductivity of the nutrient solution were analyzed by a pH meter (Starter 3100, OHAUS, USA) and a conductivity meter (DDB-303A, INESA Scientific Instrument, China).

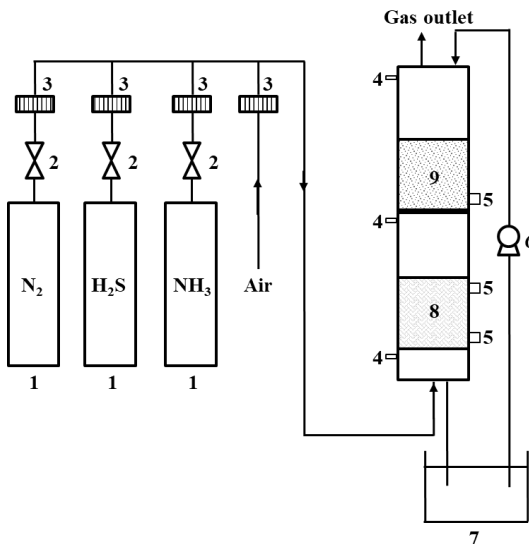


Figure 1. Schematic diagram of the biotrickling filter. (1) N<sub>2</sub>, H<sub>2</sub>S and NH<sub>3</sub> gas cylinders; (2) pressure regulator; (3) mass flow controllers; (4) air sampling ports; (5) packing media sampling ports; (6) peristaltic pump; (7) recirculation tank; (8) porcelain Rasching ring; (9) ceramsite.

#### 2.4. Microbial community analysis

In order to identify the microbial community of the BTF, the biofilms were collected from the bottom to the top sample ports on the 96th day of Stage I and the 89th day of Stage II. High-throughput sequencing was performed by Novogene Co., Ltd (Beijing, China). The V3-V4 region of the microbial 16S rRNA was amplified by PCR using the primers 341F: CCTAYGGGRBGCASCAG and 806R: GGACTACNNNGGTATCTAAT. The PCR program included an initial denaturation at 95 °C for 2 min, followed by 25 cycles at 95 °C for 30 s, 55 °C for 30 s, and 72 °C for 30 s, and a final extension at 72 °C for 5 min. PCR reactions were carried out with Phusion® High-Fidelity PCR Master Mix (New England Biolabs, USA) in duplicate.

### 3. Results and Discussion

#### 3.1. Treatment performance for simultaneous H<sub>2</sub>S and NH<sub>3</sub> removal

Table 2 shows the H<sub>2</sub>S removal efficiency of the BTF at different residence times and inlet concentrations. Outstanding H<sub>2</sub>S removal efficiencies (>99%) were obtained at all conditions. The removal efficiency of H<sub>2</sub>S with short EBRT was lower under the similar loading rate ( $P<0.05$ ). This result indicated that H<sub>2</sub>S removal was sensitive to EBRT in this BTF. And this phenomenon may be due to the solubility of H<sub>2</sub>S in water is not high. The sampling frequency of the two instruments is about once a minute, and each sampling time is more than 15 minutes.

Table 3 summarizes the outlet concentrations of H<sub>2</sub>S and NH<sub>3</sub> under various inlet concentrations at the EBRT of 20.4 s and 10.2 s. The NH<sub>3</sub> outlet concentration was less than 1 ppm under all operating conditions tested, indicating that NH<sub>3</sub> removal was not influenced by the coexistence of H<sub>2</sub>S and NH<sub>3</sub> in the system at relatively high concentrations in short EBRTs. This result was in agreement with that of Ottosen et al. (2011), who demonstrated that established filters normally have a fixed outlet concentration of NH<sub>3</sub> (typically 0.5-2 ppm) irrespective of inlet concentration and load. Similar result was also obtained by Chung et al. (Chung et al., 2005),

who reported that the NH<sub>3</sub> removal efficiency is not affected by the coexistence of H<sub>2</sub>S at sufficiently long EBRT. The pH of recirculation remained around 7.5 after nitrification occurred due to that about half of the NH<sub>3</sub> dissolved in water was degraded to nitrate to form ammonium nitrate. In addition, part of NH<sub>3</sub> may be removed by the reaction between NH<sub>3</sub> and sulfate, which is the by-product of the degradation of H<sub>2</sub>S to form ammonium sulfate.

Table 2. H<sub>2</sub>S removal under different H<sub>2</sub>S inlet concentrations and empty bed residence times.

EBRT (s)	H <sub>2</sub> S inlet concentration (ppb)	Removal efficiency (%)	EC (Elimination capacity) (mg m <sup>-3</sup> h <sup>-1</sup> )
20.4	979±93	99.96±0.17	249±42
20.4	1555±57	99.93±0.17	395±15
20.4	4461±74	99.91±0.07	1133±7
20.4	7328±121	99.76±0.01	1858±15
10.2	496±31	99.28±0.61	250±15
10.2	810±62	99.37±0.17	409±46
10.2	2112±237	99.21±0.17	1065±125
10.2	4586±86	99.50±0.04	2320±87

H<sub>2</sub>S detection limit: 3.64 ppb

Table 3. Biotrickling filter operating conditions and removal performance of NH<sub>3</sub> and H<sub>2</sub>S at the EBRTs of 20.4 s and 10.2 s.

EBRT (s)	H <sub>2</sub> S			NH <sub>3</sub>		
	Concentration (ppb)	Removal efficiency (%)	EC (mg m <sup>-3</sup> h <sup>-1</sup> )	Concentration (ppm)	Removal efficiency (%)	EC (mg m <sup>-3</sup> h <sup>-1</sup> )
20.4	923±39	99.96±0.00	235±10	18.6±0.2	99.84±0.07	2355±30
20.4	1182±96	99.91±0.01	300±25	39.0±0.7	99.35±0.05	4926±87
20.4	895±29	99.96±0.00	227±7	67.4±0.7	98.74±0.01	8463±82
10.2	609±111	99.71±0.03	309±56	11.4±0.2	99.67±0.15	2892±48
10.2	507±37	99.87±0.01	257±19	19.1±0.4	98.11±0.10	4756±92
10.2	449±62	99.93±0.03	228±32	34.1±0.3	98.11±0.02	8514±70
10.2	441±36	99.73±0.02	224±18	70.4±0.5	99.10±0.01	17741±128
10.2	877±31	99.82±0.00	445±16	33.5±0.6	98.96±0.05	8431±138
10.2	1823±15	99.88±0.00	926±7	35.3±0.4	98.75±0.03	8873±108
10.2	4429±68	98.29±0.00	2214±34	34.3±0.9	99.15±0.08	8636±232

NH<sub>3</sub> detection limit: 0.18 ppm; H<sub>2</sub>S detection limit: 3.64 ppb

### 3.2. Nitrous oxide emissions

After the introduction of NH<sub>3</sub> into the BTF, the concentration of nitrous oxide remained at a low level (<0.5 ppm), and the conversion rate of NH<sub>3</sub> to nitrous oxide was less than 1%. This level is comparable to other studies on air scrubbers at pig housing facilities (Van der Heyden et al., 2016), bioscrubber treatment (Liu et al., 2017) and are low compared to BTF with an extra denitrification step (about 24%) of incoming ammonia nitrogen (Melse and Mosquera, 2014). Considering that the treatment of NH<sub>3</sub> in pig farms may increase greenhouse gas (GHG) emissions, the use of bioscrubbers for NH<sub>3</sub> removal can remain acceptable according to the level of GHGs emitted by the pig farm and provided that less than 3% of the NH<sub>3</sub> entering the apparatus is converted into N<sub>2</sub>O (Dumont, 2018). So the 1% conversion rate is relatively small and will not aggravate the greenhouse effect.

### 3.3. Differences of microbial communities in BTF before and after NH<sub>3</sub> injection

The microorganisms in the BTF at different heights (see the sample ports in Figure 1) before and after the introduction of NH<sub>3</sub> were compared at the phylum and genus levels. *Proteobacteria* accounted for the largest proportion of microorganisms, but the proportion of microorganisms in

Stage II decreased significantly, especially in the middle of the BTF. There were 15 phyla in Stage I, which was less than 29 in Stage II, indicating that the diversity of microorganisms in the BTF increased after the introduction of ammonia. Moreover, among the top 10 genera of Stage I and II, *Rhodanobacter* was the only common microorganism, indicating that the microbial community structure had undergone tremendous changes. *Rhodanobacter* is a facultative anaerobic bacterium capable of complete denitrification. It grows anoxically by using nitrate, nitrite and nitrous oxide as sole electron acceptors (Prakash et al., 2012). *Metallibacterium* and *Thiomonas* were the dominant genera in Stage I. *Metallibacterium* is an acid-tolerant microorganism with sulfur and hydrogen oxidation genes (Bartsch et al., 2017). *Thiomonas* is a sulfur-oxidizing bacterium that grows optimally in mixotrophic media supplemented with reduced sulfur compounds and is often found in BTF used for biogas desulfurization (Giordano et al., 2018; Valle et al., 2018). In Stage I, the relative abundance of *Metallibacterium* and *Thiomonas* decreased from bottom to top in the BTF because H<sub>2</sub>S entered from the bottom. *Acidithiobacillus* and *Thiobacillus* were detected in Stage I and II, respectively, both of which were the most frequently sulfur-oxidizing bacteria found in H<sub>2</sub>S biofiltration at acidic and neutral pH conditions. In Stage I, hydrogen ions were generated during the oxidation of H<sub>2</sub>S, resulting in lower pH, while in stage II, because of the introduction of ammonia, the whole stabilized system was basically neutral, so *Thiobacillus* accounted for a large proportion. It is indicated that in these two stages, although the BTF has been capable of degrading H<sub>2</sub>S, the genus of microorganisms that play a major role has changed. In addition, *Nitrosomonas* was detected in Stage II (not in top 10 but in top 30 identified genera), a common ammonia-oxidizing bacterium that plays an important role in the oxidation of ammonia (Van der Heyden et al., 2015).

#### 4. Conclusions

Overall, excellent removal efficiencies were obtained both for H<sub>2</sub>S and NH<sub>3</sub> in the BTF during Stage I and Stage II. Specifically, the outlet H<sub>2</sub>S concentration was less than the detection limit (~3.6 ppb) and the outlet NH<sub>3</sub> concentration was less than 0.4 ppm when the inlet concentration of H<sub>2</sub>S and NH<sub>3</sub> were 1.8 ppm and 35.3 ppm, respectively, at the running empty bed residence time of 10.2 s. There were obvious differences in the microbial community structure between the Stage I and II. Therefore, suitable strains should be selected when starting the BTF with pure bacteria. The outlet H<sub>2</sub>S concentration was decreased when the inlet NH<sub>3</sub> concentration was increased ( $P<0.05$ ), likely due to the influence by pH. Most NH<sub>3</sub> was dissolved in water, and about half was oxidized to nitrate, with only a small fraction escaping or being converted to N<sub>2</sub>O. The future research direction may be to ensure the removal of H<sub>2</sub>S and NH<sub>3</sub> by the BTF in a very short residence time.

#### Acknowledgements

The research was financially supported by the National Natural Science Fund of China (No. 31672468); National Key R&D Program of China (Project No. 2017YFD0701700); and Thousand Talents Program (Youth Project 2016).

#### References

- Akdeniz, N., K.A. Janni, 2012. Full-scale biofilter reduction efficiencies assessed using portable 24-hour sampling units. Journal of the Air & Waste Management Association. 62 (2), 170–182. <http://dx.doi.org/10.1080/10473289.2011.639479>.
- APHA, 2005. *Standard Methods for the Examination of Water and Wastewater*, 21th ed. American Public Health Association, Washington, DC, 9–72 p.
- Bartsch, S., A. Gensch, S. Stephan, A. Doetsch, J. Gescher, 2017. Metallibacterium scheffleri: genomic data reveal a versatile metabolism. FEMS Microbiol Ecol. 93 (3). <http://dx.doi.org/10.1093/femsec/fix011>.
- Bittman, S., K. Jones, R. Vingarzan, D.E. Hunt, S.C. Sheppard, J. Tait, R. So, J. Zhao, 2015. Weekly agricultural emissions and ambient concentrations of ammonia: Validation of an emission inventory. Atmospheric Environment. 113, 108–117.

- Chung, Y.C., Y.Y. Lin, C.P. Tseng, 2005. Removal of high concentration of NH<sub>3</sub> and coexistent H<sub>2</sub>S by biological activated carbon (BAC) biotrickling filter. *Bioresour Technol.* 96 (16), 1812–1820. <http://dx.doi.org/10.1016/j.biortech.2005.01.003>.
- Dumont, E., 2018. Impact of the treatment of NH<sub>3</sub> emissions from pig farms on greenhouse gas emissions. Quantitative assessment from the literature data. *N Biotechnol.* 46, 31–37. <http://dx.doi.org/10.1016/j.nbt.2018.06.001>.
- Filho, J.L.R.P., L.T. Sader, M.H.R.Z. Damianovic, E. Foresti, E.L. Silva, 2010. Performance evaluation of packing materials in the removal of hydrogen sulphide in gas-phase biofilters: Polyurethane foam, sugarcane bagasse, and coconut fibre. *Chemical Engineering Journal.* 158 (3), 441–450. <http://dx.doi.org/10.1016/j.cej.2010.01.014>.
- Giordano, C., F. Spennati, G. Mori, G. Munz, C. Vannini, 2018. The microbial community in a moving bed biotrickling filter operated to remove hydrogen sulfide from gas streams. *Syst Appl Microbiol.* 41 (4), 399–407. <http://dx.doi.org/10.1016/j.syapm.2018.04.001>.
- Jaber, M.B., B. Anet, A. Amrane, C. Couriol, T. Lendormi, P.L. Cloirec, G. Cogny, R. Fillières, 2014. Impact of nutrients supply and pH changes on the elimination of hydrogen sulfide, dimethyl disulfide and ethanethiol by biofiltration. *Chemical Engineering Journal.* 258, 420–426. <http://dx.doi.org/10.1016/j.cej.2014.07.085>.
- Jin, Y., M.C. Veiga, C. Kennes, 2005. Autotrophic deodorization of hydrogen sulfide in a biotrickling filter. *Journal of Chemical Technology & Biotechnology.* 80 (9), 998–1004. <http://dx.doi.org/10.1002/jctb.1275>.
- Liu, F., C. Fiencke, J. Guo, R. Rieth, C. Cuhls, R. Dong, E.-M. Pfeiffer, 2017. Bioscrubber treatment of exhaust air from intensive pig production: Case study in northern Germany at mild climate condition. *Engineering in Life Sciences.* 17 (4), 458–466. <http://dx.doi.org/10.1002/elsc.201600169>.
- Luc, M., G. Catherine, R. Jean-Claude, F. Jean-Louis, L.C. Pierre, 2003. Biological treatment process of air loaded with an ammonia and hydrogen sulfide mixture. *Chemosphere.* 50 (1), 145–153.
- Melse, R.W., J. Mosquera, 2014. Nitrous oxide (N<sub>2</sub>O) emissions from biotrickling filters used for ammonia removal at livestock facilities. *Water Science and Technology.* 69 (5), 994–1003. <http://dx.doi.org/10.2166/wst.2013.826>.
- Ottosen, L.D.M., S. Juhler, L.B. Guldberg, A. Feilberg, N.P. Revsbech, L.P. Nielsen, 2011. Regulation of ammonia oxidation in biotrickling airfilters with high ammonium load. *Chemical Engineering Journal.* 167 (1), 198–205. <http://dx.doi.org/10.1016/j.cej.2010.12.022>.
- Prakash, O., S.J. Green, P. Jasrotia, W.A. Overholt, A. Canion, D.B. Watson, S.C. Brooks, J.E. Kostka, 2012. Rhodanobacter denitrificans sp. nov., isolated from nitrate-rich zones of a contaminated aquifer. *Int J Syst Evol Microbiol.* 62 (Pt 10), 2457–2462. <http://dx.doi.org/10.1099/ijss.0.035840-0>.
- Tsang, Y.F., L. Wang, H. Chua, 2015. Simultaneous hydrogen sulphide and ammonia removal in a biotrickling filter: Crossed inhibitory effects among selected pollutants and microbial community change. *Chemical Engineering Journal.* 281, 389–396. <http://dx.doi.org/10.1016/j.cej.2015.06.107>.
- Valle, A., M. Fernandez, M. Ramirez, R. Rovira, D. Gabriel, D. Cantero, 2018. A comparative study of eubacterial communities by PCR-DGGE fingerprints in anoxic and aerobic biotrickling filters used for biogas desulfurization. *Bioprocess Biosyst Eng.* 41 (8), 1165–1175. <http://dx.doi.org/10.1007/s00449-018-1945-9>.
- Van der Heyden, C., P. Demeyer, E.I.P. Volcke, 2015. Mitigating emissions from pig and poultry housing facilities through air scrubbers and biofilters: State-of-the-art and perspectives. *Biosystems Engineering.* 134, 74–93. <http://dx.doi.org/10.1016/j.biosystemseng.2015.04.002>.
- Van der Heyden, C., E. Brusselman, E.I.P. Volcke, P. Demeyer, 2016. Continuous measurements of ammonia, nitrous oxide and methane from air scrubbers at pig housing facilities. *J. Environ Manage.* 181, 163–171. <http://dx.doi.org/10.1016/j.jenvman.2016.06.006>.

## Calculation Method for Chicken-Perceived Light Intensity

Zhichao Li<sup>a,b</sup>, Xiaocui Wang<sup>a,b</sup>, Baoming Li<sup>a,b,c</sup>, Weichao Zheng<sup>a,b,c</sup>,  
Zhengxiang Shi<sup>a,b,c</sup>, Ziyue Cao, Qin Tong<sup>a,b,c,\*</sup>

<sup>a</sup> Key Laboratory of Agricultural Engineering in Structure and Environment, Beijing 100083, P.R. China

<sup>b</sup> College of Water Resources & Civil Engineering, China Agricultural University, Beijing 100083,  
P.R. China

<sup>c</sup> Beijing Engineering Research Center for Livestock and Poultry Healthy Environment,  
Beijing 100083, P.R. China

\* Corresponding author. Email: [tongjin@cau.edu.cn](mailto:tongjin@cau.edu.cn)

### Abstract

Poultry has superior visual function. Its visible spectrum is wider than humans (380–760 nm) and its sensitivity is high. To study chicken-perceived light intensity, seven light intensities from full-spectrum white light, monochromatic blue light and monochromatic green light were set-up. Measurement and comparison of differences between chicken-perceived light and illuminance were conducted. Results showed that the difference between them was significant ( $P<0.01$ ). Both wavelength band and light intensity had effect on the ratio of chicken-perceived light and illuminance ( $P<0.01$ ). Therefore, spectrometer and photometric unit lx used in poultry production and research were not appropriate. To scientifically set poultry house lighting conductions and reasonably evaluate the illumination environment, the actual chicken-perceived light intensity should be considered and applied.

**Keywords:** Poultry, spectral sensitivity curves, illuminance, spectrometer, chicken-perceived light intensity

### 1. Introduction

The visual function of birds is well developed. Optical information mainly acts on animals through photoreceptors (Sharp et al., 1979). There are two kinds of photoreceptors on the avian retina, namely rod and cone cells. Rod cells are sensitive to dark light (< 0.4 lx) and have the greatest sensitivity at 507 nm (blue-green light). Cone cells are sensitive to bright light (> 0.4 lx) and can distinguish color, this gives chickens amazing color perception (Hart et al., 1999; Kram et al., 2010). Human cone cells are sensitive between 400 and 730 nm, with the most sensitive at 555 nm (Sagawa et al., 1986). There are only three types of cone cells in humans, and poultry has one more type of cone cells than humans, with a peak sensitivity of 415 nm (Govardovskii et al., 1977; Hart et al., 1999). The highest sensitive spectra of birds and humans are similar at 545–575 nm, but the sensitivity of spectral of poultry at 400–480nm and 580–700 nm is stronger than that of humans (Prescott et al., 1999; Wortel et al., 1987). Lux (lx) is the international unit of illumination, usually used to measure the intensity of the light environment. There is a large number of researches, who have indicated that light plays an important role in poultry. Appropriate light intensity, color and photoperiod for poultry can promote the growth and development of chicken embryos during incubation (Duncan et al., 1978; Shafey et al., 2002), and affect the post-hatching activities, reproduction, and growth (Phillips, 1992). Especially in the modern poultry house where the artificial light is fully applied for the illumination. Therefore, the study of chicken-perceived light intensity has certain positive significance for poultry.

Illumination Ev, commonly known as Lux (lx), is an important unit to measure the human perceived light intensity of the light environment. It is calculated from the spectral output power of the light source and the sensitivity of the human eyes.

$$Ev=683.002lm/W \cdot \int_0^{\infty} \bar{V}(\lambda)\phi_{e\lambda}(\lambda)d\lambda/(4\pi r^2) \quad (1)$$

where  $V(\lambda)$  is the human photometric function (CIE, 1983);  $\phi_{e\lambda}$  is the spectral radiation power corresponding to each nm, also known as spectral radiation flux. The optimum spectral

luminescence efficiency of photopic vision is  $683.002 \text{ lm w}^{-1}$ , and  $r$  is the distance (m) of light source.

When calculating the perceptual illumination of a specific species, the specific perceptual illumination level of the light source can be calculated by using the photometric function of each species according to the spectral power distribution range of the lamp. Some scholars have validated the photometric functions of chicken (Prescott et al., 1999), turkey (Barber et al., 2006), duck (Barber et al., 2006), rat (Jacobs et al., 2001), mouse (Jacobs et al., 2004), cat (Brown et al., 1964; Pasternak et al., 1981). The results show that the visual sensitivity coefficients of different species are obviously different. Therefore, human light intensity ( $I_x$ ) cannot reflect the actual chicken-perceived light intensity (Chicken  $I_x$ ,  $Cl_x$ ) (Nuboer et al., 1992), nor can it accurately evaluate the light environment of poultry house. According to the photometric function and illumination calculation formula of human (Sagawa et al., 1986) and poultry (Prescott et al., 1999), a method for measuring the chicken-perceived light intensity was established and integrated into a conventional spectrometer. Furthermore, human perceived light intensity ( $I_x$ ) poultry perceived light intensity ( $Cl_x$ ) under three different light sources was compared by using the calculation data of integral sphere as a reference. The reliability of the measured data of the spectrometer was proved by comparing the date between these two methods. Human perceived light intensity ( $I_x$ ) and poultry perceived light intensity ( $Cl_x$ ) were measured using light meter. The ratios of the two were calculated and the differences of the ratios of different wave bands and illumination levels were compared. At present, the measurement of illumination in livestock and poultry houses relies on conventional illuminometers. There are not many instruments on the market which measure chicken-perceived light intensity. Therefore, the ratio of different spectrum can be used to convert human perceived light intensity ( $I_x$ ) to poultry perceived light intensity ( $Cl_x$ ), which helps actual production and evaluation the light environment in poultry house.

## 2. Materials and Methods

In order to scientifically set poultry house lighting conductions and reasonably evaluate the illumination environment, the corresponding relationship between illumination and chicken perceived light intensity should be found. The illumination and chicken perceived light intensity obtained by integral sphere calculation and directly measured by spectrometer were compared. Furthermore, the difference between illumination and chicken-perceived light intensity was compared under the same intensity level of the same LED.

### 2.1. Light source

Three wave bands of LEDs (Yimeixinguang Technology Co., Ltd., Beijing, China), which were white light (380–780 nm), blue light (447.5–462.5 nm) and green light (515–535 nm) were configured using iLMS lighting management software (Aviation Energy Technology Nanjing Co., Ltd.) for compensation for light fading and real-time state monitoring.

### 2.2. Formula for calculating chicken-perceived light intensity

According to the formula of human illumination, the formula of chicken-perceived light intensity at a fixed distance from the light source is as follows:

$$E_s = 683.002 \text{ lm}/W \cdot \int_0^{\infty} \bar{S}(\lambda) \phi_{e\lambda}(\lambda) d\lambda / (4\pi r^2) \quad (2)$$

where  $E_s$  is the chicken-perceived light intensity;  $\phi_{e\lambda}$  is the spectral radiation power corresponding to each nm, also known as spectral radiation flux;  $\bar{S}(\lambda)$  is the photometric function of poultry (Prescott et al., 1999). It is assumed that the optimal spectral luminescence efficiency of chicken photopic vision is the same as that of human beings ( $683.002 \text{ lm w}^{-1}$ );  $r$  is the distance of light source (m).

The proportional constant 683.002 in the formula is an internationally agreed lumen value: the wavelength of the monochromatic light output approaching 555 nm is defined as  $683.002 \text{ lm W}^{-1}$ . Because the standard CIE photon function is normalized at the same wavelength (its maximum sensitivity), the calculated value of the standard photon for photopic vision is 683.002.

In very few cases, when calculating the illumination of human scotopic condition, different values will be used, depending on the value of the photometric function at 555 nm, the peak of visual sensitivity. It is worth noting that when calculating the perceived light level of a specific species by using formula (2), the peak of the photometric function of this species should be about 555 nm.

### 2.3. Calculation and measurement of illumination and chicken-perceived light

#### 2.3.1. Calculation method using integral sphere

The white, blue and green LED were placed in the integral sphere with a diameter of 2.0 m. The intensity was adjusted to 7 levels using iLMS lighting management software spectral radiation power was measured using a LED Spectral analyzer (HAAS-1200, Hangzhou Yuanfang Photoelectric Information Co., Ltd., Hangzhou, China). Then, according to formulas (1) and (2), the illumination level ( $I_x$ ) and chicken-perceived light intensity ( $Cl_x$ ) from three LEDs were calculated.

#### 2.3.2. Spectrometer measurement method

In collaboration with Shangze Photoelectric Co., Ltd., a piece of software was developed for calculating chicken perceived light intensity and integrated into a conventional spectrometer (SRI-LM-2000, Shangze Photoelectric Co., Ltd.). It can simultaneously measure the illumination and chicken-perceived light. The LEDs were fixed on the shelf and adjusted to seven illumination using the control software in the dark condition of the Animal Behavior and Environmental Physiology Lab (China Agricultural University). The illumination level ( $I_x$ ) and chicken-perceived light intensity ( $Cl_x$ ) at 16 cm vertical distance of the LEDs were measured using a SRI-LM-2000 spectrometer.

### 2.4. Statistical analysis

SPSS (IBM statistics 25) software was used to analyze the data and results were expressed as mean  $\pm SD$ . Independent sample T test was performed for illumination and chicken-perceived light intensity under the same intensity level of the LED. A general linear model was used to analyze the effects of spectrum (LED) and intensity level on the ratio:  $Y = \mu + LED + intensity + LED * intensity + \epsilon$ ,  $\mu$  is the overall average value,  $\epsilon$  is the residual error term, LED and intensity are fixed effects, and  $LED * intensity$  is the cross-influence factor. When the effect was significantly different, multiple comparisons were further conducted.

## 3. Results and Discussion

Table 1 shows that the average values of the three repeated measurements of the spectrometer are in good agreement with the integral sphere calculated data as a reference, especially the full spectrum white light. The difference between the two methods was small. At the same time, the output values of SRI-LM-2000 spectrometer at different LEDs and intensity levels were also stable, and the difference of repeated measurement data was small. This indicated the accuracy and reliability of the data measured using SRI-LM-2000 spectrometer. The method of measuring the chicken-perceived light intensity established in this study could be used to measure the illumination in livestock and poultry house or for scientific research.

The difference between illumination and chicken-perceived light intensity under the same intensity level of the same LED is shown in Table 2. The difference between illumination and chicken-perceived light intensity at the seven intensity levels of white LED was significant ( $P < 0.01$ ); and the latter was about 1.5 times of the former. At the seven intensity levels of blue LED, the difference between illumination and chicken-perceived light intensity was significant ( $P < 0.01$ ). Compared with illumination, the change of intensity level of blue LED caused a huge increase in chicken-perceived light intensity. This indicated that poultry was extremely sensitive to blue light. This was corresponded to the known spectral sensitivity curve of poultry and human, and the sensitivity of poultry to blue light was obviously better than human beings. The difference between illumination and chicken-perceived light intensity under green LED was also significant ( $P < 0.01$ ), although the ratio of the latter to the former was about 1.0. The results showed that the

illumination and chicken-perceived light intensity had significant difference under different intensity levels of different LEDs. Current general illumination measurement methods and units could not reflect the actual chicken-perceived light intensity, especially in some monochrome light.

Table 1. Illumination and chicken-perceived light intensity obtained by spectrometer and integrating sphere and the ratio between them.

LED	Intensity level	Illumination (lx)		Chicken-perceived light intensity (Clx)		Ratio	
		Spectro-meter	Integral sphere	Spectro-meter	Integral sphere	Spectro-meter	Integral sphere
White	1	136.82	120.43	204.30	182.20	1.49	1.51
	2	261.05	248.40	388.45	374.22	1.49	1.51
	3	924.63	945.28	1359.05	1407.35	1.47	1.49
	4	1040.53	1084.62	1526.87	1612.06	1.47	1.49
	5	1181.19	1223.83	1730.60	1816.32	1.46	1.48
	6	1312.89	1362.36	1921.35	2019.78	1.46	1.48
	7	1439.51	1500.32	2102.44	2221.38	1.46	1.48
Blue	1	23.37	24.15	205.10	200.11	8.78	8.29
	2	44.78	49.91	401.30	421.78	8.96	8.45
	3	152.42	186.48	1446.14	1656.32	9.49	8.88
	4	172.83	213.37	1647.87	1904.72	9.54	8.93
	5	194.94	237.40	1865.53	2147.33	9.57	9.05
	6	210.88	264.62	2025.35	2396.00	9.60	9.05
	7	232.09	266.33	2237.15	2410.78	9.64	9.05
Green	1	191.61	230.93	194.09	234.18	1.01	1.01
	2	192.34	231.76	195.06	234.98	1.01	1.01
	3	675.52	760.04	690.17	773.43	1.02	1.02
	4	1164.54	1298.11	1192.80	1325.48	1.02	1.02
	5	1640.70	1812.84	1688.16	1856.87	1.03	1.02
	6	2095.86	2312.21	2164.70	2374.59	1.03	1.03
	7	2522.07	2787.40	2613.32	2869.65	1.04	1.03

Note: Spectrometer data was the average value of three repeated measurements and integrating sphere data was the calculated value using the spectral radiation power measured in integrating sphere.

From the results of the general linear model analysis, the influence of LED on the ratio of chicken-perceived light intensity to illumination was significant ( $P < 0.01$ ) (Table 2). The ratio of chicken-perceived light intensity to illumination was blue LED > white LED > green LED. The LED and the intensity level had significant effects on the ratio of chicken-perceived light intensity to illumination ( $P < 0.01$ ). The results of multiple comparisons of chicken-perceived light intensity to illumination value of poultry at different intensity levels under the same LED had done. It was showed that ratio of chicken-perceived light intensity to illumination in different LEDs showed a certain change trend with the intensity level. The ratio of white LED decreased with the increase of light intensity. However, the ratio of blue LED and green LED increased with the increase of light intensity.

The data showed that the ratio was relatively stable in the white and green LEDs. Lewis and Morris had proved that both poultry and human are sensitive to green light (Prescott et al., 1999). Lewis showed that the ratio in green light was close to 1 (Lewis et al., 2000); so it can be approximated that the chicken-perceived light intensity in green light is same as human perceived light intensity. The ratio of blue light fluctuated from 3.24 to 13.3. However, the results in this paper showed that the ratio was around 8.78 to 9.64 in blue LED. It was possible that the spectrum

and intensity of blue-light sources were different between this study and the previous ones. The illumination conditions in this study were 447.5–462.5 nm blue light (23.37 lx–232.09 lx) and in Lewis experiment were 440–500 nm spectrum (3.0 lx–16.4 lx). For full spectrum white light, the ratio was also stable at 1.5, because the relative visual sensitivity of poultry and human were known and the spectral range was determined. Therefore, the corresponding chicken-perceived light intensity could be obtained by multiplying the value of illumination by 1.5 in practical application.

Table 2. Comparisons of chicken-perceived light intensity and illumination measured by spectrometer under different light intensity of three LEDs.

LED	Intensity level	Illumination (lx)	Chicken-perceived light intensity (Clx)	Ratio
White	1	136.82±0.25 <sup>A</sup>	204.30±0.34 <sup>B</sup>	1.493±0.000 <sup>T</sup>
	2	261.05±0.87 <sup>A</sup>	388.45±1.41 <sup>B</sup>	1.488±0.001 <sup>U</sup>
	3	924.63±2.71 <sup>A</sup>	1,359.05±3.61 <sup>B</sup>	1.470±0.000 <sup>V</sup>
	4	1,040.53±3.05 <sup>A</sup>	1,526.87±4.32 <sup>B</sup>	1.467±0.001 <sup>W</sup>
	5	1,181.19±2.36 <sup>A</sup>	1,730.60±3.64 <sup>B</sup>	1.465±0.001 <sup>X</sup>
	6	1,312.89±2.07 <sup>A</sup>	1,921.35±2.61 <sup>B</sup>	1.463±0.001 <sup>Y</sup>
	7	1,439.51±6.79 <sup>A</sup>	2,102.44±10.81 <sup>B</sup>	1.460±0.001 <sup>Z</sup>
Mean				1.473±0.121
Blue	1	23.37±0.10 <sup>A</sup>	205.10±0.82 <sup>B</sup>	8.777±0.011 <sup>Y</sup>
	2	44.78±0.23 <sup>A</sup>	401.30±0.74 <sup>B</sup>	8.962±0.031 <sup>X</sup>
	3	152.42±0.68 <sup>A</sup>	1,446.14±2.84 <sup>B</sup>	9.488±0.024 <sup>W</sup>
	4	172.83±1.38 <sup>A</sup>	1,647.87±11.61 <sup>B</sup>	9.535±0.027 <sup>V</sup>
	5	194.94±0.33 <sup>A</sup>	1,865.53±1.53 <sup>B</sup>	9.570±0.010 <sup>UV</sup>
	6	210.88±0.76 <sup>A</sup>	2,025.35±4.38 <sup>B</sup>	9.604±0.014 <sup>TU</sup>
	7	232.09±0.45 <sup>A</sup>	2,237.15±3.44 <sup>B</sup>	9.640±0.020 <sup>T</sup>
Mean				9.368±0.330
Green	1	191.61±0.35 <sup>A</sup>	194.09±0.31 <sup>B</sup>	1.013±0.002 <sup>Y</sup>
	2	192.34±0.23 <sup>A</sup>	195.06±0.24 <sup>B</sup>	1.014±0.000 <sup>Y</sup>
	3	675.52±1.72 <sup>A</sup>	690.17±2.04 <sup>B</sup>	1.022±0.001 <sup>X</sup>
	4	1,164.54±0.98 <sup>A</sup>	1,192.80±0.99 <sup>B</sup>	1.024±0.001 <sup>W</sup>
	5	1,640.70±3.42 <sup>A</sup>	1,688.16±3.82 <sup>B</sup>	1.029±0.000 <sup>V</sup>
	6	2,095.86±1.77 <sup>A</sup>	2,164.70±1.77 <sup>B</sup>	1.033±0.000 <sup>U</sup>
	7	2,522.07±6.23 <sup>A</sup>	2,613.32±7.12 <sup>B</sup>	1.036±0.000 <sup>T</sup>
Mean				1.024±0.008

Note: <sup>A,B</sup> values with different superscripts in the same row means significant difference ( $P < 0.01$ ); <sup>T-Z</sup> values with different superscripts within one LED in the same column means significant difference ( $P < 0.01$ ).

#### 4. Conclusions

The chicken-perceived light intensity (Clx) measured by updated spectrometer were accurate and reliable in this study. The human and chicken-perceived light intensities under the same intensity level of the same LED were significantly different. The ratios between them were relatively stable in the white and green LEDs and were about 1.5 and 1, respectively. However, the ratio of chicken-perceived light intensity to illumination in blue LED varied from 8.8 to 9.6. Therefore, it was inaccurate to evaluate the chicken-perceived light intensity (Clx) using human perceived light intensity (lx) for various monochrome light application.

#### Acknowledgements

This study was supported by the National Key R&D Program of China (grant numbers 2017YFB0404000) and by the National Natural Science Foundation of China (31601981).

### References

- Barber, C.L., N.B. Prescott, J.R. Jarvis, C.L. Sueur, G.C. Perry, C.M. Wathes, 2006. Comparative study of the photopic spectral sensitivity of domestic ducks (*Anas platyrhynchos domesticus*), turkeys (*Meleagris gallopavo gallopavo*) and humans. *British Poultry Science*, 47(3), 365–374.
- Brown, J.L., F.D. Shively, R.H. Lamotte, J.A. Sechzer, 1964. Color discrimination in the cat. *Journal of Comparative & Physiological Psychology*, 144(3617), 427–429.
- CIE, 1983. The Basis of Physical Photometry. Commission Internationale de L'Eclairage (CIE) Publication 18.2, Paris, France.
- Duncan, I.J.H., C.J. Savory, D.G.M. Wood-Gush, 1978. Observations on the reproductive behaviour of domestic fowl in the wild. *Applied Animal Ethology*, 4(1), 29–42.
- Govardovski, V.I., L.V. Zueva, 1977. Visual pigments of chicken and pigeon. *Vision Research*, 17(4), 537–543.
- Hart, N.S., J.C. Partridge, I.C. Cuthill, 1999. Visual pigments, cone oil droplets, ocular media and predicted spectral sensitivity in the domestic turkey (*Meleagris gallopavo*). *Vision Research*, 39(20), 3321.
- Jacobs, G.H., G.A. Williams, J.A. Fenwick, 2001. Cone-based vision of rats for ultraviolet and visible lights. *Journal of Experimental Biology*, 204(14), 2439–2446.
- Jacobs, G.H., G.A. Williams, J.A. Fenwick, 2004. Influence of cone pigment coexpression on spectral sensitivity and color vision in the mouse. *Vision Research*, 44(14), 1615–1622.
- Kram, Y.A., M. Stephanie, J.C. Corbo, 2010. Avian cone photoreceptors tile the retina as five independent, self-organizing mosaics. *Plos One*, 5(2), e8992.
- Lewis P.D., M.T. Morris, 2000. Poultry and coloured light. *Worlds Poultry Science Journal*, 56(3), 189–207.
- Nuboer, J.F.W., M.A.J.M. Coemans, J.J. Vos, 1992. Artificial lighting in poultry houses: Are photometric units appropriate for describing illumination intensities? *British Poultry Science*, 33(1), 135–140.
- Pasternak, T., W.H. Merigan, 1981. The luminance dependence of spatial vision in the cat. *Vision Research*, 21(9), 1333–1339.
- Phillips, C.J.C., 1992. Environmental factors influencing the production and welfare of farm animals: Photoperiod. Pages 49–65 in Farm Animals and the Environment. C.J.C. Phillips and D. Piggins, ed. CAB International, Oxford, UK.
- Prescott, N.B., C.M. Wathes, 1999. Spectral sensitivity of the domestic fowl (*Gallus g. domesticus*). *British Poultry Science*, 40(3), 332–339.
- Sagawa, K., K. Takeichi, 1986. Spectral luminous efficiency functions in the mesopic range. *Journal of the Optical Society of America A Optics & Image Science*, 3(1), 71.
- Shafey, T.M., T.H. Al-Mohsen, 2002. Embryonic Growth, Hatching Time and Hatchability Performance of Meat Breeder Eggs Incubated under Continuous Green Light. *Asian Australasian Journal of Animal Sciences*, 15(12), 1702–1707.
- Sharp, P.J., C.G. Scanes, J.B. Williams, S. Harvey, A. Chadwick, 1979. Variations in concentrations of prolactin, luteinizing hormone, growth hormone and progesterone in the plasma of broody bantams (*Gallus domesticus*). *Journal of Endocrinology*, 80(1), 51.
- Wortel, J.F., H. Rugenbrink, J.F.W. Nuboer, 1987. The photopic spectral sensitivity of the dorsal and ventral retinae of the chicken. *Journal of Comparative Physiology A*, 160(2), 151–154.

# Isotopomer Analyses of N<sub>2</sub>O Produced from NH<sub>3</sub>-loaded Biofilter: Microbial Production Pathways

Xianwang Kong <sup>a</sup>, Shihao Ying <sup>a</sup>, Yicong Xin <sup>a</sup>, Zhen Cai <sup>a</sup>, Liangcheng Yang <sup>b</sup>,  
Dezhao Liu <sup>a,\*</sup>

<sup>a</sup> College of Biosystems Engineering and Food Science, Zhejiang University,  
Hangzhou, Zhejiang 310000, P.R. China

<sup>b</sup> Department of Health Sciences, Illinois State University, Normal, IL 61761, USA

\* Corresponding author. Email: [dezhao.liu@zju.edu.cn](mailto:dezhao.liu@zju.edu.cn)

## Abstract

Ammonia-loaded biofilters are potential sources of nitrous oxide (N<sub>2</sub>O) emissions as a result of nitrification and denitrification within the biofilter bed. A 204-d laboratory experiment was conducted to evaluate the relative importance of these two processes with regard to N<sub>2</sub>O production using site preference (SP, 33% for nitrification and 0% for denitrification). Two moisture levels (45% vs. 55%, two replicates) and three inlet NH<sub>3</sub> concentration levels (35, 18 and 0 ppmv) were simulated. Under operational conditions of 35 and 18 ppmv NH<sub>3</sub>, all of the four biofilters removed more than 50% of the NH<sub>3</sub> but no clear difference was seen between the two moisture treatments. The biofilters were obviously strong sources of N<sub>2</sub>O production, and more so with 55% moisture content. Interestingly, biofilters that have treated air containing NH<sub>3</sub> still presented a net source of N<sub>2</sub>O production over a period of three weeks during which NH<sub>3</sub> was absent in the inlet air. The NH<sub>3</sub>-N converted into N<sub>2</sub>O-N was calculated as 2.5–12.8%, 3.2–10.5% for replicated biofilters with 45% moisture content, and 2.9–24.2% and 4.8–17.6% for those with 55% moisture content. Based on SP values on selected sampling days, nitrification was estimated as the main source (mostly larger than 60%) of N<sub>2</sub>O emission. However, such results should be interpreted with great caution and possible reasons were discussed. Overall, this experiment demonstrated that NH<sub>3</sub>-loaded biofilters were sources of N<sub>2</sub>O emissions and use of SP values for source partition would require additional information.

**Keywords:** Nitrogen isotope, source partition, greenhouse gas, nitrification, denitrification

## 1. Introduction

Livestock produce large amount of manure rich in ammoniacal nitrogen and therefore presents a major source of anthropogenic ammonia (NH<sub>3</sub>) emissions worldwide (Poulton et al., 2014). In China, estimated by Huang et al. (2012), livestock excreta emitted 5.3 Tg of NH<sub>3</sub> during 2006 contributing 54% of the national emissions. The NH<sub>3</sub> by deposition can cause problems of water eutrophication and soil acidification, and more importantly NH<sub>3</sub> as precursor can promote the formation of particulate matter (Pinder et al., 2007).

Biofiltration can be an effective technology for minimizing odors and gases in the air stream from livestock production. Biofilters are engineered bioreactors and often filled with organic packing materials, e.g., wood chips, composts and soil. The NH<sub>3</sub> in the exhaust of a livestock building can be removed by biofilters and the processes involved include water absorption and biological transformation of NH<sub>3</sub> into nitrite (NO<sub>2</sub><sup>-</sup>) or nitrate (NO<sub>3</sub><sup>-</sup>) by nitrifying bacteria. Under proper operational conditions, e.g., adequate media moisture, pH, and temperature, biofilters often achieved more than 50% of NH<sub>3</sub> removal efficiency at field scale (Akdeniz and Janni, 2012). However, a number of studies (Maia et al., 2012a; Dumont et al., 2014; Yang et al., 2014a; Dumont, 2018) observed that NH<sub>3</sub> removal by biofilters were frequently accompanied by emissions of nitrous oxide (N<sub>2</sub>O), which is unexpected since N<sub>2</sub>O is a potent greenhouse gas (GHG) also involved in stratospheric ozone depletion (Ravishankara et al., 2009). For example, Dumont et al. (2014) calculated that the part of NH<sub>3</sub>-N converted into N<sub>2</sub>O-N ranged from 10% to 40% during piggery air biofiltration.

The N<sub>2</sub>O can be generated by nitrification process during incomplete oxidation of NH<sub>2</sub>OH to

$\text{NO}_2^-$ . The environment within a biofilter is normally regarded as aerobic favoring nitrification because of continued air flow. However, due to heterogeneous water distribution and small anaerobic zones resulted from media compaction, denitrification may prevail given the supply of organic C from packing materials as well as the nitrite or nitrate from nitrification of  $\text{NH}_3$ . In a lab study, Nicolai et al. (2006) found that total  $\text{NH}_3\text{-N}$  accumulated in the compost/woodchip media accounted for only 29% of the N removed by biofilter after 1160 h, and these unexplained N were considered lost as  $\text{NO}$ ,  $\text{N}_2\text{O}$  and  $\text{N}_2$  through denitrification. Indeed several studies reached conclusions (Akdeniz and Janni, 2012; Maia et al., 2012b) that denitrification was the main contributor to biofilter  $\text{N}_2\text{O}$  emissions during  $\text{NH}_3$  removal.

The  $\text{N}_2\text{O}$  emissions from  $\text{NH}_3$ -loaded biofilters have gained more and more attentions (Bollon et al., 2016; Dumont, 2018). As crucial factors for  $\text{NH}_3$  removal and microbial activities, effects of moisture content (Maia et al., 2012a; Yang et al., 2014a; Liu et al., 2017), pH (Yang et al., 2014b) and age (Akdeniz and Janni, 2012) of biofilter bed on  $\text{N}_2\text{O}$  emissions were specifically investigated. For instance,  $\text{N}_2\text{O}$  emissions may significantly increase when media moisture exceeded a certain level, e.g., 55%, reported by Yang et al. (2014a); and lower pH, at 4.5 and 6.0 compared with 8.0 and 9.5, favored  $\text{N}_2\text{O}$  emissions of  $\text{NH}_3$ -loaded biofilter, possibly through an inhibition effect on  $\text{N}_2\text{O}$  reductase. To date so far, however, no studies have provided direct evidence about the relative importance of nitrification and denitrification to biofilter  $\text{N}_2\text{O}$  emissions triggered by  $\text{NH}_3$  removal and how this would change in response to differed biofilter environment.

Yoshida and Toyoda (2000) suggested that intramolecular distributions of  $^{15}\text{N}$  in  $\text{N}_2\text{O}$  could offer additional information on the sources and sinks of this greenhouse house gas (GHG). This intramolecular distribution of  $^{15}\text{N}$  is expressed as site preference ( $\text{SP}=\delta^{15}\text{N}^a-\delta^{15}\text{N}^b$ ) and therefore defined as the difference between relative abundance of  $^{15}\text{N}$  in the central and terminal N atoms of the liner  $\text{N}_2\text{O}$  molecule ( $^b\text{N}^a\text{N-O}$ ). Later, Sutka et al. (2006) experimentally proved that determination of  $\text{N}_2\text{O-SP}$  could be used to quantitative apportion  $\text{N}_2\text{O}$  as SP of ~33% and ~0% are characteristic of nitrification and denitrification, respectively. As a valid and non-invasive method, use of SP value for  $\text{N}_2\text{O}$  source partition soon became popular and has been widely applied in soil systems (Quan Van et al., 2017) as well as in wastewater treatment (Wunderlin et al., 2013).

Here, we present a lab study where  $\text{N}_2\text{O}$  emissions from  $\text{NH}_3$ -loaded biofilters (45% vs. 55% moisture of packing materials) were periodically monitored during a 204-d operation. Three  $\text{NH}_3$  concentration levels, e.g., 35 ppm, 18 ppm and 0 ppm, were tested and the SP values of emitted  $\text{N}_2\text{O}$  were determined under each  $\text{NH}_3$  concentration level. The main objectives were 1) to quantitatively distinguish the  $\text{N}_2\text{O}$  emissions between nitrification and denitrification from  $\text{NH}_3$ -loaded biofilters using SP values; and 2) to observe how this would respond to media moisture and  $\text{NH}_3$  concentrations.

## 2. Materials and Methods

### 2.1. Packing materials

Raw packing materials of pine wood chips and peat soil were purchased from an online shop. In order to get homogeneous materials, peat soil was first passed through 2 mm, 0.9 mm, 0.45 mm sieves and then mixed at ratio of 1:1:1 (in weight) and saved for later use. For wood chips 10 mm, 8 mm, 6 mm and 4 mm sieves were used and the subsequent mixing ratio was also 1:1:1:1 (in weight). The total C, N contents of the wood chips and peat soil were 47.2%, 0.32% and 24.5%, 1.31%, respectively. The initial pH of wood chips and peat soil (in water 1: 4, w: v) was 5.8 and 5.1, respectively. The wood chips and peat soil were then mixed together with a ratio of 1: 4 on dry weight basis, yielding a final C: N ratio of 26.1. This mixture was later used for packing of the biofilters.

## 2.2. Biofilter design and operations

There were two treatments of media moisture (i.e., 45%, 55%) with two replicates each. The four cylindrical biofilters (I.D. 15 cm) were made of polymethyl methacrylate and the schematic overview of the gas line was shown in Figure 1. The total packing depth was 20 cm, equivalent to an effective biofiltration volume of 3.5 L, and the packing density  $0.25 \text{ g cm}^{-3}$  (dry weight). The media was split into four portions with equal weight and the subsequent packing was therefore done individually for each 5-cm depth. The biofilter was gently shaken so that the media was loosely packed to the desired depth.

After adjusted to the target moisture, the packing media received activated sludge (0.5 g sludge  $\text{kg}^{-1}$  media) collected from the secondary settling tank of a local waste water treatment plant in Hangzhou, China, for inoculation. The activated sludge was evenly sprayed onto the media and the excessive water was removed by evaporation at room temperature.

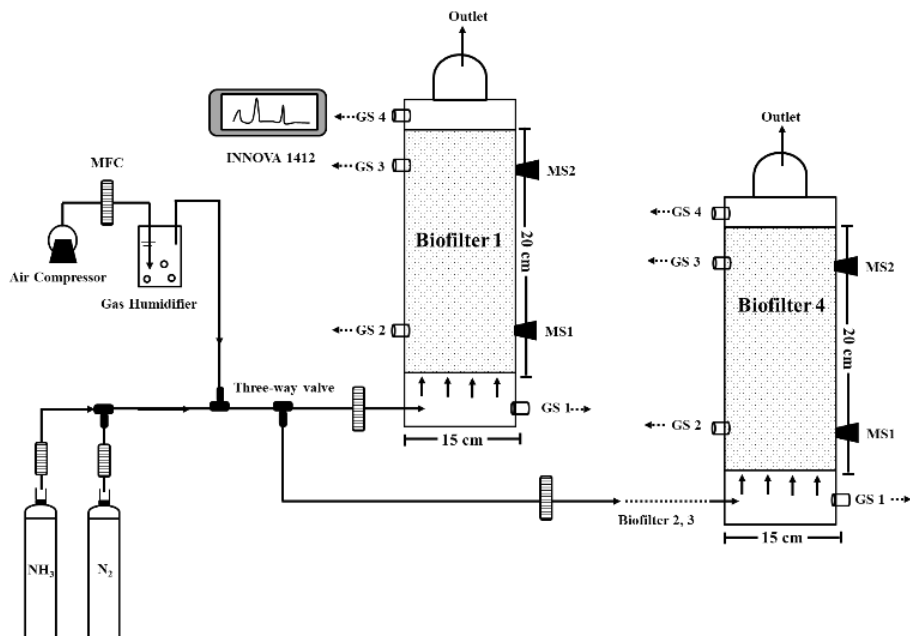


Figure 1. Schematic overview of lab setup. Arrow indicates the direction of gas flow. There are four gas sampling ports (GS): GS 1 for sampling inlet gas, GS 2 and 3 for sampling gas at distance of 5 and 15 cm from the bottom of the packing media, respectively, and GS 4 for sampling outlet gas. Two media sampling ports (MS) are located at the same height as the gas sampling ports.

The desired  $\text{NH}_3$  concentrations (35 ppm and 18 ppm) of biofilters inlet air were obtained by diluting the gas from a certified  $\text{NH}_3$  gas cylinder ( $10\% \text{ v/v}$ ,  $\text{N}_2$  balanced) (Jingong Gas Company Co., Ltd, Hangzhou, China). Because only a very small volume of the gas was required from the gas cylinder, a two stage dilution was performed (Figure 1) in order to achieve a stable  $\text{NH}_3$  concentration in the gas stream, e.g., the gas from  $\text{NH}_3$  cylinder was first mixed with  $\text{N}_2$  gas (99.999%; Jingong Gas Company Co., Ltd, Hangzhou, China) and then further diluted by the compressed air. A stainless steel container was used for humidifying the inlet air to a relative humidity (RH) around 45–50% before the gas entered the biofilters. The total air flow for each biofilter was set at  $5.0 \text{ L min}^{-1}$  corresponding to an EBRT (empty bed residence time) of ca. 40 s. The indoor temperature was recorded at 0.5-h intervals, and the temperature and humidity of inlet

air was checked twice during the day and the gas humidifier was refilled with water when necessary. The water loss from each biofilter was compensated by water spraying every 12 h. The gas flow were all regulated by mass flow controllers (MFC) (CSA200, Beijing Sevenstar Electronics Co., Ltd., China) and the accuracy of MFC is at *ca.* 1%.

The experiment started on 14<sup>th</sup> Nov. 2018 with a 3-d measurement of background production of N<sub>2</sub>O and NH<sub>3</sub>. Afterwards, 35 ppm NH<sub>3</sub> was supplied to each biofilter as described above. On day 140, the NH<sub>3</sub> concentration of inlet air was changed to 18 ppm, and again on day 181 no NH<sub>3</sub> was present in the inlet air.

### 2.3. Gas sampling and measurement

The NH<sub>3</sub> and N<sub>2</sub>O concentrations were measured regularly and simultaneously with an online infrared photo-acoustic gas-monitor (INNOVA 1412, LumaSense Technologies, Inc., USA). For one sampling port (Figure 1), the measurement was performed and continued for *ca.* 15 min (or until steady output), and then the sampling tube was switched to another sampling port. The last five measurements were averaged and considered as the final result. On day 64, 72, 78, 93, 107, 126, 140, 158, 180, outlet gas (GS 4, Figure 1) were sampled and analyzed for SP values of emitted N<sub>2</sub>O using IRMS.

### 2.4. Data analyses

Statistical data analyses were all performed by SPSS 19.0, and a level of  $\alpha = 0.05$  was used for describing significant difference.

## 3. Results and Discussion

### 3.1. NH<sub>3</sub> removal by biofilters

Figure 2 shows the NH<sub>3</sub> concentrations of biofilter inlet and outlet air (those at 5 cm and 15 cm depth data are not shown here) during the whole experiment. The abrupt drop of inlet NH<sub>3</sub> concentration indicated changes in NH<sub>3</sub> gradient as described in section 2.2.

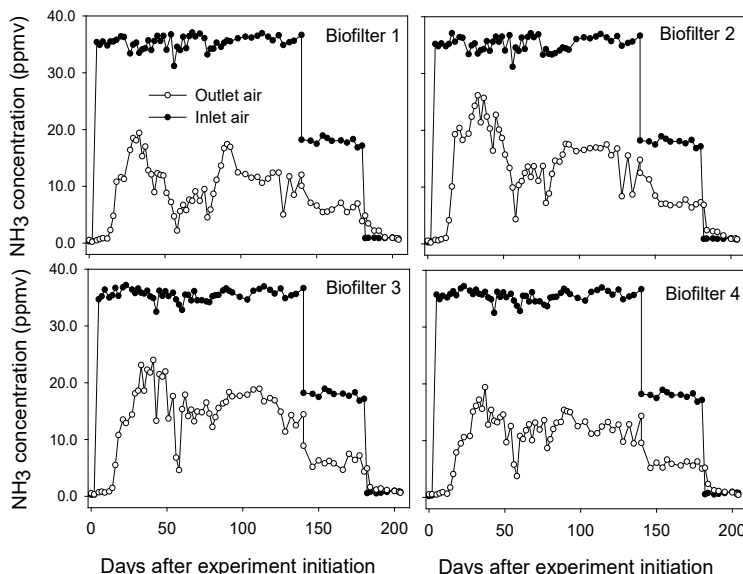


Figure 2. NH<sub>3</sub> concentrations of inlet and outlet air during the whole experiment. The moisture content of packing materials were 45% and 55% in biofilters 1, 2 and in biofilters 3, 4, respectively.

For all biofilters, there were no obvious background emissions of NH<sub>3</sub> during the first 3-d operation. When ca. 35 ppmv NH<sub>3</sub> was introduced to the biofilters, more than 90% of NH<sub>3</sub> was removed in the first two weeks (Figure 1) for all biofilters. At this stage, NH<sub>3</sub> should have been mostly removed via absorption into the water film covering the packing media (Maia et al., 2012a), since NH<sub>3</sub> is highly water soluble. The time needed for saturated absorption of NH<sub>3</sub> in this experiment was therefore about two weeks.

In general, the four biofilters shared a similar dynamic pattern of outlet NH<sub>3</sub> concentrations (Figure 1), and the variations were partly due to changes of indoor temperature (data not shown). The averaged NH<sub>3</sub> removal efficiency (after saturated absorption) was 68.9%, 55.2%, 53.7% and 64.7% for biofilters 1, 2, 3 and 4, respectively, under operational conditions of 35 ppmv NH<sub>3</sub> (n=43). When the inlet NH<sub>3</sub> concentration changed to 18 ppmv, the corresponding removal efficiency was 64.3%, 55.1%, 65.4%, 65.7%, respectively. These values were comparable to those found in the literature (Chen et al., 2009; Akdeniz and Janni, 2012). Clearly increased moisture content in the packing materials did not dramatically improved the NH<sub>3</sub> removal efficiency.

### 3.2. N<sub>2</sub>O emissions from NH<sub>3</sub>-loaded biofilters

Similar to NH<sub>3</sub> emissions, the four biofilters given the targeted moisture content in this experiment were not natural sources of N<sub>2</sub>O before NH<sub>3</sub> was supplied to them (Figure 3). Obvious N<sub>2</sub>O emissions were only detected 36 days (Figure 3) after introduction of 35 ppmv NH<sub>3</sub>. Therefore before this time point, either the slow growth of nitrifiers or limited NO<sub>2</sub><sup>-</sup>/NO<sub>3</sub><sup>-</sup> availability to denitrifiers had constrained the N<sub>2</sub>O production from the biofilters.

Although the four biofilters had similar trend of N<sub>2</sub>O in the outlet air, biofilters 3 and 4, which had higher moisture content in the packing materials, peaked with higher N<sub>2</sub>O concentrations in the outlet air (Figure 3), consistent with the findings by Liu et al. (2017) and Yang et al. (2014a). Increased moisture content retarded the O<sub>2</sub> diffusion into biofilm and O<sub>2</sub>- limited conditions would induce more N<sub>2</sub>O production from both nitrification and denitrification (Zhu et al., 2013).

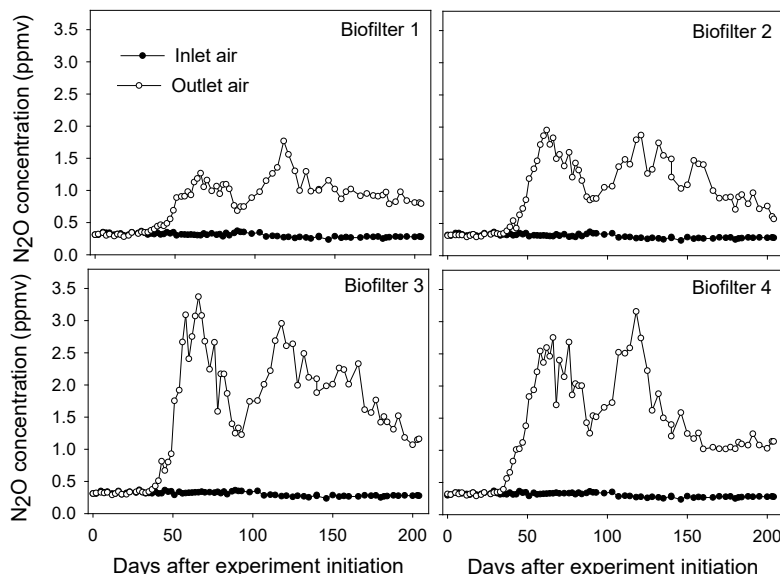


Figure 3. N<sub>2</sub>O concentrations of inlet and outlet air during the whole experiment. The moisture content of packing materials were 45% and 55% in biofilters 1, 2 and in biofilters 3, 4, respectively.

After changing into 18 ppmv NH<sub>3</sub> on day 140, N<sub>2</sub>O concentrations slightly decreased. Interestingly, over a period of three weeks after NH<sub>3</sub> was completely cut off (day 181), the four biofilters still had considerable amount of N<sub>2</sub>O present in the outlet air. These results indicated that biofilters once dumped after usage was still a potential source of N<sub>2</sub>O, which should be taken into account when dealing with overall assessment on environmental impact of biofilters.

Across the experiment, the NH<sub>3</sub>-N converted into N<sub>2</sub>O-N was calculated as 2.5–12.8%, 3.2–10.5%, 2.9–24.2% and 4.8–17.6% for biofilters 1, 2, 3 and 4, respectively. These results together confirmed the information in the literature (Akdeniz and Janni, 2012; Yang et al., 2014a; Dumont, 2018) that NH<sub>3</sub>-loaded biofilters were non-negligible source of N<sub>2</sub>O emissions.

### 3.3. SP values of emitted N<sub>2</sub>O and microbial production pathways

Results of SP at the stage of 0 ppmv NH<sub>3</sub> were not available at the moment. According to Sutka et al. (2006), N<sub>2</sub>O generated from nitrification and denitrification has SP value of 33% and 0%, respectively. In this experiment, firstly the two replicated biofilter of each moisture content coincided well on the SP values (Figure 4). Secondly, the overall SP of the four biofilters ranged from 17.7% to 33.2%, and the variations may indicate a shift of biological process that was mainly responsible to N<sub>2</sub>O production. For instance, a declined trend of SP values would suggest that denitrification were becoming more important regarding N<sub>2</sub>O production, and a reverse trend may indicate that nitrification contributed more and more to N<sub>2</sub>O production.

When NH<sub>3</sub> supply changed from 35 ppmv to 18 ppmv (day 141), SP values were expected to decrease since N<sub>2</sub>O derived from nitrification would have also decreased as NH<sub>3</sub> input deceased. However, it was not the case (Figure 4). Based on SP values, the estimated contribution of nitrification-derived N<sub>2</sub>O on selected sampling days all exceeded 60% (Figure 4, lower panel). These results seemed to conflict with the observations that packing materials with higher moisture content promoted N<sub>2</sub>O production (Figure 3). In addition, the apparent production of N<sub>2</sub>O after NH<sub>3</sub> was cut off from the inlet air also indirectly showed the importance of denitrification.

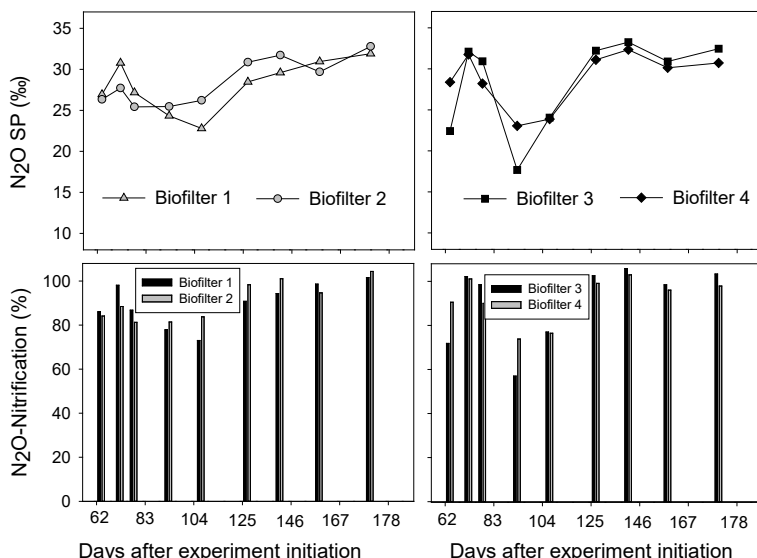


Figure 4. Changes of SP values of emitted N<sub>2</sub>O on selected sampling days (upper panel), and the estimated portion of nitrification-derived N<sub>2</sub>O (lower panel). The moisture content of packing materials were 45% and 55% in biofilters 1, 2 and in biofilters 3, 4, respectively.

Therefore the SP values, used for the first time in a biofilter system for N<sub>2</sub>O source partition,

should be interpreted with great caution in view of the limited data base from this single experiment. Jinuntuya-Nortman et al. (2008) demonstrated that N<sub>2</sub>O reduction to N<sub>2</sub> would enrich <sup>15</sup>N in the  $\alpha$  position, therefore increase the SP values, and more so if N<sub>2</sub>O reduction rate was higher. In addition, N<sub>2</sub>O derived from fungal denitrification has SP value similar to nitrification (Quan Van et al., 2017). Often <sup>18</sup>O-N<sub>2</sub>O signature (data not shown) was used for distinguishing nitrification and fungal denitrification (Quan Van et al., 2017).

#### 4. Conclusions

Biofilters could effectively remove NH<sub>3</sub> and the two moisture contents (45%, 55%) used in this experiment did not show clear difference with regard to NH<sub>3</sub> removal efficiency. The NH<sub>3</sub>-loaded biofilters were non-negligible source of N<sub>2</sub>O production even after the biofilters were dumped after service. Surprisingly, SP values suggested that nitrification was the main source of N<sub>2</sub>O production from all biofilters. These results should be interpreted with great caution due to limited data in this experiment and other possible influencing factors on N<sub>2</sub>O-SP values, as discussed above.

#### Acknowledgements

The research was financially supported by the National Natural Science Fund of China (No. 31672468), National Key R&D Program of China (Project No. 2017YFD0701700), and Thousand Talents Program (Youth Project 2016).

#### References

- Akdeniz, N., K.A. Janni, 2012. Full-scale biofilter reduction efficiencies assessed using portable 24-hour sampling units. Journal of the Air & Waste Management Association. 62 (2), 170–182. <http://dx.doi.org/10.1080/10473289.2011.639479>.
- Bollon, J., A. Filali, Y. Fayolle, S. Guerin, V. Rocher, S. Gillot, 2016. N<sub>2</sub>O emissions from full-scale nitrifying biofilters. Water Res. 102, 41–51. <http://dx.doi.org/10.1016/j.watres.2016.05.091>.
- Chen, L., S. Hoff, L. Cai, J. Koziel, B. Zelle, 2009. Evaluation of wood chip-based biofilters to reduce odor, hydrogen sulfide, and ammonia from swine barn ventilation air. Journal of the Air & Waste Management Association. 59 (5), 520–530. <http://dx.doi.org/10.3155/1047-3289.59.5.520>.
- Dumont, E., S. Lagadec, P. Landrain, B. Landrain, Y. Andrès, 2014. N<sub>2</sub>O generation resulting from piggy air biofiltration. Chemical Engineering Journal. 248, 337–341. <http://dx.doi.org/10.1016/j.cej.2014.03.058>.
- Dumont, E., 2018. Impact of the treatment of NH<sub>3</sub> emissions from pig farms on greenhouse gas emissions. Quantitative assessment from the literature data. N Biotechnol. 46, 31–37. <http://dx.doi.org/10.1016/j.nbt.2018.06.001>.
- Huang, X., Y. Song, M. Li, J. Li, Q. Huo, X. Cai, T. Zhu, M. Hu, H. Zhang, 2012. A high-resolution ammonia emission inventory in China. Global Biogeochemical Cycles. 26 (1), 1–14. <http://dx.doi.org/10.1029/2011gb004161>.
- Jinuntuya-Nortman, M., R.L. Sutka, P.H. Ostrom, H. Gandhi, N.E. Ostrom, 2008. Isotopologue fractionation during microbial reduction of N<sub>2</sub>O within soil mesocosms as a function of water-filled pore space. Soil Biology & Biochemistry. 40 (9), 2273–2280. <http://dx.doi.org/10.1016/j.soilbio.2008.05.016>.
- Liu, T., H. Dong, Z. Zhu, B. Shang, F. Yin, W. Zhang, T. Zhou, 2017. Effects of biofilter media depth and moisture content on removal of gases from a swine barn. J Air Waste Manag Assoc. 67 (12), 1288–1297. <http://dx.doi.org/10.1080/10962247.2017.1321591>.
- Maia, G.D., G.B.t. Day, R.S. Gates, J.L. Taraba, M.S. Coyne, 2012a. Moisture effects on greenhouse gases generation in nitrifying gas-phase compost biofilters. Water Res. 46 (9), 3023–3031. <http://dx.doi.org/10.1016/j.watres.2012.03.007>.
- Maia, G.D.N., G.B. Day V, R.S. Gates, J.L. Taraba, 2012b. Ammonia biofiltration and nitrous oxide generation during the start-up of gas-phase compost biofilters. Atmospheric Environment. 46, 659–664. <http://dx.doi.org/10.1016/j.atmosenv.2011.10.019>.
- Nicolai, R.E., Clanton, C.J., Janni, K.A., Malzer, G.L., 2006. Ammonia removal during biofiltration as affected by inlet air temperature and media moisture content. Transactions of ASABE. 49 (4): 1125–1138.
- Paulot, F., D.J. Jacob, R.W. Pinder, J.O. Bash, K. Travis, D.K. Henze, 2014. Ammonia emissions in the United States, European Union, and China derived by high-resolution inversion of ammonium wet deposition

data: Interpretation with a new agricultural emissions inventory (MASAGE\_NH3). *Journal of Geophysical Research: Atmospheres*. 119 (7), 4343–4364. <http://dx.doi.org/10.1002/2013jd021130>.

Pinder, R.W., P.J. Adams, S.N. Pandis, 2007. Ammonia emission controls as a cost-effective strategy for reducing atmospheric particulate matter in the eastern United States. *Environ Sci Technol.* 41 (2), 380–386. <http://dx.doi.org/10.1021/es060379a>.

Quan Van, N., D. Wu, X. Kong, R. Bol, S.O. Petersen, L.S. Jensen, S. Liu, N. Brueggemann, R.N. Glud, M. Larsen, S. Bruun, 2017. Effects of cattle slurry and nitrification inhibitor application on spatial soil O<sub>2</sub> dynamics and N<sub>2</sub>O production pathways. *Soil Biology & Biochemistry*. 114, 200–209. <http://dx.doi.org/10.1016/j.soilbio.2017.07.012>.

Ravishankara, A.R., J.S. Daniel, R.W. Portmann, 2009. Nitrous oxide (N<sub>2</sub>O): The dominant ozone-depleting substance emitted in the 21<sup>st</sup> century. *Science*. 326 (5949), 123–125. <http://dx.doi.org/10.1126/science.1176985>.

Sutka, R.L., N.E. Ostrom, P.H. Ostrom, J.A. Breznak, H. Gandhi, A.J. Pitt, F. Li, 2006. Distinguishing nitrous oxide production from nitrification and denitrification on the basis of isotopomer abundances. *Applied and Environmental Microbiology*. 72 (1), 638–644. <http://dx.doi.org/10.1128/aem.72.1.638-644.2006>.

Wunderlin, P., M.F. Lehmann, H. Siegrist, B. Tuzson, A. Joss, L. Emmenegger, J. Mohn, 2013. Isotope signatures of N<sub>2</sub>O in a mixed microbial population system: constraints on N<sub>2</sub>O producing pathways in wastewater treatment. *Environ Sci Technol.* 47 (3), 1339–1348. <http://dx.doi.org/10.1021/es303174x>.

Yang, L., A.D. Kent, X. Wang, T.L. Funk, R.S. Gates, Y. Zhang, 2014a. Moisture effects on gas-phase biofilter ammonia removal efficiency, nitrous oxide generation, and microbial communities. *J Hazard Mater.* 271, 292–301. <http://dx.doi.org/10.1016/j.jhazmat.2014.01.058>.

Yang, L., X. Wang, T.L. Funk, 2014b. Strong influence of medium pH condition on gas-phase biofilter ammonia removal, nitrous oxide generation and microbial communities. *Bioresour Technol.* 152, 74–79. <http://dx.doi.org/10.1016/j.biortech.2013.10.116>.

Yoshida, N., S. Toyoda, 2000. Constraining the atmospheric N<sub>2</sub>O budget from intramolecular site preference in N<sub>2</sub>O isotopomers. *Nature*. 405 (6784), 330–334. <http://dx.doi.org/10.1038/35012558>.

Zhu, X., M. Burger, T.A. Doane, W.R. Horwath, 2013. Ammonia oxidation pathways and nitrifier denitrification are significant sources of N<sub>2</sub>O and NO under low oxygen availability. *Proceedings of the National Academy of Sciences of the United States of America*. 110 (16), 6328–6333. <http://dx.doi.org/10.1073/pnas.1219993110>.

# A Preliminary Study on Dispersion Modeling of Hydrogen Sulfide from a Six-story Pig House in China

Dejia Liu <sup>a</sup>, Li Rong <sup>b</sup>, Günther Schauberger <sup>c</sup>, Chuandong Wu <sup>d</sup>, Yicong Xin <sup>a</sup>,  
Xiusong Li <sup>e</sup>, Bin Chen <sup>f</sup>, Dezhaoliu <sup>a,\*</sup>

<sup>a</sup> Zhejiang University, College of Biosystems Engineering and Food Science,  
Hangzhou, Zhejiang 310000, P.R. China

<sup>b</sup> Aarhus University, Department of Engineering, Aarhus 8000, Denmark

<sup>c</sup> University of Veterinary Medicine, WG Environmental Health, Unit for Physiology and Biophysics,  
Vienna A-1210, Austria

<sup>d</sup> University of Science & Technology Beijing, Department of Chemistry, Beijing 100083, P.R. China

<sup>e</sup> Big Herdsman Machinery Co. Ltd., Qingdao, Shandong 266000, P.R. China

<sup>f</sup> Zhejiang Huatong Meat Products Co. Ltd., Yiwu, Zhejiang 322000, P.R. China

\* Corresponding author. Email: [dezhaoliu@zju.edu.cn](mailto:dezhaoliu@zju.edu.cn)

## Abstract

With the rapid development of intensive pig production in recent years in China, odor pollutants emitted from pig houses have become one of the primary sources of air pollution. The storied buildings typically have a more significant number of feed animals inside, and therefore lead to even higher emissions of odor pollutants. Because these storied buildings are usually not far from the residential area, it is imperative to predict how the odor pollutants disperse to the neighborhood. This study used a six-story pig house as the emission source and simulated the emission of H<sub>2</sub>S (as one representative of the significant odor pollutants emitted from these pig houses) from the storied pig house as a point source. The calculation applied the meteorological and geographical conditions of the study area and used the Gaussian dispersion model to simulate the dispersion of H<sub>2</sub>S. Results show that the H<sub>2</sub>S concentration is relatively high at a distance of 10 m to 30 m away from the pig farm. The H<sub>2</sub>S concentration in the morning is the highest with its highest value exceeding 25 ppb and that at noon being the lowest with its highest value around 10 ppb. Moreover, the downwind H<sub>2</sub>S concentration is inversely proportional to wind speed.

**Keywords:** Hydrogen sulfide, air dispersion model, six-story pig house, gaussian dispersion model

## 1. Introduction

Concentrated Animal Feeding Operation (CAFOs) are widely present all over the world due to the high population demand for food and products of animals origin (Wu et al., 2019). However, CAFOs have generated several environmental concerns, including odor nuisance, which affects people health and quality of life (Guffanti et al., 2018). These years, storied animal buildings are becoming more and more popular for they can have a larger number of animals in them and therefore lead to higher emissions of odor pollutants. Because these storied buildings are usually not far from the residential area, it is imperative to predict how the odorants diffuse to the neighborhood.

Aerial emissions from CAFOs are composed of a mixture of hydrogen sulfide (H<sub>2</sub>S), ammonia, volatile organic compounds (VOCs), and particulates including bioaerosols that arise during biodegradation of manure (Schiffman et al., 2005). Hydrogen sulfide (H<sub>2</sub>S) is a colorless, corrosive, and toxic gas with a smell of rotten eggs. The high concentration of H<sub>2</sub>S is an active nerve agent, affecting people's physical and mental health. At lower concentration, it stimulates the eye and respiratory mucosa (Zhou, 2015). The higher the concentration, the more obvious the effect on the central nervous system, leading to the central nervous system, breathing system and myocardial damage and other hazards (Qu et al., 2008). At the same time, H<sub>2</sub>S will cause secondary pollution to the ecological environment (Dong, 2008). For example, the oxidation of H<sub>2</sub>S in the atmosphere forms acid rain, which is harmful to the construction industry and the

aquaculture industry. Hydrogen Sulfide in pig houses is produced by microorganisms in an anaerobic environment, reducing sulfate in water and decomposing sulfur-containing organic matter in the feces. If the feces is not cleaned in time, H<sub>2</sub>S will volatilize, and anaerobic treatment will also produce a large amount of H<sub>2</sub>S, which is quite harmful (Yan et al., 2014).

An atmospheric dispersion model is a mathematical tool for quantitatively describing the entire process of atmospheric pollutants from the source to the receiving site. It describes the transport, dispersion, and dilution of pollutants by the atmosphere. The Gaussian dispersion model is one of the most commonly used atmospheric dispersion models based on statistical theory. The theoretical basis of it is that in a flat and open plain area the laws of dispersion, distribution, and concentration of pollutants accord with the normal distribution. The Gaussian dispersion model is based on the following four hypotheses: 1) uniform and stable continuous discharge of pollution sources; 2) the process of pollutant transport and dispersion follows the law of conservation of mass; 3) stable wind direction and wind speed; 4) concentration distribution in horizontal and vertical directions accord with normal distribution. For small-scale atmospheric dispersion simulation and the evaluation of the point source pollution dispersion on surrounding areas, Gaussian dispersion model is widely used.

## 2. Methods

### 2.1. Site description

This pig farm is located in the southeast of Yiwu, Zhejiang Province, China, with a latitude of 29.22° and longitude of 120.03°. Yiwu is located in the central part of Zhejiang Province, with a total area of 1105.46 km<sup>2</sup>, 55 km from Jinhua City and 158 km from Hangzhou, the provincial capital. The city is surrounded by mountains on the east, south, and north. It is a typical mountainous area with various landforms. Yiwu has a subtropical monsoon climate, mild and humid, with four distinct seasons. The annual average temperature is about 17 °C, and the annual average precipitation is between 1100–1600 mm.

The farm has 20 buildings, each of which was designed to be six-story with 1,200 pigs on each floor and it was designed to accommodate 144,000 pigs in total. However, according to our survey, there were only 3,913 sows and 5,800 piglets in it. The simulation was based on the actual stock density.

### 2.2. Hydrogen sulfide emission rate

To estimate the H<sub>2</sub>S emission rate, a factor called emission factor is needed. There are some studies on the emission factor in the pig farm. One of them, carried out in two pig farms in Zhejiang province, shows that the ammonia emission factor in sow houses and nursery houses is 17.3 g d<sup>-1</sup> per pig and 2.2 g d<sup>-1</sup> per pig, respectively (Dai, 2010). Because there is a lack of H<sub>2</sub>S emission factor in similar livestock production practices. The ammonia emission factors were utilized to estimate the H<sub>2</sub>S emission rate by the correlation of ammonia and H<sub>2</sub>S emissions (Feilberg et al., 2017). The H<sub>2</sub>S emission rate for this modeling practices was 484.6 µg s<sup>-1</sup>.

### 2.3. Meteorological data

#### 2.3.1. Wind speed and direction

According to the wind speed and wind direction data of the site for 365 days in 2018 provided by the Zhejiang Meteorological Bureau, the frequency of each wind direction and the hourly average wind speed of each wind direction are obtained, as is shown in Table 1.

Then the wind direction with the highest frequency is obtained, and the average wind speed in this direction in the morning, noon, and evening are calculated and shown in Table 2. Among them, the average wind speed in the morning takes the average of 6 a.m. and 9 a.m. wind speeds, the average wind speed at noon the average of 12 p.m. and 3 p.m. wind speeds and the average wind speed at night the average of 6 p.m. and 9 p.m. wind speeds.

Table 1. Frequency and average wind speed of each wind direction.

From	To	Frequency (%)	Hourly average wind speed ( $\text{m s}^{-1}$ )
11.25°	33.75°	18.18	1.4
33.75°	56.25°	9.33	1.3
56.25°	78.75°	3.34	1.5
78.75°	101.25°	3.56	1.2
101.25°	123.75°	7.63	1.5
123.75°	146.25°	10.94	1.5
146.25°	168.75°	5.10	1.6
168.75°	191.25°	2.55	1.3
191.25°	213.75°	1.10	1.3
213.75°	236.25°	1.61	1.0
236.25°	258.75°	3.08	1.1
258.75°	281.25°	3.40	1.5
281.25°	303.75°	3.07	1.1
303.75°	326.25°	2.91	1.5
326.25°	348.75°	3.41	1.1
348.75°	11.25°	20.79	1.8

Table 2. The wind speed in the most frequent wind directions.

U ( $\text{m s}^{-1}$ )	Morning			Noon			Evening		All Day
	6 a.m.	9 a.m.	12 p.m.	15 p.m.	18 p.m.	21 p.m.			
U max	2.5	3.0	3.9	3.7	3.4	5.7			5.7
U min	0.1	0.1	0.1	0.1	0.1	0.1			0.1
U average	0.7	1.1	1.9	1.8	0.9	1.1			1.1

### 2.3.2. Atmospheric stability class

Atmospheric stability class is a measure of the thermal properties of the atmosphere. It is one of the main meteorological factors affecting the transport and dispersion of pollutants. The classification method of atmospheric stability class recommended in current Chinese standard GB T3840–91 is the Pasquill (PS) method. Atmospheric stability is divided into six levels, including strong instability, instability, weak instability, neutrality, comparative stability, and stability, representing A, B, C, D, E, and F respectively. According to the GB T3890–91, the stability class is determined by the corresponding solar altitude angle and solar radiation level. It is worth mentioning that when the atmospheric stability is neutral or stable, the convection of the atmosphere will be suppressed, the pollutants will not easily spread, thus easily causing air pollution or mixing into the clouds to reduce the rainfall and strengthening the ground pollution (Zhu, 1989). According to the research, the atmospheric stability of Hangzhou is mostly neutral and stable (Ma et al., 2012). Because we were unable to obtain relevant meteorological data, the atmospheric stability was assumed to be neutral in the modeling of H<sub>2</sub>S concentration in the three periods of a day and we compared the trend of H<sub>2</sub>S concentration dispersion under six different atmospheric stability class in the end.

### 2.4. Gaussian dispersion model

If it is used to simulate the dispersion of pollutants in a specific area, the Gaussian dispersion model coordinate system should be established first. The odor pollution of the six-story pig house in Yiwu is regarded as a continuous point source. The projection of the pollution point source on the ground is taken as the coordinate origin, and the main wind direction of the simulation area being selected as the positive direction of the X-axis, the tangential direction of the leading wind direction on the ground surface being taken as the Y-axis, and the vertical direction of the surface water level being taken as the Z-axis. The primary simulation of this study evaluates the dispersion characteristics of H<sub>2</sub>S, so the Gaussian plume model with continuous point source continuous

emission is used.

When the atmosphere is stable and the pollution source discharges continuously, the spatial distribution of the pollutants is stable. Its concentration does not change with time in a specific spatial position. Therefore, when the atmospheric conditions are borderless, the algorithm for expressing the pollutant dispersion model of a stable point source is as follows:

$$C_{(x,y,z)} = \frac{q}{2\pi u \sigma_y \sigma_z} \exp \left[ -\frac{1}{2} \left( \frac{y^2}{\sigma_y^2} + \frac{z^2}{\sigma_z^2} \right) \right] \quad (1)$$

where  $C$  is downwind concentration of the  $\text{H}_2\text{S}$  ( $\mu\text{g m}^{-3}$ );  $q$  is  $\text{H}_2\text{S}$  emission rate ( $\mu\text{g s}^{-1}$ );  $y$  is horizontal transversal distance vertical to the average wind direction (m);  $z$  is human's respiratory height (m);  $\sigma_y$  is transversal dispersion parameter;  $\sigma_z$  is vertical dispersion parameter. The dispersion parameter  $\sigma_y$  and  $\sigma_z$  is given by

$$\sigma_y = \gamma_1 x^{\alpha_1} \quad (2)$$

$$\sigma_z = \gamma_2 x^{\alpha_2} \quad (3)$$

where  $\alpha_1, \alpha_2, \gamma_1, \gamma_2$  can be found in Table D1 of Appendix D in the China national standard GB/T 3840–91 by using the corresponding atmospheric stability class.

The factors affecting the dispersion of the atmosphere include meteorological factors and geographical factors. Therefore, in the process of simulation, it is necessary to make corrections to the parameters and determine the specific values for different terrains and meteorological conditions according to actual conditions.

### 3. Results & Discussion

The dispersion trend of  $\text{H}_2\text{S}$  at the highest frequency wind was simulated first. As shown in Figures 1–3, the  $\text{H}_2\text{S}$  concentration decreases continuously as the downwind distance increases. When the distance exceeds 200 m, it drops to a very low level. When the distance exceeds 1000 m, it is close to 0 ppb. Moreover, wind speed significantly affects the  $\text{H}_2\text{S}$  concentration and dispersion. The downwind  $\text{H}_2\text{S}$  concentration is inversely proportional to wind speed. Because the higher the wind speed is, the stronger the ability of atmospheric dispersion and dilution, on the contrary, the weaker the ability of dispersion dilution.

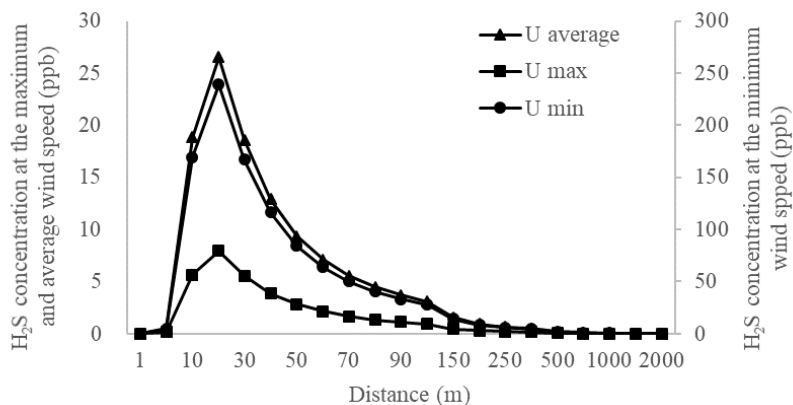


Figure 1.  $\text{H}_2\text{S}$  dispersion in the morning.

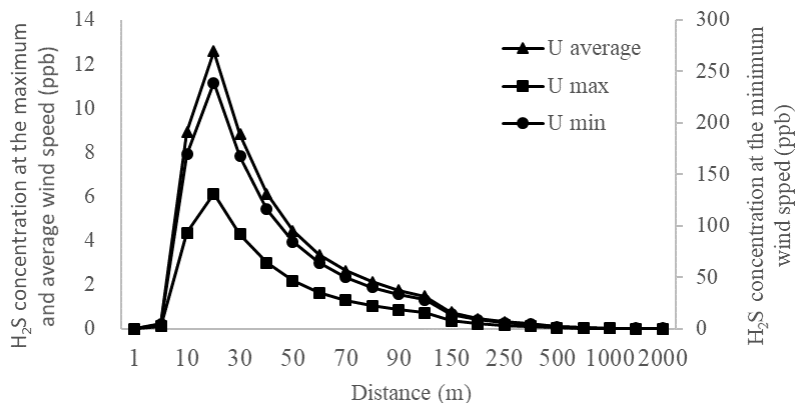
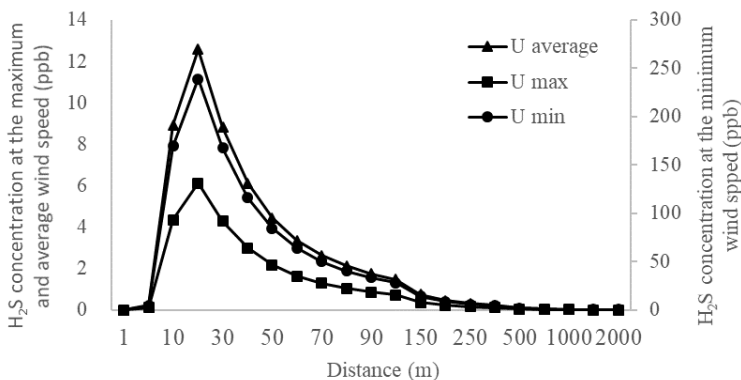
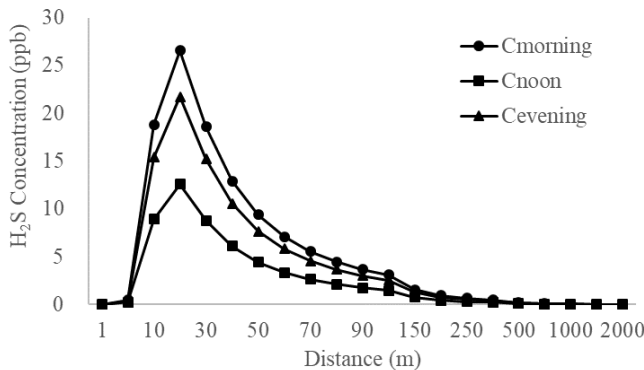
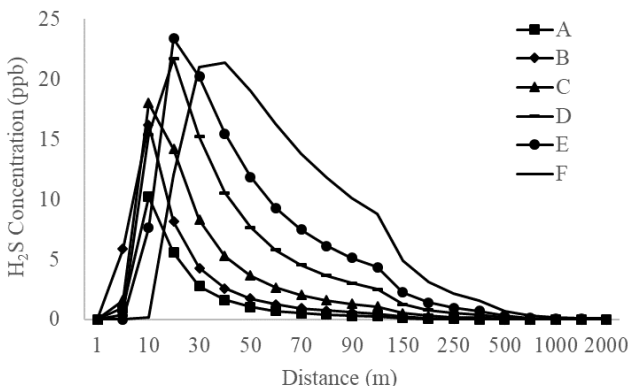
Figure 2. H<sub>2</sub>S dispersion at noon.Figure 3. H<sub>2</sub>S dispersion in the evening.

Figure 4 shows the comparison of H<sub>2</sub>S concentrations in the three different periods of a day. It is indicated that the H<sub>2</sub>S dispersion trends over those three time periods are the same. However, the H<sub>2</sub>S concentration in the morning is the highest with its highest value exceeding 25 ppb, that in the evening being the second highest with its highest value close to 20 ppb and that at noon being the lowest with its highest value around 10 ppb. H<sub>2</sub>S concentration reached the highest value at 20 m away from the pig farm while within 20 m to 200 m, it decreases with the increase of distance. Given that the H<sub>2</sub>S concentration limit is 20 mg m<sup>-3</sup> (around 14.4 ppb) in the Emission Standard for Odour Pollutants (GB 14554–93), odor pollution is severe at a distance of 10 m to 30 m away from the pig farm.

Finally, we compared the trend of H<sub>2</sub>S concentration dispersion under six different atmospheric stability classes. The results are shown in Figure 5. It is observed that when the atmospheric stability is neutral and stable conditions, both the peak concentrations of H<sub>2</sub>S and the range of pollution are higher than those when the atmospheric stability is unstable. Therefore, it is confirmed that when the atmospheric stability is neutral and stable, atmospheric convection is suppressed, resulting in the non-dispersion of pollutants and enhanced air pollution.

Figure 4. H<sub>2</sub>S dispersion in the three periods.Figure 5. H<sub>2</sub>S dispersion in different atmospheric stability class.

#### 4. Conclusions

This paper reports a preliminary study of dispersion of H<sub>2</sub>S emitted from a six-story pig building in Yiwu, China. The pig building was regarded as a continuous point source and the Gaussian dispersion model was used to predict downwind concentrations of H<sub>2</sub>S in response to different downwind distances and atmospheric stability conditions. The following observations were obtained through this modeling study.

The concentration of H<sub>2</sub>S decreases continuously as the downwind distance increases. Moreover, the H<sub>2</sub>S concentration in the morning was the highest in this area and the H<sub>2</sub>S concentration peaked at a position about 20 m away from the point source and then decreased with the increase of the downwind distance. When the downwind distance exceeds 200 m, the H<sub>2</sub>S concentration can be ignored. Because the high level of H<sub>2</sub>S concentration (>14.4 ppb of GB 14554–93 threshold), odor pollution may be considered severe at a distance of 10 m to 30 m away from pig farm. The H<sub>2</sub>S concentration in the morning is the highest with its highest value exceeding 25 ppb, that in the evening being the second highest with its highest value close to 20 ppb and that at noon being the lowest with its highest value around 10 ppb. The downwind H<sub>2</sub>S concentration is inversely proportional to wind speed. It was also found that when the atmospheric stability is neutral and stable, both the peak concentration of the H<sub>2</sub>S and the range of pollution are higher than those when the atmospheric stability is unstable.

At present, the modeling and simulation of dispersion of H<sub>2</sub>S emitted from the six-story pig buildings is in the preliminary stage. Therefore, in-depth research and field validation of the modeling results should be done in the future to improve the accuracy of the model further.

### Acknowledgment

The research was financially supported by the National Natural Science Fund of China (No. 31672468); National Key R&D Program of China (Project No. 2017YFD0701700); Thousand Talents Program (Youth Project 2016).

### References

- Dai, X.R., 2010. Study on Ammonia Emission Factors in Concentrated Pig Farm. MS Thesis, College of Biosystem Engineering and Food Science, Zhejiang University, Hangzhou, Zhejiang, China.
- Dong, N., 2008. Study on the Treatment of Hydrogen Sulfide Odor Air Using Modified Activated Alumina Adsorbent, MS Thesis, College of New Energy and Environment, Jilin University, Changchun, Jinlin, China.
- Feilberg, A., M.J. Hansen, D.Z. Liu, T. Nyord, 2017. Contribution of livestock H<sub>2</sub>S to total sulfur emissions in a region with intensive animal production. *Nature Communications*. 8. <http://dx.doi.org/10.1038/s41467-017-01016-2>
- Guffanti, P., V. Pifferi, L. Falciola, V. Ferrante, 2018. Analyses of odours from concentrated animal feeding operations: A review. *Atmospheric Environment*. 175, 100–108. <http://dx.doi.org/10.1016/j.atmosenv.2017.12.007>.
- Ma, X.J., X.G. Jiang, Y.Q. Jin, L.H. M., T. Chen, Y.J. H., 2012. Dispersion modeling and health risk assessment of dioxin emissions from a municipal solid waste incinerator in Hangzhou, China. *Journal of Zhejiang University SCIENCE A*. 13 (01), 69–78. <http://dx.doi.org/10.1631/jzus.a1100201>
- Qu, K., S.W. Lee, J.S. Bian, C.M. Low, P.T. Wong, 2008. Hydrogen sulfide: neurochemistry and neurobiology. *Neurochem Int*. 52 (1–2), 155–165. <http://dx.doi.org/10.1016/j.neuint.2007.05.016>.
- Schiffman, S.S., C.E. Studwell, L.R. Landerman, K. Berman, J.S. Sundy, 2005. Symptomatic effects of exposure to diluted air sampled from a swine confinement atmosphere on healthy human subjects. *Environ Health Perspect*. 113 (5), 567–576. <http://dx.doi.org/10.1289/ehp.6814>.
- Wu, C.D., M. Brancher, F. Yang, J. Liu, C. Qu, G. Schaubberger, M. Piringer, 2019. A Comparative Analysis of Methods for Determining Odour-Related Separation Distances around a Dairy Farm in Beijing, China. *Atmosphere*. 10 (5). <http://dx.doi.org/10.3390/atmos10050231>.
- Yan, Z.Y., L.S. Xu, Z.D. Li, X.F. Liu, Y.X. Yuan, X.L. Wei, 2014. Progress in Research and Application of Controlling Odor from Livestock Manure. *Chinese Journal of Applied & Environmental Biology*. 20 (02), 322–327. <http://dx.doi.org/10.3724/SP.J.1145.2014.00322>.
- Zhou, B., 2015. Study and application of air pollution control technology in pig farm, College of Biosystem Engineering and Food Science, Zhejiang University, Hangzhou, Zhejiang, China.
- Zhu, S.F., 1989. The Frequency Distribution of Atmospheric Stability and Its Regional Characteristics in Zhejiang Province. *Environmental Pollution & Control*. 11 (05), 14–17. <http://dx.doi.org/10.15985/j.cnki.1001-3865.1989.05.004>.

# Effects of Different Color LED lights on Layer Chickens During Brooding and Rearing Periods

**Yongxiang Wei<sup>a,b,c</sup>, Weichao Zheng<sup>a,b,c,\*</sup>, Baoming Li<sup>a,b,c</sup>, Qin Tong<sup>a,b,c</sup>**

<sup>a</sup> Department of Agricultural Structure and Environmental Engineering,  
College of Water Resources & Civil Engineering, China Agricultural University, Beijing 100083,  
P.R. China

<sup>b</sup> Key Laboratory of Agricultural Engineering in Structure and Environment,  
Ministry of Agriculture and Rural Affairs, Beijing 100083, P.R. China

<sup>c</sup> Beijing Engineering Research Center on Animal Healthy Environment, Beijing 100083, P.R. China

\* Corresponding author. Email: [weichaozheng@cau.edu.cn](mailto:weichaozheng@cau.edu.cn)

## Abstract

Behavior, growth, and production performance of poultry are affected by light environment. The influence of light is a resultant of light intensity, light color, and photoperiod. With light-emitting diode (LED) lamp being applied in poultry housing systems, specific light color for each period of layer chickens is desired. The objective of this study was to investigate effects of different color LED lights on layer chickens during their brooding and rearing periods. Fifty-two hens were raised in each of the 4 treatment groups with 3 replicates, White (400–700 nm) light at 0–20 weeks (WL treatment as the control); blue-green (435–565 nm) light at 0–13 weeks followed by yellow-orange (565–630 nm) light at 14–20 weeks (BG-YOL treatment); yellow-orange LED (565–630 nm) light at 0–20 weeks (YOL treatment); and blue-green (435–565 nm) light at 0–20 weeks (BGL treatment). The results showed that the serum immunoglobulins (Ig) concentrations of layer chickens in BG-YOL treatment and BGL treatment were more than those in WL treatment ( $P < 0.05$ ). Serum glucose (GLU) concentration levels following the WL and BGL treatments were less than those following YOL treatment ( $P < 0.05$ ). Compared with WL treatment, YOL treatment increased bone mineral density of layer chickens ( $P < 0.05$ ), and BG-YOL treatment could promote development of sexual organ (oviduct and ovary) of laying hens ( $P < 0.05$ ). For the age of 50% of chickens starting to lay eggs, YOL treatment was earlier than the other three treatments. This study demonstrated that appropriate staged spectral control using LED lights could have positive effects on caged laying chickens during their brooding and rearing periods.

**Keywords:** Pullets, light-emitting diode, light spectrum, bone quality, immune performance

## 1. Introduction

Lighting is one of the essential environmental factors in poultry houses. Behavior, growth and development, and production performance of poultry are affected by light (Lewis et al., 1998; Olanrewaju et al., 2006; Parvin et al., 2014). Nowadays, because of its high energy efficiency, long operating life, availability in different peak wavelength, low electricity consumption and low rearing cost (Hassan et al., 2013, 2014; Sultana, et al 2013; Huber-Eicher et al., 2013; Liu et al., 2017), light-emitting diode (LED) light is gradually replacing conventional incandescent and fluorescent lights in the poultry industry (Li et al., 2018; Yang et al., 2016).

While the white LED and monochrome LED lights are widely applied in poultry production (Hassan et al., 2013, 2014; Liu et al., 2017), these lights may not meet the requirement on welfare and health of layer chickens, especially for the brooding and rearing periods (0–20 week), when staged spectral control is required to meet the growth of immune and digest system or skeletal and sexual development over the increasing chicken age. Some studies have shown that blue and green light can improve the growth of layer chickens, help to calm them down, and promote their immune performance (Hassan et al., 2013; Xie et al., 2008; Zhang et al., 2014). Red light can promote the sexual development and maturity of pullets (Hassan et al., 2013; Min et al., 2012; Gongruttananun, 2011). Moreover, many color LED lamps are currently available commercially to meet light environmental requirement of modern poultry houses (Rozenboim et al., 1998).

Therefore, we hypothesized that different color LED lights given during different growing stages could promote growth and sexual development of layer chickens. However, limited information about the effect of staged spectral light control on performance of layer chickens is available, especially during the brooding and rearing periods.

In this study, the effects of different color LED lights on the blood parameters, skeletal development parameters, and sexual development parameters in laying hens were evaluated. The objectives of the study were: a) to select appropriate light color for laying hens during brooding and rearing periods; b) to carry out staged spectral light control to enhance biology system development of layer chickens, in order to provide a theoretical basis on the application of LED lights for the layer chickens during brooding and rearing periods.

## 2. Materials and Methods

### 2.1. Hens and treatments

All the hens in this experiment were managed by trained staff with standing guidelines for Jinghong laying hens (Beijing Yukou Poultry Co., Ltd., Beijing, China). Fifty-two hens were raised in each of the 4 treatment groups with 3 replicates, white (400–700 nm) light at 0–20 weeks (WL treatment as the control); blue-green (435–565 nm) light at 0–13 weeks followed by yellow-orange (565–630 nm) light at 14–20 weeks (BG-YOL treatment); yellow-orange LED (565–630 nm) light at 0–20 weeks (YOL treatment); and blue-green (435–565 nm) light at 0–20 weeks (BGL treatment). A shading cloth was installed between the adjacent individual cages to avoid unintended irradiation to hens from the lamps in other cages. The surface of the light was wiped by 75% alcohol regularly to avoid excessive dust affecting its light intensity. Each treatment had 4 cages (length × width × height = 72 × 65 × 40 cm) distributed at the 4 tiers of the stacked cage system and 4 different treatments were randomly assigned in the one same chamber (other two chambers as two replicates) (Figure 1).

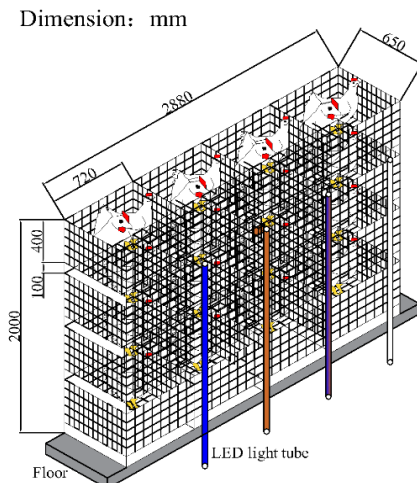


Figure 1. Oblique view of the 4 treatments in one chamber.

Air temperature of the three chambers was maintained between 16 °C and 36 °C and the relative humidity of the three chambers was maintained between 40% and 60% during the whole experiment. Light tube with specific color was provided by LEDs (220 V 15 W, Huazhaohong Optoelectronic Technology Co., Ltd., Wuxi, China) in each chamber. The lighting intensity measured by an illuminometer (SRI 2000, Shangze Photoelectric Co., Ltd.) was averaged 5–60 lux at the level of the birds' head in the middle of each tier cages, which was adjusted with the

age of the layer chickens. Spectral characteristics involved in this study are shown in Figure 2. Hens were fed twice per day at 08:00 am and 02:00 pm, and unlimited water was provided during the whole experiment period. The photoperiodic and light intensity are shown in Table 1.

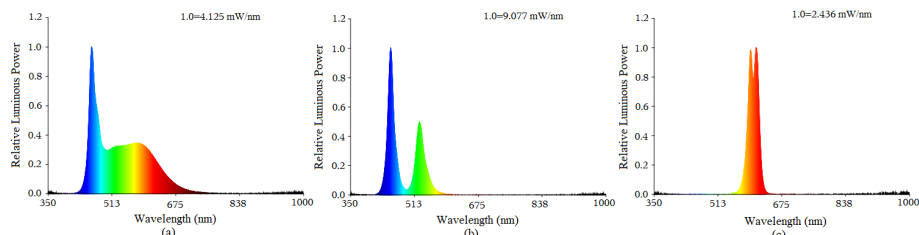


Figure 2. Spectral characteristics: (a) white light-emitting diode light (WL); (b) blue-green light-emitting diode light (BGL); (c) yellow-orange light-emitting diode light (YOL).

Table 1. Photoperiodic and light intensity.

Day (d) or week (wk)	Photo-periodic (h)	Light (lux)	Day (d) / week (wk)	Photo-periodic (h)	Light (lux)
1–3 d	24	40–60	6 wk	12	5–10
4–7 d	22	40–60	7 wk	10	5–10
2 wk	20	20–40	8–13 wk	9	5–10
3 wk	18	10–20	14–18 wk	9	5–10
4 wk	16	5–10	19 wk	10	10–20
5 wk	14	5–10	20 wk	11	10–20

## 2.2. Data collection and measurements

*Blood parameters:* Blood samples were collected in anticoagulant blood vessels from the right jugular vein of the same one bird which was randomly chosen in each cage at the age of 7 weeks (50 days), 13 weeks (92 days), and 20 weeks (141 days) during the experiment, respectively. The collected samples were stored under conditions of -20 °C before being delivered to Beijing Huaying Biotechnology Research Institute (Beijing, China) for test at the same day. Immunoglobulins G (IgG) was determined at the age of 7, 13, and 20 weeks, respectively. Glucose (GLU), total protein (TP), triglyceride (TG), phosphorus (P), and calcium (Ca) were measured at the age of 20 weeks.

*Skeletal development parameters:* A bird randomly selected from each cage was euthanized at the age of 7, 13, and 20 weeks during the experiment, respectively. Its left tibia was removed and the tibia traits (bone mineral density, bone mineral content and bone area) were detected by a dual-energy X-ray bone mineral density instrument (Lunar-iDXA, GE, USA).

*Sexual development parameters:* Laying chickens were killed humanely by neck dislocation, and the length and weight of oviduct and the weight of ovary were recorded at the age of 20 weeks. The age of first and 50% of chickens starting to lay eggs in each treatment was recorded.

## 2.3. Statistical analysis

Data are presented as means  $\pm$  Standard Error (SE). Statistical analyses were performed by SPSS (IBM SPSS Statistics 16.0, USA). Data were analyzed by one-way repeated measures analysis of variance (ANOVA). Differences between weeks within the groups were analyzed by independent-samples T test. Means were considered as significantly different at  $P < 0.05$ .

## 3. Results and Discussion

### 3.1. Blood parameters

It is well known that an antibody, an immunoglobulin, is an important component of the body's humoral immune system to protect body from bacteria and viruses. And the immunoglobulin

concentrations reflect the performance of the immune system. Figure 3 shows the changes of immunoglobulins G (IgG) level under different LED light treatment. No significant difference in IgG level was detected in different treatment group at 7 weeks and 20 weeks of age. However, at 13 weeks of age, the IgG contents under BGL group and BG-YOL group were more than that under WL group. This confirms the results of previous study that immune function of poultry could be affected by light color (Cao et al., 2008; Rozenboim et al., 1999), and blue light can enhance the immune response (Hassan et al., 2013; Xie et al., 2008; Zhang et al., 2014). These might have been due to the calming effect of the blue treatment on chicken activity (Prayitno et al., 1997). Moreover, blue light (BL) would alleviate the negative effects induced by the stress response, subsequently leading to a well-balanced immune response status. Hence, BL may play a vital role in alleviating the stress response and improve immune level in poultry (Xie et al., 2008).

In addition, the photoreceptors in the hypothalamus are more sensitive to blue and green light than red light (Osorio et al., 2008). Thus, it may be concluded that short-wavelength (blue and green) light might keep chickens calm and quiet, and reduced response on environment to promote immune performance of pullets.

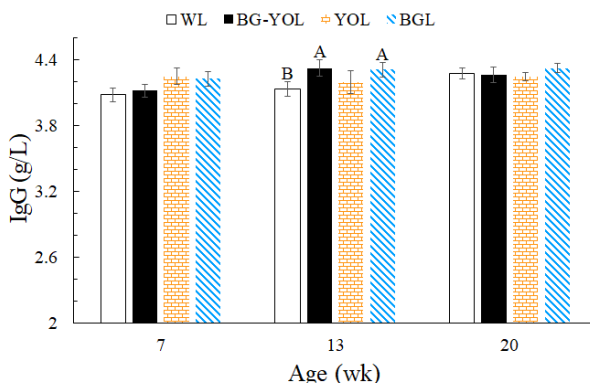


Figure 3. Effect of different color LED treatments on serum IgG content in laying hens.

Note: White (400–700 nm) light at 0–20 weeks (WL treatment as the control); blue-green (435–565 nm) light at 0–13 weeks followed by yellow-orange (565–630 nm) light at 14–20 weeks (BG-YOL treatment); yellow-orange LED (565–630 nm) light at 0–20 weeks (YOL treatment); and blue-green (435–565 nm) light at 0–20 weeks (BGL treatment). Data are presented as means  $\pm$  SE. Different capital letters indicate significant differences ( $P < 0.05$ ).

The biochemical blood parameters of the laying hens during the full trial period (0–20 weeks) are summarized in Table 2. The total protein (TP) at 20 weeks of age significantly differed amongst YOL group and other two treatments (BG-YOL group and BGL group). At the age of 20 weeks, serum blood glucose (GLU) concentrations following the YOL group treatment was improved, which corresponded to the results of Hassan et al., (2013). One reason was that hens raised under a red light were more active to generate more energy (Sultana et al., 2013). There were significantly differences in triglyceride (TG) at 20 weeks of age between the BL group and other three groups. It may have been due the calming effect of the short-wavelength on poultry activity (Prayitno et al., 1997), which would cause fat accumulation of body in laying hens. At 20 weeks of age, YOL treatment increased serum calcium (Ca) concentrations and decreased serum phosphorus (P) concentrations, which was consistent with the previous research that both P and Ca showed antagonism effects (Li et al., 2014). On the other hand, the increase of Ca absorption will promote skeleton mineralization (Zhang et al., 2006). Therefore, YOL may be useful for the skeleton growth and development of layer chickens.

Table 2. Effects of different color LED lights on the biochemical blood parameters of laying hens at 20 weeks of age.

Parameter	Treatment group			
	WL	BG-YOL	YOL	BL
TP ( $\text{g L}^{-1}$ )	39.54±0.86	37.59±0.84 <sup>b</sup>	37.91±1.11 <sup>b</sup>	40.67±0.84 <sup>a</sup>
GLU ( $\text{mmol L}^{-1}$ )	15.82±0.18 <sup>a</sup>	15.53±0.37	15.71±0.15 <sup>a</sup>	14.92±0.20 <sup>b</sup>
TG ( $\text{mmol L}^{-1}$ )	13.49±2.10 <sup>b</sup>	11.76±2.25 <sup>b</sup>	13.09±2.92 <sup>b</sup>	20.54±2.01 <sup>a</sup>
Ca ( $\text{mmol L}^{-1}$ )	8.27±0.73 <sup>b</sup>	7.91±0.74 <sup>b</sup>	10.18±0.87 <sup>a</sup>	9.64±0.43
P ( $\text{mmol L}^{-1}$ )	4.33±0.16	4.32±0.12	4.06±0.16 <sup>b</sup>	4.56±0.12 <sup>a</sup>

Note: White (400–700 nm) light at 0–20 weeks (WL treatment as the control); blue-green (435–565 nm) light at 0–13 weeks followed by yellow-orange (565–630 nm) light at 14–20 weeks (BG-YOL treatment); yellow-orange LED (565–630 nm) light at 0–20 weeks (YOL treatment); and blue-green (435–565 nm) light at 0–20 weeks (BGL treatment). Data are presented as means ± Standard Error (SE). Different lowercase letters indicate significant differences ( $P < 0.05$ ). The same as the following Tables.

### 3.2. Skeletal development parameters

The effect of different color LED lights on the skeletal parameters of laying hens during brooding and rearing periods is shown in Table 3. The bone mineral density, bone mineral content, and bone area in general are used to evaluate the bone status (Park et al., 2003). There were no significant changes in bone mineral density (BMD) between 7 weeks and 13 weeks of age. However, at 20 weeks of age, BMD of layer chickens in YOL group was more than BMD of layer chickens in WL group. No significant difference in bone mineral content and area level was detected in different treatment groups ( $P > 0.05$ ).

The previously published results demonstrated that bone development of chickens during brooding and rearing periods determined the egg production performance and mortality in the late egg production stage (Hester et al., 2011). In addition, BMD, a very important measure of bone quality, is usually proportional to bone quality (Riczu et al., 2004) and positively related to bone breaking strength (McCoyetal, 1996). And raised in cages is main reason resulting osteoporosis of chickens (Rennie et al., 1997), rather than nutrition, though poor nutrition (in terms of calcium and phosphorus content or availability) may exacerbate the osteoporosis condition (Bishop et al., 2000). Allowing birds more exercise will improve bone strength (Whitehead et al., 2000). Moreover, hens raised under a red light were more active and performed more walking behaviors (Sultana et al., 2013). Thus, it is believed that YOL can increase activity amount of chickens to increase BMD content.

It was proved that hens spent more inactive time sitting or sleeping under blue light, whereas birds illuminated with red light were more active and engaged in more ground scratching behaviors (Hassan et al., 2014; Sultana et al., 2013). Hence, YOL would have a positive effect on improving bone quality of pullets. However, longer-term studies and a larger sample size probably will be needed to validate that possibility.

### 3.3. Sexual development parameters

There were no significantly changes in sexual organ development in different groups at the age of 16 weeks (Table 4). At the age of 20 weeks, the length of oviduct, the weight of oviduct, and the weight of ovary of laying hens under BG-YOL group were more than those under WL group. It disconfirmed previously published results that gonadal development was not affected by the light color (Pyrzak et al., 1986), the difference of light sources, photoperiod, light intensity, age, and nutrition maybe the reasons to cause different observation by the two studies. In addition, YOL can penetrate the skull of poultry on the hypothalamus, stimulating hormone secretion (Lewis et al., 2000). Therefore, when the light stimulates the hypothalamus, the body secretes

gonadotropin-releasing hormone (GnRH), which promotes the secretion of follicle-stimulating hormone (FSH) and luteinizing hormone (LH) in the anterior pituitary, and finally promotes the development oviduct and ovary.

Table 3. Effects of different color LED treatments on the skeletal parameters of laying hens during brooding and rearing periods.

Age (week)	Treatment group	Bone mineral density (g cm <sup>-2</sup> )	Bone mineral content (g)	Area (cm <sup>2</sup> )
7	WL	0.144±0.002	0.76±0.02	5.27±0.14
	BG-YOL	0.143±0.002	0.79±0.03	5.49±0.14
	YOL	0.142±0.001	0.75±0.02	5.26±0.13
	BGL	0.141±0.002	0.78±0.03	5.57±0.18
13	WL	0.169±0.002	1.33±0.03	7.87±0.13
	BG-YOL	0.171±0.003	1.32±0.04	7.70±0.16
	YOL	0.172±0.001	1.29±0.02	7.51±0.09
	BGL	0.169±0.003	1.29±0.03	7.62±0.14
20	WL	0.206 <sup>b</sup> ±0.005	1.64±0.05	7.92±0.09
	BG-YOL	0.210±0.004	1.57±0.06	7.47±0.23
	YOL	0.215 <sup>a</sup> ±0.003	1.64±0.06	7.60±0.26
	BGL	0.209±0.002	1.66±0.04	7.97±0.17

Unlike mammals, the non-visual effects of hens are more important than visual effects, and the perception of light during reproduction does not depend on the photoreceptors of the eye (Jácome et al., 2014). Studies have shown that the photoreceptor of the hypothalamus is a bioconverter that converts photon energy into nerve impulses, which would affect and control the endocrine system of ovarian activity, which in turn affects the reproductive, behavioral, and secondary sexual characteristics of laying hens (Morris, 1973). Long-wavelength light can pass through the skull more easily than the short-wavelength light, and act on the hypothalamus extra-retinal photoreceptors (Huber-Eicher et al., 2013; Lewis et al., 2000, Mobarkey et al., 2010). Therefore, yellow-orange light is more likely to act on hypothalamus than blue-green light and white light, and promotes the sexual maturity of laying hens.

Table 4. Effects of different color LED treatments on the sexual organs of laying hens at 16 and 20 weeks of age.

Age (week)	Treatment group	The length of oviduct (cm)	The weight of oviduct (g)	The weight of ovary (g)
16	WL	10.07±0.46	1.8±0.17	0.9±0.12
	BG-YOL	9.95±0.58	1.9±0.13	0.8±0.07
	YOL	9.17±0.45	1.8±0.11	0.9±0.09
	BGL	9.50±0.31	1.7±0.09	0.8±0.07
20	WL	42.42 <sup>b</sup> ±7.18	36.6 <sup>b</sup> ±10.08	19.0 <sup>b</sup> ±6.21
	BG-YOL	59.17 <sup>a</sup> ±3.83	63.3 <sup>a</sup> ±9.37	25.0 <sup>a</sup> ±6.46
	YOL	45.67 <sup>b</sup> ±14.09	45.1 <sup>b</sup> ±19.42	20.2±8.85
	BGL	62.17 <sup>a</sup> ±4.56	60.6 <sup>a</sup> ±10.66	22.6±5.46

Table 5 shows the effect of different color LED treatments on the reproduction performance. The age of 50% of chickens starting to lay eggs under BG-YOL group and YOL group was earlier than the other two groups. The YOL group improved production uniformity, the BG-YOL group and the WL group were the second, and the BGL group was the last. These results confirmed that long wavelength (red, orange, and yellow) light can promote sexual development (Liu et al., 2017), because the long wavelength stimulated extra retinal photoreceptors, which reflect on the pituitary

gland and deep brain and influence gonadal hormone (FSH, LH, and estradiol (E2)) secretion and subsequent rapid development of the oviduct and ovary to promote laying eggs (Hartwig et al., 1979).

Furthermore, it had also been demonstrated that red, orange, or yellow light, as a long-wavelength radiation, can pass through hypothalamic extra-retinal photoreceptors of poultry and stimulate the hypothalamus-pituitary growth axis to release related hormone (Lewis et al., 2000), thereby having an accelerating effect on activity stimulation, sexual development and maturity of poultry (Baxter et al., 2014; Li et al., 2014). The results in this study also supported the above theoretical analysis. However, the age of 50% of pullets starting to laying eggs under blue and green light was earlier than those under white light, which disconfirmed the previous observation that short-wavelength could delay sexual maturity of poultry (Min et al., 2012). There might exist a threshold for visual sensitivity in poultry's response to long-wavelength radiation, only when the intensity of short-wavelength light reached a certain level, long-wavelength light effects may occur (Liu et al., 2017; Benoit., 2006). More research about comprehensive effect between light intensity and color on laying hens is needed to confirm appropriate spectrum parameters.

Table 5. Effects of different color LED treatments on the reproduction performance.

Treatment group	The age of first egg (d)	The age of 50% egg (d)	The age from first egg to 50% egg (d)
WL	127	137	10
BG-YOL	124	133	9
YOL	126	133	7
BGL	121	135	14

Note: White (400–700 nm) light at 0–20 weeks (WL treatment as the control); blue-green (435–565 nm) light at 0–13 weeks followed by yellow-orange (565–630 nm) light at 14–20 weeks (BG-YOL treatment); yellow-orange LED (565–630 nm) light at 0–20 weeks (YOL treatment); and blue-green (435–565 nm) light at 0–20 weeks (BGL treatment).

#### 4. Conclusions

This study investigated the effects of different color LED lights on the growth and development of laying chickens during brooding and rearing periods (0–20 week). The results demonstrated that staged spectral control using LED lights could be beneficial to the growth of pullets. The blue-green light (BGL) at 0–13 week slightly increased the serum immunoglobulins (Ig) concentrations and serum glucose (GLU) concentration levels of layer chickens. The yellow-orange light (YOL) at 14–20 weeks increased bone mineral density concentrations, promoted sexual organ development (oviduct and ovary), advanced production age and improved production uniformity of layer chickens. Results of this research should stimulate further studies on the effects of exposure of chickens to different color LED lights. Further research on how the hormone in serum and body to be synthesized is needed to promote welfare and health of laying hens.

#### Acknowledgements

The animal study proposal was approved by The Laboratory Animal Ethical Committee of China Agricultural University. This study was funded by the National Key R&D Program of China (2017YFB0404000). Thanks to the colleagues of Shangzhuang experimental station and the department of Agricultural Structure and Bioenvironmental Engineering, College of Water Resources and Civil Engineering, China Agricultural University, Beijing, China.

#### References

- Lewis, P. D., T. R. Morris, 1998. Responses of domestic poultry to various light sources. World's Poultry Science Journal. 54(01), 7–25.

- Olanrewaju, H. A., S. Wongpichet, J. P. Thaxton, W. A. Dozier, S. L. Branton, 2006. Stress and acid-base balance in chickens. *Poultry Science*. 85(7), 1266–1274.
- Parvin, R., M. M. H. Mushtaq, M. J. Kim, H. C. Choi, 2014. Light emitting diode (LED) as a source of monochromatic light: a novel lighting approach for behaviour, physiology and welfare of poultry. *World's Poultry Science Journal*. 70(03), 543–556.
- Sultana, S., M. R. Hassan, H. S. Choe, M. I. Kang, K. S. Ryu, 2013. Effect of various LED light color on the behavior and stress response of laying hens. *Indian Journal of Animal Sciences*. 83(8), 829–833.
- Sultana, S., M. R. Hassan, H. S. Choe, K. S. Ryu, 2013. The effect of monochromatic and mixed LED light colour on the behaviour and fear responses of broiler chicken. *Avian Biology Research*. 6(3), 207–214.
- Hassan, M. R., S. Sultana, H. S. Choe, K. S. Ryu, 2013. Effect of monochromatic and combined light colour on performance, blood parameters, ovarian morphology and reproductive hormones in laying hens. *Italian Journal of Animal Science*. 12(56), 359–364.
- Hassan, M. R., S. Sultana, H. S. S. Choe, K. S. Ryu, 2014. Effect of combinations of monochromatic LED light color on the performance and behavior of laying hens. *The Journal of Poultry Science*. 51(3), 321–326.
- Huber-Eicher, B., A. Suter, P. Spring-Stähli, 2013. Effects of colored light-emitting diode illumination on behavior and performance of laying hens. *Poultry Science*. 92(4), 869–873.
- Liu, K., H. Xin, J. Sekhon, T. Wang, 2017. Effect of fluorescent vs. poultry-specific light-emitting diode lights on production performance and egg quality of W-36 laying hens. *Poultry Science*. 97(3), 834–844.
- Min, J. K., M. S. Hossan, A. Nazma, C. N. Jae, T. B. Han, K. K. Hwan, ... S. S. Ok, 2012. Effect of monochromatic light on sexual maturity, production performance and egg quality of laying hens. *Avian Biology Research*. 5(2), 69–74.
- Gongruttananun, N., 2011. Influence of red light on reproductive performance, eggshell ultrastructure, and eye morphology in Thai-native hens. *Poultry Science*. 90(12), 2855–2863.
- Rozenboim, I., E. Zilberman, G. Gvaryahu, 1998. New monochromatic light source for laying hens. *Poultry Science*. 77(11), 1695–1698.
- Prayitno, D., C. Phillips, D. Stokes, 1997. The effects of color and intensity of light on behavior and leg disorders in broiler chickens. *Poultry Science*. 76(12), 1674–1681.
- Manser, C. E., 1996. Effects of lighting on the welfare of domestic poultry: A Review. *Animal Welfare*. 5(4), 341–360.
- Xie, D., Z. X. Wang, Y. L. Dong, J. Cao, J. F. Wang, J. L. Chen, Y. X. Chen, 2008. Effects of Monochromatic Light on Immune Response of Broilers. *Poultry Science*. 87(8), 1535–1539.
- Zhang, Z., J. Cao, Z. Wang, Y. Dong, Y. Chen, 2014. Effect of a combination of green and blue monochromatic light on broiler immune response. *Journal of Photochemistry and Photobiology B: Biology*. 138, 118–123.
- Prayitno, D., C. Phillips, D. Stokes, 1997. The effects of color and intensity of light on behavior and leg disorders in broiler chickens. *Poultry Science*. 76(12), 1674–1681.
- Cao, J., W. Liu, Z. Wang, D. Xie, L. Jia, Y. Chen, 2008. Green and Blue Monochromatic Lights Promote Growth and Development of Broilers Via Stimulating Testosterone Secretion and Myofiber Growth. *The Journal of Applied Poultry Research*. 17(2), 211–218.
- Rozenboim, I., I. Biran, Z. Uni, B. Robinzon, O. Halevy, 1999. The effect of monochromatic light on broiler growth and development. *Poultry Science*. 78(1), 135–138.
- Park, S., S. Birkhold, L. Kubena, D. Nisbet, S. Ricke, 2003. Effect of storage condition on bone breaking strength and bone ash in laying hens at different stages in production cycles. *Poultry Science*. 82(11), 1688–1691.
- Hester, P. Y., D. A. Wilson, P. Settar, J. A. Arango, N. P. O'Sullivan, 2011. Effect of lighting programs during the pullet phase on skeletal integrity of egg-laying strains of chickens. *Poultry Science*. 90(8), 1645–1651.
- Riczu, C. M., J. L. Saunders-Blades, A°. K. Yngvesson, F. E. Robinson, D. R. Korver, 2004. End-of-Cycle Bone Quality in White- and Brown-Egg Laying Hens. *Poultry Science*. 83(3), 375–383.
- Whitehead, C. C., R. H. Fleming, 2000. Osteoporosis in cage layers. *Poultry Science*, 79(7), 1033–1041.
- Mccoy, M. A., G. A. C. Reilly, D. J. Kilpatrick, 1996. Density and breaking strength of bones of mortalities among caged layers. *Research in Veterinary Science*. 60(2), 185–186.
- Rennie, J. S., R. H. Fleming, H. A. McCormack, C. C. McCorquodale, C. C. Whitehead, 1997. Studies on effects of nutritional factors on bone structure and osteoporosis in laying hens. *British Poultry Science*. 38(4), 417–424.
- Bishop, S. C., R. H. Fleming, H. A. McCormack, D. K. Flock, C. C. Whitehead, 2000. Inheritance of bone characteristics affecting osteoporosis in laying hens. *British Poultry Science*. 41(1), 33–40.

- Hartwig, H. G., T. van Veen, 1979. Spectral characteristics of visible radiation penetrating into the brain and stimulating extraretinal photoreceptors. *Journal of Comparative Physiology.* 130(3), 277–282.
- Jácome, I. M. T. D., L. A. Rossi, R. Borille, 2014. Influence of artificial lighting on the performance and egg quality of commercial layers: a review. *Brazilian Journal of Poultry Science.* 16(4), 337–344.
- Morris, T. R., 1973. The Effects of ahemeral light and dark cycles on egg production in the Fowl. *Poultry Science.* 52(2), 423–445.
- Pyrzak, R., T. D. Siopes, 1986. The effect of light color on egg quality of turkey hens in cages. *Poultry Science.* 65(7), 1262–1267.
- Baxter, M., N. Joseph, V. R. Osborne, G. Y. Bédécarrats, 2014. Red light is necessary to activate the reproductive axis in chickens independently of the retina of the eye. *Poultry Science.* 93(5), 1289–1297.
- Lewis, P. D., T. R. Morris, 2000. Poultry and coloured light. *World's Poultry Science Journal.* 56(03), 189–207.
- Li, G., B. Li, Y. Zhao, Z. Shi, Y. Liu, W. Zheng, 2018. Layer pullet preferences for light colors of light-emitting diodes. *Animal.* 1–7.
- Li, D., L. Zhang, M. Yang, H. Yin, H. Xu, J. S. Trask, ... Q. Zhu, 2014. The effect of monochromatic light-emitting diode light on reproductive traits of laying hens. *The Journal of Applied Poultry Research.* 23(3), 367–375.
- Yang, Y. F., J. S. Jiang, J. M. Pan, Y. B. Ying, X. S. Wang, M. L. Zhang, ... X. H. Chen, 2016. The relationship of spectral sensitivity with growth and reproductive response in avian breeders (*Gallus gallus*). *Scientific Reports.* 6(1).
- Li, M., Y. Gao, G. Lan, Z. B. Gu, 2014. Effects of ultraviolet-B radiation on immunity and carcass characteristics in quail. *The Journal of Applied Poultry Research.* 23(3), 429–436.
- Zhang, L., Z. Shi, X. Wang, A. Geng, B. Li, 2006. Effects of Ultraviolet Radiation on Skeleton Development of Broiler Chickens. *Agricultural Sciences in China.* 5(4), 313–317.
- Osorio, D., M. Vorobyev, 2008. A review of the evolution of animal colour vision and visual communication signals. *Vision Research.* 48(20), 2042–2051.
- Benoit, J., 2006. The role of the eye and of the hypothalamus in the photostimulation of gonads in the duck. *Annals of the New York Academy of Sciences.* 117(1), 204–215.
- Mobarkey, N., N. Avital, R. Heiblum, I. Rozenboim, 2010. The role of retinal and extra-retinal photostimulation in reproductive activity in broiler breeder hens. *Domestic Animal Endocrinology.* 38(4), 235–243.

# Development of a Farm Scale, Quasi Mechanistic Model for Estimation of NH<sub>3</sub> Emission from Commercial Manure-Belt Layer Facilities

Xinjie Tong <sup>a</sup>, Lingying Zhao <sup>a,\*</sup>, Albert Heber <sup>b</sup>, Ji-Qin Ni <sup>b</sup>

<sup>a</sup> Department of Food, Agricultural and Biological Engineering, The Ohio State University, Columbus, OH 43210, USA

<sup>b</sup> Department of Agricultural and Biological Engineering, Purdue University, West Lafayette, IN 47907, USA

\* Corresponding author. Email: [zhao.119@osu.edu](mailto:zhao.119@osu.edu)

## Abstract

Poultry production significantly contributes to atmospheric ammonia (NH<sub>3</sub>) emission which has caused serious concerns on human health, animal health, and the environment. An effective tool is urgently needed for the estimation of NH<sub>3</sub> emission from poultry facilities for the development of effective mitigation strategies and fair regulation. A laboratory-scale mechanistic NH<sub>3</sub> emission model was previously developed, but the input factors require extensive monitoring and laboratory work and therefore cannot be conveniently used by producers or regulatory agencies. In this study, a farm-scale NH<sub>3</sub> emission estimation model was developed for estimating NH<sub>3</sub> emission from cross-ventilated manure-belt caged layer houses based on the mechanistic model. Sub-models were developed to estimate the inputs of mechanistic model from farm-scale conditions that are commonly monitored during poultry production. Computational fluid dynamics models and analysis of manure characteristics and amount were used to estimate airflow conditions and NH<sub>3</sub> emission areas in a layer house. The model was able to estimate hourly and daily NH<sub>3</sub> emission from cross-ventilated manure-belt layer houses with input information on ambient air temperature, house ventilation rate, a specific date, and manure management practices with acceptable accuracy ( $P$ -value = 0.15–0.61). Overall uncertainty of 32% was obtained for the model based on the uncertainty of individual sub-model along with their corresponding sensitivity. The model had an acceptable performance during ordinary egg production, but needs to be further developed for special events such as molting and the introduction of the new flocks.

**Keywords:** Regulation, ammonia emission mechanism, computational fluid dynamics, emission area, house ventilation, egg production

## 1. Introduction

Poultry production significantly contributes to ammonia (NH<sub>3</sub>) emission in the atmosphere, and has caused concerns on human health, animal health, and the environment (OSHA, 2019; Maliselo and Nkonde, 2015). An attempt was made by U.S.EPA in 2017 to regulate NH<sub>3</sub> emission from animal facilities by requiring a mandatory reporting of NH<sub>3</sub> emission by animal farms under the Emergency Planning and Community Right to Know Act (EPCRA). However, the attempt failed as no reliable tool was available for producers or the regulatory agencies to estimate NH<sub>3</sub> emissions from different farms. The capability of estimating NH<sub>3</sub> emission from animal facilities becomes a necessity down the road, not only because it is the essential knowledge for effective management, mitigation, and regulation, but it is also a crucial input for atmospheric models to study the fate and transport of NH<sub>3</sub> in the atmosphere.

In the National Air Emission Monitoring Study (NAEMS) (Ni et al., 2011; Heber et al., 2008), long-term high-quality measurement data of NH<sub>3</sub> emissions from different animal facilities were obtained. Although these measurements are limited in representing NH<sub>3</sub> emission from other animal facilities with different species, weather conditions, housing structure, and farm management practices (Ni et al., 2012; Chepere et al., 2011), they can be used to develop and validate NH<sub>3</sub> emission models for estimations of NH<sub>3</sub> emissions from farms.

Among various kinds of models, the mechanistic model has advantages in accounting for key

processes involved in the NH<sub>3</sub> emission mechanisms. Tong et al. (2019a) developed a mechanistic model for estimating NH<sub>3</sub> emissions from layer manure under lab-scale conditions with various environmental conditions and manure properties. The major limitation of the mechanistic model is that it requires inputs on manure properties which are not commonly monitored during poultry production management. The air temperatures and velocities inside cages are also required inputs of the mechanistic model, and they are usually unknown to producers because they cannot be obtained with limited field measurements due to large spatial variations caused by non-uniform ventilation patterns (Tong et al., 2019b, 2019c). Alternatively, computational fluid dynamics (CFD) modeling has been proved with adequate capability of predicting three-dimensional distributions of airflow and environmental conditions in animal production facilities (Tong et al., 2019b, 2019c, 2019d; Blanes-Vidal et al., 2008; Bjerg et al., 2002). In order to allow producers and regulatory agencies to conveniently estimate NH<sub>3</sub> emissions without extra laboratory work or monitoring, the key inputs of the mechanistic model need to be estimated based on farm-scale factors that can be easily obtained at farms through statistical modeling of manure properties and CFD modeling of thermal environment.

This study aims to develop a farm-scale NH<sub>3</sub> emission estimation model based on the mechanistic model (Tong et al., 2019a) to estimate NH<sub>3</sub> emission from typical commercial manure-belt caged layer houses. The model can be used as an effective tool for better management and fair regulation of NH<sub>3</sub> emissions from manure-belt layer houses in the U.S.

## 2. Materials and Methods

### 2.1. Mechanistic model for estimating ammonia emissions

According to the mechanistic model developed by Tong et al. (2019a), NH<sub>3</sub> emissions from layer manure was estimated using Eq. (1). The key inputs to the mechanistic model of estimating NH<sub>3</sub> emission from layer manure included air temperature and velocity at bird zone, and manure pH and moisture content (MC) (Tong et al., 2019a).

$$ER = \left\{ \left[ 1 + \frac{10^{-pH}}{K_d} \right]^{-1} \times \left( \frac{[TAN]}{1 - MC/100} \right) \times K_h \times 1000 \times \left( \frac{100 - MC}{MC} \right) - C_{g,\infty} \right\} \times K_G \quad (1)$$

where  $ER$  is NH<sub>3</sub> emission rate, mg m<sup>-2</sup> h<sup>-1</sup>;  $pH$  is pH value of layer manure;  $K_d$  is the value of the dissociation constant of poultry manure as a function of manure pH and moisture content (MC);  $[TAN]$  is the wet-based concentration of TAN which is the summation of the concentration of liquid-phase NH<sub>3</sub>, liquid-phase NH<sub>4</sub><sup>+</sup>, and solid-phase NH<sub>4</sub><sup>+</sup>, and was assumed to be 6943 µg g<sup>-1</sup>;  $MC$  is wet-based moisture content of layer manure, %;  $K_h$  is the Henry's Law constant as a function of air temperature, (g NH<sub>3</sub>-N m<sup>-3</sup> air) / (g NH<sub>3</sub>-N m<sup>-3</sup> solution);  $C_{g,\infty}$  is the NH<sub>3</sub> concentration in the free air stream of the layer house, mg m<sup>-3</sup>;  $K_G$  is convective mass transfer coefficient as a function of air temperature and velocity, m h<sup>-1</sup>;  $T$  is the air temperature at bird zone, °C; and  $v$  is the average air velocity inside the cages, m s<sup>-1</sup>.

### 2.2. Manure-belt layer houses

The two cross-ventilated manure-belt layer houses (Ni et al., 2017) were 140.2 m long, 19.5 m wide, and 11.5 m high at the ridge and 7 m high at sidewalls. Laying hens were stocked in seven rows and ten tiers of cages, with five tiers of cages at the upper level and five tiers of cages at the lower level. Manure belts were moved 1/3 of the total length every day except for Sunday for manure removal. A total of 88 exhaust fans with a diameter of 1.32 m were installed in each of the houses: eight fans in the east end wall and 40 fans in each of two side walls. Among them, 14 fans were operated with variable speed, with 7 fans in each of two side walls (Ni et al., 2017).

Seven adjustable inlet openings were placed in the ceiling, with one above each row of cages. The operations of exhaust fans were controlled in 12 stages based on indoor air temperature settings and sensor measurements. Molting happened in 01/10/09–02/28/09 (month/date/year) in

house 1 and in 12/05/09–01/16/10 in house 2. New birds were introduced at the beginning of the monitoring study (01/01/08) in house 1 and in 10/4/08–10/24/08 in house 2.

### 2.3. Determination of house ventilation rate

The exhaust fans were monitored individually (Ni et al., 2017) using vibration sensors (Model OSU–06, Ohio State University, Columbus, OH, USA) (Chen et al., 2010), magnetic proximity sensors (Model MP100701, Cherry Co. Pleasant Prairie, WI, USA), and/or impeller anemometers (Model 27106RS, R.M. Young Co., Traverse City, MI, USA). Pressure sensors (Model 260, Setra Systems, Inc. Boxborough, MA, USA) were used to measure house static pressures across the walls. FANS tester (Lim et al., 2010; Gates et al., 2004) was utilized for the verification of airflow rates of selected fans. Detailed information can be found in Chai et al. (2012).

### 2.4. Estimation of thermal and airflow conditions inside cages using CFD simulations

#### 2.4.1. CFD simulations

The CFD models developed by Tong et al. (2019b, 2019c) had acceptable accuracy in estimating the spatial distributions and seasonal variations of airflow, thermal environment, and air pollutant concentrations in commercial manure-belt layer houses as indicated by a normalized mean square error of 0.001–0.134 for all variables with units of  $\text{m s}^{-1}$  for airflow,  $^{\circ}\text{C}$  for temperature,  $\text{g g}^{-1}$  for humidity, and ppm for  $\text{NH}_3$  concentrations. These CFD models were used for predicting air conditions (i.e., temperature and velocity) in cages under various weather conditions and ventilation rates. Modifications on the boundary conditions were performed to account for different bird numbers, house dimensions, and the applied ventilation rates in different houses. Multiple cases (Table 1) were simulated using the CFD models with typical outdoor weather conditions encountered by cross-ventilated manure-belt layer houses in different seasons.

Table 1. Boundary conditions of the CFD simulation cases

Case #	$T_{\text{amb}}$ ( $^{\circ}\text{C}$ )	$Q$ ( $\text{m}^3 \text{s}^{-1}$ )	Number of operating exhaust fans		Opened Inlet #
			Side wall	End wall	
1	30	687	80	8	7
2	30	573	80	0	7
3	26	360	50	0	7
4	20	132	18	0	7
5	5	89	14	0	4
6	-15	60	14	0	2

#### 2.4.2. Division of cages into multiple zones

The cages in one-quarter houses were divided into 15 zones, indicated with capital letters (Table 2), based on their similarities in environmental conditions to account for the spatial variation of air velocity and temperature in cages in the whole house. One quarter of the house was defined as the one-quarter portion of the house after cutting the house along the building width and length through the center point. The zone splitting method allowed for standard deviation to be smaller than  $2.5^{\circ}\text{C}$  for air temperature and  $0.2 \text{ m s}^{-1}$  for air velocity within each zone in more than 90% of time in summer. Since the numbers of cages are not the same for different zones, the proportion of the cages included in each zone was weighted for the determination of total  $\text{NH}_3$  emission.

Table 2. Zone splitting of cages in the one-quarter houses.

	Tier 1, 2	Tier 3, 4, 5	Tier 6, 7	Tier 8, 9	Tier 10
Row 1	A	B	C	D	E
Row 2, 3	F	G	H	I	J
Row 4 (half)	K	L	M	N	O

### 2.4.3. Interpolation of air temperatures and velocities in cages

Air temperatures and velocities in cages under the simulation conditions used in the cases (Table 1) were directly extracted from CFD simulations. When the ambient temperature and house ventilation rate were different from the simulation conditions, the air temperatures and velocities in cages were estimated using linear interpolation, Eqs. (2–3) and Eq. (4), respectively, based on the results obtained from simulation cases. To avoid extrapolation of the mechanistic model (Tong et al., 2019a), the in-cage air temperatures and air velocities were restricted to the range of 22.0–33.5°C and 0.25–1.17 m s<sup>-1</sup>, respectively.

$$T_{i,v>0.2} = T_{amb} + \left\{ (T_{i,a} - T_{amb,a}) - \frac{(T_{i,a} - T_{amb,a}) - (T_{i,b} - T_{amb,b})}{(Q_b - Q_a)} \times (Q - Q_a) \right\} \quad (2)$$

$$T_{i,v\leq0.2} = T_{i,a} + \frac{(T_{i,a} - T_{i,b})}{(T_{amb,a} - T_{amb,b})} \times (T_{amb} - T_{amb,a}) \quad (3)$$

where  $T_{i,v>0.2}$  and  $T_{i,v\leq0.2}$  are the estimated air temperature in cages in zone  $i$  when  $v > 0.2 \text{ m s}^{-1}$  and  $v \leq 0.2 \text{ m s}^{-1}$ , respectively;  $T_{amb}$  is the given ambient temperature, °C;  $T_{i,a}$  and  $T_{i,b}$  are the air temperature in cages in zone  $i$  in case a and b, where  $T_{amb,a} < T_{amb} < T_{amb,b}$ , respectively, °C;  $T_{amb,a}$  and  $T_{amb,b}$  are the ambient temperature used in case a and b, respectively, °C;  $Q$  is the given house ventilation rate, m<sup>3</sup> s<sup>-1</sup>; and  $Q_a$  and  $Q_b$  are the ventilation rates used in case a and b, respectively, m<sup>3</sup> s<sup>-1</sup>.

$$v_i = v_{i,a} + \frac{(v_{i,b} - v_{i,a})}{(Q_b - Q_a)} \times (Q - Q_a) \quad (4)$$

where  $v_i$  is the air velocity in cages in zone  $i$  to be estimated given house ventilation rate  $Q$ , m s<sup>-1</sup>;  $v_{i,a}$  and  $v_{i,b}$  are the in-cage air velocities in zone  $i$  in case a and b, respectively, m s<sup>-1</sup>;  $Q$  is the given house ventilation rate, m<sup>3</sup> s<sup>-1</sup>;  $Q_a$  and  $Q_b$  are the ventilation rates used in case a and b, respectively, with  $Q_a < Q < Q_b$ , m<sup>3</sup> s<sup>-1</sup>.

### 2.5. Estimation of manure characteristics and emission areas

Both of manure pH and MC were estimated based on characterization of manure samples taken in the layer houses. Manure samples were sampled randomly from multiple locations on each manure belt, and five belts located at different rows and tiers were sampled to generate the final manure sample. A total of 9 samples were taken for a mixed sample for characterization at each of 12 sampling events. The manure samples were stored in a sealed bag and placed in a cooler during transportation. They were then delivered to a quality certified laboratory in a timely manner for characterization of pH and MC to avoid the change in manure properties. More details about manure sampling and characterization are available in Heber (2010). The emission area of NH<sub>3</sub> was estimated based on manure production rate and manure removal frequency. According to observations during field measurement, manure produced by layers per day covered approximately 1/3 of the total surface area of the belts.

### 2.6. Integration of the sub-models to form the farm-scale NH<sub>3</sub> emission model

The total NH<sub>3</sub> emission was estimated with a one-hour resolution (Eqs. (5–6)) by summing up the NH<sub>3</sub> emission rates from all zones of cages as defined in Table 2. The daily NH<sub>3</sub> emission rate was obtained by averaging the hourly NH<sub>3</sub> emission within each day.

$$ER'_i = 2.4 \times 10^{-5} \cdot ER_i \cdot A \cdot \beta \quad (5)$$

$$ER' = \sum_{n=1}^N (n_i \cdot ER'_i) \Bigg/ \sum_{n=1}^N n_i \quad (6)$$

where  $ER'_i$  is the  $\text{NH}_3$  emission rate of the whole house assuming all the cages have conditions same as those in  $i^{th}$  zone,  $\text{kg d}^{-1}$ ;  $A$  is the total surface area of manure belts in the whole house,  $\text{m}^2$ ;  $\beta$  is the coefficient accounting for coverage of manure on the belts;  $ER'$  is the hourly  $\text{NH}_3$  emission rate of the whole house,  $\text{kg d}^{-1}$ ;  $N$  is the total number of zones; and  $n_i$  is the weighting coefficient accounting for number of cages included in  $i^{th}$  zone.

## 2.7. Model validation and uncertainty analysis

The performance of the CFD simulations and linear interpolation methods was evaluated by comparing the estimated in-cage air temperatures with the field measurements. Validation of  $\text{NH}_3$  emission was performed both on an hourly basis and a daily basis by comparing the estimations with the hourly and daily averages of  $\text{NH}_3$  emission measurement. The agreement between the measurements and estimations was assessed using five statistics, including fractional bias (FB), geometric mean bias (MG), normalized mean square error (NMSE), geometric variance (VG), and fraction of two (FAC2) (Chang and Hanna, 2004). In addition, the paired t-test was performed in JMP 11.0 Statistical Analysis Software to compare the measurements and estimations of in-cage air temperatures. Nonparametric Wilcoxon Signed Rank test was conducted in JMP to compare the measurement and estimations of  $\text{NH}_3$  emissions. A significance level of 0.05 was used for all the statistical tests. The data at special events such as molting and the introduction of new flocks were removed for model validation. Because of potential correlations of the time-series data, the data recorded 7 days before and after the special events were also removed based on the assumption that the effects of special events on manure properties and  $\text{NH}_3$  emission processes have lagging period of less than one week.

Model uncertainty was analyzed by Eq. (7) using the uncertainty attributed by the estimation of each input factor weighted by their relative sensitivity to  $\text{NH}_3$  emission (JCGM, 2008).

$$u_c(NH_3ER) = \sqrt{[c_r u(T)]^2 + [c_v u(v)]^2 + [c_{pH} u(pH)]^2 + [c_{MC} u(MC)]^2} \quad (7)$$

where  $u_c(NH_3ER)$  is the combined uncertainty in estimating  $\text{NH}_3$  emission, %;  $c_x$  is the sensitivity coefficient of input factor  $x$  in the mechanistic model, %; and  $u(x)$  is the standard deviation of input factor  $x$ .

## 3. Results and Discussion

### 3.1. Validation of CFD simulations and linear interpolations

The CFD simulations and linear interpolations had adequate accuracy in estimating air temperatures in cages as all of the statistical criteria were met (Table 3).

Table 3. Model performance in estimating in-cage air temperatures.

Criteria	Temperature ( $^{\circ}\text{C}$ )	$\text{NH}_3$ ER-Hourly ( $\text{kg d}^{-1}$ )	$\text{NH}_3$ ER-Daily ( $\text{kg d}^{-1}$ )
NMSE (< 0.25)	0.01	0.67	0.49
FB  (< 0.3)	0.03	0.26	0.22
MG (0.7–1.3)	0.97	1.12	1.06
VG (< 4)	0.94	1.25	1.13
FAC2 (0.5–2.0)	0.97	1.46	1.20
P-value (> 0.05)	0.94	0.15	0.61

The criteria in parenthesis indicate adequate model performance (Hanna and Chang, 2011)

### 3.2. Manure pH and MC and emission area

Obvious seasonal variation of manure pH was found with the highest pH occurred in winter and the lowest pH occurred in summer (Figure 1). The relationship of manure pH with month was

fitted using Eq. (8) which explained 92.4% of the total variations in manure pH. To account for seasonal variations in manure pH, it was estimated based on the measurement data as a constant manure pH for each month. In particular, the input of manure pH was 8.21, 8.13, 7.85, 7.33, 7.37, 7.19, 7.18, 7.31, 7.51, 7.75, 7.98, and 8.15 for months from January to December, respectively. Manure MC ranged from 62.4 to 76.1% with an average of 72.1% (Figure 1). The input for manure MC was 67.2% to avoid extrapolation of the mechanistic model (Tong et al., 2019a). The input for manure emission area was 2/3 of the surface area of belts.

$$pH_{m'} = -0.0077m^3 + 0.1331m^2 - 0.5245m + 7.7671 \quad (8)$$

where  $pH_{m'}$  is the manure pH in month  $m'$ ;  $m$  is a constant corresponding to each month  $m'$  with the following relationship:  $m = m' - 4$  for May to December,  $m = m' + 8$  for January to April.

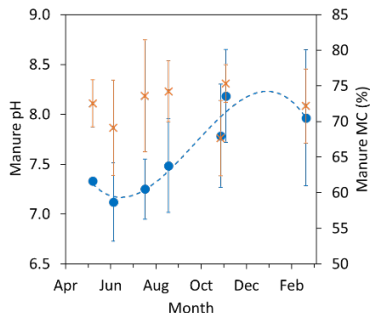


Figure 1. Change of manure pH (●) and moisture content (MC) (✖) with month. The error bars indicate standard deviation of measurements for manure samples taken on the same day.

### 3.3. Validation of NH<sub>3</sub> emission estimation

The general trend in NH<sub>3</sub> emission was mostly captured by the model except for the high peaks of NH<sub>3</sub> emission measured in Dec. 2008 with both hourly and daily resolutions (Figure 2).

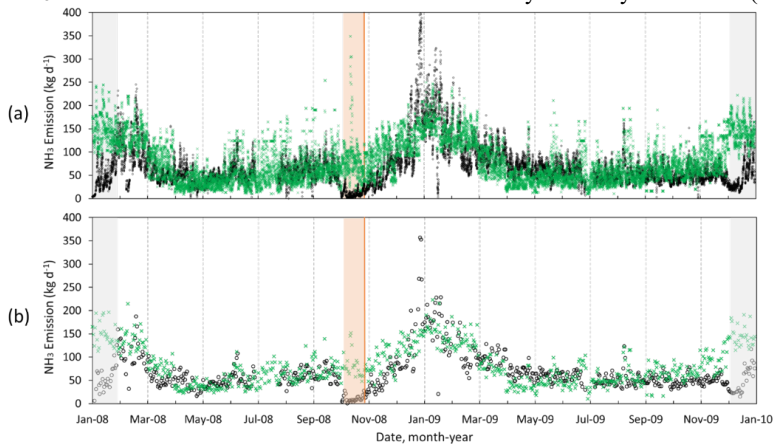


Figure 2. Comparison between the measured NH<sub>3</sub> emission (○) and the estimated NH<sub>3</sub> emission (✖) in house 2 based on (a) hourly averages and (b) daily averages. Molting period: ■; introducing flocks: □ where the line (—) indicates the end of the introduction period.

The underestimation of NH<sub>3</sub> emission was likely due to the uncertainty of the estimated manure pH values which was the most sensitive input to the mechanistic model (Tong et al., 2019a). It was also noticed that the model significantly overestimated NH<sub>3</sub> emissions during the special events, such as molting and introduction of the new flock. During molting, layers were provided with limited feed, and thus manure production was significantly decreased which led to a reduction in NH<sub>3</sub> emission (Ni et al., 2017; Li et al., 2013). The lower NH<sub>3</sub> emission during the introduction of new flock could be explained by less number of layers which corresponded to lower manure production. All of these changes due to special events were not included in the model, which might cause the overestimation of the NH<sub>3</sub> emissions during these periods.

Based on the agreement between measurements and estimations of NH<sub>3</sub> emissions (Table 3), the model was adequate in estimating both the daily and hourly NH<sub>3</sub> emissions, although the estimation was more accurate for daily emissions than hourly emissions.

### 3.4. Model uncertainty

The overall uncertainty (Table 4) of the farm-scale model was 31.8%. This indicated that an additional 31.8% error in NH<sub>3</sub> emission was introduced when using farm-scale factors to estimate the inputs of the mechanistic model (Tong et al., 2019a).

Table 4. Uncertainty of the farm-scale model.

	Standard Deviation	Change in <i>ER</i> (%)
pH	0.10	11.7
Moisture Content	2.8%	0.93
Temperature	2.1°C	27.2
Air Velocity	0.14 m s <sup>-1</sup>	11.6
Overall Uncertainty		31.8%

## 4. Conclusions

The developed farm-scale NH<sub>3</sub> emission estimation model was based on the mechanistic model, and can be used for estimating ammonia emission from typical manure-belt layer houses with cross ventilations. The input factors of the farm-scale NH<sub>3</sub> emission model were ambient temperature, house ventilation rate, date, manure production rate, and manure removal schedule that are accessible to producers and regulatory agencies.

The farm-scale model had a 32% uncertainty in NH<sub>3</sub> emission estimation based on the sensitivity of the multiple input factors of the mechanistic model. The model was suggested to be adequate for predicting both daily (*P*-value = 0.61) and hourly (*P*-value = 0.15) NH<sub>3</sub> emissions, with the daily estimations being more accurate than the hourly estimations.

Overall, the model had adequate performance in estimating NH<sub>3</sub> emissions in cross-ventilated manure-belt layer houses during ordinary productions. Overestimation of NH<sub>3</sub> emissions was observed during special events of molting and the introduction of new flocks.

## Acknowledgements

This study was supported by the USDA-NIFA Grant 2018-67019-27803. The authors are thankful for the managers and staff of the collaborating poultry farm for their support and assistance to the project.

## References

- Bjerg, B., K. Svidt, G. Zhang, S. Morsing, J.O. Johnsen, 2002. Modeling of air inlets in CFD prediction of airflow in ventilated animal houses. Computers and Electronics in Agriculture. 34 (1–3), 223–235. [https://doi.org/10.1016/S0168-1699\(01\)00189-2](https://doi.org/10.1016/S0168-1699(01)00189-2).
- Blanes-Vidal, V., E. Guijarro, S. Balasch, A.G. Torres, 2008. Application of computational fluid dynamics to the prediction of airflow in a mechanically ventilated commercial poultry building. Biosystems Engineering. 100(1), 105–116. <https://doi.org/10.1016/j.biosystemseng.2008.02.004>.

- Chai, L., J.-Q. Ni, C.A. Diehl, I. Kilic, A.J. Heber, Y. Chen, E.L. Cortus, B.W. Bogan, T.T. Lim, J.C. Ramirez-Dorronsoro, L. Chen, 2012. Ventilation rates in large commercial layer hen houses with two-year continuous monitoring. *British Poultry Science*. 53(1), 19–31. <https://doi.org/10.1080/00071668.2011.643766>
- Chang, J.C., S.R. Hanna, 2004. Air quality model performance evaluation. *Meteorology and Atmospheric Physics*. 87 (1–3), 167–196. <https://doi.org/10.1007/s00703-003-0070-7>.
- Chepere, J.H., H. Xin, H. Li, 2011. Ammonia emissions of laying-hen manure as affected by accumulation time. *The Journal of Poultry Science*. 48(2), 133–138. <https://doi.org/10.2141/jpsa.010087>.
- Gates, R.S., K.D. Casey, H. Xin, E.F. Wheeler, J.D. Simmons, 2004. Fan assessment numeration systems (FANS) design and calibration specifications. *Transactions of the ASAE*. 47(5), 1709–1715.
- Hanna, S.R., and J. Chang, 2011. Setting acceptance criteria for air quality models. In *Air Pollution Modeling and its Application XXI*. NATO Science for Peace and Security Series C: Environmental Security, Steyn, D. and Trini Castelli, S. Eds. Dordrecht: Springer: 479–484.
- Heber, A.J., 2010. Emissions data from two manure-belt layer houses in Indiana. Final report for site IN2B of the National Air Emissions Monitoring Study. U.S.EPA, Durham, NC. <https://archive.epa.gov/airquality/af02012/web/pdf/in2bsummaryreport.pdf>. Accessed May 10, 2019.
- Heber, A.J., W.W. Bogan, J.-Q. Ni, T.T. Lim, J.C. Ramirez-Dorronsoro, E.L. Cortus, C.A. Diehl, S.M. Hanni, C. Xiao, K.D. Casey, C.A. Gooch, L.D. Jacobson, J.A. Koziel, F.M. Mitloehner, P.M. Ndegwa, W.P. Robarge, L. Wang, R. Zhang, 2008. The national air emissions monitoring study: overview of barn sources. In *Livestock Environment VIII – Proceedings of the 8th International Symposium*. Iguassu Falls, Brazil, 31 August – 4 September. 199–206. <http://doi.org/10.13031/2013.25499>.
- JCGM, 2008. Evaluation of measurement data — Guide to the expression of uncertainty in measurement. International Organization for Standardization Geneva ISBN, 50(September), 134. <https://doi.org/10.1373/clinchem.2003.030528>.
- Li, Q.F., L. Wang-Li, B.W. Bogan, K. Wang, L. Chai, J.-Q. Ni, A.J. Heber, 2013. The national air emissions monitoring study's southeast layer site: part IV. Effects of Farm Management. *Transaction of ASABE*. 56(2010), 1199–1209.
- Lim, T.T., J.-Q. Ni, A.J. Heber, Y. Jin, 2010. Applications and calibrations of the fans and traverse methods for barn airflow rate measurement. In *International Symposium on Air Quality and Manure Management for Agriculture*. St. Joseph, Mich.: ASABE, Dallas, Texas.
- Maliselo, P.S., G.K. Nkonde, 2015. Ammonia production in poultry houses and its effect on the growth of *Gallus Gallus Domestica* (broiler chickens): a case study of a small scale poultry house in Riverside, Kitwe, Zambia. *International Journal of Scientific & Technology Research*. 4(4), 141–145.
- Ni, J.-Q., 1999. Mechanistic models of ammonia release from liquid manure: a review. *Journal of Agricultural Engineering Research*. 72(1), 1–17. <https://doi.org/06/jaer.1998.0342>.
- Ni, J.-Q., L. Chai, L. Chen, B.W. Bogan, K. Wang, E.L. Cortus, A.J. Heber, T.T. Lim, C.A. Diehl, 2012. Characteristics of ammonia, hydrogen sulfide, carbon dioxide, and particulate matter concentrations in high-rise and manure-belt layer hen houses. *Atmospheric Environment*. 57, 165–174. <https://doi.org/10.1016/j.atmosenv.2012.04.023>.
- Ni, J.-Q., E.L. Cortus, A.J. Heber, 2011. Improving ammonia emission modeling and inventories by data mining and intelligent interpretation of the national air emission monitoring study database. *Atmosphere*. 2(2), 110–128. <https://doi.org/10.3390/atmos2020110>.
- OSHA, 2019. How much ammonia is too much? Part 2. <https://www.osha.gov/sites/default/files/2019-03/fs4-howmuch2.pdf>. Accessed May 10, 2019.
- Tong, X., L. Zhao, A.J. Heber, J.-Q. Ni, 2019a. Mechanistic modeling of ammonia emission from laying hen manure at laboratory scale. *Biosystems Engineering*. Under revision.
- Tong, X., S.W. Hong, L. Zhao, 2019b. CFD modelling of airflow pattern and thermal environment in a commercial manure-belt layer house with tunnel ventilation. *Biosystems Engineering*. 178, 275–293. <https://doi.org/10.1016/j.biosystemseng.2018.08.008>.
- Tong, X., S.W. Hong, L. Zhao, 2019c. CFD modelling of airflow, thermal environment, and ammonia concentration distribution in a commercial manure-belt layer house with mixed ventilation systems. *Computers and Electronics in Agriculture*. 162, 281–299. <https://doi.org/10.1016/j.compag.2019.03.031>.
- Tong, X., S.W. Hong, L. Zhao, 2019d. Using CFD simulations to develop an upward airflow displacement ventilation system for manure-belt layer houses to improve the indoor environment. *Biosystems Engineering*. 178, 294–308. <https://doi.org/10.1016/j.biosystemseng.2018.08.006>.

# Effects of Electrode Materials and Dimensions on Water Droplet Charging for Dust Removal

Xiaochuan Li <sup>a,b</sup>, Reyna Knight <sup>b</sup>, Lingying Zhao <sup>b,\*</sup>, Jeb Hocter <sup>b</sup>

<sup>a</sup> School of Chemical Engineering and Technology, China University of Mining and Technology,  
Xuzhou, Jiangsu 221008, P.R. China

<sup>b</sup> Department of Food, Agricultural, and Biological Engineering,  
The Ohio State University, Columbus, OH 43210, USA

\* Corresponding author. Email: [zhao.119@osu.edu](mailto:zhao.119@osu.edu)

## Abstract

Droplet charging is an effective method to enhance dust removal efficiency using a water spray scrubber. However, the effects of the dimensions and materials of different electrodes on droplet charging efficiency have not been studied systematically. In this study, ring-shaped electrodes were selected to study effects of electrode material (copper, stainless steel, and graphite) and electrode dimensions on droplet charging efficiency. A Faraday pail charge measurement device was used to measure the droplet charge generated by the three different electrodes. A one-factor-at-a-time experimental design of experiments was used to determine effects of charging voltage, electrode material and dimensions, and nozzle height on water droplet charging efficiency. The charging characteristics of the three different material electrodes with the same size as well as one type of electrode with different dimensions were compared. The results show that the maximum charge-to-mass ratio (CMR) values of the 304 stainless steel and graphite electrodes (0.435 and 0.429 mC kg<sup>-1</sup>) are 20% higher than the copper electrode (0.344 mC kg<sup>-1</sup>). 304 stainless steel and copper electrodes had better charge stability. The smaller the diameter (200, 150, and 100 mm) of the 304 stainless steel electrodes, the higher the maximum CMR (0.233, 0.275, and 0.364 mC kg<sup>-1</sup>) would be. The electric field intensity around the electrode could be changed by changing the nozzle height. The continuous jet tip should be placed at the location of strongest electric field intensity to obtain higher CMR. The results will be used to design effective an electrostatic spray scrubber for mitigation PM emissions.

**Key words:** Droplets charging, CMR, copper, stainless steel, graphite

## 1. Introduction

Dust is a significant problem in agricultural food production, mining, building construction, and other industrial operations. Dust emissions negatively affect human and animal health and the environmental quality (Cai et al., 2019; Ru et al., 2017; Liu et al., 2019). A variety of dust capture and removal methods and equipment with different working mechanisms have been invented for different industrial processes, such as filters, wet scrubbers, and electrostatic precipitators. However, the removal efficiency of particles smaller than 1 μm rapidly decreases for conventional gas cleaning systems such as inertial scrubbers, bag filters, or electrostatic precipitators (Balachandran et al., 2003; Huang et al., 2002), which cannot satisfy the requirements for industrial applications. The need for removing small dust particles (below 1 μm) has been increasing.

Research has been conducted to improve the dust capture process through charging droplets in a spray separator (Yang et al., 2019), and reducing secondary escape of dust particles from electrostatic precipitators (Zheng et al., 2019). Electrostatic spraying in a dusty air stream is an effective method to enhance fine particle removal using electrostatic forces. The device for the realization of this process is called an electrostatic spray scrubber (ESS). Almuhanne et al. (2012), Di Natale et al. (2015), and Ru et al. (2017) reported their experimental studies and indicated that ESS is a promising technology to effectively capture particles smaller than 1 μm.

It has been widely used in agricultural applications to improve pesticide spraying adhesive ability in recent years. Some experimental studies were conducted in the fine dust removal using the charged spray, such as poultry facilities (Ru et al., 2017). It is necessary to research the

chargeability of the droplet by the high voltage. And those research results can provide important insight to the pesticide spraying and dust removal spraying equipment design.

Charging is an important process for effective operation of an ESS. There are many factors that affect droplet charging. Electrode voltage has a significant effect on spray charge and generally higher voltages, up to a limit, result in higher spray charge (Carroz and Keller, 1978; Almekinders et al., 1992). Electrode materials and dimensions are the other significant factors. Appropriate electrode material may enhance the chargeability of water droplets. At present, copper, stainless steel, and brass are the most common materials used for electrodes in electrostatic nozzles (Almuhanne et al., 2012; Marchewicz et al., 2019; Chen et al., 2019). Nickel and aluminum were also used to make electrodes for high voltage applications with different dimension and shapes (Patel et al., 2013; Patel et al., 2016).

In addition, the distance between the electrode and the nozzle is another factor affecting droplet charging (Alharbi et al., 2014). As the distance increases, the charge-to-mass ratio (CMR), which is estimated as the ratio of spray current to the mass flow rate of the droplets, increases because the electric field becomes stronger at the breakup points of water film. However, when distance reaches a limit, the saturation of specific charge can be noticed (Andrzej et al., 2013). A too short distance between the electrode and the jet led to charging instability, because some of the charged droplets deposited on the electrode and caused charge transfer to the electrode along with occasional sparkover (Penney et al., 1944). Additionally, water flow rate, droplet size, droplet distribution, and water conductivity are also affecting factors. (Andrzej et al., 2013; Marchewicz et al., 2019; Devanand and Divaker, 2010).

Although high-voltage charging of droplets has been investigated in many studies, the effect of electrode materials and dimensions on droplet charging is not fully understood. The objectives of this study are to quantify performances of 304 stainless steel (304 SS), copper, and high-purity graphite electrodes with different diameters in terms of water droplet charging. The study results will provide guidance for the development of electrostatic spray scrubbers for industrial applications of dust control.

## 2. Experimental Method

### 2.1. Experimental facilities

The experimental system consisted of a spray system including nozzle (TX-VK6), a pressure gauge and pump, a high-voltage power supply, and ring electrodes. The schematic diagram of the system is shown in Figure 1. The flow pattern of the TX-VK6 nozzle was hollow cone; the pressure was set to 300 kPa; and the flow rate measured in the experiment ranged from 0.3843 to 0.4113 kg min<sup>-1</sup>. The charging current measurement device (an electrometer) was connected to a mesh and the Faraday pail. Microcurrent resulted from microcharge carried by the droplets and transferred from the inner cylinder of the Faraday pail to the outer cylinder was measured using the electrometer.

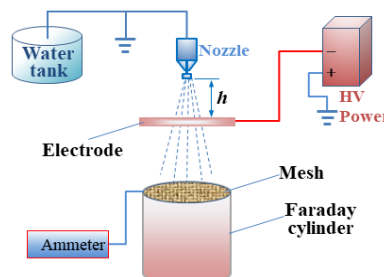


Figure 1. Schematic diagram for the droplet charging experiment.

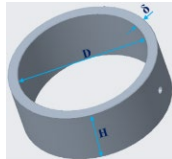
## 2.2. Experimental materials and electrode dimensions

In this study, graphite, 304 SS, and copper were used as electrode materials. Physical properties of the electrode materials are shown in Table 1. The density of graphite is about 1/4 of those of the metal materials, and its electrical resistivity is 13.7 and 571.43 times that of 304 stainless steel and copper, respectively. To test different dimensions of the electrodes, ring-shaped electrodes were used and designed with various thicknesses depending on mechanical properties of the electrode materials. Effects of the electrode diameter and the position of the electrode relative to the spray nozzle (i.e. nozzle height) on droplet charge were studied. The dimensions and a physical photograph of the ring electrodes are shown in Table 2 and Figure 2, respectively.

Table 1. Physical properties of the electrode materials.

	Ash content (ppm)	Density (g cm <sup>-3</sup> )	Resistivity ( $\mu\Omega \cdot m$ )
Graphite	60–80	1.84	10
Steel 304		7.93	0.73
Copper		8.6	0.0175

Table 2. The dimensions of the experimental electrodes.

Electrode No.	Material	D (mm)	H (mm)	$\Delta$ (mm)	
Steel 304 A		200	10	8	
Steel 304 B	304 Stainless	150	10	8	
Steel 304 C	Steel	100	10	8	
Steel 304 D		100	45	3	
Graphite	Graphite	100	45	8	
Copper A	Copper	100	45	3	

  
Steel 304

  
Graphite

  
Copper

  
Steel 304

Figure 2. The physical photograph of the experimental electrodes.

The electrode is positioned right underneath the spray nozzle aligned with the vertical axis of the electrode. The vertical position of the nozzle could be adjusted up and down. The nozzle height ( $h$ ) was defined as the vertical distance between the nozzle tip and the upper end face of the electrode (Figure 1). Zero height was defined where the bottom of the nozzle tip coincided with the upper end face of electrode. The direction upwards from the nozzle was defined as the positive direction, and downwards the negative direction. Droplet charge was measured under different  $h$  values.

Pure water was used for the experiment. Water conductivity was adjusted to 0.05 S m<sup>-1</sup> by adding NaCl. The water temperature was 18±2°C, and density ranged from 1000.74–1002.48 kg m<sup>-3</sup>.

## 2.3. Experimental design

A one-factor-at-a-time experimental design with four factors was used in this study to investigate the effects of the factors on the charging efficiency. The four factors tested were electrode material, electrode diameter (D), nozzle height ( $h$ ), and supply voltage (V). Two series of tests were designed. One test changed the nozzle height  $h$  and supply voltage for different materials (304 SS, graphite, and copper) and another for different electrode diameters (200, 150, and 100 mm).

For current measurement, the sampling time of the electrometer was set to 3 s. The average within 3 s was taken as the display value. Six groups of data were recorded continuously and the

averages and errors were calculated.

#### 2.4. Data analysis

The CMR of the charged droplets was determined based on the current carried by droplets over the mass flow rate.

$$CMR = \frac{I}{(q/60)1000} \quad (1)$$

where  $CMR$  is the charge-to-mass ratio ( $\text{mC kg}^{-1}$ );  $q$  is the mass flow rate of droplets ( $\text{kg min}^{-1}$ );  $I$  is the measured current,  $\mu\text{A}$ .

### 3. Results and discussion

#### 3.1. Effects of electrode materials on droplets charging

Copper and 304 SS are both commonly used electrode materials for droplet charging, whereas the use of graphite as electrode material has not been reported yet. The CMR measurements of the three types of electrodes with a diameter of 100 mm and a height of 45 mm are shown in Figure 3.

Apparently, CMRs of the three electrode materials showed similar variation trends with the increase of applied voltage. Within the experimental voltage range, when the  $h$  value was 0–22.5 mm, CMR first increased and then decreased, whereas when the  $h$  value was below 45 mm, the CMR showed a near-linear increase.

The reason for the increase of CMR with voltage was that as the voltage increased, the electric field intensity of the space where the electrode was located increased. As a result, the polarization of the spray jet tip (before separation into droplets) was enhanced, and the charge carried by the droplets then increased. After the voltage reached a certain level, the influence of high-voltage electrodes on the polarization features of ambient air began to manifest. As the voltage further increased, the polarization degree of the air molecules was enhanced, leading to a reduction of dielectric constant  $\varepsilon$  of the air as well as the decline of electric field intensity between the electrodes. And this is the major reason for the gradual decline of CMR after peaking. When the voltage level exceeded the polarization limit of the air molecules, the air began to break down with discharge between the electrodes. This is the extreme voltage that can be applied by induction charging.

The  $h$  values with a range of 0–22.5 mm resulted in higher efficiencies of charging, because the nozzle was located at the position with the highest electric field intensity. At this position, the maximum CMR for copper, 304 SS, and graphite were 0.344, 0.435 and 0.429  $\text{mC kg}^{-1}$ , respectively. The CMR values were close for 304 SS and graphite, while the CMR value for copper was lower by about 20% as compared with the other two.

Although the 304 SS and graphite electrodes had similar CMRs, the charging stability of the 304 SS electrode under high voltage was far greater than that of the graphite electrode. As shown in Figure 3 (c), when the voltage was higher than 12 kV, the errors of CMR with graphite electrode gradually increased. For example, at the  $h$  value of 15 mm, when the voltage was 12 kV, CMR fluctuated within the range of 0.423–0.436  $\text{mC kg}^{-1}$ , and the errors were below 8% of the average; when the voltage increased to 15 kV, the CMR measurements fluctuated significantly within the range of 0.171–0.415  $\text{mC kg}^{-1}$ , and the error was as high as 96.4% of the average. In contrast, the maximum error of CMR for the 304 SS electrode was only 22.8% of the average within the experimental range, which was far smaller than that of graphite. It is easy to see that 304 SS and copper electrodes resulted in more stable droplet charging. The charging stability of different electrode materials has rarely been studied in existing literature, and the influence factors for charging stability needs to be further analyzed.

#### 3.2. CMR at different electrode dimensions of 304 stainless steel

The effect of 304 SS electrode dimensions (diameters of 200, 150, and 100 mm) on charging

was examined, and the results are shown in Figure 4. As the diameter increased, the CMR of droplets decreased rapidly. Within the experimental voltage range, the maximum CMRs were 0.233, 0.275, and 0.364 mC kg<sup>-1</sup> with electrode diameter of 200, 150, and 100 mm. According to the analysis, as the electrode diameter decreased, higher electric field intensity was produced by the electrode under the same voltage. As a result, the charge density  $q$  of the electrode increased, which was conducive to the improvement of CMR of droplets.

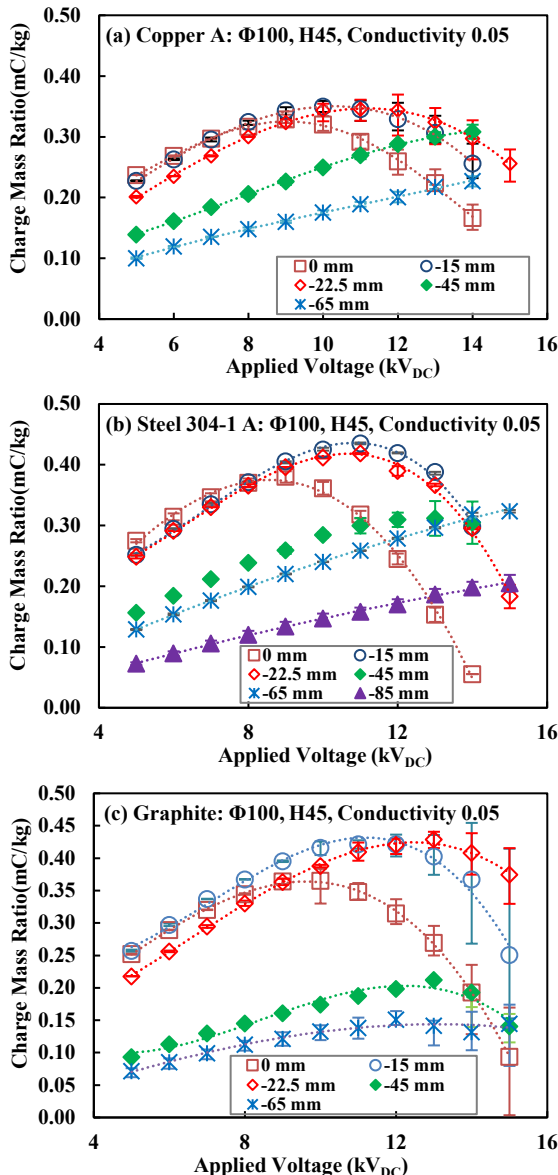


Figure 3. CMR under the electrode of (a) copper, (b) 304 stainless steel, and (c) graphite.

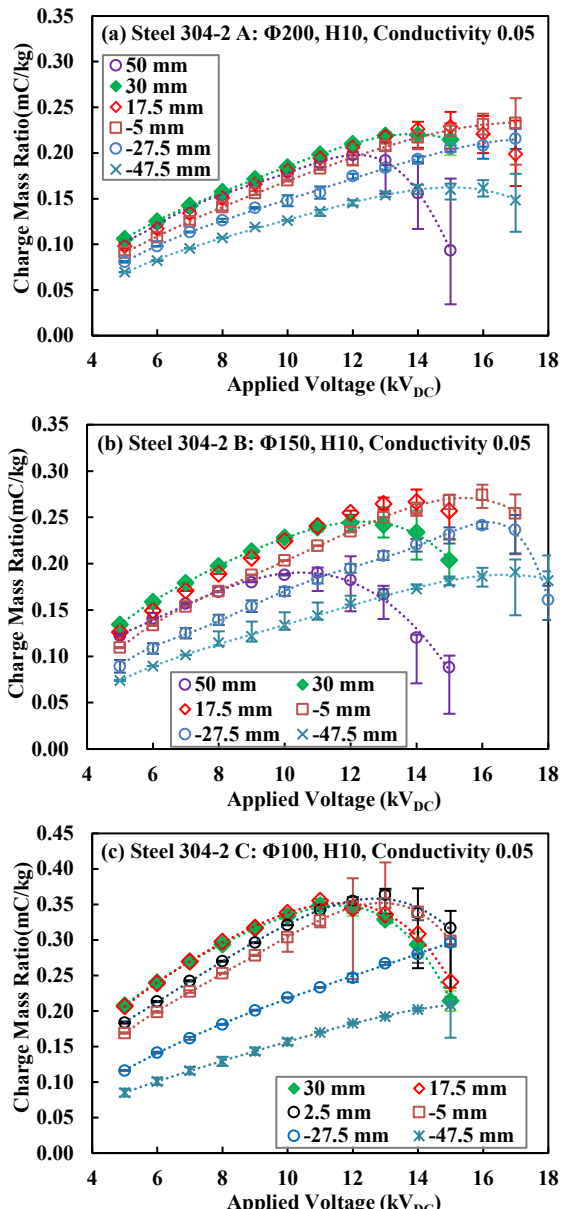


Figure 4. CMR with the 304 SS electrode at (a) 200, (b) 150, and (c) 100 mm inner diameter.

For the electrode of this dimension, a better charging effect could be obtained with the  $h$  values of -5 to 30 mm. When  $h$  values were above 30, there would be a fan-shaped jet from the nozzle, and a large amount of droplets were sprayed on the electrode or outside the electrode. Moreover, the electrode was far away from the nozzle, which was not conducive to charging. As shown in Figure 4(b), when the  $h$  value was 50 mm, CMR remained low. When the  $h$  value lied within the range of -5 to 30 mm, the nozzle was closer to the electrode, and a higher charge density was

formed on the electrode, thus strengthening the droplet charging effect. As shown in Figure 4(a), (b) and (c), there were large CMR values with the  $h$  values of -5 to 30 mm regardless of voltage. For example, within the voltage range of 3–12 kV, the maximum CMR was reached at the  $h$  value of 30 mm; the maximum CMR was reached at the  $h$  value of 17.5 mm within the voltage range of 14–15 kV (electrode diameter 200 mm) and voltage range of 12–14 kV (electrode diameter 150 mm); when the electrode diameters were 200 mm and 150 mm, the maximum CMR was reached at the  $h$  value of -5 mm as the voltage further increased.

Moreover, the larger the electrode diameter, the wider the voltage range capable of maintaining induction charging and the higher the voltage corresponding to peak CMR. For example, with the  $h$  value of 17.5 mm, the voltages corresponding to peak CMR for the electrode diameters of 200, 150, and 100 mm were 15, 14, and 11 kV, respectively.

### 3.3. Effects of nozzle height on CMR

The electric field intensity around the nozzle could be changed by changing the  $h$  value, which further influenced the droplet charge during spraying. As shown in Figure 5, nozzle and electrode served as the two poles of a capacitor, between which an electric field with intensity  $E$  was formed. Changing  $h$  values was done to change the distance between the two poles. The larger the distance, the smaller the charge  $Q$  of the capacitor and the smaller the charge density  $q$  of the electrode. As a result, the electric field intensity  $E$  around the nozzle would be smaller. At this time, the polarization effect of the spray jet tip (before droplet separation from the jet) was weakened, resulting in smaller charge of droplets after separation, and vice versa.

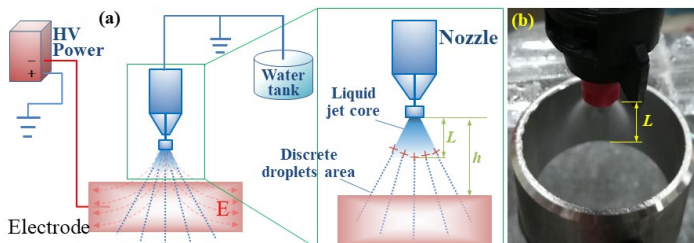


Figure 5. Effect model of the nozzle height on the CMR.

It was noticed that the initial segment of jet from the pressure type nozzle existed in the form of continuous jet (known as liquid jet core area). When this part of jet was exposed to the electric field, a large amount of positive charges would accumulate on the continuous jet tip. When the continuous jet at the positively charged tip was separated into discrete droplets, the droplets would acquire a certain amount of positive charges. This is the basic principle of induction charging. Since the continuous jet had a certain length  $L$  (Figure 5), higher CMR could be obtained if the continuous jet tip was placed where the electric field intensity was the highest. As shown in Figures 3 and 4, the position with the highest CMR was found near the  $h$  value of -15mm. At this position, the continuous jet tip of the nozzle was located near the middle of electrode (about -22.5 mm). This result can provide guidance for installation of the spray nozzle of an ESS.

## 4. Conclusions

With the electrode diameter of 100 mm, the maximum CMR values of the 304 SS and graphite electrodes were 0.435 and 0.429 mC kg<sup>-1</sup>, respectively. Comparatively, the maximum CMR of copper electrode was lower by about 20% (0.344 mC kg<sup>-1</sup>). 304 SS and copper electrodes had better charge stability.

The electrode diameter could change CMR of droplets by influencing electric field intensity. Within the experimental range of electrode dimensions (200, 150, and 100 mm), the smaller the diameter of the 304 SS electrode, the higher the maximum CMR (0.233, 0.275, and 0.364 mC kg<sup>-1</sup>, respectively) would be.

The electric field intensity around the electrode could be changed by changing the nozzle height  $h$ , which further influenced the charge during spraying. The initial segment of jet from the pressure type nozzle existed in the form of continuous jet. When installing the nozzle, the continuous jet tip should be placed where the electric field intensity was the strongest so as to obtain higher CMR.

### Acknowledgments

This work was supported by USDA-NIFA Grant 2016-67021-24434, and Key Research and Development Program of Xuzhou (Social Development) KC18221.

### References

- Alharbi, A., T. Soban, and R. Ohyama. 2014. Experimental studies on influence of different conductivities on water mist charging with electrostatic induction. In *2014 IEEE Conference on Electrical Insulation and Dielectric Phenomena (CEIDP)*. 558–61. IEEE.
- Almekinders, H., H.E. Ozkan, D.L. Reichard, T.G. Carpenter, and R.D. Brazee. 1992. Spray deposit patterns of an electrostatic atomizer. *Transactions of the ASAE*. 35: 1361–1367.
- Almuhamma, E.A., A.H. Amer Eissa, A.O. Alghannam, and A.M. Al-Amri. 2012. Optimization of Dust Removal in Poultry Houses Using Electrostatic Wet Scrubber. *Journal of Applied Sciences Research*. 8(12): 5651–5660.
- Andrzej, K., J. Anatol, T. Arkadiusz, A. Marchewicz, M. Szudyga, and T. Antes. 2013. Charged spray generation for gas cleaning applications. *Journal of Electrostatics*. 71: 260–264.
- Balachandran, W., A. Jaworek, A. Krupa, A., J. Kulon, and M. Lackowski. 2003. Efficiency of smoke removal by charged water droplets. *Journal of Electrostatics*. 58: 209–220.
- Cai, P., W. Nie, D. Chen, S. Yang, and Z. Liu. 2019. Effect of air flow rate on pollutant dispersion pattern of coal dust particles at fully mechanized mining face based on numerical simulation. *Fuel*. 239, 623–635.
- Carroz, W. J., N. Keller. 1978. Electrostatic induction parameters to attain maximum spray charge. *Transactions of the ASAE*. 21: 63–69.
- Chen, F., H. Chen, L. Zhang, S. Yin, S. Huang, G. Zhang, and Q. Tang. 2019. Controllable distribution of ultrafine diamond particles by electrostatic spray deposition. *Powder Technology*. 345: 267–273.
- Devanand, M., D. Divaker. 2010. Effects of electrode voltage, liquid flow rate, and liquid properties on spray chargeability of an air-assisted electrostatic-induction spray-charging system. *Journal of Electrostatics*. 68: 152–158.
- Di Natale, F., C. Carotenuto, L. D'Addio, A. Jaworek, A. Krupa, M. Szudyga, and A. Lancia. 2015. Capture of fine and ultrafine particles in a wet electrostatic scrubber. *Journal of Environmental Chemical Engineering*. 3: 349–356.
- Huang, S.H., C. C. Chen. 2002. Ultrafine aerosol penetration through electrostatic precipitators. *Environmental Science & Technology*. 36(21): 4625–4632.
- Liu, Q., W. Nie, Y. Hua, H. Peng, C. Liu, and C. Wei. 2019. Research on tunnel ventilation systems: dust diffusion and pollution behavior by air curtains based on CFD technology and field measurement. *Building and Environment*. 147: 444–60.
- Marchewicz, A.; A.T. Sobczyk, A. Krupa, A. Jaworek. 2019. Induction charging of water spray produced by pressure atomizer. *International Journal of Heat and Mass Transfer*. 135: 631–648.
- Patel, M.K., C. Ghanshyam, and P. Kapur. 2013. Characterization of electrode material for electrostatic spray charging: Theoretical and engineering practices. *Journal of Electrostatics*. 71: 55–60.
- Patel, M.K., M. Kundu, H. K. Sahoo, and M. K. Nayak. 2016. Enhanced performance of an air-assisted electrostatic nozzle: Role of electrode material and its dimensional considerations in spray charging. *Engineering in Agriculture, Environment and Food*. 9: 332–338.
- Penney G. 1944. Electrostatic liquid spray precipitator. US. Patent No. 2357 354.
- Ru, Y., L. Zhao, L. J. Hadlocon, H. Zhu, and S. K. Ramdon. 2017. Laboratory evaluation of electrostatic spray wet scrubber to control PM emissions from poultry facilities. *Environmental Technology*. 38(1): 23–33.
- Vaaraslahti, K., A. Laitine, and J. Keskinen. 2002. Spray charging of droplets in wet scrubber. *Journal of the Air & Waste Management Association*. 52:175–180.
- Yang, S., W. Nie, S. Lv, Z. Liu, H. Peng, X. Ma, P.Cai, and C. Xu. 2019. Effects of spraying pressure and installation angle of nozzles on atomization characteristics of external spraying system at a fully-mechanized mining face. *Powder technology*. 343: 754–64.
- Zheng, C., D. Duan, Q. Chang, S. Liu, Z. Yang, X. Liu, W. Weng, and X. Gao. 2019. Experiments on Enhancing the Particle Charging Performance of an Electrostatic Precipitator. *Aerosol and Air Quality Research*. 19 (6): 1411–1420.

# Modeling a Wire-Plate Electrostatic Precipitator for Poultry PM Collection Using COMSOL

Reyna M. Knight, Lingying Zhao \*

Department of Food, Agricultural, and Biological Engineering, The Ohio State University,  
Columbus, OH 43210, USA

\* Corresponding author. Email: [zhao.119@osu.edu](mailto:zhao.119@osu.edu)

## Abstract

Poultry production facilities generate significant emissions of particulate matter (PM). Electrostatic precipitation has shown promise as an effective technology for PM mitigation. However, most previous electrostatic precipitators (ESPs) are for industrial applications and there is a distinct lack of research on optimizing the design of an ESP to mitigate poultry PM. This study utilizes COMSOL 5.3a to model the PM collection processes using a wire-plate ESP under conditions similar to those within a poultry production facility. The collection efficiencies for both PM<sub>2.5</sub> and PM<sub>10</sub>, the electric power consumption, and the specific corona power were determined from the simulation. This study provides an effective method of modeling ESP designs and performances for poultry PM control.

**Keywords:** Particulate matter; dust; poultry housing; mitigation; simulation; computational fluid dynamics (CFD)

## 1. Introduction

Particulate matter (PM), commonly referred to as dust, is a significant air pollutant in poultry housing facilities. These particles are generated primarily through processes such as feeding, ventilation, human worker and bird activity, and manure management. The most commonly studied particles are those smaller than 10 µm in diameter, known as PM<sub>10</sub>, and those smaller than 2.5 µm in diameter, known as PM<sub>2.5</sub>. Inhalation of poultry PM is linked to increased rates of several respiratory ailments in workers, including bronchitis, asthma, and organic dust toxic syndrome (Radon et al., 2001). Additionally, these particles can act as vectors of pathogen transmission, allowing harmful microorganisms to transmit throughout the facility, potentially infecting birds with diseases such as avian influenza (Spekreijse et al., 2013). Effective poultry PM control would greatly reduce the chances of these adverse effects impacting poultry facilities.

Electrostatic precipitators (ESPs) have long been used for PM mitigation in industries such as mining and coal-fired power plants. ESP systems for these applications have typically been optimized enough that very high PM collection efficiencies are common, such as a PM collection efficiency greater than 99% reported for an ESP system in a coal-fired power plant (Wang et al., 2015). However, the use of ESP systems for mitigation of PM in animal housing facilities is relatively new and has yet to achieve the high collection efficiencies seen in other industrial applications due to the facts that poultry PM has distinct characteristics in comparison with industrial PM, in terms of organic nature, particle size, concentration, and aerodynamic environment. Manuzon et al. (2014) optimized and tested a very small scale (0.0929 m<sup>2</sup>) ESP module for PM mitigation in a manure-belt layer house and reported collection efficiencies of 86% for PM<sub>2.5</sub> and 84% for PM<sub>10</sub>. These high PM collection efficiencies suggest that optimization of ESPs for mitigation of poultry PM is promising, but a significant amount of work is still needed to scale-up the ESP and achieve poultry PM collection efficiencies at or above 90%.

COMSOL (version 5.3a, COMSOL Inc., Burlington, MA) is a user-friendly, multiphysics simulation software, which can simulate electrical, mechanical, fluid, and chemical applications and processes. It contains several modules that come with the relevant equations preprogrammed for ease of use. Lancereau et al. (2013) and Kherbouche et al. (2016) developed COMSOL models for a wire-cylinder ESP. Relatively few studies have attempted to utilize such software to model a wire-plate ESP system and perform subsequent optimization, with no studies specifically

focusing on poultry PM mitigation.

This study aims to develop a COMSOL model to predict the PM collection efficiencies and specific corona power of an ESP module for mitigation of PM emissions from poultry production facilities. The COMSOL model can be used to assess designs of ESPs for optimization and further physical prototype construction.

## 2. Materials and Methods

### 2.1. Geometry and meshes of an ESP cell

Figure 1 illustrates the dimensioned geometric design for a cell of the simulated wire-plate ESP module.

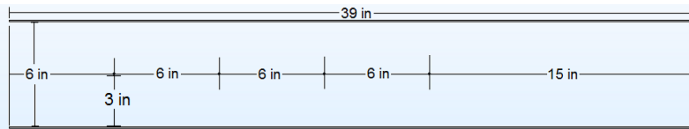


Figure 1. Basic geometric layout of the simulated ESP module.

The wire electrodes were modeled as 304L stainless steel wires with a diameter of 0.965 mm (0.038 in.). This diameter is close to the smallest commercially available diameter wire that can adequately maintain tension. The collector plates were modeled as 304L stainless steel plates with a thickness of 2.29 mm (0.090 in.) and a length and height of 99.1 cm (39 in.), giving an aspect ratio of 1.

The geometry meshes were created in three separate portions. The first mesh was applied to the air within the precipitator and consisted of 2,747,063 volume mesh elements. The second mesh was applied to the boundary between the air and the wire electrodes and consisted of 93,632 boundary mesh elements. The third mesh was applied to the boundary between the air and the collector plates and consisted of 40,728 boundary mesh elements. The mesh elements are smaller in size and greater in number near the wire electrodes.

### 2.2. Airflow simulation in the ESP module

The airflow through the ESP module is modeled using the default settings for COMSOL's  $k-\epsilon$  turbulent flow model. The turbulent intensity is set at 0.01 and the turbulent length scale is defined as 0.07 times the hydraulic diameter of the ESP module, as done by Dastoori et al. (2013). The air velocity was set at an initial value of  $2 \text{ m s}^{-1}$ , which was near the higher end of the range of typical ESP air velocities ( $1\text{--}2 \text{ m s}^{-1}$ ) and near the optimized air velocity ( $1.7 \text{ m s}^{-1}$ ) for an ESP in a poultry facility identified by Manuzon et al. (2014). A previous study also showed that operating an ESP at air velocities greater than  $2 \text{ m s}^{-1}$  can lead to greater re-entrainment of collected PM (Manuzon and Zhao, 2009). Wall functions are applied at the surfaces of the wire electrodes and the collector plates. The Reynolds averaged Navier-Stokes (RANS) equations were solved using a stationary algebraic multigrid solver. The stationary RANS equations are shown in Equations 1 and 2.

$$\rho_{air}(\vec{U} \cdot \nabla)\vec{U} = -\nabla p + \mu_{air}\nabla^2\vec{U} + \rho_{ion}\vec{E} \quad (1)$$

$$\nabla \vec{U} = 0 \quad (2)$$

where  $\rho_{air}$  is the density of air ( $1.205 \text{ kg m}^{-3}$ );  $\vec{U}$  is the air velocity ( $\text{m s}^{-1}$ );  $p$  is the absolute air pressure ( $101.325 \text{ kPa}$  for ambient air);  $\mu_{air}$  is the dynamic viscosity of air ( $18.2 \mu\text{Pa s}$ );  $\rho_{ion}$  is the ionic space charge density ( $\text{C m}^{-3}$ ); and  $\vec{E}$  is the electric field strength ( $\text{V m}^{-1}$ ).

### 2.3. Electric field simulation

As pointed out by Manuzon et al. (2014), the optimal value of electric field strength for corona generation in an ESP is typically just below the value of the sparking electric field strength. The sparkover electric field strength calculation was performed using Equation 3, adapted from Turner

et al. (2000). Using values of 298.15 K and 1 atm for temperature and pressure, respectively, the sparking electric field strength for a wire-plate ESP is  $5.447 \text{ kV cm}^{-1}$  ( $13.84 \text{ kV in}^{-1}$ ). Thus, a value of  $5.433 \text{ kV cm}^{-1}$  ( $13.8 \text{ kV in}^{-1}$ ) was chosen as the electric field strength between the wire electrodes and collector plates, requiring an applied voltage of 41.4 kV at each of the wire electrodes.

$$E_s = 6.3 \cdot \left( \frac{273}{T} P \right)^{1.65} \quad (3)$$

where  $E_s$  is the sparking electric field strength ( $\text{kV cm}^{-1}$ );  $T$  is the temperature (298.15 K); and  $P$  is the pressure (1 atm).

The electrostatic characteristics of the ESP module are solved for using an approach modeled after that of Skodras et al. (2006). The electric field strength at the surface of the wire electrodes must be consistent in each simulation, matching the value determined by a formula known as Peek's Law, shown as Equation 4 below, where  $E_0$  is the electric field strength in  $\text{V m}^{-1}$ ,  $f$  is the dimensionless wire fatigue factor,  $\delta$  is the relative air density, and  $r_w$  is the wire electrode radius in m. The constant space charge density at the surface of the wire electrodes that gives the correct electric field strength is set using an iterative approach following the approach of Rubinetti et al. (2015), using a tolerance of 0.0025%. The dimensionless wire fatigue factor was set at 0.6, as done by Rubinetti et al. (2015). Poisson's equation, shown as Equation 5 below, is coupled with the charge continuity equation, shown as Equation 6 below. These equations are simultaneously solved using a stationary multifrontal massively parallel sparse (MUMPS) direct solver. Boundary conditions were set to give zero flux of electric potential at the inlet and outlet and zero flux of space charge density at the inlet, outlet, and collector plate surfaces, as shown in Table 1.

$$E_0 = 3 \times 10^6 \cdot f \cdot \left( \delta + 0.03 \sqrt{\frac{\delta}{r_w}} \right) \quad (4)$$

$$\nabla^2 V = -\frac{\rho_{ion}}{\epsilon_0 \epsilon_{air}} \quad (5)$$

$$\nabla(\rho_{ion} \cdot (-\nabla V + \vec{U}_{air})) - D_{ion} \cdot \nabla \rho_{ion} = 0 \quad (6)$$

where:  $E_0$  is the electric field strength at the wire electrode surface ( $\text{V m}^{-1}$ );  $f$  is the wire fatigue factor (0.6, as recommended by Rubinetti et al., 2015);  $\delta$  is the relative air density;  $r_w$  is the radius of the wire electrode (m);  $V$  is the electric potential or voltage (V);  $\rho_{ion}$  is the ionic space charge density ( $\text{C m}^{-3}$ );  $\epsilon_0$  is the vacuum permittivity ( $8.854 \times 10^{-12} \text{ F m}^{-1}$ );  $\epsilon_{air}$  is the dielectric constant of air (1.00059);  $U_{air}$  is the air velocity ( $\text{m s}^{-1}$ ); and  $D_{ion}$  is the ionic diffusivity ( $10 \text{ m}^2 \text{ s}^{-1}$ , as done by Skodras et al., 2006).

## 2.4. Boundary conditions

Table 1. Boundary conditions used in the simulation of the ESP module.

Boundary	Airflow	Electric potential (V)	Space charge density ( $\rho_v$ )	Particles
Inlet	$U_x = 2 \text{ m s}^{-1}$	$\frac{\partial V}{\partial n} = 0$	$\frac{\partial \rho_v}{\partial n} = 0$	Enter
Outlet	$P = 101,325 \text{ Pa}$	$\frac{\partial V}{\partial n} = 0$	$\frac{\partial \rho_v}{\partial n} = 0$	Escape
Wire Electrodes	Wall functions	$V = 41.4 \text{ kV}$ (constant)	Constant (from Peek's Law)	Reflect
Collector Plates	Wall functions	$V = 0$ (constant)	$\frac{\partial \rho_v}{\partial n} = 0$	Trap

## 2.5. Simulation of particle charging

The poultry PM was assumed to have a dielectric constant of 4. Both diffusion charging and field charging are considered, although the charges of the particles are assumed to have a negligible effect on the electric field and/or space charge density. Particle charges are calculated

throughout the time-dependent simulation at each time step using Cochet's combined charging model, shown in Equations 7, 8, and 9 below. Long and Yao (2010) have shown that this charging model would provide accurate results while limiting computational complexity in these simulations. This electric charge contributes to an electric force that pulls the charged particles toward the grounded plate surface, the value of which is determined by Equation 10. Equations 11, 12, 13, and 14 were used to calculate the drag force on each particle and Equation 15 was used to calculate the combined gravitational and buoyant force on each particle. Conservation of momentum is confirmed by performing a force balance calculation on each particle at every time step using Equation 16, as outlined by Arif et al. (2016). The simulations were run until all particles have either been collected by the plates or have escaped the ESP module. The total simulation time was 0.61 s.

$$q_p(t) = q_{sat} \left( \frac{t}{t+\tau} \right) \quad (7)$$

$$q_{sat} = \left[ \left( 1 + \frac{2\lambda}{1+2\lambda/d_p} \right)^2 + \frac{2}{1+2\lambda/d_p} \frac{K_p-1}{K_p+2} \right] \pi \varepsilon_0 E d_p^2 \quad (8)$$

$$\tau = \frac{4\varepsilon_0}{\rho_{ion} b_{ion}} \quad (9)$$

$$F_E = q_p \vec{E} \quad (10)$$

$$F_D = \frac{m_p}{\tau_p} (\vec{U}_{air} - \vec{U}_p) \quad (11)$$

$$\tau_p = \frac{4\rho_p d_p^2}{3\mu_{air} C_D Re_r} \quad (12)$$

$$C_D = \frac{24}{Re_r} (1 + 0.15 Re_r^{0.687}) \quad (13)$$

$$Re_r = \frac{\rho_{air} \|\vec{U}_{air} - \vec{U}_p\| d_p}{\mu_{air}} \quad (14)$$

$$F_g = m_p g \frac{\rho_p - \rho_{air}}{\rho_{air}} \quad (15)$$

$$m_p \frac{dU_p}{dt} = F_D + F_g + F_E \quad (16)$$

where:  $q_p$  is the particle charge (C);  $q_{sat}$  is the particle saturation charge (C);  $\tau$  is the charging time constant (s);  $\lambda$  is the ionic mean free path (0.1  $\mu\text{m}$ , as recommended by Long and Yao, 2010);  $d_p$  is the particle diameter (m);  $K_p$  is the particle dielectric constant (assumed to be 4.0);  $\varepsilon_0$  is the permittivity of vacuum ( $8.854 \times 10^{-12} \text{ F m}^{-1}$ );  $E$  is the electric field strength ( $\text{V m}^{-1}$ );  $\rho_{ion}$  is the ionic space charge density ( $\text{C m}^{-3}$ );  $b_{ion}$  is the ion mobility ( $0.00022 \text{ m}^2 \text{ V}^{-1} \text{ s}^{-1}$  as done by Skodras et al., 2006);  $t$  is time (s);  $F_E$  is the electric force (N);  $F_D$  is the drag force (N);  $m_p$  is the particle mass (kg);  $\tau_p$  is the particle velocity response time (s);  $U_{air}$  is the air velocity ( $\text{m s}^{-1}$ );  $U_p$  is the particle velocity ( $\text{m s}^{-1}$ );  $\rho_p$  is the particle density ( $1403.2 \text{ kg m}^{-3}$ );  $\mu_{air}$  is the dynamic viscosity of air ( $18.2 \mu\text{Pa s}$ );  $C_D$  is the Schiller-Naumann drag constant;  $Re_r$  is the relative Reynolds number;  $\rho_{air}$  is the density of air ( $1.205 \text{ kg m}^{-3}$ );  $F_g$  is the combined gravitational and buoyant force; and  $g$  is the gravitational acceleration constant ( $9.80665 \text{ m s}^{-2}$ ).

### 3. Results and Discussion

The electrical characteristics are important in determining the feasibility of an ESP design. The surfaces of the wire electrodes must have space charge densities and electric field strengths that satisfy Peek's law in order for the results of the particle collection simulations to be considered valid. Figures 2, 3, and 4 show contour plots for voltage, electric field strength, and space charge density, respectively.

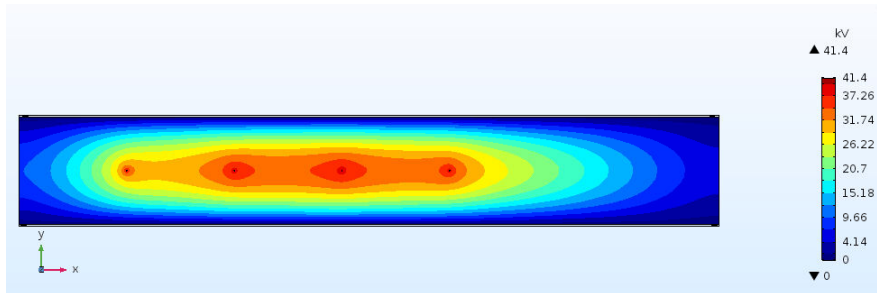


Figure 2. Contour plot of voltage distribution within the simulated ESP module.

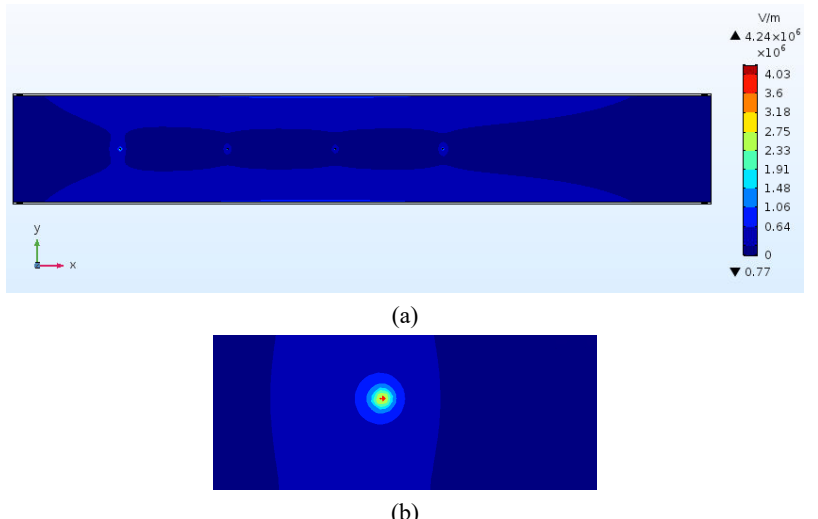


Figure 3. Contour plot of electric field strength distribution within the simulated ESP module showing the entire module (a) and a zoomed in view near the wire electrode surface (b).

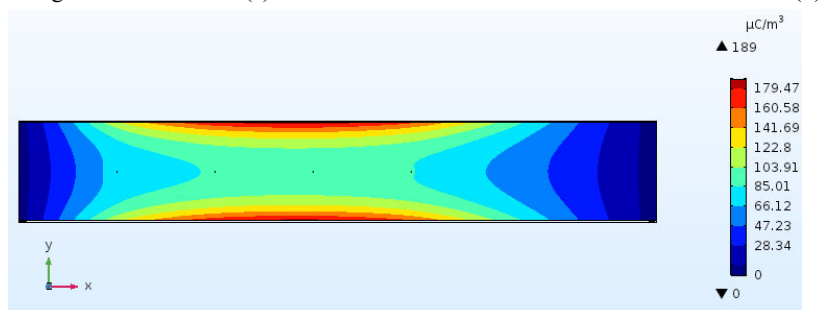


Figure 4. Contour plot of space charge density distribution within the simulated ESP module.

As expected, the voltage is highest (41.4 kV) at the surfaces of the wire electrodes and decreases as the distance from the wire electrode surface increases, reaching a minimum of 0 at the surfaces of the grounded collector plates. The electric field strength is also greatest ( $4.24 \times 10^6$  V m<sup>-1</sup>) at the surfaces of the wire electrodes and matches the value specified by Peek's Law. The electric field strength rapidly decreases as the distance from the wire electrode surface

increases, reaching a minimum of nearly 0 at the inlet and outlet. The space charge density followed a distribution very similar to that of the electric field strength, with the highest space charge density ( $189 \mu\text{C m}^{-3}$ ) at the surfaces of the wire electrodes and the lowest at the inlet and outlet.

COMSOL was used to generate contour plots of air velocity and static pressure distributions as well as particle trajectory plots to allow for a more detailed examination of the final positions of all simulated particles. Figure 5 shows a contour plot of the air velocity and Figure 6 shows a contour plot of the static pressure to demonstrate the airflow patterns within the simulated ESP module. Figure 7 shows particle trajectory plots indicating the final position and status of all simulated particles for both PM<sub>2.5</sub> and PM<sub>10</sub>.

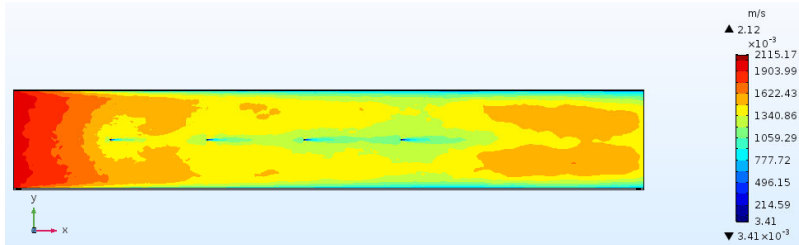


Figure 5. Contour plot of air velocity distribution within the simulated ESP module.

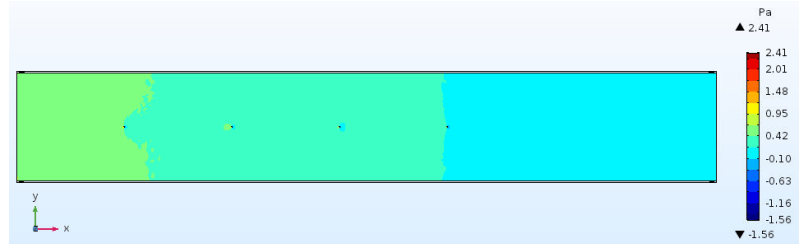


Figure 6. Contour plot of static pressure distribution within the simulated ESP module.

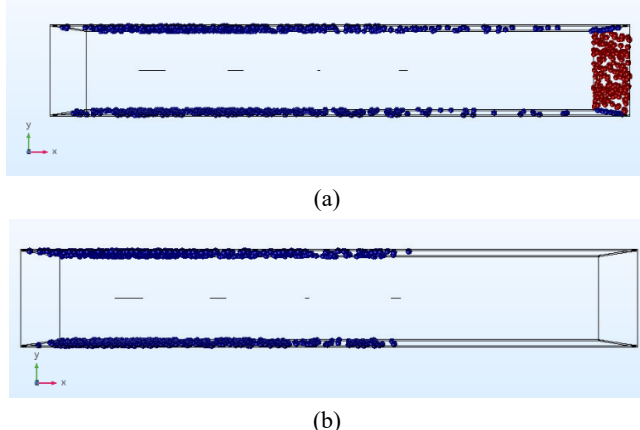


Figure 7. Particle trajectory plots showing the final positions of all particles, with blue particles having been collected and red particles having escaped, for (a) PM<sub>2.5</sub> and (b) PM<sub>10</sub>.

The particle collection process was more successful at collecting PM<sub>10</sub> than PM<sub>2.5</sub>, which is

expected, since the difficulty of collecting a particle is inversely related to its diameter. All of the 10 µm diameter particles were successfully collected on the collector plates, while some of the 2.5 µm diameter particles managed to escape the ESP and were not successfully collected. This resulted in a PM<sub>10</sub> collection efficiency of 100% and a PM<sub>2.5</sub> collection efficiency of 80.5%. The air velocity distribution shows an initial air velocity of 2 m s<sup>-1</sup>, which decreases moving further into the channel between the collector plates. Wake effects are visible after each wire electrode, showing that the wire electrodes disturb the airflow pattern, causing turbulent effects that significantly decrease the air velocity behind the wire electrodes. The air velocity decreased moving closer to the surfaces of the collector plates, reaching essentially zero velocity at the boundary layer between the airstream and the collector plate. The static pressure change was minimal, with the highest static pressure found to be 2.41 Pa and the lowest found to be a pressure drop of 1.56 Pa. This suggests that the ESP module would cause a very small pressure drop. The ESP was found to consume 56.5 W of electric power in order to treat an air flow rate of 1087 m<sup>3</sup> h<sup>-1</sup>, giving a specific corona power of 0.052 W (m<sup>3</sup> h<sup>-1</sup>)<sup>-1</sup>.

#### 4. Conclusions

An ESP module consisting of two 99.1 cm × 99.1 cm (39 in. × 39 in.) steel plates placed 15.24 cm (6.0 in.) apart with four 0.965 mm (0.038 in.) diameter steel wires halfway between the plates was simulated in COMSOL. Distributions of voltage, electric field, space charge density, air velocity, and static pressure were determined. At an initial air velocity of 2 m s<sup>-1</sup> and an applied voltage of 41.4 kV, the ESP module was found to collect 100% of the PM<sub>10</sub> and 80.5% of the PM<sub>2.5</sub> while consuming 56.5 W with a pressure drop of no more than 2.41 Pa.

#### Acknowledgements

This study was performed as part of a project funded by USDA-NIFA Grant 2016-67021-24434. The authors would like to thank the Ohio Supercomputer Center and Dr. Zhenyu Liu of Shanxi Agricultural University.

#### References

- Arif, S., D.J. Franken, R.C. Everson, H.W.J.P. Neomagus, L.A. le Grange, A. Arif, 2016. CFD modeling of particle charging and collection in electrostatic precipitators. *Journal of Electrostatics*. 84, 10–22. <http://doi.org/10.1016/j.elstat.2016.08.008>.
- Dastoori, K., B. Makin, M. Kolhe, M. Des-Roseaux, M. Conneely, 2013. CFD modelling of flue gas particulates in a biomass fired stove with electrostatic precipitation. *Journal of Electrostatics*. 71 (3), 351–356. <http://doi.org/10.1016/j.elstat.2012.12.039>.
- Kherbouche, F., Y. Benmimoun, A. Tilmantine, A. Zouaghi, N. Zouzou, 2016. Study of a new electrostatic precipitator with asymmetric wire-to-cylinder configuration for cement particles collection. *Journal of Electrostatics*. 83, 7–15. <http://doi.org/10.1016/j.elstat.2016.07.001>.
- Lancereau, Q., J.M. Roux, J.L. Achard, 2013. Electrohydrodynamic flow regimes in a cylindrical electrostatic precipitator. *IEEE Transactions on Dielectrics and Electrical Insulation*, 20 (4), 1409–1420. <http://doi.org/10.1109/TDEI.2013.6571463>.
- Long, Z., Q. Yao, 2010. Evaluation of various particle charging models for simulating particle dynamics in electrostatic precipitators. *Journal of Aerosol Science*. 41 (7), 702–718. <http://doi.org/10.1016/j.jaerosci.2010.04.005>.
- Manuzon, R., L. Zhao, 2009. Laboratory evaluation and modeling of electrostatic precipitation of PM emissions from poultry buildings. *ASHRAE Transactions*. 115 (2), 831–850.
- Manuzon, R., L. Zhao, C. Gecik, 2014. An optimized electrostatic precipitator for air cleaning of particulate emissions from poultry facilities. *ASHRAE Transactions*. 120 (1), 490–503.
- Radon, K., C. Weber, M. Iversen, B. Danuser, S. Pedersen, D. Nowak, 2001. Exposure assessment and lung function in pig and poultry farmers. *Occupational and Environmental Medicine*. 58 (6), 405–410. <http://doi.org/10.1136/oem.58.6.405>.
- Rubinetti, D., D.A. Weiss, and W. Egli, 2015. Electrostatic precipitators - Modelling and analytical verification concept. In COMSOL Conference 2015. Grenoble, France, October 14–16.

Skodras, G., S.P. Kaldis, D. Sofialidis, O. Faltsi, P. Grammelis, G.P. Sakellaropoulos, 2006. Particulate removal via electrostatic precipitators - CFD simulation. *Fuel Processing Technology.* 87 (7), 623–631. <http://doi.org/10.1016/j.fuproc.2006.01.012>.

Spekreijse, D., A. Bouma, G. Koch, A. Stegeman, 2013. Quantification of dust-borne transmission of highly pathogenic avian influenza virus between chickens. *Influenza and Other Respiratory Viruses.* 7 (2), 132–138. <http://doi.org/10.1111/j.1750-2659.2012.00362.x>.

Turner, J.H., P.A. Lawless, T. Yamamoto, D.W. Coy, G.P. Greiner, J.D. McKenna, W.M. Vatavuk, 2000. Chapter three: Control of particulate matter: Electrostatic precipitators. *Air Pollution Engineering Manual.* 2nd Ed., 86–98. New York, NY: Wiley-Interscience.

Wang, C., X. Liu, D. Li, J. Si, B. Zhao, M. Xu, 2015. Measurement of particulate matter and trace elements from a coal-fired power plant with electrostatic precipitators equipped the low temperature economizer. *Proceedings of the Combustion Institute.* 35 (3), 2793–2800. <http://doi.org/10.1016/j.proci.2014.07.004>.

## Ammonia Transport from Multi-Floor Pig Houses Based on CFD Simulations

Yicong Xin <sup>a</sup>, Li Rong <sup>b,\*</sup>, Dejia Liu <sup>a</sup>, Xiusong Li <sup>c</sup>, Bin Chen <sup>d</sup>, Xianwang Kong <sup>a</sup>,  
Shihao Ying <sup>a</sup>, Dezhao Liu <sup>a,\*</sup>

<sup>a</sup> College of Biosystems Engineering and Food Science, Zhejiang University,  
Hangzhou, Zhejiang 310058, P.R. China

<sup>b</sup> Department of Engineering, Aarhus University, Aarhus 8000, Denmark

<sup>c</sup> Big Herdsman Machinery Co., Ltd., Qingdao, Shandong 266000, P.R. China

<sup>d</sup> Zhejiang Huatong Meat Products Co., Ltd., Yiwu, Zhejiang 322000, P.R. China

\* Corresponding authors. Email: [Li.Rong@eng.au.dk](mailto:Li.Rong@eng.au.dk), [dezhao.liu@zju.edu.cn](mailto:dezhao.liu@zju.edu.cn)

### Abstract

The fast growth of livestock industry and meat demand in China brings new challenges such as air emission problem to the neighborhood. Due to the lack of sufficient land especially in the East China area, the highly-intensive livestock houses such as multi-floor buildings for raising pigs have become attractive. However, this may also pose greater challenges to the local environment due to the dispersion of air pollutants emitted from such high-rise pig production buildings. Assessment and thereby mitigation of the influence of the emitted air pollutants on the surrounding neighborhood will therefore be essential for the sustainable design and development of the multi-floor buildings. This study used Computational Fluid Dynamics (CFD) to investigate the ammonia level, released from the multi-floor pig house and dispersed to the neighborhood. Navier-Stokes equations, Species transport equations and standard k-ε turbulence model were chosen and applied in this research. The numerical results of velocity and concentration distribution were presented and analyzed. The results from this study provide theoretical based understanding of ammonia transport from multi-floor pig houses to the neighborhood.

**Keywords:** Animal building, computational fluid dynamics, dispersion, pollutant, simulation

### 1. Introduction

Livestock industry is essential for the economy and sustainable development of China. In recent years, livestock industry has a rapid growth towards modernization and intensification (Zhou et al., 2014). At the same time, China has become the biggest market in the whole world regarding the consumption of meat products, as people living standards unceasingly enhanced and the demand for meat greatly increased (Du et al., 2019). The fast growth of livestock industry and meat demand also put new challenges to the local areas especially to areas lack of land in East China. Therefore, the traditional farming may no longer meet the needs for the rapid development of livestock industry. Multi-floor building to raise pigs has already attracted investors as this type of buildings save the floor space and improve the production efficiency per unit of land area. Multi-floor buildings greatly changed the infrastructure inside and outside of the buildings and intensified the ventilation air volume flows greatly. This poses great challenges to the control of the environmental of the production houses within each of the multi-floor buildings and the emissions of pollutants. Therefore, it is imperative to demonstrate that this new design can fulfill the requirements of the emissions to the atmosphere (Norton et al., 2010).

Livestock houses release a large amount of air pollutants, such as ammonia, hydrogen sulfide, and greenhouse gases, and lead to ambient air quality problems (Zhang et al., 2012). Knowledge about dispersion of air emissions from the multi-floor production buildings is needed to assess the emission impacts on local air quality for development of mitigation strategies. (Tominaga and Stathopoulos, 2009).

The wind flows in the atmospheric boundary layer over buildings are inherently complex because the wind flow patterns and the vortices produced by an array of buildings ventilation fans are naturally transient, so it is difficult to get a large amount of measured data of wind velocity

and direction to reproduce the atmospheric air motion (Lateb et al., 2016). In practice, full-scale measurements, wind tunnel experiments and Computational Fluid Dynamics (CFD) simulation tools can be applied to investigate the airflow conditions around buildings. The full-scale measurements are usually performed under real conditions, but it is expensive and time-consuming. Wind tunnel experiments of air emission dispersion may not always be representative of the full-scale phenomena, so the numerical modeling techniques became a better choice with high efficiency (Norton et al., 2007). In recent years, with the advancement of CFD, it has been increasingly applied for simulating the emissions of air pollutants (e.g., carbon dioxide and ammonia) in street canyons and urban geometry (Ntinis et al., 2017). The CFD may be an alternative tool to study the dispersion of air emissions from multi-floor production buildings as it can provide the information of distribution of several parameters (e.g., air speed, temperature, humidity, concentration) around the buildings with complex geometric shapes at the same time and at every point in the whole computational domain as well (Gaultieri, 2010).

While the multi-floor pig building has not been widely adapted by the animal production industry in China, it has been in place in Zhejiang Province. This study is to simulate airflow pattern around one single multi-floor pig house using CFD technique to predict the velocity and ammonia distribution. The simulation also includes the prediction of the distance and concentration of the ammonia dispersion.

## 2. Materials and Methods

### 2.1. Geometry model and site location of the multi-floor pig building

The multi-floor pig building is located in Yiwu, Zhejiang Province. The simplified geometry model of the multi-floor pig house is shown in Figure 1. The length, width and height of the building are 118 m, 62 m, and 21 m, respectively. To achieve better simulation result, the pig building was simplified as a cuboid due to the external structure of the building. This building consists of two smaller symmetrical pig houses with a gases emission area in the middle of these two pig houses, and the emission area was simplified into an emission surface. There is an empty area simplified into an empty cube in each pig house, which is subtracted from the whole geometry model. The aim of this study is mainly about predicting the dispersion of ammonia around the building, and the ammonia was discharged to the atmosphere mainly through the release area, so the inside of the pig house was not simulated. The Reynold number based on  $H_b$  (building height) and  $U_b$  (inflow velocity at  $z = H_b$ ) is  $2.0 \times 10^7$ . The average velocity at the 10 m is  $1.5 \text{ m s}^{-1}$  according to the measured data of the local meteorological information.

The power law exponent of the vertical profile of the inflow velocity is 0.15. Ammonia is selected as the target pollutant released at a concentration of 5 ppm. There are 192 large size fans with ventilation rate of 27,700 cfm and 96 small size fans with ventilation rate of 5,850 cfm. The total mass flow rate of the emission outlet is  $3581.9 \text{ kg s}^{-1}$  by calculation according to the ventilation rate of fans and the area of the emission outlet supposing fans are fully open.

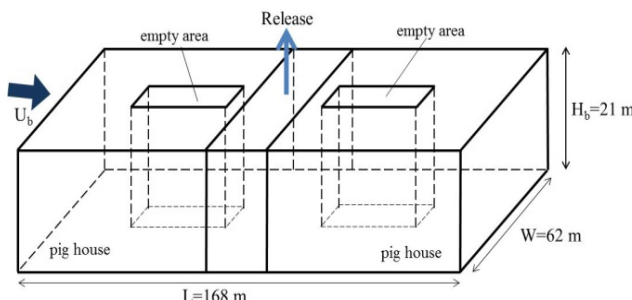


Figure 1. Flow field considered and notation.

## 2.2. Numerical methods and boundary conditions

This three-dimensional simulation of the outdoor environment for the multi-floor pig house was conducted by the commercial code Fluent 15.0 and the code used for the calculation is based on a finite volume approach for solving the flow and concentration equation on structured rectangular grids. The computational domain and the boundary conditions are shown in Figure 2(a). The dimensions of the computational domain were length, 706.08 m, width, 313.72 m, height, 168 m. The emission area was simplified into the emission surface; however, in order to simplify the boundary condition setting, the emission surface was regarded as a case of emission point source because the computational domain is large enough. The emission concentration of ammonia was assumed as 5 ppm which is within the ammonia emission range of most pig houses in China (Melse et al., 2012; Zhifang Shi, 2017); in addition, the emission concentration in this study could be lower due to an optimized manure collection.

Symmetry boundary was used for sides and the standard wall function was used for wall boundary. This domain was discretized into  $430(x) \times 215(y) \times 85(z)$  grid cells and the total grid numbers was 7,353,584. The boundary conditions in this research were summarized in Table 1. Steady Reynolds-averaged Navier-Stokes (RANS) method was applied in this research. The standard k-e model was used for the turbulence modeling. In addition, The QUICK scheme was used for discretizing the convection of momentum and concentration equations. The second order centered difference scheme was used for other term. Semi-Implicit Method for Pressure Linked Equations (SIMPLE) methods was used for the pressure-velocity correction. Iterations were considered to be in convergence when the residual for energy equation arrived at  $10^{-6}$  and the residual for other equation arrived at  $10^{-3}$  for the simulation, in addition, the variables need tend to be constant. Representative planes and lines selected in this study are shown in Figure 2(b).

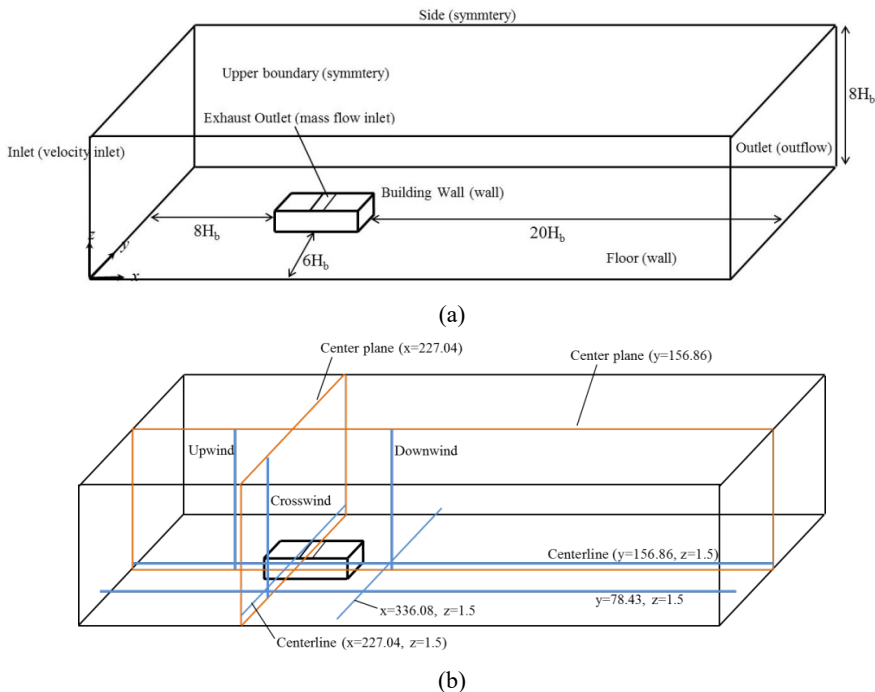


Figure 2. (a) Computational domain and boundary conditions; (b) Representative planes and lines.

Table 1. List of boundary conditions.

Position	Boundary conditions
Inlet	Velocity inlet ( $1.5 \text{ m s}^{-1}$ at the height of 10 m; power law at 0.15)
Outlet	Outflow
Exhaust outlet	Mass flow inlet (flow rate $3581.9 \text{ kg s}^{-1}$ ; ammonia concentration 5 ppm )
Side and top	Symmetry
Walls and floor	Non-slip wall, adiabatic

### 3. Results and Discussion

#### 3.1. Velocity distribution

The complexity of the flow around an obstacle or group of obstacles has been recognized because the wind flow exhibits a wide range of physical phenomena including strong pressure gradients, unsteady flow regions. Thus, velocity distribution is important for studying the wind-flow field around a building.

Figures 3 and 4 are the velocity distribution at two center planes ( $y=156.86 \text{ m}$  and  $x=227.04 \text{ m}$ ), respectively. The high level of velocity magnitude appears at the emission outlet and the lower velocity region with vortexes is behind the building and in the empty cubes. However, the high velocity is more favorable to the rapid dilution and dispersion of ammonia. As it can be seen in Figure 4, the velocity distribution is symmetric and the velocity magnitude is lower above the building, which could be due to the obstruction of the building.

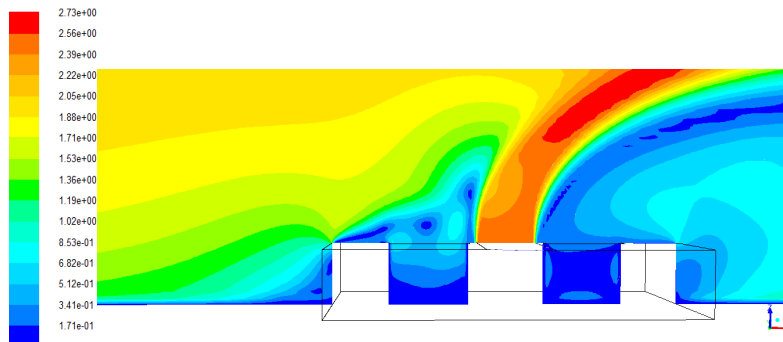


Figure 3. Velocity ( $\text{m s}^{-1}$ ) distribution at  $y=156.86 \text{ m}$ .

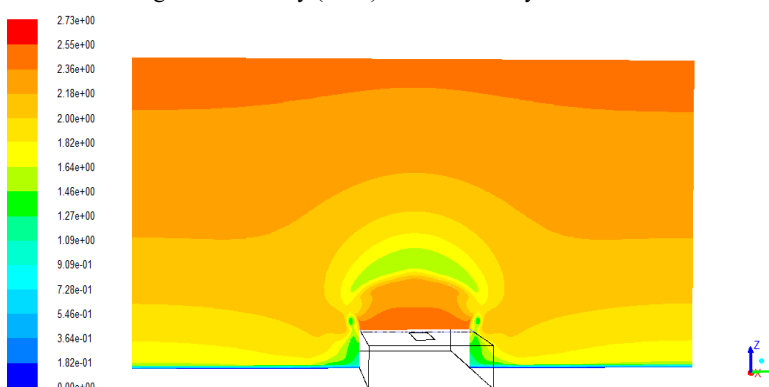


Figure 4. Velocity ( $\text{m s}^{-1}$ ) distribution at  $x=227.04 \text{ m}$ .

### 3.2. Ammonia concentration distributions

#### 3.2.1. Ammonia concentration distribution along the height

In order to show the ammonia concentration distribution along the height, three lines were chosen to represent the ammonia concentration of the upwind, downwind and crosswind of the exhaust outlet, respectively. The line named upwind in figure 2(b) is from point (118, 156.86, 0) to point (118, 156.86, 168) on the center plane representing the upwind concentration. The line named crosswind is from point (227.04, 76, 0) to point (227.04, 76, 168) representing the crosswind concentration, and the line named downwind that from point (336.08, 156.86, 0) to point (336.08, 156.86, 168) is also on the center plane to represent the downwind concentration.

As shown in Figure 5, the ammonia concentration is lower in upwind and crosswind direction than the downwind with the maximum ammonia concentration of about 0.0002 ppm, indicating that there is not so much ammonia spreading to those regions. This is consistent with previous research result (Tominaga and Stathopoulos, 2009) that the standard  $k-\epsilon$  model fails to represent the concentration upwind of the outlet, so the flow patterns of upwind and crosswind are different from downwind. As for the downwind direction, the ammonia concentration increases first and then decreases with the height increasing and reaches maximum value at height of 86 m. This is mainly because the emission outlet is at the roof of the building and the ammonia emission velocity direction is vertically upward, the area with the highest concentration of the selected line is above the height of the building and then the concentration decreases with the height increasing. However, when the height is above 120 m, the ammonia concentrations of the downwind directions are similar.

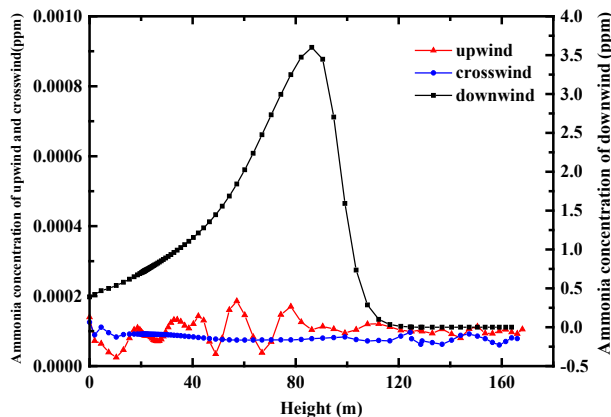


Figure 5. Ammonia concentration distributions along the height.

#### 3.2.2. Ammonia concentration distribution along the length

The two parallel lines at the plane of  $z=1.5$  m are used to show the concentration varies with length since 1.5 m is the average human breathing height. And the x-coordinate values are all from 0 m to 706.08 m but the y-coordinate values of the three lines are 78.43 m and 156.86 m, respectively.

The Figure 6 shows that the ammonia concentration upwind is almost 0 ppm on centerline, indicating that the dispersion of ammonia is mainly affected by the wind direction when the wind direction is determined. The ammonia spreads along the wind direction of the airflow; therefore, the concentration is highest at the emission source, and then decreases with the length increasing. This demonstrates that fully developed flow is conducive to the dilution of ammonia concentration. However, contrary to the centerline, the ammonia concentration at  $y=78.43$  m increases with the length increasing, but the maximum concentration on this line is only about

0.003 ppm. The reason of the increase may be the dispersion of ammonia concentration across the width in the downwind direction.

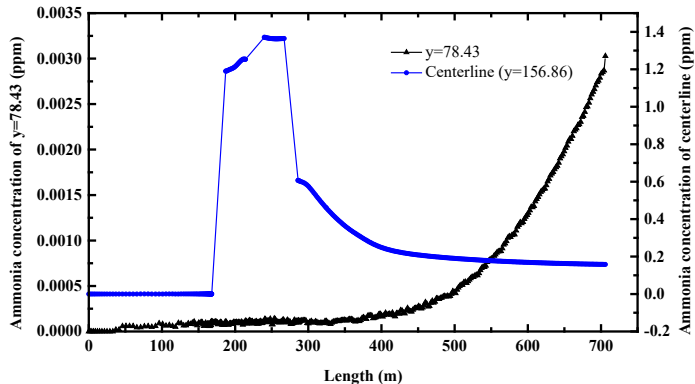


Figure 6. Ammonia concentration distribution along the length.

### 3.2.3. Ammonia concentration distribution along the width

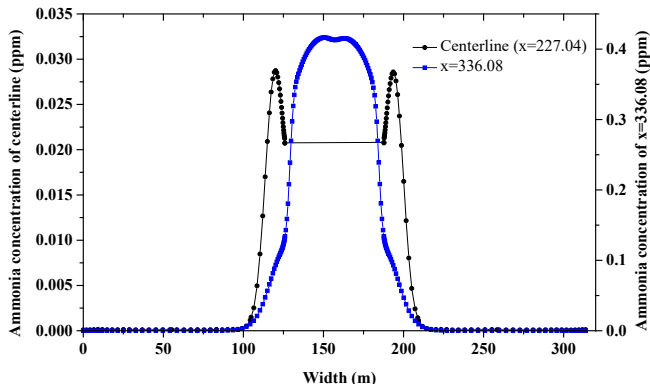


Figure 7. Ammonia concentration distributions along the width.

The centerline ( $x=227.04$  m) and another line ( $x=336.08$  m) at the plane of  $z=1.5$  m are used to show the concentration varies with width. And the  $y$ -coordinate values are all from 0 m to 313.72 m. The Figure 7 shows that the symmetry of the simulation is good, and this may be because the geometric model is symmetric and the boundary conditions of both sides are the same. The ammonia concentration distributions of the two lines have the same variation tendency, that is, the concentration is high in the middle and low on both sides. The reason may be that the emission outlet is at the center of both the two lines and the ammonia would spread out on both sides. And the existence of the building would affect the concentration distribution on the centerline so that concentration decreased as it gets closer to the wall.

## 4. Summary and Conclusions

In this study, a three-dimension CFD model was build based on the real dimension of a multi-floor pig building to get the velocity distribution and ammonia concentration distribution around the building. The high velocity appears at the emission outlet and the lower velocity region is behind and above the building due to the building obstruction. As for the ammonia distribution, the ammonia concentration in downwind is higher than in upwind and crosswind. In addition, the concentration is highest at the emission source and decreases with the length increasing on the

centerline. However, as for the regions of two empty cubes, the velocity is low but the ammonia concentration reaches about 1.4 ppm in those regions. Whether this structural design adversely affects the dispersion of ammonia remains to be further studied.

### Acknowledgements

The research was financially supported by the National Natural Science Fund of China (No. 31672468); National Key R&D Program of China (Project No. 2017YFD0701700); Thousand Talents Program (Youth Project 2016).

### References

- Du, L., C. Yang, R. Dominy, L. Yang, C. Hu, H. Du, Q. Li, C. Yu, L. Xie, X. Jiang, 2019. Computational Fluid Dynamics aided investigation and optimization of a tunnel-ventilated poultry house in China. Computers and Electronics in Agriculture. 159, 1–15.
- Gualtieri, C., 2010. RANS-based simulation of transverse turbulent mixing in a 2D geometry. Environmental Fluid Mechanics. 10 (1–2), 137–156.
- Lateb, M., R.N. Meroney, M. Yataghene, H. Fellouah, M.C. Boufadel, 2016. On the use of numerical modelling for near-field pollutant dispersion in urban environments – A review. Environmental Pollution. 208 (Pt A), 271–283.
- Melse, R.W., J.P.M. Ploegaert, N.W.M. Oginck, 2012. Biotrickling filter for the treatment of exhaust air from a pig rearing building: Ammonia removal performance and its fluctuations. Biosystems Engineering. 113 (3), 242–252.
- Norton, T., D.-W. Sun, J. Grant, R. Fallon, V. Dodd, 2007. Applications of computational fluid dynamics (CFD) in the modelling and design of ventilation systems in the agricultural industry: A review. Bioresource Technology. 12 (98), 2386–2414.
- Norton, T., J. Grant, R. Fallon, D.-W. Sun, 2010. Assessing the ventilation performance of a naturally ventilated livestock building with different eave opening conditions. Computers and Electronics in Agriculture. 71 (1), 7–21.
- Ntinias, G.K., X. Shen, Y. Wang, G. Zhang, 2017. Evaluation of CFD turbulence models for simulating external airflow around varied building roof with wind tunnel experiment. Building Simulation. 11 (5), 1–9.
- Tominaga, Y., T. Stathopoulos, 2009. Numerical simulation of dispersion around an isolated cubic building: Comparison of various types of k- $\epsilon$  models. Atmospheric Environment. 43 (20), 3200–3210.
- Zhang, T., M.D. Bu, W. Geng, 2012. Pollution status and biogas-producing potential of livestock and poultry excrements in China. Chinese Journal of Ecology. 5 (31), 1241–1249.
- Shi, Z., Z. Ji, L. Xi, 2017. Study on the characteristics and influencing factors of NH<sub>3</sub> emission from industrialized pig farm. Chinese Journal of Animal Science. 53 (8), 100–104.
- Zhou, J., Y.P. Chen, S.J. Ding, 2014. Analysis on influencing factors of pig livestock intensification in China. Statistics & Information Forum. 1 (29), 63–69.

## The Dose-effect Relationships between Green Light and Metabolism Rate in Chick Embryos

Tao Wang <sup>a</sup>, Zhentao Zhong <sup>a</sup>, Qiong Liu <sup>a</sup>, Yue Yu <sup>a</sup>, Jinming Pan <sup>a,\*</sup>

<sup>a</sup> College of Biosystems Engineering and Food Science, Zhejiang University,  
Hangzhou, Zhejiang 310058, P.R. China

\* Corresponding author. Email: [panhouse@zju.edu.cn](mailto:panhouse@zju.edu.cn)

### Abstract

Green light during artificial incubation can affect the development of chick embryos. However, there has been relatively little work systematically assessing dose-effect relationships between green light and metabolism rate in chick embryos. Eggs (n=800) were incubated under photoperiods of either 0 h of light and 24 h of darkness (0L:24D), 6 h of light and 18 h of darkness (6L:18D), 12 h of light and 12 h of darkness (12h:12h), or 18 h of light and 6 h of darkness (18L:6D). In accordance with dose-effect on embryonic development, the response of carbon dioxide production rate to variations in illuminance was consistent with lipid reserve in yolk residue and hepatic glycogen in chick embryos. This sensitivity to green light indicates that the variation in illuminance within certain range of green light can have a significant impact on embryonic development and metabolic rate in chick embryos during artificial incubation. The results of this study indicate that providing 18 h of light during incubation can significantly improve the development and metabolism of the chick embryos.

**Keywords:** Artificial incubation, eggs, lighting circle, lighting duration, sensitivity to light

### 1. Introduction

More and more reports show that adding green light during artificial incubation will affect the development of avian embryos. Rozenboim et al. (1999; 2003; 2004; 2013) found that hatching poultry eggs in green light compared to hatching in a traditional dark environment, embryo development and growth after hatching were all better. Zhang et al. (2012; 2014) found that certain green light stimulation during incubation could promote the growth of muscles, especially the pectoral muscle during the breeding period. Bai et al. (2016) further found that the green light stimulation during incubation increased various muscle indicators and promoted the proliferation of muscle satellite cells. The above studies mainly focused on the effects of different spectra on embryonic development and determined the superior role of green light in promoting embryonic development and explored the mechanism of green light on the embryonic weight gain. However, there are relatively few studies on the effects of different green light doses (green light duration) on embryonic development.

Embryonic Metabolism has been measured in the form of heat, oxygen consumption or carbon dioxide (CO<sub>2</sub>) production (Wangensteen and Rahn, 1970; Rahn et al., 1974; Bucher and Barnhart, 1984). In the literature, there are fewer studies on the metabolism of poultry. To investigate the effect of the green light on the metabolism of poultry, we designed a device to measure the production of CO<sub>2</sub> during incubation of poultry eggs, which could be used to explore the mechanism of green light to promote the development of poultry.

Overall, it remains challenging to the optimal green light dose to embryo development in artificial incubation. The objective of this study was therefore to determine the appropriate dose of green light to promote the development and metabolism of chicken.

### 2. Materials and Methods

All experimental protocols were approved by the committee for the Care and Use of Animals of Zhejiang University. The methods were carried out in strict accordance with the guidelines of the Association for the Study of Animal Behavior and Use of Zhejiang University.

## 2.1. Eggs

A total of 800 hatching eggs produced by the 48-week-old Lingnanhuang broiler breeder (Zhejiang Qunda Animal Husbandry Co., Jiaxing, China) were selected by weight ( $62 \pm 2$ g). The weight screening was completed at 9:00 am on the day of egg production and was transported to Zhejiang University (Hangzhou, Zhejiang) after the disinfection (methanol plus potassium permanganate fumigation). The eggs were labelled and randomly divided into 4 treatment groups with 200 in each treatment. There were 4 replicates in each treatment and 50 eggs per replicate.

## 2.2. Light stimulus treatments

In this experiment, 4 treatment groups with three different doses of light and one dark treatment group (control group) were set according to the duration of the green light. The daily duration of light in the G6 group was 6 hours (6L:18D), that in the G12 group was 12 hours (12L:12D), that in the G18 group was 18 hours (18L:6D), and that in the D group (the control group) was full darkness (0L:24D). Incubation light environment was consistent with previous reports (Yu et al., 2018) in our laboratory and is briefly described below. Two LED pipes were installed in each incubator. Each treatment included 2 egg trays with 4 replicates. The LED pipes in each light stimulus treatment were adjusted with a pulse-width modulation controller to achieve 120–200lux light intensity levels. The light intensity measurements were performed with a luxmeter (model MS6610, Precision Mastech Enterprises, Hong Kong, China).

## 2.3. Incubation

The four experimental groups were placed in separate commercial incubators (NK-hatching, Dezhou Nongke Incubation Equipment Co., Shandong, China). Incubation equipment and conditions were the same with previous reports (Yu et al., 2018) in our laboratory. In brief, the internal dimensions of the incubators were 1100 mm long  $\times$  1000 mm width  $\times$  950 mm height. The incubators were automatically maintained at  $37.8^\circ\text{C} \pm 0.1^\circ\text{C}$  and  $60\% \pm 2\%$  relative humidity (RH) during the entire incubation period. The eggs were candled (Cool-Lite tester, GQF Manufacturing, Savannah, Ga.) on day 8 (E8) during incubation, and nonviable eggs were removed. The turning time during incubation was 2 h, and eggs were no longer turned after day 18.

## 2.4. Respiratory Rate Determination

The device for measuring the metabolic  $\text{CO}_2$  production of embryos is shown in Figure 1, in which: A is a filtering device used to filter  $\text{CO}_2$  in the air; B is a respiratory chamber, transparent glass material, allows green light to pass through; C is an absorption device, used to absorb the  $\text{CO}_2$  produced by embryo metabolism; D is an air pump, which controls the pumping rate.

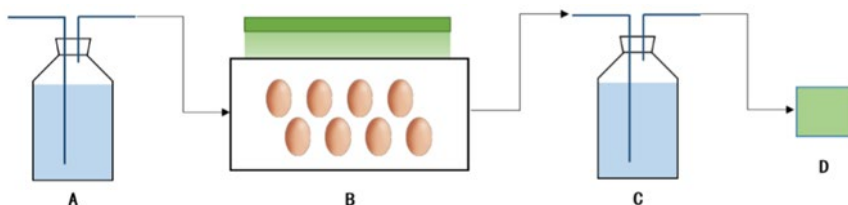


Figure 1. A system for measuring  $\text{CO}_2$  production by embryos. (A)  $\text{CO}_2$  filter; (B) respiration chamber; (C)  $\text{CO}_2$  absorption; (D) air pump.

Alkali solution (10mL) was took out from the absorption device C in Figure 1 and the double indicator method was used to obtain the concentration of  $\text{CO}_2$  in the solution. The phenolphthalein was used as the indicator and standard hydrochloric acid solution was dripped until the solution is pink, at which time,  $\text{CO}_3^{2-}$  is converted into  $\text{HCO}_3^-$ . Methyl orange was further added as an

indicator, and a standard hydrochloric acid solution was added dropwise until the solution became red, and the volume  $V_2$  of the standard hydrochloric acid solution was added dropwise for the second time. The formula for the respiration rate of a single embryo is as follows:

$$V_{CO_2} = \frac{V_2 \times C_{HCl} \times 22.4 \times M}{T \times N \times m} \quad (1)$$

where,  $V_{CO_2}$  is the respiration rate per chick embryo,  $V_2$  is the volume of hydrochloric acid solution used for titrating  $CO_3^{2-}$ ,  $C_{HCl}$  is the concentration of the standard hydrochloric acid solution,  $M$  is the volume of alkaline solution in the adsorption device,  $T$  is the absorption time, and  $N$  is the number of chicken embryos,  $m$  is the volume of solution that we took out from the absorption device.

On the 8<sup>th</sup>, 10<sup>th</sup>, 12<sup>th</sup>, 14<sup>th</sup>, 16<sup>th</sup> and 18<sup>th</sup> days of incubation (E8, E10, E12, E14, E16, E18), 32 eggs were selected from each treatment and were checked to confirm that the chicken embryos have survived. The 32 eggs came from 4 replicates in each treatment (8 eggs per replicate). The  $CO_2$  production of each replicate chicken embryo was determined separately.

## 2.5. Sampling and measurements

On E10, E14 and E18 and hatching day (H0), 2 eggs were taken from each replicate in the location with the same light intensity (8 eggs from each treatment), respectively. Eggs from each treatment group were crushed at the blunt end of the eggshell, stripped of the shell membrane, and the embryos were killed after cervical disconnection. Weighing and dissection were performed. According to the methods reported (Yu et al., 2018). Each embryo's body weight, yolk weight, heart weight and liver weight were measured. Then we calculate the liver weight ratio (ratio of liver weight to body weight).

## 2.6. Statistical analysis

Each data was plotted using the GraphPad Prism 7.0 software and a two-way analysis of variance was performed.  $P<0.05$  indicates a statistical difference between treatments. A linear or non-linear regression model was used to fit the correlation curve between green light dose at each sampling point and embryo development, respiratory rate, and embryonic nutrition. The Pearson correlation model was used to analyze the correlation between green light dose and each index. A  $P<0.05$  means significant correlation between the two groups.

## 3. Results and Discussion

### 3.1. Green light exposure improved body weight and dose of light linearly related to body weight

As shown in Figure 2, E14 (Figure 2 (a)) and E18 (Figure 2 (b)) incubation period, there was a positive correlation between green light dose and body weight, but they were not significant ( $P>0.05$ ). There was a significant positive correlation between green light dose and body weight during hatching ( $P<0.01$ ). On H0 (Figure 2 (c)), body weight of chicks was significantly higher in the G18 group than in the dark group ( $P<0.05$ ).

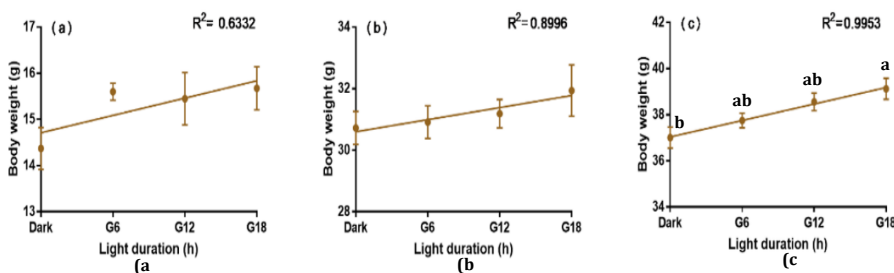


Figure 2. Linear regressions of green light dose and body weight of chick embryos. (a) E14; (b) E18; (c) H0. Bars with different letters are significantly different from each other.

### 3.2. Green light elevated the absorption of the yolk by the embryo in E18

On E18, the greater the dose of green light, the better the embryo's absorption of the yolk. The green light dose was negatively correlated with the yolk weight (Figure 3 (a)). The weight of yolk in the G18 group was significantly lower than that of the Dark group. On the day of hatching (H0; Figure 3 (b)), the yolk of the three different doses of the green light groups was slightly lower than that of the dark group, but there was no significant correlation between the dose and the weight of the yolk, and there was no significant difference between the groups.

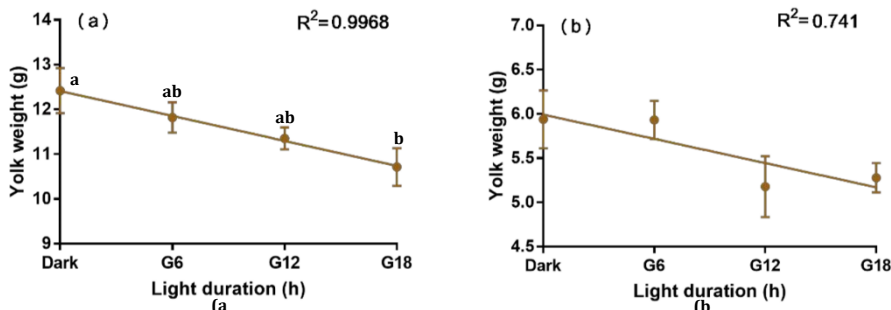


Figure 3. Linear regression of green light dose and yolk weight of chick embryos. (a) E18; (b) H0. Bars with different letters are significantly differently from each other.

### 3.3. Liver and embryo ratio on the hatching day was enhanced following green light exposure

On E14 and E18, there was no significant difference in liver weight ratio between groups. However, on H0, liver weight ratios in the G12 and G18 groups were significantly higher than those in the G0 and G8 groups. More than 12 hours of daily green light exposure to hatching promoted the development of the embryonic liver of chicken embryos in the later stages of embryonic development.

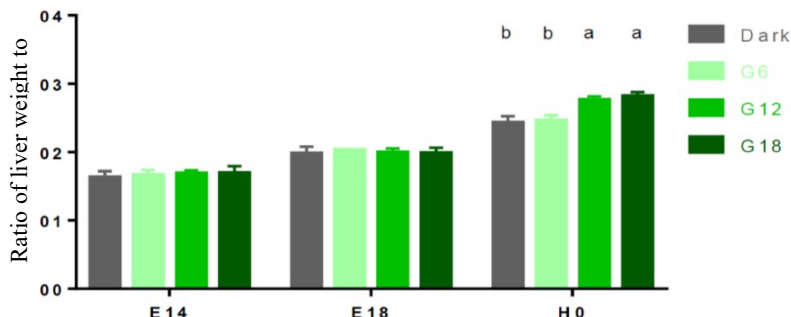


Figure 4. Effects of green light dose on ratio of liver to body weight of embryos. Bars with different letters are significantly differently from each other.

### 3.4. Green light exposure improved the respiration rate of the embryo

The effects of green light dose on the CO<sub>2</sub> yield on the chick embryo E8 to 20<sup>th</sup> day of incubation (E20) stage are shown in Figure 5. Overall, the CO<sub>2</sub> production rates of chick embryos in the green light treatment groups were higher than that in the dark treatment group, and the longer the green light duration, the higher the CO<sub>2</sub> yield. The CO<sub>2</sub> yields of E8, E14, E16, and E20 showed a significant linear positive correlation with green light duration ( $R^2=0.9784, P<0.05$ ;  $R^2=0.9951, P<0.01$ ). The G18 had the highest CO<sub>2</sub> production. The CO<sub>2</sub> yields of chick embryos

in each green group on E10 and E12 were generally higher than those in the dark group. On E10, the respiratory rate was the highest in the G6 and G12 groups, and the highest were served in the G6 and G18 on the E12.

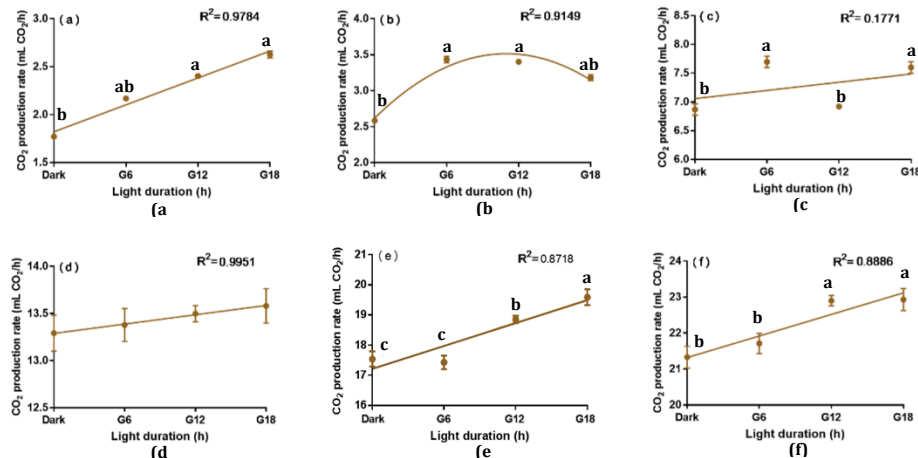


Figure 5. Relationships between green light dose and CO<sub>2</sub> production rate of chick embryos during incubation. (a) E8; (b) E10; (c) E12; (d) E14; (e) E16; (f) E20. Bars with different letters are significantly differently from each other.

### 3.5. Green light exposure reduced yolk lipid residues

The relationship between the dose of green light and the total lipid mass of yolk is shown in Figure 6. On E14, there was no significant difference in total lipid mass between dose groups, and there was no correlation. On E18 and H0, lipid residue in G18 group was significantly lower than that in Dark group ( $P<0.01$ ). At the same time, green light dose and yolk weight were significantly negative correlation ( $R^2=0.9857$ ,  $P<0.05$ ;  $R^2=0.9726$ ,  $P<0.05$ ).

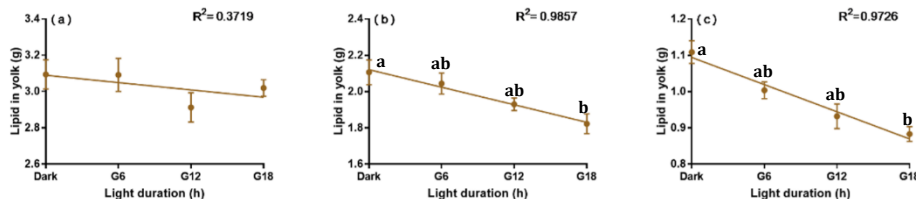


Figure 6. Relationship between green light dose and total lipid in yolk from incubation to hatch. (a) E14; (b) E18; (c) H0. Bars with different letters are significantly differently from each other.

### 3.6 Green light elevates hepatic glycogen mass in chick embryos

The relationships between the dose of green light and the total hepatic glycogen mass of yolk are shown in Figure 7. Embryos on E18 had greater hepatic glycogen mass than those on E14 and H0. On E14, there was no significant difference in total hepatic glycogen among the groups, but there was a significant linear positive correlation between total hepatic glycogen mass of yolk and green light duration( $R^2 = 0.9681$ ,  $P < 0.05$ ). On E18, the difference in green light duration caused a significant difference in total hepatic glycogen content. There was no significant difference between the G6 group with short green light duration and the Dark group, but there was significantly higher hepatic glycogen content in the G18 group than in the Dark and G6 groups ( $P < 0.01$ ). On H0, the hepatic glycogen contents in the high-dose green light group (G12

and G18) were significantly higher than that in the short-duration green light group and the dark group.

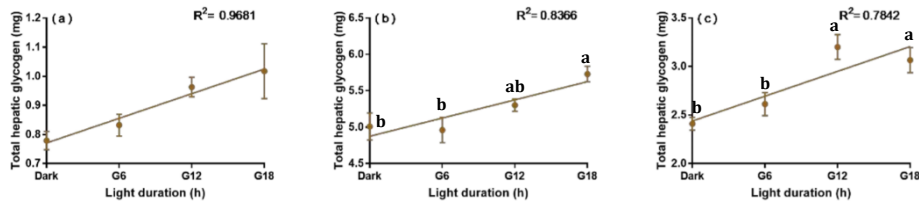


Figure 7. Relationships between green light dose and total hepatic glycogen from incubation to hatch. (a) E14; (b) E18; (C) H0. Bars with different letters are significantly different from each other.

#### 4. Conclusions

This study investigated the impacts of dose of green light on the development and metabolism of chicken. It was discovered that the dose of green light is positively correlated with embryonic development and metabolism. In accordance with dose-effect on embryonic development, the response of carbon dioxide production rate to variations in illuminance was consistent with lipid reserve in yolk residue and hepatic glycogen in chick embryos. This sensitivity to green light indicates that the variation in illuminance within certain range of green light can have a significant impact on embryonic development and metabolic rate in chick embryos during artificial incubation. The results of this study indicate that providing 18 h of light during incubation can significantly improve the development and metabolism of the chick embryos.

#### References

- Bai, X., Y. Wang, Z. Wang, J. Cao, Y. Dong, Y. Chen, 2016. In ovo exposure to monochromatic lights affect posthatch muscle growth and satellite cell proliferation of chicks: role of IGF-1. *Growth Factors*. 34 (3–4), 107–118.
- Bucher, T.L., M.C. Barnhart, 1984. Varied egg gas conductance, air cell gas tensions and development in *Agapornis roseicollis*. *Respiration Physiology*. 55 (3), 277–289.
- Rahn, H., C. Paganelli, A. Ar, 1974. The avian egg: air-cell gas tension, metabolism and incubation time. *Respiration Physiology*. 22 (3), 297–309.
- Rozenboim, I., I. Biran, Z. Uni, B. Robinzon, O. Halevy, 1999. The effect of monochromatic light on broiler growth and development. *Poultry Science*. 78 (1), 135–138.
- Rozenboim, I., R. Huisenga, O. Halevy, M. El Halawani, 2003. Effect of embryonic photostimulation on the posthatch growth of turkey pouls. *Poultry Science*. 82 (7), 1181–1187.
- Rozenboim, I., Y. Piestun, N. Mobarkey, M. Barak, A. Hoyzman, O. Halevy, 2004. Monochromatic light stimuli during embryogenesis enhance embryo development and posthatch growth. *Poultry Science*. 83 (8), 1413–1419.
- Rozenboim, I., M. El Halawani, Y. Kashash, Y. Piestun, O. Halevy, 2013. The effect of monochromatic photostimulation on growth and development of broiler birds. *General and Comparative Endocrinology*. 190, 214–219.
- Wangensteen, O.D., H. Rahn, 1970. Respiratory gas exchange by the avian embryo. *Respiration Physiology*. 11 (1), 31–45.
- Yu, Y., Z. Li, Z. Zhong, S. Jin, J. Pan, X. Rao, Y. Yu, 2018. Effect of monochromatic green LED light stimuli during incubation on embryo growth, hatching performance, and hormone levels. *Transactions of the ASABE*. 61(2): 661–669.
- Zhang, L., H. Zhang, X. Qiao, H. Yue, S. Wu, J. Yao, G. Qi, 2012. Effect of monochromatic light stimuli during embryogenesis on muscular growth, chemical composition, and meat quality of breast muscle in male broilers. *Poultry Science*. 91 (4), 1026–1031.
- Zhang, L., H. Zhang, J. Wang, S. Wu, X. Qiao, H. Yue, J. Yao, G. Qi, 2014. Stimulation with monochromatic green light during incubation alters satellite cell mitotic activity and gene expression in relation to embryonic and posthatch muscle growth of broiler chickens. *Animal Science*. 8 (1), 86–93.

# Modelling the Reduction of Ammonia Emission of a Naturally Ventilated Cow House Using an Acidified Water Curtain

Bert van 't Ooster <sup>a,\*</sup>, Roland W. Melse <sup>b</sup>, Sjoerd Bokma <sup>b</sup>, Marjolein Derkx <sup>a</sup>,  
Yeb P. Andela <sup>a</sup>, Jeroen A. A. Verstegen <sup>a</sup>, Peter W. G. Groot Koerkamp <sup>a</sup>

<sup>a</sup> Department of Plant Sciences, Farm Technology Group, Wageningen University and Research, 6708PB Wageningen, The Netherlands

<sup>b</sup> Wageningen Livestock Research, Livestock & Environment, Wageningen University & Research, 6708PB Wageningen, The Netherlands

\* Corresponding author. Email: [Bert.vanOoster@wur.nl](mailto:Bert.vanOoster@wur.nl)

## Abstract

In the Netherlands, the dairy sector contributes roughly 50% to the ammonia emission of the agricultural sector. Ammonia emission causes eutrophication and acidification of vulnerable nature. Current innovative floors reduced ammonia emission, but not enough. This study explored, by means of simulation, the ammonia emission reduction of an innovative type of air scrubber existing of an acidified water curtain, consisting of free falling droplets of a sulphuric solution (pH 3), in the ventilation openings of a naturally ventilated dairy cow house. Based on a full year simulation, the emission reduction induced by the water curtain was estimated for a dairy cow house with 120 cows. The sensitivity of ammonia removal efficiency was determined for the parameters, height of the vents, water flow and distribution, pH of washing fluid, ammonia source strength and type of vents where scrubbing was active. The most important parameters for ammonia removal were retention time, contact area and acidity of wash water. The water curtain reduced the emission up to 60% yearly, and can be combined with other solutions to further reduce ammonia emission if needed. Validation of the models and testing of suggested designs is needed.

**Keywords:** Acidification, air pollution, air scrubber, dairy, natural ventilation, simulation

## 1. Introduction

In the Netherlands, agriculture is the main source of ammonia emission. Fifty percent of this source is originating from the dairy sector, of which roughly half is emitted from the housing systems and manure storages. Ammonia emission may cause eutrophication and acidification of vulnerable nature. Since 1990 the total emission originating from dairy farming was strongly reduced, mainly by novel slurry application techniques (Webb et al., 2010). Other innovative measures like low emission floors (Groenestein et al., 2011), automatic controlled natural ventilation (Samer et al., 2012; Steinemann et al., 2014), and reducing rumen-degradable proteins in diet of the cows (van Duinkerken et al., 2005) do not reduce the ammonia emission below 3 kg per cow per year. So, other measure and options are needed.

In this research we explored by means of a model study and small experiments the potential of a low pressure air scrubber as an abatement measure for ammonia emission while preserving natural ventilation and open side-walls of the dairy cow houses. Generally, three types of air scrubbers can be distinguished, chemical air scrubbers, biological air scrubbers, and spray towers (Melse and Ogink, 2005; Hadlocon et al., 2014; Van der Heyden et al., 2016). An acidified water curtain with a working principle close to that of a spray tower, so without packing material, might work as an air scrubber in combination with natural ventilation (Hadlocon et al., 2014). Our model study aimed to determine the potential of this idea by estimating the annual ammonia removal efficiency of an acidified water curtain implemented in the outlet openings of a dairy cow house.

## 2. Materials and Methods

### 2.1. Design of the water curtain

We designed the water curtain for our simulation study with the help of a detailed tree of objectives (addressing safety of animals, environment and humans, and effectiveness) that were

transferred and used for a quantified and specific brief of requirements. Most important requirements were a max. pressure drop of 1 Pa by the water curtain, a minimum empty bed retention time of 0.4 s and at least 8 m<sup>2</sup> contact area per m ventilation opening to reach at least 60% reduction of ammonia emission. Based on lab tests, the droplet size of a curtain was set at a minimum of 500 µm to minimize drift below 3.3% at an air speed of 1.45 m s<sup>-1</sup>.

## 2.2. Modelling the water curtain system

The transfer of ammonia molecules in the air into the acid liquid and physical aspects of the water curtain were described with chemical-physical equations based on literature of (Melse and Ogink, 2005), in particular the two film theory, Fick's law, and Henry's law (Coulson et al. (1996); Satter (1996) and van Lenthe (2008)). Potential evaporation from the water curtain was determined theoretically using Penman (1948) for open surfaces restricted by adiabatic cooling at wet bulb temperature. A detailed description of the equations of ammonia transfer and wash water control can be obtained from the corresponding author.

## 2.3. Modelling the dairy cow house

The Climsim model (Van 't Ooster, 1994; Van Loon et al., 2007) is a dynamic finite element indoor climate model for naturally ventilated monospaced buildings. It was used in this study to determine the natural ventilation rates and gaseous emissions from a dairy cow house. Several simplifications of the real life situation were made, e.g. ammonia source strength is assumed to be uniformly distributed in space and time. Inputs of Climsim were housing specifications (building dimensions and materials), outdoor weather data (temperature, humidity, wind speed, wind direction and solar radiation), and animal heat, vapour and CO<sub>2</sub> production. The ventilation mechanism simulates pressure differences and air flow rates for each opening of the cow house.

The model was extended in order to implement the effect of an acidified water curtain. A predefined source strength of ammonia volatilized from the cow house floor was used to determine the ammonia emission. The ammonia mass balance (Eq. 1) was used to find the concentration of ammonia inside the cow house. It was assumed that ammonia was perfectly mixed within the house volume.

$$V \cdot \rho \cdot \frac{dC_{NH_3,in}}{dt} = \phi_{air,in} \cdot \rho \cdot C_{NH_3,envir} + M_{prod} - \phi_{air,out} \cdot \rho \cdot C_{NH_3,in} \quad (1)$$

With  $V$  the cow house volume (m<sup>3</sup>),  $\rho$  air density (kg m<sup>-3</sup>),  $\phi_{air,in}$  the inlet airflow (m<sup>3</sup> s<sup>-1</sup>),  $C_{NH_3,envir}$  the ammonia concentration outside (kg kg<sup>-1</sup>),  $M_{prod}$  the ammonia volatilized from floor and manure pit (kg s<sup>-1</sup>),  $\phi_{air,out}$  outgoing airflow (m<sup>3</sup> s<sup>-1</sup>),  $C_{NH_3,in}$  the inside ammonia concentration (kg kg<sup>-1</sup>). Multiplying the airflow in each opening ( $I, J$ ) at each time  $t$  by the concentration corrected for opening specific washing efficiency  $\eta(I, J, t)$ , results in the emission per opening (Eq. 2). In this equation  $I$  defines the opening number in length direction and  $J$  defines the opening number across the cow house, being sidewalls and ridge. For each time step, the ammonia emission of the cow house was calculated by summing the emission of the individual openings (Eq. 3). Total ammonia emission during the simulated period [ $t_0; t_f$ ] was found by numerical integration of the emissions per time step (Eq 4).

$$E(I, J, t) = \rho(t) \cdot \phi_{air,out}(I, J, t) \cdot C_{NH_3,in}(t) \cdot (1 - u \cdot \eta(I, J, t)) \quad (\text{kg s}^{-1}) \quad (2)$$

$$E(t) = \sum_1^J \sum_1^I E(I, J, t) \quad (\text{kg s}^{-1}) \quad (3)$$

$$E = \int_{t=t_0}^{t=t_f} E(t) \cdot \Delta t \quad (\text{kg}) \quad (4)$$

The model determines whether an opening is an inlet, outlet or a combined inlet and outlet

(in-outlets). The user may select which openings to wash: all openings, outlets only, outlets plus in-outlets or no opening at all. The acidified water curtain was switched on and off when an opening changes status or when wind speed was too high by means of control  $u$ . A counter for each opening recorded the water curtain activity. The starting and stopping process itself was assumed to be instantly. The equations defining the efficiency of the acidified water curtain (Section 2.2), were clustered as one function. For buffer control constant pH was applied. Finally, an estimation of operational variable costs was made.

#### 2.4. Case study: housing characteristics, sensitivity analysis and scenarios

For the model calculations, a time step of one minute was applied. Every hour, the requested output was logged including hourly ammonia emission, inside and outside temperatures, air density, relative humidity, ventilation flow, ammonia emitted and ammonia captured. A full year was simulated to find hours of low ventilation, ventilation rates and ammonia emission per cow.

A rectangular building with gable roof for 120 cows was simulated (Figure 1). The building was split in 13 sections in the length direction to generate 26 side openings. No ridge opening was considered in the default model settings. Since, due to thermal buoyancy, a ridge opening improved the ventilation at low wind speeds, one scenario with a non-washed ridge opening was simulated. Doors were assumed to be closed and the roof to be insulated. The flow resistance of openings was set to 3 for the side openings and to 6 for the optional ridge.

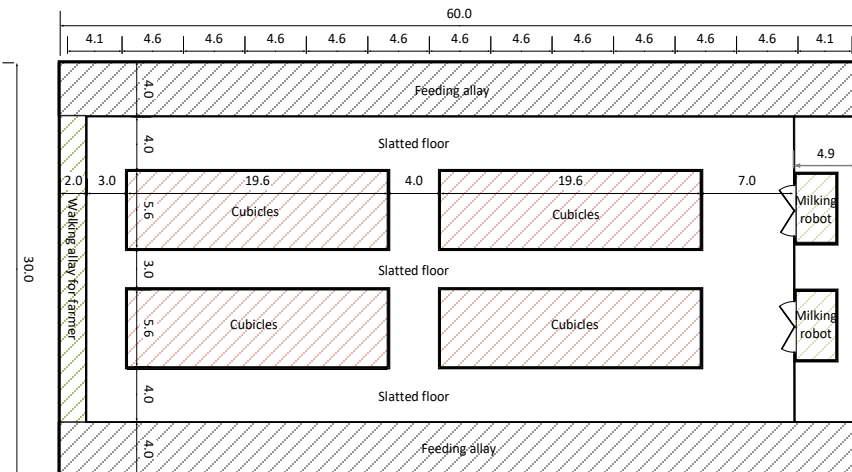


Figure 1. The layout of the simulated dairy cow house with 136 cubicles (2.8 m by 1.15 m), and two automatic milking systems. The feeding alleys were 4 m wide. The side walls were 1.5 m high with a 2.5 m opening. Eaves height was 4 m, roof slope 20°, ridge height 9.46 m.

For the outdoor climate, a statistically representative dataset with weather data per hour for one complete year was used (Breuer and van de Braak, 1989). The cow house was located in Wageningen, NL with a North-South ridge orientation, which was favourable for the ventilation due to wind. No shading objects were taken into account and background ammonia concentration was neglected. Total heat production of the herd was estimated at 165 kW, based on milk yield 23.85 kg per cow per day and body weight 650 kg (Salvink et al., 1999). A default ammonia source strength of 13 kg per year per cow was assumed, equally distributed over time.

The acidified water curtain was applied in outlets or in-outlets. The water curtain was either nozzle based or a rain ceiling. A nozzle sprayed in an angle of 80° and had a 2 bar water pressure drop, a water flow of 0.0741 L s<sup>-1</sup> and an estimated initial velocity of droplets of 1 m s<sup>-1</sup>. A buffer volume of 10 m<sup>3</sup> acidified water was installed and controlled for a constant pH of 3. Other building

modifications such as drift collecting gutters or spraying ceilings were not considered to affect the ventilation nor the water curtain efficiency. Drift was assumed zero.

Only the variable costs (electricity used to pump water through the nozzles ( $0.0577 \text{ € kWh}^{-1}$ ), sulphuric acid (98%) use for the washing fluid ( $3.69 \text{ € L}^{-1}$ ), and water ( $0.562 \text{ € m}^{-3}$ )) were taken into account. Liquid disposal costs or investment costs of the system were not taken into account.

With respect to the efficiency of the acidified water curtain, only the result of the mechanistic scrubber model is presented. The washing efficiency was determined for each opening and each time step. Both the yearly mean and variation in the washing efficiency were computed.

To verify the functioning of the model, a one-at-a-time sensitivity analysis was done. The single effect of changing the following input variables was analysed: pH of the water (2–6), initial water velocity (0–3 m s<sup>-1</sup>), water curtain width, opening types with active curtain, opening height, ammonia source strength (5–13 kg y<sup>-1</sup> per cow), and a non-scrubbed ridge opening 21.6 cm wide.

If not more than six fluctuations in opening status occurred per hour, the acidified water curtain was switched off in case when the opening was an inlet. Two additional strategies were simulated: 1) all cow house openings were scrubbed, and 2) only outlets were scrubbed. These simulations were compared to the results of the simulation with default settings for resource use.

Two scenarios were defined, one aiming for maximum reduction of ammonia emission and one aiming to minimize costs. To ensure a suitable climate for the animals, the opening height was increased to 2.8 m. To increase efficiency, the number of nozzles was doubled to 30 per meter of opening. In the second scenario the costs were reduced by reducing the number of nozzles to 5 per meter of opening and only outlet openings were washed instead of both outlets and in-outlets.

One of the key features of the acidified water curtain is the nozzle setting. In order to provide insight in the effect of the nozzle settings, four alternative nozzle settings were tested. Two work pressures for the Teejet XR8015 nozzle, 1 bar and 3 bar (Teejet Technologies, 2014), each with its estimated settings for liquid flow, droplet size and start velocity (Table 1).

Table 1. The estimated nozzle settings for four alternative scenarios. Low and high pressure represent operational pressure of the XR8015 nozzle, while droplet ceiling, low and high flow, specify the settings for a conceptual low pressure water curtain.

Nozzle settings	Default	Low pressure	High pressure	Droplet ceiling, high flow	Droplet ceiling, low flow	Unit
Pressure	2	1	3	0	0	bar
Flow per nozzle	0.0741	0.056	0.1	$7.7 \cdot 10^{-4}$	$3.8 \cdot 10^{-4}$	L s <sup>-1</sup>
Start velocity	1	0.5	3	0.2	0.2	m s <sup>-1</sup>
Droplet size	500	650	400	1200	1200	μm
Number of nozzles	15	12	24	3000	3000	-

Also, two scenarios for a low pressure droplet ceiling were simulated. This ceiling has 3000 holes spread over an area of 1 m by 0.3 m. A water flow of  $7.7 \cdot 10^{-4} \text{ L s}^{-1}$  or  $3.8 \cdot 10^{-4} \text{ L s}^{-1}$  results in approximately  $8 \text{ m}^2$  or  $4 \text{ m}^2$  of contact area, in case droplets have a diameter of 1200 μm.

### 3. Results and Discussion

#### 3.1. Scenario results

Table 2 shows the simulation results for the default model settings *versus* the scenarios with high reduction of ammonia emission and low cost. Default settings reduced ammonia emission by 56%, from 13 to 5.7 kg per cow per year. The efficiencies per opening had an average of 65%, with a standard deviation of 20%. The goal to reduce emission with sixty percent was almost reached. The electricity demand to pump the water through the system was  $9 \cdot 10^5 \text{ MJ}$  (or 242 kWh per thousand litre milk), almost three times the current electricity usage in dairy cow houses with an automatic milking system. Controlling the buffer water for a constant pH of 3 resulted in

acceptable water usage for nitrogen discharge. If acid was added till the maximum amount of allowed salinity threshold of 58.8 g [N] L<sup>-1</sup> was reached, a buffer of ten cubic meter dissolved 715 kg of ammonia. In case of a constant pH, the buffer was only refreshed once and it is therefore a good method to store the captured ammonia. For default settings, the acid usage (H<sub>2</sub>SO<sub>4</sub>) was 2515 kg y<sup>-1</sup>. The operational costs were estimated at €22.66 per kg reduced ammonia emission and 1.9 euro cents per litre milk produced. The number of changes in opening status was simulated. Only in 16% of the time, openings changed status 1 or more times per hour and never 4 or more times. Controllability of the curtain was not at stake.

Table 2. Outputs of 3 simulations of one year with default model settings (a), the high reduction scenario (b), and the low costs scenario (c). In (b) outlets and in-outlets were washed, 30 nozzles per m opening, opening height 2.8 m. In (c) 5 nozzles per m opening, opening height 2.8 m.

Scenario	Default	High reduction	Low cost	Unit
Hours of low ventilation	44	32	32	h
Max. ventilation rate per cow	11512	12897	12897	m <sup>3</sup> h <sup>-1</sup>
Min. ventilation rate per cow	116	101	101	m <sup>3</sup> h <sup>-1</sup>
Ammonia captured (per cow)	873 (7.3)	1080 (9.0)	348 (2.9)	kg y <sup>-1</sup>
Yearly average efficiency	56	69	22	%
Electricity usage	896747	1819459	212976	MJ
Acid usage (H <sub>2</sub> SO <sub>4</sub> )	2515	3109	1001	kg
Discharge volume	20	20	10	m <sup>3</sup>
Evaporated volume	462	979	133	m <sup>3</sup>
Costs per unit of captured NH <sub>3</sub>	22.66	33.43	15.95	€ kg <sup>-1</sup>
Costs per litre of milk	0.019	0.035	0.005	€ L <sup>-1</sup>

The ‘high reduction’ scenario reached an efficiency of 69% and reduced the ammonia emission per cow from 13 to 4 kg y<sup>-1</sup>. Compared to the default model settings the operation costs increased due to the increased acid use and increased electricity usage to €33.43 per kg reduced ammonia emission or 3.5 euro cents per litre milk. Minimizing costs by minimizing the water curtain width resulted in a low efficiency of 22%, reducing ammonia emission per cow with no more than 2.9 kg y<sup>-1</sup>. The costs were reduced to €15.95 per kg ammonia captured or 0.5 euro cents per litre milk produced. The 2 bar pressure drop in the nozzles in the default simulation alone, is responsible for an electricity usage of 215 kWh per 1000 kg milk or €14.62 per kg ammonia captured. A strong reason to use low water pressure as well.

Regarding the efficiency, the high pressure nozzle, producing a lot of small droplets, was effective but its operational costs were the highest. If a droplet ceiling with low water pressure is effective in practice, this would be a good alternative to reduce operational costs. On the other hand, the efficiency will be lower at equal water flow rate as shown in Table 3.

Table 3. Simulation output nozzle pressures of 1 bar (low) and 3 bar (high) for a Teejet XR8015 nozzle and for a droplet ceiling with high and low washing liquid flow.

Model settings	Low pressure	High pressure	Ceiling, high flow	Ceiling, low flow	Unit
Ammonia captured	811	935	664	451	kg y <sup>-1</sup>
Yearly average efficiency	52	60	43	29	%
Electricity usage	601000	1399000	203000	100000	MJ
Acid usage (H <sub>2</sub> SO <sub>4</sub> )	2336	2692	1912	1298	kg
Discharge volume	20	20	10	10	m <sup>3</sup>
Evaporated volume	461	474	448	221	m <sup>3</sup>
Costs per unit of captured NH <sub>3</sub>	18.11	30.19	11.18	9.75	€ kg <sup>-1</sup>
Costs per litre of milk	0.014	0.027	0.007	0.004	€ L <sup>-1</sup>

The simulations show that it is possible to scrub a significant percentage of the ammonia out the ventilation air. The trade-off between costs for pumping the washing liquid and scrubbing efficiency needs attention as well as the physical realization of the acidified water curtain.

### 3.2. Sensitivity analysis

The simulations for scrubbing 1) all, 2) outlets only or 3) outlet and in-outlet openings showed that washing outlets only, decreased the efficiency from 56% to 44%, also the evaporated volume and operational costs decreased. Scrubbing all openings is not practical since no more ammonia is captured but operational costs rise with over 1 € kg<sup>-1</sup> ammonia captured.

**Opening height:** Decreasing the opening height of the default dairy cow house, led to lower ventilation rates and increased scrubbing efficiency (Table 4). Openings of 1.5 m high or smaller, lead to a considerable increase in the number of hours with a ventilation rate per cow below the 555 m<sup>3</sup> h<sup>-1</sup>. But on the other hand, a washing efficiency increase of 5% to 9% was realised. Since the opening height of 2.5 m show many hours with ventilation rate above 2000 m<sup>3</sup> h<sup>-1</sup> per cow, limiting the ventilation for hours with high ventilation rates is recommended in case a cow house with similar opening sizes is realized in practice. Therefore, ventilation control with wind mesh curtains might be favourable for the inside climate and for the acidified water curtain efficiency.

Table 4 Results with four different opening heights. Low ventilation is less than 555 m<sup>3</sup> h<sup>-1</sup> per cow. Number of hours the indoor climate exceeds thresholds not satisfying animals' demands.

Opening height	2.5	2	1.5	1	2.5 (incl. ridge)	m
Yearly average efficiency	59	61	64	68	50	%
Hours of low ventilation	44	193	1191	2211	33	h

**Source strength:** Changing the ammonia source strength in the model did not affect the yearly average efficiency. A difference in costs per reduced unit of ammonia was observed, since ammonia captured decreased more than the operational costs.

**pH:** A pH ranging from 2 to 6, showed a drop of two percent points in efficiency. The acid usage decreased proportionally.

**Ventilation:** The calculated ventilation rate did not show a clear relation with washing efficiency, however, the specific air flow in individual openings (kg s<sup>-1</sup> m<sup>-2</sup>) did, as shown in Figure 2. Low air speed was important both for washing efficiency and stability of the curtain.

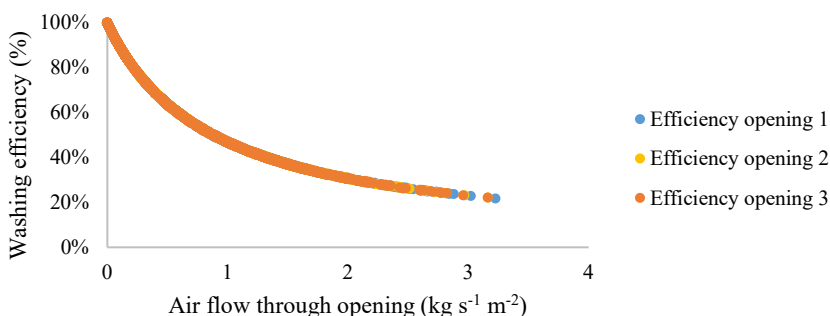


Figure 2. Efficiency of the acidified water curtain against the specific air flow in individual openings (kg s<sup>-1</sup> m<sup>-2</sup>). Efficiency of the first three openings on the West side of the cow house.

**Evaporation:** The water evaporated from the water curtain per day differed in time. Higher summer time evaporation was related to solar radiation more than to higher temperatures. Evaporation increased with radiation. In case no radiation was present, night time, the evaporation was close to zero. Shading the water curtain could be an effective measure to reduce evaporation.

**Initial droplet velocity:** Increasing the initial velocity of the droplets reduced washing

efficiency from 59% at 0 m s<sup>-1</sup> to 50% at 3 m s<sup>-1</sup>. A higher start velocity resulted in a smaller airborne time of the droplets, which decreases the contact area. Less water usage and less acid usage decreased the cost, but the decreased washing efficiency caused the costs per reduced ammonia to increase from 21.84 to 24.56 € kg<sup>-1</sup> ammonia captured.

Water curtain width: The curtain width was adjusted by varying number of nozzle rows. Each row of nozzles consisted of 5 nozzles per m with 0.1 m work width. Figure 3 shows the relation between number of nozzles and yearly average efficiency and the operational costs per unit of ammonia reduced. A higher number of nozzles, showed a higher yearly average efficiency, but also higher operational costs caused by a higher consumption of acid and electricity. It can be observed that the efficiency increase is asymptotic, while the costs increase was close to linear. Therefore a trade-off shows with smallest distance between the curves at 10 to 15 nozzles per m.

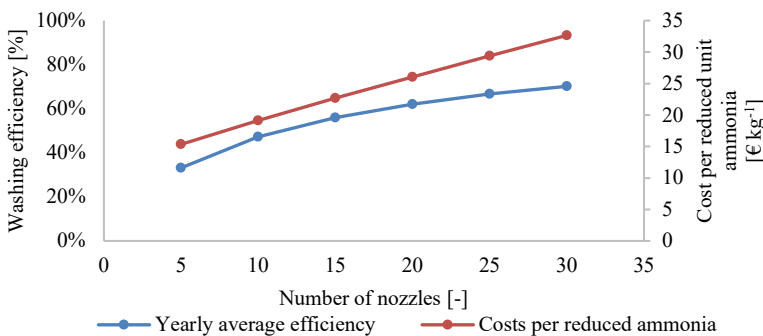


Figure 3. Average yearly washing efficiency (%) and the costs (€ kg<sup>-1</sup>) for captured ammonia against the number of nozzles applied per one meter of acidified water curtain length.

#### 4. Conclusions

The water curtain alone cannot serve as the only abatement measure to reduce ammonia emission from dairy housing systems to less than 3 kg ammonia per cow per year. According to the model, a yearly average efficiency of 60% is possible by implementing an acidified water curtain. Experiments are needed to control drift and allow sufficient natural ventilation.

The spraying nozzle solution operated at a work pressure of 2 bar, initial velocity of 1 m s<sup>-1</sup>, droplet size of 500 µm, and a flow of 0.0741 L s<sup>-1</sup>. The specifications of the simulated droplet ceilings need validation, to indicate whether they are realistic. The model predicted up to 43% removal efficiency for the droplet ceiling at lower operation cost.

Both outlets and in-outlets of a dairy cow house should be scrubbed. Running the water curtain without ventilation control is not realistic, due to high ventilation rates and a clear benefit for the scrubbing process of lowering ventilation rate. Decreasing the air speed through the acidified water curtain increases removal efficiency. Smaller opening heights resulted in a lower ammonia emission. No effect of the ammonia source strength was observed with respect to removal efficiency. Water usage of the water curtain strongly increased when exposed to solar radiation.

Efforts to maximize removal efficiency increased operational costs per kg ammonia removed. Increasing the contact area leads to a higher removal efficiency. A larger contact area is realised by, increasing the wash water flow, decreasing initial velocity of the droplets and decreasing droplet size. Increasing droplet size decreases drift. Decreasing contact area decreases theoretical ammonia removal efficiency as well as evaporation rate. The water distribution system has a major influence on the operational costs, caused by the operating pressure and the water flow.

Scenarios on water distribution settings, showed that a higher removal efficiency increased operational costs. For nozzles spraying water, a removal efficiency of about 60% was simulated

at estimated operational costs of €23 kg<sup>-1</sup> ammonia captured. A concept droplet ceiling showed a removal efficiency of 30–43% and estimated costs of €9.75–11.18 € kg<sup>-1</sup> ammonia captured.

### Acknowledgements

This research was part of the Dutch project Environmental Dairy Design '20, a public-private partnership (PPP) of enterprises in the agro-sector and Wageningen UR, co-financed by the Dutch top sector Agro & Food. The authors acknowledge this PPP for making this project possible.

### References

- Breuer, J.J.G., N.J. van de Braak, 1989. Reference year for dutch greenhouses. *Acta Horticulturae* (248), 101–108. <http://dx.doi.org/10.17660/ActaHortic.1989.248.9>.
- Coulson, J.M., J.F. Richardson, J.R. Backhurst, J.H. Harker, 1996. *Chemical engineering / Vol. 1, Fluid flow, heat transfer and mass transfer*. Oxford [etc.]: Butterworth Heinemann.
- Groenestein, C.M., M.C.J. Smits, J.F.M. Huijsmans, O. Oenema, 2011. Measures to reduce ammonia emissions from livestock manures: now, soon and later. 488. Wageningen UR Livestock Research.
- Hadlocon, L.J.S., R.B. Manuzon, L. Zhao, 2014. Optimization of ammonia absorption using acid spray wet scrubbers. *Transactions of the ASABE*. 57 (2), 647–659.
- Melse, R.W., N.W.M. Ogink, 2005. Air scrubbing techniques for ammonia and odor reduction at livestock operations: Review of on-farm research in the netherlands. *Transactions of the ASAE*. 48 (6), 48.
- Penman, H.L., 1948. Natural evaporation from open water, bare soil and grass. *Proc. R. Soc. Lond. A*. 193 (1032), 120–145.
- Saltvik, K., S. Pedersen, J.M. Bruce, 1999. Environment for Animals. In: *Handbook of Agricultural Engineering*. Ed., Bartali, E.H. 31–87.
- Samer, M., C. Ammon, C. Loebis, M. Fiedler, W. Berg, P. Sanftleben, R. Brunsch, 2012. Moisture balance and tracer gas technique for ventilation rates measurement and greenhouse gases and ammonia emissions quantification in naturally ventilated buildings. *Building and Environment*. 50, 10–20. <https://doi.org/10.1016/j.buildenv.2011.10.008>.
- Satter, I.H.G., 1996. Biowassers in Nederland, Agrotechniek & fysica, Wageningen University and Research, Wageningen.
- Steinemann, B., A. Gattinger, M. Krauss, A. Berner, F. Leiber, V. Maurer, M. Meier, B. Oehen, L. Bautze, U. Niggli, 2014. Mitigating the impact of agriculture on air quality and climate change: Solutions for improved Nitrogen management.
- Teejet Technologies, 2014. Catalog 51A. In: Technologies, T. Ed., Illinois, USA, 164 p.
- Van 't Ooster, A., 1994. Using natural ventilation theory and dynamic heat balance modelling for real time prediction of ventilation rates in naturally ventilated livestock houses.
- Van der Heyden, C., B. Vanthillo, J.G. Pieters, P. Demeyer, E.I. Volcke, 2016. Mechanistic modeling of pollutant removal, temperature, and evaporation in chemical air scrubbers. *Chemical Engineering & Technology*. 39 (10), 1785–1796.
- van Duinkerken, G., G. Andre, M.C. Smits, G.J. Monteny, L.B. Sebek, 2005. Effect of rumen-degradable protein balance and forage type on bulk milk urea concentration and emission of ammonia from dairy cow houses. *Journal Dairy Science*. 88 (3), 1099–1112.
- van Lenthe, C., 2008. Design of an ammonia air scrubber with rotating packing material, Farm Technology, Wageningen University & Research, Wageningen.
- Van Loon, W.K.P., A. Van 't Ooster, E. Dekker, 2007. Site influence on wind induced pressure distribution on a dairy house. In: *Agricontrol 2007 Proceedings of the 2nd IFAC Intern. Conf. on Modeling and Design of Control Systems in Agriculture, Osijek, Croatia, 3–5 Sep. 2007*. 83–89.
- Webb, J., B. Pain, S. Bittman, J. Morgan, 2010. The impacts of manure application methods on emissions of ammonia, nitrous oxide and on crop response – a review. *Agriculture, Ecosystems & Environment*. 137 (1), 39–46.

## Evaluation of Indoor Environment of A Six-Story Swine Barn and Associated Impact on the Surrounding Environment

Kaiying Wang <sup>a\*</sup>, Xiaoshuai Wang <sup>a</sup>, Xiaorong Dai <sup>b</sup>, Leiping Wang <sup>b</sup>, Jiegang Wu <sup>a</sup>, Ailun Wang <sup>a</sup>, Xiusong Li <sup>c</sup>, Zhihua Yang <sup>d</sup>, Bin Chen <sup>d</sup>, Kangning Huan <sup>c</sup>

<sup>a</sup> College of Biosystems Engineering and Food Science, Zhejiang University,  
Hangzhou, Zhejiang 310058, P.R. China

<sup>b</sup> Ningbo Research Center for Urban Environment, Chinese Academy of Science,  
Ningbo, Zhejiang 361020, P.R. China.

<sup>c</sup> Big Herdsman Machinery Co. Ltd., Qingdao, Shandong 266108, P.R. China

<sup>d</sup> Zhengkang (Yiwu) Pig Industry Co. Ltd., Yiwu, Zhejiang 322000, P.R. China

\* Corresponding author. Email: [zjuwky@zju.edu.cn](mailto:zjuwky@zju.edu.cn)

### Abstract

Increasing land-use cost forced some large animal feeding operations (AFOs) to change the barns from typical one story to multiple stores in the southern China recently, referred as multi-story animal barns (MSAB). The MSAB is getting popular in the southeast of China and attracts increasing public attention. Because of its great holding capacity with large numbers of animals, the MSAB can greatly save the footprint of animal buildings, as compared with typical one story animal barns. However, no study has been done to understand the performance of this kind of novel barn. Although each barn in the building has its individual ventilation system, it is highly possible that the indoor environments of the individual barns might be different caused by the interactions of individual barn ventilation fans clustered in the center of the building to form a courtyard exhausted channel. . Besides, as a large air pollutant source, the impact of the air emissions from such high rise building on the surrounding environment is unknown as existing knowledge of air emissions is limited to the conventional none story barn, not a multi-story barn.

Therefore, this work aims to evaluate 1) the indoor environmental condition of the MSAB including the distribution of air temperature, humidity, velocity and air pollutant concentrations (i.e., VOCs, NH<sub>3</sub>, H<sub>2</sub>S); 2) the impacts of the emitted air pollutants (i.e., odor, VOCs, NH<sub>3</sub>, H<sub>2</sub>S et al.) on the surrounding environment. Field measurements both inside and outside of the facility were conducted in September 2019. For the indoor measurements, TSI were used to measure the indoor air temperature, humidity, and velocity, Dyllos were used to measure the indoor PM (PM<sub>2.5</sub> and PM<sub>10</sub>) concentrations, FTIR was used to measure indoor NH<sub>3</sub>, H<sub>2</sub>S and other gases. For the outdoor measurements, VOCs were measured using both PTR-MS and online GS-MS; NH<sub>3</sub> was measured using a specially configured chemiluminescence analyzer with an external thermal convertor (Model T201, API, Japan); H<sub>2</sub>S was measured by (API). With these filed measurement data, Computational Fluid Dynamics (CFD) technique was used to extend the study for advanced understanding of indoor environmental conditions and air pollution distribution in the vicinity of the building with spatial resolution. In addition, dispersion of the building emissions will be modelled by AREMOD, aiming at establishing the setback distance for biosecurity and odor annoyance of the MSAB.

The CFD simulation results showed differences of airflow patterns and the hygrothermal conditions occurred from story to story, although their ventilation systems were the same. Therefore, in order to perform a uniform and comfortable environment for animals, each story of an MSAB should have a specific ventilation design. Findings from this research will provide fundament knowledge to better design the MSAB buildings and to better assess the environmental impacts of air emissions from MASB.

**Keywords:** multi-story animal barns (MSAB), indoor environment, Computational Fluid Dynamics (CFD), air emission, air dispersion modeling, NH<sub>3</sub>, H<sub>2</sub>S, VOCs, PM<sub>10</sub>, PM<sub>2.5</sub>

**Theme III:**

**Impacts of Production Systems and  
Management Practices**



# Design and Experimental Study of Clam Automatic Cleaning Equipment

Hanbing Zhang<sup>a,b</sup>, Jialin Tian<sup>b</sup>, Jian Zhang<sup>b</sup>, Xiuchen Li<sup>a,b</sup>, Guochen Zhang<sup>a,b</sup>, Yanfei Ren<sup>b</sup>, Gang Mua<sup>b\*</sup>

<sup>a</sup> School of Mechanical and Power Engineering, Dalian Ocean University,

Heishijiao Street No.52 Dalian, Liaoning 16023, P.R. China

<sup>b</sup> R&D Center of Fisheries Equipment and Engineering, Liaoning 116023, P.R. China

\*Corresponding author. Email: [mugang@dlou.edu.cn](mailto:mugang@dlou.edu.cn)

## Abstract

Cleaning is a key process in the post-harvesting of shellfish. Due to the less-advanced technologies and equipment, China mainly relies on manual cleaning at present, leading to problems such as low operating efficiency and high labor intensity. In this paper, an innovative rotary shellfish automatic cleaning equipment was designed and the fresh Philippine clam were cleaned. The results showed that the cleaning rate and crushing rate were 14.10% and 0.19%, respectively, provided the rotary speed, inclination angle and water flow rate of the drum were 45 rpm, 6° and 1200 L hr<sup>-1</sup>, respectively. Compared with the manual cleaning effect and efficiency, which has prominently improved, it is of great significance to raise the mechanized production level of China's shellfish industry.

**Keywords:** Shellfish, drum, cleaning efficiency, automatic cleaning equipment

## 1. Introduction

With the continuous increase of clam breeding and yield, the clam breeding yield in China reached  $5.36 \times 10^6$ t in 2018 (FFA, 2018). With its strong adaptability, short breeding period and high yield, clam larvae is the most productive single species of cultured shellfish in China (Yan, 2014). At present, most clam cleaning in China relies on manual operation, and there is no specific cleaning equipment for clam (Liu, 2008). The existing cleaning equipment is mainly used for cleaning vegetables and fruits (Jiang, 2006 and Mulugeta and Geyer, 2005), which is not suitable for large-scale clam cleaning production. Although researchers from countries including Europe, United States, and Japan have studied cleaning equipment earlier (Tao, 2008; Falconer et al., 2004; Einarsson; 1995 and Wenstrom and Gorton, 2000), the machines have serious problems of wasting water and poor cleaning efficiency. Based on the biological characteristics of the Philippines clam and actual production conditions, this paper documents the design of a set of automatic roller combined with high pressure water cleaning equipment, studied the drum rotating speed, water flow, roller angle, material quantity for the influence on breakage and cleaning rate, as well as determined the optimum technology parameters of cleaning clam, aiming at providing a reference for the design of the automatic shellfish cleaning equipment research and development.

## 2. System Design

### 2.1. Overall design scheme

The drum structure, combined with high pressure water cleaning, were applied to this design, for the drum can make the materials constantly rolling in the process of working, with mutual friction, and the high pressure jet nozzle can supply high pressure-water at the same time. Therefore the clam surface sediment can be removed to a higher degree, which can conform to the requirement of cleaning. The structure of this device is simple and compact, highly automatic, and can achieve ideal target of cleaning (Gao et al., 2015).

### 2.2. Structural design

The cleaning equipment is shown in Figure 1. When the submersible is working, motor drives the drum to rotate at the same time, and then the conveying device will transport freshly collected

clams into the working drum. Entered from the higher end of the drum, the clam will come out from the lower end, after being washed by the High pressure nozzle, which will be then conveyed to the subordinate device through conveyor belt. The lower end of the drum is the sewage impurity recycling device, which filters the dirt and impurities, and the filtered water is can be discharged for recycling.



Figure 1. Photograph of the clam cleaning machine tested.

### 3. Experimental Study on Clams Cleaning

#### 3.1. Materials and equipment

##### 3.1.1. Test materials

The materials tested are 1 kg fresh (containing impurities and sediment) clams collected from a clam farm in Dalian.

##### 3.1.2. Test equipment

The clam cleaning equipment developed (Figure 1) is installed with (Model X680), inverter, rotor flow meter, and electronic day equalizer (TCS-KS100).

#### 3.2. Method of test

##### 3.2.1. Test design

Control variable method was adopted to conduct the cleaning test by changing the drum rotating speed (20–80 rpm), water flow (400–2000 L hr<sup>-1</sup>), drum inclination (3–12°) and feed amount (3.5–10.5 kg), to analyze the influence of different parameters on the cleaning rate and crushing rate of clams.

Based on the single factor test and the Box-Behnken central combination test principle, the horizontal response surface test of three factors (drum rotation speed, inclination angle and water flow Design) was selected, and the response surface analysis of cleaning rate and crushing rate was conducted by the Design Expert 8.0.6 software to obtain the optimal combination of various factors. The variables tested for each level were listed in Table 1.

Table 1. Factor level code.

Level	Rotation speed (r min <sup>-1</sup> )	Roller angle (°)	Water flow (L hr <sup>-1</sup> )
-1	30	3	800
0	45	6	1200
1	60	9	1600

##### 3.2.2. Index measurement method

The cleaning rate and crushing rate of clams are calculated by equations (1) and (2) (Yang, 2016).

$$\text{Cleaning rate} = [(W_0 - W_1 - W_2)/W_0] \cdot 100\% \quad (1)$$

$$\text{Crushing rate} = (W_2/W_0) \cdot 100\% \quad (2)$$

where,  $W_0$  is the mass of clam before cleaning, kg;  $W_1$  is the mass of clam after cleaning, kg; and  $W_2$  is the mass of crushed clam, kg.

The cleaning quality requirements of clam shell are as follows: The dirty and other sundries on the surface of clam shell shall be cleaned up to show bright color; the cleaning rate shall not be less than 10%, and the crushing rate shall be less than 3%. In order to meet the above requirements, the drum rotating speed, water flow, drum inclination angle and the material quantity shall be reasonably matched.

### 3.3. Single factor test results and analysis

The cleaning effect of roller speed on clam is shown in Figure 2a. Results show that the roller speed will make a nonlinear effect on the clam cleaning rate. When the roller speed was less than 50 rpm, the clam cleaning rate was high, which could be more than 13%, and the crushing rate was low (< 1.7%); when the roller speed exceeded, the cleaning rate dropped significantly, while the crushing rate increased; when the speed reached 80 rpm, the cleaning rate fell below 3%, while the crushing rate increased to 12%. When the roller speed increased, the cleaning rate would decrease, while the crushing rate would rise. One possible reason is that when the drum speed increases, the retention time of clam in the drum is shortened, and the collision degree between clams and drum is intensified, so the cleaning effect is reduced. Under the test conditions, it is more suitable to control the drum speed at 30–60 rpm.

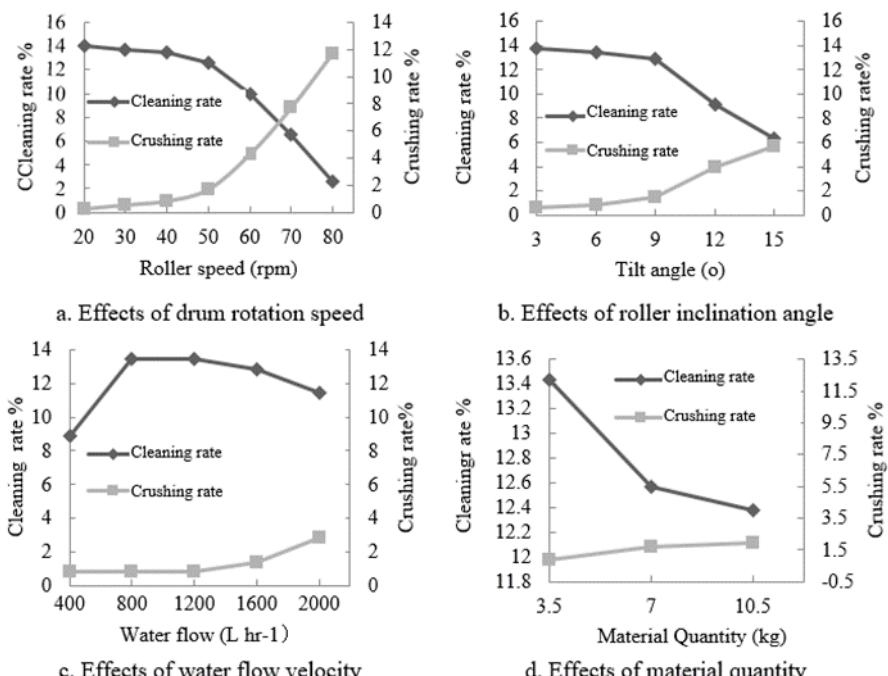


Figure 2. The influence of various factors on cleaning rate and breakdown rate.

The cleaning effect of dip angle on clam is shown in Figure 2b. Results show that there is a nonlinear relationship between roller speed and clam cleaning rate and crushing rate. When the tilt angle was 3°, the optimal cleaning efficiency (13.71 %) and the lowest crushing rate (0.57 %) were obtained. When the tilt angle continued to increase, the cleaning effect would decrease. When the tilt angle was 3–9°, the cleaning rate would be more than 10%. As the tilt angle increased, the crushing rate would increase slowly, which approached an ideal state. When the angle exceeded 12°, the cleaning effect was not ideal and the crushing rate was high. Because when the angle is too large, the clam in the drum cleaning time will be shortened, and the cleaning

effectiveness would decrease .Considering the cleaning rate, crushing rate and cleaning time, the drum rotating speed should be set at 3 – 9°.

Under the circumstances that the roller speed was 40rpm, the tilt angle was 6° and the material quantity was 3.5kg, and the water flow was set as 400, 800, 1200, 1600 and 2000 L hr<sup>-1</sup> respectively, the cleaning effect is shown in Figure 2c. It can be seen from the results in the Figure that there is a nonlinear relationship between water flow rate and clam cleaning rate. Under the condition of small flow rate (400–800 L hr<sup>-1</sup>), the cleaning rate increased significantly. When the flow rate was 800–2000 L hr<sup>-1</sup>, the cleaning rate would be more than 10%, and the crushing rate was almost unchanged. When the flow rate was 400–1600 L hr<sup>-1</sup>, the crushing rate was all less 3%, reaching the ideal state. In excess of 1800 L hr<sup>-1</sup>, the cleaning effect was not ideal. Because when the water flow is excessive, it will accelerate the speed and time of the clam to pass through the drum .Considering the cleaning rate, crushing rate and cleaning time, the water flowrate shall be set at 800–1600 L hr<sup>-1</sup>.

Under the circumstances that the drum rotating speed was 40rpm, the water flow was 800 L hr<sup>-1</sup>, and the tilt angle was 6 °, and the material volume was set at 3.5 and 7, 10.5 kg respectively, the cleaning effect is shown in Figure 2d. Results show that, there is a nonlinear relationship between the amount of material and the cleaning rate and the crushing rate of clam. When the amount of material increased, the shell friction between clams was not enough, and the cleaning effect would decrease. When the material quantity was 3.5–10.5kg, the cleaning rate and crushing rate could reach the ideal state. Considering the cleaning rate, crushing rate, cleaning time and cost saving, the material quantity shall be set at 3.5 kg.

### 3.4. Response surface test results and analysis

Three test factors including roller speed, water flow and drum tilt angle were selected in this experiment, and comprehensive scores of cleaning rate and crushing rate were taken as response values. The random combination test sequence included 17 test points, which consisted of 12 factorial points and 5 center points. Response surface analysis of clam cleaning rate and crushing rate was conducted by design expert 8.0.6 software, and the best combination of various factors was obtained on this basis .The test results are shown in Table 2.

Range R reflects the effect of various parameters in the test. From range R value in table 2, it could be concluded that the intensity of influence of various parameters on cleaning rate and crushing rate within the range of the test is in general following this pattern: roller speed > inclination angle>water flow at the drum speed, while both the optimal cleaning rate and crushing rate were the 17th group, with the cleaning rate of 14.29 %, the crushing rate of 0%, the cleaning effect of which is of great significant. Therefore, the optimal parameters are roller speed of 45rmp, tilt angle of 6°, and water flow of 1200 L hr<sup>-1</sup>, which can make the cleaning effect become extremely efficient.

Figures 3 and 4 show the response surface diagram of the influence of drum rotating speed and drum tilt angle on cleaning rate and crushing rate when the water flow is 1200 L hr<sup>-1</sup>. The water flow was 1200 L hr<sup>-1</sup>; contour line shape could reflect the strength of interaction effect, and the ellipse could mean significant interaction between the two factors, while the circle means unapparent interaction.

When the flow rate was constant, the interaction between roller speed and inclination angle was extremely sensitive. With the decrease of roller speed, the inclination angle decreased, which had a more significant impact on the cleaning rate and crushing rate. When the roller speed was between 33–44 rpm and the inclination angle was between 3–7°, the crushing rate would be as low as 0%. When the roller speed was 30–46 rpm, the cleaning rate would decrease first and then would increase with the decrease of inclination angle. When the roller speed was more than 60rpm, the cleaning rate would decrease with the increase of the tilt angle .when the roller speed was 30–45rpm, the inclination angle was between 3–8°, the cleaning rate would be over 14%, which was the highest cleaning rate. The results show that when the water flow is constant,

appropriately reducing the drum speed and tilt angle is helpful to improve the cleaning rate and crushing rate. This is because if the roller speed is too fast and tilt angle are too big, the crushing rate will be significantly increased and the cleaning rate will be significantly reduced, which is consistent with the previous analysis results.

Table 2. Response surface test design and test results.

Test No.	Factors			Cleaning rate	Crushing rate
	Rotation speed	Angle	Flow		
1	-1	1	0	13.14	1.14
2	-1	1	0	13.14	1.14
3	0	0	0	14.00	0.29
4	0	0	0	14.00	0.29
5	-1	-1	0	13.71	0.57
6	0	1	1	12.57	1.71
7	1	1	0	8.57	5.71
8	1	0	-1	10.29	4.00
9	0	-1	-1	14.00	0.29
10	0	1	-1	12.86	1.43
11	0	0	0	14.00	0.29
12	1	-1	0	10.86	3.43
13	1	0	1	9.14	5.14
14	-1	0	1	13.43	0.86
15	-1	0	-1	14.00	0.29
16	0	0	0	13.71	0.57
17	0	0	0	14.29	0
Cleaning rate k <sub>-1</sub>	13.57	12.93	12.79		
Cleaning rate k <sub>0</sub>	13.62	12.98	12.92		
Cleaning rate k <sub>1</sub>	9.71	11.79	12.07		
Range R	3.90	1.20	0.85		
crushing rate k <sub>-1</sub>	0.71	1.36	1.50		
crushing rate k <sub>0</sub>	0.67	1.30	1.37		
crushing rate k <sub>1</sub>	4.57	2.50	2.21		
Range R	3.90	1.20	0.85		

Note: K<sub>n</sub> represents the average values of cleaning rate and crushing rate corresponding to the nth level of factor drum speed A, drum tilt angle B and water flow C respectively.

#### 4. Conclusions

This paper documents the design of an automatic shell cleaning equipment which combined a drum cleaning structure with the high pressure water jet, which means automatic clam cleaning can be realized. Through single factor and response surface experiments, the optimal cleaning process was determined as follows: roller speed of 45rpm, tilt angle of 6°, water flow of 1200 L hr<sup>-1</sup>. This equipment can realize automatic clam cleaning, reduce labor intensity, at the same time, it is hoped to improve the efficiency of shellfish cleaning in the process of further optimization of equipment.

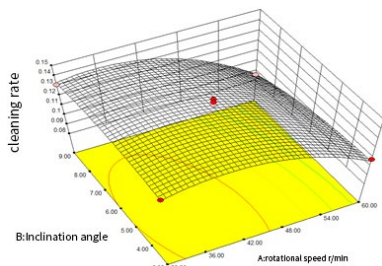


Figure 3. Response surface of interaction between drum speed and tilt angle when the flow rate is  $\text{L hr}^{-1}$

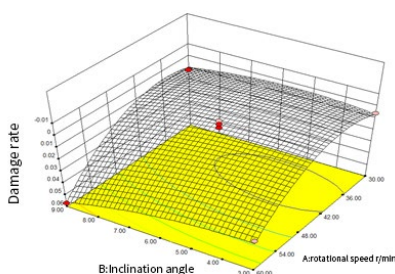


Figure 4. response surface of impact of drum speed and inclination angle on damage rate when flow rate is  $\text{L hr}^{-1}$

### Acknowledgements

This work was supported by the Commission of Science and Technology of Liaoning Province of China (Grant No. 2015103021), the Commission of Ocean and Fisheries of Liaoning Province of China (Grant No. 201509), the Educational Commission of Liaoning Province of China (Grant No. L201621) and the Key Laboratory of Mari culture & Stock Enhancement in North China's Sea, Ministry of Agriculture, P. R. China (Grant No. 2014-MSENC-KF-07).

### References

- Einarsson, G. 1995. Separating and cleaning device for shellfish. United States Patent: CA19830423883, 1995-10-15.
- Falconer, R. M. N. A. 2004. Method and apparatus for shucking shellfish. United States Patent: WO9400022, 2004-01-06.
- Gao, Z. Y., C.X. Ban, Q. Zhou, Y. Z. Li, C.S. Yang. 2015. Analysis of the movement track in the drum of cassava washer. Research on Agricultural Mechanization. (5), 58–60.
- Jiang, Z. 2006. Vegetable washing machine design. Science and Technology Information. 9 (1),51.
- Liu, T. C., 2008. Research and analysis on jet impact of high pressure water jet cleaning machine Clean of the World. 24 (12), 26–29.
- Ministry of agriculture fishery administration, 2019. China fishery statistics yearbook Beijing: China agricultural press. 23–30.
- Mulugeta, E., and M. Geyer. 2005. Characterizing the Washing Processes of Vegetables and potatoes. Biosystems engineering. 91 (4), 441–445.
- Tao, J. 2008. Study on purification technology of oyster Food science and technology. 7,108–112.
- Wenstrom R T, and T.S. Gorton. 2000. Method for shucking shellfish. United States Patent: D3528124, 2000-09-15.
- Yan, X.W. 2014. Current situation, problems and prospects of clam breeding industry Academic exchange meeting on Marine and lake ecological safety under global changes.
- Yang, S. H. 2016. Experimental study and prototype design of bay scallop cleaning. Journal of Hebei Agricultural University. 39 (3), 112–116.

## Best Available Techniques (BAT) for Emission Reduction of Livestock Farming Industry in Denmark

Peter Kai, Guoqiang Zhang \*

Department of Engineering, Aarhus University, Aarhus 8000, Denmark

\* Corresponding author. Email: [Guoqiang.zhang@eng.au.dk](mailto:Guoqiang.zhang@eng.au.dk)

### Abstract

With Integrated Pollution Prevention and Control Directive (IPPC), the Europe Union (EU) commission has defined the obligations that industrial and agricultural activities with a high pollution potential must comply. In Denmark, considerable research and development investigations regarding reducing pollutant emissions from livestock production industry have been conducted in the last 2 decades, which results in a list of available techniques that can mitigate the emission in varied degree.

The Danish Environmental Protection Agency (EPA) has analysed and summarised the environmental performance of different techniques that covering the areas of feeding practice, housing systems, manure storage and application. The analysis of the different technologies has been described in so called technology sheets for the best available techniques (BAT).

Based on the published researches and the technique documentations the Danish EPA has conducted standardized BAT-assessments for the prevailing combinations of types and sizes of livestock farms in Denmark. These BAT-conclusions include quantitative BAT-emission limit values for ammonia and phosphorous together with qualitative BAT-assessments for nitrate leaching and the consumption of water and energy.

The standardized BAT-assessments were formulated as guidelines to the competent authorities and are published on the Danish EPA's homepage [www.mst.dk](http://www.mst.dk) together with technical and economical documentation. The purpose of the guidelines and documentations is to assist the local authority in setting the BAT requirements and to ensure a uniform and a standard practice in defining the BAT requirements for livestock facilities. This paper summarised all the techniques related to pig housing and air cleaning, including assessments in practical applications and provides readers an overview on Danish BAT and application of environmental technologies.

**Keywords:** Animal housing, environmental friendly production, ammonia and odour, air quality, mitigation technology

### 1. Introduction

Environmental issues are great challenges for livestock industry worldwide. Ammonia ( $\text{NH}_3$ ), odour, dust and greenhouse gases emissions from livestock production should be reduced to mitigate the environment impacts on atmosphere and global climate warming.

With the Industrial Emissions Directive (IE directive), the EU commission has defined obligations that industrial and agricultural activities with a high pollution potential must comply. Livestock farmers in EU countries must fulfil legal binding requirements expressed in the BAT conclusions for intensive rearing of poultry or pigs as defined in the EU commission implementation decision (EU, 2017). The decision defines intensive rearing as activities with more than 40,000 places for poultry, more than 2,000 places for fattening pigs (over 30 kg), or more than 750 places for sows.

As an example, activities associated with the production of fattening pigs with more than 2,000 pig places the binding requirement known as the BAT ammonia emission limit (BAT-AEL) falls within the range 0.1 to 2.6 kg  $\text{NH}_3$  animal place<sup>-1</sup> year<sup>-1</sup> (EU 2017).

The implementation decision does not define emission factors for different housing systems or reduction performance of the defined BAT. The competent authorities shall establish emissions limits to secure that the emissions under normal production conditions do not exceed emissions

associated with the application of BAT. The member states may define individual requirements, as long as the emissions falls within the BAT-AEL. The implementation of the decision requires established procedures by the member countries to ensure that the livestock farmers meet the requirement within the BAT-AEL range.

In Denmark, considerable research and development investigations regarding reducing pollutant emission from livestock production industry have been conducted in the last 2 decades. A number of available technologies have been analysed, evaluated, and adapted into the technology list for reduction of emissions from livestock farming, focusing on NH<sub>3</sub> and odour emissions.

The Danish Environmental Protection Agency (EPA) has analysed and summarised the environmental performance of different techniques that covers the areas of housing systems, manure storage and application. The analysis of the different technologies has been described in so-called Technology Sheets as potential BAT candidates based on which NH<sub>3</sub> emission limits are defined. The objectives of this paper are to provide readers an overview of these listed techniques and to discuss the potentials and limitations for theirs applications in practices. The main focus is more on the technologies in pig housing and air cleaning.

## 2. A Brief Introduction to NH<sub>3</sub> Regulation Related To Animal Production In Denmark

When a farmer wishes to build a new animal production facility or expanding an existing one, he/she must obtain a production permit including meeting requirements for maximum NH<sub>3</sub> emissions from the production facility. The requirements depends on the animal category and size of production facility, and further on the distance to nearby legally protected nitrogen sensitive nature areas. The farmer must choose a combination of housing system and Environmental technologies (ET) to meet the requirements to ensure that the NH<sub>3</sub> emission is below certain threshold values stated in a Ministerial order (Denmark, 2019). The NH<sub>3</sub> emission factor for the relevant housing system, which is in planning and further to choose ETs amongst those listed on the Danish EPA Environmental Technology List (Danish EPA, 2019).

As a ground rule, emission factors for housing systems as well as reduction efficiencies for environmental technologies are based on on-farm testing following test procedures defined in the so-called VERA test protocol (VERA, 2019). The NH<sub>3</sub> emission factor for a specific housing system is normally based on the annual NH<sub>3</sub> emission measured at four animal houses of the specific housing system. For environmental technologies, the protocol requires a minimum of two locations where the technology installed/applied in an animal room or house is tested against an un-treated reference room or house. For animal housing systems, the resulting NH<sub>3</sub> emission factor is kg NH<sub>3</sub>-N per year per m<sup>2</sup> production area (i.e., animal accessible area). For ETs, the efficiency is defined as the percent reduction in NH<sub>3</sub> emission compared with a reference housing system without the ET installed.

Ammonia emission factors for animal housings are listed in a section of the Ministerial order on “permission and approval of livestock farming” (Denmark, 2019). Currently 58 emission factors for different animal categories and housing systems are listed in the Ministerial order. The approved ETs are listed on the EPA Environmental Technology List (EPA, 2019). Currently, 19 ETs are listed including 12 focused at reducing the volatilization of NH<sub>3</sub> and odour from animal houses, five air-cleaning systems, and two slurry storage technologies.

## 3. Application of BAT in Denmark

In Denmark, national BAT-AELs are defined for all animal categories and for animal production facilities with an NH<sub>3</sub> emission exceeding 750 kg NH<sub>3</sub>-N per year (911 kg NH<sub>3</sub>). Thus, the Danish regulation on BAT extends beyond pigs and poultry as defined in the IE directive EU, 2017).

The Danish BAT-AEL has been established based on a technological, economical evaluation of combinations of animal housing and technologies. For each animal category, a reference system

is defined, normally considered the most abundant housing system associated with a specific animal category. As an example, for growing/finishing pigs in slurry based production systems the reference system is a pen with fully drained floor, i.e., a combination of drained floor with max 10 % slotted area and slatted floor with approx. 20 % slotted area (fully slatted floor is no longer allowed in Danish pig houses).

The Danish government has defined two criteria for establishing national BAT-AELs: 1) The costs associated with any ET should not exceed 100 DKK kg<sup>-1</sup> NH<sub>3</sub>-N emission (11 € kg<sup>-1</sup> NH<sub>3</sub>), and 2) the total costs of applying ET(s) should not exceed 1–1.5 % of the production costs. For fattening pigs this is equivalent to approx. 8 DKK (1.07 €) per fattening pig. Production costs tend to decrease with increased production on a location, thus the BAT-AEL depends on the size of the production facility.

Further, the BAT-AEL depends on the manure system (slurry vs. deep-litter based), and whether the animal house is planned or existing. The law differentiate between manure systems because current ETs are developed for animal houses in which the manure is treated as slurry. Consequently, deep-litter based housing systems have fewer options to reduce the emission. In addition, it is generally easier to implement ET in new buildings compared with existing ones. These considerations are reflected in the Danish BAT-AELs.

Table 1 provides an overview of the BAT-AELs for pig production facilities (new installations) as defined by the Ministerial order (Denmark, 2019). Animal housing systems with slurry the BAT-AELs generally decreases as the production area increases. For the litter-based systems, no approved ETs are currently available and therefore, the BAT-AELs is constant and equal to the standard NH<sub>3</sub> emission factor for the housing system if self.

Table 1. Pigs BAT-AEL and associated production areas.

Animal typ-manure type	BAT-AEL (kg NH <sub>3</sub> -N a <sup>-1</sup> m <sup>-2</sup> )	Production area (m <sup>2</sup> )	BAT-AEL (kg NH <sub>3</sub> -N a <sup>-1</sup> m <sup>-2</sup> )	Production area (m <sup>2</sup> )
Sows, lactating - slurry	0.59	≤1200	0.47	≥3600
Sows, gestating and dry - slurry	0.87	≤1900	0.70	≥5700
Sows, gestating and dry – deep litter	1.40*			
Weaners - slurry	0.58	≤2600	0.50	≥7800
Weaners – deep litter	1.40			
Fattening pigs - slurry	1.62	≤1300		≥4500
Fattening pigs – deep litter	2.30*		1.06	
Fattening pigs, organic	1.30*			

\* The BAT-AEL for deep litter is same as the housing system as is.

In Figure 1, the BAT-AEL for fattening pig pens and the standard NH<sub>3</sub> emission factor for fattening pig pens with fully drained floor is depicted (solid lines) together with the total NH<sub>3</sub> emission per year with increasing number of animal places (dotted lines). Note the units in Table 1 and Figure 1 are not the same.

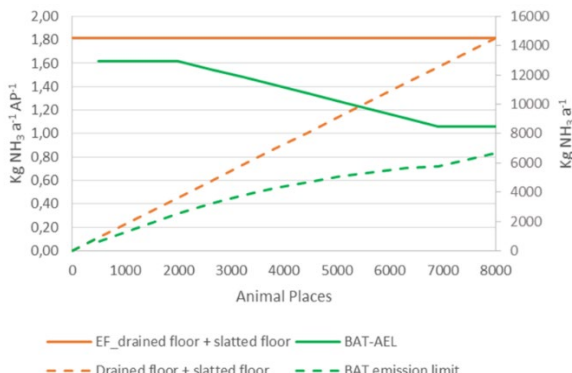


Figure 1. Consequence of BAT-AEL for fattening pig pens with fully drained floor  
(1AP = 0.65 m<sup>2</sup>).

#### 4. Overview of BAT and Related Research & Development (R&D)

ETs related to animal farming are generalised into four categories, i.e., emission control focussed at the housing system, air cleaning, manure storage, and field application. The mitigation technologies for manure storage and field application are rather straight forward, i.e., using coverage for manure tanks and direct slurry injection into the soil for field application. However, the methods and techniques using in animal housing for emission reduction are more comprehensive and therefore, this paper will focus on BAT for NH<sub>3</sub> and odour emission reduction from animal housing including air cleaning of exhaust air from the animal housing.

The available technologies varied a lot among the different categories, due to the complexity of each category. All the technologies in the list have a strong linkage to the national and international R&D in the fields and have active stockholders to move them forward for practice application and approval by the authority.

##### 4.1. Housing systems

Most investigations and consequently the mitigation technologies for reduction of emission are within livestock housing system, including floor design, manure managements as well as ventilation etc. As indicated earlier in this paper, the basic housing design including floor design influences the emission of NH<sub>3</sub> and odour resulting in different emission factors. For fattening pigs, the highest NH<sub>3</sub> and odour emissions are observed in pens with combination of slatted floor and drain floor. The high emissions is a result of a large emitting surface area of the manure pit. With solid floor in the pen, the emitting surface of slurry in the manure pit is reduced and hence the total emission (Table 2).

It is generally considered that with 25% to 50% of solid floor, NH<sub>3</sub> emission can be reduced 16% comparing to a housing with 1/3 drain floor and 2/3 slatted floor (Poulsen 2016); and 27% comparing to a pen with fully slatted floor (Poulsen, 2016). Note, that fully slatted floor is no longer allowed in both new and existing pig buildings.

An investigation report by Danish Research Pig Research Centre for an field test in summer 2009 (Pedersen & Jensen, 2010) showed that fattening pigpens with 58% solid floor resulted in 35–40 % less NH<sub>3</sub> emission comparing with the pigpens with drain floor.

###### 4.1.1. In house manure slurry cooling

Investigations have showed that cooling slurry manure in pit significantly reduces the NH<sub>3</sub> emission from animal housing. Slurry cooling is carried out by inserting PEL tubes in the floor of the slurry pit. By recirculating water at a low temperature through the tubes, energy is extracted from the slurry causing the slurry temperature to decrease, which in effect reduces the NH<sub>3</sub>

volatilization from slurry. A test carried out in a commercial pregnant sow unit for loose sows showed that the NH<sub>3</sub> emission was reduced by 23 % and 33 % applying cooling rates at 21 and 37 W m<sup>-2</sup> slurry pit, respectively (Holm, 2016). Another investigation of applying manure slurry cooling in a fattening pig housing with an average cooling rate of 27 W m<sup>-2</sup> slurry pit resulted in an average emission reduction of 19 % and 20 %, for NH<sub>3</sub> and odour respectively (Holm et al., 2017). An investigation conducted in an experimental farm at Danish Pig research Centre (Grønhoj) showed that, NH<sub>3</sub> and odour emission were about 51 and 22 % lower in the fattening pig section with manure slurry cooling compared with a section without cooling. The average cooling rate was 55 W m<sup>-2</sup> slurry pit (Jørgensen et al., 2013).

Table 2. NH<sub>3</sub> and odour emission factors associated with different floor systems for fattening pigs and weaned pigs (Denmark, 2019).

Floor type	NH <sub>3</sub> emission factor (kg NH <sub>3</sub> -N yr <sup>-1</sup> m <sup>-2</sup> )	Odour emission factor (OU <sub>E</sub> s <sup>-1</sup> ·m <sup>-2</sup> )
<b>Fattening pigs</b>		
Partly slatted floor (1/3 drain floor*)	2.3	43
Partly slatted floor (25–49% solid floor)	1.9	29
Partly slatted floor (50–75% solid floor)	1.4	29
<b>Weaners</b>		
Partly slatted floor (50% drain floor)	1.2	21
Two-climate pen with partly slatted floor (65% solid floor)	0.56	21

\* Drain floor is a type of slatted floor with 50% less slot opening area.

In the DEPA Environmental Technology List, the effect is estimated as a reduction of NH<sub>3</sub> up to 34% as a function of cooling power. The following equation has been derived from the investigations (DEPA, 2019):

$$R = 0.85x - 0.004x^2 \quad (1)$$

where R is the reduction in NH<sub>3</sub> emission in percent of the standard NH<sub>3</sub> emission factor, x is the cooling power rate in W m<sup>-2</sup> slurry pit.

Pig farmers may apply slurry cooling in order to meet the BAT-AEL requirements in new and existing pig houses (DEPA, 2019).

#### 4.1.2. Manure slurry additive (Acidification)

Acidification has proved to be one of the most effective methods to reduce NH<sub>3</sub> emission from pig houses (Kai et al., 2008). “JH forsuring NH<sub>4</sub><sup>+</sup>”, a commercial acidification system, has been investigated at pig farms. The system empty the slurry pits to a process tank located outside the pig house. In the process tank, the pH of the slurry is reduced by adding sulfuric acid to a pH of 5.5 is reached. After acidification the slurry is pumped back to the slurry pits in the pig house. In investigations carried out at both commercial pig farms and an experimental test farm, the slurry acidification system proved to reduce NH<sub>3</sub> emission 64 – 71 % compared with untreated reference sections (Pedersen & Albrechtsen, 2012; Riis, 2016).

Slurry acidification has not shown odour reducing potential (Riis, 2016), however combining slurry acidification with solid-liquid separation during the acidification process, have shown to effectively reduce the odour emission by 51 % (Jonassen, 2016; DEPA, 2019). The system is called SmellFighter and is developed by JH Agro.

#### 4.1.3. Partial pit air exhaust for air cleaning

The concept of partial pit air exhaust technique was introduced for investigations in Denmark in 2006, associated with a large national project “Reduction of Odour Source in and Emission from Swine buildings (ROSES)” to aim at to collect most pollutant air near to the emission source

for further cleaning treatment (Zhang, 2006). The housing system has two ventilation exhaust channels: room air exhaust and pit air exhaust, Figure 2. The principle idea was to apply partial air exhaust opening(s) in slurry pit headspace and using a limited ventilation airflow rate to remove the high concentrated pollutant air near to surface of slurry and slatted floor. The flowrate of room air exhaust is regulated according indoor thermal condition. The pit exhaust is operated in a constant level when both exhausts are in operation. Very often, the designed airflow capacity of a pit exhaust is about 10% of the total designed capacity for the housing system. However, this partial pit air exhaust rate can be regulated down to 5% according to the winter climate condition and indoor air quality. A summary of the Danish investigations on the techniques has been reported by Zhang et al. (2017). Principally, a partial pit exhaust can be applied in both mechanically ventilated buildings and naturally ventilated buildings.

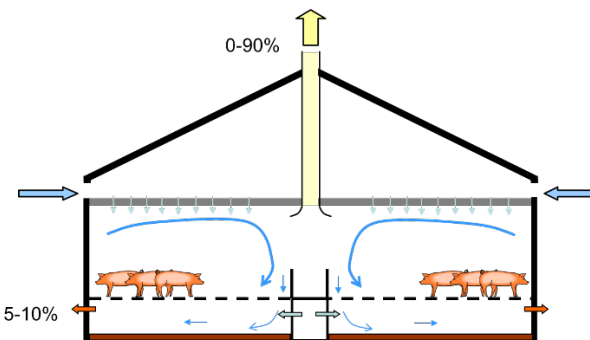


Figure 2. Concept of the pig housing with a partial pit air exhaust with roof top room air exhaust and air supply from ceiling room via diffusion ceiling.

Through the many case installation and measurements, the partial pit exhaust techniques has been adopted in the BAT list in 2014. Overall, the system performs well in Danish pig housing systems. However, the NH<sub>3</sub> removal efficiency via pit exhaust may vary depending upon room airflow patterns and ventilation flowrates (Zhang et al., 2017). In principle, this technology can be also applied in a naturally ventilated housing system. The main challenge is on optimal design and control of the system to achieve the most effective pollutant air collection by the pit exhaust, since indoor airflow pattern control in such a system is not easy. Currently, there is a research and development project in Denmark working on it – a hybrid ventilation system for pig production.

#### 4.1.4. Regular removal of manure slurry from animal house

Removal of slurry in livestock housing systems for fattening pigs weekly (flush tube barns) can reduce the odour emission by 20 % if the manure pit is emptied every week compared with every six weeks (DEPA, 2019).

#### 4.1.5. Other techniques

Most investigations and consequently the environmental technologies for reduction of emission are within livestock housing system, including floor design, manure managements as well as ventilation etc. The main focus has been on reduction of emission source area or removal of the emission source frequently.

##### a. Manure in-house separation

In house manure separation has been investigated using several different manure belt designs. Kai (2010) investigated a belt system with a slope under slatted floor to regularly remove manure and drain the liquid manure (urine & water) from the dry matter rich faeces. The system improved both indoor air quality and reduced emission of NH<sub>3</sub> and odour. The disadvantage is the costs of investment and maintenance.

*b. Removing emission source at defined time intervals – manure scraper under floor*

A pig housing concept with a pit manure escape unit and drain channels in pit to separate the manure was investigated (Pedersen & Kai, 2012). Results showed both significant improvement of indoor air quality and reduction of NH<sub>3</sub> emission.

#### 4.2. Air cleaning

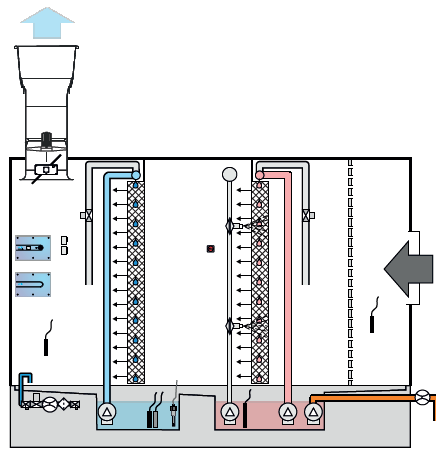
For purification of exhaust air at the end of ventilation system, varied air cleaning technologies have been proposed and investigated in the last decades, including wet scrubber (water spray), wet pad (with chemical additive or biological processing), mainly aiming at reduction of NH<sub>3</sub> and odour emissions from livestock housing systems.

An investigation of a prototype air cleaning system for emission control in livestock buildings was conducted in a pig rearing building (Ogawa et al, 2011). The system uses a two-step process: (1) absorption and (2) nitrification. The absorption process takes place in a scrubber, in which NH<sub>3</sub> is removed by a water spray. The nitrification process takes place in water purification unit, in which the NH<sub>3</sub> in water is oxidized to nitrites and nitrates using a microbiological process. Scrubbers or spray towers can be installed in ventilation stacks. Water purification unit is a central unit, which recycles water with a controlled pH to the spray towers. In tests, the water purification unit was able to maintain the spray water at pH < 7.5, which enabled 55–95% NH<sub>3</sub> removal efficiency.

Zhao et al. (2011) investigated three multi-stage scrubbers and evaluated their effectiveness in terms of emissions reductions for airborne dust, total bacteria, NH<sub>3</sub>, and CO<sub>2</sub> from pig houses in winter. The three multi-stage scrubbers were one double-stage scrubber (acid stage+ bio-filter), one double-stage scrubber (acid stage + bio-scrubber), and one triple-stage scrubber (water stage + acid stage + bio-filter). Results showed that these scrubbers reduced concentrations of PM<sub>10</sub> by 61% to 93%, concentrations of PM<sub>2.5</sub> by 47% to 90%, concentrations of airborne total bacteria by 46% to 85%, and concentrations of NH<sub>3</sub> by 70% to 100%. No effects on reduction of CO<sub>2</sub> concentration was found.

Many similar investigations have been reported, e.g., Melse et al. (2012), Ottosen et al. (2011), Van der Heyden et al. (2016). Today an optimal filtering technique can remove 95% or more NH<sub>3</sub> from the exhaust ventilation air of a livestock unit. In Denmark, a few commercial air purification products have been listed on the DEPA ET-list. Figure 2 shows two purification system with different approaches and designs, both of them are included on the DEPA environmental technology list (DEPA, 2019).

Using such cleaning approach, dimension of the system design corresponding the ventilation airflow rate and average air speed through the system are important, since that will affect the contacting (residence) time between air and cleaning material surface. Besides, the porosity in using wet pad/panel or vapour sizes in using water sprayer should be considered in system design.



(a)



(b)

Figure 3. Examples of air cleaning systems, by (a) SKOV A/S; (b) AgriFarm A/S.

## 5. Conclusions

The best available technologies that applied for reduction livestock farming emission, focusing on NH<sub>3</sub> emission from housing system in Denmark, are reviewed. These technologies are (1) cleaning techniques for removing NH<sub>3</sub> and odour from exhaust ventilation air channels; (2) using partial pit air exhaust to lead an amount of the most pollutant exhaust air for cleaning treatment; (3) in-house-cooling of manure slurry in pit; (4) acidification of manure slurry; (5) regularly removal of manure. Relative reports, scientific publications are also reviewed and discussed.

## References

- Aarnink, A.J.A., M.J.M. Wagemans. A.J. og van den Berg. 1997. Housing for growing pigs meeting the needs for animal, stockman and environment. ASAE International Livestock Environment Symposium V, Minneapolis, Bloomington, Minnesota, 29–31 May. p 86–92.
- Danish EPA - Danish Environmental Agency, 2019. Best Available (Environmental) Technology (BAT) -Environmental Technologies for Livestock production industry. <https://eng.mst.dk/trade/agriculture/environmental-technologies-for-livestock-holdings/list-of-environmental-technologies/> accessed in June 25, 2019.
- Denmark, 2019. Ministerial order on permission and approval of livestock farming” (Bekendtgørelse om tilladelse og godkendelse m.v. af husdyrbrug- BEK nr 1467 af 06/12/2018). <https://www.retsinformation.dk/Forms/R0710.aspx?id=205574> Accessed July 16 2019.
- EU, 2017. Commission Implementing Decision (EU) 2017/302 of 15 February 2017 establishing best available techniques (BAT) conclusions, under Directive 2010/75/EU of the European Parliament and of the Council, for the intensive rearing of poultry or pigs. <http://eur-lex.europa.eu/legal-content/EN/TXT/PDF/?uri=CELEX:32017D0302&from=EN> Accessed July 16 2019.
- Holm M; K.B. Sørensen, M.B.F. Nielsen. 2017. Ammoniak- og lugtreduktion ved gyllekøling i slagtesvinestalde (Ammonia and odour reduction by manure cooling in fattening pig houses). Report No. 1105, Danish Pig Research Centre.
- Jonassen, K. 2016. Lugtreduktion ved separation af forsuret gylle (Odour reduction by solid-liquid separation of acidified slurry). Report 1080, Danish Pig Research Centre.
- Jørgensen M, A.F. Riis, P. Pedersen. 2013. Effekten af gyllekøling i slagtesvinestier med drænet gulv i lejearéal (Effects of manure cooling in fattening pigpen with drain floor at laying area). Experience No. 1312. Danish Pig Research Centre.
- Kai, P., P. Pedersen, J.E. Jensen, M.N. Hansen, and S.G. Sommer. 2008. A whole-farm assessment of the efficacy of slurry acidification in reducing ammonia emissions. European Journal of Agronomy. 28:148–154.
- Kai, P., 2010. In-house manure separation of finishing pig buildings. Project Report. Department of Biosystems Engineering, Aarhus University.
- Melse RW, J.P.M. Ploegaert, N.W.M. Ogink. 2012. Biotrickling filter for the treatment of exhaust air from a pig rearing building: Ammonia removal performance and its fluctuations. Biosystems Engineering 113:242–52.
- Ottosen LDM, S. Juhler L.B. Guldborg, A. Feilberg, N.P. Revsbech, L.P. Nielsen. 2011. Regulation of ammonia oxidation in biotrickling airfilters with high ammonium load. Chemical Engineering Journal 167:198–205.
- Okawa H, P.J. Dahl, T. Suzuki, P. Kai, H. Takai. 2011. A microbiological-based air cleaning system using a two-step process for removal of ammonia in discharge air from a pig rearing building. Biosystems Engineering, 109:108–19.
- Pedersen, P., 2007. Tilsætning af brintoverlitr til forsuret gylle i slagtesvinestald med drænet gulv (Addition of hydrogen peroxide to acidified slurry in pig finisher house with drain floor). Report No. 792, Dansk Pig Production. pp. 14.
- Pedersen, P., 2010. Fast gulv er ikke driftsikkert for alle svineproducenter (Solid floor is not reliable for all pig production). Note No. 1016. Danish Pig Research Centre.
- Pedersen, P. and T.L. Jensen. 2010. Forskellige gulv typer med og uden gulvudsugning i en sommerperiode (Different floor types in summer period with and without pit air exhaust). Report No. 883. Danish Pig Research Centre.
- Pedersen P, K. Albrechtsen. 2012. JH forsuringssanlæg i slagtesvinestald med drænet gulv (JH Acidification system in fattening pig house with drain floor). Report 932. Danish Pig Research Centre.
- Pedersen P, P. Kai, 2012. Separation af ajle og fast gødning med gødningsbånd (Separation of liquid and solid manure using manure belt), Report 958. Danish Pig Research Centre.

Poulsen HD. 2015. Normtal for husdyrgødning (Environmental data for livestock manure). Aarhus University. <http://anis.au.dk/normtal/>

Riis, A.L. 2016. Effekt af JH forsuring NH<sub>4</sub><sup>+</sup> i slagtesvinestalde med drænet gulv (Effect of JH acidification NH<sub>4</sub><sup>+</sup> in fattening pig houses with fully slatted floor). *Report 1078*, Danish Pig Research Centre.

Van der Heyden C, E. Brusselman, EIP Volcke, P. Demeyer. 2016. Continuous measurements of ammonia, nitrous oxide and methane from air scrubbers at pig housing facilities. *Journal of Environmental Management* 181:163–71.

VERA - Verification of Environmental Technologies for Agricultural Production. 2019. VERA test protocol for Livestock Housing and Management Systems. <http://www.vera-verification.eu/test-protocols/>, accessed in June 25, 2019.

Zhao Y, AJA Aarnink, MCM de Jong, NWM Ogink, PWGG Koerkamp. 2011. Effectiveness of Multi-Stage Scrubbers in Reducing Emissions of Air Pollutants from Pig Houses. *Transactions of the ASABE*, 54:285–93.

Zhang G. 2006. Reduction of odour source in and emissions from swine buildings – ROSES. DaNet News Letter, Dec. 2006. Danish Institute of Agricultural Sciences, Bygholm, Horesens, Denmark.

Zhang G; B. Bjerg B and C. Zong. 2017. Partly pit exhaust improves indoor air quality and effectiveness of air cleaning in livestock housing – a review. *Applied Engineering in Agriculture*. 33(2): 243–256.

# Outcome-Based Measures of Animal Welfare: the Challenges and the Opportunities

Janice C. Swanson\*

Department of Animal Science and Department of Large Animal Clinical Sciences

Michigan State University, East Lansing, MI 48824, USA

\* Corresponding author. Email: [swansoj@msu.edu](mailto:swansoj@msu.edu)

## Abstract

Over the last decade there has been a trend to transition animal care guidelines, standards, and audits from using a predominantly environment or resource-based approach to an animal outcomes-based approach for the assessment of animal welfare. An outcome-based measure focuses on one (or more) outcomes of the processes used by farmers to meet an expected level of animal welfare. The outcome represents the experiences of the animal living under the prescribed standards of management and care. For example, a numerical space requirement, its assessment and corresponding audit point determines whether the required space (resource) per animal unit has been met. The actual physical condition (outcome) of the animal(s) living according to the space requirement is not measured. Years of implementation of animal welfare assessment and audit programs have revealed the limitations to using a predominantly resource-based or process oriented approach as it does not adequately capture the welfare outcomes for the animal. The variability of housing systems, practices and processes employed by farms has tipped the scales toward adopting more animal outcomes-based measures. The challenge is to identify which measures of animal welfare are best suited for use as an outcome, validating those measures, and then training assessors and auditors to effectively, and with consistency, assess the measure(s). The opportunity is an outcomes-based approach can provide more flexibility in the assessment and auditing of animal welfare and may encourage positive outcomes in animal care to emerge at the farm level.

**Keywords:** Animal welfare, assessment, measures, outcome, farm animals

## 1. Introduction

Many countries have implemented laws, codes, or industry guidelines that provide direction and guidance on how farm animals should be kept and cared for. In the most advanced cases corresponding enforcement of these laws, codes and industry guidelines take the form of a third party inspection of the farm(s). The assessment tool used by an assessor or auditor is composed of criteria that are observed or measured at the farm level. The on-farm inspection constitutes an assessment of the farmer's compliance with laws, standards and guidelines functioning in their country, state and/or locale. In some cases the on farm assessment may also represent the animal welfare compliance expectations set by a food company as a condition of doing business within its supply chain. Regardless of the mode, the criteria used to assess animal welfare must be validated for what they are intended to measure, and whether or not it is useful in making determinations about the farmer's compliance with producing a state of good animal welfare.

## 2. Measuring Animal Welfare

### 2.1. Background

Social expectations for the treatment and care of farmed livestock continues to rise globally. At first, laws or guidelines were developed to set baseline recommendations for the care of farmed animals and to provide public assurance that basic animal needs were met. Of particular focus were farm species kept in intensive, indoor production systems (poultry, dairy cattle, veal calves, and swine). Recommendations for the care of these livestock typically focused on the provisioning of resources and management practices required to house, feed, water and provide space for animals to live (Rushen et al. 2011).

The Five Freedoms (FF) were developed by the U.K. appointed Brambell Committee (Brambell, 1965) and were the first set of aspirational targets developed to guide livestock production practice. The FF were driven by public concern for the welfare of intensively raised livestock. The initial issuance of the FF focused upon the normal postural adjustments that should be permitted to livestock living under intensive conditions. The FF were later revised by the Farm Animal Welfare Council (FAWC, 1993). FAWC retained the original intent of the technical committee recommendations and broadened them to be meaningful to all aspects of livestock production.

Unique to the FF is the inclusion of general principles that consider the psychological wellbeing of an animal in addition to its physiological needs. Of special note is the emphasis on the animal's experience evident in Freedom's 4 and 5.

1. Freedom from thirst, hunger and malnutrition - By ready access to a diet to maintain full health and vigour.
2. Freedom from thermal and physical discomfort – By providing a suitable environment including shelter and a comfortable resting area.
3. Freedom from pain, injury and disease – By prevention or rapid diagnosis and treatment.
4. Freedom from fear and distress – By providing sufficient space, proper facilities and the company of the animal's own kind.
5. Freedom to express normal behavior - By ensuring conditions which avoid mental suffering.

In many respects the FAWC FF changed the world of farm animal welfare from one in which provisions (resources) to animals mattered most to one in which farmers and ranchers also become responsible for the animal's quality of life. As demands increased for research to provide scientific evidence to meet the FF, scientists rebooted their training to focus on the behavior, physiology, health, husbandry and care of farm animals (Webster, 2016). The FF developed by the FAWC spread globally and often serve as the guiding principles for laws, standards and guidelines in force today. One important example is the World Organization for Animal Health, better known by its French acronym OIE, adopted the FF (OIE 2018a) as its foundation for the development of global terrestrial and aquatic animal standards.

At present some animal welfare scientists have proposed a revision of the FF to more accurately capture the current state of progress in animal welfare assessment under an increasingly complex social and political environment. For example, Mellor (Mellor, 2016, 2017) has proposed a model revising the FF into a set of domains with corresponding aims to address the problem of literal interpretation of the word "Freedom" and to address the current state of scientific advancements in the assessment and auditing of animal welfare. Although the FAWC likely did not intend the term "freedom" to mean animals must be completely free of, for example, distress, however as written it does allow for a literal interpretation. In addition, Green and Mellor (2011) observed that new scientific information has enhanced our understanding of what constitutes a better 'quality of life' for an animal including the assessment of their positive affective states. As currently written the FAWC FF largely describe outcomes reflecting negative affective states that animals ought to be free of (Webster, 2016).

Since the development of the FAWC FF numerous animal welfare assessment programs and schemes have emerged. Some driven by laws, others by market forces, and some by voluntary efforts of the industry to self-police (Mench, 2008). As animal welfare is multidimensional a variety of measures are utilized to assess the welfare of livestock and poultry. Based on the scientific and practical evidence, criteria and tools have been developed to assist in assessing the welfare of livestock. The intent of this paper is not to focus on the different animal welfare assessment or auditing programs but to examine the challenges and opportunities for the use of animal outcome-based measures in addition to proven environmental, resource, and management measures. As written, the FAWC FF represent the first set of published animal outcomes to assure

the welfare of farmed livestock and poultry.

## 2.2. Environmental-based measures and outcomes-based measures

The simplest type of animal welfare measure to implement is one that is clear, universally understood by the user, and is observed with little subjectivity and variability. It is likely why quantitative environment-based measures (which includes provisioning of resources and management practice) have been heavily utilized in the development of legal standards and voluntary guidance documents (Blatchford, 2017). The assessor (or law enforcer) and the farmer have a common understanding of what is and what is not compliant. However, the provisioning of a resource or the specification of a management procedure only provides a starting point from which to assess animal welfare. An environment-based measure is not a direct observation of an animal's welfare. Space, feeder, bunk, or watering allocations per animal, thresholds for air quality and ventilation rates, litter, and other such measures are deemed as important environmental conditions to support good welfare. What it does not capture is the actual state or experience of the animal(s) living within the prescribed environment. So what is a measure that will inform us if the provisioned resources and management have successfully sustained a good quality of life for the animal(s)? An animal outcome-based measure.

The concept of animal welfare is naturally animal-based. Therefore more organizations including the World Organization for Animal Health are incorporating an animal outcomes-based approach to fully assess animal welfare.

*"For the OIE animal welfare standards to be applicable globally, they should emphasise favourable outcomes for the animals, although, in some circumstances, it may be necessary to recommend specific conditions of the animals' environment and management. Outcomes are generally measured by assessing the extent to which animals experience the "five freedoms" described in Article 7.1.2." (OIE, 2018b)*

An outcome-based measure focuses on one (or more) outcomes of the processes used by farmers to meet an expected level of animal welfare. It is the effect upon, or the outcome for, the animal that is its focus. Typically this would mean direct assessment of the animal(s) using scientifically established physical or behavioral measures of their welfare state. Important to the assessment process is that the selected measure to determine whether an outcome has been met is validated and proven to be accurate. In some respects setting a desired welfare outcome for the animal mimic's the backward design model used for building an educational curriculum. Desirable sets of animal welfare outcomes and their corresponding measures are established first then the processes or environmental requirements (resource- and management-based measures) to meet those outcomes are identified for assessment too. The most accurate measures for each animal outcome should be selected and used by assessors to conduct on-farm or slaughter plant assessments.

## 2.3. Examples of outcome-based measures

Animal outcome-based measures have been incorporated into animal welfare assessment tools. Examples will be provided using three types of farm animals to illustrate how outcome-based measures are used to assess animal welfare.

Litter (a resource) is typically a required housing element on broiler chicken and indoor cage free egg farms. Litter serves several purposes including the encouragement of behavior such as scratching and dustbathing, provides comfort, and absorbs fecal material. In many guidelines or standards the amount of litter (resource-based measure) may be specified by percent floor space to be covered or another criterion. Sometimes recommendations for litter depth and type are also part of the standard. Moreover, there may be management-based requirements that litter must be replaced at certain intervals and managed to avoid caking and wet spots. Poor litter management, has been implicated in poor broiler welfare (Winder, et al. 2018). So these environmentally-based measures will be used by an animal welfare assessor to check-off whether the standards pertaining

to litter have been met by the farm. However simply meeting these requirements for litter does not tell us what the experience or outcome is for the chickens living on the litter.

Poor litter conditions have been linked to painful foot pad pathologies the most notable being foot pad dermatitis (de Jong et al. 2014; 2012 a, b). The outcome desired for the chicken is to be free of painful foot pad pathologies. Moreover, thresholds of acceptability or failure are often established based on parameters such as the percent of flock affected and the severity of the pathology. Thus the percentage of chickens in the flock that have foot pad health problems (based on a flock sampling procedure and scoring) and severity of the condition (based upon a lesion score) would be the measured criteria that tells us if the desired outcome has been achieved. In the case of both types of chickens scoring the foot pads for lesions provides important information about the farm litter conditions and its impact on chicken welfare. Foot pad lesion scoring can be conducted at the slaughter plant (broilers) or during the farm inspection of live birds. (Butterworth, 2018; Blatchford, 2017; Saravia et al. 2016).

Another outcome-based measure used in poultry production focuses on feather condition. Feathers can be scored to assess dirtiness, physical condition, and patterns of feather loss due to behavioral problems like feather-pecking (Hartcher et al. 2016). The desired outcome for the bird is to have clean feathers in good physical condition and to be fully plumed. Scoring systems have been developed for feather condition. The most commonly adopted scoring systems for foot pad lesions and feather condition, and perhaps the best researched to date, are the Welfare Quality® assessment protocols (Welfare Quality®, 2009). The assessment protocols are designed to encourage farmers to conduct self-assessments of their facilities and flock. Welfare Quality® uses a combination of resource, management, and outcome-based measures to assess and improve poultry welfare.

Outcome-based measures are often integrated with environment-based measures. Drawing from the examples above, cleanliness of plumage, hock burns, and foot pad health relate to litter and other conditions found on the farm (Saravia, et al. 2016). Together assessments of litter conditions and the animal outcomes help the farmer to identify the source of the problem, to implement changes, and be observant of whether or not foot and leg health and feather condition improve for the flock by changes in litter or other management practices. Recent reviews of poultry welfare assessment have been published by Butterworth (2018) and Blatchford (2017).

In poultry, swine, and dairy cattle locomotion or gait scoring systems are used to assess the prevalence of lameness in the flock or herd. Lameness can be attributed to foot and leg conformation (genetics), physical environment, age of animal, body weight, stocking density, and other etiologies. In dairy cattle lameness has been a particularly vexing issue. In free stall housing systems, the types of flooring, floor composition and grooving patterns for traction, free stall design, cow to free stall ratio, bedding type, wetness and alley cleaning can contribute to the development of lameness (Endres, 2017). In most standards of care these features of the dairy's physical environment will be assessed using environment-based measures. Lameness, a painful condition, is used as an animal outcome-based measure that can inform a farmer whether the physical and/or managed environment is preventing or potentially causing lameness. Locomotion scoring protocols have been developed for assessing the severity of lameness in dairy cattle (Zinpro, 2019 a; Welfare Quality® 2009b), swine (Zinpro, 2019b; Welfare Quality®, 2009c) and poultry (Welfare Quality®, 2009a).

Other outcomes-based measures used in swine production include body lesion and tail biting lesion scoring, mortality and morbidity rates, and pig performance parameters such as feed conversion ratio and average daily gain among others. For recent reviews of outcomes-based assessment of swine welfare see Pairis-Garcia and Moeller (2018) and Temple et al. (2018).

## 2.4. Challenges and opportunities of outcomes-based measures

The challenge of using outcome-based measures is identifying which measures of animal welfare are best suited for use to assess an outcome. Before an outcome measure is used it must

first be properly tested and validated then followed by training of assessors and auditors to effectively, efficiently and with consistency assess the measure(s). For example, locomotion scoring for lameness (Cook, 2018). The goal is to assess lameness with accuracy and consistency to reduce variability among observers and prevent interpretive problems. Another challenge is outcomes-based measures often take more time and training to detect the individual deviations from normal, for example, of birds housed in a large flock (Linares, et al. 2018).

The most challenging measures are those that may lend themselves to broad interpretation. Behavior has been included in outcome-based measures to assess farm animal welfare. As mentioned earlier, they are part of the FAWC FF including freedom from fear and distress. Thus published assessment protocols such as Welfare Quality® (2009a-c) include measures to assess behavior including fearfulness. Behavioral measures often utilize observations of the presence or absence of a behavior along with measures of their frequency and intensity. For example, sickness behavior may include postural attitudes, behavioral depression or excitement, anorexia and other behavioral signs and coupled with physical signs including injury and poor body condition. Successfully and consistently identifying and assessing sickness within a commercial flock or herd can be challenging (Linares, et al. 2018).

Pain also presents challenges to the assessment of animal welfare. Keel bone injury is painful for laying hens (Toscano, 2018). One widely used method of assessing keel bone damage is by physical palpation of the hen's keel bone then scoring it according to a keel bone scoring system (Casey-Trout, et al. 2015). However the accuracy and repeatability of palpation and observing birds for behavioral signs of pain (Casey-Trott and Widowski, 2016) can be difficult under commercial conditions. Although these measures are challenging for auditors and farmers to assess there is hope to be found in the new and emerging smart technologies that practically, precisely, and with high repeatability and consistency assess measures such as keel bone damage or behavior to determine the welfare status of the animal (Sassi, et al. 2016; Berkman 2014).

The opportunity of an outcomes-based approach is it can provide more flexibility in the assessment and auditing of animal welfare across a range of farm and management conditions. It may also encourage innovation of animal care to emerge from the farm level. Let us consider space requirements. Stocking density, or space allotment per animal, has been one of the most contentious and debated issues in animal welfare. It is rare that a guideline, directive, law or standard would not specify a specific allotment of living space per animal. But does this resource-based measure accurately assess, for example, a broiler chicken's welfare?

Dawkins et al. (2004) published a ground-breaking study of how using a single resource-based measure, stocking density, may not be an effective welfare assessment criterion for broiler chickens. Subsequent studies addressing stocking density of broiler chickens reveal that measures of animal health (as an example) have not led to identifying a specific space allotment threshold that will assure good broiler health and welfare (see reviews by Dawkins, 2018; Estevez, 2007). Stocking density for many of the farm species presents the same challenge. It is not only the quantity of space that matters but a multitude of other factors play a role in determining the outcome for the animal including social behavior, animal genetics, quality of the designed environment, differences in farm management practices, etc. (Estevez, 2007).

Space is a complex issue and the use of a combination of outcome-based measures may be more effective in determining whether a farm has provided appropriate space considering the conditions, management practices, facilities, and type of animal it is raising. The drawback is that a single quantitative measure like stocking density is valued for its ease of use and its transparent uniform nature. Thus it should be replaced by environment- and outcome-based measures that can be reliably combined to assess the welfare outcomes for the animals across varying farm management and housing landscapes. And provide latitude for the farmer to find innovative ways to achieve good welfare for the animals. The most important point is that by using an outcomes-based approach it provides direct information about the animal's welfare state.

Ample opportunity exist for the use of outcome-based measures to help navigate differences in housing and management systems. Stringent resource-based measures validated in one type of system may not apply to newer designs. This is especially true for evolving laying hen, pig and dairy housing systems. However, for an outcomes-based approach to be successful the measures must be practical to use, validated through rigorous testing to determine if it reliably informs us about the welfare outcome its meant to measure, demonstrates high repeatability among assessors using the measure, and is not unduly influenced or changed by circumstances (Cook, 2018).

When properly tested and validated, outcomes-based approaches may relieve farmers from having to meet stringent one-size-fit all animal welfare standards and allow for the generation of innovative farm environments, management practices, and solutions to problems.

### 3. Conclusions

Animal welfare is an animal-based phenomenon. The primary social concerns and expectations are typically focused on the animal and the improvement of its welfare. To meet social expectations for the provision of a good quality of life for farm animal(s), outcomes-based measures have great potential to provide a high level of public assurance. They can be important purveyors of information on how farmers are meeting this public, and often legal, obligation through measuring the experience of the animal. This is one of many reasons that caused the shift of OIE toward the use of outcome-based measures to assure the welfare of animals (OIE, 2018b).

Outcomes based measures of animal welfare are currently in use in protocols developed for the on-farm assessment of animal welfare. Some measures are easier to assess than others. Scientific advancement in the assessment of farm animal welfare and practical information emerging from farms will continue to shape which types of measures or combinations thereof are best suited to determine the welfare status of farmed livestock. Environment-based measures (resources and management) will continue to play an important role in the assessment of animal welfare. When used in combination with outcomes-based measures a more holistic understanding of animal welfare develops.

Finally, animal welfare assessment protocols by their very nature must be living documents that require on-going review and revision to keep abreast of scientific advancement. And the practical feedback emerging from on-farm assessments will play an important role in the continuous improvement of farm animal welfare.

### References

- Berckmans, D. 2014. Precision livestock farming technologies for welfare management in intensive livestock systems. Review Scientific and Technical, Office International des Epizooties. 33, 189–196.
- Blatchford, R. 2017. Poultry welfare assessments: Current use and limitations. Animal Behavior and Well-Being Symposium. Journal of Animal Science. 95, 1382–1387. <https://dx.doi.org/10.2527/jas2016.0957>.
- Brambell, F.W.R. Report of the Technical Committee of Enquiry into the Welfare of Livestock kept under Intensive Conditions. HMSO: London, U.K. 1965.
- Butterworth, A. 2018. Chapter 6. Welfare assessment of poultry on farm. In: Advances in Poultry Welfare. Ed. J. A. Mench. Woodhead Publishing Series in Food Science Technology and Nutrition, Advances in Farm Animal Welfare series. Elsevier Ltd. UK. Pp 113–130.
- Casey-Trott, T.M., J. Heerkens, M.T. Petrik, P. Regmi, L. Schrader, M.J. Toscano and T.M. Widowski. 2015. Methods for assessment of keel bone damage in poultry. Poultry Science. 71, 461–472. <https://dx.doi.org/10.3382/ps/pev223>.
- Casey-Trott, T.M. and T.M. Widowski. 2016. Behavioral differences of laying hens with fractured keel bones within furnished cages. Frontiers of Veterinary Science. 3, 42. <https://dx.doi.org/10.3389/fvets.2016.00042>.
- Cook, N. 2018. Chapter 2. Assessment of cattle welfare: Common animal-based measures. In: Advances in Poultry Welfare. Ed. J. A. Mench. Woodhead Publishing Series in Food Science Technology and Nutrition, Advances in Farm Animal Welfare series. Elsevier Ltd. UK. Pp 27–53.
- de Jong, I.C., H. Ginnick, and J. van Harn. 2014. Wet litter not only influences foot pad dermatitis but also reduces overall welfare, technical performance and carcass yield in broilers. Journal of Applied Poultry Research. 23, 51–58.

- Dawkins M.S., C.A. Donnelly, and T.A. Jones. 2004. Chicken welfare is influenced more by housing conditions than by stocking density. *Nature*. 427, 342–344.
- de Jong, I.C., J. van Harn, H. Ginnick, V.A. Hindle, A. Lourens. 2012a. Foot pad dermatitis in Dutch broiler flocks: Prevalence and factors of influence. *Poultry Science*. 91, 1569–1547.
- de Jong, I.C., van Harn, H. Ginnick, A. Lourens. 2012b. Measuring footpad lesions in commercial broiler houses. Some aspects of methodology. *Animal Welfare*. 21, 325–330.
- Endres, M. 2017. The relationship of cow comfort and flooring to lameness disorders in dairy cattle. *Veterinary Clinics: Food Animal Practice*. 33, 227–233. <http://dx.doi.org/10.1016/j.cvfa.2017.02.007>
- Farm Animal Welfare Council (FAWC). Second Report on Priorities for Research and Development in Farm Animal Welfare; DEFRA: London, U.K. 1993.
- Green, T.C. and D.J. Mellor. 2011. Extending ideas about animal welfare assessment to include ‘quality of life’ and related concepts. *New Zealand Veterinary Journal*. 59, 316–324. <https://doi.org/10.1080/00480169.2011.610283>.
- Hartcher, K.M., S.J. Wilkerson, P.H. Hemsworth and G.M. Cronin. 2016. Severe feather pecking in non-cage hens and some associated and pre-disposing factors: A review. *World’s Poultry Science Journal*. 72, 103–114. <https://doi.org/10.1017/S0043933915002469>.
- Linares, J.A., S. Dougherty and S. Millman. 2018. Chapter 7. Poultry welfare assessment on the farm: Focusing on the individual. In: Advances in Poultry Welfare. Ed. J. A. Mench. Woodhead Publishing Series in Food Science Technology and Nutrition, Advances in Farm Animal Welfare series. Elsevier Ltd. UK. Pp 130–148.
- Mellor, D. 2017. Operational details of the Five Domains model and its key applications to the assessment and management of animal welfare. *Animals*. 7, 60. <https://doi.org/10.3390/ani7080060>.
- Mellor, D. 2016. Moving beyond the “Five Freedoms” by updating the “Five Provisions” and introducing aligned “Animal Welfare Aims”. *Animals*. 6, 59. <https://doi.org/10.3390/ani6100059>.
- Mench, J.A. 2008. Farm animal welfare in the USA: Farming practices, research, education, regulation and assurance programs. *Applied Animal Behaviour Science*. 113, 298–312. <https://doi.org/10.1016/j.applanim.2008.01.009>.
- OIE, 2018a. Article 7.1.2. Guiding principles for animal welfare. Chapter 7.1 Introduction to the Recommendations for Animal Welfare. OIE Terrestrial Animal Health Code 11/12/2018. P 1.
- OIE, 2018b. Article 7.1.4. Guiding principles for the use of measures of animal welfare. Chapter 7.1 Introduction to the Recommendations for Animal Welfare. OIE Terrestrial Animal Health Code 11/12/2018. P 2.
- Pairis-Garcia, M. and S. Moeller. 2018. The Common Swine Industry Audit: Future steps to assure positive on-farm animal welfare utilizing validated, repeatable and feasible animal based measures. *Animal Behavior and Well-Being Symposium. Journal of Animal Science*. 95, 1372–1381. <https://doi.org/10.2527/jas2016.0906>.
- Rushen, J., A. Butterworth and J.C. Swanson. 2011. Farm animal welfare assurance: Science and application. *Animal Behavior and Well-Being Symposium. Journal of Animal Science*. 89, 1219 –1228. <https://doi.org/10.2527/jas2010.3589>.
- Saraiva, S., C. Saraiva and G. Stilwell. 2016. Feather conditions and clinical scores as indicators of broiler welfare at the slaughterhouse. *Research in Veterinary Science*. 107, 75–79. <http://doi.org/10.1016/j.rvsc.2016.05.005>.
- Sassi, N.B., X. Averos and I. Estevez. 2016. Review. Technology and poultry welfare. *Animals*. 6, 62. <https://doi.org/10.3390/ani6100062>.
- Temple, D., P. Llonch, E. Mainau and X. Manteca. 2018. Chapter 12. On-farm and post-mortem health assessment. In: Advances in Pig Welfare. Ed. M. Spinka. Woodhead Publishing Series in Food Science Technology and Nutrition, Advances in Farm Animal Welfare series. Elsevier Ltd. UK. Pp 357–379.
- Webster, J. 2016. Opinion: Freedoms, Dominions and “A life worth living”. *Animals* 6, 35. <https://doi.org/10.3390/ani606>.
- Welfare Quality®. Welfare Quality® Assessment Protocol for Poultry (broilers, laying hens). Welfare Quality® Consortium. Lelystad, The Netherlands. 2009a.
- Welfare Quality®. Welfare Quality® Assessment Protocol for Pigs. Welfare Quality® Consortium. Lelystad, The Netherlands. 2009b.
- Welfare Quality®. Welfare Quality® Assessment Protocol for Cattle. Welfare Quality® Consortium. Lelystad, The Netherlands. 2009c.
- Winder, C.B., J.M. Sargeant, A. Novy, C.M. Logue, Y. Sato and A. O'Connor. 2018. The efficacy of litter management to prevent disease and/or antibiotic use in broiler poultry: A protocol for a systematic

review. Veterinary Diagnostic and Production Animal Medicine Reports. 20. Iowa State University. [https://lib.dr.iastate.edu/vdpam\\_reports/20](https://lib.dr.iastate.edu/vdpam_reports/20).

Zinpro. First Step® Locomotion Scoring of Dairy Cattle. 2019a. <https://www.zinpro.com/lameness/dairy/locomotion-scoring>. Accessed June 28, 2019.

Zinpro. Feet First® Swine Locomotion Scoring System. 2019b. <https://www.zinpro.com/lameness/swine/locomotion-scoring>. Accessed June 28, 2019.

# Impacts of Exercise or Pasture Access on the Welfare of Transition Dairy Cows

Peter D. Krawczel \*, Ramdi A. Black

Department of Animal Science, The University of Tennessee, Knoxville, TN 37996, USA

\* Corresponding author. Email: [krawczel@utk.edu](mailto:krawczel@utk.edu)

## Abstract

Transition cows are the cows most susceptible to disease and prevalence has not changed over the past decade. However, increased physical activity during late gestation may represent a management option to improve transition. Therefore, the objectives of this study were to determine the effect of exercise, pasture turnout, or total confinement on physical fitness, behavior, and horn growth and wear and sole thickness during the dry period. Pasture turnout tended to reduce anaerobic metabolism 60 min after exercise and exercise and pasture turnout resulted in less variable heart rate during and after exercise compared with confined cows. Physical activity during late gestation may allow cows to maintain a certain level of fitness. Physical activity did not alter behavior during the dry period. Exercise cows experienced greater hind hoof horn wear than confined and pasture cows but had more equal rates of horn growth and wear. Sole thickness was not altered with exercise or pasture turnout but tended to increase for cows in total confinement. Future research should investigate the impact of pasture turnout during periods cows are more active to increase the level of physical activity.

**Keywords:** Physical fitness, behavior, calving, hoof health

## 1. Introduction

Consumers are increasingly concerned about how their food is raised and produced (Frewer et al., 2005). While access to pasture may address this concern by providing what could be viewed as a more natural life to cattle, further benefits may be gained by an increase in physical activity from greater access to pasture. This gain might be generated primarily from improved physical fitness resulting from increased physical activity. Barker et al. (1975) exercised prepartum heifers 4-to-8-wk a distance of 1.6 km at 5.5 km h<sup>-1</sup>, which improved ease of parturition, placental release, and feed efficiency in these heifers. Davidson and Beede (2009) exercised late-gestation, non-lactating dairy cows and observed that exercised cows, from use of a mechanical walker, had lower heart rates (HR) during an exercise challenge on a treadmill, returned to resting HR quicker, and had lower L-lactate concentrations during and following exercise challenge relative to non-exercised paired controls. While this suggests controlled exercise can improve physical fitness, the approach used to achieve this gain is not practical on commercial dairy farms due to required labor. Alternative management strategies that increase overall physical activity, such as pasture access, provide a more reasonable approach to achieve this end for dairy producers.

A reduction in the occurrence of disease during the first two weeks of lactation was reported when tie-stall housed cows were provided daily access to pasture (Gustafson, 1993). Gustafson (1993) walked cows out to pasture 1 km per d, allowing cows to walk back to the barn over the following 2 h, and, while physical activity was not intense, cows still benefited from this low intensity activity. Further, providing outdoor access to tie-stall cows resulted fewer hock lesions, fewer lame cows, and lower mastitis prevalence (Popescu et al., 2013).

The majority of US dairy cattle are housed in confinement (tie stalls, stanchions, or freestall barns with no access to pasture; 58.9%; USDA, 2016), which offer little access to exercise other than walking to the milking parlor, waterer, feed resources, and social interactions. With the majority of cows housed on concrete flooring (55.6%), few cows have access to softer standing surfaces such as rubber flooring (13.9%), dirt (20%), or pasture (5.1%; USDA, 2010). Concrete flooring can often result in unequal hoof horn growth and wear and heel erosion (Hahn et al., 1986, van Amstel et al., 2016). Standing and walking on hard surfaces (Greenough and Vermunt,

1991) and walking along rough cow tracks (Chesterton et al., 1989) can negatively impact lameness. However, offering cows access to softer surfaces can improve hoof health.

Transitioning to pasture housing for 3 weeks was sufficient to improve locomotion compared with a total confined control group (Hernandez-Mendo et al., 2007), which may be related to increased activity, as cows housed on pasture are more active than those in confinement (Hernandez-Mendo et al., 2007, Legrand et al., 2009, Black and Krawczel, 2016). Cows given access to exercise 2× or 7× per week tended to have a shorter claw diagonal than non-exercised cows kept in tie-stalls on rubber mats (Loberg et al., 2004). Shorter and steeper claws show less susceptibility to disease (Politiek et al., 1986) and may be improved with increased physical activity. Therefore, allowing cows access to increased physical activity through pasture turnout may improve hoof health while walking cows excessively on concrete or hard surfaces may lead to negative hoof outcomes.

Pasture access may be a more viable management decision, resulting in similar health benefits to an exercise routine through improved physical fitness; however, a direct comparison of exercise and pasture access has not yet been studied. The objective of this study was to determine the effect of daily exercise, pasture access, or total confinement on physical fitness, behavior, and hoof health during the dry period.

## 2. Materials and Methods

### 2.1. Animals, housing, and management

Twenty-nine primiparous and 31 multiparous, pregnant, non-lactating Holstein ( $n = 58$ ) and Jersey-Holstein crossbred ( $n = 2$ ) dairy cows were assigned to either control ( $n = 20$ ), exercise ( $n = 20$ ), or pasture ( $n = 20$ ) treatments at dry-off using rolling enrollment from January to November 2015. Cows were balanced on parity ( $1.8 \pm 0.9$ ), projected ME FCM ( $13,831 \pm 2,028$  kg per lactation), and projected calving date. Cows were managed with a 60-d dry period ( $58.5 \pm 5.4$  d) divided into far-off (dry-off to 2 weeks before parturition) and close-up periods (two weeks before projected parturition).

Cows were housed in a naturally ventilated, 4-row, head-to-head freestall barn with drive-through feed bunk at the University of Tennessee's Little River Animal and Environmental Unit (Walland, TN). Deep-bedded sand freestalls were 2.4 m long and 1.2 m wide with a 1.2 m high neck rail positioned 1.7 m from the curb and a 0.6 m high PVC tube brisket board placed 1.7 m from the curb. Fresh sand was added once per week with manure removed from stalls twice daily before milking the lactating herd (0730 and 1730 h). Fans turned on automatically when temperatures rose above 23 °C. Throughout the study period, study cows were housed in with pens measuring 12.1 m wide and 19.4 m long, enclosing 24 freestalls and 26 0.6 m wide headlocks, and containing 2 waterers, one on each end. Study cows were comingled unless the pen was split into far-off and close-up groups, leaving 12 freestalls and 13 headlocks for each group. Cows were maintained below 80% stocking density, based headlock and freestall availability.

Cows were fed twice daily at 0730 and 1530 h. Far-off cows were fed a TMR from dry-off to two weeks before projected parturition consisting of 4.5 kg ryegrass hay, 3.4 kg orchardgrass hay, 2.3 kg corn silage, and 2.7 kg dry cow grain per cow per day. Close-up cows were fed a TMR up to parturition consisting of 3.6 kg orchardgrass hay, 1.8 kg clover, 11.3 kg corn silage, and 3.0 kg dry cow grain per cow per day. All cows had ad lib access to water, except exercise treatment cows during exercise.

### 2.2. Experimental treatments

Before enrollment, all cows had been housed in the same freestall barn with no previous experience with exercise, aside from pasture access during the dry period before the previous calving. Cows were enrolled into treatments on the day of dry-off. Cows assigned to control remained in the pen at all times, except for general management reasons (i.e. cleaning, rebedding

stalls) when cows were moved to an adjacent lane for a maximum of 30 min. Cows were permitted to eat, drink, and move around the pen during exercise times. Cows assigned to exercise were removed from the pen 5× per week, Monday through Friday, and walked for at targeted 1.5 h at  $3.25 \text{ km h}^{-1}$  beginning at 1200 h along the path denoted by a dashed black line in, measuring 250 m for each lap. Cows were walked in a group using the cows' flight zones and implements (i.e. rattle paddle) to encourage walking. Exercise pace was calculated by the total exercise time divided by the distance walked. During periods of high heat load, determined subjectively through cow heat stress behavior (i.e. increased respiration rate, panting) and exerciser comfort, cows were offered water at the point where the walking path met the entrance to the milking parlor from a 19 L bucket. Cows did not have access to feed during the exercise period.

Cows on pasture were moved into a 2.11 hectare pasture (Pasture 1) from January to April 2015 and a 0.42 hectare pasture (Pasture 2) from April to December 2015 5× per week, Monday to Friday. Pasture 1 was 330 m from the barn to the pasture gate while Pasture 2 was 15 m from the barn to the pasture gate. Pasture 1 had rolling hills and a 0.75 hectare wooded area while pasture 2 had a shade structure and trees around one side of the fence line. Both pastures were seeded with orchardgrass and KY-31 fescue and managed by the farm manager for a height of 0.3 to 0.5 m. Cows were put on pasture before and returned to the barn after exercising cows from the exercise treatment group. Cows were put on pasture for a target of 1.5 h, excluding travel time to and from the paddock, beginning at 1200 h. Both pastures had access to water and grass.

To assess fitness, all cows were subjected to an exercise challenge at dry-off and 42 d after dry-off. During the exercise challenge, challenged cows and exercise treatment cows were exercised simultaneously.

### 2.3. Blood sampling

On d 0 and 42, cows were moved into a palpation chute and fitted with an indwelling jugular catheter the morning before exercise challenge. Cows were released back into their pen until 10 min prior to exercise where they were either restrained in the headlocks in the pen or moved to the palpation chute for blood collection. After exercise, cows were moved back into the palpation chutes for blood collection. Ten minutes prior to exercise, immediately after, and 60 min after exercise, 8 mL of blood were collected into 20 mL syringes and immediately transferred to a 6 mL sodium heparin blood tube (BD Vacutainer, BD, Franklin Lakes, NJ) and 2 mL potassium oxalate/sodium fluoride blood tube (BD Vacutainer, BD, Franklin Lakes, NJ). An additional 2 mL of blood was collected into 20 mL syringes 3, 6, 9, 12, and 15 min following exercise and immediately transferred into a 2 mL potassium oxalate/sodium fluoride blood tube.

After collection, sodium heparin blood tubes were centrifuged, plasma separated into microcentrifuge tubes, and tubes frozen at -80 °C. Plasma total cortisol concentration was determined by a radioimmunoassay procedure using a commercially available kit (ImmunChem Cortisol 125 | RIA Kit, BP Biomedical, LLC, Orangeburg, NY). Inter- and intra-assay CV for the low control (7 ng mL<sup>-1</sup>) was 42.9% and 47.6%, respectively, and 13.7% and 13.8%, respectively, for the high control (25 ng mL<sup>-1</sup>). A 0.2 mL whole blood sample from potassium oxalate/sodium fluoride blood tubes was used to determine L-lactate concentration using the Lactate Scout (range: 0.5 to 25 mmol L<sup>-1</sup>; EKF Diagnostics GmbH, Mannheim, Germany) (Burfeind and Heuwieser, 2012). The meter would not read below 0.5 mmol L<sup>-1</sup>, therefore, all samples that read as low (<0.5 mmol L<sup>-1</sup>) were removed (68.2% of all recorded data).

### 2.4. Heart rate

On d 0 and 42, cows were fitted with a wireless electrocardiogram monitor (Polar V800, Polar Electro, Port Washington, NY) after catheter insertion to monitor HR. Hair was clipped from the left wither down to the left elbow, approximately 7.5 cm wide, and the area drenched with water to allow increased contact between the skin and monitor electrodes. Heart rate was recorded every 1 s to a watch attached to the band at the right wither. Data were recorded for 10 minutes preceding exercise challenge, the entire length of exercise challenge, and the following 60 min.

## 2.5. Behavior

Cows were fitted with accelerometers (IceTag, IceRobotics, Edinburgh, Scotland) 3 d prior to dry-off. Activity was summarized by day from dry-off to the day prior to calving into lying time ( $\text{h d}^{-1}$ ), lying bout frequency (bouts  $\text{d}^{-1}$ ), lying bout duration (min bout $^{-1}$ ), and steps ( $n \text{ d}^{-1}$ ). All lying bouts under 2 min were removed (Endres and Barberg, 2007)

## 2.6. Hoof measures

Hoof growth and wear and sole thickness were measured on d 2 and 44, relative to dry-off. Cows were moved into a mobile, stand-up leg chute between 1000 and 1100 h before daily treatments were imposed. Only the rear hooves were measured, as rear hooves show greater wear and growth patterns and would display more difference over 42 d than front hooves (Hahn et al., 1986). To measure hoof growth and wear, each back claw was grooved horizontally and vertically using a power file, according to van Amstel et al. (2016). Grooves were ground at a 1 mm depth to ensure grooves did not extend past the hoof wall or fade before the lines were measured at d 44. The first vertical line (line B) was ground parallel to the heel, midway between the heel and toe. The second vertical line (line A) was ground parallel to the heel between the first line and the toe. The horizontal line was ground just below the periople of the coronary band. After grooving, the following measures were taken: coronary band to horizontal line using line B (B1), coronary band to horizontal line using line A (A1), horizontal line to edge of the hoof wall using line B (B2), and horizontal line to the edge of the hoof wall using line A (A2). Line segments were used using a ruler (accurate to 0.1 mm) on d 2 and 44. Caudal and cranial growth and wear were calculated using calculations described by van Amstel et al. (2016).

Sole thickness was measured using a 7.0-MHz curvilinear probe on each day, as described by van Amstel et al. (2004). Hooves were cleaned off using a brush with water and alcohol applied to the sole to improve probe contact. The probe was placed approximately 3.75 cm below the apex of the toe and on the inside of the abaxial line. Sole thickness was measured as the area between the outer margin of the ultrasound image and the inner sole seen as a thin continuous hyperechoic Kofler et al. (1999). All four rear claws were measured.

## 2.7. Statistical analyses

The experimental and observational units of this study were the cow. Data were analyzed using the MIXED procedure of SAS (SAS 9.4, SAS Inst., Cary, NC). Cow within treatment was considered a random variable. Explanatory variables included day (d 0 to 58 relative to dry-off), treatment (control, exercise, pasture), and their interaction to analyze lying behaviors (lying time, lying bout frequency, lying bout duration, steps). Finally, explanatory variables included treatment and day (d 0 and 42 relative to dry-off, d 0, 7, 14, 28, and 60 relative to calving) and their interaction to analyze their effect on BCS and gait score.

Mean, max, and min HR were determined using PROC MEANS of SAS (SAS 9.4, SAS Inst., Cary, NC), with results reported as means  $\pm$  SD. The observational and experimental unit of this study was the cow. Data were analyzed using PROC MIXED of SAS. Cow within treatment and exercise challenge day was considered random in all models. Explanatory variables included treatment (control, exercise, pasture), exercise challenge day (d 0 and 42), time (lactate: -10, 0, 3, 6, 9, 12, 15, and 60 min), and exercise pace. Explanatory variables and all interactions between explanatory variables were tested ( $P < 0.05$ ) using backward elimination. Resulting values are reported as least squares means  $\pm$  SE.

Cow within treatment was considered a random variable. Explanatory variables included treatment (control, exercise, pasture) to analyze hoof growth and wear. Sole thickness was analyzed using treatment, day (d 2 and 44), and their interactions as explanatory variables. Results are reported as least squares means  $\pm$  SE. A paired TTEST procedure in SAS was used to determine if hoof horn growth and wear were different on the cranial and caudal aspects of the hoof for each treatment. Results are reported as mean  $\pm$  SE. Means are considered different at  $P$

$\leq 0.05$  and a tendency at  $P \leq 0.10$ .

### 3. Results and Discussion

#### 3.1. Treatments

Exercise cows walked for  $1.4 \pm 0.1$  h at  $1.88 \pm 0.58$  km  $h^{-1}$ . Exercise periods began, on average, at 12:18:50 h, ranging from 10:12 to 14:39 h, and, on average, ended at 13:43:11, ranging from 11:16 to 16:03 h. Pasture cows spent a mean of  $2.0 \pm 0.3$  h on Pasture 1, entering the pasture, on average, at 12:55:58 h, ranging from 11:24 to 14:41 h, and, on average, exiting the pasture at 14:56:17 h, ranging from 13:56 to 17:12 h. Cows spent a mean of  $1.7 \pm 0.3$  h on Pasture 2, entering the pasture, on average, at 11:58:40 h, ranging from 10:04 to 14:32 h, and, on average, exiting the pasture at 13:40:01, ranging from 11:21 to 16:07 h. On exercise challenge days, cows were walked  $3.1 \pm 0.7$  km over  $1.4 \pm 0.1$  h at a pace of  $2.16 \pm 0.45$  km  $h^{-1}$ .

#### 3.2. Exercise challenge

L-lactate concentrations did not differ by treatment (control:  $0.92 \pm 0.09$  mmol L $^{-1}$ ; exercise:  $0.98 \pm 0.08$  mmol L $^{-1}$ ; pasture:  $0.84 \pm 0.10$  mmol L $^{-1}$ ;  $P = 0.54$ ), day (d 0:  $0.92 \pm 0.08$  mmol L $^{-1}$ ; d 42:  $0.91 \pm 0.07$  mmol L $^{-1}$ ;  $P = 0.90$ ), time (-10 min:  $0.99 \pm 0.09$  mmol L $^{-1}$ ; 0 min:  $0.88 \pm 0.10$  mmol L $^{-1}$ ; 3 min:  $0.88 \pm 0.11$  mmol L $^{-1}$ ; 6 min:  $0.89 \pm 0.12$  mmol L $^{-1}$ ; 9 min:  $0.71 \pm 0.13$  mmol L $^{-1}$ ; 12 min:  $0.90 \pm 0.13$  mmol L $^{-1}$ ; 15 min:  $0.98 \pm 0.09$  mmol L $^{-1}$ ; 60 min:  $1.08 \pm 0.10$  mmol L $^{-1}$ ;  $P = 0.45$ ), or pace ( $P = 0.50$ ).

The walking challenge did not alter L-lactate concentrations and no groups increased over a mean concentration of 1.0 mmol L $^{-1}$ , which may suggest that no group entered a period anaerobic metabolism. Conversely, an increase of 3.25 mmol L $^{-1}$  in L-lactate from the start to end of a 1 h treadmill exercise test, changing from 0.68 to 3.94 mmol L $^{-1}$  in non-pregnant, non-lactating dairy cows was evident when cows were subjected to a challenge on a mechanical walker Davidson and Beede (2003). Pregnant, non-lactating dairy cows exercised 3.25 km  $h^{-1}$  for 1.25 to 1.5 h every other day for 70 d experienced a change in response to exercise with an increase in lactate of 3.3 mmol L $^{-1}$  on d 0 to an increase of 1.7 mmol L $^{-1}$  on d 60 (Davidson and Beede, 2009). Simmental oxen worked 1 h three times a week doing draft work experienced an increase in lactate from 0.81 to 3.60 mmol L $^{-1}$  during exercise (Zanzinger and Becker, 1992). In the current study, cows walked considerably slower ( $2.16 \pm 0.45$  km  $h^{-1}$ ) than in previous evaluations of physical fitness or exercise (Anderson et al., 1979, Davidson and Beede, 2003, Davidson and Beede, 2009). This suggests the pace of the challenge in the current study did not present a sufficient workload to shift cows into an anaerobic effort. Using a low stress method of exercise execution prevented cows from experiencing chronic stress, which can cause hyper-reactivity of the adrenal cortex to other stressors (Broom, 1988), exaggerating issues during periods of immunosuppression, such as calving (Aleri et al., 2016). While this method may have prevented cows from experiencing anaerobic metabolism, it also prevented cows from experiencing negative impacts of chronic stress.

Mean HR during exercise stayed similar from d 0 to d 42 for exercise and pasture cows but increased for control cows. This may allude to maintenance of cardiac capacity in pasture and exercise compared with control. However, mean HR did not increase meaningfully from the pre-exercise to exercise periods, indicating cows did not increase their workload enough to initiate a strong cardiac response. In the current study, mean HR during exercise are lower than those previously reported during an exercise challenge (Davidson and Beede, 2003, Davidson and Beede, 2009), ranging between 170 to 182 bpm. During those studies, cows were subjected to greater workloads with walking speeds of 5 km  $h^{-1}$  using a treadmill with incline. In the current study, cows did not experience similar workloads to induce a similar cardiac change.

#### 3.3. Behavior

Treatment and treatment  $\times$  day did not affect lying time ( $P \geq 0.12$ ; or lying bout frequency ( $P \geq 0.12$ ) though both were affected by day ( $P < 0.0001$ ). Cows laid down for the least amount of

time and had the fewest lying bouts on d 0 and 58, relative to dry-off. A treatment  $\times$  day effect existed for lying bout duration ( $P = 0.01$ ) and steps ( $P < 0.0001$ ). Exercise cows took the most steps during exercise days ( $P < 0.0001$ ), compared with pasture and control, except for d 0 and 42 where all cows were exercised. Pasture cows took more steps than control cows on turnout days ( $P < 0.10$ ). All cows took a similar number of steps during the 2 d when treatments were not applied (Saturday and Sunday;  $P > 0.10$ ). Control cows had longer lying bouts on d 19 and shorter lying bouts on d 51 compared with exercise and pasture cows ( $P \leq 0.04$ ), longer lying bouts on d 22 and shorter lying bouts on d 25 compared with pasture cows ( $P \leq 0.03$ ), and shorter lying bouts on d 56 compared with exercise cows ( $P < 0.01$ ). Pasture and exercise cows had similar lying bout durations throughout the dry period ( $P > 0.05$ ).

It was predicted that exercise cows would have a greater number of steps on exercise days than control groups. However, pasture cows did not experience the same level of physical activity as those exercised, potentially due to environment (i.e. heat, snow) or distance from the barn. Cows were only required to walk a maximum of 330 m to the paddock (660 m roundtrip) from January to April and 15 m to the paddock (30 m roundtrip) from April to December, which is less than the 2 and 3 km implemented to see changes in health in a previous study (Gustafson, 1993). Cows were free to move once in the paddock, but, due to the time of treatment implementation (average: 11:58:40 to 13:40:01 h), cows may have been less willing to walk and explore due to heat load during warmer months and snow cover during colder months. However, even when kept on pasture during the entire dry period, cows only walked between 3,000 and 2,300 steps per day during the far-off and close-up periods, respectively (Black and Krawczel, 2016), which was reached by cows in the current study, indicating cows were hyperactive during turnout compared with cows regularly housed on pasture. Addition of resources that require more travel (i.e. water located further away, feed supplement, heifers/calves in adjacent pen) may encourage cows to participate in more physical activity. Further, turnout during the cooler evening hours may encourage activity, as this is when cows are more likely to graze (Walker et al., 2008) and prefer to be on pasture (Legrand et al., 2009).

Treatment did not affect lying time or lying bout duration and frequency, which is contradictory to previous research where pasture cows spent less time lying during the dry period than confined cows (Black and Krawczel, 2016). This was likely due to a portion of pasture cows' diets coming from grazing, where, while cows could graze in the current study, it is not assumed that a significant proportion of the diet came from grazing; however, this was not measured. In the current study, cows typically spent less than 2 h on pasture and this may not have been enough time to alter their time budget while in the barn.

### 3.4. Hoof measurements

Five cows were excluded from hoof growth and wear and sole thickness data (control = 1, exercise = 2, pasture = 2) as cows' hooves were trimmed before d 42 of the study. Treatment did not affect cranial horn growth (control:  $0.97 \pm 0.08$  mm; exercise:  $1.11 \pm 0.08$  mm; pasture:  $0.97 \pm 0.08$  mm;  $P = 0.40$ ) or caudal horn growth (control:  $1.02 \pm 0.09$  mm; exercise:  $1.23 \pm 0.10$  mm; pasture:  $1.01 \pm 0.10$  mm;  $P = 0.20$ ). Cranial horn wear was greater for exercise cows ( $1.08 \pm 0.06$  mm) than control ( $0.69 \pm 0.06$  mm) and pasture cows ( $0.76 \pm 0.06$  mm;  $P < 0.0001$ ). Caudal horn wear was greater for exercise cow ( $1.05 \pm 0.06$  mm) than control ( $0.69 \pm 0.05$  mm) and pasture cows ( $0.77 \pm 0.05$  mm;  $P < 0.0001$ ). Growth and wear did not differ on the cranial aspect of the horn for exercise cows (difference:  $0.03 \pm 0.08$  cm;  $P = 0.72$ ); however, the caudal aspect of the horn tended to grow  $0.18 \pm 0.10$  cm more than the horn wore ( $P = 0.08$ ). Horn growth was greater for the cranial and caudal aspect of the horn in pasture ( $0.22 \pm 0.06$  and  $0.24 \pm 0.06$  cm, respectively;  $P < 0.001$ ) and control cows ( $0.28 \pm 0.06$  and  $0.33 \pm 0.06$  cm;  $P < 0.0001$ ). Sole thickness tended to be affected by treatment  $\times$  day ( $P = 0.07$ ) where control cows tended to increase sole thickness from d 2 to d 44.

Exercise cows experienced a more even horn growth and wear rate compared with control

and pasture cows. Normal claws are characterized by equal rates of growth and wear (Vermunt and Greenough, 1995) and an imbalance can cause horn lesions (Bazeley and Pinsent, 1984, Greenough and Vermunt, 1991). Increased horn growth and wear can occur when housed on concrete compared with a softer surface, such as a rubber mat (van Amstel et al., 2016). Further, walking surface may be even more important around calving when horn quality is weakened from systematic changes with calving and lactogenesis, increasing the likelihood of white line disease and horn lesions (Webster, 2001). The current study, however, determined that regular exercise of cows on concrete contributed to an improved growth and wear rate of the horn, potentially improving hoof health. This is in contrast to previous research indicating improved hoof characteristics and health with access to pasture or a straw yard (Hahn et al., 1986). This may indicate that, during the dry period, additional locomotor activity on a concrete surface does not impair the hoof health of cows. However, it should be noted that the current study did not record hoof disorders, such as horn lesions, white line disease, or other disorders caused by environmental factors, and additional work looking at hoof disorders is needed to fully understand the interaction of exercise and hoof health.

Walking on concrete has been previously associated with thin soles (van Amstel et al., 2006). Soles provide protection to the claw capsule (Toussaint Raven, 1989) and thin soles are more prone to injury and contusion, particularly in environments with hard or irregular surfaces (Toussaint Raven, 1989). However, neither exercised nor pasture cow experienced a reduction in sole thickness, illustrating that the exercise and pasture regimens used did not have a negative impact on hoof health. Control cows did experience a tendency to increase sole thickness, but all cows were above the minimum of 7 mm to provide adequate protection to the claw capsule (Toussaint Raven, 1989).

#### 4. Conclusions

Physical activity during the dry period may help cows maintain a minimum level of physical ability during a relatively sedentary period of life. Exercise and pasture turnout increased daily steps over control without negatively affecting lying behaviors. Exercise cows experienced greater hind hoof horn wear than control and pasture cows but had more equal rates of horn growth and wear. Sole thickness was not altered with exercise or pasture turnout but tended to increase for cows in total confinement and all cows remained above the minimum thickness to provide adequate protection to the claw capsule. Further research into the consequence of physical inactivity on cow performance and health and how pasture turnout may help alleviate inactivity should be pursued.

#### References

- Aleri, J. W., B. C. Hine, M. F. Pyman, P. D. Mansell, W. J. Wales, B. Mallard, and A. D. Fisher. 2016. Periparturient immunosuppression and strategies to improve dairy cow health during the periparturient period. Research in Veterinary Science. 108:8–17.
- Anderson, M. J., R. C. Lamb, and J. L. Walters. 1979. Effect of prepartum exercise on feed intake and milk production of multiparous cows. Journal of Dairy Science. 62(9):1420–1423.
- Barker, B. O., R. C. Lamb, and C. H. Mickelsen. 1975. Effect of prepartum exercise on first calf heifers. Journal of Dairy Science. 58(5):749.
- Bazeley, K. and P. J. Pinsent. 1984. Preliminary observations on a series of outbreaks of acute laminitis in dairy cattle. Veterinary Record. 115(24):619–622.
- Black, R. and P. Krawczel. 2016. A case study of behaviour and performance of confined or pastured cows during the dry period. Animals 6(7):41.
- Broom, D. M. 1988. The scientific assessment of animal welfare. Appl. Anim. Behav. Sci. 20(1):5–19.
- Burfeind, O. and W. Heuwieser. 2012. Validation of handheld meters to measure blood l-lactate concentration in dairy cows and calves. Vet. Rec. 95(11):6449–6456.
- Chesterton, R. N., D. U. Pfeiffer, R. S. Morris, and C. M. Tanner. 1989. Environmental and behavioural factors affecting the prevalence of foot lameness in New Zealand dairy herds — a case-control study. New Zealand Veterinary Journal 37(4):135–142.

- Davidson, J. A. and D. K. Beede. 2003. A system to assess fitness of dairy cows responding to exercise training. *Journal of Dairy Science*. 86(9):2839–2851.
- Davidson, J. A. and D. K. Beede. 2009. Exercise training of late-pregnant and nonpregnant dairy cows affects physical fitness and acid-base homeostasis. *Journal of Dairy Science*. 92(2):548–562.
- Endres, M. I. and A. E. Barberg. 2007. Behavior of dairy cows in an alternative bedded-pack housing system. *Journal of Dairy Science*. 90(9):4192–4200.
- Frewer, L. J., A. Kole, S. M. A. V. d. Kroon, and C. d. Lauwere. 2005. Consumer attitudes towards the development of animal-friendly husbandry systems. *Journal of Agricultural and Environmental Ethics*. 18(4):345–367.
- Greenough, P. R. and J. J. Vermunt. 1991. Evaluation of subclinical laminitis in a dairy herd and observations on associated nutritional and management factors. *Veterinary Record*. 128(1):11–17.
- Gustafson, G. M. 1993. Effects of daily exercise on the health of tied dairy cows. *Preventive Veterinary Medicine*. 17(3–4):209–223.
- Hahn, M. V., B. T. McDaniel, and J. C. Wilk. 1986. Rates of hoof growth and wear in Holstein cattle. *Journal of Dairy Science*. 69(8):2148–2156.
- Hernandez-Mendo, O., M. A. G. von Keyserlingk, D. M. Veira, and D. M. Weary. 2007. Effects of pasture on lameness in dairy cows. *Journal of Dairy Science*. 90(3):1209–1214.
- Kofler, J., P. Küpper, and W. Henninger. 1999. Ultrasonographic imaging and thickness measurement of the sole horn and the underlying soft tissue layer in bovine claws. *The Veterinary Journal*. 157(3):322–331.
- Legrand, A. L., M. A. G. von Keyserlingk, and D. M. Weary. 2009. Preference and usage of pasture versus free-stall housing by lactating dairy cattle. *Journal of Dairy Science*. 92(8):3651–3658.
- Loberg, J., E. Telezhenko, C. Bergsten, and L. Lidfors. 2004. Behaviour and claw health in tied dairy cows with varying access to exercise in an outdoor paddock. *Applied Animal Behavior Science*. 89(1–2):1–16.
- Političek, R. D., O. Distl, T. Fjeldaas, J. Heeres, B. T. McDaniel, E. Nielsen, D. J. Peterse, A. Reurink, and P. Strandberg. 1986. Importance of claw quality in cattle: Review and recommendations to achieve genetic improvement. Report of the E.A.A.P. working group on “claw quality in cattle”. *Livestock Production Science*. 15(2):133–152.
- Popescu, S., C. Borda, E. A. Diugan, M. Spinu, I. S. Groza, and C. D. Sandru. 2013. Dairy cows welfare quality in tie-stall housing system with or without access to exercise. *Acta Veterinaria Scandinavica*. 55(1):43.
- Toussaint Raven, E. 1989. Structure and function. Pages 24–26 in *Cattle Foot Care and Claw Trimming*. Farming Press, Ipswich, UK.
- USDA. 2016. Dairy cattle management practices in the United States, Dairy 2014. USDA-APHIS-VS, CEAH, Fort Collins, CO.
- van Amstel, S., C. Young, C. Scully, and B. Rohrbach. 2016. Comparison of the rate of claw horn growth and wear and sole thickness in dairy cattle housed in a free stall barn with concrete and rubber flooring. *PeerJ Preprints* 4(e2061v1).
- van Amstel, S. R., J. K. Shearer, and F. L. Palin. 2004. Moisture content, thickness, and lesions of sole horn associated with thin soles in dairy cattle. *Journal of Dairy Science*. 87(3):757–763.
- van Amstel, S. R., J. K. Shearer, F. L. Palin, J. Cooper, and G. Rodgers. 2006. The effect of parity, days in milk, season and walking surface on thin soles in dairy cattle. Pages 142–143 in *Proc. 14th International Symposium and 6th Conference on Lameness in Ruminants*, Colonia del Sacramento, Uruguay.
- Vermunt, J. J. and P. R. Greenough. 1995. Structural characteristics of the bovine claw: Horn growth and wear, horn hardness and claw conformation. *British Veterinary Journal* 151(2):157–180.
- Walker, S. L., R. F. Smith, J. E. Routly, D. N. Jones, M. J. Morris, and H. Dobson. 2008. Lameness, activity time-budgets, and estrus expression in dairy cattle. *Journal of Dairy Science*. 91(12):4552–4559.
- Webster, A. J. 2001. Effects of housing and two forage diets on the development of claw horn lesions in dairy cows at first calving and in first lactation. *The Veterinary Journal*. 162(1):56–65.
- Zanzinger, J. and K. Becker. 1992. Blood parameters in draught oxen during work: Relationship to physical fitness. *Comparative Biochemistry and Physiology*. A 102(4):715–719.

# **Optimisation of Environment-Animal-Welfare Interactions in High-Performance Dairy Cows Housed in Naturally Ventilated Barns**

**Thomas Amon<sup>a,b,\*</sup>, Qianying Yi<sup>a</sup>, Julia Heinicke<sup>a</sup>, Severino Pinto<sup>a,b</sup>, Gundula Hoffmann<sup>a</sup>, Sabrina Hempel<sup>a</sup>, Theresa Müschner Siemens<sup>a</sup>, David Janke<sup>a</sup>, Christian Ammon<sup>a</sup>, Barbara Amon<sup>c,d</sup>**

<sup>a</sup> Department of Engineering for Livestock Management, Leibniz Institute for Agricultural Engineering and Bioeconomy (ATB), Potsdam 14469, Germany

<sup>b</sup> Department of Veterinary Medicine, Free University Berlin, Berlin 14163, Germany

<sup>c</sup> Department of Technology Assessment and Substance Cycles, Leibniz Institute for Agricultural Engineering and Bioeconomy (ATB), Potsdam 14469, Germany

<sup>d</sup> Faculty of Civil Engineering, Architecture and Environmental Engineering, University of Zielona Góra, Zielona Góra 65-417, Poland

\* Corresponding author. Email: [tamon@atb-potsdam.de](mailto:tamon@atb-potsdam.de)

## **Abstract**

The Leibniz Institute for Agricultural Engineering and Bioeconomy (ATB) works on a range of interdisciplinary and transdisciplinary basic and applied research projects which deal with emissions, animal welfare and veterinary issues. Through active participation in Food and Agriculture Organization (FAO) of the United Nations, The Intergovernmental Panel on Climate Change (IPCC), The United Nations Economic Commission for Europe (UNECE), and European Union (EU) Commission initiatives, ATB research is closely linked to international activities. In this paper, the main focus is on the research of livestock-environment interactions. Firstly, potentials of digitisation, e.g. by means of sensor technology, are used to detect animal-specific adaptive reactions of dairy cows. Sensor information of animals such as milk yield, physiological parameters (breathing and heart rate) and behaviour (standing, lying, and moving) are analysed by means of mathematical modelling and numerical simulation for sustainable optimisation of innovative livestock systems. This information can be used for barn construction and livestock management (ventilation and cooling) in response to climate change. Secondly, livestock-environment interactions require measurements, modelling, and reduction of emissions (NH<sub>3</sub>, CH<sub>4</sub>, N<sub>2</sub>O, bio-aerosols, PM). On-farm measurements, mechanistic modelling using computational fluid dynamics simulations, application of reaction kinetic models as well as the biophysical characterisation of aerosols are used for this purpose. Investigations reported by this paper demonstrate the application of established methods in dairy farming for the management and optimisation of livestock production and husbandry processes. The investigations contribute to the improvement of animal welfare and the reduction of negative environmental effects. This "dairy cattle husbandry" system is beneficial to the development of a transparent, economical, animal- and environmental-friendly food production chain.

**Keywords:** Livestock-environment interaction, sensor technology, emission, animal welfare, dairy cattle husbandry

## **1. Introduction**

Increases in the consumption of animal products and the use of environmental resources render the sustainability of livestock production increasingly important (Thompson and Nardone, 1999). Meanwhile, animal welfare is receiving more concern than ever since it is not only related to animal well-being, but also linked with animal health, animal productivity, and feeding efficiency (Norton and Berckmans, 2018). In addition, the negative effects caused by animal husbandry, such as air pollution, global warming, infectious diseases, and antibiotic resistance, etc. should be minimised. To reduce the environmental and health risks and the related costs, an indispensable in-depth understanding of the complex interactions between humans, animals,

plants as well as environment, economy and society is required (Zinsstag et al., 2011). Therefore, the One Health concept, which applies multidisciplinary and interdisciplinary approaches to integrate the agricultural system into human and veterinary medicine (Palatnik-de-Sousa and Day, 2011), was proposed.

The research area “Animal Welfare and Animal Husbandry” at ATB deals with questions concerning animal well-being and sustainable animal husbandry. Dairy cows are one of the largest sectors in animal husbandry, and their welfare is receiving a growing attention (Norton and Berckmans, 2018). Through the early detection of behavioural deviations or pathological processes of individual cows, an early reaction by humans and/or technology can be established to guarantee animal welfare and health based on their needs (Norton and Berckmans, 2018). In ATB research, individual animal indicators such as activity, respiration rate, body temperature, rumination activity, heart rate variability, and performance are analysed together with barn climate parameters in order to derive information on dairy cattle welfare, and further to develop measures for the improvement of their welfare. The investigations are mainly carried out in the welfare barn at the “Agricultural Research and Education Center for Animal Breeding and Husbandry” (LVAT) in Groß Kreutz (near Berlin, Germany). The use of artificial intelligence and innovative technologies and modelling approaches will enable the fusion of sensors and the automatic recognition of animal welfare in the future.

Ventilation can improve the productivity and welfare of animals by removing excess heat, moisture and pollutants (Yi et al., 2019a). Dairy cattle buildings are often naturally ventilated, which makes it challenging to determine ventilation rate and control indoor climate because the microclimate inside the barn is strongly influenced by outdoor climate conditions (Hempel et al. 2018). Moreover, naturally ventilated dairy housing is a large contributor of ammonia ( $\text{NH}_3$ ), greenhouse gas emissions, dust, odour, and other gaseous pollutants (König et al., 2017). These pollutants can cause secondary particulate matter formation, terrestrial acidification and eutrophication, reduce biodiversity, and result in global warming (Poore and Nemecek, 2018). Therefore, to improve indoor microclimate and reduce negative impacts on the environment, a deep understanding of air movements with respect to variable weather conditions and ventilation openings is important.

The research area “Barn Climate and Emissions” at ATB uncovers improvement strategies for indoor microclimate and reduction potentials for environmentally and climate-relevant gases, infectious bio-aerosols and multi-resistant germs by dynamically characterising and modelling airflows in interaction with atmospheric conditions. The effects of dynamic changes of boundary conditions on the distribution of tracer gases and air exchange rates in the barn, especially in the animal occupied zone (AOZ) as well as reduction potentials in connection with dispersion processes are investigated. In addition, the effect of animals as heat sources, mobile pollutant sources and flow obstacles on the airflows and gas emissions will be investigated. The modelling of complex transport processes of gases, dusts, heat, water vapour and infectious agents is based on a comprehensive understanding of the system. For this purpose, the three-pillar-approach, as shown in Figure 1, has been developed by ATB, and will be continuously further developed. It combines on-farm research on the real system, investigations on the physical model in a large boundary layer wind tunnel and numerical modelling. The on-farm measurements on airflows, climate, and gaseous emissions are mainly carried out in a commercial naturally ventilated dairy barn (NVDB) in Dummerstorf, northeast Germany.

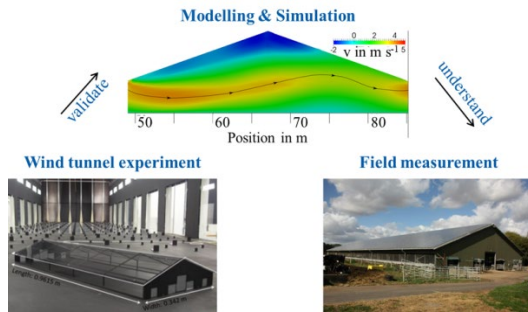


Figure 1. Three-pillar-approach.

Existing challenges require a deeper understanding of interactions between environmental factors and farm animals. The overall objective of this research is to develop sustainably intensified agricultural systems including animal husbandry in a One Health concept with a Global Health perspective. An interdisciplinary team at ATB from the fields of agricultural sciences, meteorology, biology, engineering, data science and veterinary medicine is involved in the research work on livestock-environment interactions.

## 2. Animal Welfare

With the increase of milk yield and stocking density, as well as with global warming, dairy cows are more susceptible to heat stress. Heat stress can impair animal welfare and milk production, increase incidence of health problems such as metabolic disorders and lameness, and cause economic losses (de Andrade Ferrazza et al., 2017). Thus, reducing the burden of dairy cow heat stress is a central topic in ATB research.

### 2.1. Temperature-humidity index

The heat stress level of dairy cows can be quantitatively assessed by a range of thermal indices (Wang et al., 2018a). The temperature-humidity index (THI) is one of the most widely used indices (Mader et al., 2006), and thus was used in ATB research in the form of Eq. (1) (National Research Council, 1971).

$$THI = (1.8 \cdot T + 32) - (0.55 - 0.0055 \cdot RH) \cdot (1.8 \cdot T - 26) \quad (2)$$

where  $T$  is the dry bulb temperature of the air, °C;  $RH$  is the relative humidity, %.

The climate data within the barn in terms of  $T$  and  $RH$  were measured at eight locations 3.4 m above the floor (Heinicke et al., 2018; Heinicke et al., 2019; Pinto et al., 2019a) or at nine locations 3.0 m above the floor (Pinto et al., 2019b). The average values of all locations were used for THI calculations.

### 2.2. Indicators of heat stress

Heat-stressed dairy cows dissipate surplus body heat into environment and reduce heat generation rate by adjusting their behaviour (body posture, lying bout, movement, etc.), making physiological responses (e.g., increased body temperature and respiration rate, decreased dry matter intake and milk production, loss of weight, sweating) and immune responses (changed blood hormone concentration) (Kadzere et al., 2002; Sejian et al., 2012). Therefore, dairy cows' activity data, physiological reactions, and immune responses can be used as indicators of heat stress (Wang et al., 2018b; Herbut et al., 2019). Through the early detection of heat stress in individual cows, an early reaction by humans and/or technology can be established to mitigate heat stress and guarantee animal welfare and production stability.

As a sensitive indicator of heat stress, dairy cow activities ( $y_{ijklmn}$ ) including the resting behaviour (total lying time, number of lying bouts, lying bout duration) and number of steps per cow per day were recorded by the activity sensor IceTag3D™ (IceRobotics, Edinburgh, UK) in

ATB research (Heinicke et al., 2019). The experiments were carried out in the experimental dairy barn in Groß Kreutz, in which 51 German Holstein-Friesian cows were housed. Additionally, the individual cow factors, e.g. milk yield level ( $Milk_i$ ), lactation state ( $L_j$ ), days in milk ( $DIM_k$ ), pregnancy status ( $G_l$ ), and estrus status ( $I_m$ ) were monitored because they also affect the metabolic heat production process. All the above mentioned parameters were included in a linear mixed model, as described by Eq. (2) (Heinicke et al., 2019), for the assessment of effects of heat load on animal activity.

$$\begin{aligned} y_{ijklmn} = & \mu + a \cdot THI_t + b \cdot THI_{t-1} + c \cdot THI_{t-2} + d \cdot THI_{t-3} + Milk_i + L_j + DIM_k + G_l + I_m + f_{ijkl} \cdot HLD_t^{THI \in [68,72]} \\ & + g_{ijkl} \cdot HLD_t^{THI \in [72,80]} + h_{ijkl} \cdot HLD_t^{THI \geq 80} + i_{ijkl} \cdot HLD_{t-1,t-2,t-3}^{THI \in [68,72]} + j_{ijkl} \cdot HLD_{t-1,t-2,t-3}^{THI \in [72,80]} + k_{ijkl} \cdot HLD_{t-1,t-2,t-3}^{THI \geq 80} + cow_n + e_{ijklmn} \end{aligned} \quad (2)$$

where  $\mu$  is the mean value of each animal activity;  $t$  is the measurement day;  $THI$  and  $HLD$  are temperature-humidity index and heat load duration, respectively;  $a$  to  $d$  and  $f$  to  $k$  are regression coefficients of  $THI$  and  $HLD$ , respectively;  $cow_n$  is the random cow effect;  $e$  is the model error.

The effects of heat stress and individual cow factors on the total daily lying time are shown in Figure 2 (Heinicke et al., 2019). It was found that cows suffering from heat load had shorter lying time than cows without heat load. When additional heat load was accumulated three days before the measurement day, reduced activity responses to heat load (i.e. delayed heat load effects) were observed. This was reflected by the lying time increasing from 479 to 568 min  $d^{-1}$ , from 531 to 582 min  $d^{-1}$ , and from 472 to 561 min  $d^{-1}$  for the reference group, lactation  $\geq 4$  group, and  $DIM > 150$  group, respectively. In addition, it was found that dairy cows with low milk yield level had a longer lying time than normal- and high-yielding cows. When there was no heat load, dairy cows in the periods of an advanced lactation stage (lactation  $\geq 4$ ) and of long days in milk ( $DIM > 150$ ) laid down 52 min and 19 min more than the reference group (lactation = 1,  $DIM < 150$ ). The results showed that the lying time of dairy cows was affected by both the heat load and individual cow factors. Similar results were also obtained in the estimation of lying bout number, lying bout duration, and the number of steps (Heinicke et al., 2019).

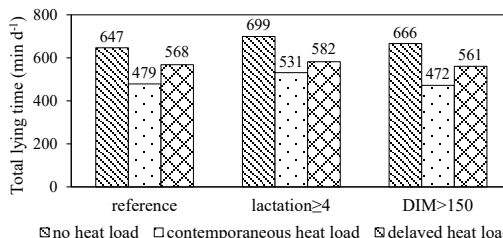


Figure 2. Daily total lying time predicted by Eq. (2) under different heat load conditions for the reference group, lactation  $\geq 4$  group, and  $DIM$  (days in milk)  $> 150$  group. Reference group has normal milk yield level, lactation state of 1, no pregnancy and estrus (Heinicke et al., 2019).

As another reliable and early indicator of heat stress, the respiration rate (RR) of dairy cows was measured by counting their right thoracoabdominal movements for 30 seconds and multiplying by 2 (Pinto et al., 2019a; Pinto et al., 2019b). As described in Figure 3 (Pinto et al., 2019a), the RR showed high variabilities for the same THI, especially for higher THI conditions. The RR increased with the increase of THI for both standing cows and lying cows. In addition, it was observed that standing cows had a lower RR than lying cows when THI was less than 80 (Pinto et al., 2019a).

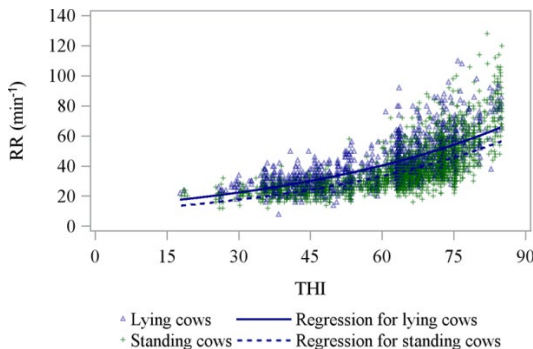


Figure 3. Respiration rate (RR) of individual cows in relation to temperature-humidity index (THI) for both lying and standing body postures (Pinto et al., 2019a).

Since counting flank movements is time-consuming, labour-intensive, and non-continuous, ATB developed a new differential pressure sensor for monitoring the RR (Strutzke et al., 2019). The sensor can carry out automatic, continuous and long-term RR measurements.

### 2.3. Reduction of heat stress

Evaporative cooling by installing cooling fans with sprinklers is one of the commonly used methods to alleviate heat stress of dairy cows. ATB tested two cooling frequencies: 3 times cooling ( $3\times$ cool) or 8 times cooling ( $8\times$ cool) per day in an Israeli NVDB (20 Israeli Holstein cows were housed) during summer to optimise the cooling efficiency (Pinto et al., 2019b). The RR, cow body posture (standing or lying), and location (cowshed or cooling yard) were recorded and shown in Table 1 (Pinto et al., 2019b). It was found that during cooling periods (cows were in the cooling yard), no significant difference in RR was observed. By contrast, during pre-cooling and post-cooling periods (cows were in the cowshed), the RRs of cows treated with the  $8\times$ cool strategy were significantly lower than those treated with the  $3\times$ cool strategy. Thus, the  $8\times$ cool frequency had better cooling effects in terms of respiration rate reduction for dairy cows during hot periods.

Table 1. Effects of two cooling frequencies ( $3\times$ cool and  $8\times$ cool) on the respiration rate of standing and lying cows in cooling yard and cowshed. The numbers in parentheses are standard errors (Pinto et al., 2019b).

	Cooling yard			Cowshed		
	$3\times$ cool	$8\times$ cool	P-value	$3\times$ cool	$8\times$ cool	P-value
Standing cows	47.1 (0.66)	43.9 (0.37)	>0.05	73.1 (0.64)	60.2 (0.72)	<0.001
Lying cows	-	-	-	65.6 (0.65)	51.6 (0.57)	<0.001

### 3. Barn Climate and Gaseous Emissions

Indoor airflow pattern and microclimate of NVDBs are strongly dependent on outdoor wind and weather conditions, configurations of the building and openings, animals, internal partitions, and the surrounding environment. Thus, to maintain a desired thermal condition and good indoor air quality, it is important to implement the adaptation strategy for changing boundary conditions. During this process, the information on air exchange and airflow characteristics, especially in the AOZ is required. Moreover, this information is important for quantification and reduction of gaseous emissions from NVDBs together with gas concentration data. The three-pillar-approach, combining field measurements, wind tunnel experiments, and Computational Fluid Dynamics (CFD) simulations, was developed and applied in ATB research.

### 3.1. Determination of air exchange rate

The air exchange rate (AER) of a NVDB can be determined by the CO<sub>2</sub> mass balance method, as described by Eq. (3) (Pedersen and Sällvik, 2002):

$$AER = \frac{N \cdot P_{CO_2}}{(C_{CO_2,in} - C_{CO_2,out}) \cdot V} \quad (3)$$

where *AER* is the number of air exchange per hour, h<sup>-1</sup>; *N* is the number of cows; *P<sub>CO<sub>2</sub></sub>* is the CO<sub>2</sub> production rate per cow, g cow<sup>-1</sup> h<sup>-1</sup>; *C<sub>CO<sub>2</sub>,in</sub>* and *C<sub>CO<sub>2</sub>,out</sub>* are the CO<sub>2</sub> concentrations inside and outside of the barn, g m<sup>-3</sup>; *V* is the volume of the barn, m<sup>3</sup>.

The accurate determination of AER relies on precisely measured CO<sub>2</sub> concentrations inside and outside of the barn. To determine the representative CO<sub>2</sub> sampling positions and sampling durations, as well as their effects on uncertainties of AER, on-farm measurements in an experimental dairy barn in Dummerstorf (Northeast Germany) were carried out. Eight indoor CO<sub>2</sub> measurement positions at a height of 3 m above the floor were uniformly distributed. Four outdoor CO<sub>2</sub> sampling positions were arranged at each side of the barn. Daily CO<sub>2</sub> concentrations were measured using a Fourier Transform Infrared spectrometer (Gasmet Technologies, Vantaa, Finland) from June 2014 to May 2015 (König et al., 2018). It was found that indoor CO<sub>2</sub> concentrations were spatially non-homogeneous and the pattern was greatly dependent on wind directions (Figure 4) (König et al., 2018). Smaller deviations from the mean CO<sub>2</sub> concentrations were observed in the centre of the barn, whereas larger deviations occurred near the edges of the barn. The outdoor CO<sub>2</sub> concentrations measured at the gable walls resulted in higher AERs than those measured at the side walls (König et al., 2018). Larger AER differences caused by different sampling strategies/locations and wind directions were observed in our later research (Janke et al., 2018).

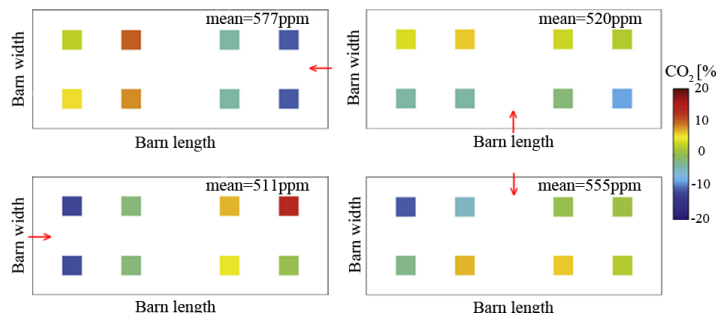


Figure 4. Spatial distributions of CO<sub>2</sub> concentration deviations from their spatial mean values for different wind directions. Red arrows represent wind directions (König et al., 2018).

Figure 5 shows the effects of sampling duration on the uncertainty of AER estimation (König et al., 2018). The results showed that the longer the measurement duration, the smaller the uncertainties. The year-round measurements had an uncertainty of 5% in the AER determination. By contrast, measuring three days per season resulted in 20% uncertainty.

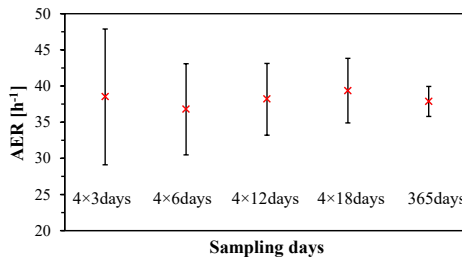


Figure 5. The air exchange rate (AER) determined based on different sampling days. Red crosses represent mean values. The number ‘4’ means four seasons (König et al., 2018).

As another air exchange rate determination method, the orifice equation with a pre-defined discharge coefficient is often used in NVDBs. However, dairy buildings are commonly equipped with large openings, which result in uncertainties when using this method. To figure out the uncertainties, we carried out both wind tunnel experiments and CFD simulations based on a 1:40 scaled model of the NVDB in Dummerstorf, focusing on the discharge coefficient investigations. The results showed that when using the orifice equation in the estimation of AER for NVDBs, the discharge coefficient value should be specified based on both opening configurations and the wind direction (Yi et al., 2018b; Yi et al., 2019b).

Apart from the barn AER, local AERs in AOZs were also investigated. We found that the range of local AERs was heterogeneously distributed and dependent on many factors, e.g. the AOZ location, wind speed and direction, and building length to width ratio (Doumbia et al., 2019).

### 3.2. Investigation of airflows

The effects of opening configuration on airflow fields were investigated in a large boundary layer wind tunnel at ATB. Air velocities inside and around the scaled model in a vertical plane were measured by a 2D Laser Doppler Anemometer (Dantec Dynamics, Skovlunde, Denmark). As shown in Figure 6, a cross-ventilation airflow pattern was observed when sidewalls were fully opened, whilst a clock-wise air recirculation zone with lower air velocities occurring near the windward side was found when sidewalls were half opened (Yi et al., 2018a). The results contribute to the development of adaption strategies for varied outdoor climate conditions.

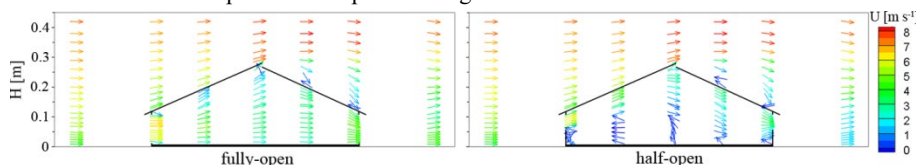


Figure 6. Air velocity fields of scaled dairy barn model for fully-open and half-open sidewall cases (Yi et al., 2018a).

### 3.3. Estimation of gaseous emissions

In order to mitigate gaseous emission, an accurate estimation of the emission rate is important. From our extensive field measurements, the exponential and parabolic dependencies on the outdoor temperature were found for NH<sub>3</sub> and CH<sub>4</sub>, respectively (Hempel et al., 2016). Based on those empirical relations, we projected for around 30·10<sup>6</sup> dairy cattle in Europe future emission increase only by changing barn climate of up to 16 Gg NH<sub>3</sub> and 0.1 Gg CH<sub>4</sub> per year under IPCC’s worst climate change scenario (Hempel et al., 2019). We also found that emission factors, for example for NH<sub>3</sub>, were largely dependent on gas sampling strategies (Janke et al., 2018). This information helps to provide more accurate, economical, and environmental assessments of innovative livestock husbandry.

#### 4. Conclusions

In this paper, we addressed crucial research questions related to animal welfare, barn climate, and influences of livestock farming on the environment. The research was performed at ATB by an interdisciplinary team (animal science, engineering, data science, veterinary medicine, etc.). The combined method of on-farm measurements, laboratory experiments in a large boundary layer wind tunnel, as well as numerical and statistical modelling was applied to bridge the gap between different research methodologies. ATB incorporated an assessment of animal heat stress, indoor climate conditions, barn designs, and gas sampling strategies in terms of animal welfare and barn climate improvement, as well as airflows and gas emissions determination. Comprehensive investigations about heat stress of dairy cows using sensor technology help to improve animal welfare and livestock productivity. An in-depth understanding of interrelations between barn climates and atmospheric conditions contributes to better design and control of animal houses. ATB research contributes to the development of a sustainable optimisation approach to achieve an economical, animal- and environmental-friendly livestock housing system in future.

#### Acknowledgements

The authors gratefully acknowledge the financial support from the research project “Optimized animal-specific barn climatization facing temperature rise and increased climate variability” (OptiBarn) in the FACCE ERA-NET Plus Initiative, from the Federal Office for Agriculture and Food (BLE), DE-Grant No. 2814ERA02C, Germany, and from the research project “Determination of air exchange rates in naturally ventilated barns – Validation of prediction models” (BeLuVa), German Research Foundation (Deutsche Forschungsgemeinschaft, DFG), project number 397548689, Grant No. AOBJ: 645856, Bonn for this research.

#### References

- de Andrade Ferrazza, R., H.D.M. Garcia, V.H.V. Aristizábal, C. de Souza Nogueira, C.J. Veríssimo, J.R. Sartori, R. Sartori, J.C.P. Ferreira, 2017. Thermoregulatory responses of Holstein cows exposed to experimentally induced heat stress. *Journal of Thermal Biology.* 66, 68–80.
- Doumbia, M., S. Hempel, D. Janke, T. Amon, 2019. Prediction of the local air exchange rate in animal occupied zones of a naturally ventilated barn. In *XXXVIII CIOSTA & CIGR V International Conference.* Rodos, Greece, 24–26 June.
- Heinicke, J., G. Hoffmann, C. Ammon, B. Amon, T. Amon, 2018. Effects of the daily heat load duration exceeding determined heat load thresholds on activity traits of lactating dairy cows. *Journal of Thermal Biology.* 77, 67–74.
- Heinicke, J., S. Ibscher, V. Belik, T. Amon, 2019. Cow individual activity response to the accumulation of heat load duration. *Journal of Thermal Biology.* 82, 23–32.
- Hempel, S., C.K. Saha, M. Fiedler, W. Berg, C. Hansen, B. Amon, T. Amon, 2016. Non-linear temperature dependency of ammonia and methane emissions from a naturally ventilated dairy barn. *Biosystems Engineering.* 145, 10–21.
- Hempel, S., M. König, C. Menz, D. Janke, B. Amon, T.M. Banhazi, F. Estellés, T. Amon, 2018. Uncertainty in the measurement of indoor temperature and humidity in naturally ventilated dairy buildings as influenced by measurement technique and data variability. *Biosystems Engineering.* 166, 58–75.
- Hempel, S., C. Menz, S. Pinto, E. Galán, D. Janke, F. Estellés, T. Müschner-Siemens, X. Wang, J. Heinicke, G. Zhang, B. Amon, A. del Prado, T. Amon, 2019. Heat stress risk in European dairy cattle husbandry under different climate change scenarios - uncertainties and potential impacts. Preprint in Earth System Dynamics Discussions (under review for the journal *Earth System Dynamics*). 1–38.
- Herbut, P., S. Angrecka, D. Godyn, G. Hoffmann, 2019. The physiological and productivity effects of heat stress in cattle – a review. *Annals of Animal Science.* 19 (3), 579–594.
- Janke, D., D. Willink, S. Hempel, C. Ammon, B. Amon, T. Amon, 2018. Influence of wind direction and sampling strategy on the estimation of ammonia emissions in naturally ventilated barns. In: *EurAgEng 2018 conference.* Wageningen, the Netherlands, July 8–12. pp. 762–767.
- Kadzere, C., M. Murphy, N. Silanikove, E. Maltz, 2002. Heat stress in lactating dairy cows: a review. *Livestock Production Science.* 77 (1), 59–91.

- König, M., K. Bonkoß, T. Amon, 2017. Wind tunnel measurements on reduction of near surface concentrations through naturally barrier on emissions from naturally ventilated barn. In *International Workshop on Physical Modelling of Flow and Dispersion Phenomena*, Nantes, France, August 23–25.
- König, M., S. Hempel, D. Janke, B. Amon, T. Amon, 2018. Variabilities in determining air exchange rates in naturally ventilated dairy buildings using the CO<sub>2</sub> production model. Biosystems Engineering. 174, 249–259.
- Mader, T.L., M.S. Davis, T. Brown-Brandl, 2006. Environmental factors influencing heat stress in feedlot cattle. Journal of Animal Science. 84 (3), 712–719.
- Norton, T., D. Berckmans, 2018. Engineering advances in precision livestock farming. Biosystems Engineering. 173, 1–3.
- National Research Council, 1971. *A Guide to Environmental Research on Animals*. National Academy of Science, Washington, DC.
- Palatnik-de-Sousa, C.B., M.J. Day, 2011. One Health: the global challenge of epidemic and endemic leishmaniasis. Parasites & Vectors. 4 (1), 197.
- Pedersen, S., K. Sällvik, 2002. CIGR 4th report of working group on climatization of animal houses. Heat and moisture production at animal and house levels. Horsens, Denmark. December.
- Pinto, S., G. Hoffmann, C. Ammon, B. Amon, W. Heuwieser, I. Halachmi, T. Banhazi, T. Amon, 2019a. Influence of barn climate, body postures and milk yield on the respiration rate of dairy cows. Annals of Animal Science. 19 (2), 469–481.
- Pinto, S., G. Hoffmann, C. Ammon, W. Heuwieser, H. Levit, I. Halachmi, T. Amon, 2019b. Effect of two cooling frequencies on respiration rate in lactating dairy cows under hot and humid climate conditions. Annals of Animal Science. 19 (3), 821–834.
- Poore, J., T. Nemecek, 2018. Reducing food's environmental impacts through producers and consumers. Science. 360 (6392), 987–992.
- Sejian, V., S.M.K. Naqvi, T. Ezeji, J. Lakritz, R. Lal, 2012. *Environmental Stress and Amelioration in Livestock Production*. Berlin: Springer.
- Strutzke, S., D. Fiske, G. Hoffmann, C. Ammon, W. Heuwieser, T. Amon, 2019. Development of a noninvasive respiration rate sensor for cattle. Journal of Dairy Science. 102 (1), 690–695.
- Thompson, P.B., A. Nardone, 1999. Sustainable livestock production: methodological and ethical challenges. Livestock Production Science. 61 (2–3), 111–119.
- Wang, X., B.S. Bjerg, C.Y. Choi, C. Zong, G. Zhang, 2018a. A review and quantitative assessment of cattle-related thermal indices. Journal of Thermal Biology. 77, 24–37.
- Wang, X., H. Gao, K.G. Gebremedhin, B.S. Bjerg, J. Van Os, C.B. Tucker, G. Zhang, 2018b. A predictive model of equivalent temperature index for dairy cattle (ETIC). Journal of Thermal Biology. 76, 165–170.
- Yi, Q., M. König, D. Janke, S. Hempel, G. Zhang, B. Amon, T. Amon, 2018a. Wind tunnel investigations of sidewall opening effects on indoor airflows of a cross-ventilated dairy building. Energy and Buildings. 175, 163–172.
- Yi, Q., G. Zhang, M. König, D. Janke, S. Hempel, T. Amon, 2018b. Investigation of discharge coefficient for wind-driven naturally ventilated dairy barns. Energy and Buildings. 165, 132–140.
- Yi, Q., H. Li, X. Wang, C. Zong, G. Zhang, 2019a. Numerical investigation on the effects of building configuration on discharge coefficient for a cross-ventilated dairy building model. Biosystems Engineering. 182, 107–122.
- Yi, Q., X. Wang, G. Zhang, H. Li, D. Janke, T. Amon, 2019b. Assessing effects of wind speed and wind direction on discharge coefficient of sidewall opening in a dairy building model – a numerical study. Computers and Electronics in Agriculture. 162, 235–245.
- Zinsstag, J., E. Schelling, D. Waltner-Toews, M. Tanner, 2011. From “one medicine” to “one health” and systemic approaches to health and well-being. Preventive Veterinary Medicine. 101 (3–4), 148–156.

## **Image Analysis of Heavy Broiler Behavior under Summer Heat Stress Condition**

**Yingying Liu<sup>a,b</sup>, Bin Cheng<sup>a</sup>, Derek West<sup>a</sup>, Suraiya Akter<sup>a</sup>, Lingjuan Wang-Li<sup>a,\*</sup>, Alejandro H. Cordova-Noboa<sup>c</sup>, Edgar Oviedo-Rondon<sup>c</sup>**

<sup>a</sup> Department of Biological and Agricultural Engineering, North Carolina State University, Raleigh, NC 27695, USA

<sup>b</sup> Department of Electrical Engineering, Nanjing Agricultural University, Nanjing, Jiangsu 210031, P.R. China

<sup>c</sup> Prestage Department of Poultry Science, North Carolina State University, Raleigh, NC 27695, USA

\* Corresponding author. Email: [lwang5@ncsu.edu](mailto:lwang5@ncsu.edu)

### **Abstract**

North Carolina (NC) is one of the largest broiler producing states in the United States (U.S.). Broilers adapt to a relatively narrow range of temperatures, heat or cold stress may occur when the thermal condition is beyond the optimum environmental temperatures. In the hot and humid summer climate in NC, it is very challenging to keep heavy broilers (with a final age of 63 days and body weight of 5.44 kg, 12 lb.) cool. Heat stress causes a series of behavioral, physiological, neuroendocrine, and molecular responses that compromises animal welfare. Funded by a US Department of Agriculture (USDA), the research group at NC State University are working on assessing and developing an engineering solution for mitigating heat stress to enhance welfare and performance of heavy broilers in the age of 42–61d. This reported study is a subset of the USDA project, aiming at evaluating a set of heavy broiler behavioral welfare parameters in responses to air velocity (AV) treatments under the heat stress condition. The experiment was conducted in 6 identical mechanically ventilated environmental chambers for two AV treatments with 3 chambers per treatment and 44 broilers per chamber from 28 d–61d of broiler ages. Starting at 42 d, video cameras placed in each chamber were used to record undisturbed comfort and exploratory broiler behaviors over 24-h periods twice each week. Behavioral time budget, duration and frequency of activity/resting, ingestion (feeding/drinking) were evaluated to determine broiler responses to the heat stress under the two AV treatments. To describe the broiler's behavior, occupation rate, cluster degree, and activity amount were calculated using image processing technique. Images of the broilers' position distribution in drinking zone and feeding zone at different time of day were analyzed to show the impacts of heat stress and AV treatments. Broilers' body surface temperature (BST) were measured using thermal infrared cameras. The BST maps at different zones and times were used to explain the broiler behavior under the heat stress. Data were summarized as the percentage of time used by the majority of the broilers in the individual chambers at a 10-minute interval. It was observed that broilers under the heat stress liked to stay around the waterline. They were more crowded and less active under the low AV treatment. It is expected that results of this study will advance our understanding of heat stress and the AV treatments on heavy broiler behavior and welfare.

**Keywords:** Heavy broiler, heat stress, image analysis, occupancy rate, cluster degree, activity amount.

**Theme IV:**

**Manure Management and Utilization**



# Impact of Fieldwork Day Constraints on Manure Application Regulations

Raymond E. Massey <sup>a,\*</sup>, Haluk Gedikoglu <sup>b</sup>

<sup>a</sup> Division of Applied Social Science, University of Missouri, Columbia, MO 65211, USA

<sup>b</sup> Department of Economics, Konya Food and Agriculture University, Konya 42080, Turkey

\* Corresponding author. Email: [masseyr@missouri.edu](mailto:masseyr@missouri.edu)

## Abstract

At first glance, limiting manure application to the annual crop nutrient needs should minimize the chance of nutrients leaving the field and entering water bodies. This paper evaluates that assumption by including the feasibility of complying with various proposed manure application limits. Three manure application limit rules will be evaluated: an annual nitrogen limit rule, an annual phosphorus limit rule and a phosphorus banking rule.

Time needed to field apply specific quantities of manure is estimated using engineering coefficients for each application limit rule. Each rule will affect by the number of hectares accessed annually and over time, and the number of hours necessary to land apply manure. Feasibility analysis incorporates two datasets that incorporate uncertainty into the model. Data from the U.S. Department of Agriculture on Days Suitable for Fieldwork will be used to estimate the probability of successfully completing land application within specified time periods appropriate for crop fertility and environmental protection. Data from the U.S. National Weather Service provide probabilities of a 0.5 inch rainfall occurring during the application period. These two probability estimates are used to determine the joint probability of the successful completion of manure application.

We illustrate the model using production achievements of a typical hog farm in north central Missouri applying pit manure to corn land in a corn-soybean rotation. Our illustration indicates that a phosphorus banking regulation would return the greatest net income from manure and have the greatest probability of a successful completion.

**Keywords:** Climate, hog, phosphorus, nitrogen, economic, environment

## 1. Introduction

Two characteristics of manure tend to be the focus of its odd place as a source of crop nutrients. First, manure has a low value: mass ratio. Commodities possessing a low value: mass ratio limit the distance the manure can be economically transported, resulting in localized markets (Keplinger and Hauck, 2006). Second, the nitrogen (N):phosphorus (P) ratio of manure does not match the N:P ratio needed by crops. Farmers must choose a nutrient to use to determine their application rate. The P index measures the risk of P moving offsite. When the P index is rated medium risk or less, the manure application can be based on N Limit (USDA, 2013). Otherwise, P based manure application should be done (USDA, 2013). Choosing N as the limiting nutrient typically means P is applied in quantities greater than needed by crops. Choosing P as the limiting nutrient means that N is under-applied on crops needing N fertilizers. P based applications are expected to reduce P runoff by ensuring that all P applied is removed by harvested crops in the year the P is applied.

Over application of both manure supplied N and P on fields may cause environmental pollution, causing it to be the target of environmental regulation (Tang et al., 2018; Amann et al., 2018). Norwood and Chvosta (2005) showed that regulations designed to reduce P loading could result in unintended consequences, such as increased N runoff. Unintended consequences occur when policy writers do not consider how managers will respond to regulations given their resources, constraints and incentives.

If P based manure applications do reduce runoff on a per land unit basis, this does not equate

to reducing total P runoff from a manure source. Pollution is the result of all land under production. Mandating practices like P based applications could increase the number of hectares receiving manure, leading to greater pollution.

Previous studies analyzed the economics of manure management for individual farm profitability (Fleming, et al., 2018) or the environmental quality (Wang and Baerenklau, 2014), but not both. The primary objective of this paper is to analyze both economic profitability and the impact of manure management on environmental quality for alternative manure application rules. This paper seeks to further understand the constraints and incentives that farmers face when making manure management decisions. Specifically, we elaborate on the time constraints. Time constraints affect both the profitability of decision makers and the environmental impact of decisions made. Farmers are assumed profit maximizers. Economic studies that indicate that farmers over-apply manure reveal a lost economic opportunity to the decision makers or improperly specify the cost and return that farmers face. This study attempts to incorporate time as a constraint into the costs associated with manure management.

## 2. Materials and Methods

### 2.1. Manure application rules

The most common manure management limit is a N limit (*N Limit*), when allowed by the P index (USDA, 2013). If the P index does not allow for N Limit, an Annual P Limit rule is dictated. Some have recommended an Annual P Limit for all manure applications. We envision a modification to the Annual P Limit rule which we call the P Banking rule.

An N Limit rule specifies that land-applied manure not exceed the N uptake of the crop following application. This normally supplies more P than will be removed by the crop in that year. If the same ground receives an N Limit of manure annually, P accumulates in the soil and increases the probability of P runoff into waters.

An Annual P Limit rule specifies that cropland receive only as much manure supplied P as will be removed by a single year's crop harvest. Annual P Limits usually supply less N than necessary for the crop to obtain optimum yield goals. Commercial N fertilizer applications, in addition to manure application, ensure all the N needs of the crop are met. Annual P Limits do not reduce the total amount of P applied each year to land from an animal feeding operation. Rather they apply the same amount of P from the manure storage structure on more units of land, each hectare receiving a reduced rate.

A P Banking rule limits manure supplied P to the quantity that can be removed by various crops before a subsequent manure application can be applied. It allows sufficient manure application to meet the N uptake of the crop grown in the year of application. Commercial N applications are unnecessary on the land that received manure in the year it received manure. The total number of hectares needed *over the planning horizon* for the P Banking rule is identical to that of the Annual P Limit rule. The number of hectares accessed *in any one year* for the P Banking rule is identical to that of the N Limit rule.

The difference in the amount of land required for the N limit rule and either P limit rules depend on the manure and harvested crop characteristics.

The impact of manure regulations on land requirements has been well documented (Fleming et al., 1998; Norwood and Chvosta, 2005). What has not been as explicitly studied is the impact of more land on time constraints. Time is implied in the fact that accessing more land with lower application rates will require greater travel distances and in-field application time. This is handled by using custom rates charging a base rate and a distance rate rather than specifically looking at the increased hours responsible for this increased charge. Fleming et al. (1998) acknowledge that costs might increase with tighter time constraints but do not consider them.

Application time in the field under various application rules is an important factor. Applying manure to more hectares will increase the amount of application time in the field. The Annual P

Limit rule requires access to more fields each year but each field receives less manure each year than if the N Limit or P Bank rules are enforced. Application time in the field will increase if the farmer is required to cover multiple times as many hectares as before. While lower application rates might allow for quicker application per hectare, the total time will likely increase due to the decreased field efficiency.

## 2.2. Model

We use a double-objective framework and look for the highest net economic returns to manure supplied nutrients and the highest probability of not having a run-off event from manure application. Our economic model that estimate benefits and costs, closely follow Fleming et al. (1998). Please see them for detailed model equations.

Net economic return is defined as the total benefit from manure minus the cost of manure application. The total benefit from manure is the foregone commercial fertilizer needed for crop production times the cost of commercial fertilizers. Not all manure applied to cropland is valued because it may not be needed. Manure applied to legumes does not have any N value because legumes do not require N fertilizer. Manure supplied P does not have value if it is applied in excess of crop needs before subsequent applications of manure are applied. Generally, N is fully valued when needed as a crop nutrient and P and K are valued to the extent that they are removed by crop harvest before subsequent manure applications. It is assumed that buildup of P and K are not needed so excess P and K are not economically valued.

To estimate the value of the manure supplied nutrients applied to the corn-soybean cropping system rotation, a spreadsheet entitled Value of Manure (Massey, 2008a) is used. This spreadsheet allows the user to enter crop production and fertility needs along with the characteristics of the manure resource (Table 1). We use an Aerway system to incorporate the manure into the soil and conserve N.

Table1. Summary of N supply from manure and crop nutrient need and removal.

Supply or removal	Plant available N (PAN)	Phosphorus	Potassium
Pit manure supply	2.4 kg PAN m <sup>-3</sup>	2.9 kg P <sub>2</sub> O <sub>5</sub> m <sup>-3</sup>	2.8 kg K <sub>2</sub> O m <sup>-3</sup>
Corn need/removal	16.1 kg PAN Mg <sup>-1</sup>	6.6 kg P <sub>2</sub> O <sub>5</sub> Mg <sup>-1</sup>	4.8 kg K <sub>2</sub> O Mg <sup>-1</sup>
Soybean removal	0*	13.3 kg P <sub>2</sub> O <sub>5</sub> Mg <sup>-1</sup>	23.3 kg K <sub>2</sub> O Mg <sup>-1</sup>

\* N need set to zero because soybean, a legume, does not require N fertilization

We pay particular attention to the land base needed because it is central to the feasibility of different rules. First, we calculate the quantity of land necessary to accept manure according to each rule. We then calculate the quantity of hectares that must be “searched” in order to actually find that many hectares. Search hectares is a function of the percentage of nearby land designated cropland, the percentage of cropland that is suited to receiving manure and the percentage of suitable land that is actually available for receiving manure. Following Fleming, et al. (1998) we assume that manure is applied to 1 of every 8 hectare of land. In other words, if 10 hectares of land will be receiving manure, 70 hectares will have been passed over. This increases the distance that manure may have to be hauled in order to reach the 10 hectares.

The cost of manure application accounts for the time necessary for loading manure into spreaders, transporting the manure from the source to the fields in the spreaders and using the spreaders to apply manure to the fields. The search hectares concept increases the cost as distance to suitable land increases. To estimate the cost of applying manure to the land, a spreadsheet, containing an engineering-economic model, entitled Manure Cost Distribution Analyzer (Massey, 2008b) is used. The total number of hours needed for manure application is expensed at a custom rate of \$100 hr<sup>-1</sup> (Battel and Stein, 2018).

The net economic return calculation gives an indication of the purely financial decision before the farmer. It values all hours as equal. However, not all hours are equal. During critical time periods, farmers will trade money or other benefits to reduce hours. So a farmer may choose an

alternative that does not have the highest net economic return if it reduces hours during a critical time.

The amount of manure that enters water is dependent on the amount of manure on a particular field and the probability that a particular field will experience a runoff causing precipitation event. The probability of manure runoff increases when a rainfall event of a sufficient quantity occurs before land applied manure has time to be incorporated into the soil. The probability of a runoff event increases with 1) soil type and slope and 2) physical proximity to water bodies and 2) temporal proximity of manure application to a runoff causing rainfall event. The regulatory rules of manure application may affect each of the above factors affecting the probability of a runoff event. Manure application rules that require lighter applications require more land to be searched and accessed, and more time.

As more land is required, the amount of land suitable to receiving manure decreases. Environmentally sensitive land (e.g. greater slope or closer to water bodies) that may have been avoided under an N Limit rule might be used under an Annual P Limit rule because of the difficulty in finding suitable land. Land that may have utilized the N (e.g. corn ground) may be not be used in order to access land closer to the manure source (e.g. land growing soybeans or alfalfa).

Increasing the number of hours required to land apply manure may also increase the probability of a runoff event. The time between when manure is applied prior to a runoff event diminishes with increased hours necessary for application. Farmers are more likely to apply prior to a forecasted runoff event simply because the additional time needed for application offers little choice. Farmers also are likely to work more hours in a day to complete the land application of manure, increasing the likelihood of working in the dark when leaks may go unnoticed.

Successful completion is defined as the probability that the work can be done within the probable fieldwork days as estimated by the USDA while not increasing the probability of a runoff causing rainfall event. As more hours are needed the probability of a rainfall causing rainfall event increases.

We estimate the probability of a successful completion in two steps. First, we estimate the probability of finishing manure application during a specified period. We used the eight week period during October and November to illustrate manure application following harvest. A spreadsheet program developed at the University of Missouri (Carpenter and Massey, 2007) estimated the probability of completing the manure application using fieldwork day data (USDA, 2109) and assuming that application occurred during daylight hours.

Next we estimate the probability of a rainfall event expected to cause a runoff event occurring within 24 hours of manure application. For illustration, we use a permit rule currently in use in Michigan that prohibits application within 24 hours of a 1.27 cm rainfall forecast event (Michigan Department of Natural Resources, 2010). The probability of a runoff causing event within 24 hours of application will increase as the number of hours required for land application increases.

A Markov chain model is used to determine the probability of a 1.27 cm rainfall occurring within 1 day of a dry day suitable for manure application (Gabriel and Neumann, 1962). It is recognized that the amount of rainfall needed to create a runoff event is dependent on many factors. We chose 1.27 cm as a proxy that can be expanded in later work to more accurately model runoff events. National Weather Service rainfall data necessary to determine the probability of a 1.27 cm rainfall event within the land application window was obtained from AgEBB (2019).

### 2.3. Decision rule

The results will be evaluated under a traditional risk-return framework. More net economic benefit is preferred to less; less risk of an unsuccessful completion of manure application is preferred to more. A policy scenario is preferred to another if simultaneously its net economic benefit to the farmer is greater than another scenario and its risk of unsuccessful completion of

manure application is less than that same scenario.

#### 2.4. Application to Missouri

The following example is to illustrate the methodology employed.

We assume that 4164 m<sup>3</sup> of farrow-to-finish swine pit manure is land applied to corn ground in a corn-soybean rotation each year. The manure provides 2.4 kg m<sup>3</sup> of plant available nitrogen (PAN) and 2.9 kg P2O5 m<sup>3</sup> (see Table 1).

Using removal rates reported in Table 1, corn production at 9.4 Mg ha<sup>-1</sup> is assumed to need 184.9 kg PAN ha<sup>-1</sup> and remove 62.2 kg P2O5 ha<sup>-1</sup> and 45.4 kg K2O ha<sup>-1</sup>. Soybean production at 3.0 Mg ha<sup>-1</sup> is assumed to need no N and remove 40.4 kg P2O5 ha<sup>-1</sup> and 70.6 kg K2O ha<sup>-1</sup>.

Manure is injected using a 22.7-m<sup>3</sup> tanker with Aerway applicator. Field receiving manure are assumed to be 16.2 ha in size. One of every eight fields is available for land application of manure. The distance to each field is estimated using a grid pattern around the manure source. When the closest field is used, the next seven closest fields are deemed unavailable; then the ninth field is available for manure, and so forth.

For N limit rule, manure is applied to corn ground only. The ground that receives manure in one year does not receive manure the subsequent year because it would not obtain the economic benefit of the N in the manure.

For the P Banking rule, manure is applied to corn ground only. The ground that receives manure in year one will not receive manure again until year 5. Two cycles of a corn-soybean rotation are required to remove all the P applied in year one.

For the Annual P rule, manure is applied to corn ground only. The application is provides less N that is required by the corn so a commercial application of fertilizer would be necessary to all corn land.

### 3. Results and Discussion

Table 2 presents the results of the illustration of the model. The application rate for manure is 75.8 m<sup>3</sup> ha<sup>-1</sup> for the Nitrogen Limit and the P Bank rules. The application rate is 22.0 m<sup>3</sup> ha<sup>-1</sup> for the Annual P Limit – about 30 percent of the application rate for the N limit and P Bank rules. The land needed each year are 55.0 ha for both the N Limit and P Bank rules; 189.4 ha are needed for the Annual P Limit rule. The number of search hectares necessary to find sufficient land application hectares is 440, 880 and 1515 for the N Limit, P Bank and Annual P Limit rules, respectively. The larger search areas result in longer travel distances and road travel time. The Annual P Limit road travel time of 28.1 hr is 205% that of the N Limit road time of 13.7 hr. The P Bank road travel time of 20.9 hr is 153% that of the N Limit. The annual Field Time is the same for the N Limit and P Bank scenarios at 48.2 hours; it rises to 117.9 hours for the Annual P Limit.

Assuming a custom application charge of \$100 hour<sup>-1</sup>, the distribution cost is \$9240 for the N Limit, \$17,660 for the Annual P Limit and \$9965 for the P Bank scenario. Using fertilizer prices of \$.79 kg N, \$.95 kg P2O5 and \$.73 kg K2O, the total benefit of meeting crop nutrient needs by manure is \$15,998 for the N Limit, \$27,698 for the Annual P Limit and \$27,102 for the P Bank scenario. The net economic benefit of manure use is \$6758 for the N Limit, \$10,038 for the Annual P Limit and \$17,137 for the P Bank scenario.

The PDFM software (Carpenter and Massey, 2007) estimated that the probability of completing of manure application activities within the October-November window to be 100% for both the N Limit and P Bank scenarios and 93% for the Annual P Limit Scenario. The 93% chance of completing the Annual P Limit scenario indicates that about 1 in 20 years the manure application will not be successfully completed according to regulations due to weather problems.

Using 30-year (1980 to 2010) historical rainfall for Columbia, MO, the probability of a rainfall event following the application of manure was estimated at 5.8% for the N Limit and P Bank scenarios; 6.1% for the Annual P Limit scenario. The difference in probability of a runoff event

is small, less than 1%, but still greater for the Annual P Limit rule. The annual P Limit rule marginally increase the probability that farmers will not be able to apply manure in an environmentally beneficial manner.

Table 2. Results of analysis of land application of swine pit manure to corn-soybean production in Missouri.

	N Limit	Annual P Limit	P Bank
Application Rate ( $\text{m}^3 \text{ ha}^{-1}$ )	75.8	22.0	75.8
Land needed/year ( $\text{ha yr}^{-1}$ )	55.0	189.4	55.0
Search Area (ha)	440.3	1515.1	880.6
Median Distance Travelled (ha)	0.9	1.9	1.4
Road Travel Time (hr $\text{yr}^{-1}$ )	13.7	28.1	20.9
Field Time (hr $\text{yr}^{-1}$ )	48.2	117.9	48.2
Total Time (hr $\text{yr}^{-1}$ )	92.4	176.6	99.7
Distribution Cost (\$ $\text{yr}^{-1}$ )	9240.0	17660.0	9965.0
Total Benefit (\$ $\text{yr}^{-1}$ )	15998.0	27698.0	27102.0
Net Benefit (\$ $\text{yr}^{-1}$ )	6758.0	10038.0	17137.0
Probability of completing within application window	100%	93%	100%
Probability of runoff event following application	5.8%	6.1%	5.8%

The efficient set (highest net economic benefit, highest probability of successful completion without runoff increased) is the P Bank rule (Figure 1). The P Bank scenario was preferred to both the N Limit and Annual P Limit rules because it had the highest net benefit and greater than or equal to probability of successful completion. Theoretically, though not empirically in this example, the P Bank could have had lesser probability of successful completion than the N Limit because it required more hours to perform.

According to the risk-return framework, the N Limit rule cannot be determined to be preferable to the Annual P Limit rule. The Annual P Limit has higher net economic income than the N Limit but it also has a lesser probability of successful completion.

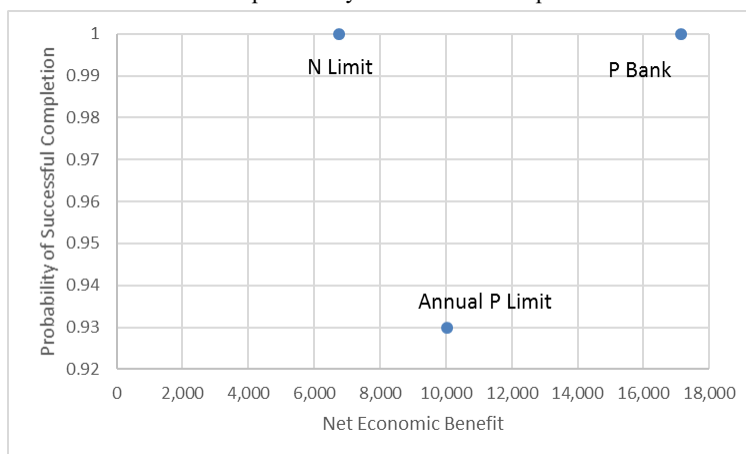


Figure 1. Efficient set of manure application rules

#### 4. Conclusions

Our results indicate that P Banking is preferable to both N Limit and Annual P Limit. Because

most farmers practice an N Limit for manure management, we can assume that the value of time is greater than we estimate it to be. Otherwise, they would voluntarily practice P Banking. The imposition of an Annual P Limit would spread manure over more hectares but it does not follow that it will reduce environmental hazard. The probability of a rainfall event causing runoff increases relative to both the N Limit and P Banking rules.

Our results are another example of how well intentioned regulations may have unintended consequences.

## References

- AgEBB, 2019 Agricultural Weather Stations Data Archive. Downloaded data at <http://agebb.missouri.edu/weather/realtime/mizzou.asp>. Accessed January 11, 2019.
- Amann, A., Zoboli, O., Krampe, J., Rechberger, H., Zessner, M., and L. Egle, 2018. Environmental Impacts of Phosphorus Recovery from Municipal Wastewater. *Resources, Conservation & Recycling*, 130, 127–139.
- Carpenter, Brent and Ray Massey, 2007. Fieldwork Days and Machinery Capacity. University of Missouri. Guide 363.
- Battel, Bob and Dennis Stein, 2018. 2018 Custom Machine and Work Rate Estimates. Michigan State University Extension. Fact Sheet #18-01. [https://www.canr.msu.edu/field\\_crops/uploads/files/2018%20Custom%20Machine%20Work%20Rates.pdf](https://www.canr.msu.edu/field_crops/uploads/files/2018%20Custom%20Machine%20Work%20Rates.pdf)
- Fleming, R. A., Bruce A. Babcock and Erda Wang, 1998. Resource or Waste? The Economics of Swine Manure Storage and Management. *Review of Agricultural Economics*. 20(1), 96–113.
- Gabriel, K. R. and J. Neumann, 1962. A Markov chain model for daily rainfall occurrence in Tel Aviv. *Monthly Weather Review*. 92(4), 169–176.
- Keplinger, K. O. and L. M. Hauck, 2006. The Economics of Manure Utilization: Model and Application. *Journal of Agricultural and Resource Economics*. 31(2), 414–440.
- Massey, Raymond E., Value of Manure. 2008. Spreadsheet program for EXCEL. University of Missouri Commercial Agriculture Program. <https://extensiondata.missouri.edu/Pro/Swine/Docs/ManureValueEstimator.xlsx>
- Massey, Raymond E., 2008. Manure Distribution Cost Analyzer. Spreadsheet Program for EXCEL. University of Missouri Commercial Agriculture Program. <https://extensiondata.missouri.edu/Pro/Swine/Docs/ManureCostAnalyzer.xlsx>
- Michigan Department of Natural Resources, 2010. NPDES General Permit: Concentrated Animal Feeding Operations. [http://www.michigan.gov/documents/deq/wb-npdes-cafo-generalpermit-MIG019000-2010\\_316373\\_7.pdf](http://www.michigan.gov/documents/deq/wb-npdes-cafo-generalpermit-MIG019000-2010_316373_7.pdf). Accessed January 10, 2011.
- Norwood, F. B. and J. Chvosta, 2005. Phosphorus-based applications of livestock manure and the law of unintended consequences. *Journal of Agricultural and Applied Economics*. 37, 79–90.
- Tang, C., G. E. Lade., D. Keiser, C. Kling, Y. Ji, and Y. Shr, 2018. Economic Benefits of Nitrogen Reduction in Iowa. Center for Agricultural and Rural Development, Iowa State University. <https://www.card.iastate.edu/products/publications/texts/water-quality-report.pdf>.
- Wang, J. and K. A. Baerenklau, 2014. How Inefficient Are Nutrient Application Limits? A Dynamic Analysis of Groundwater Nitrate Pollution from Concentrated Animal Feeding Operations. *Applied Economic Perspectives and Policy*. 37(1), 130–150.
- USDA. NASS. 2019 Crop Progress and Condition Reports. Downloaded data at [http://www.nass.usda.gov/Publications/State\\_Crop\\_Progress\\_and\\_Condition/index.asp](http://www.nass.usda.gov/Publications/State_Crop_Progress_and_Condition/index.asp).
- USDA. NRCS. 2013. *Natural Resources Conservation Service Conservation Practice Standard: Nutrient Management* (Code 590). Washington, DC.

# Isolation, Identification and Optimization of Heat-tolerant Bacteria in Composting of Pig manure

Yifan Zhang <sup>a</sup>, Zengli Ouyang <sup>a</sup>, Xuehua Mei <sup>a</sup>, Jianan Tang <sup>a</sup>, Maixun Zhu <sup>a</sup>,  
Yong Huang <sup>a,\*</sup>, Weichao Zheng <sup>b</sup>, Zonggang Li <sup>b</sup>

<sup>a</sup> Chongqing Academy of Animal Science, Chongqing, Shichuan 402460, P. R. China

<sup>b</sup> College of Water Resources and Civil Engineering, China Agricultural University,  
Beijing 100083, P. R. China

\* Corresponding author. Email: [huangyongcqbb@126.com](mailto:huangyongcqbb@126.com)

## Abstract

Laboratory experiments were conducted to screen and identify heat-tolerant bacteria for composting of pig manure. Ten strains, denoted as K1–K10, were isolated with a water bath at 90 °C for 90 min from all samples obtained from the composting piles of pig manure at different fermentation stages. Starch hydrolysis, protein hydrolysis, cellulose degradation, and oil hydrolysis tests were performed to comparatively analyze and evaluate the ten strains. Bacterial physiological, biochemical identification, and 16S rDNA analysis were used to identify the target strains. Results showed that the K8 bacteria, identified as *Bacillus cereus*, had good performance on cellulose degradation and starch hydrolysis, and could also partly decompose proteins and oils. The K10 bacteria, identified as *Bacillus amyloliquefaciens*, had powerful ability to hydrolyze starch, and could also partly break down proteins, oils and celluloses. Both K8 and K10 bacteria were proved to be environmentally safe.

**Keywords:** Composting, pig manure, *bacillus cereus*, *bacillus amyloliquefaciens*, heat-tolerance

## 1. Introduction

Composting of pig manure is a biological process by microbial metabolism to degrade organic waste in pig manure or crop straw, and reduce air emissions from organic waste. Meanwhile, heat generated in the composting process can increase the composting pile temperature to kill pathogens effectively (Weng et al., 2018). Transformation of the organic waste in the composting raw materials into a stable and humus-rich organic fertilizer by fermentation is one of the effective ways to mitigate the adverse environmental impacts of livestock and poultry organic waste.

Pig manure contains large amounts of cellulose, protein, starch and oils (Zhang et al., 2017). During the long-term accumulation and fermentation process, the manure pile forms different heat producing layers. The position and thickness of the high temperature layer may change dynamically during the composting fermentation period, and high temperature promotes the fermentation of the pig manure. Water content of the compost pile decreases with the composting fermentation duration, resulting in a higher air permeability, leading to biological aerobic high-temperature fermentation (Wang, et al., 2006). Therefore, the screening and identifying heat-tolerant bacteria may improve composting speed by enhancing high-temperature fermentation of pig manure.

Limitations of composting of pig manure include slow fermentation process, long decay time, and low compost quality. The objective of this research was to isolate and identify dominant strains to promote compost fermentation, shorten the cycle of decomposition, and improve the quality of compost.

## 2. Materials and Methods

### 2.1. Pre-isolated strains source and sampling

The Pre-isolated strains samples were collected from manure files with heap fermentation at four pig farms in Rongchang District, Chongqing, China. Three dunghills were randomly selected for sampling at warm-up phase, high-temperature phase and low-temperature phase, respectively. Samples were collected from the surface, middle and bottom of each dunghills.

## 2.2. Preparation of media

Gelatin medium was prepared to determine the protein hydrolysis level of bacteria. Each 1000 mL gelatin medium contained 5.0 g trypsin, 3.0 g beef extract, 120.0 g gelatin and 872.0 g distilled water. The pH value of the medium was adjusted to 7.1 ~ 7.5. The gelatin medium was sterilized at 115 °C for 20 min.

Each 1000 mL hydrolyzed fat medium contained 10.0 g trypsin, 5.0 g beef extract, 5.0 g sodium chloride, 10 g peanut oil, 1.6% neutral red aqueous solution, 1.7% agar. The pH value of the medium was adjusted to 7.2. The hydrolyzed fat medium was sterilized it at 121 °C for 15 min.

Each 1000 mL hydrolyzed starch medium contained 10.0 g trypsin, 5.0 g beef extract, 5.0 g sodium chloride, 5.0 g soluble starch, 1.7% agar. The pH value of the medium was adjusted to 7.2. The hydrolyzed starch medium was sterilized it at 121 °C for 15 min.

Each 1000 mL cellulose Congo red medium contained 1.0 g sodium nitrate, 1.2 g disodium hydrogen phosphate, 0.9 g potassium dihydrogen phosphate, 0.5 g magnesium sulfate, 0.5 g potassium chloride, 0.5 g yeast extract, 0.5 g acid hydrolyzed casein, 5.0 g sodium carboxymethylcellulose, 0.2 g Congo red, 1.7% agar. The pH value of the medium was adjusted to 7.2. The cellulose Congo red medium was sterilized it at 121 °C for 15 min.

Each 1000 mL spore medium contained 0.5 g trypsin, 0.5 g yeast extract, 0.5 g glucose, 0.02 g  $(\text{NH}_4)_2\text{SO}_4$ , 0.02 g  $\text{MgSO}_4 \cdot 7\text{H}_2\text{O}$ , 0.1 g  $\text{K}_2\text{HPO}_4$ , 1.7% agar. The pH value of the medium was adjusted to 7.2. The spore medium was sterilized it at 115 °C for 15 min.

## 2.3. Selection of the heat-tolerant bacteria

Each sample weighing 1.0 g was mixed with 10 mL physiological saline and vibrated for 3 min. Then, the mixture was water bathed at 90 °C for 10 min. A 100  $\mu\text{L}$  of each sample was evenly spread on the medium plate and cultured at 37 °C for 24 h. A single colony grown on the bacterial culture medium was selected and preserved for using.

## 2.4. Isolation and purification of the heat-tolerant bacteria

The bacteria were selected and purified with streak plate method and the final isolated bacteria were preserved at -40 °C. The ten strains of bacteria were isolated and labeled as K1, K2.....K10.

## 2.5. Heat-tolerant test of bacteria

The isolated bacteria were separately inoculated in LB liquid medium and cultured at 45 °C, 50 °C, and 55 °C for 24 hours, respectively. The heat-tolerant test of the particular bacteria was repeated 3 times. The concentration of the bacteria after cultured for 24 hours was used to measure the heat-tolerant ability of the bacteria.

## 2.6. Degradation test of heat-tolerant bacteria

Bacterial biochemical test and observation were used to determine the degradation level of heat-tolerant bacteria, including starch hydrolysis, protein hydrolysis, cellulose hydrolysis, oil hydrolysis. Each duplicate of 10  $\mu\text{l}$  bacteria sample was evenly spread on/in hydrolyzed starch medium plates, a hydrolyzed fat medium plates, a cellulose Congo red medium plates, and gelatin liquid medium. Three replicates were conducted for each test and the plates and tube with medium and bacteria were cultured at 37 °C for 3 days.

## 2.7. Environmental safety test

A fermentation pit with a dimension of  $4 \times 2 \times 1.5$  m ( $L \times W \times D$ ) was constructed to simulate fermentation test with the two selected strains K8 and K10. A blower and tubing were equipped for oxygen supplement from the bottom. Sawdust was added into the pig manure to achieve C/N ratio between 23 and 27. About 0.1% bacteria was mixed with the mixture (pig manure and sawdust), then was moved to a sift screen in the fermentation pit with covered surface for 12 h. The inside temperature of the manure pile was monitored every day. Each 100 g sample of pig

manure collected at the front, back, left, right and center of the manure pile was mixed for pH, *E. coli* concentration and aphid eggs measurement.

## 2.8. Identification of strains

Colony morphology and Gram staining were performed on the selected strains. Bacterial biochemical tubes were used for biochemical identification, and physical and chemical characteristics of bacteria were analyzed using methods in Berger's System Bacteriology Manual. The total DNA of the isolated bacteria was extracted according to the instructions of the bacterial genome extraction kit, and the 16S rDNA gene sequence of the isolated strain was amplified by the universal primers. The reaction used 2  $\mu$ L of DNA template, 1  $\mu$ L of upstream and downstream primers, 25  $\mu$ L of 2  $\times$  Taq PCR Master Mix and 21  $\mu$ L of ddH<sub>2</sub>O. The reaction conditions were pre-denaturation at 95 °C for 5 min, then maintained at 94 °C for 30 s, 58 °C for 30 s, and 72 °C for 30 s. This process was cycled 30 times and extended at 72 °C for 10 min. The PCR product was sequenced by Bioengineering Co., Ltd (Shanghai). The sequencing results were analyzed by BLAST in NCBI, and the phylogenetic tree was constructed by the N-J method by means of MEGA 6.0 software.

## 3. Results

### 3.1. Bacterial heat-tolerant test results

Bacterial heat-tolerant ability of the ten isolated strains of bacteria are shown in Figure 1. All ten strains of bacteria could reproduce well at 45 °C and the lowest concentration among the ten strains of bacteria was  $3.29 \times 10^7$  CFU L<sup>-1</sup> at 45 °C after 24 hours' culture. The concentrations of K8 and K10 bacteria were  $9.1 \times 10^6$  CFU L<sup>-1</sup> and  $1.18 \times 10^7$  CFU L<sup>-1</sup> at 55 °C after 24 hours' culture, which was much higher than the other strains of bacteria.

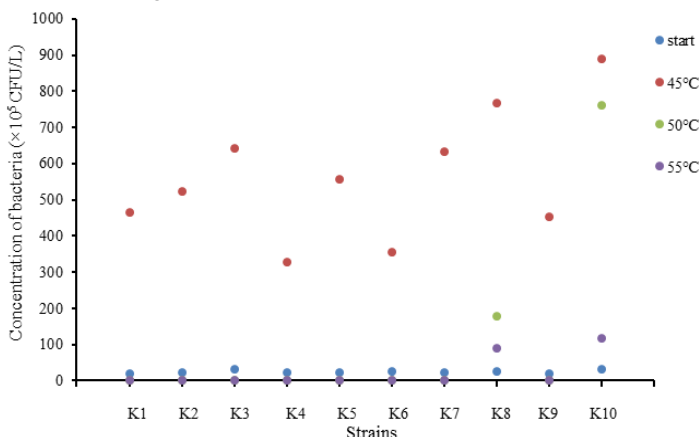


Figure 1. The bacterial heat-tolerant ability of the ten isolated strains of bacteria.

### 3.3. Starch hydrolysis analysis

The results of starch hydrolysis are shown in Table 1. Halo was found in the medium plates inoculated with strains of K5, K6, K7, K8, K9 and K10. The halo diameter of K8 strain was larger than the other strains ( $P < 0.05$ ), while there was no difference among the colony diameters of all ten strains ( $P > 0.05$ ). The Up of K10 and K8 strains were  $2.58 \pm 0.21$  and  $1.77 \pm 0.15$ , which were larger than the other strains ( $P < 0.05$ ).

### 3.3. Gelatin liquefaction analysis

Eleven gelatin tubes, including 10 bacterial culture tubes and 1 blank control tube, were placed into a refrigerator at 4 °C for 1 hour. Gelatin liquefaction results are shown in Table 2. The gelatin tubes containing strains of K5, K6, K7, K8, K9 and K10 failed to coagulate.

Table 1. Test results of hydrolyzed starch.

Strains	Halo average (D, cm)	Colony diameter (d, cm)	Up=D d <sup>-1</sup>
K1	0.61±0.10a	0.61±0.12a	1.00±0.13a
K2	0.63±0.13a	0.63±0.14a	0.99±0.21a
K3	0.60±0.09a	0.60±0.19a	1.00±0.17a
K4	0.61±0.14a	0.61±0.07a	1.01±0.16a
K5	0.85±0.20b	0.62±0.18a	1.37±0.17b
K6	0.65±0.15a	0.60±0.16a	1.08±0.23a
K7	0.68±0.09a	0.62±0.15a	1.10±0.09a
K8	1.10±0.12c	0.61±0.11a	1.77±0.15c
K9	0.82±0.13b	0.61±0.12a	1.34±0.18b
K10	1.60±0.12d	0.62±0.14a	2.58±0.21d

Note: Different lowercase letters in the same column indicate significant difference ( $P < 0.05$ ).

Table 2. Results of gelatin liquefaction.

Number	K1	K2	K3	K4	K5	K6	K7	K8	K9	K10	CK
solidification	+	+	+	+	-	-	-	-	-	-	+

Note: CK: control group without bacteria. “+” means the gelatin coagulation result was positive. “-” means the result was negative.

### 3.4. Cellulose degradation analysis

The results of cellulose degradation on cellulose Congo red medium are shown in Table 3. The halo diameter of K6, K7, K8 were  $0.94 \pm 0.19$ ,  $1.33 \pm 0.22$ ,  $1.52 \pm 0.18$  cm, respectively, which were larger than the other strains ( $P < 0.05$ ). There was no difference in colony diameters among all the ten strains ( $P > 0.05$ ). The Up of K6, K7, K8 strains were  $1.57 \pm 0.18$ ,  $2.15 \pm 0.11$ ,  $2.45 \pm 0.14$ , respectively, which were larger than the other strains ( $P < 0.05$ ).

Table 3. Test results of cellulose degradation.

Strains	Halo average (D, cm)	Colony diameter (d, cm)	Up=D d <sup>-1</sup>
K1	0.62±0.12a	0.62±0.15a	1.00±0.08a
K2	0.63±0.15a	0.63±0.17a	1.00±0.19a
K3	0.60±0.16a	0.60±0.18a	1.00±0.11a
K4	0.63±0.09a	0.63±0.16a	1.00±0.15a
K5	0.68±0.12a	0.62±0.11a	1.10±0.18a
K6	0.94±0.19b	0.60±0.18a	1.57±0.18b
K7	1.33±0.22c	0.62±0.22a	2.15±0.11c
K8	1.52±0.18d	0.62±0.19a	2.45±0.14d
K9	0.63±0.16a	0.63±0.07a	1.00±0.16a
K10	0.66±0.11a	0.60±0.15a	1.10±0.16a

Note: Different lowercase letters in the same column indicate significant difference ( $P < 0.05$ ).

### 3.5. Oil hydrolysis analysis

The results of oils hydrolysis are shown in Table 1. The change of the color occurred on the medium plates inoculated with K6, K8, K9, K10 strains, indicating that oil could be degraded by the strain of K6, K8, K9, K10.

Table 4. Test results of oils hydrolysis.

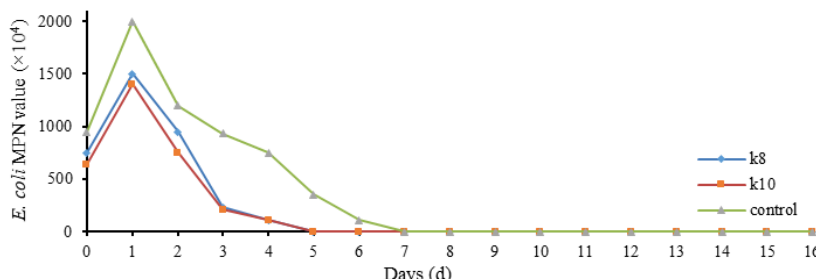
Number	K1	K2	K3	K4	K5	K6	K7	K8	K9	K10
Colony color	-	-	-	-	-	pink	-	pink	pink	pink

Note: “-” means the colony color has not changed.

### 3.6. Environmental safety analysis

#### 3.6.1. *E. coli* MPN (Most Probable Number) value changes

The *E. coli* MPN values during fermentation are shown in Figure 2. In the early stage of pig manure fermentation, *E. coli* rapidly multiply due to the increase of temperature. However, the *E. coli* in the three trials were killed by high temperature due to the continuous fermentation. The *E. coli* MPN value of K8 and K10 groups at the third day and the *E. coli* MPN value of control group at the sixth day met the requirements of *E. coli* inspection project in China's harmless treatment.

Figure 2. *E. coli* MPN value during fermentation.

#### 3.6.2. Aphid egg mortality changes

Aphid egg mortality during fermentation is shown in Figure 3. The ascaris sum are endoparasites and cannot be parasitized in the external environment. The high temperature generated during the fermentation of pig manure can kill the ascaris suum eggs. The mortality in the K8 and K10 groups exceeds 90% on the 8th day. The control group only reached 60%. Until the 15th day, the mortality in the K8 and K10 groups was greater than 95%, which meet the requirements of the ascaris suum eggs mortality project in China's harmless treatment. While the control group did not reach 90%, and it requires continuous fermentation to kill the ascaris sum eggs.

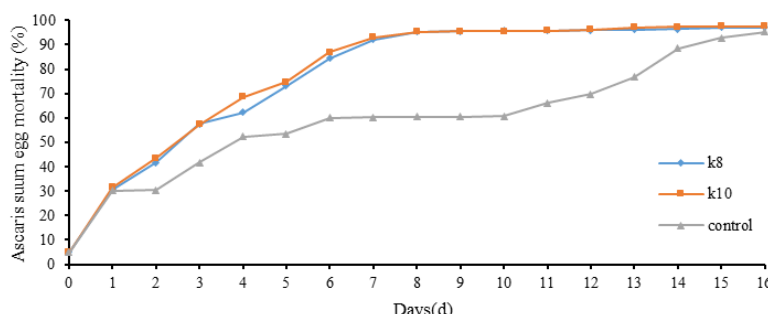


Figure 3. Aphid egg mortality during fermentation.

### 3.7. Identification of efficient strains

#### 3.7.1. Morphology and related physical and chemical properties

The colonies of the strains K8 and K10 on the plate medium were all white with the wrinkled surface, and the Gram stain was positive. The physiological and biochemical characteristics of

strains K8 and K10 are shown in Table 5 and Figure 4.

Table 5. Analysis of physiological and biochemical characteristics.

Items	K8	K10	Items	K8	K10
Starch hydrolysis	+	+	Hydrogen sulfide	-	-
Arginine double hydrolase	-	-	Sucrose	+	+
Lysine decarboxylase	-	+	Nitrate reduction	+	+
Glucose gas production	-	-	Inulin	-	-
Citrate utilization	-	-	Arabic candy	-	-
Urease	-	-	Salicin	-	+
Indole	-	-	Glycerin	+	+
Gelatin hydrolysis	+	+	Fructose	+	-
Mannitol	-	+	Semi-solid agar	+	+

Note: “+” means the reaction result was positive , “-” means negative.

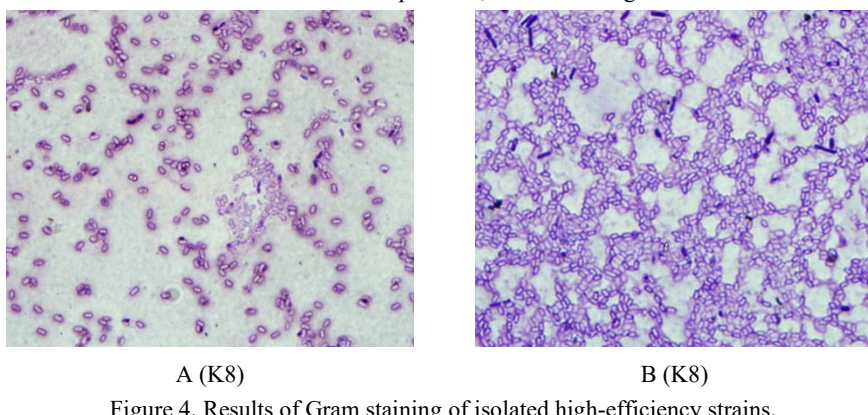


Figure 4. Results of Gram staining of isolated high-efficiency strains.

### 3.7.2. 16S rDNA and phylogenetic analysis

The 16S rDNA universal primer PCR was used to screen the strains to amplify the expected DNA fragments. The length of the rDNA sequence of the K8 strain was 1411 bp and the K10 strain was 1431 bp. The homology alignment showed that K8 had a homology of 99% with *Bacillus cereus* and a homology of K10 with K8 as high as 99%. Figure 5 shows that the 16S rDNA phylogenetic tree analysis showed that the K8 strain was clustered with KJ524513.1 *Bacillus Cereus*, and the K10 strain was clustered with MH144247.1 *Bacillus amyloliquefaciens*.

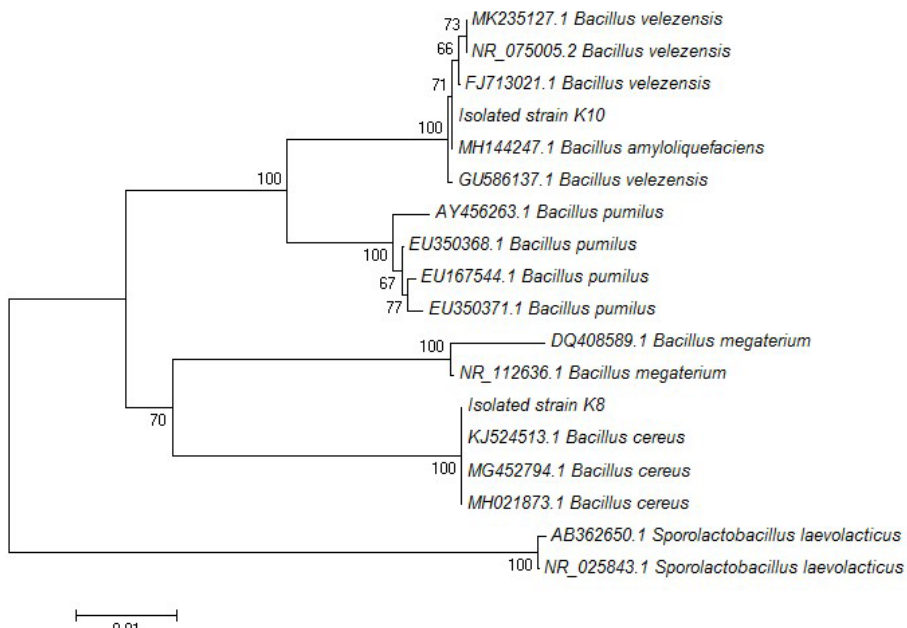


Figure 5. The bacterial evolutionary tree.

#### 4. Discussion

Bacteria, which can effectively degrade starch, protein, cellulose and fat were screened according to She et al. (2013). Proteins and polysaccharides degradation were mainly determined by the ability of gelatin and starch degradation due to the large amount of proteins and polysaccharides in the feces. The fermentation excipients contained a large amount of cellulose. The degradation of cellulose was another assessment index in the process of fecal degradation. The strains of bacteria with high performance of gelatin, starch and cellulose degradation were the preferred.

In this experiment, K8 and K10 isolated from the composting of pig manure were the potential strain of bacteria for pig manure fermentation due to strong degradation ability of starch, protein, cellulose and test. Most indexes of strains K8 and K10 were in accordance with *Bacillus cereus* and *Bacillus starch*, respectively. For further exactly identification, 16S rDNA analysis were used and the strain of K8 and K10 were identified as *Bacillus cereus* and *Bacillus amyloliquefaciens*, respectively. The strain of *Bacillus cereus* could also play a role on rapid heating and cycle shortening of composting fermentation (Gao et al., 2015). The metabolites of *Bacillus* starch hydrolysate could inhibit the growth of many harmful bacteria (Yang et al., 2017). In recent years, *Bacillus* was widely used in biological control, because it could secrete many kinds of bacteriostatic substances and has the ability to induce crops to produce resistance (Qiao et al., 2013). *Bacillus* could reproduce and grow rapidly when the condition was suitable, and also could produce spores and enter dormancy when cope with the bad environment (Yang et al., 2013). The results showed that these two strains of *Bacillus* could be used in the rapid composting of pig manure, and the expansion of practical production and application was in progress.

#### 5. Conclusions

Both strains of K8 and K10 isolated from the composting of pig manure were proved to be heat-tolerant. The strains of K8 and K10 were identified as *Bacillus cereus* and *Bacillus*

*amyloliquefaciens*, respectively. Both *Bacillus cereus* and *Bacillus amyloliquefaciens* were capable of starch, protein, cellulose, and oil hydrolysis. Particularly, *Bacillus cereus* was more capable of cellulose hydrolysis than *Bacillus amyloliquefaciens*, and *Bacillus amyloliquefaciens* was more capable of starch hydrolysis than *Bacillus cereus*. Both *Bacillus cereus* and *Bacillus amyloliquefaciens* were confirmed to be environmentally safe.

#### Acknowledgements

This study was funded by Key Social R&D Projects of Chongqing Municipal People's Livelihood (cstc2018jscx-masd0079).

#### References

- Gao, X., L. S. Zhao, L. Duo, 2015. Intensification, isolation and identification of drought-resistant microorganisms in municipal solid waste compost. Journal of Tianjin Normal University, Natural Science Edition. 35(02), 81–84.
- Qiao, J., Y. Liu, Y. Xia, S. Mu, Z. Chen, 2013. Root colonization by *Bacillus amyloliquefaciens* B1619 and its impact on the microbial community of tomato rhizosphere. Acta Phytophylacica Sinica. 40(6), 507–511.
- She, T., X. Ge, M. Li, S. Zhang, Y. Chu, H. Guo, X. Wang, K. Feng, 2013. Screening of strains of cellulase-producing bacteria in compost of sewage sludge and straw and optimization of cellulase-producing conditions. Journal of Ecology and Rural Environment. 29(6), 768–772.
- Wang K., F. Zhu, W. Wang, Z. Xue, 2006. Variotions of layer temperature during pig manure composting with different amendments. Transactions of the CSAE. 22(1), 186–188.
- Weng, Y., S. Tan, Y. Qiu, B. Liu, L. Yang, X. Liu, Y. Yang, 2018. Screening, identification and composting application of a straw degradation heat-tolerant bacteria. Jiangsu Agricultural Sciences. 46(22), 296–300.
- Yang, D., C. Zhang, Z. Xu, Y. Zhao, H. Sun, Y. Xie, 2017. Isolation and identification of a strain of *Bacillus amyloliquefaciens* and its biological characteristics. Acta Agriculturae Jiangxi. 29(9), 69–74.
- Yang, L., H. Zheng, Y. Zhang, L. Fu, J. Huang, X. Zhou, F. Yang, 2013. Optimization of conditions on spore production from *Bacillus coagulans* using solid state fermentation method. Acta Ecologiae Animalis Domestici. 7(34), 49–53.
- Zhang P., W. Liu, X. Li, Y. Liu, S. Zhang, X. Zhang, D. Shan, 2017. Screening and identification of efficient cellulose degrading bacteria. Soils and Fertilizers Sciences in China. 2, 149–156.

# A Dispersion-Based Model for Assessing the Impact of Odor from Swine Operations

Amy La, Qiang Zhang \*

Department of Biosystems Engineering, University of Manitoba, Winnipeg, Manitoba R3T 5V6, Canada

\* Corresponding author. Email: [Qiang.Zhang@UManitoba.ca](mailto:Qiang.Zhang@UManitoba.ca)

## Abstract

Odor emission from swine operations is on the top list of public concerns on the environmental impact of intensive livestock operations. Given the difficulties in quantifying odor in the ambient environment, assessing odor impact is challenging for both researchers and regulatory agencies. This paper presents a dispersion-based model for assessing odor impact of swine operations. An intensive literature review was conducted to compile data for developing an odor emission rate model for various swine housing systems and manure storages. Based on the characteristics of the swine operation, including the type and size of operation, manure collection system, and ventilation system, odor emission rate(s) is estimated. The emission rate is then used in AERMOD to simulate odor dispersion in a 10 km by 10 km grid centered around the swine facility. Based on the simulation results, the model presents an interactive screen on which the user may examine the odor concentrations and occurrence frequencies at any point within the grid. The user may also select different odor impact criteria, such as odor concentration exceedance threshold and allowable hours of odor exceedance, to determine the separation (setback) distances between the swine facility and the surrounding residences/communities to minimize odor impact. The setback zones are graphically presented over a Google map image.

**Keywords:** Swine operation, odor emission, air dispersion, setback distance

## 1. Introduction

Intensification of livestock operations and increasing urbanization has resulted in considerable attention to odor emission from livestock operations (Mackie et al., 1998). Odor has been a major environmental concern to the general public and is often an obstacle for new development or expansion of livestock operations. Odor from livestock operations are the result of numerous odorous compounds generated from anaerobic decomposition of manure. Schiffman et al. (2001) identified 331 VOCs (volatile organic compound) and fixed gases from swine facilities in North Carolina. Some common odor compounds identified in hog odor include ammonia, hydrogen sulfide, volatile fatty acids, p-cresol, indole, skatole, and diacetyl (Priest et al., 1994). In concentrations at or above their chemical toxicity thresholds, these compounds can directly cause adverse health effects. The concentrations of odorous compounds in communities downwind from livestock operations are generally much lower than their toxicity thresholds, but they can induce odor sensations, which may trigger health symptoms by a variety of physiological mechanisms. By definition, odor is the sensations and perceptions that occur when a mixture of odorous compounds (odorants) stimulate receptors in the nasal cavity of a person. In other words, odor is a complex psychophysical variable, not a simple physical or chemical variable. In addition, once odorous compounds leave the livestock facilities, they will disperse in the atmosphere and may further be modified due to various chemical and physical processes. Therefore, assessing the impact of livestock odor is extremely challenging, considering the psychophysical nature of odor and the complexities of atmospheric dispersion processes. The objective of this study was to develop a model for assessing odor impact on the communities/residences near swine operations by considering: (1) the tolerance of residents to odor; and (2) atmospheric dispersion of odor. The original version of this model was reported by Gao et al. (2012). This paper reports the updated version of the model.

## 2. Materials and Methods

### 2.1. Overall model structure

The proposed model has three key components: (1) estimation odor emission; (2) simulation odor dispersion, and (3) quantification of acceptable odor exposure (Figure 1). After the user enters the farm information, including the type and size of swine operation, manure handling and storage system, and ventilation system, the model estimates the odor emission rate for each building and manure storage on the farm. The emission rates are then used in dispersion modeling to predict odor concentration and occurrence frequency in a 10 km by 10 km grid centered at the farm. The user is then prompted to specify or select a criterion for acceptable odor exposure. Finally, the predicted odor exposure (concentration and frequency) is compared with the acceptable odor exposure to assess the impact of odor. The details of three key model components are discussed in the following subsections. The model was programmed in a software platform called Suneido<sup>TM</sup> (<https://suneido.com>).

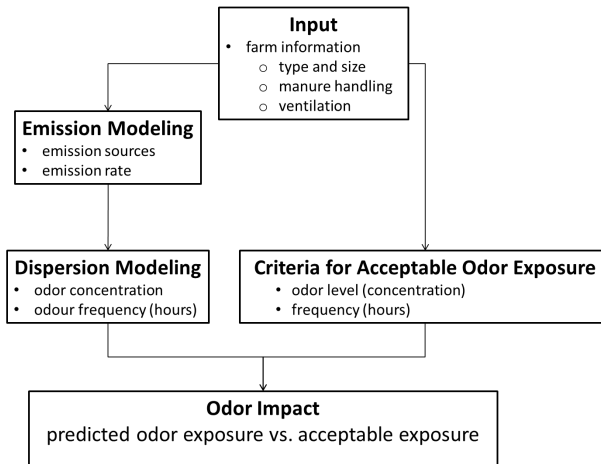


Figure 1. Overall model structure for assessing odor impact.

### 2.2. Emission modeling

The emission model estimates the emission rates of different types of swine buildings and manure storages based on the data published in the literature. An extensive literature review was conducted to compile data from journal and conference papers with measurements of odor emission rates for swine operations. For each paper that presented odor emission rate measurements, the following details were noted: (1) study of interest, (2) the location, (3) building type, (4) ventilation type, (5) manure collection system, and (6) whether the odor emission rate averages presented were annual, seasonal, or monthly averages of measurements. Odor emission rates were standardized as  $\text{OU m}^{-2} \text{s}^{-1}$ . If the data was presented in other unit(s), a conversion was performed. In cases where the data were presented in a plot, the data were extracted using Plot Digitizer ([plotdigitizer.sf.net](http://plotdigitizer.sf.net)). After the literature review was completed, the average odor emission rates were categorized into three groups: annual, seasonal, and monthly odor emission rates. The odor emission rates for buildings were then further categorized based on the housing function (gestation, farrowing, nursery, and finisher). Lastly, the emission rates were sub-categorized based on the building ventilation system, manure collection/storage, and floor slating type.

### 2.3. Dispersion modeling

AERMOD was used through a Windows interface program AERMOD View (Lakes

Environmental, Waterloo, Ontario) to conduct odor dispersion modeling. AERMOD Modeling System is a US-EPA preferred/recommended model for air quality dispersion modeling (US-EPA, 2019). The simulations were specifically conducted for the Province of Manitoba, Canada. To deal with variations in meteorological conditions across the province, the province was divided into six “meteorological” regions. Prognostic Mesoscale Meteorological (PMM) data was purchased from Lakes Environmental (Waterloo, Ontario) to run AERMOD dispersion simulations for the six regions. The coordinates of the locations representing each region and a grid resolution of 4 km were provided to Lakes Environmental to generate PMM data using the Weather Research and Forecasting Model (WRF) for the period from January 1, 2013 to December 31, 2017.

To avoid requiring the user to perform dispersion modeling every time, a set of generic simulations was performed for a standardized areal emission source of 100 m by 100 m (typical size of a swine farm) with a unit emission rate of  $1 \text{ OU m}^{-2} \text{ s}^{-1}$  at a release height of 2.0 m for a domain of 10 km by 10 km. A receptor grid of 51 columns and 51 rows was implemented within the 10 km by 10 km domain. This corresponded to a receptor being placed every 200 m at a height of 1.22 m. There was a total of 2601 receptor points at which odor concentration was calculated. The results of the generic simulations were stored in a data file (database) for later use (Section 3).

#### 2.4. Acceptable odor exposure limit

The acceptable odor exposure for neighbors/communities is a critical element in assessing the odor impact. To establish the acceptable level of odor exposure, two factors are considered in the current model: the odor level and the occurrence frequency at which the odor becomes a concern. Specifically, the odor exceedance hour (OEH) is calculated as the number of hours in a specific time frame (e.g., monthly or yearly) that the odor concentration exceeds an “exceedance threshold” (e.g.,  $1 \text{ OU m}^{-3}$ ). OEH is expressed as % of the total hours in the time frame. It should be noted that selecting the odor concentration exceedance threshold is somehow “arbitrary”, depending on several factors, including land use (e.g., rural vs. urban) and livestock species. The following table compiled by Sommer-Quabach et al. (2014) is provided to assist the user in selecting the acceptable odor exposure limit.

Table 1. Examples of acceptable odor exposure (limits) in some European countries  
(Sommer-Quabach et al., 2014).

Country	Protection level	Exceedance threshold ( $\text{OU m}^{-3}$ )	Exceedance hour (%)
Germany	Rural area	0.25	20
Ireland	Rural area, existing swine operations	6	2
	Residential area, proposed swine operation	3	2
Belgium	Pigs	6	2
Netherlands	Low population area, Proposed swine operations	1	2
	Low population area, Existing swine operations	3.5	2
	No serious odor annoyance	1	2

#### 3. Illustration of Model Application

When the program is launched, the user is first presented with a screen to enter the farm information, including the housing type, manure collection system, ventilation system, floor area, number of animals, and manure storage type and dimensions (Figure 2). The program calculates the emission rate for each building and manure storage as the information is entered and presents

the calculated rates on the screen. The user is asked if any odor abatement technologies are used. If yes, the program searches a database where odor reduction coefficients of various abatement technologies are stored and uses the reduction coefficients to modify the odor emission rate(s). The content of this database has been compiled from the data reported in the literature. Alternatively, the user can specify an odor reduction coefficient for a specific abatement technology no matter if the technology is already in the database or not. Once the farm information is completed, the user is prompted to select: (a) Annual Average; (b) Monthly; or (c) Seasonal (user defined) emission rate for use in the subsequent calculation of odor concentration based on the pre-run dispersion simulations.

The screenshot shows a software window with a red border. At the top, there are three tabs: 'Farm Buildings', 'Manure Storage', and 'References'. Below the tabs is a table with the following data:

Housing Type	Manure Collection System	Ventilation System	Odour Control Technology	Reduction	Flo
Sow, farrow to nursery	Shallow pit, partially-slatted...	Mechanical	None	.000	

In the center of the window, the text 'Summary of odour emission rates and entered parameters' is displayed in red. Below this, there are two sections: 'Swine Building Specifications' and 'Building Dimensions'.

**Swine Building Specifications**

Housing Type	Sow, farrow to nursery
Manure Collection System	Shallow pit, partially-slatted nursery
Ventilation System	Mechanical
Odour Control Technology	None
(1-Reduction)	1.000
Reduction	.000

**Building Dimensions**

Floor Area	9.923	m <sup>2</sup>
Number of animals	3.175	
animal units factor	.313	
Animal Units	993.78	

**Enter parameters here**

Figure 2. Screenshot of input screen where farm information is entered and odor emission rates are calculated.

Once the emission rate(s) is calculated, the program calls the database where the dispersion simulation data is stored (see Section 2.3 for dispersion simulations), and calculates the odor concentrations at all receptor points in the 10 km by 10 km grid defined in Section 2.3. The calculated odor concentrations are presented as an inactive plot. Specifically, when dragging the cursor over the plot, the program shows the x-and y-coordinates of the location relative to the swine operation and the hourly odor concentration at that location (Figure 3).

The user can then proceed to the next screen to select or specify the odor exceedance threshold ( $\text{OU m}^{-3}$ ), based on which the program calculates the odor exceedance hours (%) at all receptor points. The calculated odor exceedance hours are then presented as an inactive plot, on which the user can examine the odor exceedance hours at any location within the 10 km by 10 km grid by pointing the mouse cursor to the location, similar to the plot shown in Figure 3.

The last section is the calculation of Setback Distance (SD) by comparing the predicted odor exceedance hour ( $\text{OER}_{\text{pred}}$ ) against the specified odor exceedance hour ( $\text{OER}_{\text{spec}}$ ) at each and every receptor points. Specifically, the SD is the boundary that separates the region of  $\text{OER}_{\text{pred}} < \text{OER}_{\text{spec}}$  from the region of  $\text{OER}_{\text{pred}} > \text{OER}_{\text{spec}}$ . The determined SD is overlaid on a Google Earth map image (Figure 4). Different SD's can be calculated if the user specifies different  $\text{OER}_{\text{spec}}$  values and the program can also overlay the SD's based on the local regulations/guidelines on the same map.

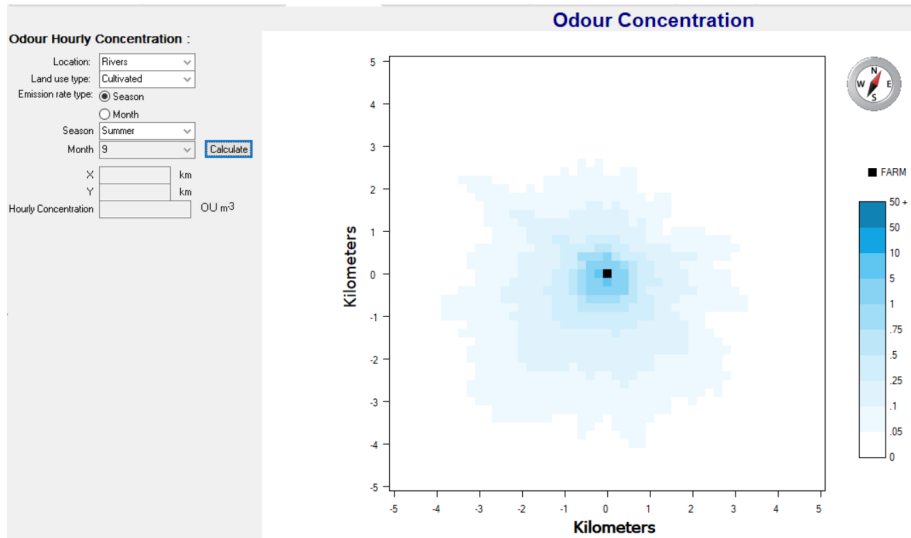
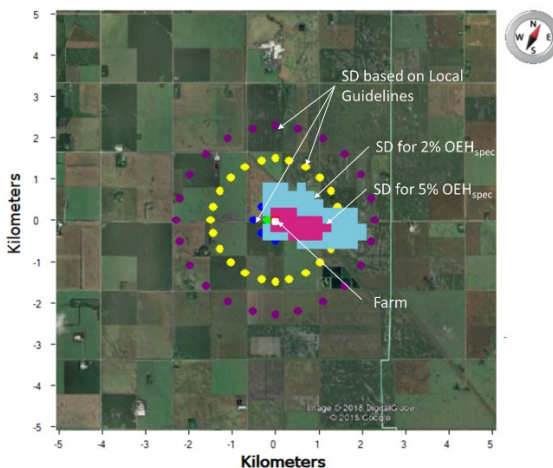


Figure 3. Predicted odor concentration in a 10 km by 10 km grid.

Figure 4. Screenshot pf predicted SD's (setback distance) for 2% and 5% OEH<sub>spec</sub> (odor exceedance hours specified by the user).

#### 4. Summary

A model was developed for assessing odor impact by swine operations. The model consists of three key elements: (i) odor emission rate estimation based on the data published in the literature; (ii) odor dispersion simulated by AERMOD; and (iii) odor impact criteria based on recommendations by several European countries. The model predicts odor distributions and occurrence frequency within a 10 km by 10 km grid centered around the swine facility. Odor impact is presented as interactive plots of odor concentrations and odor exceedance frequencies which is defined as the percent of hours of odor exceeding a specified exceedance threshold in a specific timeframe. The user may examine the odor impact at any location within the grid. The user may also select different odor impact criteria, such as odor concentration exceedance

threshold and allowable hours of odor exceedance, to determine the setback (separation) distances between the swine facility and the surrounding residences/communities. The results are graphically presented over a Google Earth map image.

### Acknowledgements

We wish to thank Van Doan, Petra Loro, Clay Sawka, and Timi Ojo from Manitoba Agriculture for their technical assistance and valuable suggestions, and to acknowledge the financial support from the Manitoba Livestock Manure Management Initiative (MLMMI). A special thank-you goes to John Carney of MIMML for assisting us in initiating this project.

### References

- Gao, Z., Q. Zhang, H. Guo, and A. La. 2012. Development of a dispersion-based setback distance model for mitigating odor impact from livestock operations. Paper No. 2012-A-269-AWMA, 2012 Air & Waste Management Associations Conference & Exhibition, San Antonio, TX, June 19–22. 8 pp.
- Mackie, R. I., P.G. Stroot, V.H. Varel. 1998. Biochemical identification and biological origin of key odor components in livestock waste. *Journal of Animal Science* 76(5):1331–1342.
- Priest, J.B., J. Zhu, R. Maghirang, L.L. Christianson, and G.L. Riskowski. 1994. Agricultural environments and their effects on animals, plants, workers, and the structure. ASAE Meeting Paper No. 94-4587. American Society of Agricultural Engineers, St. Joseph, MI.
- Schiffman, S.S., J.L. Bennett, J.H. Raymer. 2001. Quantification of odors and odorants from swine operations in North Carolina. *Agricultural and Forest Meteorology* 108(3):213–240.
- Sommer-Quabach, E., M. Piringer, E. Petz, G. Schuberger. 2014. Comparability of separation distances between odour sources and residential areas determined by various national odour criteria. *Atmospheric Environment* 95: 20–28.
- US-EPA. 2019. Support Center for Regulatory Atmospheric Modeling (SCRAM). <https://www.epa.gov/scram/air-quality-dispersion-modeling-preferred-and-recommended-models>, Accessed July 1, 2019.

# Economic Conditions for Implementing Solid-Liquid Separation Barn

Ryamond E. Massey <sup>a,\*</sup>, Teng-Teeh Lim <sup>b</sup>, Joe Zulovich <sup>b</sup>

<sup>a</sup> Division of Applied Social Sciences, University of Missouri, Columbia, MO 65211, USA

<sup>b</sup> Division of Food Systems and Bioengineering, University of Missouri, Columbia, MO 65211, USA

\* Corresponding author. Email: [masseyr@missouri.edu](mailto:masseyr@missouri.edu)

## Abstract

A University of Missouri study evaluated separation efficiency and operation of a 1200-hd solid-liquid separation pig finishing barn. Of particular interest was the feasibility of nutrient/liquid utilization from the separated liquid manure. The construction and operating costs of the separation system and the land application costs and nutrient values of both solid and liquid manure portions were compared to a deep-pit barn system. To better evaluate the solid-liquid separation facility, we compared the economic results of an unseparated manure system with a solid-liquid manure system. Existing economic models were used to estimate the benefit of the nutrients supplied by the manure, the costs of land applying the manure and the payback period for initial investments under different scenarios.

The 1200-hd farm had a 13.5 year payback period when it was built as a single barn/farm. Factors that affect the economic feasibility of the separation system include cost of the barn and equipment, quantity of manure, nutrient needs of nearby soils, predominate cropping system, percentage of land available for receiving manure solids and liquid components, and size/type of equipment used for manure application.

A sensitivity analysis revealed that further hauling distances reduced the payback period, making the separation system a more desirable investment. Larger farms able to capture economics of scale also reduced the payback period. This paper confirms that larger operations with multiple barns would have shorter payback period utilizing the solid-liquid separation barns.

**Keywords:** Cost, benefit, simulation, payback period, pig farm, nutrient management

## 1. Introduction

Manure as a crop fertilizer presents two challenges relative to using commercial crop fertilizers. First, manure has a low value:mass ratio. While the nitrogen (N), phosphorus (P) and potassium (K) fractions of manure are valuable fertilizers, they constitute only a small percentage of the mass of manure, especially for pig and dairy operations. Commodities with a low value:mass ratio can economically be transported only short distances and therefore are economically limited to localized markets.

Second, manure's N:P ratio may not match the N:P ratio needs for individual crops or cropping systems. Applying sufficient N for a corn crop will provide more P than that corn crop needs and removes. Farmers must choose either N or P content of manure to determine the application rate on any one crop or cropping system, aware that the other nutrient will be either under or over supplied.

Separating manure into its liquid and solid fractions impacts both of these challenges. The liquid and solid fractions will each have different N:P ratios than the unseparated manure (Brown et al., 2018). This will affect the application rate and, perhaps, the nutrient used to determine application rate. The separated liquid manure will have a lower value:mass ratio than unseparated manure and therefore is transported shorter distances to maximize its economic benefit/cost ratio. However, the solid fraction of the manure will have a higher value:mass and lower N:P ratios, which can be economically transported greater distances than the unseparated manure.

This paper expands on research published by Brown, et al. (2018) on a finishing hog barn in Missouri that implemented a solid-liquid separation system. Their research results will be

incorporated into an economic simulation model that estimates the costs and benefits of both fractions of the manure. The model helps determine the impacts of various management decisions such as cropping system, hauling distance and manure incorporation on the payback period for the additional investment necessary to separate liquids and solids. The objective is to determine the relative importance of various factors that influence the economic decision to incorporate solid-liquid separation into a manure management plan.

We compare a baseline system where the unseparated manure was surface applied to land eight km away to a system where the solid fraction of separated manure was hauled eight km and the liquid fraction was hauled 1.8 km. The solid-liquid system attempts to conserve manure supplied nutrients via injection of the liquid fraction and incorporation of the solid fraction. The purpose of the alternative system was to improve nutrient management flexibility and environmental quality while increasing net farm income.

## 2. Materials and Methods

### 2.1. Manure and cropping systems characteristics

Brown et al. (2018) conducted a two year study with the objectives of evaluating performance of a solid-liquid separation finishing barn in improving manure nutrient management, potential nutrient/water recycling based on filtration, and barn construction and operating costs. The researchers monitored a full-scale barn in Missouri to determine the production of liquid and solid fractions and the nutrient contents of each.

The baseline scenario was a typical 1200-head grow-finish facility with deep-pit under fully slatted floor, popular in the Mid-Western region of the U.S. They estimated the cost of a deep pit for the baseline scenario at \$45,000, amortized to \$2,250 year<sup>-1</sup>. The baseline scenario assumed 1,802 m<sup>3</sup> (476,000 gallon) of deep-pit slurry manure hauled eight km to access corn fields needing N, P and K fertility (Brown et al., 2018).

The alternative was a 1200-head grow-finish liquid-solid separation facility. The solid-liquid manure facility included \$11,000 for a conveyor system, \$32,000 for a solid manure storage shed, and \$62,000 for an uncovered liquid pit. Amortized cost of the solid-liquid manure storage and separation equipment was \$5,800 year<sup>-1</sup>. Maintenance and operating expenses for the liquid/solid system above those for the baseline scenario were estimated to be \$1,673 annually. The liquid-solid separation manure storage system created two streams of manure that were stored and land applied. The liquid fraction was assumed stored in a nearby uncovered concrete tank collecting rain water, resulting in 1,756 m<sup>3</sup> (464,000 gallon) annually land applied. The annual solid fraction amounted to 413 m<sup>3</sup> annually land applied (Brown et al., 2018).

Table 1 presents the nutrient contents of the unseparated manure and the liquid and solid fractions of the separated manure. Nutrients important for crop fertilization exist predominately in the solid fraction of the manure. The solid fraction of the manure contains 15.8 kg N m<sup>-3</sup>, 13.5 kg diphosphorus pentoxide (P<sub>2</sub>O<sub>5</sub>) m<sup>-3</sup> and 8.4 kg potash or potassium oxide (K<sub>2</sub>O) m<sup>-3</sup> compared to the liquid fraction containing only 3.3 kg N m<sup>-3</sup>, 1.5 kg P<sub>2</sub>O<sub>5</sub> m<sup>-3</sup> and 3.3 kg K<sub>2</sub>O m<sup>-3</sup>. The liquid fraction of the manure contains almost all nitrogen (97%) in the ammonium form (3.2 kg NH<sub>4</sub> m<sup>-3</sup>) while the solid fraction of the manure contains about 43% of total nitrogen in the ammonium form (6.8 kg NH<sub>4</sub> m<sup>-3</sup>).

Table 1. Summary of nutrient contents of the unseparated, solid and liquid manure samples.

Type of Manure	Total Nitrogen (kg N m <sup>-3</sup> )	Ammonium (kg NH <sub>4</sub> m <sup>-3</sup> )	Phosphorus (kg P <sub>2</sub> O <sub>5</sub> m <sup>-3</sup> )	Potassium (kg K <sub>2</sub> O m <sup>-3</sup> )
Liquid manure	3.3	3.2	1.5	3.3
Solid manure	15.8	6.8	13.5	8.4
Unseparated manure	5.9	3.7	4.1	4.2

Table 2 presents the crop need or nutrient removal rate of corn and soybeans (Silva, 2017). All manure was assumed applied to a corn-soybean crop rotation. Manure was applied to supply plant available nitrogen (PAN) at the recommended quantity necessary for expected yield. Corn needs nitrogen fertilization at the rate of 16.1 kg PAN Mg<sup>-1</sup> of expected yield. Because soybeans need no N fertilizer, manure was not applied to soybeans and its need was set to zero. Phosphorus and K were valued nutrients to both corn and soybeans because they were removed in the harvested grain or oilseed. Corn removes 6.6 kg P<sub>2</sub>O<sub>5</sub> Mg<sup>-1</sup> of grain harvested and 4.8 kg K<sub>2</sub>O Mg<sup>-1</sup> of grain harvested. Soybeans remove 13.3 kg P<sub>2</sub>O<sub>5</sub> Mg<sup>-1</sup> of grain harvested and 23.3 kg K<sub>2</sub>O Mg<sup>-1</sup> of grain harvested. It was assumed the no buildup of P and K was necessary and only crop need or removal applications of nutrients from manure were applied to maintain fertility.

Table 2. Summary of nutrient need or removal per Mg of corn and soybeans harvested and for total two year crop rotation.

Crop	Corn	Soybean	Total
Yield (Mg ha <sup>-1</sup> )	9.4	3.0	--
Nitrogen need			
(kg PAN Mg <sup>-1</sup> )*	16.1	0**	--
(kg PAN ha <sup>-1</sup> )*	151.3	0**	151.3
Phosphorus removal			
(kg P <sub>2</sub> O <sub>5</sub> Mg <sup>-1</sup> )*	6.6	13.3	
(kg P <sub>2</sub> O <sub>5</sub> ha <sup>-1</sup> )	62.2	40.4	102.6
Potassium removal			
(kg K <sub>2</sub> O Mg <sup>-1</sup> )*	4.8	23.3	
(kg K <sub>2</sub> O ha <sup>-1</sup> )	45.4	70.6	116.0

\* PAN is Plant Available Nitrogen

\*\* N need was set to zero because soybean, a legume, does not require N fertilization.

## 2.2. Simulation model

The economic evaluation compares a typical 1200-head grow-finish under barn deep pit facility with a 1200-head grow-finish solid-liquid separation facility. The net value of manure was calculated as the fertilizer value of the manure less application cost.

Manure was applied in the corn year of land planted to a corn-soybean rotation because corn requires N fertilization and soybean does not. Applying manure to corn ground uses the N portion of the manure. Manure was not applied to the individual fields in the year they were planted to soybeans. Fifty percent of the organic N was assumed available to plants in the year of application. Ninety percent of ammonium N (NH<sub>4</sub>) was assumed available to plants when the manure was applied using an Aerway applicator (an Aerway applicator punctures the soil so surface applied manure quickly moves into the soil) or surface applied and incorporated within 24 hours.

Nutrient removal was based on 9.4 Mg ha<sup>-1</sup> corn yields and 3.0 Mg ha<sup>-1</sup> soybean yields. Using removal rates reported in Table 2 N need and P and K removal over the two year cropping cycle are 151.3 kg PAN ha<sup>-1</sup>, 102.6 kg P<sub>2</sub>O<sub>5</sub> ha<sup>-1</sup> and 116.0 kg K<sub>2</sub>O ha<sup>-1</sup>.

Nutrients were valued only if they were needed or removed by the crop. Applied nutrients in excess of crop need or removal were not valued. The nutrient values were estimated as the five-year (2014–2018) average market values for commercial fertilizers – \$0.79 kg<sup>-1</sup>, \$0.95 kg<sup>-1</sup>, and \$0.73 kg<sup>-1</sup> for N, P<sub>2</sub>O<sub>5</sub>, and K<sub>2</sub>O, respectively (USDA). Micronutrients were not considered.

The baseline scenario assumed 1,802 m<sup>3</sup> of covered pit slurry manure transported eight km or more to access fields planted in a corn-soybean rotation and needing N, P and K fertilizer. Manure was hauled and applied with a 22.7-m<sup>3</sup> (6000-gallon) tanker and surface applied. Over time, the fields near the barn have become high in phosphorus, causing the need to transport the manure at least eight km every year.

In the separation facility, the 1,755 m<sup>3</sup> liquid fraction of the manure was stored outside and also collected rainwater. The 412 m<sup>3</sup> solid fraction of the manure was stored in a covered storage shed. The solid fraction of the manure was transported eight km or more to access fields planted in a corn-soybean rotation. The liquid manure was hauled 1.6 km to land planted in a corn-soybean rotation. Liquid manure was hauled a shorter distance because the liquid fraction N:P ratio and incorporation with an airway allows manure supplied P was removed in two years by the corn-soybean rotation. The liquid fraction was better balanced to the nutrient needs of the cropping system.

As in the baseline scenario, liquid manure was land applied using a 22.7-m<sup>3</sup> (6000-gallon) tanker. It differs in that the liquid fraction was incorporated using an Aerway applicator. However, solid manure was hauled and surface applied using an 18.9-m<sup>3</sup> side discharge spreader. It was incorporated within 24 hours using a disk.

To estimate the value of the manure supplied nutrients applied to the corn-soybean cropping system rotation, a spreadsheet entitled Value of Manure (Massey, 2008) was used. This spreadsheet allows the user to enter crop production and fertility needs (Table 2) along with the characteristics of the manure resource (Table 1). The manure was applied to corn to meet the nitrogen fertility needs. Applying manure to meet the nitrogen needs may apply more phosphorus than the corn will remove. Remaining P and K were valued to the extent they were removed by the subsequent crop harvest.

To estimate the cost of applying manure to the land, a spreadsheet entitled Manure Cost Distribution Analyzer (Massey, 2008) was used. This spreadsheet employs an engineering-economic model to estimate the time necessary for loading manure into spreaders, transporting the manure from the source to the fields in the spreaders, using the spreaders to apply manure to the fields, and travel of spreaders to return to source. The total number of hours needed for manure application was expensed at a custom rate of \$120 hr<sup>-1</sup> (Plastina et al., 2018).

Payback period was calculated by dividing the additional investment necessary for a solid-liquid separation facility (compared to unseparated under barn pit) by the net income available to pay for that investment. The shorter the payback period, the more viable the investment.

Table 3. Summary of manure and land management requirements for 1200-head grow-finish facility.

	Baseline: unseparated manure	Separated manure		
		Total separated manure	Liquid fraction	Solid fraction
Distance to fields (km)	8	--	1.6	8
Manure quantity (m <sup>3</sup> )	1,802	2,168	1,755	413
Tanker size (m <sup>3</sup> )	22.7	--	22.7	18.9
Application rate (m <sup>3</sup> ha <sup>-1</sup> )	34.1		51.4	14.0
Application time (hr <sup>-1</sup> )	97.9	79.0	44.7	34.3
Land required				
Annually (ha yr <sup>-1</sup> )	52.8	63.6	34.1	29.4
Rotation (ha rotation period <sup>-1</sup> )	105.6*	186.0	68.2*	128.6**

\* Assumes manure was applied every other year to a corn-soybean rotation.

\*\* Assumes manure was applied every fourth year to a corn-soybean rotation.

### 3. Results and Discussion

#### 3.1. Annual net value of manure

Manure in the baseline scenario was applied at the rate of 34.1 m<sup>3</sup> ha<sup>-1</sup>. This application supplied all necessary N for producing 9.4 Mg ha<sup>-1</sup> corn. Not all P and K applied was removed by

the two-year rotation of corn and soybean production. This is one reason that the baseline is considered unsustainable. Over time, P and K build up in the soil creates an environmental hazard. In addition, not all P and K nutrients were valued because not all were needed for crop production. This suggests the farmer was not maximizing the value of the manure resource.

The baseline scenario applies 1,802 m<sup>3</sup> of unseparated manure to 52.8 ha of corn ground each year. The total fertilizer value of all the manure produced in the baseline scenario, based on removal by both corn and soybeans, was \$15,971 yr<sup>-1</sup> (Table 4), or \$302.65 ha<sup>-1</sup>. All the plant available nitrogen (151 kg ha<sup>-1</sup>) was valued (\$120.09 ha<sup>-1</sup>) in the year applied. Phosphorus and potassium were applied in excess of crop removal. Only crop removal value of phosphorus (103 kg ha<sup>-1</sup> valued at \$97.75 ha<sup>-1</sup>) and potassium (117 kg ha<sup>-1</sup> valued at \$84.81 ha<sup>-1</sup>) was considered an economic benefit to the business.

Table 4. Summary of annual economic benefits and costs of manure from 1200-head grow-finish facility applied to a corn-soybean rotation.

	Unseparated manure	Total separated manure	Liquid fraction	Solid fraction
Fertilizer value (\$ yr <sup>-1</sup> )	15,971	20,876	9,537	11,339
Application cost (\$ yr <sup>-1</sup> )*	11,748	10,571	5,364	5,207
Net value	4,223	10,305	4,173	6,132

\*Custom application charge was \$100 hr<sup>-1</sup>

The hours to load the tanker, transport the manure eight km to nearby fields for land application using an Aerway applicator was 97.9 hr yr<sup>-1</sup>. Assuming a custom application rate of \$120 hr<sup>-1</sup>, the total application cost was \$11,748 yr<sup>-1</sup>. The baseline scenario manure net value was \$4,223 yr<sup>-1</sup>.

In the liquid-solid separation facility, the 1,755 m<sup>3</sup> liquid portion of the manure was applied to 34.1 ha of corn ground each year at the rate of 51.4 m<sup>3</sup> ha<sup>-1</sup>. The total fertilizer value of the liquid portion was \$9,537 yr<sup>-1</sup>, or \$279.51 ha<sup>-1</sup>. All the plant available nitrogen (151 kg ha<sup>-1</sup>) was valued (\$120.09 ha<sup>-1</sup>) in the year applied. All P<sub>2</sub>O<sub>5</sub> supplied (78.7 kg ha<sup>-1</sup>) was also valued (\$74.61 ha<sup>-1</sup>). Only K<sub>2</sub>O supplied by manure (170 kg ha<sup>-1</sup>) exceeded removal (117 kg ha<sup>-1</sup>) by the corn-soybean rotation earning an economic benefit of \$84.81 ha<sup>-1</sup>.

The hours to load the tanker, transport the liquid fraction of the manure 1.6 km to fields for land application using an Aerway applicator was 44.7 hr yr<sup>-1</sup>. Assuming a custom application rate of \$120 hr<sup>-1</sup>, the total application cost was \$5,364 yr<sup>-1</sup>. The liquid fraction of the manure has a net of \$4,173 yr<sup>-1</sup>.

In the liquid-solid separation facility, the 413 m<sup>3</sup> solid portion of the manure was applied to 29.4 ha of corn ground each year at the rate of 14.0 m<sup>3</sup> ha<sup>-1</sup>. Manure was applied every fourth year to a corn-soybean rotation so 128.6 ha of crop ground are needed for land application of the solid manure. The total fertilizer value of the solid portion was \$11,339 yr<sup>-1</sup>, or \$385.11 ha<sup>-1</sup>. All the plant available nitrogen (151 kg ha<sup>-1</sup>) was valued (\$120.09 ha<sup>-1</sup>) in the year applied. Phosphorus concentrated in the solid fraction of the manure also exactly meets the crop removal during the four-year rotation. Crop removal value of P (189 kg ha<sup>-1</sup> valued at \$179.15 ha<sup>-1</sup>) and K (118 kg ha<sup>-1</sup> valued at \$85.87 ha<sup>-1</sup>) was considered an economic benefit to the business.

The hours to load the 18.9-m<sup>3</sup> side discharge spreader, transport the solid fraction of the manure eight km to a field for land application, apply the manure and return was 34.3 hr yr<sup>-1</sup>. Assuming a custom application rate for manure of \$120 hr<sup>-1</sup> and \$37.07 ha<sup>-1</sup> for disketing, the total application cost was \$5,207 yr<sup>-1</sup>. The solid fraction of the manure has a net value of \$6,132 yr<sup>-1</sup>.

### 3.2. Marginal analysis and payback period

The total separated manure scenario yielded an annualized manure value of \$20,876 and an

annual cost of \$10,571. The net value of the solid-liquid separated manure was \$10,305 yr<sup>-1</sup> compared to a net value of \$4,223 yr<sup>-1</sup> for the baseline, unseparated manure. The marginal net value of the solid-liquid separation manure system over the baseline unseparated manure system was \$6,081 yr<sup>-1</sup>.

Brown, et al. (2018) estimated that the solid-liquid separation system would require an investment of \$105,000 compared to an investment of \$45,000 for under barn pit storage. The additional \$60,000 investment needs to be recovered by the marginal benefit of the solid-liquid separation manure system. In addition to the initial investment, the solid-liquid separation incurs an additional maintenance expense of \$1,673 yr<sup>-1</sup>.

The payback period was the additional investment (\$60,000) divided by \$4,408, the difference of the marginal benefit of the manure (\$6081 yr<sup>-1</sup>) minus the additional annual maintenance (\$1,673 yr<sup>-1</sup>). The payback period was estimated to be 13.6 years.

The payback period of 13.6 years is not financially optimal. Payback periods of less than 10 years and closer to 5 years are desirable for business investments. A sensitivity analysis of certain assumptions was conducted next to determine what factors might reduce payback periods to desirable levels.

### 3.3. Sensitivity analysis

For brevity reasons, only the results of the sensitivity analysis are provided. All factors except those noted were the same as in the above simulations. The results of various changes can be seen in Table 5. Marginal refers to the difference between the results of the solid-liquid separated manure and the unseparated manure.

Increased land application distance increases application costs. The initial analysis assumed that the manure would be applied eight km from the source of the manure. When multiple barns were congregated at a farm, more land application fields that are further away are likely needed to receive the relatively larger amount of manure. If the distance to haul the unseparated manure and the solid fraction of the separated manure was doubled to 16 km, the application cost would increase more for the unseparated manure than for the solid fraction because the quantity of the unseparated manure is over four times that of the solid fraction of the separated manure. This would result in a marginal application savings.

The marginal manure application savings for a 1200-head grow-finish facility when hauling the manure 16 km was estimated to be \$5,603 yr<sup>-1</sup>, providing a marginal net value of manure of \$10,508 yr<sup>-1</sup>. No other costs or benefits are expected to change. The payback period was estimated to be 6.8 years. Comparing the payback period of 6.8 years for manure hauled 16 km to the payback period of 13.6 years for manure hauled eight km illustrates how solid-liquid separation systems may be more feasible for farmers who have to haul more manure farther distances to sustainably land apply it.

Increased size of operation may also affect the payback period. The increased size would increase the total fertilizer value and total application costs relative to a smaller facility. The expense to install solid-liquid systems would likely be less expensive for larger facilities due to economies of scale.

For illustration, we modeled a 4800-head grow-finish facility. We assumed that the cost of installing and maintaining the manure system in the larger facility would provide a 10% savings. We estimated the investment needed to install a solid-liquid separation system for a 4800-head grow-finish facility to be 90% of four times the expense of the 1200-head grow-finish facility. We estimated the payback period for the larger facility assuming both an eight km and a 16 km manure hauling distance.

Referring to Table 5, the payback period for a 4800-head grow-finish facility with solid-liquid separation hauling manure eight km was estimated to be 10.4 years. Comparing the 10.4 year payback period for the 4800-head facility to the 13.6 year payback period of the 1200-head facility

illustrates how solid-liquid separation systems may be more feasible for larger farmers who can take advantage of economies of scale and additional land needing manure supplied nutrients.

If the 4800-head facility also must haul the manure 16 km the payback period was reduced even further to 6.1 years.

The solid-liquid separation system values all N and P in both the liquid and solid portions when applied to a corn-soybean rotation as described above. The unseparated manure over-applies P and, therefore, not all was valued. We chose to estimate the impact of a 10% increase in the value of P on the payback period of the 4800-head facility hauling manure 16 km. The payback period was further reduced to 5.9 years from the 6.1 year payback period of the same system with less valuable P.

Table 5. Sensitivity analysis of various factors on the net benefit of manure and the payback period of the necessary investment in solid-liquid separation.

	Size of facility (head)				
	1200	1200	4800	4800	4800
Economic Measure	Distance manure hauled (km)				
	8	16	8	16	16
P <sub>2</sub> O <sub>5</sub> price (\$ kg <sup>-1</sup> )	.95	.95	.95	.95	1.06
Marginal fertilizer value (\$ yr <sup>-1</sup> )	4905	4,905	19,619	19,619	20,857
Marginal application savings (\$ yr <sup>-1</sup> )	1,177	5,603	7,266	2,2182	22,182
Marginal net value (\$ yr <sup>-1</sup> )	6,082	10,508	26,885	41,801	43,039
Maintenance of S-L system (\$ yr <sup>-1</sup> )	1,673	1,673	6,023	6,023	6,023
Benefit available to repay investment (\$ yr <sup>-1</sup> )	4,409	8,835	20,862	35,778	37,016
Additional investment (\$)	60,000	60,000	217,637	217,637	217,637
Payback period (yr)	13.6	6.8	10.4	6.1	5.9

#### 4. Conclusions

Solid-liquid separation of manure changes the product delivered to plants, altering the rates applied, the quantity of land needed for manure application, and the value and cost of manure management. This analysis shows that the total value of the separated manure exceeds the total value of the unseparated manure in all situations modeled. The solid-liquid separation manure fractions were applied to less land in any one year, resulting in reduced land application costs. More land was needed during the rotation (time before the manure could be applied to the same piece of land) for a solid-liquid separation system. This additional land receiving manure was partly responsible for the increased value of the manure applied.

The combination of higher fertilizer value from the separated solid and liquid fractions of the manure combined with lower annual application costs, provided a net benefit that could be used to repay the investment in manure separation systems. The payback period of 13.6 years for the initial analysis of a single barn only indicated separation was not a strong investment. However, changes could be made that decreased the payback period and increased its attractiveness.

The necessity to haul manure further distances to sustainably land apply was the strongest factor in decreasing the payback period. However, our analysis also showed that taking advantage of the economies of scale for larger pork facilities also reduces payback period. Given that larger operations are more likely to have to travel long distances to sustainably land apply manure, solid-liquid separation needs to be further investigated.

A weaker factor influencing payback period was the value of P fertilizer. Increasing P fertilizer cost by 10%, increased the value of manure without increasing application costs allowing a slight reduction in payback period.

Other factors that make solid-liquid separation more economically feasible that were modeled

but not reported here include the size of the manure transportation equipment, various cropping systems and their nutrient needs, and incorporation vs surface application of the manure. The results indicate that further work is necessary to determine when solid-liquid separation makes economic sense and compare with other manure land application system such as drag-line, and feasibility of further processing the separated solid manure into organic fertilizer or compost by products. This is especially true when the animal farms tend to become larger in size and more congregated at certain areas.

### References

- Brown, J., T. Lim, J. Zulovich, and C. Costello. 2018. Sustainability Evaluation of a Solid-Liquid Manure Separation Operation. National Pork Board Research Report NPB#16-094.
- Massey, Raymond E. Value of Manure. 2008. Spreadsheet program for EXCEL. University of Missouri Commercial Agriculture Program. <https://extensiondata.missouri.edu/Pro/Swine/Docs/ManureValueEstimator.xlsx>. Accessed June 24, 2019
- Massey, Raymond E. Manure Distribution Cost Analyzer. 2008. Spreadsheet Program for EXCEL. University of Missouri Commercial Agriculture Program. <https://extensiondata.missouri.edu/Pro/Swine/Docs/ManureCostAnalyzer.xlsm>. Accessed June 24, 2019
- Plastina, A., A. Johanns and C. Welter. 2018. 2018 Iowa Farm Custom Rate Survey. Iowa State University Extension and Outreach. Ag Decision Maker File A3-10.
- Silva, George. 2017. Nutrient Removal Rates by Grain Crops. Michigan State University Extension. [https://www.canr.msu.edu/news/nutrient\\_removal\\_rates\\_by\\_grain\\_crops](https://www.canr.msu.edu/news/nutrient_removal_rates_by_grain_crops). Accessed June 18, 2019.
- USDA. Quickstats. <https://quickstats.nass.usda.gov/>. Accessed June 24, 2019.

# Preparation of UiO-66 (Zr) Series MOFs and Their Adsorption of Heavy Metals in Animal Wastewater

Leiping Wang<sup>a,b</sup>, Yifeng Jiang<sup>b</sup>, Jianrong Li<sup>a</sup>, Dezhao Liu<sup>c</sup>, Zun Man<sup>c</sup>, Xiaorong Dai<sup>a,\*</sup>

<sup>a</sup> Center for Excellence in Regional Atmospheric Environment & Key Laboratory of Urban Environment and Health, Institute of Urban Environment, Chinese Academy of Sciences, Xiamen, Fujian 361021, P.R. China

<sup>b</sup> College of Environment, Zhejiang University of Technology, Hangzhou, Zhejiang 310014, P.R. China

<sup>c</sup> College of Biosystems Engineering and Food Science, Zhejiang University, Hangzhou, Zhejiang 310058, P.R. China

\* Corresponding author. Email: [xrdai@zjue.ac.cn](mailto:xrdai@zjue.ac.cn)

## Abstract

With the continuous development of intensive livestock and poultry breeding production, large amount of heavy metals such as copper (Cu), zinc (Zn) and iron (Fe) were used as feed additives to improve the feed efficiency and animal growth rate, as well as to prevent animals from disease. Most of these superfluous heavy metals (HMs), however, were excreted to the environment through animal feces and urine. Thus when the HMs from animal wastewaters accumulate in the soil, they can be absorbed by crops and plants. Then, they will affect animals and human health directly through the food chain. This study has investigated the feasibility of metal organic framework (MOF) materials for the adsorption and removal of HMs in animal wastewater. The Zr-MOFs, including UiO-66, UiO-66-NH<sub>2</sub>, UiO-66-NO<sub>2</sub> and UiO-66-COOH were prepared by hydrothermal method. The effects of different pH (2–10), retention time (10–600 min) and initial concentrations (0–10 g L<sup>-1</sup>) of Zr-MOFs on the adsorption efficiency of HMs in animal wastewater were investigated. Results show that availability of UiO-66-COOH on the removal of various HMs in animal wastewater has more limitations than the other three materials. The removal efficiency of UiO-66, UiO-66-NH<sub>2</sub> and UiO-66-NO<sub>2</sub> on heavy metals Mn, Zn, As, Sb and Pb in animal wastewater, reached over 80%. The removal effect of UiO-66-NO<sub>2</sub> on HMs, such as copper (Cu) and arsenic (As), was higher than that of UiO-66 and UiO-66-NH<sub>2</sub>. The adsorption effects of UiO-66, UiO-66-NO<sub>2</sub> and UiO-66-COOH on HMs in animal wastewater were negligible under the influence of pH.

**Keywords:** Zr-based metal-organic frameworks, heavy metal ion removal, adsorption, UiO-66, swine wastewater.

## 1. Introduction

With the increase consumption of pork in Chinese market, intensive livestock production has developed rapidly in China. In order to reduce the occurrence of livestock diseases and increase animals' growth rate, various trace elements (i.e., Cu, Zn, and As) were added in commercial feed products used in the large-scale farms. However, due to the poor metabolism, more than 90% of these additives are excreted in animal manure, resulting in the high concentration of heavy metals (HMs) in animal wastewater. Subsequent use of animal wastewater as agricultural irrigating and fertilizing can lead to a number of environmental problems, including salt toxicity to plants and accumulation of heavy metals in ground water and soil (Li et al., 2019). Therefore, removal of heavy metals from animal wastewater before released to the environment is crucial.

In recent years, porous materials composed of metal organic frameworks (MOFs) have attracted considerable attention in separation, energy conversion, catalysis, sensing, organic degradation, biomedical applications, and metal ion adsorption due to their unique structural properties (Ma et al., 2009). Many studies have shown that MOF-type materials can be used to adsorb and remove harmful metal ions from the environment because of its high surface area, low bulk density and the ability to capture target components in both physical and chemical adsorption states (Fang et al., 2005; Zhang et al., 2015; Kobielska et al., 2018). In addition, appropriate

modification of MOFs with specific functions can improve the adsorption performance (Saleem et al., 2016). Among these MOFs, UiO-66 ( $\text{Zr}_6\text{O}_4(\text{OH})_4(\text{CO}_2\text{C}_6\text{H}_4\text{CO}_2)_6$ ) has attracted wide attention in the field of adsorption due to its good selectivity, large working capacity, low regeneration cost and easy modification (Bai et al., 2016; Embaby et al., 2018). Besides, different types of functional groups (i.e., -Br, -COOH, -NO<sub>2</sub>, -NH<sub>2</sub>, etc.) were applied as simple modification method to obtain high adsorption capacity and selective sites for specific pollutants (Katz et al., 2013; Reinsch et al., 2015; Lin et al., 2016). In this study, batch adsorption experiments were conducted to compare the adsorption performance of UiO-66, UiO-66-NO<sub>2</sub>, UiO-66-COOH and UiO-66-NH<sub>2</sub> on heavy metals removal in swine wastewater. The effects of adsorption parameters such as pH, initial concentration of MOFs and contact time on the metal ions sorption were investigated. These pioneering experimental results would shed light on the MOFs material applications in the complicated animal wastewater treatment.

## 2. Materials and Methods

### 2.1. Materials

Zirconium chloride (99.9%), p-phthalic acid (99%), 2-aminoterephthalic acid (98%), nitroterephthalic Acid (98%), trimellitic acid (98%), N,N-dimethylformamide (99.5%) were supplied by Aladdin Company (Shanghai, China), and acetone (99.5%) was bought from TEDA High Purity Solvents (America). Hydrochloric acid (HCl, 36%–38%), ethanol (99.5%) and methanol (99.5%) were purchased from Sinopharm Chemical Reagent Co., Ltd. (China). All reagents were used as received without further purification.

### 2.2. Preparation of adsorbent

UiO-66 was prepared based on the previously reported method (Kandiah et al., 2010; Katz et al., 2013). A 10 mmol of  $\text{ZrCl}_4$  and 10 mmol of terephthalic acid were dissolved in 60 mL of N'N'-dimethylformamide, and the mixture was thoroughly stirred. The resulting solution was transferred to a 100 mL stainless steel polytetrafluoroethylene-lined autoclave and reacted at 120 °C for 24 h. After cooling to room temperature, the obtained solid was centrifuged, washed with N'N'-dimethylformamide and methanol three times, dried overnight and then triturated to give UiO-66 as a white powder. The synthesis of UiO-66-NH<sub>2</sub>, UiO-66-NO<sub>2</sub> and UiO-66-COOH was done following the same procedure and keeping the same conditions as preparing UiO-66, except replacing terephthalic acid with 2-aminophthalic acid, 2-Nitrophthalic acid and 1,2,4-benzenetricarboxylic acid, respectively.

### 2.3. Heavy metals adsorption process

The animal wastewater sample used in this experiment was collected from a local swine farm in Fenghua area in Ningbo City. The batch adsorption tests in this study were all conducted at room temperature. A 200 mL liquid sample was placed in 500 mL beaker, and after the adsorbent was added, the mixture was stirred by magnetic stirring at a speed of 200 r min<sup>-1</sup>. The removal efficiency (R, %) of heavy metals was calculated by the following formula:

$$R = \frac{C_0 - C_e}{C_0} \times 100\% \quad (3)$$

where  $C_0$  is the initial metal ion concentration ( $\mu\text{g L}^{-1}$ ) and  $C_e$  is the final equilibrium concentration ( $\mu\text{g L}^{-1}$ ). All metal ion concentrations were determined by inductively coupled plasma mass spectrometry (ICP-MS, Thermo icap Q) before and after adsorption. The pH of the wastewater was adjusted by using 1 M HCl solution and 1 M NaOH before MOFs was added for evaluating the pH effect on the removal efficiency.

### 2.4. Characterization

The micrographs of the synthesized Zr-MOF samples were obtained using a scanning electron microscopy (SEM) instrument (S-4800, Hitachi, Japan).

### 3. Results and Discussion

#### 3.1. Morphology and structure of Zr-MOFs

The surface morphology of synthesized UiO-66 series adsorbents were captured by SEM image as shown in Figure 1. The crystal structure of UiO-66-NO<sub>2</sub>, UiO-66-COOH and UiO-66-NH<sub>2</sub> exhibited the same spatial arrangement of inorganic building units as UiO-66. However, the primary particle size differed among them. The UiO-66 featured nanoscaled crystals size in the range of 15–50 nm in size, while UiO-66-NO<sub>2</sub>, UiO-66-COOH and UiO-66-NH<sub>2</sub> were approximately 100 nm. The increased size in the functionalized UiO-66 series is attributed to the additional elements from 2-aminophthalic acid, 2-Nitrophthalic acid and 1,2,4-benzenetri carboxylic acid ligand in UiO-66-NH<sub>2</sub>, UiO-66-NO<sub>2</sub> and UiO-66-COOH.

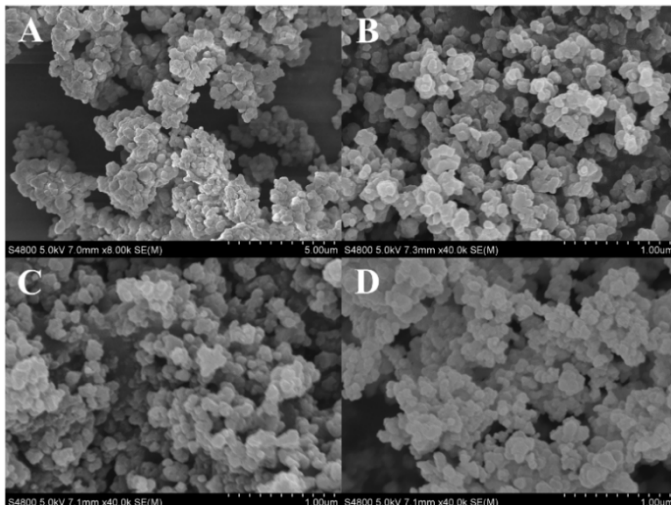


Figure 1. The SEM images of synthesized UiO-66 series adsorbents: (A). UiO-66; (B). UiO-66-COOH; (C). UiO-66-NH<sub>2</sub>; (D). UiO-66-NO<sub>2</sub>.

#### 3.2. Removal of HMs from animal wastewater

Table 1 presents the initial concentrations and the removal rate of heavy metals in animal wastewater by UiO-66 series adsorbents. The initial concentrations of twelve metal ions (Cr, Mn, Fe, Co, Ni, Cu, Zn, As, Cd, Sb, Ba and Pb) were measured, and the primary mental ions were Fe, Zn and Cu, with concentrations of 1000.8 µg L<sup>-1</sup>, 570.17 µg L<sup>-1</sup>, and 120.08 µg L<sup>-1</sup>, respectively. Results showed that the removal efficiency of UiO-66, UiO-66-NH<sub>2</sub> and UiO-66-NO<sub>2</sub> and UiO-66-COOH on arsenic (As) and antimony (Sb) was over 93%, on manganese (Mg), zinc (Zn), and lead (Pb) was over 83%, on barium (Ba) was over 70%, on iron (Fe) and copper (Cu) was over 60%, and on cobalt (Co) was over 50%. The adsorption efficiency of UiO-66 below 50% included two metal ions (Co and Cd), which had a relatively low initial concentrations in the animal wastewater. Similar results were obtained with other three adsorbents. The results also showed that functional groups (-NH<sub>2</sub>, -NO<sub>2</sub> and -COOH) did not improve the adsorption efficiency significantly as compared with UiO-66.

#### 3.3. Effect of dosage of adsorbents on HMs removal

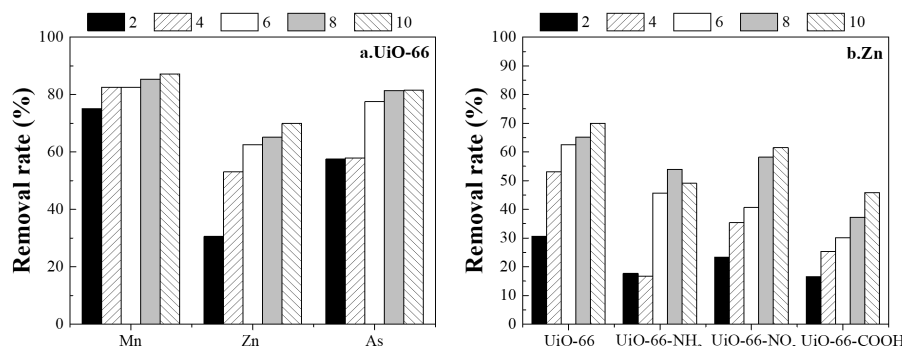
Effects of the initial adsorbent concentrations (a.k.a. dosage of adsorbents) on the removal of HMs (Mn, As and Zn as examples) by the UiO-66 are shown in Figure 2a. The adsorption amount of Zn increased markedly with increasing of initial UiO-66 concentration. While, removal rates of Mn affected by the initial concentrations were not significantly different between the dosages

in  $4 \text{ g L}^{-1}$  and  $6 \text{ g L}^{-1}$ , and the dosages in  $8 \text{ g L}^{-1}$  and  $10 \text{ g L}^{-1}$ . When the initial  $\text{UiO-66}$  concentration was up to  $10 \text{ g L}^{-1}$ , the equilibrium removal rate of Mn and As onto the  $\text{UiO-66}$  was 82.48% and 57.94%, respectively. Generally, the removal rate of HMs increased along with the increasing of initial adsorbent concentrations, this could attribute to the increased contact between heavy metals and chelating sites on adsorbents, and finally the adsorption reached saturation owing to the insufficient driving force of the concentration gradient of heavy metal in solution.

Table 1. Removal efficiencies of heavy metals by the Zr-metal organic framework materials.

Heavy metal	Concentration ( $\mu\text{g L}^{-1}$ )	R (%)		
		UiO-66	UiO-66-NH <sub>2</sub>	UiO-66-NO <sub>2</sub>
Chromium (Cr)	8.50	68.16	67.71	49.92
Manganese (Mn)	46.04	95.08	87.41	94.63
Iron (Fe)	1000.80	82.45	61.80	77.54
Cobalt (Co)	6.32	49.09	68.30	58.98
Nickel (Ni)	21.94	63.75	41.80	38.13
Copper (Cu)	120.08	68.45	59.76	68.69
Zinc (Zn)	570.17	85.54	83.40	87.21
Arsenic (As)	14.30	95.37	95.60	97.10
Cadmium (Cd)	0.35	36.09	20.92	45.31
Antimony (Sb)	1.37	96.13	93.70	96.84
Barium (Ba)	15.94	74.99	71.14	73.62
Lead (Pb)	7.37	89.09	83.87	90.46

As shown in Figure 2b, with the initial concentration (dosage) of adsorbents increased from  $2 \text{ g L}^{-1}$  to  $10 \text{ g L}^{-1}$ , the removal rate of heavy metals by the four adsorbents were also increased. When the amount of adsorbents were  $10 \text{ g L}^{-1}$ , the removal rates of Zn by  $\text{UiO-66-NO}_2$ ,  $\text{UiO-66-COOH}$  and  $\text{UiO-66-NH}_2$  were 61.52%, 45.84% and 49.10% respectively, while the removal rate of Zn by  $\text{UiO-66}$  was 69.90%. At the initial concentration of  $2 \text{ g L}^{-1}$ ,  $4 \text{ g L}^{-1}$ ,  $6 \text{ g L}^{-1}$ ,  $8 \text{ g L}^{-1}$  and  $10 \text{ g L}^{-1}$ , the equilibrium removal rate of Zn onto the  $\text{UiO-66}$  was 30.55%, 53.05%, 62.56%, 65.12% and 69.90%, respectively.

Figure 2. Removal rates of Mn, Zn, and As by  $\text{UiO-66}$  series materials at different dosages of adsorbents ( $\text{g L}^{-1}$ ).

### 3.4. Effect of the solution pH values

The pH of the solution plays an important role in the adsorption process. It not only affects the surface charge of the adsorbent, but also affects the degree and morphology of metal ions in

the solution (Kołodyńska et al., 2012). Normally, UiO-66 adsorbent is electrically neutral in aqueous solution (Zou and Liu, 2019). As shown in Figure 3a, with the increase of solution pH value, the removal rates of Cr by UiO-66-COOH and UiO-66-NH<sub>2</sub> increased, while the removal rate of UiO-66 decreased. Under the different pH conditions, Cr in the solution exists in the form of HCrO<sup>4-</sup>, Cr<sub>2</sub>O<sub>7</sub><sup>2-</sup> or CrO<sub>4</sub><sup>2-</sup>. When the solution is acidic, the surface charge of UiO-66 triggers protonic reaction and promotes the electrostatic adsorption of Cr (Sari and Tuzen, 2008). Simultaneously, with the increase of pH value, the existence of OH<sup>-</sup> competes with CrO<sub>4</sub><sup>2-</sup>, resulting in the reduction of Cr removal rate (Fan et al., 2017). The influence of pH on the removal rates of Zn by UiO-66, UiO-66-COOH and UiO-66-NH<sub>2</sub> are exhibited in the Figure 3b. The removal rates of Zn by UiO-66 series MOFs all reached over 70%, indicating that the pH value has little influence on the adsorption of Zn in solution. The best removal rates of UiO-66, UiO-66-NH<sub>2</sub> were obtained at pH 8. This may be due to the high pH that caused the Zn<sup>2+</sup> to react to form Zn(OH)<sub>3</sub><sup>-</sup> and Zn(OH)<sub>4</sub><sup>2-</sup>.

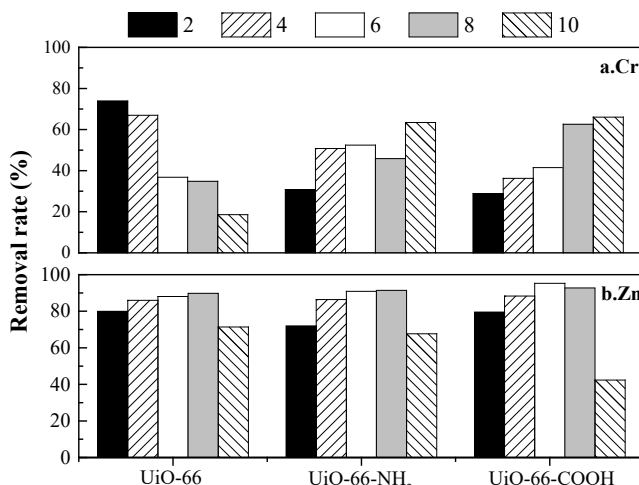


Figure 3. Removal rates of Zn and Cr by UiO-66, UiO-66-NH<sub>2</sub> and UiO-66-COOH at different pH values.

### 3.5. Effect of reaction time on HMs removal

Figure 4 shows the effect of contact time on the adsorption of heavy metals by UiO-66. All the adsorption tests on time series were carried out at room temperature and pH 8. As shown in Figure 4, the removal rates of As, Mn and Pb improved dramatically in the initial 60 min, then the removal rates reached 92.82%, 93.89% and 89.72% at equilibrium respectively. Owing to saturation of the adsorption sites at the later stage of adsorption test, the removal rate remained stable from 90 min to 270 min. Therefore, the removal rate of Cr by UiO-66 was significantly improved at 90 min, and the equilibrium rate finally reached 88.22%. The maximum removal rate of Fe by UiO-66 was only 64.25%, which is lower than that of other five metal ions listed in Figure 4. The possible reasons might be the high initial concentration of Fe in the wastewater and co-existing ions' competition on the adsorbents. The adsorption of most heavy metals by UiO-66 reached a balance at 120 min, and the removal rates were above 70% except for iron. Therefore, in practical application or experiment, 2 hours can be selected as the best processing time.

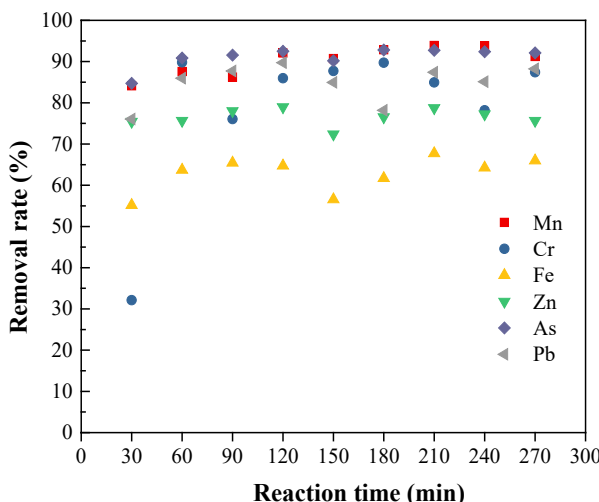


Figure 4. Removal rates of heavy metals by UiO-66 at different retention time.  
(Note: initial UiO-66 concentration = 4 g L<sup>-1</sup>).

#### 4. Conclusions

UiO-66 series metal organic framework materials (MOFs) were studied to remove heavy metals in swine wastewater. The results showed that the removal rates of heavy metals such as Mn, Zn, As, Sb and Pb in animal wastewater by UiO-66 series MOFs reached more than 80%. While at a pH range of 2–8, the removal efficiency of Zn was not significantly affected, at a pH of 10, the removal of Zn by all four adsorbents decreased. With the initial concentration of adsorbents increased from 2 g L<sup>-1</sup> to 10 g L<sup>-1</sup>, the removal rates of heavy metals by the four adsorbents were also increased. The adsorption of heavy metals by UiO-66 reached a balance at 120 min. Results suggest that 2 hours is an appropriate retention time in practical or experimental application in the future.

#### Acknowledgements

This study is supported by the National Science Foundation for Young Scientists of China (Grant No. 41605094).

#### References

- Bai, Y., Y. Dou, L.H. Xie, W. Rutledge, J.R. Li, H.C. Zhou, 2016. Zr-based metal-organic frameworks: design, synthesis, structure, and applications. *Chem Soc Rev.* 45 (8), 2327–2367. <http://dx.doi.org/10.1039/c5cs00837a>.
- Embabay, M.S., S.D. Elwany, W. Setyaningsih, M.R. Saber, 2018. The adsorptive properties of UiO-66 towards organic dyes: A record adsorption capacity for the anionic dye Alizarin Red S. *Chinese Journal of Chemical Engineering.* 26 (4), 731–739. <http://dx.doi.org/10.1016/j.cjche.2017.07.014>.
- Fan, S., Y. Wang, Y. Li, J. Tang, Z. Wang, J. Tang, X. Li, K. Hu, 2017. Facile synthesis of tea waste/Fe<sub>3</sub>O<sub>4</sub> nanoparticle composite for hexavalent chromium removal from aqueous solution. *RSC Advances.* 7 (13), 7576–7590. <http://dx.doi.org/10.1039/c6ra27781k>.
- Fang, Q., G. Zhu, M. Xue, J. Sun, Y. Wei, S. Qiu, R. Xu, 2005. A metal-organic framework with the zeolite MTN topology containing large cages of volume 2.5 nm<sup>3</sup>. *Angew Chem Int Ed Engl.* 44 (25), 3845–3848. <http://dx.doi.org/10.1002/anie.200462260>.

- Kandiah, M., M.H. Nilsen, S. Usseglio, S. Jakobsen, U. Olsbye, M. Tilset, C. Larabi, E.A. Quadrelli, F. Bonino, K.P. Lillerud, 2010. Synthesis and Stability of Tagged UiO-66 Zr-MOFs. *Chemistry of Materials*. 22 (24), 6632–6640. <http://dx.doi.org/10.1021/cm102601v>.
- Katz, M.J., Z.J. Brown, Y.J. Colon, P.W. Siu, K.A. Scheidt, R.Q. Snurr, J.T. Hupp, O.K. Farha, 2013. A facile synthesis of UiO-66, UiO-67 and their derivatives. *Chemical Communications*. 49 (82), 9449–9451. <http://dx.doi.org/10.1039/c3cc46105j>.
- Kobielska, P.A., A.J. Howarth, O.K. Farha, S. Nayak, 2018. Metal–organic frameworks for heavy metal removal from water. *Coordination Chemistry Reviews*. 358, 92–107. <http://dx.doi.org/10.1016/j.ccr.2017.12.010>.
- Kołodyńska, D., R. Wnętrzak, J.J. Leahy, M.H.B. Hayes, W. Kwapiński, Z. Hubicki, 2012. Kinetic and adsorptive characterization of biochar in metal ions removal. *Chemical Engineering Journal*. 197, 295–305. <http://dx.doi.org/10.1016/j.cej.2012.05.025>.
- Li, J., Y. Xu, L. Wang, F. Li, 2019. Heavy metal occurrence and risk assessment in dairy feeds and manures from the typical intensive dairy farms in China. *Environ Sci Pollut Res Int*. 26 (7), 6348–6358. <http://dx.doi.org/10.1007/s11356-019-04125-1>.
- Lin, K.A., Y.T. Liu, S.Y. Chen, 2016. Adsorption of fluoride to UiO-66-NH<sub>2</sub> in water: Stability, kinetic, isotherm and thermodynamic studies. *Journal of Colloid and Interface Science*. 461, 79–87. <http://dx.doi.org/10.1016/j.jcis.2015.08.061>.
- Ma, L., C. Abney, W. Lin, 2009. Enantioselective catalysis with homochiral metal–organic frameworks. *Chem Soc Rev*. 38 (5), 1248–1256. <http://dx.doi.org/10.1039/b807083k>.
- Reinsch, H., B. Bueken, F. Vermoortele, I. Stassen, A. Lieb, K.-P. Lillerud, D. De Vos, 2015. Green synthesis of zirconium-MOFs. *CrystEngComm*. 17 (22), 4070–4074. <http://dx.doi.org/10.1039/c5ce00618j>.
- Saleem, H., U. Rafique, R.P. Davies, 2016. Investigations on post-synthetically modified UiO-66-NH<sub>2</sub> for the adsorptive removal of heavy metal ions from aqueous solution. *Microporous and Mesoporous Materials*. 221, 238–244. <http://dx.doi.org/10.1016/j.micromeso.2015.09.043>.
- Sari, A., M. Tuzen, 2008. Biosorption of total chromium from aqueous solution by red algae (*Ceramium virgatum*): Equilibrium, kinetic and thermodynamic studies. *Journal of Hazardous Materials*. 160 (2–3), 349–355. <http://dx.doi.org/10.1016/j.jhazmat.2008.03.005>.
- Zhang, Y., X. Zhao, H. Huang, Z. Li, D. Liu, C. Zhong, 2015. Selective removal of transition metal ions from aqueous solution by metal–organic frameworks. *RSC Advances*. 5 (88), 72107–72112. <http://dx.doi.org/10.1039/c5ra09897a>.
- Zou, D., D. Liu, 2019. Understanding the modifications and applications of highly stable porous frameworks via UiO-66. *Materials Today Chemistry*. 12, 139–165. <http://dx.doi.org/10.1016/j.mtchem.2018.12.004>.

**Theme V:**  
**Precision Livestock Farming**



## A Novel Quantification Method for Keel Bone Fracture and Deformation of Laying Hens

Kailao Wang <sup>a,b</sup>, Brett C. Ramirez <sup>b</sup>, Hongwei Xin <sup>c,\*</sup>, Rebecca Parsons <sup>d</sup>, Jinming Pan <sup>a</sup>, Yibin Ying <sup>a,c,\*</sup>

<sup>a</sup> Department of Biosystems Engineering, Zhejiang University, Hangzhou, Zhejiang, 310058, P.R. China

<sup>b</sup> Department of Agricultural and Biosystems Engineering, Iowa State University, Ames, IA 50011, USA

<sup>c</sup> Institute of Agriculture, University of Tennessee, Knoxville, TN 37996, USA

<sup>d</sup> Veterinary Diagnostic and Production Animal Medicine, Iowa State University, Ames, IA 50011, USA

<sup>c</sup> Faculty of Agricultural and Food Science, Zhejiang A&F University, Zhejiang, 311300, P.R. China

\* Corresponding authors. Email: [hxin2@utk.edu](mailto:hxin2@utk.edu); [ybying@zju.edu.cn](mailto:ybying@zju.edu.cn)

### Abstract

Keel bone (KB) damage is prevalent in all types of laying hens housing systems and is perceived to lead to compromised hen welfare. Research on KB damage quantification is limited, compared to the conventionally used, subjective discretized scoring criteria. A novel apparatus and method were developed to quantify KB damage. The number of fractures in proximal aspect, middle portion, and distal aspect were counted for each KB. The deformation area at side view and ventral view were quantified too. A normalized deformation index was developed to represent the overall deformation amount. The newly developed characteristics were more representative for the KB damage severity than a 4-level criterion. In the future, the developed quantification method will assist with providing more precise research which related to KB damage severity.

**Keywords:** Keel bone fracture, keel bone deformation, animal welfare

### 1. Introduction

Keel bone (KB) damage is prevalent in all types of commercial production systems with 6–59% of laying hens having some KB deformity (Heerkens et al., 2016; Riber and Hinrichsen, 2016) and 36–97% having fractures (Torrey et al., 2017; Riber et al., 2018; Buijs et al., 2019) depending on bird age and housing system style.

Fractures are characterized by sharp bends or clear displacements of the KB. Collision with housing system structures is a major cause of KB fractures (Flening et al., 2004; Harlander-Matauschek et al., 2015; Stratmann et al., 2015). Deformation is less studied compared to fractures. A normal KB is linear, but deformation can lead to deviations, or curvature. Fracture or sudden impact injury has been shown to cause KB deformation (Casey-Trott et al., 2015).

Some KB damage quantification methods were introduced in former studies. Richards et al. (2011) manually scored each fracture on a KB into 3 levels using radiographic images (0, no damage; 1, mild damage; 2, severe damage). Heerkens et al. (2016) applied the 3-point scale method to quantify KB deformation. The ventral ridge curve of the KB was compared to the connecting line of distal tip and carina sterna. The largest distance from the point on the keel ridge to the connecting line was recorded as a deviation. The deviation was then scored as “no deviation” (<0.5 cm), “mild deviation” (0.51 to 1 cm), “severe deviation” (>1 cm). Chargó et al. (2019b) also adopted the 3-point scale method to score the KB deviation with 3D images from computed tomography (CT) scanning. Regmi et al. (2016) analyzed the KB deformities with the 3D images from quantitative CT scans. The angle of KB with carina sterni was measured to quantify the deformation. The presence of fractures and the angle of deformation were combined to score the KB damage severity from Score ‘0’ to ‘4’. Rufener et al. (2018, 2019) developed an online tutorial and recalibration tool to train KB fracture scoring skill with radiographic images. Due to the complexity of specific fracture characteristics like number, location, direction, width of the fracture gap, and dislocation, the aggregate fracture severity of a KB was determined subjectively into score 0 to 5 rather than any quantitative method. Chargó et al. (2019a) quantified the number of fractures in 3 portions of KB (proximal aspect, middle portion, and distal aspect)

with 3D images from CT scanning. Comparison of the aforementioned methods, the 3-point scale method adequately quantifies KB deformation severity. It is able to assign every KB a specific deformation value. Conversely, because the fracture severity quantification is complicated, quantification methods generally include the number or the location of fractures.

In this study, we developed an apparatus and a novel methodology to quantify the severity of KB deformation and number of fractures at three locations. The results were compared with the damage evaluation results from a four-level criterion. We aimed to prove the quantification method was more representative for KB damage severity than the traditional method.

## 2. Materials and Methods

Animal use was approved by the Iowa State University Institutional Animal Care and Use Committee (IACUC protocol No. 18-382).

### 2.1. Source of KBs

Two batches of 18 Dekalb White laying hens ( $n = 36$ ) were obtained from a local commercial cage-free facility. Starting bird age was 57 (Batch 1) and 54 weeks old (Batch 2). The average body weight of the birds was  $1670 \pm 23$  g (Mean  $\pm$  SD). Birds were euthanized and necropsied, the harvested KBs were preserved for evaluation.

### 2.2. Birds selection criterion

A 4-level criterion was used to assess KB damage severity: Score 0, non-fractured and non-deformed; Score 1, non-fracture but deformed; Score 2, fractured but non-deformed; Score 3, fractured and deformed.

Birds were selected with relatively better and relatively worse KB by palpation. In order to simplify the selection procedure, the 4-level criterion was condensed to only 2 levels: birds with better KB (Score 0–2, no apparent deformation, sharp bends, or periosteal scars) and worse KB (Score 3, especially many apparent fractures or great deformation).

### 2.3. Imaging system for KB damage quantification

A novel evaluation system was created to quantify KB damage, rather than using the existing 4-level, discrete criteria. An imaging system was built to acquire 2 orthographic-view images of dissected, clean KBs (Figure 1). The system consisted of a digital camera (HD Pro Webcam C920, Logitech, Lausanne, Switzerland), a servomotor (HS-805MG, Hitec, South Korea), a binder clip (2 cm wide), adjustable KB fixing arm, and a computer. Software (Logitech Capture; v1.0.553, Logitech, Lausanne, Switzerland) on the computer was used to capture the images from the camera. The servomotor was controlled by a microprocessor (Arduino Uno) and slowly rotated 90 degrees and stopped to provide the 2 orthographic views for the camera: ventral ridge view and side view (Figure 2). The binder clip was fixed to the servomotor and rotated with it. The apex carinae of KB was clamped by the binder clip. The adjustable KB fixing arm ensured the caudal tip of the KB fixed at the same height of apex carinae. The binder clip and the fixing arm guaranteed the repeatability of KB fixing.

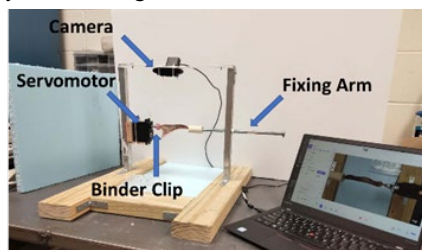


Figure 1. Imaging system for KB damage quantification. It is comprised a digital camera, a servomotor, a binder clip, and a fixing arm.

### 2.3.1. Deformation amount

Five characteristics were extracted from each KB, defined as: ventral ridge curve (VRC), tip-to-tip connecting line (TTCL), side-view concave connecting line (SVCCL), ventral-view deformation area (VVDA), and side-view deformation area (SVDA) (Figure 2). These characteristics are all measured and assessed in pixels. The VRC describes the curve length of the KB ridge. With no KB deformation, the VRC coincided with TTCL, and concaveness is not observed in the side view. To quantify the deformation amount in the ventral view, the VVDA enclosed by VRC and TTCL was measured. To quantify the deformation amount for the side view, the SVCCL was drawn to enclose the concave. The enclosed area was named as SVDA. Greater deformation led to larger magnitudes of VVDA and SVDA.

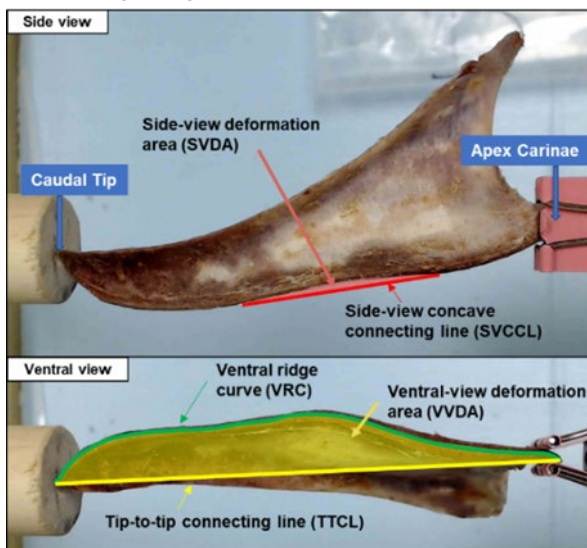


Figure 2. Keel bone deformation quantification method to measure the area of deformation form both side view and ventral view. The ventral ridge curve (VRC), tip-to-tip connecting line (TTCL), side-view concave connecting line (SVCCL), ventral-view deformation area (VVDA), and side-view deformation area (SVDA) were extracted from the images.

Lines and areas were manually drawn in ImageJ (1.52g, National Institutes of Health, Bethesda, Maryland, USA) software. The function Measure in ImageJ was used to measure the 5 characteristics in pixels. Due to high KB length variability (TTCL, range from 1,237 to 1,565 pixels), the same degree of deformation (same shape of VVDA) of 2 birds with different length of KB may lead to different deformation area. To normalize the deformation degree between KBs, the sum of VVDA/TTCL and SVDA/TTCL was denoted as the normalized deformity index (NDI), and the ratio of TTCL and VRC was denoted as shrink ratio (SR).

### 2.3.2. Fracture location

The location of each fracture was carefully confirmed with an experienced assessor before quantifying the fracture location. The fracture points were manually annotated in the ventral view image in light green color along the KB ridge (Figure 3). Three sections were defined along the TTCL from the apex carinae to the caudal tip, namely distal aspect (first 1/3 section), middle portion (middle 1/3 section), and proximal aspect (last 1/3 section). We projected the fracture points to the TTCL and counted the number of fractures located at each section. The names of the 3 sections of KB were adopted from Chargo et al. (2019a), but the definitions were modified. We divided a KB into 3 equal sections rather than specific distance from caudal tip or apex carinae.

Scripts were written to automatically process the fracture location in MATLAB 2018b (The MathWorks, Inc., Natick, MA, USA). First, the manually annotated TTCL and fracture points were extracted respectively by RGB color thresholding. Second, calculated the x-coordinate projection length of the TTCL by subtracting the x coordinate value of its left tip from right tip. Third, extracted the centroids of the fracture points. Fourth, calculated the projection length of fracture points on KB by subtracting x coordinate value of TTCL left tip from x coordinate value of each fracture point. At last, the fracture point projection lengths were divided by TTCL projection length and the results were split into the three predefined sections. The number of fractures in each section was counted.

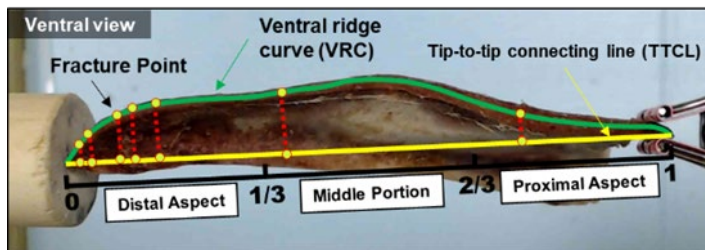


Figure 3. Keel bone fracture quantification method to count the number of fractures on distal aspect, middle portion, and proximal aspect.

## 2.4. Statistical analysis

All statistical analyses were performed in MATLAB 2018b. A one-way ANOVA was applied to assess the damage severity difference between better and worse KBs from the palpation result. Normality and homogeneity of variance of the data were examined before ANOVA.  $P$ -value of less than 0.05 was considered significant.

## 3. Results and Discussion

### 3.1. Palpation and expert evaluation

In-farm palpation (prior to bringing birds to experimental pens) was performed by an inexperienced person. The person was unable to score the KB with high accuracy, but was able to differ good KBs from bad KBs. Half of the 36 birds in this experiment were regarded to have evidently better KB condition than the other half. After the experiment, the experienced assessor dissected the 36 laying hens and evaluated the 36 KBs. According to the 4-level criterion, a total of 33, 1, 1, and 1 KBs were scored as level 3, 2, 1, 0, respectively.

### 3.2. KBD quantification indicators: better reflecting the real damage severity

Damage severity of all the 36 KBs were quantified. Figure 4 shows KBs of Score 0 and Score 3. The KB with Score 0 was better than the 2 KBs of Score 3. Moreover, the 2 KBs of Score 3 had apparent damage severity difference, including number of fractures and deformation severity.

We compared the quantification results of the 16 better KBs from palpation results with the 16 worse KBs (Table 1). Significant differences among KB categories were found for both NDI ( $P = 0.001$ ) and total fracture numbers ( $P = 0.001$ ). The characteristics to quantify fracture and deformity found the better KB were at least half the magnitude of the worse KBs, except middle portion fractures. The length characteristics showed no significant difference between better KBs and worse KBs. Although almost all the KBs were defined as badly damaged (Score 3), they had different damage severity among each other according to the quantification results. Locating intact KB in flock of laying hens aged 55+ weeks was challenging. Especially when following the current rigid definition of deformity. Fractures at caudal tips were prevalent and some were too minor to be identified by palpation. Slight deformation and one fracture will cause a KB to attain a Score 3. A continuous value is more representative of true KB damage severity. Significant difference ( $P < 0.05$ ) of deformity and fracture severity were found between the relatively better

KBs and worse ones, although almost all KBs were scored as badly damaged (Score 3).

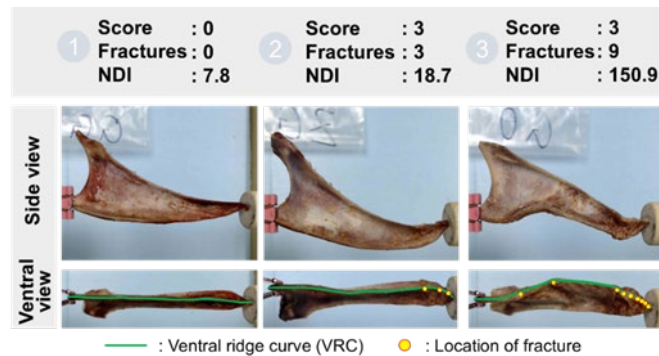


Figure 4. Example of damage severity for three KBs scored as 0, 3, and 3. Varying levels of damage severity difference.

Table 1. Quantification results of deformation, fracture, and length of the relatively better KBs and worse ones by palpation.

Quantification Characteristics	16 better KBs by palpation (13/16 with Score 3)	16 worse KBs by palpation (16/16 with Score 3)	P-value
	Mean ± SE	Mean ± SE	
Deformation	SVCCL <sup>[1]</sup>	317.4 ± 47.7	808.8 ± 42.6
	SVDA <sup>[1]</sup>	2,542 ± 688	< 0.001
	VVDA <sup>[1]</sup>	37,078 ± 8,603	0.001
	NDI	27.91 ± 6.23	0.001
	Distal	2.222 ± 0.358	0.008
	Middle	0.111 ± 0.111	0.135
	Proximal	0.056 ± 0.056	< 0.001
	Total	2.389 ± 0.380	0.001
	TTCL <sup>[1]</sup>	1,433 ± 15	0.089
Fracture No.	VRC <sup>[1]</sup>	1,446 ± 16	0.105
	SR <sup>[1]</sup>	0.991 ± 0.001	0.469

<sup>[1]</sup> The measured length and area were in unit of pixel. SVCCL, side view concave connecting line; SVDA, side view deformation area; VVDA, ventral view deformation area; NDI, normalized deformation index; TTCL, tip-to-tip connecting line; VRC, ventral ridge curve; SR, shrink ratio

#### 4. Conclusions

A novel KB damage quantification method was developed. The damage quantification results were more representative than the 4-level criterion. The number of fractures at three different locations were counted and the deformation area at side view and ventral view were quantified. The newly developed characteristics were validated to be more representative for the KB damage severity than a 4-level criterion. The developed quantification method will assist the more precise research which related with KB damage severity in the future.

#### Acknowledgments

Partial financial support for the experiment was provided by the National Key R&D Plan of China (Grant No. 2016YFD0700203). We are grateful to Iowa Cage-Free LLC for providing the laying hens and feed. Furthermore, we gratefully acknowledge the financial support of the China Scholarship Council for Kailao Wang during his joint PhD program at Iowa State University.

## Reference

- Buijs, S., J. L. T. Heerkens, B. Ampe, E. Delezie, T. B. Rodenburg, and F. A. M. Tuyttens, 2019. Assessing keel bone damage in laying hens by palpation: effects of assessor experience on accuracy, inter-rater agreement and intra-rater consistency. *Poultry Science*. 98 (2), 514–521. <https://doi.org/10.3382/ps/pey326>
- Casey-Trott, T., J. L. T. Heerkens, M. Petrik, P. Regmi, L. Schrader, M. J. Toscano, and T. Widowski, 2015. Methods for assessment of keel bone damage in poultry. *Poultry Science*. 94 (10), 2339–2350. <https://doi.org/10.3382/ps/pev223>
- Charge, N. J., C. I. Robison, H. O. Akaeze, S. L. Baker, M. J. Toscano, M. M. Makagon, and D. M. Karcher, 2019a. Keel bone differences in laying hens housed in enriched colony cages. *Poultry Science*. 98 (2), 1031–1036. <https://doi.org/10.3382/ps/pey421>
- Charge, N. J., C. I. Robison, S. L. Baker, M. J. Toscano, M. M. Makagon, and D. M. Karcher, 2019b. Keel bone damage assessment: consistency in enriched colony laying hens. *Poultry Science*. 98 (2), 1017–1022. <https://doi.org/10.3382/ps/pey373>
- Fleming, R. H., H. A. McCormack, L. McTeir, and C. C. Whitehead, 2004. Incidence, pathology and prevention of keel bone deformities in the laying hen. *British Poultry Science*. 45 (3), 320–330. <https://doi.org/10.1080/00071660410001730815>
- Harlander-Mataushek, A., T. B. Rodenburg, V. Sandilands, B. W. Tobalske, and M. J. Toscano, 2015. Causes of keel bone damage and their solutions in laying hens. *World's Poultry Science Journal*. 71 (3), 461–472. <https://doi.org/10.1017/S0043933915002135>
- Heerkens, J. L. T., E. Delezie, T. B. Rodenburg, I. Kempen, J. Zoons, B. Ampe, and F. A. M. Tuyttens, 2016. Risk factors associated with keel bone and foot pad disorders in laying hens housed in aviary systems. *Poultry Science*. 95 (3), 482–488. <https://doi.org/10.3382/ps/pev339>
- Regmi, P., N. Nelson, J. P. Steibel, K. E. Anderson, and D. M. Karcher, 2016. Comparisons of bone properties and keel deformities between strains and housing systems in end-of-lay hens. *Poultry Science*. 95 (10), 2225–2234. <https://doi.org/10.3382/ps/pew199>
- Riber, A. B., T. M. Casey-Trott, and M. S. Herskin, 2018. The influence of keel bone damage on welfare of laying hens. *Frontiers in Veterinary Science*. 5, 6. <https://doi.org/10.3389/fvets.2018.00006>
- Riber, A. B., and L. K. Hinrichsen, 2016. Keel-bone damage and foot injuries in commercial laying hens in Denmark. *Animal Welfare*. 25 (2), 179–184. <https://doi.org/10.7120/09627286.25.2.179>
- Richards, G. J., M. A. Nasr, S. N. Brown, E. M. G. Szamocki, J. Murrell, F. Barr, and L. J. Wilkins, 2011. Use of radiography to identify keel bone fractures in laying hens and assess healing in live birds. *Veterinary Record*. 169, 279. <http://dx.doi.org/10.1136/vr.d4404>
- Rufener, C., S. Baur, A. Stratmann, and M. J. Toscano, 2018. A reliable method to assess keel bone fractures in laying hens from radiographs using a tagged visual analogue scale. *Frontiers in Veterinary Science*. 5, 124. <https://doi.org/10.3389/fvets.2018.00124>
- Rufener, C., S. Baur, A. Stratmann, and M. J. Toscano, 2019. Keel bone fractures affect egg laying performance but not egg quality in laying hens housed in a commercial aviary system. *Poultry Science*. 98 (4), 1589–1600. <https://doi.org/10.3382/ps/pey544>
- Stratmann, A., E. K. F. Fröhlich, A. Harlander-Mataushek, L. Schrader, M. J. Toscano, H. Würbel, S. G. Gebhardt-Henrich, 2015. Soft perches in an aviary system reduce incidence of keel bone damage in laying hens. *PLoS One*. 10 (3), e0122568. <https://doi.org/10.1371/journal.pone.0122568>
- Torrey, S., T. M. Casey-Trott, T. M. Widowski, V. Sandilands, and M. T. Guerin, 2017. Rearing system affects prevalence of keel-bone damage in laying hens: a longitudinal study of four consecutive flocks. *Poultry Science*. 96 (7), 2029–2039. <https://doi.org/10.3382/ps/pex026>

# Sequential Patterns of Broilers Behavior under Comfort and Stress Conditions

Daniella Jorge de Moura <sup>a,\*</sup>, Tatiane Branco <sup>a</sup> Irenilza de Alencar Naas <sup>b</sup>,  
Stanley Robson de Oliveira Medeiros <sup>c</sup>

<sup>a</sup> Agricultural Engineering College, State University of Campinas, Campinas, Sao Paulo 04.661-100, Brazil

<sup>b</sup> Paulista University, Sao Paulo City, Sao Paulo 13. 083-886, Brazil

<sup>c</sup> Embrapa – Informatics in Agriculture, Campinas, Sao Paulo 04.661-100, Brazil

\* Corresponding author. Email: [djmoura@unicamp.br](mailto:djmoura@unicamp.br)

## Abstract

The sequence pattern mining method aims to identify frequent sequences that exceed a user-specified support threshold. The present study used the same approach based on sequential standards to estimate the heat stress of broilers from a resulting behavioral pattern. Experimental data were recorded in a climate chamber where the behavior of broilers were recorded when exposed to thermal stress (cold and heat), and the thermal neutral (comfort) was set as control. The Generalized Sequential Patterns (GSP) algorithm was used to evaluate the heat stress of broilers in the third and fourth weeks of growth. The results indicated that the mining of pattern sequences is a useful and straightforward technique to estimate the welfare of broiler chickens, allowing the identification of temporal relations between thermal stress and the consequent behavior of the broiler. Temperature 8 °C below the thermal comfort zone showed that the broiler remained lying down most of the time, walking only to the drinker and feeder trough. Broilers exposed to temperatures above the thermal comfort zone (8 °C) tend to decrease locomotor activities, showing lower welfare status.

**Keywords:** Animal welfare, behavioral pattern, data mining algorithm, detection of sequential frequency

## 1. Introduction

Thermal stress conditions negatively affect the development and productive performance of broiler chickens. At the first weeks of growth, low rearing temperatures might severely impact the bird's performance since the thermoregulatory system is not well developed (Cassuce et al., 2013). In the last weeks of growth, the exposure to high rearing temperatures might affect the performance since the bird's ability to dissipate heat decreases considerably (Renaudeau et al., 2012). Heat stress is one of the most critical issues when determining broiler welfare since it may easily lead to high flock mortality (Quinteiro-Filho et al., 2010).

Previous knowledge of broiler behavior is a way to identify stressful situations that might affect the productive performance and well-being of broiler chickens (Bracke and Hopster, 2006). The change in behavior is one of the first responses in the occurrence of stress and can be identified using video cameras. Amongst the most frequent behaviors observed to identify the thermal stress in broilers, besides water and food consumptions, is the changes in pecking, dust bathing, scratching, locomotion and grouping activity (Maria et al., 2004; Costa et al., 2012). Behavior analysis is a useful tool in understanding how animals perceive the rearing environment (Bizeray et al., 2002; Pereira et al., 2013). Since the environment implies a direct influence on the physiological responses of broilers, the sequence of behaviors, with the change of environment, might provide interesting source of information regarding the adjustments made during a known period. The evaluation and the interactive controls of the thermal comfort of animals could be done considering the animals as biosensors and the behavioral response as an input to real-time decision-making (Xin and Shao, 2002; Cordeiro et al., 2011).

Developed by Agrawal and Srikant (1995), the sequence pattern mining approach has the purpose of identifying frequent sequences that exceed a user-specified support threshold. The support of a sequence is the percentage of a finite ordered list of elements in the database that

contain the sequence. The generalized sequential pattern algorithm (GSP) has been used in predicting climate pattern (Kaur, 2012; Chauhan and Thakur, 2014), in classifying malicious sequential pattern for automatic malware detection (Fan et al., 2016), in predicting next prescribed medications (Wright et al., 2015), and in recommending personalized learning material (Salehi et al., 2014). However, although it may be a promising tool, we did not find the use of GSP in mining behavioural pattern in broiler production in current literature. Therefore, the present study aimed to apply the GSP algorithm for evaluating the sequential pattern of broiler behaviour under heat stress.

## 2. Materials and Methods

### 2.1. Birds and husbandry

A total of 27 broiler chickens (Cobb® genetic strain with mixed-sex flock) were selected from an experimental broiler house. The birds were reared in an open-sided house, fed ad libitum with commercial feed-ration, and had constant access to clean water. The broilers were 21 and 28 days old when exposed to the experimental trial. The experiment was part of an extensive research approved by the UFSM ethics committee (087/2012).

### 2.2. Experimental set-up

The broilers were distributed in three boxes, each one with nine birds, inside a climatic chamber. The room had the dimensions of 0.8 m wide × 1.1 m long × 1.1 m high. The thermal isolation was done using 0.10 m Styrofoam between two walls of plywood. The environmental control of the room was done using commercial air-conditioning and monitored with digital thermometers outside the room. Inside the chamber, in the experimental boxes, there were a tubular feeder and nipple drinkers. The birds stayed initially two days reared under neutral thermal conditions before the exposure to the heat stress. The heat stress was applied during three consecutive days when the behavior of the broilers was recorded and analyzed. A video camera with an infrared sensor was positioned facing the birds. The camera resolution was 704 × 480 pixels and recorded 30 frames per minute, 24 hours per day. The stress consisted of increasing 8 °C above the thermal neutral temperature (Table 1). Air relative humidity remained with the range of 64 to 80%; 67 to 86%, and 50 to 80% during the thermal neutral raring condition, stress by cold, and stress by heat, respectively.

Table 1. Values of temperature used to stress the broilers at 21 and 28 days-old.

Age (day)	Thermal neutral* (°C)	Cold stress (°C)	Heat stress (°C)
21	21.0 ± 1.1	13.0 ± 0.8	29.0 ± 1.1
28	20.0 ± 1.3	12.0 ± 2.3	28.0 ± 1.0

\*Values based on Cobb (2016)

The behavioral parameters were evaluated by the scan sampling method (Altmann, 1974). The evaluations consisted of 15 continuous minutes every 3 hours for each stress tested. The dark period (8 hours; Cobb, 2016) was not analyzed, as it did not allow individual identification of the bird. The total hours analyzed for each week was 17 hours.

The final data set was composed of 11 behavioral attributes (Table 2); which is related to an ethogram consisting of basic behaviors, based on previous studies related to the well-being of broilers (Weeks et al., 2000, Bokkers and Koene 2003, Pereira et al., 2005).

The data sets were built after the organisation of information from the observed behaviours of the 21- and 28-day-old broilers. Data were processed using the analysis of sequential patterns applying the GSP algorithm (Table 3).

A model based on sequential standards was developed to estimate the welfare of broiler chickens through their behavior. Considering that there is a repetition of the behavior of the broilers exposed to the stress during the present study, the sequence of observed behavior under ideal rearing environment (thermal neutral) and cold or heat stress was analyzed.

Table 2. Descriptive ethogram of the observed behaviors for the composition of the dataset.

		Observed behaviors
Eating and drinking behavior		
Eating (Co)	The bird is in front of the feeder and ingests feed	
Drinking (B)	The bird is in front of the drinker and ingests water	
Foraging (Ci)	The bird stands in upright position, uses both feet to peck at or move litter material in search of food	
Activity behavior		
Laying down (D)	The bird lies in the litter while the head rests on the ground or is erected	
Walking (A)	The bird moves at a slow pace	
Running (C)	The bird moves at a fast pace	
Normal behavior (bird in comfort)		
Preening (Lp)	The bird cleans and align the feathers using the beak	
Litter pecking (Bc)	The bird pecks the litter with the beak	
Dust bathing (BC)	Bathing in the dust with the use of wings, head, neck and legs	
Stretching (Esp)	The bird stretches one wing and one leg of the same body hemisphere	
Laying laterally (DL)	The bird lays laterally with a stretched leg	

Table 3. Partial data set for thermal neutral and stress exposure in the rearing environment.

21 days-old bird behavior	28 days-old bird behaviour
Bird 1, "Co, D"	Bird 1, "Co, D"
Bird 2, "Co, A"	Bird 2, "Co, D"
Bird 3, "D, A"	Bird 3, "D, A"
Bird 4, "A, B"	Bird 4, "Ep, A"
Bird 5, "Co, A"	Bird 5, "Lp, D"
Bird 5, "Co, A"	Bird 9, "A, Co"

The sequence pattern mining approach is to find frequent sequences that surpass a user stated support threshold. The support of a sequence is the percentage of a finite ordered list of elements in the database that contain the sequence. The generalized sequential pattern algorithm (GSP) has been used as following:

- A sequence s is an ordered list of item-sets described as  $s = e_1, e_2, \dots, e_n$ , where the element (transaction)  $e_1$  occurs before the element  $e_2$ .
- Each element  $e_i$  is a group of events (items)  $(x_1, x_2, \dots, x_q)$ .
- The number of elements of the sequence is the length of the sequence.
- Sequence  $a = e_1, e_2, \dots, e_n$  is called subsequence of sequence  $b = e_1, e_2, \dots, e_m$ , which is a sequence of a.
- The sequence database contains tuples in the form.
- In the database of sequences, where each sequence is a list of transactions ordered by the transaction-time, and each transaction is a set of items.
- The frequent patterns support must be greater or equal to the minimum support threshold defined by the user.
- The time sliding window between every two adjacent actions must be longer or shorter than a given gap (Srikant and Agrawal, 1996; Bureva et al., 2015).

The GSP algorithm mines sequential patterns by adopting a candidate subsequence generation and-test approach (Agrawal and Srikant, 1995). At first, GSP scans the database for the named items, meeting the user's minimum support sequences of events. A seed set is used in the next steps. All mined seed set in the previous step will be used for generating candidate sequences. Each candidate sequences contain a minimum one seed sequential pattern from the generated seed

set in the previous step. The candidate sequences have equal lengths, increased k+1 time in each following step. The sequences that do not fit the minimum support threshold are pruned. The process is repeating until there is a lack of new sequences or it cannot generate more candidate sequences (Bureva et al., 2015).

In this study, for instance, the sequence s= means that it is normal the bird shows the behaviors in that order. Such a sequence has the size of three different actions. The support value of a sequence s reveals the frequency. To calculate the support of a sequence Equation 1 was used.

$$support(s) = \left[ \frac{\text{number of occurrences}}{\text{Total of sequences in the data set}} \right] \rightarrow [0,1] \quad (1)$$

The software Weka® (Frank et al., 2016) was used to process the data.

### 3. Results

The approach of using GSP algorithm indicates that a sequential pattern is characterized by events that occur in time and appear with significant frequency in a database; these patterns can be used to predict a future event based on the previous ones. From such assumption, from the 11 analyzed behaviors the pattern “Laying down (D)” was the most frequent with support higher than 25%. The behaviors of “Foraging (Ci)”, and “Running (C)” was the only behavioral pattern not found in any of the studied scenarios and had a frequency lower than 25%.

Table 4. Behavioural pattern with sequence size equal to 1 for broilers exposed to thermal neutral rearing environment, cold and heat stress at ages of 21 and 28 days-old.

21 days-old	28 days-old
Behaviour under thermal neutral rearing environment	
Eating, Walking, Laying down.	Eating, Laying down.
Laying down, Walking, Drinking,	Laying down, Stretching, Walking, Laying down.
Laying down.	Laying down, Preening, Walking, Drinking.
Laying down, Preening.	Laying down, Walking, Eating, Laying down.
Cold stress	Eating, Laying down, Eating, Walking, Drinking.
Laying down, Walking, Eating.	Eating, Laying down.
Eating, Walking, Laying down.	Laying down, Walking, Drinking, Walking, Laying down.
Laying down, Walking, Drinking,	Laying down, Eating, Laying down, Preening.
Walking, Laying down.	Laying down, Eating, Laying down, Walking, Drinking, Walking, Laying down.
Heat stress	
Laying down, Walking, Drinking,	Eating, Laying down.
Laying down.	Dust bath, Laying laterally, Walking, Eating.
Laying down, Preening, Walking,	
Eating.	

In a thermally neutral environment, seven behaviour patterns were found for broilers 21days-old with a sequence size equal to 1, while 18 behaviour patterns were found for broilers 28 days-old. In cold stress rearing environment, the found behavioural patters were 11 and 10, for broilers 21 and 28 days-old, respectively. When exposed to heat stress, there were found two and six behavioral patterns, for broilers 21 and 28 days-old, respectively. Most of the behaviors were repeated along the trial. Therefore, pruning was added, and we show here the most relevant ones (Table 4).

Similar sequence of behavioral pattern such as Laying down → Walking → Drinking → Laying down; Eating → Walking → Laying down; and Laying down → Preening was found in thermal neutral rearing environment and both stress exposures; however, with less frequency of occurrence when the broilers were under stress (cold or heat), independent of age. The highest

frequency during heat stress exposures was that the bird remained inactive (Lying down), indicating that the environment was not favorable to increase the body-sensible heat production. The repetitive sequence behavior observed in broilers 28 days-old was ". The behavioral pattern of "Laying laterally" was only observed in broilers under heat stress. Such behavior seems natural since birds exposed to acute or chronic heat stress tend to increase the body surface to dissipate heat.

#### 4. Discussion

Although broiler chickens spend most of their time resting (Bizeray et al., 2002), Barbosa Filho et al. (2007) report that the lying behavior can be considered normal under thermal stress conditions, in order to facilitate heat exchange with the litter, which would undoubtedly be at a lower temperature than the body of the animal. Such a condition would favor the exchange of heat by conduction. Pereira et al. (2005) reported a positive correlation between temperature and "Dust bath" and "Drinking" behaviors and negatively correlated with "Running" behavior.

The decrease of broiler locomotor activities during heat stress is an attempt to reduce the heat generated by the movements (Maria et al., 2004). Such behavior might also occur as indicative of cold stress when the birds cluster together to minimize heat loss (Schiassi et al., 2015). It was also observed in the evaluated cold stress exposure that the birds diminished the exploratory behavior of the surrounding. Probably because the birds remained lying down for a long time and only getting up to drink and eat.

It is known that the longer in thermal discomfort, whether by cold or heat, the productivity of the bird decreases, resulting in problems of health, performance and well-being (Quintero-Filho et al., 2010). Therefore, it is vital to evaluate the thermal comfort within broiler chicken houses, since it is a highly significant factor in determining the success of broiler production (Nascimento et al., 2011). The importance of evaluating the behavior of broiler chickens shows that the higher the repertoire of behaviors performed by the birds, the greater the indicative of the birds being in a better condition of well-being (Zhao et al., 2014). The higher the intensity, duration and incidence of a known behavior, the better indication we might have of the bird welfare status (Bracke and Hopster, 2006). Although broilers can adapt the behavior to the variations of the thermal rearing environment, the exposure a large fluctuation in the temperature of the internal environment is not recommended (Quintero-Filho et al., 2010).

The present analysis characterizes only the frequency of the behavior related to the rearing environment, not focusing on the physiological responses (feed consumption, weight gain and feed conversion) that might lead to production losses. Such losses are difficult to forecast through behavioral analysis (Schiassi et al., 2015). The thermal environment has a direct influence on broiler behavior, which validates the feasibility of finding welfare indicators based on the behavior of birds (Pereira et al., 2005).

As a result of genetic improvement, the temperature range during production currently recommended by the genetic strain as optimal may be outdated (Cassuce et al., 2013), which indicates the importance of continuing research in this direction. By mapping the change, the temperature and duration of thermal stress it is possible to find arrays of behavioral pattern. Another factor to observe is that broiler chickens can acclimatize to a certain intensity of thermal stress (acute stress). Short-term adaptations lead the animal to show physiological, behavioral and immunological changes to survive stressful events. Long-term adaptations occur during animal life and include a reduction in metabolic rate, changes in behavioral response, and overall morphology of the animal (Renaudeau et al., 2012). There is the need to determine the temperature ranges and exposure periods in which the short-term thermoregulatory mechanisms of broilers (physiological and/or behavioral) are efficient in maintaining the homeothermic with minimum production cost.

The present study contributes to indicate a level of behavioral compensation to the effects of acute heat or cold stress. Also, further studies are required on levels of intensity of exposure to

thermal stress to identify the onset of relevant, productive losses that might justify mitigating stress actions. Some shown behaviors may not have been a result of the video analysis application methodology (15 continuous minutes every 3h), and a continuous record and analysis might be suggested as future research.

Regarding the use of GSP for analyzing the behavioral frequency, the proposed algorithm scales linearly with the number of data sequences, discovers a sequential pattern, and has excellent scale-up properties concerning the present average data sequence size (Chauhan and Thakur, 2014). Although there are other options of sequential pattern-based approach (modified Apriori and PrefixSpan algorithms), such alternatives are applied to discover underlying patterns instead of on-going frequency pattern, as behavior (Salehi et al., 2014; Fan et al., 2016). The use of GSP is recommended when a particular condition occurs in a stepwise fashion, where one behavior leads to another (Wright et al., 2015), or to identify patterns of ordered events (Kaur, 2012).

## 5. Conclusions

The sequencing pattern mining is a promising and straightforward technique to estimate the behavioral pattern of broiler chickens, allowing the identification of temporal relationships between thermal stress and individual behavior. Temperature 8 °C below the thermal comfort zone showed that the bird remained lying down and clustered most of the time, walking only to the drinker and feeder trough. Temperatures 8 °C above the thermal comfort zone have shown that the bird tends to decrease locomotor activities, showing lower welfare rates.

## Acknowledgements

The authors would like to thank the CAPES/CNPq for the financial support this research. We are also grateful to the UFSM Polytechnic College for their support of the research project.

## References

- Agrawal, R. and R. Srikant, 1995. Mining Sequential Patterns. In Proceedings of the 11th International Conference on Data Engineering. Taipei, March 6–10. IEEE. 3–14.
- Altmann, J., 1974. Observational Study of Behavior: Sampling Methods. *Behaviour*, 49 (3/4), 227–267.
- Barbosa Filho, J. A., I. J. O. Silva, M. A. N., Silva, and C. J. M. Silva, 2007. Avaliação dos comportamentos de aves poedeiras utilizando sequência de imagens. *Engenharia Agrícola*, 27 (1), 93–99.
- Bizeray, D., I. Estevez, C. Leterrier, C. and J.M. Faure, 2002. Effects of increasing environmental complexity on the physical activity of broiler chickens. *Applied Animal Behaviour Science*, 79 (1), 27–41.
- Bracke, M. B. M. and H. Hopster, 2006. Assessing the importance of natural behavior for animal welfare. *Journal of Agricultural and Environmental Ethics*, 19 (1), 77–89.
- Bureva, V., E. Sotirova and P. Chountas, 2015. Generalized net of the process of sequential pattern mining by generalized sequential pattern algorithm (GSP). In: Filev D. et al. (eds) Intelligent Systems' 2014. Advances in Intelligent Systems and Computing, Warsaw, Poland, September 24–26. IEEE. 323.
- Cassuce, D. C., , I. F. F. Tinoco, F.C. Baêta, S. Zolnier, P.R. Cecon, P. R., and M.F.A. Vieira, 2013. Thermal comfort temperature update for broiler chickens up to 21 days of age. *Engenharia Agrícola*, 33 (1), 28–36.
- Chauhan, D., and J. Thakur, 2014. Boosting decision tree algorithm for weather prediction. *Journal of Advanced Database Management and Systems*, 1 (3) 2393–8730.
- Cobb - Vantress, 2016. Inc. Broiler Management Guide. 69p.
- Cordeiro, M. B., I. F. F. Tinoco, R. M., Filho and F.C. Sousa, 2011. Análise de imagens digitais para a avaliação do comportamento de pintainhos de corte. *Engenharia Agrícola*, 31(3) 418–426.
- Costa, L. S., D.F. Pereira, L.G.F. Bueno and H. Pandorfi, H., 2012. Some aspects of chicken behavior and welfare. *Brazilian Journal of Poultry Science*, 14 (3), 159–232.
- Fan, Y., Y. Ye and Chen, L., 2016. Malicious sequential pattern mining for automatic malware detection. *Expert Systems with Applications*, 52 (1) 16–25.
- Frank E., M. A. Hall and I. H. Witten, 2016. The WEKA Workbench. Online Appendix for "Data Mining: Practical Machine Learning Tools and Techniques", Morgan Kaufmann, Fourth Edition, 2016.
- Maria, G. A., J. Escos, and C.L. Alados, 2004. Complexity of behavioural sequence and their relation to stress conditions in chicken (*Gallus gallus domesticus*): A non-invasive technique to evaluate animal welfare. *Applied Animal Behavior Science*, 86 (1/2), 93–104.

- Nascimento, G. R. T., I.A. Nääs, D.F. Ferreira, W.M. Dutra Junior and A.P.A.Maia, 2011. Previsão de conforto térmico de frangos de corte utilizando mineração de dados. *Brazilian Journal of Biosystems Engineering*, 5 (1), 36–46.
- Pereira, D. F., B. C. B. Miyamoto, G. D. N. Maia, G.T. Sales, M.M. Magalhães and R.S. Gates, 2013. Machine vision to identify broiler breeder behavior. *Computers and Electronics in Agriculture*, 99 (1), 194–199.
- Pereira, D. F., I.A.Nääs, C.E.B. Romanini, D.D. Salgado and G.O.T. Pereira, 2005. Indicadores de bem-estar baseados em reações comportamentais de matrizes pesadas. *Engenharia Agrícola*, 25 (2), 308–314.
- Quinteiro-Filho, W. M., A. Ribeiro, V. Ferraz-de-Paula, M.L. Pinheiro, M. Sakai, L.M.R., Sá, A.J.P. Ferreira and J. Palermo-Neto, 2010. Heat stress impairs performance parameters, induces intestinal injury, and decreases macrophage activity in broiler chickens. *Poultry Science*, 89 (9), 1905–1914.
- Renaudeau, D., A. Collin, S. Yahav, V. Basilio, J.L. Gourdin, and R.J. Collier, 2012. Adaptation to hot climate and strategies to alleviate heat stress in livestock production. *Animal*, 6 (5), 707–728.
- Salehi, M., I.N. Kamalabadi, and M.B.G. Ghoushchi, 2014. Personalized recommendation of learning material using sequential pattern mining and attribute based collaborative filtering. *Education and Information Technologies*, 19 (4), 713–735.
- Schiassi, L., T. Yanagi Junior, P.F.P. Ferraz, A.T. Campos, G.R. Silva, and L. H. P. Abreu, 2015. Broiler behavior under different thermal environments. *Engenharia Agrícola*, 33 (3) 390–396.
- Srikant, R. and R. Agrawal, 1996. Mining Sequential Patterns: Generalizations and Performance Improvements. In *Proceedings of the Fifth International Conference on Extending Database Technology (EDBT)*, Avignon, France, March 25–29. 1 –17.
- Verma, M. and D. Mehta, 2014. Sequential Pattern Mining: A Comparison between GSP, SPADE and Prefix SPAN. *International Journal of Engineering Development and Research*, 2 (3), 3016–3036.
- Weeks, C. A., T.C. Danburi, H.C. Davies, P. Hunt, S.C. Kestin, 2000. The behaviour of broiler chicken and its modification by lameness. *Applied Animal Behaviour Science*, 67 (1/2) 111–125.
- Wright, A. P., A.T. Wright, A.B. McCoy, D.F. Sittig, 2015. The use of sequential pattern mining to predict next prescribed medications. *Journal of Biomedical Informatics*, 53 (2), 73–80.
- Xin, H., and J. Shao, 2002. Real-time assessment of swine thermal comfort by computer vision. In *Proceedings of the World Congress of Computers in Agriculture and Natural Resources*, March 13–15, ASAE, 362–369.
- Zhao, Z., J. Li, X. Li, and J. Bao, 2014. Effects of housing systems on behaviour, performance and welfare of fast-growing broilers. *Asian-Australasian Journal of Animal Sciences*. 27 (1), 140–146.

# Preliminary Study on a Data-driven Prediction Method for the Early Detection of Coccidiosis in Intensive Livestock Systems

Ferrante Valentina <sup>a</sup>, Grilli Guido <sup>b</sup>, Borgonovo Federica <sup>a\*</sup>, Pascuzzo Riccardo <sup>c</sup>,  
Guarino Marcella <sup>a</sup>

<sup>a</sup> Department of Environmental Science and Policy, Università degli Studi di Milano, Milan 20133, Italy

<sup>b</sup> Department of Veterinary Medicine, Università degli Studi di Milano, Milan 20133 , Italy

<sup>c</sup> Fondazione IRCCS Istituto Neurologico Carlo Besta, UOC Neuroradiologia, Milan 20133, Italy

\* Corresponding author. Email: [federica.borgonovo@unimi.it](mailto:federica.borgonovo@unimi.it)

## Abstract

Coccidiosis in poultry is still one of the main enteric diseases that can influence the performance of animals raised under intensive production system. Unfortunately, these enteric pathologies are not preventable, and diagnosis is available only when the disease is full-blown. The available diagnostic methods such as oocyst count and lesion scoring are extremely time-consuming and costly. For this reason, the use of a prediction method, that works in real-time, could provide valuable and rapid information for farmers with clear and suitable alerts in their daily routine. The quick reaction to any change in the health, well-being or productive states is the fundamental element for reduction of drugs usage, prevention and control of coccidiosis, and improvement of animal welfare. The main object of this research was to assess the possible relationship between the air quality data and the number of oocysts hosted in three different broiler houses. Prototypes have been developed and tested in three different experimental poultry farms based on collected data of the Volatile Organic Compounds (VOCs - organic chemicals and detectable to the human nose and to an electronic device such as electronic nose) emitted from broilers during the entire life cycle of the animals. A data-driven machine learning algorithm was built to relate VOCs data to the number of oocysts during time. For each broiler production cycle, the results showed that variations in the VOCs were related to the change of oocysts number, and specific critical VOCs values were associated to abnormal levels of oocysts count at an early stage of the disease. In conclusion, the results of this study support the feasibility of building an automatic data-driven machine learning algorithm for early warning of coccidiosis for intensive broiler production.

**Keywords:** Early warning system, PLF, poultry, enteric diseases, volatile organic compounds, coccidiosis, data-driven machine learning algorithm.

## 1. Introduction

In intensive poultry farming, enteric disorders represent a major health issue; these pathologies could be caused by bacteria, viruses, and parasites and are a major cause of performance reduction. One of the most common enteric disorders in poultry farming is coccidiosis. Even if coccidiosis has been known for many years, it is still the most economical important parasitic disease affecting poultry production worldwide.

This enteric disease is caused by protozoa of the family Eimeriidae and Coccidia that are present in almost every poultry farm. In the modern intensive farming system, the environmental condition and the high number of reared animals might promote the development of coccidiosis (McDougald and Fitz-Coy, 2013). Clinical disease occurs only after the ingestion of a relatively large number of sporulated oocysts by susceptible birds and the infectious process may last up to 4-7 days in host cells with extensive damage to the intestinal mucosa (Chapman, 2014). Symptoms of coccidiosis depend on the degree of damage and inflammation, which could result in loss of appetite and diarrhea with consequent drop in productive performances of the birds, characterized by poor weight gain and poor feed conversion efficiency, intestinal malabsorption, reduced nutrient digestion, etc. (Williams, 2005). Furthermore, subclinical infestations have consequences on poultry performance with serious economic losses, poor product quality and increase of carcass

condemnation at slaughter (Williams, 1999). Moreover, the interpretation of the impact of subclinical coccidiosis is difficult and the diagnosis is available only when the pathology is full-blown.

Today there are two prevention measures of coccidiosis, namely vaccination and chemoprophylaxis (anticoccidial products or anticoccidials in the ration) (De Gussem, 2007; Haug et al., 2008). However, this last clashes with the public's concern regarding the drug usage in intensive farming because the antimicrobials and anticoccidial drugs in animals pose a potential risk for public health, and it contributes to the selection and spread of resistant microbes in the environment (Speksnijder et al., 2014). Antimicrobials resistance is, therefore, a global health problem integrating human, animal and environmental health.

Nowadays, the available technique of diagnosis is to count the oocysts in the faeces or evaluate the lesions provoked by coccidia in different intestinal tracts in dead/culled animals (Johnson and Reid, 1970). However, these unethical methods are time-consuming, and only some qualified laboratories are able to perform this practice. It is, therefore, necessary to incentivize the development of new vaccines, diagnostics, novel therapies and stewardship methods (Laxminarayan et al., 2016) that are able to promptly detect the onset of the infestation.

Several studies have explored the possibility of diagnosing pathologies in livestock and in humans via identification of Volatile Organic Compounds (VOCs) produced by pathogens, host-pathogen interactions and biochemical pathways (Guffanti et al., 2018). Volatile Organic Compounds are present in blood, breath, stool, sweat, skin, urine and vaginal fluids of humans and animals, and their qualitative and quantitative composition is influenced by pathophysiological responses to infections, toxins or endogenous metabolic pathway perturbations (Ellis et al., 2014).

Odour and air quality from livestock can give an indication on the health of animals, and the odour from litter is indeed influenced by the features of manure. Therefore, enteric problems are characterised by different chemical odour properties (Sohn et al., 2008). In this scenario, a system based on sensors was developed for an early and non-invasive warning for enteropathies in intensive broiler farms. The use of this innovative approach might provide fast and reliable results on coccidiosis diagnosis. The goals of this study were to assess the possible relationship between the air quality data and the number of oocysts hosted in three different broiler houses and to evaluate the applicability of an early warning to detect coccidiosis in intensive broiler farming.

## 2. Materials and Methods

The trial was carried out in three different intensive poultry farms located in northern Italy, where Ross 308 were reared. One complete life cycle of the broilers in two different houses (Farm 1 and 2) and two cycles in the same house (Farm 3) were monitored. All the farms were equipped with forced ventilation by negative-pressure systems. Table 1 describes the characteristics of the buildings and the management of the broiler houses.

### 2.1. Animal management

Nutrition management of the birds was similar for all houses during the experiment and management programmes were designed to prevent the development of coccidiosis, which also resulted in the improvement of gut health and feed utilization of animals. The animals in the three farms were fed with the same diet with the addition of anticoccidials in the ration to prevent coccidiosis infection. The anticoccidial was added to the feed from the first day up to the 7 days before the birds being slaughtered. The management allows a direct comparison among results.

The feeding program was divided into three periods: i) in the first period (0 to 10 days old), the animals were fed with a starter; ii) in the 2nd period (10 to 24–26 days old), the animals were fed with a feed for growth to ensure that the nutrients intake supported the growth of the birds; and finally iii) in the third period the animals were fed with finishing feed, which started from the 26 days of age until slaughter.

Table 1. Building and management of the surveyed broiler houses.

Farm	Province	Dimensions (m)		Animals (n)	Cycle duration (d)	Litter	Maximum density (head m <sup>-2</sup> )
		Length	Width				
1	Mantova	145	14	27,000	48	Wood shaving	13.3
2	Brescia	60	13	10,000	48	Rice hull	12.8
3	Mantova	110	14	27,000	49 (cycle 1) 47 (cycle 2)	Wood shaving	17.5

## 2.2. Faeces samples

To evaluate the possible presence of coccidiosis, a pool of faeces was collected weekly from each barn at 5 different zones. The pool consisted of a set of 50 faeces (25 from cecum). Oocysts count of the collected samples in vials were performed in the laboratory of avian pathology, following the Mc Master method (Holdsworth et al., 2004). The number of oocysts, expressed as oocysts g<sup>-1</sup> [faeces] (opg), was used as a gold standard to indicate the health status of broiler (infected/not infected) and as a reference compared to the volatile organic compounds (VOCs) analysis performed on air samples.

## 2.3. Air sampling

The prototype were placed in the middle of the buildings to collect the air into the device. Air samples were continuously collected throughout the production cycle, through a polytetrafluoroethylene tube (Teflon) connected to the device. The air was sampled at a height of 40 cm above the floor (birds' level) and drawn into a small chamber consisting of the electronic non-specific sensor array. This array of sensors is sensitive to a wide range of VOCs and change their electrical characteristics due to the superficial reaction as a result of gas absorption. The electrical signals produced from the sensors were recorded every 10 seconds for further analysis. The system is based on a patent technology (International Publication Number: WO2017/212437).

## 2.4. Statistical analysis

The data obtained with the prototype on air samples collected in the farms were processed using multivariate statistical techniques, specifically Principal Component Analysis (PCA). PCA was performed on the scaled data of the sensors' responses for each cycle separately, to obtain a reduced representation of the data. Moreover, a monotone cubic spline interpolation of the sampled oocysts number was performed to obtain a continuous representation of the response variable in the considered time domain. Finally, a k-nearest neighbors algorithm (k-nn) was applied to predict the number of oocysts based on the scores of the first two or three principal components (PCs). The number k of nearest neighbors considered in the final model was optimized separately for each cycle, through a leave-one-group-out cross-validation procedure, where the data of one day at the time were excluded. Then, 2-dimensional of predicted oocysts numbers in the space of the first two or three PCs, respectively, were generated on a uniform grid with a step equal to 2% of the PC scores range. Contour levels were drawn at 1000 and 10000 predicted oocysts, where the former may be considered a candidate threshold for early warning of coccidiosis. Accuracy error was computed locally around the 1000 level for each map on the training data.

The analysis was carried out in R 3.2.3, using packages "factoextra" and "kknn" for running and visualizing the results of the PCA and k-nearest neighbors algorithm, respectively.

## 3. Results and Discussion

### 3.1. Oocyst count

The number of oocysts in the fecal samples acquired at variable days was displayed in Figure

1. In particular, in farm 1 as well as in the other two farms, the opg was 0 at week 1 and then increased to the highest values of 31,875 in farm 1 and 31,000 in farm 2 at the week 4 or 5. The following sampling (week 6) resulted in an average value of 1,000 opg counted.

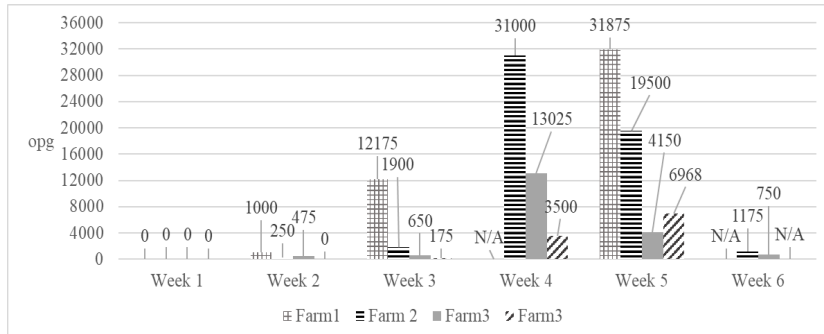


Figure 1. Oocyst count in all the three farms during the production cycle.

### 3.2. Interpolation of the oocysts number

The oocysts number was interpolated for the identification of new data points of the Cartesian plane starting from a discrete set of known data points. The number of oocysts corresponding to each measurement was interpolated from the count available (white crosses) between days 0 and 28 or 35, to obtain the new data points (black line), as shown in Figure 2.

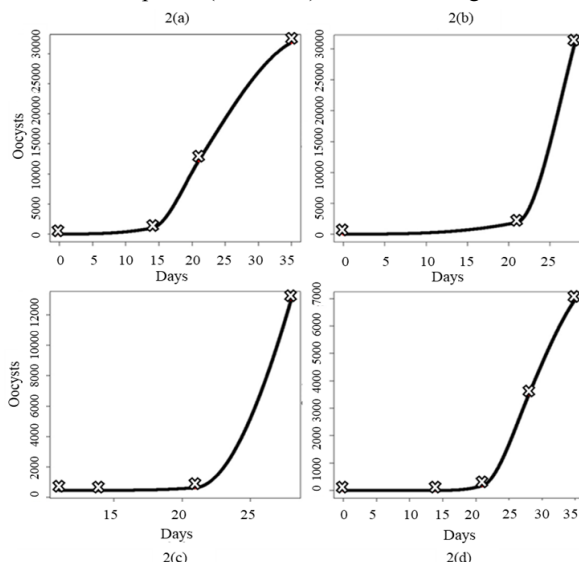


Figure 2. Oocysts interpolation: number of oocysts interpolated (black line) from the oocysts count available (white crosses) for Farm 1 (2a), Farm 2 (2b) and Farm 3 (first cycle 2c; second cycle 2d).

### 3.3. Principal component analysis

PCA was made on the scaled data of the sensors' responses, acquired in the interval between day 0 and the day at which the oocysts count was maximum. Each broiler house was analyzed separately. PCs describe directions of data variation and present the influences of the original

features. Such influences, or loadings, are the weights used to combine linearly the sensors' responses and associated to the importance of each input in generating the PCs. From the comparison between the PCA biplots of the cycles (Figure 3), there were similarities (possibly changing the sign) in the combinations used to generate the principal components among cycles. The first component (PC1) was approximately an average of the signals, while the second (PC2) was a contrast between inputs 3 and 6 against the others. These similarities among cycles are important findings in terms of reproducibility of the study.

Farm 1: The first two PCs explained almost 93% of the data variance, which increased to 96.4% if the third PC was included. Individual measurements were represented in terms of their first two components in Figure 3a, colored by interpolated number of oocysts.

Farm 2: The first two PCs explained 94.8% of the data variance, and it increased to 97.8% if the third PC was included. Individual measurements were represented in terms of their first two components in Figure 3b, colored by interpolated number of oocysts.

Farm 3 first cycle: The first two PCs explained 96.9% of the data variance, which increased to 98.9% if the third PC was included. Individual measurements were represented in terms of their first two components in Figure 3c, colored by interpolated number of oocysts.

Farm 3 second cycle: The first two PCs explained 96.8% of the data variance, which increased to 98.7% if the third PC was included. Individual measurements were represented in terms of their first two components in Figure 3d, colored by interpolated number of oocysts.

According to the Gold Standard (oocysts count), PCA showed good ability to discriminate between air samples from infected and not infected animals with coccidiosis. Visual inspection of the PCA results suggested that variations in the scores of the first two PCs of the sensors' data were related to a change in the number of oocysts.

Similarities among the 2-d representations were found among cycles, pointing out how change in the sensors' responses can be used as an indication of oocysts increment.

### 3.4. Infection prediction

In order to evaluate whether the system was able to early identify the coccidia infection in intensive poultry farms, the  $k$ -nearest neighbors algorithm ( $k$ -nn) was performed on the scores of the first two principal components (PCs).

The results showed that the model exhibited good predictability of the sample classification;  $k$ -nn algorithm identified the contour level of 1000 oocysts with different local average error in the 2-d space generated by the first two PCs (Table 2).

The  $k$ -nn algorithm therefore allowed to predict the number of oocysts based on the PCs of the sensors' responses and to reliably identify a possible threshold (i.e. 1000 oocysts) corresponding to an early significant increment of the number of oocysts. Such threshold was accurately identified in every cycle, suggesting the robustness and the repeatability of the study in different broiler houses.

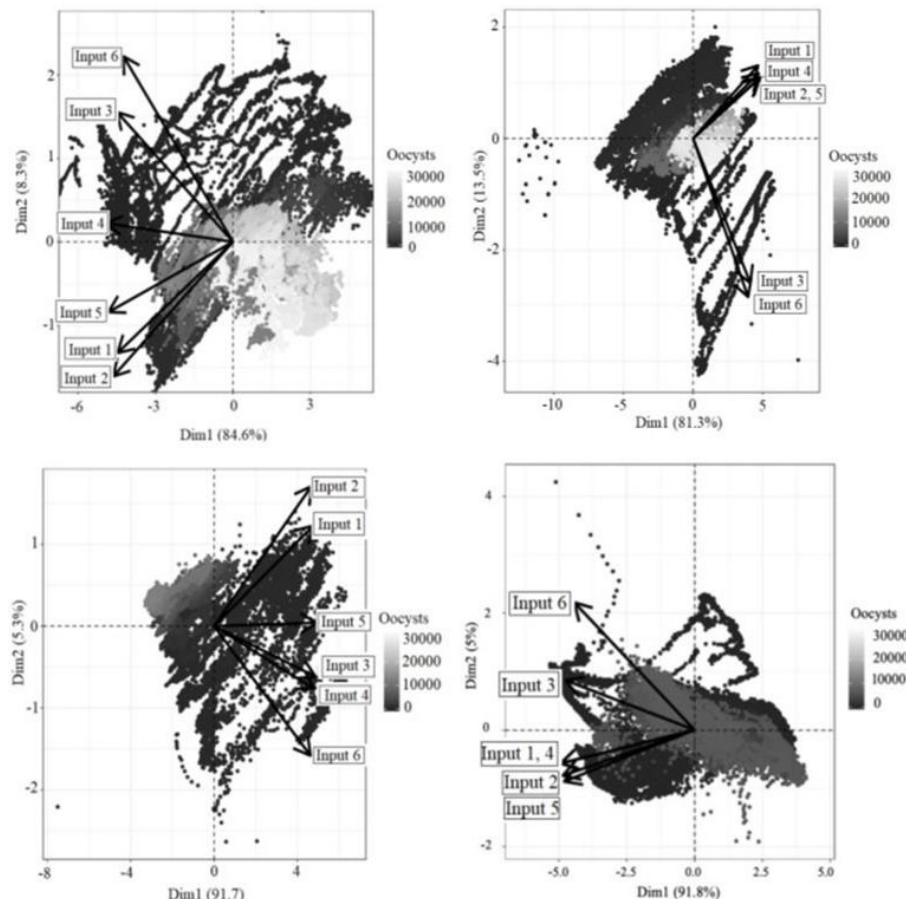


Figure 3. PCA biplots of the four cycles. Points represent the PCA scores, i.e. individual measurements of the sensors in the space generated by the first two principal components, colored by the number of oocysts interpolated at that time point. The principal directions of the original inputs are represented as arrows, whose coordinates are proportional to the loadings.  
Farm 1 (3a); Farm 2 (3b); Farm 3 (first cycle 3c; secondo cycle 3d).

Table 2. List of the 2-d models' parameter ( $k$ ) and the average local error around the 1000-level of the  $k$ -nearest neighbors algorithm for each cycle.

Broiler house	Variance explained %	Optimal $k$	Average local error
1	93.0	24	1083
2	94.8	50	1823
3 – Cycle 1	96.9	30	458
3 – Cycle 2	96.8	50	1700

#### 4. Conclusions

This study shows that the system was able to discriminate between VOCs emitted from infected or not infected animals with coccidiosis, and its application in poultry farming could be very advantageous. Air analysis revealed that this discrimination was related to a significant

change in the number of oocysts, at a very early stage. This system is very well suited for the methodologies and the goals of Precision Livestock farming. In fact, this tool might provide a real-time monitoring system that is aimed to improve animal health by giving alerts when the infection arises, and then the veterinary can take immediate action.

In conclusion, the results of this study supported the feasibility of building an automatic data-driven machine learning algorithm for early warning of coccidiosis in broiler farming. In future studies, further information should be considered when building such a model, including the temporal dependency of the data and the broiler house effect.

### Acknowledgements

This research did not receive any specific grant from funding agencies in the public, commercial, or not-for-profit sector.

### References

- Chapman, H.D., 2014. Milestones in avian coccidiosis research: A review. *Poultry science*. 93, 501–511. <http://doi.org/10.3382/ps.2013-03634>.
- De Gussem, M., 2007. *Coccidiosis in poultry: Review on diagnosis, control, prevention and interaction with overall gut health*.
- Elaine Rose, M., P. Hesketh, 1976. Immunity to coccidiosis: stages of the life cycle of *Eimeria maxima* which induce, and are affected by, the response of the host. *Parasitology*. 73, 25–57. <http://doi.org/10.1017/s0031182000051295>.
- Ellis, C.K., R.S. Stahl, P. Nol, W.R. Waters, M.V. Palmer, J.C. Rhyan, K.C. VerCauteren, M. McCollum, M.D. Salman, 2014. A Pilot Study Exploring the Use of Breath Analysis to Differentiate Healthy Cattle from Cattle Experimentally Infected with *Mycobacterium bovis*. *PLOS ONE*. 9 (2), e89280. <http://doi.org/10.1371/journal.pone.0089280>.
- Guffanti, P., V. Pifferi, L. Falciola, V. Ferrante, 2018. Analyses of odours from concentrated animal feeding operations: A review. *Atmospheric Environment*. 175, 100–108. <http://doi.org/10.1016/j.atmosenv.2017.12.007>.
- Haug, A., A.-G. Gjævre, P. Thebo, J.G. Mattsson, M. Kaldhusdal, 2008. Coccidial infections in commercial broilers: epidemiological aspects and comparison of *Eimeria* species identification by morphometric and polymerase chain reaction techniques. *Avian Pathology*. 37 (2), 161–170. <http://dx.doi.org/10.1080/03079450801915130>.
- Holdsworth, P.A., D.P. Conway, M.E. McKenzie, A.D. Dayton, H.D. Chapman, G.F. Mathis, J.T. Skinner, H.C. Mundt, R.B. Williams, 2004. World Association for the Advancement of Veterinary Parasitology (WAAVP) guidelines for evaluating the efficacy of anticoccidial drugs in chickens and turkeys. *Veterinary Parasitology*. 121 (3–4), 189–212. <http://dx.doi.org/10.1016/j.vetpar.2004.03.006>.
- Johnson, J., W.M. Reid, 1970. Anticoccidial drugs: Lesion scoring techniques in battery and floor-pen experiments with chickens. *Experimental Parasitology*. 28 (1), 30–36. [https://doi.org/10.1016/0014-4894\(70\)90063-9](https://doi.org/10.1016/0014-4894(70)90063-9).
- Laxminarayan, R., D. Sridhar, M. Woolhouse, 2016. Achieving global targets for antimicrobial resistance. *Science*. 353. <http://dx.doi.org/10.1126/science.aaf9286>.
- McDougald, L., S. Fitz-Coy, 2013. Coccidiosis: protozoal infections. *Diseases of Poultry*, 13th edn. Blackwell, New York, 1148–1166.
- Sohn, J.H., N. Hudson, E. Gallagher, M. Dunlop, L. Zeller, M. Atzeni, 2008. Implementation of an electronic nose for continuous odour monitoring in a poultry shed. *Sensors and Actuators B: Chemical*. 133 (1), 60–69. <https://doi.org/10.1016/j.snb.2008.01.053>.
- Speksnijder, D., D. J. Mevius, C. J. M. Bruschke, J. A. Wagenaar, 2014. Reduction of Veterinary Antimicrobial Use in the Netherlands. The Dutch Success Model. *Zoonoses and Public Health*. 62. <http://dx.doi.org/10.1111/zph.12167>.
- Williams, R., 1999. A compartmentalised model for the estimation of the cost of coccidiosis to the world's chicken production industry. *International Journal for Parasitology*. 29 (8), 1209–1229.
- Williams, R., 2005. Intercurrent coccidiosis and necrotic enteritis of chickens: Rational, integrated disease management by maintenance of gut integrity. *Avian pathology: Journal of the W.V.P.A.* 34, 159–180. <http://dx.doi.org/10.1080/03079450500112195>.

# Evaluation of Convolutional Neural Networks for Detecting Floor Eggs of Cage-Free Hen Housing Systems

Guoming Li <sup>a</sup>, Yang Zhao <sup>a,\*</sup>, Yan Xu <sup>b</sup>, Qian Du <sup>b</sup>

<sup>a</sup> Department of Agricultural and Biological Engineering, Mississippi State University,  
Hood Road, MS 39762, USA

<sup>b</sup> Department of Electrical and Computer Engineering, Mississippi State University,  
Hood Road, MS 39762, USA

\* Corresponding author. Email: [yzhao@abe.msstate.edu](mailto:yzhao@abe.msstate.edu)

## Abstract

Automatic systems for floor egg detection and collection in cage-free hen housing rely on robust computer vision systems and modeling tools. The objectives of this study were to 1) select an optimal convolutional neural network (CNN) floor-egg detector by comparatively evaluating three CNN detectors to detect floor eggs under a typical cage-free housing environment, and 2) investigate the performances of the selected CNN detector for floor egg detection under different settings reflecting a range of common cage-free environments and conditions. For objective 1, 700 images containing floor eggs were used to evaluate the performances of the single shot detector floor-egg detector (SSD detector), faster region-based CNN floor-egg detector (faster R-CNN detector), and region-based fully convolutional network floor-egg detector (R-FCN detector) in a Python-based computing environment. The most optimal floor-egg detector was selected based upon the trade-offs of accuracy and processing speed for floor egg detection. For objective 2, the performances of the optimal floor-egg detector on floor egg detection (accuracy and root mean square error “RMSE”) were determined at different camera height, camera tilting angle, light intensity, litter condition, egg color, buried depth, egg number in an image, egg proportion in an image, egg shell cleanness, and egg connection in an image. The results show that the SSD detector had the fastest processing speed (26.1 s for 350 testing images) but the lowest accuracy (82.3%) among all three detectors. The R-FCN detector had the slowest processing speed (83.9 s for 350 testing images). The faster R-CNN detector had the highest accuracy (99.9%) and a medium processing speed (63.2 s for 350 images) and thus was selected as the optimal detector for floor egg detection. The faster R-CNN detector detected the floor eggs almost perfectly under different cage-free environments and conditions, except for brown eggs at 1-lux light intensity. It is concluded that a properly selected CNN floor-egg detector may accurately detect floor eggs in cage-free housing environments and may serve as a useful tool for automatic floor egg collection systems.

**Keywords:** Floor egg, convolutional neural network, tensorflow, detector evaluation, detector performance

## 1. Introduction

Cage-free (CF) housing system is one of alternative egg production systems where hens can express more natural behaviors compared with those in conventional cage systems (Hartcher and Jones, 2017). While hens are provided with litter floor in CF systems, they may lay eggs on the floor (Lentfer et al., 2011; Oliveira et al., 2018). Unlike eggs laid in nestboxes that are automatically conveyed to egg processing rooms, floor eggs must be collected manually by caretakers, which is time-consuming and laborious. Therefore, improving collection method for floor eggs is among primary concerns for egg producers. One potential solution is to detect and collect floor eggs using robots.

Robotic systems have been developed for various agricultural applications, e.g., sweet pepper detection and harvest (Bac et al., 2017), maize field navigation (Hiremath et al., 2012), and floor egg detection and collection (Vroegindeweij et al., 2018). These robotic systems typically consist of vision-based detectors to detect objects of concern (Vroegindeweij et al., 2018). The

performance of the object detection is subject to operation environments and conditions (Hiremath et al., 2012). Environments and conditions of floor egg collection in CF housing are complicated and may vary in terms of light distribution, egg cleanliness, egg color, egg size, etc (Vroegindeweij et al., 2014). Robust algorithms that can handle the complex situations in CF housing are needed for accurately detecting floor eggs.

Convolutional neural networks (CNN) have widely been used for object detection in past years. With CNN-based detectors, objects of concern in images/videos are accurately detected, classified, and localized using bounding boxes (Huang et al., 2017a). Although CNN-based detectors have been applied to detect a variety of objects, e.g. license plates (Kurpiel et al., 2017), animal behaviors (Stern et al., 2015), and fingerprints (Chugh et al., 2017), they have not been utilized to detect floor eggs in CF systems.

The objectives of this study were to 1) select an optimal detector from the three CNN floor-egg detectors (i.e., single shot detector “SSD detector”, faster region-based CNN “faster R-CNN detector”, and region-based fully convolutional network “R-FCN detector”) by comparatively evaluating their performances to detect floor eggs under a typical cage-free housing environment; and 2) investigate the performances of the selected CNN floor-egg detector for floor egg detection under different settings reflecting a range of common cage-free environments and conditions.

## 2. Materials and Methods

### 2.1. Experimental system setup

Figure 1a shows the imagery system setup for this experiment. A webcam (HD Webcam C615-Black, Logitech International S.A., Silicon Valley, California, USA) was used to collect floor egg images (1920×1080 pixels, Figure 1b). Litter was obtained from a commercial CF farm. The computer system used for detector training and testing consisted of 32 GB RAM, Intel(R) Core (TM) i7-8700K processor, and a NVIDIA GeForce GTX 1080 GPU card. Python v3.6.8 with TensorFlow-GPU v1.13.1, cuDNN v7.4, and CUDA v10.0 were installed in the PC. Brown and white eggs for the tests were procured from a grocery store.

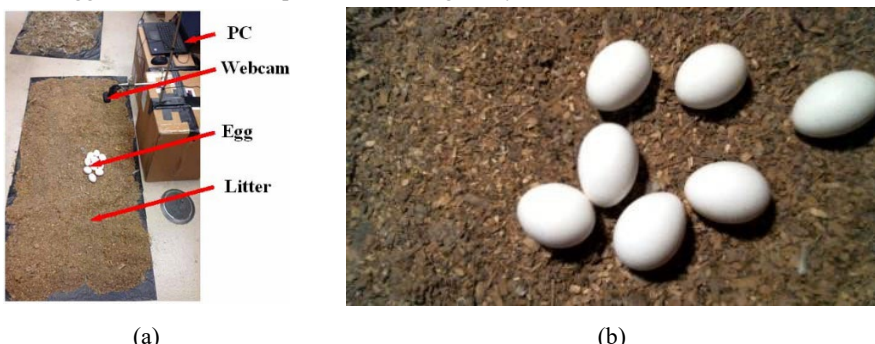


Figure 1. A photo of the imagery system setup (a) and a top-view image of floor eggs (b).

### 2.2. Experimental settings

#### 2.2.1. Settings for comparing the three CNN floor-egg detectors (*Objective 1*)

The camera was installed ~30 cm above the litter with its lens pointing downward to capture top views of floor eggs on the litter. Light intensity was set to 15 lux at bird head level (~30 cm height) (Hy-line International, 2016). One to seven (1–7) brown eggs were placed on the litter surface. Seven hundred (700) pictures were taken. Half of the pictures were used for training and the other half for testing.

## 2.2.2. Settings for evaluating the optimal CNN floor-egg detector (Objective 2)

After detector comparison, the most optimal CNN floor-egg detector was selected. The accuracy and root mean square error (RMSE) of the deviation between the manually-labelled egg center and the detected egg center were evaluated under different settings (i.e., camera height, camera tilting angle, light intensity, litter condition, egg color, buried depth, egg number in an image, egg proportion in an image, egg shell cleanliness, and egg connection in an image) for floor egg detection. Each setting was examined with brown and white eggs. One hundred (100) images were taken for each type of egg in each setting. Half of the images were used for training and the other half for testing. Details of the settings are shown in Table 1.

Table 1. Settings for evaluating the selected convolutional neural network (CNN) floor-egg detector.

Settings		Description
Camera settings	Camera height	30, 50, and 70 cm
	Camera tilting angle	0, 30, and 60°
Environmental settings	Light intensity	1, 5, 10, 15, and 20 lux
	Litter condition	with and without feather
Egg settings	Buried depth	0, 2, 3, and 4 cm
	Egg number in an image	0, 1, 2, 3, 4, 5, 6, and 7
	Egg proportion in an image	30%, 50%, 70%, and 100%
	Egg shell cleanliness	with and without litter
	Egg connection in an image	separated and connected

Note: camera tilting angle is the dihedral angle between the plane of the camera and the horizontal plane. All tests were conducted under a condition of 30-cm camera height, top camera view, 15-lux light intensity, litter without feather, and five eggs (white and brown), unless specified in ‘Description’ otherwise.

## 2.3. Convolutional neural network floor-egg detector

Three CNN-based detectors, i.e. the SSD, faster R-CNN, and R-FCN detectors, were used in this case. A CNN consists of an input layer, multiple pairs of convolutional and pooling layers, a fully connected layer, and an output layer (Figure 2). During the detection process, an input image was convolved with different feature extractors/filters to construct feature maps, which were processed with different convolutional and pooling layers and activation functions. Then these maps were processed with different filters, strides, pooling, and activation functions. The resultant maps were fully connected with different weights to get desired outputs (Huang et al., 2017a). The SSD detector, with the Mobilenet V1 feature extractor, directly produced a set of bounding boxes and scores for the presence of objects using a feedforward convolutional network (Liu et al., 2016). The faster R-CNN detector, with the Inception V2 feature extractor, used a unified neural network for both region proposals and object detection tasks, which can speed up region selections and reduce computational cost. The R-FCN detector, with the Resenet101 feature extractor, was a region-based fully convolutional network, which can predict objects by using relative spatial information. The three detectors were selected based on the accuracy and speed trade-offs as reported by Google TensorFlow (Huang et al., 2017b).

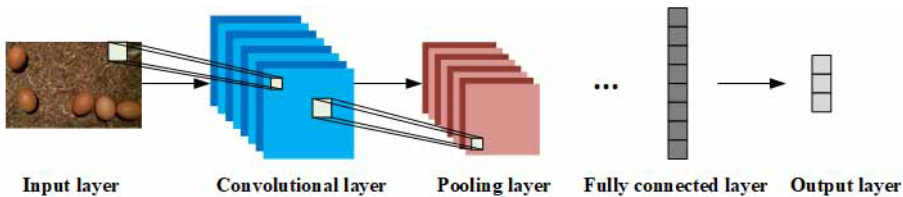


Figure 2. An example structure of a convolutional neural network.

## 2.4. Data preparation

In this study, we used Google TensorFlow Object Detection Application Programming Interface, an open source framework for object detection, to train the CNN floor-egg detectors. The framework has provided the three above-mentioned CNN detectors, which are pretrained based on Common Objects in Context (COCO) dataset and can be easily modified and fine-tuned for our dataset (Huang et al., 2017b). Eggs in the images were manually labelled with a series of bounding boxes, resulting in each egg having its label name (“egg” in this case) and four bounding box coordinates ( $x_{\min}$ ,  $y_{\min}$ ,  $x_{\max}$ , and  $y_{\max}$ ). The labelled images were split into training and testing sets (50%:50%) and serialized into TFRecord files, which are Tensorflow’s own binary storage formats. The files were used for detector training and testing.

## 2.5. Detector training

Three hundred and fifty (350) images were used to train the detectors for the objective 1, and 50 images in each setting (3,300 in total) were used for the objective 2. The training files were prepared as mentioned in Section 2.4 and used as input for detector training with 200,000 iterations, after which the training loss became stable and the detectors were well trained. The trained detectors were saved as inference graphs and output as .pb files for testing.

## 2.6. Detector testing and evaluation

Three hundred and fifty (350) images were used to test the trained detectors for the objective 1, and 50 images in each setting were tested for the objective 2. The testing files were set as mentioned in Section 2.4. To determine whether an egg is correctly detected by the detectors, the intersection over union (IoU) for each bounding box was computed, with its value more than 0.5 being true positive (TP). Calculation of the IoU is illustrated in Figure 3.

$$\text{IoU} = \frac{\text{Area of Overlap} \text{ (black shadow area)}}{\text{Area of Union} \text{ (area of red box+area of blue box-black shadow area)}}$$

Figure 3. Illustration of intersection over union (IoU) calculation. Red square box is ground truth box, blue square box is detected box, and black shadow area is overlap area of manually labelled box and detected box.

The accuracy for testing each egg in the images was mainly concerned in this study and calculated as shown in Eq. (1).

$$\text{Accuracy} = \frac{TP+TN}{TP+FP+FN+TN} \quad (1)$$

where  $TP$  is true positive, i.e. number of cases that a detector successfully detects an existent egg in an image with IoU greater than 0.5;  $FP$  is false positive, i.e. number of cases that a detector reports a nonexistent egg in the image, or IoU is less than 0.5;  $FN$  is false negative, i.e. number of cases that a detector fails to detect an existent egg in the images; and  $TN$  is true negative, i.e.

number of cases that no egg is reported by both detector and manual label.

The RMSE for the center coordinate of detected eggs was obtained by comparing detected center coordinates with manually-labelled center coordinates. The calculation schedule is shown in Eq. (2).

$$RMSE = \sqrt{\frac{\sum_{i=1}^N \{(\hat{x}_i - x_i)^2 + (\hat{y}_i - y_i)^2\}}{N}} \quad (2)$$

where  $RMSE$  is root mean square error;  $\hat{x}_i$  and  $\hat{y}_i$  are the  $i^{\text{th}}$  detected center coordinate ( $x, y$ ) in the image;  $x_i$  and  $y_i$  are the  $i^{\text{th}}$  manually-labelled center coordinate ( $x, y$ ) in the image; and  $N$  is the total number of eggs in the images.

Processing time was used to evaluate the processing speed of the detectors and reported by Python 3.6 after processing 350 testing images.

### 3. Results and Discussion

#### 3.1. Sample images of floor egg detection

Figure 4 shows some sample images of floor egg detection under different situations. Eggs in the images were correctly identified with green bounding boxes using the CNN floor-egg detectors, which is useful for robots to determine coordinates of floor eggs and collect the eggs.

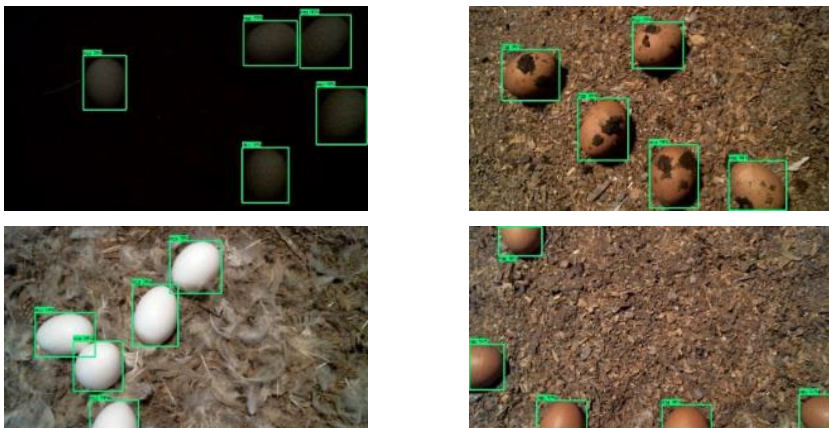


Figure 4. Sample images of floor egg detection under different settings. Eggs in the images are detected and enclosed in green bounding boxes.

#### 3.2. Testing performances for the three floor-egg detectors

Table 2 shows the testing performances for the SSD, faster R-CNN, and R-FCN detectors. Overall, the SSD detector had the lowest accuracy (82.3%) but the shortest processing time (26.1 s for 350 images). The faster R-CNN detector had the highest accuracy (99.9%) and the R-FCN detector had the longest processing time (83.9 s for 350 images). RMSEs were 4.0 mm for the SSD detector, 1.7 mm for the faster R-CNN detector, and 1.6 mm for the R-FCN detector.

Table 2. Test performances of the three convolutional neural network (CNN) floor-egg detectors.

Detector	Accuracy (%)	RMSE (mm)	Processing time for 350 images (s)
SSD	82.3	4.0	26.1
Faster R-CNN	99.9	1.7	63.2
R-FCN	90.2	1.6	83.9

Huang et al. (2017a) reported that R-FCN and SSD were faster on average while faster R-CNN was more accurate, and Mobilenet and Inception were faster feature extractors but less

accurate than Resenet. In this case, the R-FCN detector used Resenet to extract features, which may compromise processing speed. Overall, the faster R-CNN detector had decent accuracy, processing speed, and RMSE among the three floor-egg detectors, thus was selected to detect floor eggs under a range of typical conditions in commercial CF housing.

### 3.3. Performances of the faster R-CNN detector under different settings

#### 3.3.1. Detector performances with different camera settings

Table 3 shows the performances of the faster R-CNN detector under different camera heights and tilting angles. Accuracy was 100% for all camera settings and RMSE was 1.0–8.7 mm for brown and white egg detection. Although the two camera settings did not affect detection accuracy, errors for detected center coordinates of eggs increased for higher camera placements and greater titling angles. Therefore, placing a camera at ~30 cm height with its lens pointing downward may be optimal setup.

Table 3. Accuracy and root mean square error (RMSE) of floor egg detection by the faster region-based convolutional neural network (faster R-CNN) detector under different camera settings.

Settings	Brown egg		White egg	
	Accuracy (%)	RMSE (mm)	Accuracy (%)	RMSE (mm)
Camera height (cm)	30	100.0	1.0	100.0
	50	100.0	2.4	100.0
	70	100.0	7.6	100.0
Camera tilting angle (°)	0	100.0	1.0	100.0
	30	100.0	1.6	100.0
	60	100.0	2.6	100.0

Note: camera tilting angle is the dihedral angle between the plane of the camera and the horizontal plane.

#### 3.3.2. Detector performances with different environmental settings

Table 4 shows the performances of the faster R-CNN detector at different light intensities and litter conditions. Lowest accuracy (44.6%) and highest RMSE (4.6 mm) appeared when the light intensity was set to 1 lux for brown egg. Litter with feather compromised detection accuracy for both types of eggs. To improve detection accuracy, integrated lamps to light up some dark areas and blowers to clear feather may be considered for egg-collecting robots.

Table 4. Accuracy and root mean square error (RMSE) of floor egg detection by the faster region-based convolutional neural network (faster R-CNN) detector under different environmental settings.

Settings	Brown egg		White egg	
	Accuracy (%)	RMSE (mm)	Accuracy (%)	RMSE (mm)
Light intensity (lux)	1	44.6	4.6	100.0
	5	100.0	1.4	100.0
	10	100.0	1.2	100.0
	15	100.0	1.2	100.0
	20	100.0	1.1	100.0
Litter condition	w/ feather	92.8	1.7	98.4
	w/o feather	100.0	1.0	100.0

#### 3.3.3. Detector performances with different egg settings

Table 5 shows the performances of the faster R-CNN detector under different egg settings. Accuracy and RMSE varied in the ranges of 98.4–100.0% and 0.7–2.1 mm, respectively. Buried depth, egg number in an image, egg proportion in an image, egg shell cleanness, and egg

connection had little effect on detection accuracy.

Vroegindeweij et al. (2018) developed a vision system based on image processing for an egg-collecting robot and achieved 86% accuracy to detect floor eggs. The image processing algorithms were parameterized according to specific egg shape, egg color, and egg size. In commercial CF systems, floor eggs could be buried by litter/feather, contaminated by manure, and shadowed by cage structure and birds. They also vary in size, color, and orientation. The parameterized image processing algorithms may not be generalized well among such complicated scenarios (Hiremath et al., 2012). In this case, except for brown egg in 1-lux light intensity, the faster R-CNN detector can accurately detect eggs in most settings, which suggests that this detector can be generalized well among different scenarios, thus being a useful component for robotic vision systems.

Table 5. Accuracy and root mean square error (RMSE) of floor egg detection by the faster region-based convolutional neural network (faster R-CNN) detector under different egg settings.

Settings	Brown egg		White egg	
	Accuracy (%)	RMSE (mm)	Accuracy (%)	RMSE (mm)
Buried depth (cm)	0	100.0	0.7	100.0
	2	100.0	1.8	100.0
	3	100.0	1.3	100.0
	4	99.6	2.1	100.0
Egg number in an image	0	100.0	—	100.0
	1	100.0	1.0	100.0
	2	100.0	1.1	100.0
	3	100.0	1.1	100.0
	4	100.0	1.1	100.0
	5	100.0	1.2	100.0
	6	100.0	1.2	100.0
Egg proportion in an image (%)	7	100.0	1.7	100.0
	30	99.2	2.1	100.0
	50	100.0	0.8	100.0
	70	100.0	0.9	100.0
Egg shell cleanness	100	100.0	1.0	100.0
	w/ litter	100.0	1.6	100.0
	w/o litter	100.0	1.2	100.0
Egg connection	connected	100.0	1.3	98.4
	separated	100.0	1.6	100.0

#### 4. Conclusions

Three CNN floor-egg detectors (single shot detector “SSD detector”, faster region-based CNN “faster R-CNN detector”, and region-based fully convolutional network “R-FCN detector”) were compared for floor egg detection. The performances of the most optimal detector were evaluated under different commercial settings to get a well-generalized detector for the detection. Based on the experiment, we obtained following conclusions:

- Compared with the SSD and R-FCN detectors, the faster R-CNN detector had decent accuracy (99.9%) and processing speed (63.2 s for testing 350 images) with 30-cm camera height, top camera view, 15-lux light intensity, and 1–7 brown eggs on the litter surface.
- Except for brown eggs in the 1-lux light intensity, performances of the faster R-CNN detector were not profoundly affected by camera height, camera tilting angle, light intensity, litter condition, egg color, buried depth, egg number in an image, egg proportion in an image, egg shell cleanness, and egg connection in an image.

#### Acknowledgements

Financial support of this research was provided by Egg Industry Center (EIC) Research

Program, and the USDA National Programs: Food Animal Production (NP 101).

## References

- Bac, C.W., J. Hemming, B. Van Tuyl, R. Barth, E. Wais, E.J. van Henten, 2017. Performance evaluation of a harvesting robot for sweet pepper. *Journal of Field Robotics*. 34 (6), 1123–1139.
- Chugh, T., K. Cao, A.K. Jain, 2017. Fingerprint spoof detection using minutiae-based local patches. In: *2017 IEEE International Joint Conference on Biometrics (IJCB)*: IEEE. 581–589.
- Hartcher, K., B. Jones, 2017. The welfare of layer hens in cage and cage-free housing systems. *World's Poultry Science Journal*. 73 (4), 767–782.
- Hiremath, S., F. van Evert, V. Heijden, C. ter Braak, A. Stein, 2012. Image-based particle filtering for robot navigation in a maize field. In: *Proceedings of the Workshop on Agricultural Robotics (IROS 2012), Vilamoura, Portugal*. 7–12.
- Huang, J., V. Rathod, C. Sun, M. Zhu, A. Korattikara, A. Fathi, I. Fischer, Z. Wojna, Y. Song, S. Guadarrama, 2017a. Speed/accuracy trade-offs for modern convolutional object detectors. In: *Proceedings of the IEEE conference on computer vision and pattern recognition*. 7310–7311.
- Huang, J., V. Rathod, D. Chow, C. Sun, M. Zhu, A. Fathi, Z. Lu, 2017b. Tensorflow object detection api. GitHub. [https://github.com/tensorflow/models/tree/master/research/object\\_detection](https://github.com/tensorflow/models/tree/master/research/object_detection). Accessed May 5th, 2019.
- Hy-line International, 2016. Management Guide: Hy-Line W-36. [https://www.hyline.com/userdocs/pages/36\\_COM\\_ENG.pdf](https://www.hyline.com/userdocs/pages/36_COM_ENG.pdf). Accessed June 12th, 2019.
- Kurpiel, F.D., R. Minetto, B.T. Nassu, 2017. Convolutional neural networks for license plate detection in images. In: *2017 IEEE International Conference on Image Processing (ICIP)*: IEEE. 3395–3399.
- Lentfer, T.L., S.G. Gebhardt-Henrich, E.K. Fröhlich, E. von Borell, 2011. Influence of nest site on the behaviour of laying hens. *Applied Animal Behaviour Science*. 135 (1–2), 70–77.
- Liu, W., D. Anguelov, D. Erhan, C. Szegedy, S. Reed, C.-Y. Fu, A.C. Berg, 2016. Ssd: Single shot multibox detector. In: *European conference on computer vision*: Springer. 21–37.
- Oliveira, J.L., H. Xin, L. Chai, S.T. Millman, 2018. Effects of litter floor access and inclusion of experienced hens in aviary housing on floor eggs, litter condition, air quality, and hen welfare. *Poultry Science*. 98 (4), 1664–1677.
- Stern, U., R. He, C.-H. Yang, 2015. Analyzing animal behavior via classifying each video frame using convolutional neural networks. *Scientific Reports*. 5, 14351.
- Vroegindeweij, B.A., J.W. Kortlever, E. Wais, E.J. van Henten, 2014. Development and test of an egg collecting device for floor eggs in loose housing systems for laying hens. In: *Paper presented at the international conference of agricultural engineering AgEng 2014, Zurich*.
- Vroegindeweij, B.A., S.K. Blaauw, J.M. IJsselmuiden, E.J. van Henten, 2018. Evaluation of the performance of PoultryBot, an autonomous mobile robotic platform for poultry houses. *Biosystems Engineering*. 174, 295–315.

# A Rapid Test for Avian Influenza Detection of Chicken Based on Sound Analysis

Tiemin Zhang <sup>a,b\*</sup>, Junduan Huang <sup>a</sup>, Kaixuan Cuan <sup>a</sup>

<sup>a</sup>College of Engineering, South China Agricultural University, Guangzhou, Guangdong 510642, P.R. China

<sup>b</sup>National Engineering Research Center for Breeding Swine Industry, Guangzhou, 510642, P.R. China

\* Corresponding author. Email: [tm-zhang@163.com](mailto:tm-zhang@163.com)

## Abstract

The development of modern poultry-breeding industry makes the danger of avian influenza more salient towards the whole industry. In order to prevent and detect avian influenza (AI) as early as possible, this research puts forward an audio-examination method, which is capable to distinguish the sound of the infected chicken from the healthy ones. frequency-domain of the extracted sound of the chickens was used to distinguish the chickens infected with AI from the healthy ones. A Back Propagation Neural Network (BPNN) with three layers of supervised learning was designed and the backward propagation algorithm was used to train and identify the extracted features by changing the Regularization Coefficient.. The experiment results show that the audio-examination method developed in this research can identify 78.77% to 81.69% of the test sets for detecting poultry which is suspected to have avian influenza. The goal of this research was to provide the large-scale chicken farming with a rapid and efficient method for Avian Influenza detection.

**Keywords:** Chicken sound, Mel frequency cepstrum coefficient, artificial neural network, avian influenza detection.

## 1. Introduction

Highly pathogenic avian influenza (HPAI) is a new zoonosis, which has a great impact on our economy, food safety, and human's health (Brown et al., 2015). Meanwhile, in-time detection diagnosis of the disease not only closely affects the income of poultry farming industry, but also plays an important role in preventing the spread of avian influenza among human beings. The traditional diagnostic methods of poultry farming industry mainly focus on the observation of chicken's posture, comb, sound and excrement (Brown et al., 2015; Aydin et al., 2014; Aydin et al., 2015; Mdbazlur et al., 2010). However, these methods are time-consuming and inefficient, especially for large scale farms. Nowadays, with rapid development of modern electronic technology and computer science, many novel and efficient diagnostic methods were put forward. Huang et al. and Zhang et al. detected the chickens infected with the Avian Influenza base on sounds analysis (Huang et al., 2019; Zhang et al., 2019). Research has also adopted image processing technology to distinguish infected chickens by observing their posture, with an identification about 99.47% by Support Vector Machine in the test set (Bi et al., 2016; Bi et al., 2018; Zhuang et al., 2018). Banakar et al. used data mining method and Dempster-Shafer theory, with Support Vector Machine as the identification tool, to identify and classify several common diseases of chicken and led to a 91.15% identification rate (Banakar et al., 2016). Besides the graphic processing technology mentioned above, there are also other methods. Silva et al. (2008) narrowed down the range of infected pigs by measuring the cough of the pigs at different locations in a pig barn, and thus used drugs such as antibiotics in the targeted location. Vandermeulen et al. (2016), however, came up with a new method, which can automatically forecast bovine respiratory disease through a three-month recording of 62 calves' coughing.

In the reported research the sounds of both the healthy chickens and those injected with avian influenza in a coop were analyzed. Based on the analysis of time-domain and frequency-domain, an effective method to extract the target sound from a large number of sounds from a perspective of audio was established. Finally, an automatic identification method for infected and healthy chicken sounds was developed base on Back Propagation Neural Network (BPNN).

## 2. Material and Method

### 2.1. Method to obtain the sound of healthy chickens and chickens with avian influenza

Obtaining the chicken's sounds included the following three steps: First, targeted group of five-week white-feather chickens were put in a coop to get them familiar with the environment and to reduce stress reaction. The coop may house 10–100 chickens. Second, a voice recorder was installed in the coop to record the sounds of chickens. The recorder was high definition digital (32G) with a sampling frequency of 48000Hz. Third, the chickens were injected with avian influenza virus after the sounds of the healthy chickens were well obtained. The recorder recorded the infected chickens' sound until all the infected chickens died. The collected data in the paper were processed using MATLAB2016b (Mathworks, Massachusetts, USA).

### 2.2. Pre-processing of the chickens' sound

#### 2.2.1. Pre-emphasis

A pre-emphasis processing with the high-frequency range was used on the inputted digitalized sound of the chickens. The Transfer Function of high-pass filter is as shown in Eq. (1), where  $\alpha$  is the pre-emphasis coefficient, in this research,  $\alpha=0.98$

$$y(n) = x(n) - \alpha x(n-1) \quad (1)$$



Figure 1. Illustration of sound signal. (a) The original chicken's sound signal, (b) The amplitude range of the sound signal being pre-emphasized.

Figure 1a shows the timing amplitude curve of the original chickens' sound signal. When it goes across the high-pass filter, the low-frequency range is weakened down. The timing amplitude curve becomes what is presented in Figure 1b, which shows the amplitude range of the sound signal being pre-amplified

#### 2.2.2. Windowing and framing

Though time-varying is one of the characteristics of chicken sound signal, its essential features can be maintained or remain stable in a very short time span (10ms–30ms) (Allen and Rabiner, 1977; Portnoff, 1981; Quatieri, 2002; Slaney, 1993). So it can be regarded as a quasi-stable state with stability in a short time period (Gou et al., 2013). In this research, we chose 21.3ms as one frame. Thereby, Hamming windowing was used to framing the sound in this paper (Alsteris and Paliwal, 2004; Wojcicki and Paliwal, 2007). A new wave of the chicken sound is shown in Figure 2 after framing by Hamming windowing method.

#### 2.2.3 Short-term energy

Short-term energy (STE) is one of the most crucial characteristics in time-domain of sound signal (Bharali and Kalita, 2015). The STE  $E_n$  of chicken's sound signal at  $n$  moment can be calculated as shown in Eq. (2). N is the window length.

$$E_n = \sum_{m=-\infty}^{+\infty} [x(m)\omega(n-m)]^2 = \sum_{m=n-(N-1)}^n [x(m)\omega(n-m)]^2 \quad (2)$$

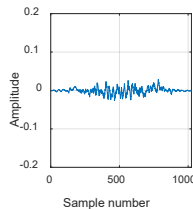


Figure 2. One frame after framed waveform.

#### 2.2.4. Short-term zero-crossing rate

Short-term zero-crossing rate (STZ) refers to the number of signals that cross zero per frame (Bharali and Kalita, 2015; Kumar et al., 2017). The STZ rate is shown in Eq. (3).

$$Z_n = \sum_{m=-\infty}^{+\infty} |\operatorname{sgn}[x(m)] - \operatorname{sgn}[x(n)]| \omega(n-m) = |\operatorname{sgn}[x(n)] - \operatorname{sgn}[x(n-1)]| * \omega(n) \quad (3)$$

where  $\operatorname{sgn}[\ ]$  is a sign function as shown in Eq. (4).

$$\operatorname{sgn}[x(n)] = \begin{cases} 1, & x(n) \geq 0 \\ -1, & x(n) < 0 \end{cases} \quad (4)$$

#### 2.2.5. Double-threshold method for endpoint detection of chicken sound based on STE and STZ rate

The double-threshold method base on both STE and STZ was use for the chicken sounds endpoint detection. The calculation flow chart is showed in Figure 3. The endpoint detection results are shown in Figure 4.

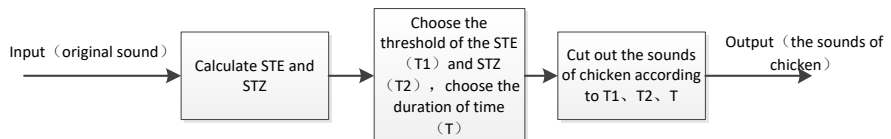


Figure 3. The calculation flow chart of double-threshold method.

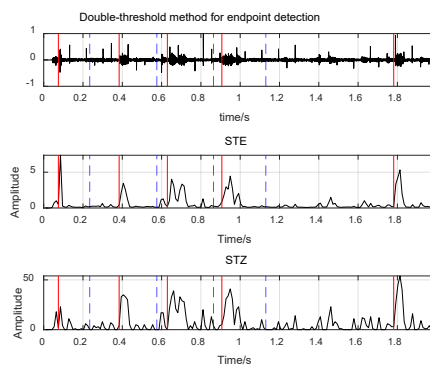


Figure 4. The endpoint detection results.

### 2.3. Extracting features of chicken's sound

Mel-Frequency Cepstral Coefficients (MFCC) is to analyze the spectrum features of sound based on human being's auditory sense (Kinnunen et al., 2012; O'Shaughnessy, 1987). Below is a brief introduction of the extraction procedure in this study.

- Pre-processing: The pre-processing includes pre-emphasis, windowing processing and framing processing.
- Calculating Fast Fourier Transform (FFT) (Allen and Rabiner, 1977; Portnoff, 1981; Quatieri, 2002; Slaney, 1993), which is as shown in Eq. (5).

$$X(i, k) = \text{FFT}[x_i(m)] \quad (5)$$

- Calculating the spectrum energy of each frame, which is as shown in Eq. (6)

$$E(i, k) = [X_i(k)]^2 \quad (6)$$

- Calculating the energy that went through Mel Filters

The spectrum energy of each frame  $E(i, k)$  separately times the frequency response function of Mel Filter  $H_m(k)$  resulting in the energy that went through Mel Filter. There are 24 Mel Filters in total and the subscript m in  $H_m(k)$  refers to the  $m^{\text{th}}$  Mel Filter. The energy that went through Mel Filters  $S(i, m)$  is counted by adding the energy of each frame that had gone through the 24 Mel Filters, which is shown in Eq. (7).

$$S(i, m) = \sum_{k=0}^{N-1} E(i, k) H_m(k) \quad (7)$$

- Calculating the Discrete Cosine Transform (DCT) cepstrum

Take the logarithm of  $S(i, m)$  and then times DCT coefficient, the Mel-Frequency Cepstral Coefficients will be figured out as shown in Eq. (8).

$$MFCC(i, n) = \sqrt{\frac{2}{M}} \sum_{m=0}^{M-1} \log[S(i, m)] \cos\left[\frac{\pi n(2m-1)}{2M}\right] \quad (8)$$

where m refers to the  $m^{\text{th}}$  Mel Filter, i to the  $m^{\text{th}}$  frame of sound signal, and n to the spectral line with DCT processing. Windowed by Hamming window with a length of 21.3ms and sampling point at 1024.

### 2.4. Identification of the sound of healthy and infected chicken

Two groups of MFCC that contain the health and the infected chickens' sounds are frame-packed to generate a matrix, with 5891 rows and 12 columns. We named it as X, and each row is a frame of the MFCC signal of chicken's sound. Then we marked a matrix which is consist of 5891 rows and 1 column as matrix Y, and marked it with 0 when it is the sound signal from the healthy chicken, and marked with 1 when it is from the infected ones. The order of the matrix X and Y was randomly reordered as the training set of this experiment.

### 2.5. Design of neural network

Because the extracted MFCC of the chickens' sound is a 12-dimentionality data, the neuron number of first layer, which is the data-input layer, was set to be 12. As for the hidden layers, however, a larger number of neurons is required so as to take a full advantage of the extracted 12-dimentionality MFCC. Therefore, 500 neurons are formed to be the hidden layer of the neural network. The last layer is the output layer which requires only one neuron to demonstrate two types of data, namely, 0 represents data from the healthy chicken's sound and 1 from the infected ones, activation function is sigmoid. The design of neural network structure of this paper is as Figure 5 shows.

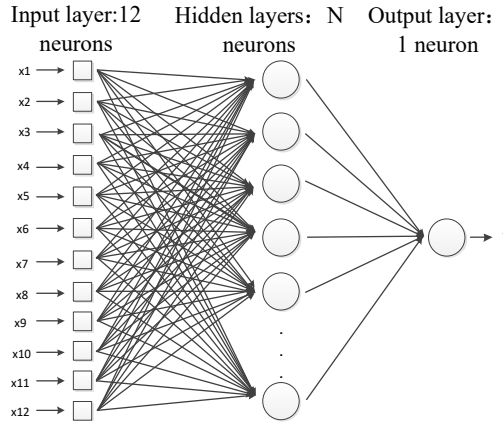


Figure 5. The design of neural network structure.

### 2.5.1. Cost function

The cost function of the three-layer neural network is shown as Eq. 9.  $x^i$  is an input vector,  $y^i$  the label,  $h_w(x)$  the network output.

$$J(w) = \frac{1}{m} \sum_{i=1}^m \left[ -y^{(i)} \log(h_w(x^{(i)})) - (1-y^{(i)}) \log(1-h_w(x^{(i)})) \right] + \frac{\lambda}{2m} \left[ \sum_{j=1}^{s_1} \sum_{k=1}^{s_2} (w_{j,k}^{(1)})^2 + \sum_{j=1}^{s_2} \sum_{k=1}^{s_3} (w_{j,k}^{(2)})^2 \right] \quad (9)$$

where  $m$  is the number of training set,  $s_1, s_2, s_3$  respectively represents the neuron number of the first, second, third layer of the network, and  $\lambda$  is the regularization coefficient.

### 2.5.2. Back propagation algorithm procedure

The training process is presented in Figure 6. There are three parts: Design of BPNN, training of BPNN and the prediction of BPNN.

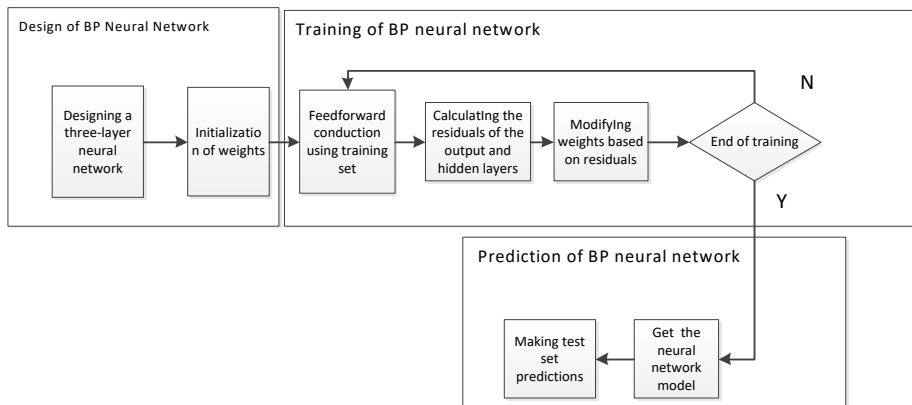


Figure 6. Training process.

### 3. Results and Discussion

#### 3.1. The learning ability of the BPNN

The coefficient  $\lambda = 2^i$ ,  $i$  ranged from -6 to 3 in 10 different regularization coefficients. With the change of the regularization coefficient in the neural network, the varying curve of identification rate for the test set are shown in Figure 7. There were 800 training times in total.

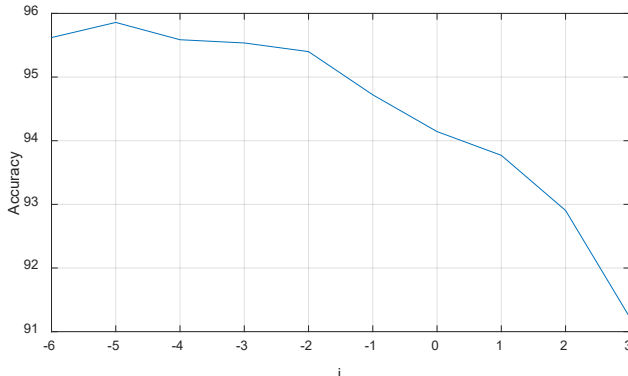


Figure 7. The accuracy with different regularization coefficients (The coefficient  $\lambda = 2^i$ ,  $i$  ranges from -6 to 3).

As can be observed in Figure 7, the accuracy first rises then falls gradually as the change of the regularization coefficient. When the regularization coefficient was  $2^{-5}$ , the accuracy reached its highest. The learning process curve is shown in Figure 8.

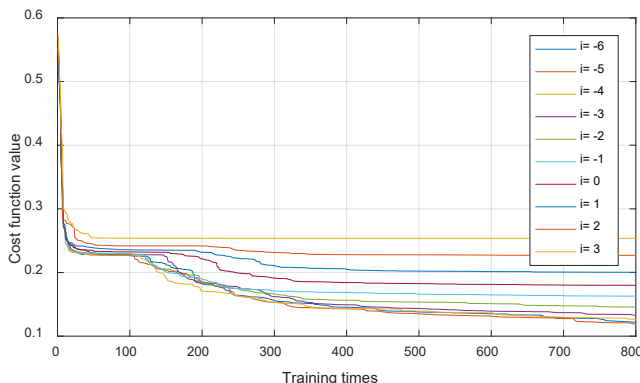


Figure 8. Neural network learning curve (The coefficient  $\lambda = 2^i$ ,  $i$  ranges from -6 to 3).

From Figure 8, we can see that the learning ability is getting stronger as the reduction of the regularization coefficient.

#### 3.2. The accuracy for the test sets

We used the method mentioned above for extracting MFCC to extract four groups of test sets which is irrelevant to the training sets. And we gained 1912 samples for each test set. Then these four test sets were identified by the neural network which has been trained by the training set

when the regularization coefficient is set:  $\lambda=2^{-6}$ ,  $\lambda=2^{-5}$ ,  $\lambda=2^{-4}$ ,  $\lambda=2^{-3}$ . The results are shown in Table 1.

Table 1. The accuracy with different regularization coefficient  $\lambda$ .

No	Lambda			
	-6	-5	-4	-3
1	81.4854	80.7008	81.6946	80.9100
2	78.7657	79.0272	79.1841	79.3410
3	79.8117	79.2887	79.6025	79.6025
4	79.55.2	79.8640	79.8640	80.0209

The neural network's identification rate for the test sets ranged from 78.77% to 81.69%, Table 1. The regularization coefficient could change the neural network's identification rate for the test sets but the change was not as salient as for the training sets. When the regularization coefficient was  $\lambda=2^{-4}$ , the identification rate for the test set proposed in this paper reached its highest at about 81.69%.

#### 4. Summary and Conclusions

This paper documents a rapid method of detecting chickens that were infected with avian influenza via sound identification. Time-domain analysis was conducted to extract the sound of chicken from the enormous original recording and to remove other noise. Frequency-domain analysis was conducted to extract features of chicken sounds to distinguish infected chickens from healthy ones. A BPNN with three layers was designed and constructed to automatically identify infected chickens. The experimental testing suggested that the identification rate ranged from 78.77% to 81.69%. The method for detecting chicken with avian influenza via sound identification developed by this research is cost-effective. It is a high-efficient and rapid method for avian influenza detection. Thus, it could be a useful tool of disease prevention for the large-scale poultry farming.

#### Acknowledgements

This work is supported by National Key Research and Development Plan [grant No. 2018YFD0500705] and Guangdong Province Special Fund for Modern Agricultural Industry Common Key Technology R&D Innovation Team [grant No. 2019KJ129], China

#### References

- Allen, J. B., and L. Rabiner, 1977. A unified approach to short-time Fourier analysis and synthesis: Proc IEEE. (65), 1558–1564.
- Alsteris, L. D., and K. K. Paliwal, 2004. Importance of window shape for phase-only reconstruction of speech, IEEE International Conference on Acoustics. IEEE Computer Society.
- Aydin, A., C. Bahr, S. Viazzi, V. Exadaktylos, J. Buyse, and D. Berckmans, 2014. A novel method to automatically measure the feed intake of broiler chickens by sound technology: Computers & Electronics in Agriculture. (101), 17–23.
- Aydin, A., C. Bahr, and D. Berckmans, 2015. A real-time monitoring tool to automatically measure the feed intakes of multiple broiler chickens by sound analysis: Computers & Electronics in Agriculture. (114), 1–6.
- Banakar, A., M. Sadeghi, and A. Shushtari, 2016. An intelligent device for diagnosing avian diseases: Newcastle, infectious bronchitis, avian influenza: Computers & Electronics in Agriculture. (127), 744–753.
- Bharali, S. S., and S. K. Kalita, 2015. Zero crossing rate and short term energy as a cue for sex detection with reference to Assamese vowels. 1–4.
- Bi, M., T. Zhang, X. Zhuang, X. Yang, L. Liang, and P. Jiao, 2016. Fast Segmentation Method of Yellow Feather Chicken Based on Difference of Color Information in Different Color Models: Transactions of the Chinese Society of Agricultural Machinery, (12), 193–298.
- Bi, M., T. Zhang, X. Zhuang, and P. Jiao, 2018. Recognition Method of Sick Yellow Feather Chicken Based on Head Features: Transactions of the Chinese Society of Agricultural Machinery, (1), 51–57.

- Brown, M., L. Moore, B. Mcmahon, D. Powell, M. Labute, J. M. Hyman, A. Rivas, M. Jankowski, J. Berendzen, and J. Loepky, 2015. Constructing rigorous and broad biosurveillance networks for detecting emerging zoonotic outbreaks: Plos One, (5), e0124037.
- Gou, C., K. F. Wang, B. Hu, G. Xiong, and F. Zhu, 2013. A fast recognition algorithm for detecting common broadcasting faults: IEEE International Conference on Service Operations.
- Huang, J., W. Wang, and T. Zhang, 2019. Method for detecting avian influenza disease of chickens based on sound analysis. Biosystems Engineering. (180), 16–24.
- Kinnunen, T., R. Saeidi, F. Sedlak, A. L. Kong, J. Sandberg, M. Hansson-Sandsten, and H. Li, 2012. Low-variance multitaper MFCC features: A case study in robust speaker verification. IEEE Transactions on Audio Speech & Language Processing. (20), 1990–2001.
- Kumar, S., S. Phadikar, and K. Majumder, 2017. Modified segmentation algorithm based on short term energy & zero crossing rate for Maithili speech signal: International Conference on Accessibility to Digital World.
- Mdbazlurr, M., H. Mda, S. Mda, and A. Mda, 2010. Digital image analysis to estimate the live weight of broiler: Computers & Electronics in Agriculture. (72), 48–52.
- O'Shaughnessy, D., 1987. Speech communication: Human and machine: New York.
- Portnoff, M., 1981. Short-time Fourier analysis of sampled speech: IEEE Transactions on Acoustics Speech & Signal Processing, v. 29, p. 364–373.
- Quatieri, T., 2002. Discrete-time speech signal processing: principles and practice, Prentice Hall.
- Silva, M., S. Ferrari, A. Costa, J. M. Aerts, M. Guarino, and D. Berckmans, 2008. Cough localization for the detection of respiratory diseases in pig houses: Computers & Electronics in Agriculture, v. 64, p. 286–292.
- Slaney, M., 1993. An Efficient Implementation of the Patterson-Holdsworth Auditory Filter Bank: Apple Computer.
- Vandermeulen, J., C. Bahr, D. Johnston, B. Earley, E. Tullo, I. Fontana, M. Guarino, V. Exadaktylos, and D. Berckmans, 2016. Early recognition of bovine respiratory disease in calves using automated continuous monitoring of cough sounds. Computers & Electronics in Agriculture. 129, 15–26.
- Wojcicki, K. K., and K. K. Paliwal, 2007. Importance of the dynamic range of an analysis window function for phase-only and magnitude-only reconstruction of speech. In IEEE International Conference on Acoustics, Speech and Signal Processing. Honolulu, USA, April 15–20. <https://doi.org/10.1109/ICASSP.2007.367016>.
- Zhuang, X., M. Bi, J. Guo, S. Wu, and T. Zhang, 2018. Development of an early warning algorithm to detect sick broilers. Computers & Electronics in Agriculture. 144, 102–113.
- Zhang Tiemin, J. Huang, 2019. Detection of chicken infected with avian influenza based on audio features and fuzzy neural network. Transactions of the Chinese Society of Agricultural Engineering. 35(2), 168–174.

# Recognition and Classification of Abnormal Droppings of Broilers Based on Deep Convolution Neural Network

Jintao Wang <sup>a</sup>, Longshen Liu <sup>a</sup>, Yi Xu <sup>b</sup>, Mingxia Shen <sup>a\*</sup>, Hongxiang Xue <sup>a</sup>, Meng Tai <sup>a</sup>

<sup>a</sup>College of Engineering, Nanjing Agricultural University, Nanjing, Jiangsu 210031, P.R. China

<sup>b</sup>New Hope Liuhe Co. Ltd., Shandong 266100, P.R. China

\* Corresponding author. Email: [mingxia@njau.edu.cn](mailto:mingxia@njau.edu.cn)

## Abstract

Digestive tract disease is a major disease in large-scale broiler breeding, which directly affects the mortality and economic benefits of broiler operation. Abnormal droppings are the main manifestation of digestive tract diseases in broilers. To solve the problem that it is difficult and time-consuming to diagnose digestive diseases manually in the current breeding mode, the deep convolution neural network model was proposed to classify the fine-grained abnormal broiler droppings images effectively. And the ultimate goal was to achieve detection and early warning of digestive diseases in broilers. The collected data of broiler droppings image were evaluated by experts, the droppings were classified into normal, and abnormal (two types). And the abnormal droppings were classified into four kinds, abnormal shape, abnormal color, abnormal water content and abnormal shape and water. The classified image data was used as training set, Faster R-CNN and Yolov3 deep convolution neural networks were used for training respectively. Optimizing the anchor box, based on the data set of broiler droppings to optimize the performance of Yolov3. Faster R-CNN achieved 99. 1% recall, 93. 3% mean Average Precision and Yolov3 achieved 88. 7% recall and 84. 3% mean Average Precision on test and verification sets. An automatic and non-contact recognition and classification model of broiler abnormal droppings was provided, which provided technical support for early warning of digestive diseases in broiler breeding.

**Keywords:** Digestive tract diseases, broiler droppings, deep convolutional neural network, faster R-CNN, Yolov3

## 1. Introduction

Broiler is an important source of meat in the world and the broiler farming is one of the pillar industries of agriculture (Lu et al., 2014; Ju et al., 2019; Lu et al., 2019). In the process of further upgrading of broiler farming, intelligent monitoring of broiler diseases has become a problem restricting its development. The digestive tract disease of broiler is one of the major diseases faced by large-scale broiler farming (Dekich et al., 1999; Lu et al., 2014). The digestive tract diseases of broilers have the characteristics of rapid spreading, high incidence and great economic impact. Its destruction and influence are second only to the respiratory disease of broiler. And it is directly related to the mortality and feed conversion of broiler. Therefore, the prevention and treatment of digestive tract disease of broiler directly affects the comprehensive benefits of breeding.

Parasites (chicken coccidiosis, etc.), bacterial and viral infections, and improper feeding and management methods can cause digestive tract diseases in broilers (Zheng and Ran, 2010). When broilers suffer from digestive tract diseases, the symptoms usually include abnormal droppings, appearance, and vocal abnormality, etc. (Lu et al., 2016). However, due to other diseases, such as respiratory diseases, the external performance of broilers will also appear appearance abnormality, and vocal abnormality, such as grunting, coughing, whining and other abnormal performance. So, it is difficult to directly determine whether broilers suffer from digestive tract diseases through physical observation and sounds. Broilers excrete more than 12 droppings a day, which can reflect the digestive tract health of broilers in real time. Therefore, judging the digestive tract health of broilers by the form of droppings is the most direct and effective way.

Normal broiler droppings are usually brown, cyan-gray, with white solids at the top and cylindrical in shape. If broilers suffer from digestive tract diseases, the droppings will show

abnormalities at once. Digestive tract diseases of different etiologies can cause droppings with different abnormal appearance. The droppings with abnormal color usually include white droppings, red droppings, green droppings, etc. Such abnormal droppings are usually caused by pathogenic bacterial infections and parasitic diseases. Abnormal-shaped droppings, such as feed-like droppings, are usually caused by unbalanced microflora in the digestive tract (Lu et al., 2014). The droppings with abnormal water content, is usually caused by mismanagement of feed which lead to the damage of the digestive.

Because of the complex feeding environment and the diversity of broiler droppings, it is a key problem to realize automatic and intelligent identification of abnormal droppings to achieve early warning of digestive tract diseases in broilers.

## 2. Materials and methods

### 2.1. Image acquisition

Image data was collected in a broiler farm in Wangguancun, Jian'an District, Xuchang City, Henan Province. The objects of image acquisition were Ross chickens from March to April 2019. The broiler farm used a multi-layer cage mode with automatic manure conveyor belts. Combining with its breeding mode (multi-layer cage mode), the image acquisition area was set above the exit area of the manure conveyor belts, as shown in Figure 1.

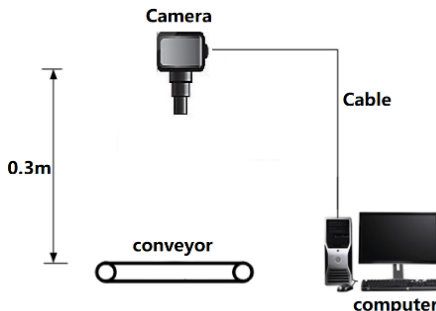


Figure 1. Experimental setup and image acquisition system

According to the living habits and excretion rules of broilers, the image acquisition time was set to 09:00–16:00 every day. Canon 5D with 24 mm fixed focus lens was used as image acquisition equipment. The distance of the image acquisition was 0.3 meters from the belt. To balance the image data of all kinds of droppings, image acquisition of abnormal droppings was emphasized in the process of acquisition. In this way, the data amount of abnormal droppings could be increased and balanced. Finally, 2796 images of broiler droppings were collected and there were 957 images of normal droppings and 1839 images of abnormal droppings.

### 2.2. Image expansion and data set preparation

Because of the complex structure of deep convolution neural network composed, a large number of parameters, including weights and deviations, need to be evaluated in training (Liu and He, 2019). Comparing with other simple structures, deep convolution neural networks need more training data to get the appropriate convergence (Wang et al., 2019). In order to achieve better recognition effect and reduce over-fitting, it was necessary to expand the data (Li and Wang, 2018). For each image, 2–4 methods such as rotation, mirror, zoom, translation, random shearing, contrast transformation and noise transformation were randomly used to expand the data. Finally, nearly 10,000 images data were obtained. After filtering the expanded image data, 7637 high-quality images were finally screened out by removing the data with poor quality caused by adding noise and have very little difference after transformation (Shelhamer et al., 2017; Du et al., 2008). Because the image data collected by SLR camera was too large, it would cost too much computing

resources for training. So, it was necessary to compress the size of the data. The original image was 5670x3240 pixels. The compressed image was 1800x1012 pixels, and the size of the image was reduced ten times. The open source software LableImage was used to deal with the image data. According to the characteristics of broiler droppings, it could be divided into five classes: normal, abnormal shape, abnormal color, abnormal water content and abnormal shape and water. When labeling, the continuous main body of droppings were labeled, and the fecal debris produced by spattering were ignored. Pascal VOC 2007 data set was selected for this research. The image and label of the data set were prepared according to the format requirements, and the data set of broiler droppings was obtained in the final (Zhenyu et al., 2017). The data set included 6307 images as training sets, 700 images as validation sets, and 630 images as test sets.

### 2.3. Construction of deep convolutional neural network

#### 2.3.1. Faster R-CNN architecture

Deep convolution neural network is an artificial neural network based on deep learning theory (Hara et al., 2015; Hui et al., 2017; Shelhamer et al., 2017; Zhenyu et al., 2017). Its artificial neurons can respond to a part of the surrounding units in the coverage area and perform well in image processing (Li and Zhang, 2017). Deep convolution neural network can be divided into two categories according to whether or not to extract the region of interest before classification and location. One is represented by Yolov3, which use the whole picture as the domain of interest to recognition and location. The other one is represented by Faster R-CNN, which extract the domain of interest first and then do the recognition and location theory (Lokanath et al., 2017; Zhenyu et al., 2017).

The structure of Faster R-CNN network was shown in Figure 2. The Region Proposal Network (RPN) was used to extract the ROI. The working process of RPN is a two-step operation, i.e., RPN Classification and RPN bounding box regression. The process of RPN Classification is a two-classification process. Firstly,  $K \times H \times W$  regions (called anchor,  $K = 9$ ,  $H$  is the height of feature map, and  $W$  is the width) should be evenly divided on feature map (Ren et al., 2017). By comparing the overlap between these anchors and ground truth, we can decide which anchors are prospects and which are backgrounds, that is, label each anchor with prospects or backgrounds. With labels, RPN can be trained to recognize foreground and background for any input (Liao et al., 2017; Ren et al., 2017).

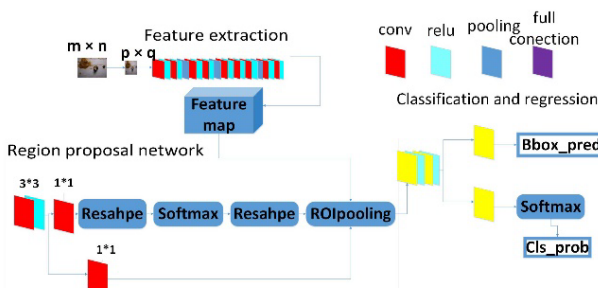


Figure 2. Overview of the proposed Faster R-CNN Network Structure

- Input Layer:

Inputting the processed data set. Pascal VOC data sets and XML tags were used.

- Convolutional layer:

Faster R-CNN supports any size of image input, but before convolution operation, the input image will be standardized, and the size of the image that is not up to the set size will be supplemented (Ohn-Bar and Trivedi, 2017). The conversion of input and output sizes, shown in Equation (1), where pad and stride are the step size of the convolution kernel and the edge of

expansion, respectively.

$$\text{output size} = \frac{(\text{input size}) - \text{ker nel size} + 2 * \text{pad}}{\text{stride}} + 1 \quad (1)$$

- Region Proposal Network (RPN)

Region Proposal Network is used to recommend region of interest (ROI). The input is feature maps and the output is multiple ROI. In the training process of RPN, anchors with the largest IoU with ground truth box (GTbox) are defined as positive samples, while negative samples are defined as IoU with GTbox less than 0.3 samples. The loss function for RPN during the training is defined as follows:

$$(\{p_i\}, \{t_i\}) = \frac{1}{N_{cls}} \sum i L_{cls}(p_i, p_i^*) + \lambda \frac{1}{N_{reg}} \sum i p_i^* L_{reg}(t_i, t_i^*) \quad (2)$$

where  $i$  is the anchor number,  $p_i$  is the probability that the  $i^{th}$  anchor number being the foreground. If the  $i^{th}$  anchor number is the foreground then  $p_i, p_i^*$  is 1, or 0.  $t_i$  is the coordinate of the predicted bounding box.  $t_i, t_i^*$  is the coordinate of ground truth,  $N_{cls}$  is the classification loss, and  $L_{reg}$  is the regression loss (Zhang et al., 2019).

- ROI Pooling

In the ROI Pooling, layer proposals generated by RPN are used to get a fixed size proposal feature map. Full connection operation can be used to identify and locate targets. There are two different sizes of proposals in the feature map, but after pooling, there are  $7 \times 7 = 49$  outputs, which can provide fixed-length input for the full connection layer.

- Classify and Output

Outputting the class of candidate region and the exacting location of candidate region in the image. The fixed-size feature maps formed by ROI Pooling layer were used for full connection operation, and specific categories are classified by Softmax. At the same time, L1 Loss is used to complete the regression of bounding box to obtain the precise position of the object (Hui et al., 2017). Outputting the results of recognition, location and classification.

### 2.3.2. Yolo-v3 architecture

Darknet 53 was chosen as the network framework of Yolov3, which consists of a series of 1x1 and 3x3 convolution layers (each convolution layer was followed by a BN layer and a Leaky ReLU). The convolution layers of Darknet53 was integrated from the convolution layers with better performance selected by various networks. Yolov3 feature interaction layer can be divided into three scales (Redmon et al., 2015).

The structure of Yolov3 is shown in Figure 3. Local feature interaction is achieved by convolution, in each scale. The local feature interaction between feature maps is realized by convolution (3\*3 and 1\*1). Using FPN algorithm, the sampled features on 97th layer are combined with the output features on 36th layer to predict large-scale targets. The sampled features on 85th layer is combined with the output features on 61th layer. Using the multiscale features to increase the abundant of features, and then the detection results of large and small targets will be getting better. Res layer just do the shortcut operation to calculate the difference and its input and output are consistent. The res layer comes from RESNET. To solve the problem of gradient dispersion or gradient explosion in the network, res layer proposes to change the layer-by-layer training of deep neural network into step-by-step training. It divides the deep neural network into several segments, each of which contains simple network layers. Then the shortcut connection is used to train each segment for residual error, and each segment learning part of the total loss. Finally, it achieves a small total loss, at the same time, the propagation of gradient is well controlled to avoid the situation that gradient disappears or explosion. The output layer directly outputs the recognition results (the type and location of the broiler droppings by predict). The output of the target box using non-maximum suppression (NMS) to predict the filter box. During the testing, setting the threshold of intersection over union (IOU) and outputting the only

prediction box for each target with NMS. IOU is defined as:

$$IOU = \frac{Overlap}{Union} \quad (3)$$

where the Overlap is the intersection between the prediction box and the real box (label box), and the Union is the union of prediction box and real box.

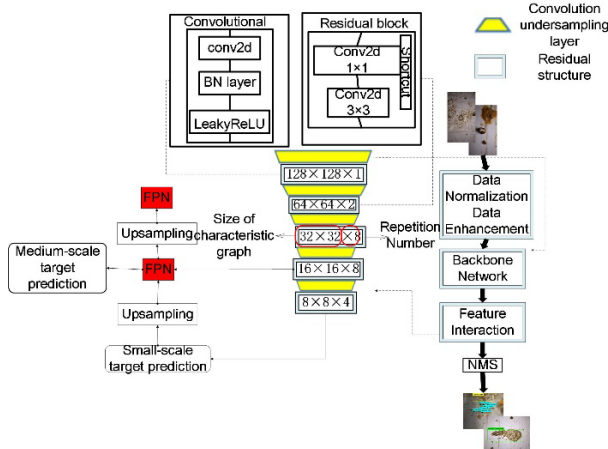


Figure 3. The overview of the proposed YOLO-V3 structure.

#### 2.4. Evaluation indicators

To evaluate the performance of broiler droppings recognition models, average precision (AP), mean average precision (mAP) and recall were applied according to Eq. 4, 5 and 6, respectively.

$$R = \frac{TPos}{Pos} \quad (4)$$

$$AP = \int_0^1 P(R)dR \quad (5)$$

$$mAP = \frac{\sum_{i=1}^c AP_i}{C} \quad (6)$$

where  $TPos$  is the result of correct classification,  $Pos$  is the positive sample, and  $C$  is the number of sample classification.

#### 2.5. Test platform

The two kinds of deep convolution neural networks were designed and constructed based on Tensorflow framework and Darknet framework. The training was set on a computer with GTX1080Ti GPU, 50GB effective memory, i7 7700k CPU and Ubuntu 16.04 operating system.

### 3. Results and discussion

#### 3.1. Analysis the performance of faster R-CNN and Yolov3

Two deep learning algorithms, Faster R-CNN and Yolov3, were trained on the image data set of broiler droppings. After 50,000 iterations of training, the test results of the model on test set and verification set were shown in Table1. The recognition performance of five kinds of broiler droppings was shown in Figure 4.

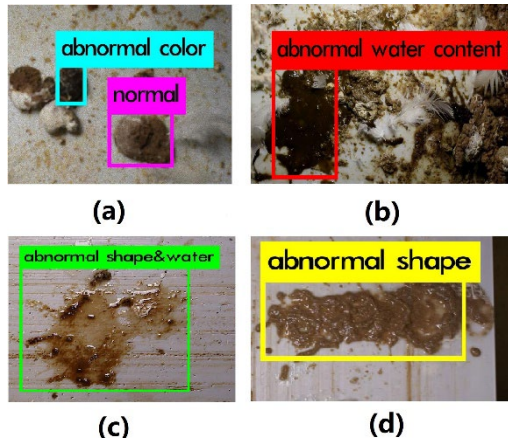


Figure 4. Broiler droppings label recognition during the testing phase based on Faster R-CNN  
 (a) abnormal color and normal color, (b) abnormal water content, (c) abnormal shape & water content, (d) abnormal shape

From Table 1, it could be found that Yolov3 training duration was longer than Faster R-CNN, but detection speed was better than Faster R-CNN. The single class AP of Faster R-CNN was higher than that of Yolov3. The mAP was 9. 07% higher on the whole test set and verification set. Faster R-CNN single and overall Recall were higher than Yolov3, which was 10. 3%. This research was applied to the cage broiler feeding line. Because the speed of the dung conveyor belt was slow, the frequency of image acquisition was higher than 2 fps, which could meet the requirements. So Faster R-CNN and Yolov3 could meet the requirement both.

Table 1. A comparison of the performance of YOLO-V3 and Faster R-CNN.

Recognition models	YOLO-V3		Faster R-CNN	
	Recall	AP	Recall	AP
Classes				
Normal	0.821	0.8285	0.989	0.8859
Abnormal shape	0.874	0.8813	0.996	0.9030
Abnormal color	0.922	0.8024	0.997	0.9815
Abnormal water content	0.927	0.8951	0.977	0.9822
Abnormal shape & water	0.895	0.8054	0.998	0.9125
Mean	0.887	0.8425	0.991	0.9332
Training duration (hr)		148		16
Detection speed (fps)		43.5		5.7

### 3.2. Comparison of different iterations

The depth of network is very important to the performance of convolutional neural network model, but with the increase of network layers, the over-fitting problem will intensify (Zhang et al., 2019). The capacity of data set, the depth of convolution layer and the number of iterations will affect the final performance. In this study, the number of training sets was 7637, the depth of Yolov3 was 106 layers except the input layer, and Faster R-CNN used resnet101 residual network with 101 layers. Figure 5 illustrates the change of total loss corresponding to different iteration number models.

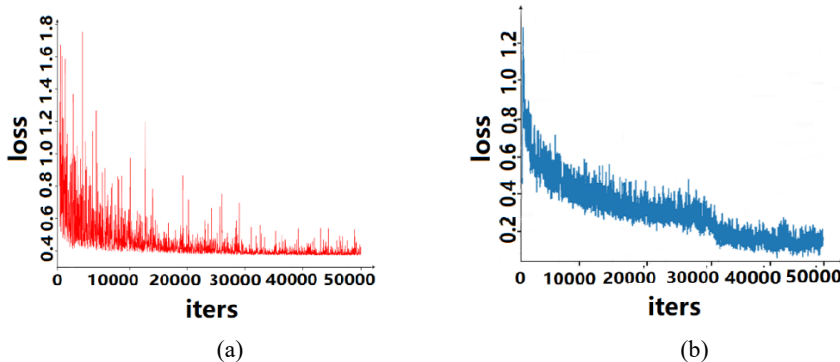


Figure 5. The average loss against the number of iterations for (a) Faster R-CNN and (b) YOLO-V3.

As shown in Figure 5, the abscissa was the number of iterations and the ordinate was the average loss value. It is easy to find that loss declined rapidly in the first 5000 iterations of Faster R-CNN, but the fluctuation was large. With training iterations increased, the loss of Faster R-CNN decreased gradually, and reached a stable level at about 30,000 times, converged to 0. 37. During the training of the Yolov3, in the first 1000 iterations, the average loss rate decreased fast, but the fluctuation was larger. During 20,000 to 25,000 iterations, the loss converged steadily to about 0. 4. However, with the increase of iterations, there was a significant non-smooth descent at 27,000 iterations. It was stable from 31,000 times and finally stabilized at about 0. 17. The weight models of Yolov3 in 23,000 iterations and the 35,000 iterations were used to test. The test object was the test set. The test results are shown in Table 2.

Table 2. Test Results for 3, 23, 000 and 35, 000 iterations weight model.

Iterations	Normal (AP)	Abnormal shape (AP)	Abnormal color (AP)	Abnormal water content (AP)	Abnormal shape & water (AP)	mAP	Recall
23,000	0.780	0.859	0.799	0.860	0.764	0.813	0.846
35,000	0.837	0.863	0.806	0.871	0.778	0.831	0.879

It was established that the weighting model of 45 000 iterations was better than that of 35 000 iterations, whether in the accuracy of single class or in the overall map and recall. Combining with Figure 5b (loss curve of Yolov3), it could be known that Yolov3 fall into the local optimal solution during the training process from 2000 to 25,000 iterations, and achieved the optimal performance at about 31,000 iterations.

#### 4. Conclusions

Digestive tract disease is one of the major diseases in broiler breeding. Monitoring technology of digestive tract diseases in broilers can promote the automation, intellectualization and precision development of broiler breeding industry. Broiler droppings can be used as an index for evaluating digestive tract diseases in broilers. In this research, broiler droppings were divided into normal and abnormal droppings, and abnormal droppings was classified into abnormal shape, abnormal color, abnormal water content and abnormal shape & water. The performances of Faster R-CNN and Yolov3 on broiler droppings data set were compared. Faster R-CNN achieved the best performance at about 30,000 iterations. On the test set, mAP was 93. 32% and recall was 0. 991. Yolov3 achieved the best performance at about 31,000 iterations. On the test set, mAP was 84. 25% and recall was 0. 887. This study provided an automatic and non-contact model for

identifying and classifying abnormal droppings in broilers, which provided technical support for early warning of digestive tract diseases in broilers.

## References

- Dekich, M.A., B. Pan, X. Suo 1999. Prevention and Control Strategies of Respiratory and Intestinal Diseases in Broilers. *China Animal Husbandry & Veterinary Medicine*, (02): 46–47.
- Du, S.-S., Z.D. Shan, Z.C. Huang, H.Q. Liu, S.L. Liu, 2008. The Algorithmic of Components Auto-classification and System Development of Electronic Components. *Development & Innovation of Machinery & Electrical Products*. 21(06): 133–135.
- Eshed O.B., T.M. Manubhai, 2017. Multi-scale volumes for deep object detection and localization. *Pattern Recognition*. 61, pp.557–572.
- Gao, Z.-Y., A. Wang, Y. Liu, L. Zhang, Y.W. Xia, 2017. Intelligent Fresh-tea-leaves Sorting System Research Based on Convolution Neural Network. *Transactions of the Chinese Society for Agricultural Machinery*. 48(7): 53–58.
- Hara, K., D. Saito, and H. Shouno, 2015. Analysis of function of rectified linear unit used in deep learning. In 2015 International Joint Conference on Neural Networks (IJCNN) (1–8). IEEE.
- Joseph R., D. Santosh, G. Ross, F. Ali, 2015. You only look once: Unified, real-time object detection. In *Proceedings of the IEEE conference on computer vision and pattern recognition* (pp. 779–788).
- Li, M., H. Zhang, 2017. Image classification based on convolution neural network of iterative optimization. *Computer Engineering and Design*. 38(01): 198–202.
- Li, X.-Y., G.B. Wang, 2018. Fine-grained Bird recognition Based on Convolution Neural Network Semantic Detection. *Science Technology and Engineering*. 18(10): 240–244.
- Liao, Z.-B., G.A. Carneiro, 2017. Deep convolutional neural network module that promotes competition of multiple-size filters. *Pattern Recognition*, 71(9): 94–105.
- Liu, Z.-C., D.J. He, 2019. Recognition Method of Cow Estrus Behavior Based on Convolutional Neural Network. *Transactions of the Chinese Society for Agricultural Machinery*. 1–12.
- Lokanath, M., K. Sai Kumar, E.S. Keerthi, 2017. November. Accurate object classification and detection by faster-RCNN. In *Materials Science and Engineering Conference Series* (Vol. 263, No. 5, p. 052028).
- Long, J., E. Shelhamer, T. Darrell, 2017. Fully Convolutional Networks for Semantic Segmentation. *IEEE Transactions on Pattern Analysis and Machine Intelligence*. 39(6): 640–651.
- Lu, G., 2019. Prevention and treatment of digestive tract diseases in Broilers. *The Chinese Livestock and Poultry Breeding*. 12(06): 40–41.
- Lu, S., W. Guo, 2014. Observation on Fecal Traits of Broiler Chickens and Differential Diagnosis of Common Diarrhea Diseases. *Henan journal of animal husbandry and veterinary medicine*. (3): 14–16.
- Qu, C., Z.F. He, S.B. Li, H.J. Li, M.X. Gong, H.L. Gong, 2019. Current status and development trend of processing and producing broilers in China. *Food and Fermentation Industries*. 45(08): 258–266.
- Ren, S.-Q., K.M. He, G. R. Ross, J. Sun 2017. Faster R-CNN: Towards Real-Time Object Detection with Region Proposal Networks. *IEEE Transactions on Pattern Analysis and Machine Intelligence*. 39(6): 1137–1149.
- Wang, Z., Y. Shi, Y. Li, 2019. Segmentation of corn leaf diseases based on improved fully convolutional neural network. *Computer Engineering and Applications*. 1–9.
- Wu, Z.-L., Y.Q. Zhang, J.L. Xu, H.P. Jia, 2014. Research on K-means Algorithm Optimization Based on OpenCL. *Papers Collection of 2013 National Annual Conference on High Performance Computing*. 8(10): 1162–1176.
- Zhang, H., K.F. Wang, F.Y. Wang, 2017. Advances and Perspectives on Applications of Deep Learning in Visual Object Detection. *Acta Automatica Sinica*. 43(08): 1289–1305.
- Zhang, Y., T. Xu, D. Feng, M. Jiang, G. Wu, 2019. Research on Faster R-CNN Object Detection Based on Hard Example Mining. *Journal of Electronics & Information Technology* (1).
- Zheng, X., G. Ran, 2010. Etiology and Prevention of Chicken Intestinal Syndrome. *The Chinese Livestock and Poultry Breeding*. 6(11): 128.

# Classification of Broiler Behaviors Using Triaxial Accelerometer and Machine Learning

Xiao Yang<sup>a</sup>, Yang Zhao<sup>a,\*</sup>, Garrett M. Street<sup>b</sup>, Yanbo Huang<sup>c</sup>

<sup>a</sup> Department of Agricultural and Biological Engineering, Mississippi State University, Hood Road, MS 39762, USA

<sup>b</sup> Department of Wildlife, Fisheries and Aquaculture, Mississippi State University, Hood Road, MS 39762, USA

<sup>c</sup> United States Department of Agriculture, Agricultural Research Service, Crop Production Systems Research Unit, Hood Road, MS 39762, USA

\* Corresponding author. Email: [yzhao@abe.msstate.edu](mailto:yzhao@abe.msstate.edu)

## Abstract

Understanding broiler behaviors and their time budget provides important implications for animal well-being and farm management. The objective of this study was to classify specific broiler behaviors via analyzing data of accelerometers using two machine learning models, K-Nearest Neighbor (KNN) and Support Vector Machine (SVM) models. Lightweight triaxial accelerometers were used to record three-dimensional accelerations of 7-week-old Ross 708 broilers at a sampling frequency of 40Hz. Total 182-minute acceleration data were labeled for four behaviors – walking, resting, feeding and drinking – and translated into six instantaneous motion features including magnitude area, vector magnitude, movement variation, energy, entropy, and tilt angle. The mean, variation, standard deviation, minimum and maximum of each above-mentioned feature and two-way correlations of three-dimensional accelerations were calculated in 3-sec sliding windows (120 samples) with 1.5-sec overlapping (60 samples), yielding total 48 statistic features for model training and testing. Seventy percent (70% or 127-minute data) of the data were used for model training, and the rest (30% or 55-minute data) were used for testing. The results show that the overall classification accuracies of KNN and SVM models were, respectively, 99% and 99% for walking, 97% and 99% for resting, 89% and 95% for drinking, and 88% and 95% for feeding. Kappa value (an indicator of agreement between observed behaviors in a video and reported behaviors by a model), sensitivity, specificity and precision of SVM model were higher than those of KNN model. In conclusion, classification of specific broiler behaviors can be achieved by recording bird triaxial accelerations and analyzing acceleration data through machine learning. Performances of different machine learning models may differ in classifying broiler walking, lying, drinking and feeding behaviors.

**Keywords:** Broiler, accelerometer, behavior, classification

## 1. Introduction

Behaviors are observable and measurable indicators of animal adaption to environmental stimuli (Benn et al., 2019). Studying animal behaviors may help better understand animal physiological health status, well-being conditions, and preference on housing systems. Animal behavior monitoring and analysis have been performed (Shimmura et al., 2008; Struelens et al., 2008) by human observation, which is however labor intensive, time-consuming and subjective (Ungar and Rutter, 2006). Recent advancement of electronics avails the use of precision agriculture tools to monitor the animal behaviors automatically.

Accelerometers measure accelerations along one or more axes that respond to both movement and gravity. They have been extensively implemented to study behaviors and motions of different animal species. For example, accelerometers were mounted to beef cattle (Watanabe et al., 2008; Robert et al., 2009; Wolfer et al., 2015) and sheep (Alvarenga et al., 2016; Giovanetti et al., 2017) to classify behaviors of eating, ruminating, sitting, standing, walking and lying. Some research has been carried out to measure the poultry activity level (Stevenson et al., 2018) and posture detection of aquatic animals, such as seals (Iwata et al., 2012) and fish (Brownscombe et

al., 2014), using accelerometers in combination with other sensors (GPS, temperature, pressure and light intensity). Dawson et al. (2007) used accelerometers to monitor the broiler terminal convulsions as an indicator of time to death after cervical dislocation. Banerjee et al. (2012) attached wireless accelerometers to laying hens reared in non-cage housing system, and classified different bird behaviors using machine learning. Accelerometers are, however, scarcely used to study behaviors of broilers. Furthermore, the performances of bird behavior classification using accelerometers and machine learning models remain explored. The objective of this study was to classify specific broiler behaviors, including walking, resting, drinking and feeding, by analyzing acceleration data using two machine learning models, k-nearest neighbor (KNN) and support vector machine (SVM). The performances of the two models were compared.

## 2. Materials and Methods

### 2.1. Animal and husbandry

Total 108 broilers were reared at two rooms ( $54 \text{ birds room}^{-1}$ ) at the stocking density of  $0.1 \text{ m}^2 \text{ bird}^{-1}$ . The broilers were 7-week-old during the experiment period. Six nipple drinkers and two tube feeders were installed in each room. Feed and water were provided *ad libitum*. All procedures of animal care and handling were approved by USDA-ARS Institutional Animal Care and Use Committee at Mississippi State.

### 2.2. Accelerometer

Lightweight triaxial accelerometers (DDAMTT,  $27 \times 26 \times 10 \text{ mm}$ ,  $\pm 16\text{g}$ , Wildbyte Technologies Ltd., Swansea, UK) were used to detect the movement of individual broilers. Each accelerometer was powered by a Li-Po battery (3.7 v, 300 mAh, LP402530,  $35 \times 20 \times 4 \text{ mm}$ ) (Figure 1a), which was able to sustain the data logging for  $\sim 72$  hours. Each pair of accelerometer and battery was sealed in a 3D printed box ( $38 \times 32 \times 18 \text{ mm}$ ) (Figure 1b) and mounted to the back of a broiler using a chicken harness (Valhoma Corporation, Tulsa, OK) (Figure 1c). The broiler accelerations in the directions of forward and backward (X), left and right (Y), and up and down (Z), were recorded. The 3D acceleration data were stored in a Micro SD card and exported as excel files using the companion software (Animal Motion Visualization, Wildbyte Technologies Ltd., Swansea, UK).

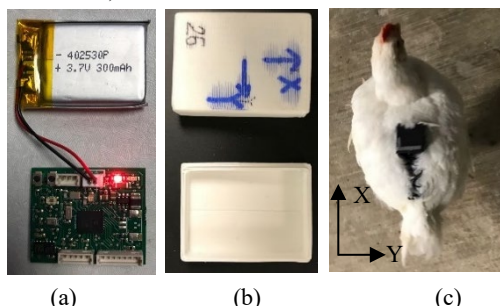


Figure 1. Photos of the accelerometer and battery (a), the 3D printed box (b), and a broiler carrying an accelerometer (c).

### 2.3. Measurements

Four broilers were randomly selected in the two experimental rooms ( $2 \text{ birds room}^{-1}$ ). Each broiler wore a chicken harness with a small pouch for holding the box of accelerometer and battery. The sampling frequency of the accelerometers was set at 40 Hz. Cameras were installed at the ceiling in each room to monitor the bird behaviors continuously.

### 2.4. Behavior description and labeling

Four specific bird behaviors, including walking, resting, drinking and feeding, were examined

in this study. Walking is considered as the act of a broiler moving for at least four successive steps without pecking at the litter floor. Resting is defined as a bird sitting on the litter. Feeding is deemed as a continuous eating event for at least 3s. Drinking is when a broiler pecks at a nipple drinker.

The four behaviors in total 182 min (436,800 instant behavior instances) of raw acceleration data were labeled, including 24.7 min of walking, 64.4 min of resting, 44.9 min of drinking and 47.2 min of feeding. Seventy percent (70%) data of each bird were combined to train the models, while the remaining 30% were used for testing.

## 2.5. Feature extraction

Data processing using machine learning was conducted in MATLAB (2016a). Six instantaneous features including magnitude area, vector magnitude, movement variation (Campbell et al., 2013), energy, entropy, and tilt angle were calculated using equations in Table 1, where  $i$  represents the moment  $i$ . The mean, variation, standard deviation, minimum and maximum of above-mentioned features and two-way correlation of 3D accelerations were calculated in 3-sec sliding windows (120 samples) with 1.5-sec overlapping (60 samples), yielding total 48 statistic features.

Table 1. Equations for calculating motion features of broilers using triaxial acceleration data. X, Y, and Z represent broiler accelerations in forward-backward, left-right, and up-down directions, respectively.

Instantaneous feature	Equation
Magnitude area	$ X_i  +  Y_i  +  Z_i $
Vector magnitude	$\sqrt{X_i^2 + Y_i^2 + Z_i^2}$
Movement Variation	$ X_{i+1} - X_i  +  Y_{i+1} - Y_i  +  Z_{i+1} - Z_i $
Energy	$(X_i^2 + Y_i^2 + Z_i^2)^2$
Entropy	$(1 + (X_i + Y_i + Z_i))^2 \times \ln(1 + (X_i + Y_i + Z_i)^2)$
Tilt angle	$\arccos\left(Z_i / \sqrt{X_i^2 + Y_i^2 + Z_i^2}\right)$

## 2.6. Machine learning models

The KNN and SVM models were used in this study. KNN is a non-parametric and lazy learning algorithm which is theoretically mature with low complexity. An instance is classified by a majority vote of its neighbors, with the instance being assigned to the class most common amongst its  $K$  nearest neighbors measured by a distance function. Briefly speaking, in a sample space, if most of its  $K$  nearest neighbor samples belong to a category, then the sample belongs to the same category (Altman, 1992). The value of  $K$  was set at 25, which had the best performance based on the training dataset. In our study. The basic idea of SVM is to transform the input data into a high-dimensional feature space using a kernel function, after which a hyperplane will be constructed between two classes of data points so that the margin separating the data points is maximized. Multi-class SVMs are usually implemented by combining several binary SVMs. In this study, one-against-all method was used, which has been widely explored to solve multi-class pattern recognition problems (Liu and Zheng, 2005). In this study, four binary classifiers were constructed to classify four behaviors, respectively. Each of them separates a single class from all remaining classes. To avoid overfitting, 5-fold cross validation was used due to the large dataset.

## 2.7. Model performance

Confusion matrices were used to evaluate the performance of classification models. From the

matrix, accuracy, sensitivity, specificity and precision are calculated using Eq. (1)–(4).

$$\text{accuracy} = \frac{(TP + TN)}{(TP + TN + FP + FN)} \quad (4)$$

$$\text{sensitivity} = \frac{TP}{(TP + FN)} \quad (2)$$

$$\text{specificity} = \frac{TN}{(TN + FN)} \quad (3)$$

$$\text{precision} = \frac{TP}{(TP + FP)} \quad (4)$$

where  $TP$  (true positive) is the number of instances that a behavior of interest was both reported by a model and observed in a video at a certain moment;  $FN$  (false negative) is the number of instances that a behavior of interest was observed but reported as other behaviors;  $FP$  (false positive) is the number of instances that a behavior of interest was reported but not observed;  $TN$  (true negative) is the number of instances that a behavior of interest was neither reported nor observed.

The Kappa value is a metric that is used to quantify the level of agreement between observed results in a video and reported results by a model (Warrens, 2011). It is calculated using Eq. (5)–(7). Altman (1990) categorized the levels of agreement as “poor” for Kappa values of 0.0–0.2, “fair” for Kappa values of 0.2–0.4, “moderate” for Kappa values of 0.4–0.6, “good” for Kappa values of 0.6–0.8, and “very good” for Kappa values of 0.8–1.0.

$$C_0 = \sum A_{mn} / N \quad (5)$$

$$C_a = \left( \sum A_{..n} \times A_{..m} \right) / N^2 \quad (6)$$

$$\text{Kappa} = \frac{(C_0 - C_a)}{(1 - C_a)} \quad (7)$$

where  $m$  represents the row of labeled behaviors in the confusion matrix;  $n$  represents the column of four classified behaviors in the confusion matrix ( $m = n = 1, 2, 3$  and 4 in this study);  $A$  represents the number of instances that classified as specific behaviors by two methods;  $N$  represents the total number of observations;  $C_0$  is the observed agreement, or the proportion of behaviors for which the two methods agree;  $C_a$  is the probability of random agreement. The performance of the models in this study was determined using only the testing data set.

### 3. Results and Discussion

#### 3.1. Data description

Example triaxial accelerations for specific broiler behaviors are shown in Figure 2. Walking behavior is identified as profound fluctuating acceleration curves in all three dimensions. Resting behavior is represented by steady acceleration curves in all three dimensions. Drinking and feeding behaviors appear similar in fluctuation amplitudes of acceleration curves; however, their baselines (or equilibriums) in forward-backward and left-right directions are slightly different, possibly because broilers need to raise heads to drink but bow to eat.

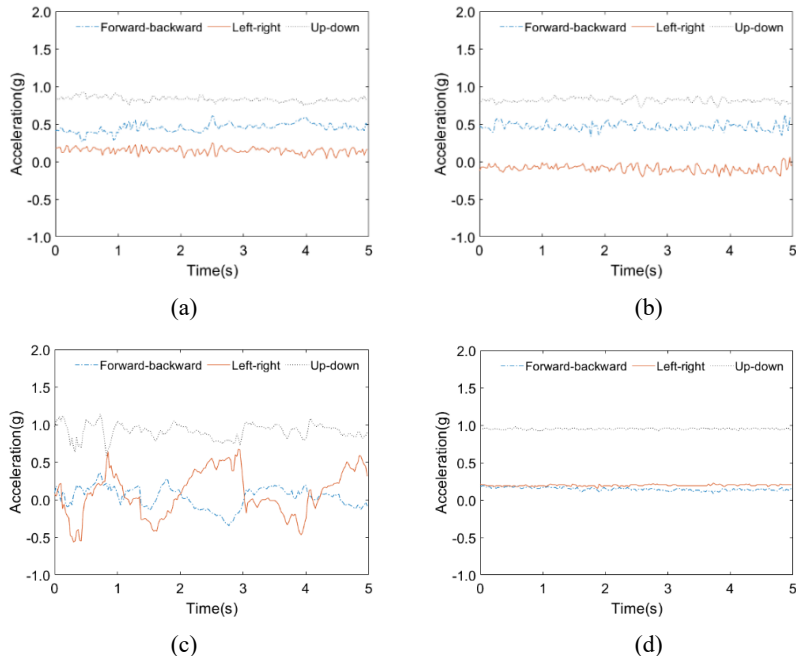


Figure 2. Example acceleration signals for broiler walking (a), resting (b), drinking (c) and feeding (d) behaviors in forward-backward, left-right, and up-down directions.

### 3.2. Behavior classification

Tables 2 and 3 show the confusion matrices of KNN and SVM by validating the model-classified behaviors against visually labeled behaviors. Both models were highly accurate in classifying walking and resting behaviors. Specifically, KNN identified 95% (281/297) walking instances, and 95% (735/774) resting instances; and SVM correctly identified 94% (278/297) walking instances and 98% (760/774) resting instances. Compared to walking and resting, drinking and feeding were classified with lower accuracies. The KNN model misclassified 20% drinking as feeding, and 18% feeding as drinking. As for SVM model 12% drinking was misclassified as feeding, and 4% feeding as drinking. Banerjee et al. (2012) also found that over 63% drinking behavior of laying hen was misclassified as feeding using acceleration data and neural network.

Table 2. Confusion matrix of k-nearest neighbor (KNN) model for classifying broiler walking, resting, drinking and feeding behaviors. Values in the table are the number of behavioral instances.

Labeled <sup>a</sup>	Classified <sup>b</sup>				
	Walking	Resting	Drinking	Feeding	Total (labeled)
Walking	281	0	14	2	297
Resting	5	735	0	34	774
Drinking	0	7	422	110	539
Feeding	0	19	103	444	566
Total (classified)	286	761	539	590	2176

<sup>a</sup> Bird behaviors labeled/observed in video files (gold standard).

<sup>b</sup> Bird behaviors reported by the model.

Table 3. Confusion matrix of Support Vector Machine (SVM) model for classifying broiler walking, resting, drinking and feeding behaviors. Values in the table are the number of behavioral instances.

Labeled <sup>a</sup>	Classified <sup>b</sup>				
	Walking	Resting	Drinking	Feeding	Total (labeled)
Walking	278	0	13	6	297
Resting	2	760	0	12	774
Drinking	0	0	474	65	539
Feeding	0	5	24	537	566
Total (classified)	280	765	511	620	2176

<sup>a</sup> Bird behaviors labeled/observed in video files (gold standard).

<sup>b</sup> Bird behaviors reported by the model.

### 3.3. Performance of classification model

The performances of KNN and SVM classification models for the four specific behaviors of broilers are shown in Table 4. Four performance indicators, accuracy, sensitivity, specificity and precision, were calculated and compared for different behaviors. Kappa value that used to evaluate the overall performance of model was also calculated.

Accuracy of KNN and SVM was, respectively, 99% and 99% for walking, 97% and 99% for resting, 89% and 95% for drinking, and 86% and 95% for feeding. Sensitivity of KNN and SVM was 95% and 94% for walking, 95% and 98% for resting, 78% and 88% for drinking and 78% and 95% for feeding. It is shown that the accuracy and sensitivity of drinking and feeding behavior were much lower than those of walking and resting. The SVM model achieved higher accuracy and sensitivity for drinking and feeding compare to the KNN model. Specificity of KNN and SVM was 99% and 99% for walking, 97% and 99% for resting, 93% and 96% for drinking, and 92% and 98% for feeding. Precision of KNN and SVM was 99% and 99% for walking, 98% and 99% for resting, 78% and 93% for drinking, and 75% and 87% for feeding. The results of Kappa values show that the strength of agreement between observed and reported behaviors were very good for both models. The SVM model had a higher Kappa value than KNN, indicating a better overall performance of SVM in broiler behavior classification.

Table 4. Performances of k-nearest neighbor (KNN) and Support Vector Machine (SVM) and models for classifying broiler behaviors.

Model	Behavior	Performance indicator				
		Accuracy (%)	Sensitivity (%)	Specificity (%)	Precision (%)	Kappa
KNN	Walking	99	95	99	99	0.81
	Resting	97	95	97	98	
	Drinking	89	78	93	78	
	Feeding	88	78	92	75	
SVM	Walking	99	94	99	99	0.92
	Resting	99	98	99	99	
	Drinking	95	88	96	93	
	Feeding	95	95	98	87	

### 4. Preliminary Observations and Recommendations

In this study, classification of specific broiler behaviors using acceleration data and two machine learning models was investigated. Classification of walking and resting behaviors were highly accurate by both models, but less accurate for drinking and feeding behaviors. To improve feeding and drinking behavior classification, larger datasets with more broilers and their motion features may be considered to train the models. Support vector machine (SVM) performed better

than k-nearest neighbor (KNN) for classifying all behaviors in terms of accuracy, sensitivity, specificity, precision and Kappa value. As concerns on animal welfare increase, continuously monitoring of natural behaviors and health status of broilers in farm conditions would be particularly important, which would rely on precision agriculture tools like accelerometer and machine learning. By combining classification models with real time measurement, the behavior recognition of broilers will be more precise.

## References

- Altman, D.G., 1990. Chapter 14: Some common problems in medical research. Practical statistics for medical research. 404–405.
- Altman, N.S., 1992. An introduction to kernel and nearest-neighbor nonparametric regression. *The American Statistician*. 46 (3), 175–185. <http://dx.doi.org/10.1080/00031305.1992.10475879>.
- Alvarenga, F., I. Borges, L. Palkovič, J. Rodina, V. Oddy, R. Dobos, 2016. Using a three-axis accelerometer to identify and classify sheep behaviour at pasture. *Applied Animal Behaviour Science*. 181, 91–99. <http://dx.doi.org/10.1016/j.applanim.2016.05.026>.
- Banerjee, D., Biswas, S., Daigle, C., & Siegfard, J. M., 2012. Ninth International Conference on Wearable and Implantable Body Sensor Networks. <https://ieeexplore.ieee.org/document/6200546>.
- Benn, A.L., D.J. McLelland, A.L. Whittaker, 2019. A Review of Welfare Assessment Methods in Reptiles, and Preliminary Application of the Welfare Quality® Protocol to the Pygmy Blue-Tongue Skink, *Tiliqua adelaidensis*, Using Animal-Based Measures. *Animals*. 9 (1), 27. <http://dx.doi.org/10.3390/ani9010027>.
- Brownscombe, J.W., L.F.G. Gutowsky, A.J. Danylchuk, S.J. Cooke, 2014. Foraging behaviour and activity of a marine benthivorous fish estimated using tri-axial accelerometer biologgers. *Marine Ecology Progress Series*. 505, 241–251. <http://dx.doi.org/10.3354/meps10786>.
- Campbell, H.A., L. Gao, O.R. Bidder, J. Hunter, C.E. Franklin, 2013. Creating a behavioural classification module for acceleration data: using a captive surrogate for difficult to observe species. *The Journal of Experimental Biology*. 216 (24), 4501–4506. <http://dx.doi.org/10.1242/jeb.089805>.
- Dawson, M.D., M.E. Lombardi, E.R. Benson, R.L. Alphin, G.W. Malone, 2007. Using Accelerometers to Determine the Cessation of Activity of Broilers. *The Journal of Applied Poultry Research*. 16 (4), 583–591. <http://dx.doi.org/10.3382/japr.2007-00023>.
- Giovanetti, V., M. Decandia, G. Molle, M. Acciaro, M. Mameli, A. Cabiddu, R. Cossu, M. Serra, C. Manca, S. Rassu, 2017. Automatic classification system for grazing, ruminating and resting behaviour of dairy sheep using a tri-axial accelerometer. *Livestock Science*. 196, 42–48. <http://dx.doi.org/10.1016/j.livsci.2016.12.011>.
- Iwata, T., K.Q. Sakamoto, A. Takahashi, E.W.J. Edwards, I.J. Staniland, P.N. Trathan, Y. Naito, 2012. Using a mandible accelerometer to study fine-scale foraging behavior of free-ranging Antarctic fur seals. *Marine Mammal Science*. 28 (2), 345–357. <http://dx.doi.org/10.1111/j.1748-7692.2011>.
- Liu, Y., Y.F. Zheng, 2005. IEEE International Joint Conference on Neural Networks. <https://doi.org/10.1109/ijcnn.2005.1555963>
- Robert, B., B. White, D. Renter, R. Larson, 2009. Evaluation of three-dimensional accelerometers to monitor and classify behavior patterns in cattle. *Computers and Electronics in Agriculture*. 67 (1–2), 80–84. <http://dx.doi.org/10.1016/j.compag.2009.03.002>.
- Shimmura, T., T. Suzuki, S. Hirahara, Y. Eguchi, K. Uetake, T. Tanaka, 2008. Pecking behaviour of laying hens in single-tiered aviaries with and without outdoor area. *British poultry science*. 49 (4), 396–401. <http://dx.doi.org/10.1080/00071660802262043>.
- Stevenson, R., H.A. Dalton, M. Erasmus, 2018. Validity of micro-data loggers to determine walking activity of turkeys and effects on turkey gait. *Frontiers in veterinary science*. 5. <http://dx.doi.org/10.3389/fvets.2018.00319>.
- Struelens, E., F. Tuyttens, L. Duchateau, T. Leroy, M. Cox, E. Vranken, J. Buyse, J. Zoons, D. Berckmans, F. Ödberg, 2008. Perching behaviour and perch height preference of laying hens in furnished cages varying in height. *British Poultry Science*. 49 (4), 381–389. <http://dx.doi.org/10.1080/00071660802158332>.

# Implication of Modern Sow's Static and Dynamic Space Usage on Gestation Stall Design

Suzanne Leonard <sup>a</sup>, Hongwei Xin <sup>b,\*</sup>, Tami M. Brown-Brandl <sup>c,\*</sup>, Brett C. Ramirez <sup>a</sup>,  
John P. Stinn <sup>d</sup>, Anna K. Johnson <sup>e</sup>

<sup>a</sup> Department of Agricultural and Biosystems Engineering, Iowa State University, Ames, IA 50011, USA

<sup>b</sup> UT AgResearch, University of Tennessee, Knoxville, TN 37996, USA

<sup>c</sup> Department of Biological Systems Engineering, University of Nebraska-Lincoln,  
Lincoln, NE 68588, USA

<sup>d</sup> Iowa Select Farms, Iowa Falls, IA 50126, USA

<sup>e</sup> Department of Animal Science, Iowa State University, Ames, IA 50011, USA

\* Corresponding authors. Email: [hxin2@utk.edu](mailto:hxin2@utk.edu); [tami.brownbrandl@unl.edu](mailto:tami.brownbrandl@unl.edu)

## Abstract

Space provided to sows in commercial housing is an economic issue as well as a welfare concern. Although the size of an average US commercial sow has changed over the last four decades, the recommended gestation stall size has not been reevaluated. In this study, a relationship between three-dimensional sow space usage and body weight was derived from monitoring of 20 individual late gestation (11–15 weeks) Landrace × Yorkshire sows (parities 0–4) with time-of-flight depth sensors. The length, width, and height of the space usage was calculated from static postures (standing and fully recumbent lying) as well as dynamic behaviors (standing up and lying down). This relationship was then used to estimate the dimensions of corresponding gestation stalls. Three common US gestation building sizes were used to demonstrate the conversion requirements by estimating the building sizes needed to house the same number of sows compared with conventional gestation stall size. Results of this study can aid industry in evaluating current gestating sow space allocations, as well as guide future facility designs.

**Keywords:** Housing, sow, Kinect V2®, welfare

## 1. Introduction

The amount of physical space allocated to individual animals is important for gestating sow housing design. Improper designs can lead to unnecessary increases in building and production costs, as well as management challenges and increased labor needs. Inadequate space also has the potential to negatively impact animal productivity and welfare (Curtis et al., 1988; Barnett et al., 2011). Thus, it is critical to understand both the static and dynamic space usage of gestating sows.

In the United States, the most commonly used guideline for commercial gestating sow space requirements is the Swine Housing and Equipment Handbook (MWPS-8). This document provides recommendations of length, width, and height dimensions for individually housed gestating sows in stalls. These recommendations were developed in the 1980s; however, 30 years later, advancements in sow genetics and changes in sow physiology emphasize the importance of revisiting these values.

An increasingly common method of evaluating animal physical space usage is with computer vision systems (Cebellos et al., 2004; Kashiha et al., 2014). Computer vision offers a non-contact, low animal stress method to measure sow space usage. Time-of-flight depth sensors, such as the Microsoft Kinect V2® (Microsoft, Redmond, WA, USA), have been shown to accurately measure height, enabling the collection of three-dimensional information (Wasenmuller and Stricker, 2016). Using depth sensors provides an additional benefit of creating a more reliable conversion from pixels to physical dimensions, as this value varies with distance from the camera. Thus, a time-of-flight depth sensor was selected for data collection in this study.

The objectives of this research were to: (1) empirically determine the static and dynamic space

usage of modern commercial gestating sows, (2) develop recommendations of new gestation stall dimensions based on sow weight, and (3) evaluate how these recommendations would affect current building configurations for rooms containing 2, 3, or 4 rows of sow stalls (MWPS-8).

## 2. Materials and Methods

### 2.1. Sensor calibration

A calibration curve was developed to convert pixel measurements to physical dimensions based on object distance from a Kinect V2® sensor. In a laboratory setting, rigid foam (19 mm thick) rectangles were used to simulate sow size for calibration. Nine sizes were created using three widths (0.5, 0.6, 0.7 m) and three lengths (1.5, 1.7, 1.9 m), placed in four different locations (center, long edge, corner, short edge) of the depth image viewable area. All posters were tested at three distances from the Kinect V2® (2.18, 1.73, 1.27 m) to simulate anticipated distance from sows. This yielded 216 possible combinations of factors; however, in some cases, the entire rectangle was not within the depth image's viewable area, resulting in 150 usable combinations. Six images were selected of each combination to develop the relationship between distance from Kinect V2® and pixel to physical dimension conversion factor.

### 2.2. Data collection and analysis

A total of four gilts and 16 sows, hereafter collectively described as sows, observed in this study ranged from parity 0 to 4 (parity 0: four gilts, parity 1: four sows, parity 2: two sows, parity 3: five sows, parity 4: five sows). All sows were commercial Landrace × Yorkshire (BW 169–251 kg, mean 212 kg; age 12–42 mo, mean 24 mo) in late gestation (wks 11–15) and were housed in groups of 12–15 in pens. Sows were individually moved to and remained in a fully slatted observation pen for 24 h. The observation pen had dimensions of 1.8 × 2.5 m, providing sufficient space for the sows to turn around without touching the pen sides if desired. A nipple drinker was provided, and sows were fed once per day prior to and immediately after observation.

One Kinect V2® and one mini-PC (ZBOX-CI325NANO, ZOTAC, Duarte, CA, USA; RAM: 8 GB, CPU: 1.8 GHz, SSD: 120 GB) were mounted 2.18 m above the floor of the observation pen, providing a top-down view of the entire pen. The mini-PC operated a program written in C# to collect one depth (512 × 424 pixels) and digital (1920 × 1080 pixels) image every 2 s (0.5 FPS). Images were stored on portable hard drives for future processing. A mobile hotspot was connected to the mini-PC to enable remote monitoring of data collection.

After collection, three frames of each static posture (standing and lying) and three sequences of each dynamic transition (standing up and lying down) were selected from each sow for analysis. Depth images were analyzed using an algorithm developed in MATLAB (R2017a, The MathWorks, Inc, Natick, MA, USA). In each image, the sow was isolated in the frame and the average distance from sow to Kinect V2® was calculated. This value was then used to convert measurements from pixels to physical dimensions. For the dynamic sequences of standing up and lying down, images were superimposed to obtain total space usage for the entire sequence. In the static posture of fully recumbent lying, it was assumed (as it commonly occurs) the sow's legs would protrude into the neighboring stall; thus, extended legs were removed from the image.

### 2.3. Development of stall designs

Summarized static and dynamic space usage results were combined to create three different stall size recommendations. For design recommendation A, the measured dimensions for all sows were evaluated and overall average values were used. Design recommendations B and C were created by dividing all sows into two groups based on weight, with B containing sows lighter than the mean weight and C containing sows heavier than the mean weight. This division was based on linear models which indicated that when exploring the effects of weight, age, and parity on sow space usage, weight was the only significant factor in this data set. Separating these two groups based on weight resulted in a smaller sow stall (B) and a larger sow stall (C). Dividing the sows based on other factors could result in different dimension recommendations; however,

literature indicates that all three factors (weight, parity, and age) are lightly related (Moustsen et al., 2011).

#### 2.4. Evaluation of building layouts

Three typical building layouts were used for stall size comparison. These standard layouts can be found in the Swine Housing and Equipment Handbook (MWPS-8; Figure 1). All layouts featured 0.91 m alleyways along the walls and between rows of stalls. For the comparison between stall sizes, the number of stalls were kept consistent while the stall size varied. Thus, differences in stall dimensions would be shown to affect overall building size.

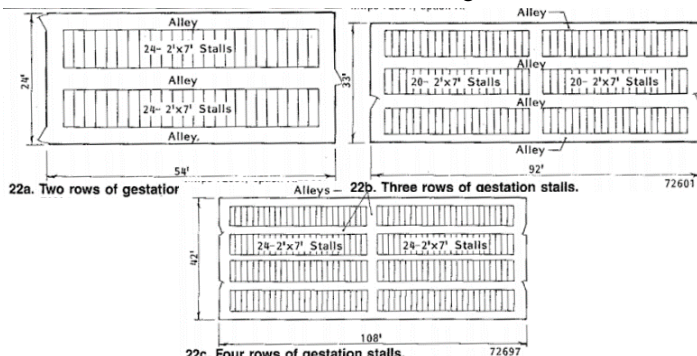


Figure 1. Three common gestation building designs used for stall size comparisons (MWPS-8).

### 3. Results and Discussion

#### 3.1. Model results

Average space usage (length, width, and height dimensions) for static lying and standing, as well as dynamic lying down and standing up, can be observed in Table 1. Stall designs must allow enough space for all four of the assessed postural behaviors, so maximum values of each dimension were adopted as the design dimensions. For all three design recommendations (A, B, C) the maximum values for all dimensions occurred in the dynamic sequence of standing up. Thus, these values were applied as the dimensions for the new stall designs.

Table 1. Average space usage for static and dynamic measurements for (A) all sows, (B) sows weighing less than the group average, and (C) sows weighing more than the group average. Values are in cm and maximum dimensions for each group are bolded. Values are presented along with 95% confidence interval.

Design		Length (cm)	CI	Width (cm)	CI	Height (cm)	CI
(avg BW: 211 kg)	Lying	166.2	17.9	69.4	12.5	36.1	7.7
	Standing	154.3	17.9	41.0	4.2	84.9	10.5
	Lying Down	173.5	22.9	83.6	17.1	86.5	9.5
	Standing Up	182.4	26.3	102.4	40.9	88.7	11.3
(lower 95% CI BW: 166 kg)	Lying	160.0	12.7	66.0	5.5	35.1	8.5
	Standing	149.4	15.9	40.5	4.4	81.1	6.9
	Lying Down	167.9	19.0	76.8	9.7	84.6	10.1
	Standing Up	172.6	13.7	100.6	47.1	85.8	10.2
(upper 95% CI BW: 255 kg)	Lying	172.3	14.0	72.8	14.2	37.2	6.7
	Standing	159.2	14.7	41.4	4.1	88.7	7.9
	Lying Down	179.0	21.9	90.5	10.9	88.4	7.5
	Standing Up	192.2	21.3	104.3	35.7	91.5	9.9

These results were obtained by providing sows with unrestricted amounts of space. Restricting the available space may alter the way the sows transition between postures, but partial restriction may or may not affect overall sow welfare. Further investigations are needed in this area.

### 3.2. Evaluation of building layouts

Conventional gestation sow stall size was compared to design recommendations A, B, and C for the three building layouts (Table 2). Stall height was nearly identical for all four designs and building height is governed by other factors (worker comfort, feed delivery system, etc.), so height was excluded from the building comparisons. Stall width was greater than conventional for all three new stall design recommendations, and as stalls are placed side by side, this factor increased the building length in all scenarios. Building length remained similar for design recommendations A, B, and C throughout (within 1 m difference), but values were greater than the conventional design, requiring a nearly 50% longer buildings to house the same number of sows in some cases.

Table 2. Comparison of conventional stall dimensions and proposed design values to accommodate all sows (A), smaller sows (B), and larger sows (C) for three building layouts.

BL-building length, m; BW-building width, m; BA-building area, m<sup>2</sup>; D-difference from conventional, m<sup>2</sup>.

Layout		Conventional	A	B	C
Stall Size	Length, m	2.13	1.82	1.73	1.92
	Width, m	0.61	1.02	1.01	1.04
	Height, m	0.91	0.89	0.86	0.91
2 row (48 sows)	BL	16.5	26.4	26.0	26.9
	BW	7.0	6.4	6.2	6.6
	BA	115.4	168.8	160.9	176.9
	D	-	53.4	45.5	61.5
3 row (120 sows)	BL	14.9	23.2	22.9	23.6
	BW	9.1	8.2	7.9	8.5
	BA	136.6	190.9	181.1	200.8
	D	-	54.2	44.5	64.2
4 row (192 sows)	BL	17.4	27.3	26.9	27.8
	BW	11.3	10.0	9.6	10.4
	BA	196.0	274.4	259.4	289.7
	D	-	78.4	63.4	93.7

Stall length was reduced for design recommendations A, B, and C, resulting in less building width when compared to conventional stalls for all layouts. However, it is important to note that these stall dimension recommendations are based only on static and dynamic posture behavior. Additional studies are required to determine if additional stall length is necessary to appropriately accommodate other behaviors such as feeding and defecating.

Building width was reduced with design recommendations A, B, and C, but this reduction was overshadowed by the increase in building length, resulting in an overall increase in building area for all layouts. Differences in overall size are illustrated in Figure 2. When housed in individual stalls, it is undesirable to have sows turn around as there is potential for increased human labor and animal stress. It unclear if the proposed increase for stall width would permit all sows to turn around, as this ability will vary with sow size, flexibility, and motivation. Further investigation is warranted.

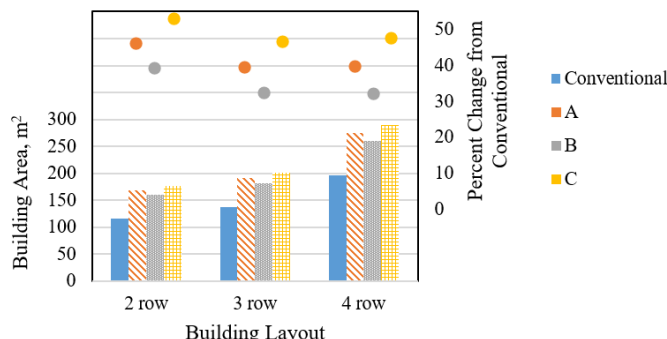


Figure 2. Building area and percent change of design values to accommodate all sows (A), smaller sows (B), and larger sows (C) compared to conventional gestation stall size.

These design values have potential implications in sow group housing as well, if it is desired that all animals should stand up and lie down without touching one another. However, there are many social factors involved with pen housing as well that should be accounted for prior to applying these design values to pen gestation.

#### 4. Conclusions

Three gestation stall design recommendations were developed to accommodate all sows (A, average BW of 211 kg), smaller sows (B, 169 kg <BW< 204 kg), or larger sows (C, 220 kg <BW< 251 kg) from sow space usage data. All three designs had greater width and less length than conventional US gestation stalls; however, the proposed designs did not evaluate space needs for other behaviors such as feeding, defecating, and turning around. The proposed designs resulted in larger building areas to house the same number of sows (compared to conventional stall sizes). Results can be used to evaluate current gestation stall housing and aid in future building designs.

#### Acknowledgements

This research was funded in part by the Iowa Pork Industry Center. The authors would like to acknowledge the contributions of the management and swine personnel at Iowa Select Farms -- Sow 11 Farm for their cooperation in system installation and animal handling.

#### References

- Barnett, J.L., P.H. Hemsworth, K.L. Butler, B.N. Schirmer, S.S Borg, G.M. Cronin, 2011. Effects of stall dimensions on the welfare of pregnant sows. *Animal Production Science*. 51 (5), 471–480. <https://doi.org/10.1071/EA07124>.
- Ceballos, A., C. Sanderson, J. Rushen, D.M. Weary, 2004. Improving stall design: use of 3-D kinematics to measure space use by dairy cows when lying down. *Journal of Dairy Science*. 87 (7), 2042–2050.
- Curtis, S.E., R.J. Hurst, H.W. Gonyou, A.H. Jensen, A.J. Muehling, 1989. The physical space requirement of the sow. *Journal of Animal Science*. 67, 1242–1248.
- Kashiha, M., C. Bahr, S. Ott, C.P.H. Moons, T.A. Niewold, F.O. Odberg, D. Berckmans, 2014. Automatic weight estimation of individual pigs using image analysis. *Computers and Electronics in Agriculture*. 107, 38–44. <http://doi.org/10.1016/j.compag.2014.06.003>.
- Moustsen, V.A., H.P. Lahrmann, R.B. D'Eath, 2011. Relationship between size and age of modern hyper-prolific crossbred sows. *Livestock Science*. 141, 272–275. <http://doi.org/10.1016/j.livsci.2011.06.008>.
- MWPS-8. 1983. *Swine housing and equipment handbook*. Midwest Plan Service Committee. <https://www-mwps.sws.iastate.edu/sites/default/files/imported/free/mwps8s.pdf>. Accessed June 10, 2019.
- Wasenmuller, O., D. Stricker, 2016. Comparison of Kinect V1 and V2 depth images in terms of accuracy and precision. *Asian Conference on Computer Vision*. [http://doi.org/10.1007/978-3-319-54427-4\\_3](http://doi.org/10.1007/978-3-319-54427-4_3).

# ROS-based Autonomous Navigation Control System for Animal Farm Inspection Robots

Tiemin Zhang <sup>a,\*</sup>, Zhong Peng <sup>a</sup>, Jinfeng Lu <sup>a</sup>

<sup>a</sup>College of Engineer, South China Agricultural University, Guangzhou, Guangdong 510642, P.R. China

\*Corresponding author. Email: [tm-zhang@163.com](mailto:tm-zhang@163.com)

## Abstract

In order to improve the detection efficiency of large-scale animal farms, this research proposes an autonomous navigation control system for inspection robots based on Robot Operating System (ROS) and laser Simultaneous Localization and Mapping (SLAM). Gmapping, Hector and Kart algorithm construction algorithms are used to simulate and construct the raster map of animal farm environment. The maps constructed are compared and analyzed from different angles, and the Kart algorithm with the best mapping effect is selected. The autonomous correction reduces the jitter error of Inertial Measurement Unit (IMU) from 10-1 to 10-4. By combining A\* algorithm with dynamic window method for path planning, the linear operation precision error of the system is within 0.7%, and the rotation precision error is within 1.1%. Experiments show that the system can basically realize function of autonomous navigation and obstacle avoidance in animal farms under the condition of using the general precision laser radar and Inertial Measurement Unit (IMU) sensor.

**Keywords:** Kart algorithm, SLAM, radar, autonomous navigation, obstacle avoidance.

## 1. Introduction

At present, most domestic animal farms still rely heavily on manual operation, with low levels of mechanization and automation, which severely limits the rapid development of animal farming. In order to transform to larger scale and modernization, the animal breeding industry must carry out comprehensive technical transformation. Therefore, it is particularly important to have an efficient automatic navigation system and the use of inspection robots for animal farms which can detect environmental conditions in many directions.

Automatic navigation technology is mostly based on the Global Positioning System (GPS) (Han et al., 2018), but it needs to be applied in a sparse outdoor environment (Liao, 2016). If applied indoors, the wall will block the GPS satellite signal, and the GPS signal directly received by the mobile robot and the GPS signal reflected by the building are superimposed multiple times, which is easy to generate multipath error (He, 2010), and cannot meet the navigation requirements. In addition, traditional inspection robots generally use wired guidance technology including electromagnetic guidance and tape guidance (Zhang, 2018).

In recent years, visual navigation technology has developed rapidly. In order to solve the current stability of the facility agricultural machinery positioning system with low positioning accuracy and high cost, a set of infinite sensor network positioning system based on NanoPAN5375 module was designed (Chen et al., 2015). In order to improve the robustness and accuracy of autonomous navigation of mechanical equipment in various environments, a series of paths such as different color marking lines, green plants and bare ground boundaries are identified and navigated (Zhang et al., 2015); Multi-sensor information such as Charge Coupled Device (CCD) image sensor, accelerometer, electronic compass and ultrasonic wave is combined (Zhang et al., 2015)]; in addition, a binocular vision recognition system for avoiding obstacles is also applied (Zhuang et al., 2015).

Nowadays, Simultaneous Localization and Mapping (SLAM) technology has become an important means to realize autonomous cruise of robot mobile platform due to its high positioning accuracy, no need to modify the application environment, high path flexibility and adaptability to complex and varied application sites. The SLAM technology can be divided into two different types of navigation and positioning technologies (Quan et al., 2016; Hess et al., 2016; Karlsson et

al., 2005), which are laser SLAM and Visual Simultaneous Localization and Mapping (VSLAM), according to the different measuring devices carried by the robot mobile platform. Laser SLAM technology has a much longer history than other SLAM technologies and the technical framework has been previously defined (Cadena et al., 2016).

With the advent of Robot Operating System (ROS) (Hellmund et al., 2016; Quigley et al., 2009), ROS is widely used as a robot development and research platform in research projects. The most representative application case is the PR2 personal robot developed by Liushu Garage Robot Development Co., Ltd. in 2008 (Cousins, 2010).

The research environment of this paper is an indoor animal farm. Through the application of laser SLAM technology, the raster map of the environment of animal farm is constructed, and the global path planning and local path planning are carried out in the constructed environment map, so that the robot can realize autonomous navigation control.

## 2. Materials and Methods

### 2.1. Hardware selection and parameters of mobile chassis

The patrol robot mobile platform designed in this experiment is shown in Figure 1. The mobile chassis has a size of  $200 \times 300 \times 120$  mm, and a two-wheel differential drive.

The control system consists of an underlying controller and an upper controller. The underlying controller uses STM32F103ZET6GY with large capacity and Cortex-M3 core framework developed by Advanced RISC Machines (ARM) company. The upper controller is a RaspberryPi 3b small single board computer produced by Eurotime Electronic Components Co., Ltd. Also included are the RPLIDAR-A2 single-line laser radar, the GY-85 nine-axis Inertial Measurement Unit (IMU) sensor and HN3808-1024-ABZ incremental encoder.



Figure 1. Inspection robot mobile chassis hardware structure

### 2.2. Test methods

The U-shaped corridor with a size of  $35.4\text{ m} \times 12.8\text{ m}$  and a total area of  $210\text{ m}^2$  is used as the test environment. By comparing the effects of raster maps constructed by different algorithms, the map construction algorithm which is most suitable for the corridor environment is selected to construct the map, and then the optimal path is found through the combination of A\* algorithm (Hart et al., 1968) and dynamic window approach (DWA) algorithm (Fox et al., 1997) to realize automatic navigation.

Four representative length dimensions are measured by a tape ruler, and two representative angle values are measured by an angle measuring instrument. Each grid occupying the background of the raster map is a square of  $1\text{ m} \times 1\text{ m}$ , and the actual size of the corresponding position in the raster map constructed by the mobile platform can be converted by referring to the grid.

During autonomous navigation, the robot mobile platform needs to constantly change the running direction to avoid obstacles in the external environment. Taking U-shaped corridor environment as the test background, six groups of repetitive experiments were measured at 360 degrees rotation test angle. Six groups of repeatability experiments were carried out with a linear driving test distance of 10 m.

### 2.2.1. Map construction of u-shaped corridor

Through the investigation and analysis of the actual environment of many poultry farms, as shown in Figure 2. The real animal farm environment has good similarity with the corridor outside the laboratory, so the corridor can truly reflect the map construction ability of mobile robots. In the experiment, Gmapping algorithm, Kart0 algorithm and Hector algorithm are used to construct occupied grid map. The linear velocity and angular velocity of the mobile platform are  $0.3 \text{ m s}^{-1}$  and  $0.4 \text{ rad s}^{-1}$  respectively. The mapping process is performed by remotely controlling the mobile platform on the PC side.



(a) Poultry farm real environment map

(b) Laboratory promenade environment

Figure 2. Electric charge

### 2.2.2. Global path planning

The experiment chooses the A\* algorithm for global path planning. The advantage is that the A\* algorithm uses the shortest path and the heuristic method to jointly guide its search when searching for the path, so that the optimal path can be obtained without traversing all the nodes in the graph. The specific formula is as follows:

$$f(n) = g(n) + h(n) \quad (1)$$

where,  $f(n)$  represents the cost estimate from the starting node via node  $n$  to the target node,  $g(n)$  represents the actual cost from the starting node to node  $n$ , and  $h(n)$  represents the estimated cost of the optimal path from node  $n$  to the target node, also known as the heuristic function.

In the process of each algorithm iteration, the A\* algorithm solves the node that minimizes  $f(n)$  according to the above formula (1), and continues to search outwards from the node until the target node is found, the specific implementation steps of the A\*algorithm are as follows:

First, create two new lists and name them CloseList and OpenList, respectively. Wherein CloseList is used to save the nodes traversed by the algorithm. OpenList is used to store nodes that may be considered by the current node. Starting from the starting point S, the starting point is treated as a node to be processed and added to the OpenList.

Then, the following procedures are repeated:

(1) Traverse each node contained in the OpenList one by one, find the node that can minimize the value of  $f(n)$ , set the minimum node found as the starting node, and move it to CloseList.(2) The eight adjacent nodes of the current node are checked one by one. If the adjacent node cannot reach or already exists in the CloseList list, the node is ignored. Conversely, do the following for the node:

a) If the adjacent node of the current node is not added to the OpenList list, the node is added to the OpenList list and the current node is taken as its parent node and the  $g(n)$  and  $f(n)$  value from the current node to the node are calculated;

b) If the adjacent nodes are already in the OpenList, the  $g(n)$  value are compared. Calculate

the  $g(n)$  value from the current node to the node, and compare the  $g(n)$  value at this time with the original  $g(n)$  value of the node. If the current  $g(n)$  value is smaller, the parent node of the node is set as the current node and the  $g(n)$  and  $f(n)$  values are recalculated.

(3) Stop the search when the following conditions are encountered:

- a) When the target node is added to the OpenList list, it indicates that the path has been found and the algorithm stops;
- b) Finding the end point fails, and the OpenList list is empty, which indicates that the path plan fails and the algorithm stops.

(4) When the path is found, starting from the end point, each node is connected along its parent node to the starting point, and the resulting connection is the optimal path from the starting node to the target node

### 2.2.3. Local path planning

The DWA is used for local path planning. The specific implementation method is to sample the angular velocity( $\omega$ ) and the linear velocity in the velocity space ( $\omega$ ) of the robot moving platform, in which the sampling velocities  $v, w$  are limited to following range.

Firstly, the moving speed  $v, w$  of the moving platform should be within a limited range, that is to say, there are maximum and minimum values.

$$V_m = \{v \in [v_{\min}, v_{\max}], \omega \in [\omega_{\min}, \omega_{\max}]\} \quad (2)$$

Secondly, due to the limitation of the motor torque, its acceleration and deceleration have a range in which the velocity can be calculated by the following formula:

$$V_d = \left\{ (v, \omega) \mid \begin{array}{l} v \in [v_c - v_b \Delta t, v_c + v_a \Delta t] \\ \omega \in [\omega_c - \omega_b \Delta t, \omega_c + \omega_a \Delta t] \end{array} \right\} \quad (3)$$

where  $v_c$  and  $\omega_c$  respectively represent the linear velocity and angular velocity of the robot mobile platform at the current time,  $\Delta t$  represents a running cycle, and other symbols represent the maximum acceleration and deceleration of the mobile robot.

In addition, the mobile platform needs to ensure that the movement can be stopped in time before hitting the obstacle during autonomous navigation. Therefore, under the condition of maximum deceleration, the running speed should have a certain range. As shown in formula (4).

$$V_a = \left\{ (v, \omega) \mid v \leq \sqrt{2 * dist(v, \omega) * v_b}, \omega \leq \sqrt{2 * dist(v, \omega) * \omega_b} \right\} \quad (4)$$

where  $dist(v, \omega)$  is the shortest distance between the running trajectory generated by the mobile platform when moving at speed  $(v, \omega)$  and the obstacle existing in the environment map.

Therefore, the speed should be the intersection of  $V_m$ ,  $V_d$  and  $V_a$ . That is to say, the effective speed set  $V_y$  can be expressed by the following formula.

$$V_y = V_m \cap V_d \cap V_a \quad (5)$$

Randomly sampling a set of velocities  $(v, \omega)$  in the acceptable velocity space  $V_y$ ; Deducing the corresponding motion trajectory of the velocity group obtained in the previous step after one cycle of operation, Then calculating the position of the obstacle closest to the motion trajectory and the distance  $dist$  between the two; Calculate the required safe braking distance  $breakdist$  when the mobile robot is operating at the sampling speed  $(v, \omega)$ . If  $dist > breakdist$ , the set speed meets the requirements. The evaluation function is used to score the corresponding trajectories in the acquired multiple sets of velocities, and the highest trajectory of the trajectories is selected, wherein the evaluation function is as shown in formula (6).

$$G(v, \omega) = \sigma(\alpha * heading(v, \omega) + \beta * dist(v, \omega) + \gamma * velocity(v, \omega)) \quad (6)$$

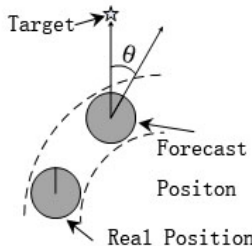


Figure 3. Schematic diagram of the angle between the end of the robot and the target point.

Wherein velocity( $v, \omega$ ) represents the forward speed of the robot;  $\alpha, \beta$ , and  $\gamma$  represent the weights of the three evaluation functions in the objective function; dist( $v, \omega$ ) represents the closest distance from the obstacle on the corresponding trajectory. Heading( $v, \omega$ ) is an azimuth evaluation function for evaluating the angle value of the target point relative to the heading of the robot when the mobile robot moves to the end of the trajectory at the selected speed ( $v, \omega$ ), and the evaluation score is negatively correlated with  $\theta$ . As shown in Figure 3.

### 3. Results and Discussion

#### 3.1. Results of raster map construction

Figure 4 shows the occupied raster map constructed by the mobile platform in the U-shaped corridor using Gmapping, Karto and Hector algorithms respectively.

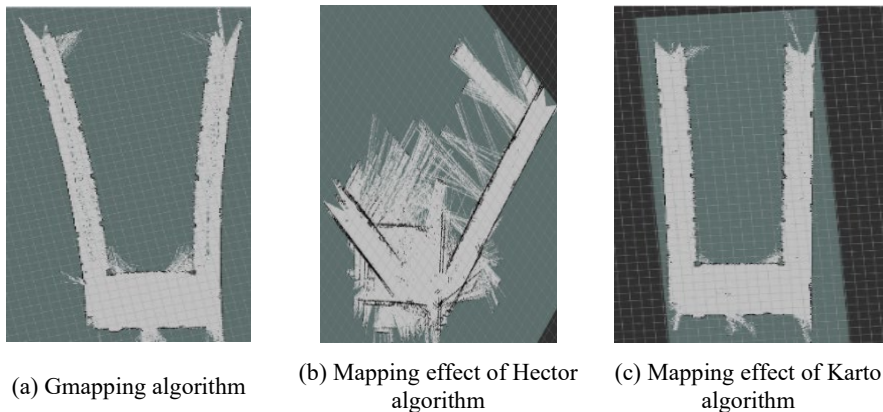


Figure 4. Mapping effects of different algorithms.

In order to better compare the differences between different algorithms, a comparative analysis is made from the five aspects of Memory Size, Offset Angle, Sensor Requirements, Completeness and Construction Area, and are summarized in Table 1. By comparing the Figure 4 and results shown in Table 1, it can be concluded that the memory required to construct the map by Karto algorithm is small compared with the Gmapping algorithm, the resulting angular deviation is the smallest, the construction area is closest to the real area and the requirements on the sensor are not high, and the integrity of the construction map is high. Although the memory required by the Hector algorithm is the smallest, the offset angle is relatively high, while it requires high accuracy of sensor, and the built map has great defects

Table 1. Comparative analysis of algorithms.

Algorithm category	Memory Size	Offset Angle	Sensor Requirements	Completeness	Construction Area
Gmapping	3.75 M	15°	No higher requirements	Partial defect	183 m <sup>2</sup>
Hector	1.00 M	37°	High precision and fast update frequency	Major defect	-
Karto	1.12 M	3°	No higher requirements	More complete	197 m <sup>2</sup>

### 3.2. Accuracy analysis of raster map

Figure 5 is a plane sketch of a U-shaped corridor. Comparing the actual measured size with the corresponding size in the raster map, Table 2 and Table 3 can be obtained. It can be seen from Table 2 and Table 3 that the maximum size error of the occupied grid map constructed by the mobile platform is 2.65%, and the angular error is 3.30%.

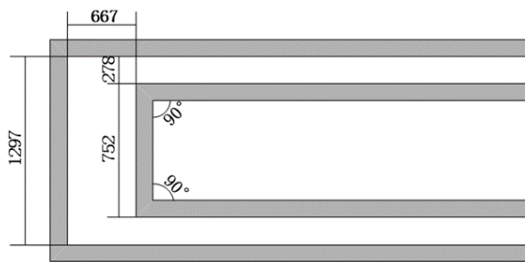


Figure 5. Plane sketch of U-shaped corridor.

Table 2. Size comparison.

No.	Actual size (cm)	Map size (cm)	Error (cm)	Percentage of error
1	667	680	13	1.90%
2	1297	1320	23	1.77%
3	278	285	7	2.51%
4	752	772	20	2.65%

Table 3. Angular comparison.

Numbering	Actual angle	Map corresponding angle	Error	Percentage of error
1	90°	93°	3°	3.3%
2	90°	93°	3°	3.3%

### 3.3. Autonomous navigation results

After the construction of the raster map occupied by U-shaped corridor, the mobile platform needs autonomous navigation test. The specific experiment steps are as follows: First, run the visual plug-in the Robit Visualization tool (Rviz) that comes with the ROS system, and load the occupied grid map of the U-shaped corridor. Then, combined with global path planning algorithm and local path planning algorithm, the optimal path from initial pose A to target pose B is planned by Rviz, which gives the initial pose A and target pose B of the mobile platform in the raster map. Finally, the mobile robot is driven to accurately move to the target pose B by using the speed corresponding to the partial path. As shown in Figure 6, the red curve in the Figure is the global planning route of the mobile platform, and the red arrowed line segment represents the route that the mobile platform has traveled. The experimental results show that the robot mobile platform can autonomously move from the starting pose A to the target pose B in the U-shaped corridor.

environment.

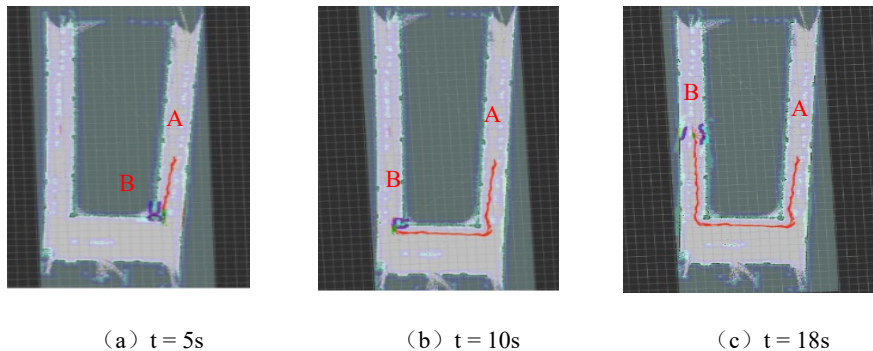


Figure 6. Autonomous navigation in the corridor environment

### 3.4. Operational accuracy analysis of mobile platform

Due to the difference in the installation accuracy of the encoders used on both sides of the mobile chassis, the difference between the mechanical structure and the motor type on the left and right sides of the chassis causes the motor speed to be different even under the same input conditions, which leads to the generation of motion errors. It can be seen from Table 4 and Table 5 that during the test, the linear running accuracy error of the system is within 0.7%, and the rotation accuracy error is within 1.1%.

Table 4. Actual rotation angle.

Numbering	Target Rotation Angle	Actual Rotation Angle	Difference
1	360°	357°	3°
2	360°	358°	2°
3	360°	358°	2°
4	360°	362°	2°
5	360°	363°	3°
6	360°	356°	4°

Table 5. Actual distance in straight line.

No.	Target Moving Distance (m)	Actual Moving Distance (m)	Error (m)
1	10	9.95	0.05
2	10	9.94	0.06
3	10	10.05	0.05
4	10	9.96	0.04
5	10	10.06	0.04
6	10	10.07	0.07

### 4. Conclusions

By using Gmapping algorithm, Hector algorithm and Kart algorithm to construct the U-shaped corridor, and compare and analyze the memory size, angle error and map integrity from the grid map, we can conclude that: The Kart algorithm has high mapping accuracy for corridor environments in larger scenes and is the best way to construct maps among the three algorithms examined. After obtaining a more accurate raster images, by combining A\* algorithm with DWA algorithm, the mobile platform can be controlled to navigate the target position and attitude accurately, which basically meets the requirements of indoor automatic navigation.

### Acknowledgements

This work is supported by National Key Research and Development Plan [grant No. 2018YFD0500705] and Guangdong Province Special Fund for Modern Agricultural Industry Common Key Technology R&D Innovation Team [grant No. 2019KJ129], China.

### References

- Cadena C, L. Carlone, H. Carrillo, 2016. At the same time, the past, present and future of positioning and mapping: towards the era of sound perception. *IEEE Transactions on robotics*.32 (6), 1309–1332.
- Chen Yu, T. Zhang, D. Sun, 2015. Design and experiment of locating system for facilities agricultural vehicle based on wireless sensor network. *Transactions of the Chinese Society of Agricultural Engineering*. 31(10), 190 – 197.
- Cousins S, 2010. ROS on the PR2 ROS Topics. *IEEE Robotics & Automation Magazine*. 17(3), 23–25.
- Fox D, W. Burgard, S. Thrun, 1997. Dynamic window method for collision avoidance. *IEEE Journal of Robotics and Automation*. 4(1),23–33.
- Han S., H. Yong, F. Hui. 2018. A review of the development of agricultural automatic navigation and unmanned vehicles. *Journal of Zhejiang University (Agriculture & Life Sciences)*. 44(04), 5–15+ 139.
- Hess W, D. Kohler, H. Rapp, 2016. Real-time cyclic closures in 2D LIDAR SLAM.2016 IEEE International Conference on Robotics and Automation (ICRA).1271–1278.
- Hellmund A M, S. Wirges, O.S. Taş , 2016. Robot operating system: A modular software framework for automated driving. 2016 IEEE 19th International Conference on Intelligent Transportation Systems (ITSC). 1564–1570.
- He L., 2010. Research on Multipath Error in High Precision GPS Measurement. *Surveying and Mapping Engineering*. 19(1), 35–38.
- Hart P E, N.J. Nilsson, B. Raphael, 1968. Heuristics to determine the formal basis of the minimum cost path. *IEEE Transactions on Systems Science and Cybernetics*. 4(2),100–107.
- Karlsson N, E. Di Bernardo, J. Ostrowski, 2005. vSLAM algorithm for robust positioning and mapping. *International Conference on Robotics and Automation (ICRA)*, 24–29.
- Liao Z., 2016. Research on laser radar/microinertia indoor autonomous mapping and navigation technology. Nanjing: Nanjing University of Aeronautics and Astronautics.
- Quan M, S. Pu, G. Li, 2016. Review of Visual SLAM. *Journal of Intelligent Systems*. 11(6),768–776.
- Quigley M, K. Conley, B. Gerkey, 2009. ROS: an open-source Robot Operating System. //ICRA workshop on open source software. 3(3.2): 5.
- Zhang Y., 2018. Innovation Path of AGV Navigation Technology. *Logistics Technology and Application*. 221(07), 16–19.
- Zhang T., X. Zhuang, 2015. High-clearance vehicle farmland path identification system based on DM642. *Transactions of the Chinese Society of Agricultural Engineering*. 31(4), 160–167.
- Zhang T., H. Li, D. Chen, 2015. Agricultural Vehicle Path Tracking Navigation System Based on Information Fusion of Multi-source Sensor. *Journal of Agricultural Machinery*. 46 (3), 37–42.
- Zhuang X., T. Zhang, 2015. Design and experiment of obstacle avoidance of binocular vision recognition system.31 (Supp.2), 24 – 30

# Is Continuous Heart Rate Monitoring of Livestock a Dream or Is It Realistic?

Luwei Nie <sup>a,b</sup>, Daniel Berckmans <sup>c</sup>, Chaoyuan Wang <sup>a,b,\*</sup>, Baoming Li <sup>a,b</sup>

<sup>a</sup> Department of Agricultural Structure and Bioenvironmental Engineering, College of Water Resources and Civil Engineering, China Agricultural University, Beijing 100083, P.R. China

<sup>b</sup> Key Laboratory of Agricultural Engineering in Structure and Environment, Ministry of Agriculture and Rural Affairs, Beijing 100083, P.R. China

<sup>c</sup> M3-BIORES, Catholic University of Leuven, Kasteelpark Arenberg 30, 3001 Leuven, Belgium

\* Corresponding author. Email: [gotowchy@cau.edu.cn](mailto:gotowchy@cau.edu.cn)

## Abstract

For all homoeothermic living organisms, heart rate (HR) is a core variable to control the metabolic energy production in the body. This metabolic energy production is crucial to realize essential body functions, including basal metabolism, thermal, physical and mental components, and also for the production term (meat, milk, eggs). In the last decades, HR monitoring for human beings has become feasible though there are still shortcomings for continuously accurate monitoring. In this paper we wonder whether it is realistic to get a continuous HR sensor for livestock. Therefore, we did a literature review of the reported techniques to monitor HR on living organisms and checked the potential to transfer the mostly adequate measures used for human beings to livestock. By considering the usability of the technology and the requirements for such a sensor, we estimate the potential based on the selected relevant references from over 200 publications on HR monitoring. Based upon its principles and applications, we grouped the techniques that are in our mind feasible for livestock. We estimated where such sensor could be positioned to start with to evolve to better solutions. We conclude that it is realistic today to develop a continuous HR sensor, being able to be integrated in an ear tag for middle size and bigger animals, for example cow, pig, sheep, goat, etc. It is obvious that one day, through further nanotechnology, the monitoring of such a crucial variable will become applicable for all living creatures.

**Keywords:** Photoplethysmography (PPG), photoplethysmographic imaging (PPGI), thermal imaging, ballistocardiography (BCG), electrocardiography (ECG), farm animals

## 1. Introduction

The world needs livestock products to feed all people, and yearly over 64 billion animals are slaughtered. FAO estimates the worldwide meat consumption may increase by 73% by 2050 (FAO, 2011), thus the food production, animal industry in particular, must become more sustainable. Currently, Precision Livestock Farming (PLF) is regarded as the heart of the engineering endeavor towards sustainability in food production by using image and sound analysis, sensors, information technology and decision-making to monitor, model and manage animal production/reproduction, health, welfare and environmental impact. All humans and homoeothermic animals generate metabolic energy to live and to produce, and the HR is a crucial variable to control the metabolic energy production in the body. With over 95% of their life, these living organisms generate the energy in the aerobic mode, by breathing air to lungs and by heart beating to cells to produce energy. For homoeothermic living organisms, HR is the crucial variable in controlling the components in the metabolic energy balance, including the basal metabolism and the immune system to stay alive, the thermal component to control its body temperature, the efficiency of the production for meat, milk, eggs, as well as the mental component. The mental component is generally connected to animal welfare, stress, the waste to manure, emissions, etc.

Current technologies for animal HR detection are mainly with the intentions of analyzing diseases, psychological and environmental stress or individual characteristics, such as the temperament and its coping strategies, which are inconvenient and inappropriate for long-term

continuous monitoring. In recent years, HR monitoring for humans has become feasible though there are still drawbacks on continuous and accurate measurement. In this paper, we present a comparative review of all techniques to measure HR on living organisms, with focus on their advantages and disadvantages, and discuss the potential to transfer some of these techniques being successfully applied in human beings to livestock. The objective of this paper is to check which techniques in our mind are applicable for the continuous HR monitoring on livestock based upon the evidences presented in literature. Additionally, we estimate the challenges and provide a solution to get such sensors.

## 2. Physiological effects

All sensing methods presented in this review is to detect the HR for living organisms, which is defined as the rate of occurrence of cardiac beats in a specific period of time, usually expressed in beats per minute (bpm). According to the principles of different sensors, acquisition of HR signals relies on specific physiological effects. Figure 1 provides an overview of different categories of physiological effects, and how they are linked to the heart, as well as the measuring techniques. Typically, such effects comprise of bioelectrical effects, mechanical effects and thermal effects (Brusser et al., 2015).

**Bioelectrical effects:** Electrical excitation of the heart causes dynamic electromagnetic fields on the body surface that can be measured by electrocardiography (ECG), such as wet/dry/non-contact electrodes.

**Mechanical effects:** Blood travelling through the vascular system causes organ motion and deformation, as well as blood volume variation. These phenomena are mechanical operations and can be subcategorized into two groups as follows.

1) **Body surface displacement:** As every heartbeat, the pulse wave travelling through the body produces subtle changes in displacements and vibrations of the body surface. Several sensor techniques rely on these effects, such as ballistocardiography / seismocardiography (BCG/SCG), Doppler radar, laser-based, as well as video-based motion.

2) **Superficial perfusion:** The ejection of blood from heart into vascular tree causes blood volume changing in the microvascular bed of the tissue. Since blood absorbs light more than surrounding tissues (Seidman et al., 2003), these microscopic changes in the optical properties of the body surface can be measured by photoplethysmography (PPG) and photoplethysmographic imaging (PPGI) methods.

**Thermal effects:** The flow of blood through the vicinity of major superficial vessels leads to changes in skin temperature that can be detected using thermal imaging technique.

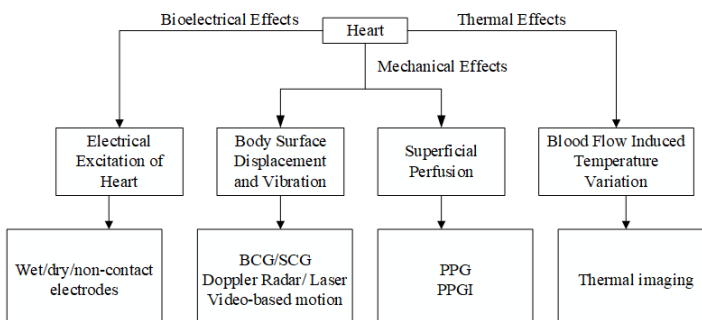


Figure 1. Overview of physiological effects and respective techniques for HR measurement.

## 3. Available Techniques to Monitor HR

This section introduces the various state-of-the-art techniques for HR monitoring as well as their principles of measurement. Here we shortly describe each technique individually, and then

discuss its advantages and disadvantages. In Section 4, comparisons of various techniques, which have the potential to be used for continuous HR monitoring on livestock, are further analyzed.

### 3.1. Optical assessment techniques

#### 3.1.1. Photoplethysmography (PPG)

Photoplethysmography is an optical measurement technique that can be used to detect blood volume changes in the microvascular bed of tissue, which is based on the principle of blood absorbing more light than surrounding tissues (Seidman et al., 2003). The measurement is done by illuminating human tissue (skin) with a light source, which is usually a red, near infrared (NIR) or green light, and a photodetector to opto-electronically detect variations in the intensity of transmitted or reflected light. The changes in light intensity are associated with small variations in blood perfusion of the tissue and provide information on the cardiovascular system, in particular, the HR. In general, PPG can be operated in a transmission or a reflection mode (Allen, 2007). In transmission mode, the light transmitted through the medium is detected by a photodetector opposite to the light source, in which a relatively good signal can be obtained. But it is restricted to certain areas (ear lobe and fingertip) of the body, where the signal can be quickly detected. A typical application of the technique is the conventional pulse oximetry sensor, while for such a system the fingertip sensor may be interfered by daily activities. In reflection mode, the photodetector detects the light that is back-scattered or reflected from tissue, which eliminates the problems associated with sensor placement, and it can be used on a variety of measurement sites. Such devices are commonly incorporated with ear-worn devices, including ear clip (Shin et al., 2009), earpiece, and earphone (Celka et al., 2004), wrist-type device (Fukushima et al., 2012), finger probe (Yousefi et al., 2014) and flexible film or patch (Xu et al., 2017).

In recent years, wearable fitness trackers and body sensor devices based on PPG have been becoming increasingly popular. There are more than ten companies commercially producing these sensors. An excellent review is provided to evaluate the accuracy, precision, and overall performance of seventeen wearable devices currently available (El-Amrawy and Nounou, 2015). In addition, wrist-wearable devices like Xiaomi and Fitbit have recently received considerable interest (Kamišalić et al., 2018). These wearable PPG methods provide good performance of accurate HR measurement for human even in the extensive exercise circumstances.

#### 3.1.2 Photoplethysmographic imaging (PPGI)

Photoplethysmographic imaging is the translation of PPG into a spatially resolved, non-contact method (Wu et al., 2000). It is based on the conventional PPG theory, i.e., the skin changes its optical properties with perfusion. Compared to PPG, the PPGI replaces the photodiode, which should be in contact with the subject's skin or clothing in a single location, with commercial cameras that can be found everywhere nowadays, such as digital camera (Sun and Zhang, 2015), webcams (Poh et al., 2010a), and cellphone cameras with dedicated light sources (e.g. green, red and/or IR wavelengths) or normal ambient light as the light source. Such a camera system is able to monitor a larger field of view of the subjects' exposed skin (usually facial area) from a distance, to record small change in light intensity values from skin and to capture physiological information (e.g. HR) over time.

Compared to conventional PPG technique, as a contactless technique, PPGI avoids the requirement of the device to be in contact with the skin and the deformation of the arterial wall. Beyond that PPGI also has several strengths: (1) cameras (particularly webcams) are ubiquitous and often inexpensive; (2) it offers detailed spatial information simultaneously from multiple sites of arbitrary size and location (Sun et al., 2012); and (3) measurements from multiple people can be performed (McDuff et al., 2015). The existing review studies (Poh et al., 2012) provide theoretical background and overview of the field. However, the acquired signal of PPGI is highly susceptible to motion-induced signal corruption, and the motion artifacts removal or attenuation is one of the most challenges in signal extracting and processing. Besides, the illumination

variations, i.e. low light levels and dynamic variations, and skin pigmentation could contaminate the pulse signal. The drawbacks limit the physiological monitoring capability of the technique in practice. A variety of signal processing methods has been proposed to remove noise and detect HR from the PPGI signals (Sun et al., 2011). Robust image and signal processing methods have the potential to address the motion artifacts and make it possible to have a good performance for HR monitoring even in extensive exercise conditions.

### 3.2. Thermal imaging

The human skin surface with a temperature of about 300K emits electromagnetic radiation in the far infrared part of the spectrum, which is not visible to the naked human eyes. The human skin temperature in the vicinity of major superficial vessels is directly modulated by the pulse blood flow. The pulse signal contained HR can be recovered from the subtle changes in skin temperature recorded with a highly sensitive thermal camera at a distance and processed through an appropriate signal analysis method. The approach is tested on motionless subjects up to 3–10 feet away from a Mid-Wave Infrared camera to measure HR from wrist, neck, and forehead area (Marc et al., 2007). The results achieve 98% agreement and mean bias is  $4.74 \pm 9.28$  bpm of HR compared to the reference signal, which is obtained with a piezoelectrical transducer.

### 3.3. Electrocardiography (ECG)

Conventional ECG method is an optimal clinical diagnostic tool to provide useful information about the cardiovascular system, characterized by its high accuracy and easy interpretation for HR measuring. The method employs Ag/AgCl electrodes with wet conductive gels fixed to specific locations of the chest, arms, or hands and legs in order to detect and record the difference of the electric potential between the points. This electrical excitation generated by the electric activity of cardiac muscular fibers causes a voltage signal that can be used to detect the HR accurately. Although the conventional ECG provides good signal quality, it is inconvenient and inappropriate for long-term monitoring, since the wet electrodes need to be directly contacted with skin. It presents movement limitations, and prolonged application of wet electrodes may cause skin irritation and signal degradation due to dehydration (Nemati et al., 2012). In order to overcome the drawbacks, dry electrodes and capacitively-coupled ECG (CECG) as two alternatives potentially provide comfortable measurement without an explicit electrolyte. However, the dry electrode technique still has to be directly contacted with skin.

Capacitively-coupled ECG is a non-contact method, which is able to detect biopotentials with an explicit gap (e.g. a thin layer of insulator) between electrodes and skin, even through hair and clothing. Compared to the wet and dry electrodes, the surface of CECG electrodes is electrically insulated and thus remains stable even in a long-term usage. Several authors have demonstrated the performance of the dry / non-contact electrodes which are comparable to clinical wet electrodes. However, a tight vest and chest band are often needed to secure the non-contact electrodes in place in the form of textile electrodes (Zheng et al., 2017). Although the CECG measurement can detect ECG signal accurately, it has shortcomings. As the high impedance, the signal quality is not comparable to conventional wet electrodes. Moreover, it is susceptibly affected by motion artifacts. Any changes in the displacement of the electrode-to-skin distance can change the coupling capacitance, hence affecting the ECG signal acquired, and friction between the electrodes and insulation also may cause artifacts.

### 3.4. Ballistocardiography (BCG) and seismocardiography (SCG)

For every heartbeat, the blood travelling along the vascular tree produces subtle changes in displacements and vibrations of the body surface. The BCG and the SCG techniques both record different aspects of the mechanical activity of the body. BCG measures whole-body recoil forces in response to blood ejection into the vascular tree, while SCG detects the positional vibrations of the chest wall in reaction to the myocardial motions (Inan et al., 2017). In principle, the recordings of the BCG and SCG contain useful physiological information, such as HR.

Although BCG and SCG measure different aspects of cardiac activity, many sensor techniques actually record a superposition of both signal sources (Tavakolian et al., 2009). Thus, both are jointly considered for signal analysis and processing. The mechanical methods, the BCG and the SCG measurement for HR monitoring, require physical coupling to the body surface and use force sensors, pressure sensors, film sensors (Brüser et al., 2012) and acceleration sensors. For not being required to be directly attached on the body surface, the sensors can be integrated into furniture, such as beds, chairs and weighting scales. Thus, the mechanical assessment of human HR allows an unobtrusive and non-contact measurement.

### 3.5. Video-based motion

The principle of extracting HR from facial video is by measuring subtle head motion caused by blood flow from the heart to the head, which is based on BCG theory. The blood circulation from the heart to the head via the abdominal aorta and the carotid arteries causes the head to move in a periodic motion. Balakrishnan et al. (2013) extracted the HR from the facial video by tracking velocities of feature points on the face region. The average HRs are closely identical to the true ones for all subjects. The mean error of average HRs is 1.5% compared to wearable ECG monitor.

### 3.6. Doppler radar and laser

During each cardiac cycle, the heart muscle pumps blood through the circulatory system, which results in displacements and vibrations of the body surface, e.g. chest wall. The phenomena can be measured by using Doppler radar and laser techniques, which is based on the Doppler effect with certain displacement resolution from a distance.

Radar-based approaches make use of electromagnetic radiation to measure body surface motion related with heart mechanical activity in a noncontact manner, so it is possible to remotely sense HR. In the past decades, there are three types of radar systems having been proposed for HR monitoring, namely constant-frequency continuous wave (CW), frequency-modulated continuous wave (FMCW), and ultrawideband (UWB) (Brüser et al., 2015). According to the Doppler theory, a target with a time-varying position reflects the transmitted signal with its phase modulated proportionally to the target displacement (Obeid et al., 2010). Continuous wave is the most commonly used method to detect HR among aforementioned three types, and it is based on the frequency shift. When CW measures velocity of target, the phase detecting radar adopts the method of analyzing phase differences between transmitted and received signals to measure the distance to a target. Due to its fine resolution, it has been employing practically in HR monitoring. Another remotely non-contact technique, which measures displacement of body surface such as chest from a distance, utilizes laser Doppler vibrocardiography. With high displacement resolution, the laser has the ability to detect subtle deflections on body area caused by the heart activity by measuring the frequency or phase differences between a reference beam and a test beam (Scalise and Morbiducci, 2008).

## 4. Transferable HR Monitoring Techniques in Livestock

### 4.1. Animal HR monitoring techniques

Heart rate is a crucial variable to quantify animal welfare and health state, as well as environmental impact. A real-time and continuous monitoring of HR of animals is a potential tool for livestock management to improve its production efficiency and welfare. Animal HR monitoring methods currently reported in literatures are mainly based on acquiring ECG signal or inter-beat intervals (IBIs) directly. Various portable devices are commercially available to record ECG signals for animals. Holter systems, widely used in human clinic, are sometimes employed for ambulatory long-term recording of ECG signal (mostly up to 24h) for animals (Konold et al., 2011). It is not practical to apply to livestock, since these systems are very expensive. Another relatively cheaper measurement is to use the monitors, which are primarily marketed for sport and relevant research in sport medicine, and fabricated by a commercial manufacturer (Polar Electro Oy, Finland) to record IBIs data, like Polar Sport Tester, Polar S810i, Polar Vantage NV and Polar

R-R Recorder are widely applied in veterinary and behavioral research, which are all using an electrode belt containing two coated electrodes that fits around the thorax of the animals. When applying such wearable techniques to livestock, it is inconvenient to mount it on animals tightly, and the obtrusive devices are also easily discovered and attracted by their mates, which may cause aggressive behaviors. Implantable telemetric transmitters, which have been applied in a wide range of small size laboratory animals, address the drawback mentioned above. But it is an invasive approach to measure HR, since surgery is needed. Recently PPG based sensors, which are positioned in ear tags, have been emerged. While due to the motion-induced artifacts, the quality of signal is not too good to accurately measure the HR of animals (Chen et al., 2017). Thus, it is necessary to develop an accurate and convenient approach for real-time continuous animal HR monitoring.

The techniques discussed in section 3 demonstrate their good performance for human HR monitoring, which provides new ideas to transfer them into livestock. For mammals, such as pigs, there are several anatomical and physiological similarities to human, including skin. Porcine skin is increasingly being employed as a model of human skin in various research fields, including pharmacology, toxicology and immunology, with particular interest in percutaneous permeation and organ transplantation for wound healing. Several anatomical and physiological similarities exist between porcine and human skin. As in humans, porcine skin is divided into three layers, i.e. the epidermis, the dermis and the hypodermis (or subcutis) from top to bottom. Human epidermis ranges from 50 to 120 $\mu\text{m}$  and the pig's is from 30 to 140 $\mu\text{m}$ . But the epidermal thickness varies considerably based on body site, and a better measure is the dermal-epidermal thickness ratio (Meyer et al., 2015). It has been reported that this ratio ranges from 10:1 to 13:1 for pigs, which is comparable to human skin. Moreover, the size, orientation, and distribution of blood vessels in the dermis of pigs are also similar to blood vessels of the human skins. Additionally, the dorsal site of pig ears represents the area of porcine tissue with the highest similarity to human skin, with regard to the thickness of the different skin layers.

#### 4.2. Comparison and discussion

The wearable PPG methods provide good performance of accuracy of HR measurement for human even in extensive exercise situations. Pig skin is known to be more similar to human skin, anatomically and physiologically. Thus, it is concluded that PPG theory has the potential in HR assessment for pigs. Nowadays, it is realistic to develop a continuous HR sensor that can be integrated in an ear tag for middle size animals and bigger, like pig, cow, sheep, goat, etc. Compared to contacting requirement of PPG, PPGI, which is a non-contact, low-cost and convenient technique, is preferable for the reasons of hygiene, animal welfare and practical installation for housed animals. From the previous researches, we can conclude that most of these methods require subjects maintaining motionless, and the distance between camera and measured subjects within several meters is another limit. This is because PPG signals are susceptible to motion-induced artifacts and illumination variations, particularly when dealing with webcams during ambient light (Bousefsaf et al., 2013). Robust image and signal processing methods are introduced to overcome drawbacks induced by light and motion artifacts. Challenges are presenting due to complicated environment of livestock, including low light levels and variations, movement of animals and their distance to cameras, thus much work on signal noise removal and processing remains to be addressed in livestock application in the future.

Thermal imaging is a passive and non-contact method, and it still presents several limitations. Its signal is susceptibility affected by physiological and environmental thermal phenomena (Liu et al., 2012). Results from related researches are derived from experimental setting in a controlled environment, where the subject remains motionless. Any spontaneous movements, such as small movements of the limbs or even stressed breathing affect the shape of the measured signal dramatically. Furthermore, the method is dependent on unwanted thermal distortions, such as sweating, external heat radiation, airflow, etc. Moreover, the infrared-based measurement is much

more expensive, as high-quality cameras must be used. We don't think it is currently practical to employ the technique particularly at farm level, due to the uncontrolled animals, environment and the high-cost cameras.

The wet and dry electrodes both require direct contact with skin, and the attachment site should be cleaned, and shaving the hair off is necessary if needed. Besides, wet electrodes need conductive gel and dry electrodes depend on sweat and moisture between the electrodes and skin, which may cause irritation and allergic reaction after prolonged usage. Although CECG is a non-contact method to detect ECG signal even through hair and clothing, it is sensitively corrupted by motion artifacts.

Ballistocardiography and SCG techniques often show high signal-to-noise ratio, which can extract HR information accurately. The signals are vulnerably affected by motion artifacts caused by body movements, position and respiratory movements, and hence the quality of the corresponding HR recordings is impacted.

Video-based motion technique for HR measuring possesses certain advantages over the PPGI methods. For example, it is invariant to illumination variance and not restricted to any particular view of the face. Furthermore, it is effective even when skin is not visible. While for PPGI, the sensitivity to color noise and changes in illumination should be considered, which requires facial skin to be exposed to the camera during tracking. However, the video-based motion approach would be highly vulnerable to internal facial motion and external movement of the head (Haque et al., 2016). In realistic scenarios, particularly in livestock farming, it is still a big challenge by using current methods to obtain high-quality video due to the unavoidable voluntary motion variations of the animals.

With regard to Doppler effect techniques, the experimental protocol in related researches requires the subjects maintaining motionless to limit the body movements, since the Doppler radar and laser which have high displacement resolution are prone to be affected by motion artifacts, and even the small movement of body can result in a high deformation of the signals. In addition, Doppler effect techniques are active measuring method since they emit energy. When applying Doppler in livestock, the direct contact of the laser to the animals' eyes is inconsistent of animal welfare. For Doppler radar, the greater the required measuring distance, the higher frequency and transmitted power are needed, which are prone to present a safety threat. Furthermore, these technologies are relatively expensive because of the special hardware.

After introducing each technique and evaluating its feasibility for implementation in livestock, we want to further compare and discuss various properties and capabilities related to application in livestock. Different technologies are shown in Table 1.

**Accuracy:** Accuracy is an essential factor for HR measurement, and an error within 5 bpm is an acceptable margin (Poh et al., 2010b). The accuracy ranges of related researches for each method which are compared to gold standard methods are listed in Table 1. The quantitative data show the ability to obtain accurate HR by using these techniques.

**Distance:** Distance between sensor and animal is an important variable for the appreciation of the different techniques and their potential applications in livestock. Since accurate measurement does not only depend on the technique itself, but also on the specific implementation. Table 1 shows the orders of magnitude for distances. According to our definition of the categories of wet/dry electrodes methods, they require direct contact with the subjects. Gaps between sensor and subject in the range of millimeters have been required by PPG, BCG/SCG and CECG methods. Significantly longer distances can be covered by the remaining systems, which are camera-based techniques like PPGI, thermal imaging and video-based motion, as well as radar and laser. Such systems can be easily operated from the distances in a range of meters.

**Movement:** It can be seen that all investigated HR monitoring techniques are to some extent sensitive to motion artifacts, hence most of them require the detected subjects maintaining motionless. Even for wearable PPG and CECG technologies, although they have good

performance even in extensive exercises, close proximity to the body surfaces is also necessary.

Costs: The category of costs are fuzzy if no limiting definitions are employed. Here we just consider the lowest possible cost for sensors while the cost of algorithm development, which is very important aspect for the commercial success of a technology, is beyond the scope of this review. Considering the measuring sensors for various techniques, the techniques PPG, PPGI, video-based motion, and BCG/SCG approach exhibit the lowest cost. PPG system consists of inexpensive phototransistors. Video-based motion and PPGI systems can be realized using consumer grade camera and webcam products that are mass produced, hence they are very inexpensive as well. The sensors used for BCG/SCG methods, such as very simple optical sensors, strain gauges pressure sensors are very cheap. We consider the techniques ECG and radar to be in the medium range of the costs. The laser is an expensive method because of its complex optical assemblies and costly devices. The most expensive method among all of the techniques is thermal imaging because a very sensitive thermal imaging camera is needed when monitoring perfusion.

According to the aforementioned properties of various techniques, a low-cost, motion-resistant and accurate sensor is needed for animal HR monitoring in livestock. For pig production, we conclude the PPG technology might be the mostly transferable since it is not only satisfying the above requirements, but also for the similarities of human and pig skins.

Table 1. Comparison of different HR monitoring techniques.

Technique	Measuring sensor	Distance	Movement	Costs	Error (bpm)
Wearable PPG	Phototransistor	mm	No limitation	low	0.07–2.7
PPGI	Camera/webcam	m	Subtle motion	low	0.16–4.63
Thermal imaging	Thermal imaging camera	m	Motionless	highest	4.74
BCG/SCG	Pressure sensor, strain gauge, optical sensor etc.	mm	Motionless	low	0.33–1.82
Video-based motion	Camera/webcam	m	Motionless	low	1.5%
Radar	Microwave sensor	m	Motionless	medium	—
Laser	Laser	m	Motionless	high	0.006–0.026
Wet ECG	Wet electrodes	0	Subtle motion	medium	—
Dry ECG	Dry electrodes	0	No limitation	medium	—
CECG	Capacitively coupled electrodes	mm	No limitation	medium	0.3–1.1

#### 4.3. Challenge and future work

According to the discussion above, we consider that it is realistic today to integrate the PPG technique into an ear tag for middle size and bigger animals, including cow, pig, sheep, goat, etc. To design such a sensor, the challenges on battery lifetime, energy to send data, working period, recovery of the sensor, re-usable characteristic and expected price, should be especially considered. To extend the battery lifetime, all components of the sensor should be chosen from low-power ones, and some battery-saving techniques are also necessary. Particularly, data communication is always a most power-hungry part, thus an extremely low-power wireless communication protocol should be developed. For the price of the sensor, the PPG is a low-cost technique. When a large amount of sensor units is manufactured, reduced price is expected, which

will allow the very small farms to use these products. We conclude that this sensor technology, being able to be integrated into an ear tag, can be employed for middle size and bigger animals, and the application would be started with cow, pig, sheep, goat, etc. Within the coming years, we expect more miniaturized hardware, so that the concept is applicable to smaller animals, such as poultry.

## 5. Conclusions

As we have seen so far, there are a significant number of different sensor technologies for HR monitoring currently under investigation, and this paper has critically reviewed the progress. Six promising measuring technologies on human beings were investigated, and the principles and theory on HR measurement were discussed. Moreover, advantages and disadvantages with further elaboration were emphasized, by comparing various properties and capabilities related to the application to livestock. We conclude that it is realistic today to develop a continuous HR sensor that can be integrated into an ear tag for middle size and bigger animals, such as cow, pig, sheep, goat, etc. Research endeavor of HR online monitoring on pigs could be as a kick-off milestone in the livestock sector, and the monitoring could become applicable for small species such as poultry when more miniaturized hardware is realized in a predictable future. We expect that this study will inspire researchers and technology companies to invest in such technology and develop prototypes of the ear tag as well as to produce the sensors later in very high numbers.

## Acknowledgements

This work was supported by the National Key R&D Program of China (2017YFD0701602).

## References

- Allen, J., 2007. Photoplethysmography and its application in clinical physiological measurement. *Physiological Measurement*. 28 (3), R1.
- Boussefsaf, F., C. Maaoui, A. Pruski, 2013. Continuous wavelet filtering on webcam photoplethysmographic signals to remotely assess the instantaneous heart rate. *Biomedical Signal Processing and Control*. 8 (6), 568–574.
- Bruser, C., C.H. Antink, T. Wartzek, M. Walter, S. Leonhardt, 2015. Ambient and Unobtrusive Cardiorespiratory Monitoring Techniques. *IEEE Reviews in Biomedical Engineering*. 8, 30–43.
- Brüser, C., A. Kerekes, S. Winter, S. Leonhardt, 2012. Multi-channel optical sensor-array for measuring ballistocardiograms and respiratory activity in bed. In: *Engineering in Medicine & Biology Society*.
- Celka, B.P., C. Verjus, R. Vetter, P. Renevey, V. Neuman, 2004. Motion resistant earphone located infrared based heart rate measurement device. In: *Lasted*.
- Chen, G.P., W.J. Qin, J. Ding, M.C. Wan, L.F. Guo, W.S. Wang, 2017. Designing and Validation of the Remote Monitoring System for Pigs' Survival Based on Io T Technology. *Scientia Agricultura Sinica*.
- El-Amrawy, F., M.I. Nounou, 2015. Are Currently Available Wearable Devices for Activity Tracking and Heart Rate Monitoring Accurate, Precise, and Medically Beneficial? *Healthcare Informatics Research*. 21 (4), 315–320.
- Fukushima, H., H. Kawanaka, M.S. Bhuiyan, K. Oguri, 2012. Estimating heart rate using wrist-type Photoplethysmography and acceleration sensor while running. In: *Engineering in Medicine & Biology Society*.
- Haque, M.A., R. Irani, K. Nasrollahi, T.B. Moeslund, 2016. Heartbeat Rate Measurement from Facial Video. *IEEE Intelligent Systems*. 31 (3), 40–48.
- Inan, O.T., P.F. Migeotte, K.S. Park, M. Etemadi, K. Tavakolian, R. Casanella, J. Zanetti, J. Tank, I. Funtova, G.K. Prisk, 2017. Ballistocardiography and seismocardiography: a review of recent advances. *IEEE Journal of Biomedical & Health Informatics*. 19 (4), 1414–1427.
- Kamišalić, A., I. Fister, M. Turkanović, S. Karakatić, 2018. Sensors and Functionalities of Non-Invasive Wrist-Wearable Devices: A Review. *Sensors*. 18 (6), 1714.
- Konold, T., G.E. Bone, M.M. Simmons, 2011. Time and frequency domain analysis of heart rate variability in cattle affected by bovine spongiform encephalopathy. *Bmc Research Notes*. 4 (1), 259–259.
- Liu, H., Y. Wang, L. Wang, 2012. A review of non-contact, low-cost physiological information measurement based on photoplethysmographic imaging. In: *Engineering in Medicine & Biology Society*.
- Marc, G., S. Nanfei, M. Arcangelo, P. Ioannis, 2007. Contact-free measurement of cardiac pulse based on the analysis of thermal imagery. *IEEE Transactions on Biomedical Engineering*. 54 (8), 1418–1426.

- Mcduff, D.J., J.R. Estepp, A.M. Piasecki, E.B. Blackford, 2015. A survey of remote optical photoplethysmographic imaging methods. In: *Engineering in Medicine & Biology Society*.
- Meyer, W., R. Schwarz, K. Neurand, 2015. The skin of domestic mammals as a model for the human skin, with special reference to the domestic pig. *Current Problems in Dermatology*. 7 (7), 39–52.
- Nemati, E., M.J. Deen, T. Mondal, 2012. A Wireless Wearable ECG Sensor for Long-Term Applications. *IEEE Communications Magazine*. 50 (1), 36–43.
- Obeid, D., S. Sadek, G. Zaharia, G.E. Zein, 2010. Multi-tunable microwave system for touch-less heartbeat detection and heart rate variability extraction. *Microwave & Optical Technology Letters*. 52 (1), 192–198.
- Poh, M.Z., D.J. Mcduff, R.W. Picard, 2010a. Advancements in noncontact, multiparameter physiological measurements using a webcam. *IEEE Transactions on Biomedical Engineering*. 58 (1), 7–11.
- Poh, M.Z., D.J. Mcduff, R.W. Picard, 2010b. Non-contact, automated cardiac pulse measurements using video imaging and blind source separation. *Optics Express*. 18 (10), 10762–10774.
- Poh, M.Z., K. Kim, A. Goessling, N. Swenson, R. Picard, 2012. Cardiovascular Monitoring Using Earphones and a Mobile Device. *IEEE Pervasive Computing*. 11 (4), 18–26.
- Scalise, L., U. Morbiducci, 2008. Non-contact cardiac monitoring from carotid artery using optical vibrocardiography. *Medical Engineering & Physics*. 30 (4), 490–497.
- Seidman, D.S., M. Jonathan, E. Zivanit, L. Arie, H.J. Vreman, D.K. Stevenson, G. Rena, 2003. A prospective randomized controlled study of phototherapy using blue and blue-green light-emitting devices, and conventional halogen-quartz phototherapy. *Journal of Perinatology Official Journal of the California Perinatal Association*. 23 (2), 123–127.
- Shin, K., Y. Kim, S. Bae, K. Park, S. Kim, 2009. *A Novel Headset with a Transmissive PPG Sensor for Heart Rate Measurement*.
- Sun, B., Z. Zhang, 2015. Photoplethysmography-Based Heart Rate Monitoring Using Asymmetric Least Squares Spectrum Subtraction and Bayesian Decision Theory. *IEEE Sensors Journal*. 15 (12), 7161–7168.
- Sun, Y., H. Sijung, A.P. Vicente, G. Stephen, C. Jonathon, Z. Yisheng, 2011. Motion-compensated noncontact imaging photoplethysmography to monitor cardiorespiratory status during exercise. *Journal of Biomedical Optics*. 16 (7), 077010.
- Sun, Y., C. Papin, V. Azorin-Peris, R. Kalawsky, S. Greenwald, S. Hu, 2012. Use of ambient light in remote photoplethysmographic systems: comparison between a high-performance camera and a low-cost webcam. *Journal of Biomedical Optics*. 17 (3), 037005.
- Tavakolian, K., B. Ngai, A. Akbardeh, B. Kaminska, A. Blaber, 2009. Comparative analysis of infrasonic cardiac signals. In: *Computers in Cardiology Conference*.
- Wu, T., V. Blazek, H.J. Schmitt, 2000. Photoplethysmography imaging: a new noninvasive and noncontact method for mapping of the dermal perfusion changes.
- Xu, H., J. Liu, J. Zhang, G. Zhou, N. Luo, N. Zhao, 2017. Flexible Organic/Inorganic Hybrid Near-Infrared Photoplethysmogram Sensor for Cardiovascular Monitoring. *Advanced Materials*. 29 (31), 1700975.
- Yousefi, R., M. Nourani, S. Ostadabbas, I. Panahi, 2014. A motion-tolerant adaptive algorithm for wearable photoplethysmographic biosensors. *IEEE Journal of Biomedical and Health Informatics*. 18 (2), 670–681.
- Zheng, J., C. Ha, Z. Zhang, 2017. Design and evaluation of a ubiquitous chest-worn cardiopulmonary monitoring system for healthcare application: a pilot study. *Medical & Biological Engineering & Computing*. 55 (2), 1–12.

# Animal Welfare Monitoring by Real-time Physiological Signals

Pieter Joosen <sup>a</sup>, Tomas Norton <sup>b</sup>, Jeremy Marchant-Ford <sup>c</sup>, Daniel Berckmans <sup>a,b</sup>

<sup>a</sup> BioRICS NV, Technologielaan 3, 3001 Heverlee, Belgium

<sup>b</sup> M3-BIORES, Catholic University of Leuven, Kasteelpark Arenberg 30, 3001 Leuven, Belgium

<sup>c</sup> USDA Livestock Behavior Research Unit, 125 South Russel Street, West Lafayette, IN 47907, USA

\* Corresponding author. Email: [daniel.berckmans@kuleuven.be](mailto:daniel.berckmans@kuleuven.be)

## Abstract

Animal welfare is important and Europe has invested a lot in methods to score or monitor animal welfare in commercial livestock houses. A main objective of Precision Livestock Farming (PLF) is to deliver a tool for active management of livestock to improve animal welfare and health and to make livestock farming more animal economically, socially and environmentally sustainable. The importance of well managed animal welfare is not limited to the ethical viewpoint but is also crucial to realize a more efficient process to produce animal products. When considering the metabolic energy balance in a homeothermic living organism, there are different components: basal metabolism, the thermal component, the physical component related to movement or delivering power, the production term (meat, milk, eggs) and finally the mental component. When applying the stress monitoring, developed for humans, on animals we see that we can monitor frustration of horses in real-time. This indicates that real-time animal welfare monitoring based upon physiological signals becomes a realistic pathway.

**Keywords:** Animal welfare monitoring, basal metabolism, precision livestock farming, metabolic energy, thermal component

## 1. Introduction

Being a technology driven method PLF takes time for technical people to tune it to the essential part which is the animal. Meanwhile it is a challenge for so called ‘animal people’ (farmers, veterinarians, animal scientist, nutritionists, immunologists, etc.) to embrace the potential that this technology has to offer. Animal scientists use many indicators related to a whole range of disorders from abnormal behaviour, diseases, production failure to poor emotional states (Botreau et al., 2007). Scientists have developed an overall assessment by manual scoring of animal welfare in livestock houses in the field. This method is interesting as a reference method or as a gold standard or for audio-visual labelling of animals in the livestock house. The approach is however not applicable for continuous monitoring of animal welfare since the scoring is done by human observers (Botreau et al., 2009).

Since 2003, when the first ECPLF2003 was organised, the proceedings of the 8 bi-annual conferences count over 1000 publications. Many more per-reviewed papers have been published from which a high number measure components related to animal welfare. With the use of cameras, microphones and sensors several methods have been developed, tested and validated to monitor components related to animal welfare. For broilers it was shown that animal feature variables like distribution and activity, measured by cameras, are useful to detect over 95 % of all noted problems in broiler houses. Gait analysis tools were developed by using cameras and accurate feed intake monitoring was realised with cameras while vocalisations were analysed for abnormal sounds (Aydin, 2017; Du et al., 2018). For fattening pigs, continuous sound analyses was developed to detect infection and this became a successful commercial product (Berckmans et al., 2015).

For pigs there were many examples of using PLF technology monitoring animal welfare related components such as detection of aggression (Oczak et al., 2014), gait analysis, weight and water intake (Viazzi et al., 2014; Oczak et al., 2014; Kashihara et al., 2013 and 2014; Ismayilova et al., 2013). For cows, PLF systems for body condition scoring, lameness monitoring, mastitis and ketosis monitoring and feed intake were developed (Van Hertem et al., 2014). We have to confess

that most of the technologies so far did not make it yet to large scale applications in livestock houses. So far we have no overall solution to monitor animal welfare in real-time with a scientifically based method. The challenge remains to get an overall animal welfare monitor based upon objective measurements.

The objective of this paper was to test whether the real-time monitoring of the metabolic energy balance offers opportunity for continuous and real-time monitoring of the mental state of animals while they are active.

## 2. Materials and Methods

### 2.1. Experimental protocol

The experimental protocol was checked and approved by the ethical commission of the Catholic University of Leuven and the Purdue Animal Care and Use committee (Protocol #111200040). Experiments were done on 2 individually-housed Large White x Yorkshire pigs, each weighing 20 kg. The pig was placed in a Pig Turn experimental pen (DeBoer et al., 2015) with enough space ( $1.12 \text{ m}^2$ ) for an individual animal while wearing a sensor integrated into a harness (Zephyr BioHarness 3). The animal's movement was measured with a 3D accelerometer positioned on the belly of the pig (100 Hz,  $\pm 16 \text{ G}$ ) while heart rate was measured with a belt around the torso just behind the front legs (1 Hz, 25–240 BPM,  $\pm 1 \text{ BPM}$  accuracy). Video recordings were taken during the entire experiment to capture animal responses.

During 3 consecutive days 4 experiments were done per day where 2 types of stressors were applied: a negative stressor and a positive stressor. The negative stressor was a loud sound (120 dB) played for 2 seconds. The positive stressor was a towel thrown in the test facility as a toy for the pigs to play with (see Table 1).

Table 1. Time schedule of the different stressors.

	9 AM	9:30 AM	10 AM	10:30 AM
Day 1	Scare (1)	Towel (1)	Scare (2)	Towel (2)
Day 2	Scare (1)	Towel (1)	Towel (2)	Scare (2)
Day 3	Towel (1)	Scare (1)	Scare (2)	Towel (2)

### 2.2. Method: decomposition of heart rate in different components

A gold standard for measuring stress, beside questionnaires for humans and audio-visual scoring of animals, is a combined measurement of EEG, ECG, respiration rate, skin conductivity, blood analysis, and/or saliva analysis. Several methods have been tested to measure stress based upon physiological data and most of them still need a combination of heart rate with respiration rate or more variables (Hovsepian et al., 2015).

In the past, it was already shown that there is a dynamic relationship between the central nervous system and the expression of emotions and that physiological variables offer potential for monitoring stress (Darwin, 1872; Porges, 1995). The decomposition of heart rate components in mental and physiological or physical components (basal metabolism, movement, power, production, thermal component) remains a challenge on moving subjects, which leads to the consequence that most methods for stress monitoring based on heart rate are limited to non-moving subjects.

We use an algorithm used to decompose the total heart rate into 3 different components: the baseline, the physical component and the mental component. The assumption in the method is that the animal is acting in the aerobic zone of metabolic energy production. This means that the inhaled air is brought into the blood in the lungs. Then the heart is pumping the blood to the cell level where the metabolic energy is produced. This means that the level of heart rate is a measure for the possible total production of metabolic energy. This metabolic energy is used for the basal metabolism (HRBM), for the thermal component (HRTHERM) to keep the body at constant temperature, for the movement energy (HRMOV), for production (HRPROD) and for the mental

component (HRMENT). This can be written as:

$$\text{HRTOTAL} = \text{HRBM} + \text{HRTHERM} + \text{HMOV} + \text{HRPROD} + \text{HRMET} \quad (1)$$

Before and during the experiment, the temperature around the animal was kept constant and since this was a short-term experiment we assumed that the production term did not vary enough during the experiment. We can simplify the equation (1) leading to (2):

$$\text{HRTOTAL} = \text{HRBM} + \text{HMOV} + \text{HRMET} \quad (2)$$

Since every animal is individually different and time varying in the responses to different stressors, the equation must adapt to the individual animal and for this individual be dynamically updated in time.

The measured variables are HRTOTAL and MOVEMENT. The HRBM, normally estimated during night sleep, was estimated here before and during the experiment since that is the non-varying baseline within the signal of total heart rate.

By monitoring in a synchronized way animal movement using a 3D accelerometer and heart rate, the dynamic responses of total heart rate and movement to stressor can be measured.

To quantify the dynamic response of heart rate to movement during the responses to stressors, a single-input single-output (SISO) linear discrete transfer function model was fitted to the data, using Equation 3:

$$y(k) = \frac{B(z^{-1})}{A(z^{-1})} u(k - \delta) + \xi(k) \quad (3)$$

where the terms  $A(z^{-1}) = 1 + a_1 z^{-1} + \dots + a_n z^{-n}$  and  $B(z^{-1}) = b_0 + b_1 z^{-1} + \dots + b_m z^{-m}$  are the polynomials of the transfer function. In these terms the  $a_1, \dots, a_n$  are the n a-parameters of the nth order A polynomial, and  $b_0, \dots, b_m$  are the m+1 b-parameters of the mth order B polynomial.  $z^{-1}$  is the backward shift operator,  $y$  is the output (heart rate) and  $u$  is the input (movement).  $k$  is the time instant of the data point,  $\delta$  is the time delay, and  $\xi$  is the noise of the output error model, which is assumed to be white.

By estimating the physical component and basal metabolism of heart rate we finally can also identify the mental component HRMENT showing the mental response to the offered stressors. For a detailed description of this method we refer to the dynamic analyses as used for mental monitoring for humans (Berckmans et. al., 2007).

### 2.3. Analysis of the mental component of heart rate to positive and negative stressors

The analysis was focused on the response of the mental component in heart rate to the different stressors. The moment at which each stressor was applied was determined based upon using labelled videos where the stressor was visible. The data were segmented in blocks around each stressor (between 2 min before and 2 min after). Visual qualitative analysis of each response was grouped per pig and per type of stressor (positive or negative).

A statistical analysis was performed for each pig, per type of stressor. The monitored mental heart rate response was grouped together in 3 groups. The first one contained the data from 1 min before application of the stressor until the moment of stress. The second group contained the data from the moment of stress until 1 min after. The third group contained the data from 1 min after application of the stressor until 2 min after.

It was statistically tested whether groups were significantly different. With the Shapiro Wilks test, the normality of each group was tested (Shapiro et al., 1965). The Friedman test was used to compare three matched groups from a non-Gaussian population (Friedman, 1937). Finally, the Wilcoxon test was used to check whether at least one group was significantly different in a post hoc test (Siegel, 1956).

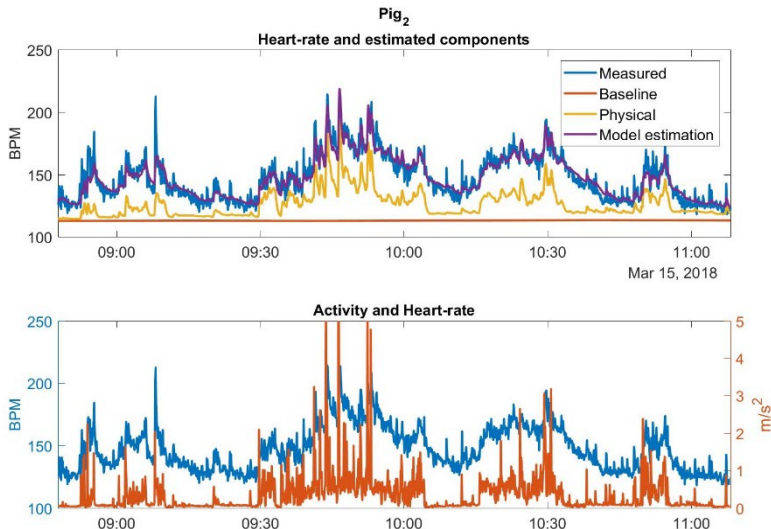


Figure 1. Top: Heart rate and estimated components of Pig 2 on Day 2. Bottom: raw activity and heart rate as measured by the Zephyr Bio Harness 3.

### 3. Results and Discussion

#### 3.1. Response of mental heart rate component to the negative stressor

The applied negative stressor (loud sound) generated in both pigs a clear increase in the mental component in heart rate after the loud sound was played. Soon after it went back to baseline levels (see Figure 2). The mental component of heart rate can be explained by the animals being scared and this was clearly measurable in real time with sensors on the animal.

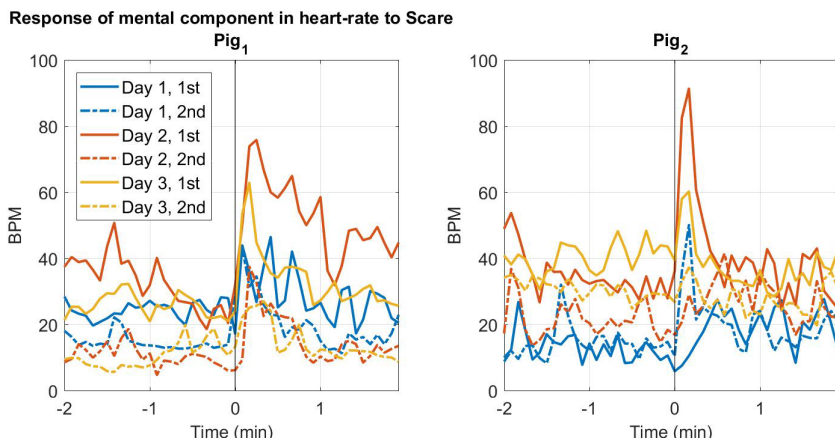


Figure 2. Responses of mental component in heart rate of both pigs to the negative stressor (scare with loud sound, applied at time 0).

#### 3.2. Responses of mental heart rate component to the positive stressor

The applied positive stressor was the access to a towel that generated a playing of the pigs with towel. There was a small increase in the mental component after the towel was thrown in the pen, and the pigs starts playing with it. Most clearly visible for Pig 2 (see Figure 3).

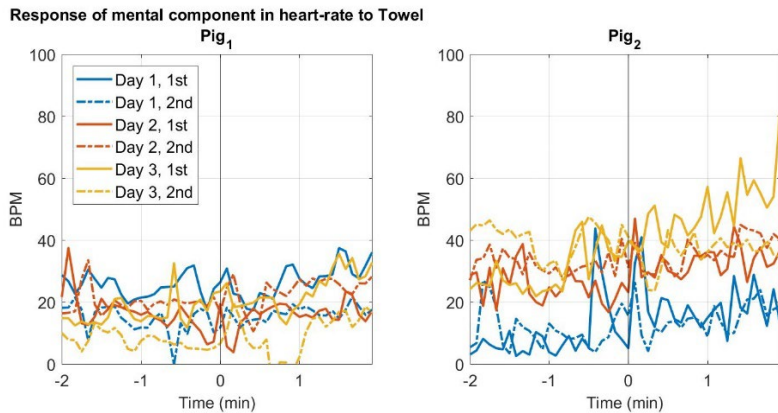


Figure 3. Responses of mental component in heart rate of both pigs to the positive stressor (playing with towel thrown in the pen at time 0).

### 3.3. Quantitative statistical analysis of mental responses to negative and positive stressors

The short loud sound as a negative stressor generates a scared response with a corresponding mental heart rate response. The mental component in heart rate increased on average by 13.3 BPM for Pig 1 and by 6.2 BPM for Pig 2 after applying the scare stressor. This increase was found to be significantly different (Figure 4).

After the negative stressor was stopped, the mental component decreased again by on average 9.4 BPM and 4.4 BPM for Pigs 1 and 2 respectively.

The access to a towel as a positive stressor results in the pigs playing with the towel. There was an increase in the mental component when the pigs started playing with the towel that was thrown in their pen. In the 2 minutes, after the towel was given, the mental heart rate increased on average 6.3 BPM and 8.5 BPM for Pigs 1 and 2 respectively compared to the period 1 min before the stressor was applied (see Figure 4 and Table 2).

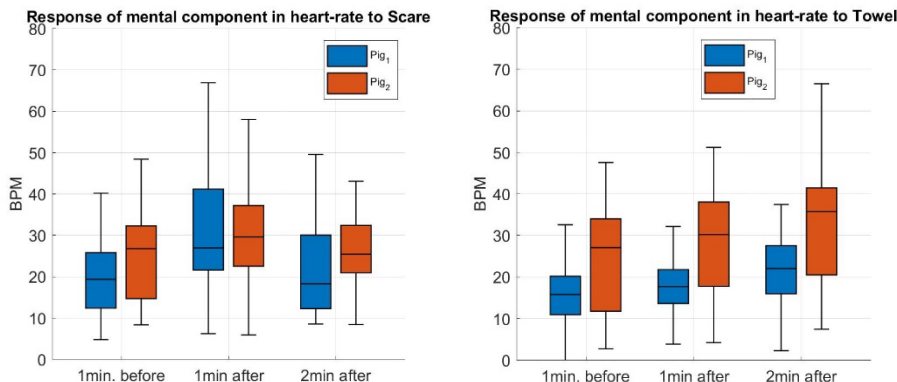


Figure 4. Responses of mental component in heart rate to negative (left) and positive (right) stressor

Table 2..Responses of mental component in heart rate (Mean  $\pm$  SD, BPM) to external stressors for 2 pigs. “abc” indicate significant differences between the groups ( $P < 0.01$ , a: 1 min before, b: 1 min after and c: 2 min after).

	Scare			Towel		
	1 min. before	1 min. after	2 min. after	1 min. before	1 min. after	2 min. after
Pig 1	18.8 $\pm$ 8.0 <sup>bc</sup>	32.1 $\pm$ 16.6 <sup>ac</sup>	22.7 $\pm$ 12.4 <sup>ab</sup>	15.7 $\pm$ 6.9 <sup>c</sup>	16.8 $\pm$ 7.8 <sup>c</sup>	22.0 $\pm$ 7.2 <sup>ab</sup>
	24.7 $\pm$ 10.9 <sup>b</sup>	30.9 $\pm$ 15.0 <sup>a</sup>	26.5 $\pm$ 8.4	25.1 $\pm$ 12.8 <sup>bc</sup>	29.1 $\pm$ 11.9 <sup>ac</sup>	33.6 $\pm$ 14.6 <sup>ab</sup>

#### 4. Conclusions

It was possible to estimate the mental component in heart rate of pigs while they were moving using wearable sensors on the body of pigs. Two pigs were exposed to a negative and a positive stressor to test whether the method allows to measure mental responses to stressors.

Both pigs respond clearly to the negative stressor. In the period of 1 minute after the stressor was applied, the mental component of heart rate increased significantly ( $P < 0.01$ ) with on average 13.3 BPM and 6.2 BPM for Pigs 1 and 2 respectively, compared to the period 1 min prior. In the period of 2 min after the stressor was applied, the mental component decreased by on average 9.4 BPM ( $P < 0.01$ ) and 4.4 BPM for Pigs 1 and 2 respectively. The mental response to this applied negative loud sound as a stressor it was a fast response, only detected immediately after the stressor is applied.

The mental component heart rate of both pigs also responded to the positive stressor, but in a different way. In the period of 2 mins after the stressor was applied, the mental component increased significantly ( $P < 0.01$ ) with 6.3 BPM and 8.5 BPM for Pigs 1 and 2 respectively, compared to the period 1 min prior to the stressor.

The mental response to the towel as a positive stressor, generated a slow response, but this may be affected by the experiment. The towel was not removed, so the pigs were continuously playing with it, as opposed to the negative stressor, which was only applied for a very short period (2 s).

#### References

- Aydin, A., 2017. Development of an early detection system for lameness of broilers using computer vision. *Computers and Electronics in Agriculture*. 136, 140–146.
- Berckmans, D., M. Hemeryck, D. Berckmans, E. Vranken, T. van Waterschoot. 2015. Animal sound...talks! Real-time sound analysis for health monitoring in Livestock. *Proc. Animal Environment and Welfare*, 215–222.
- Berckmans, D., S. Quanten, J.M. Aerts. 2007. Real-time monitoring and control of physical and arousal status of individual organisms. DK2047392, A61B5/024 International GO6F16/00, Application number DK29970784892T, Granted Patent. Pp 120.
- Botreau, R., I. Veissier, A. Butterworth, M.B.M. Bracke, L.J. Keeling. 2007. Definition of criteria for overall assessment of animal welfare. *Animal welfare*, 16 (2), 225–228.
- Botreau, R., I. Veissier, P. Perny 2009. Overall assessment of animal welfare: strategy adopted in Welfare Quality (R). *Animal welfare*, 18 (4), 363–370
- Darwin, C., 1872. *The Expression of the Emotions in Man and Animals*. London, John Murray; Reprinted Chicago, IL, University of Chicago Press, 1965.
- DeBoer, S.P., J.P. Garner, R.R. McCain, D.C. Lay Jr., S.D. Eicher, J.N. Marchant-Forde. 2015. An initial investigation into the effects of social isolation and enrichment on the welfare of laboratory pigs housed in the Pig Turn System assessed using tear staining, behaviour, physiology and haematology. *Animal Welfare*, 24, 15–27.
- Du, X.D., F.D. Lao, G.H. . 2018. A Sound Source Localisation Analytical Method for Monitoring the Abnormal Night Vocalisations of Poultry. *SENSORS*, 18, 9, 2906.

- Fernandez, A.P., T. Norton, E. Tullo, T. Van Hertem, A. Youssef, V. Exadaktylos, E. Vranken, M. Guarino, D. Berckmans. 2018. Real-time monitoring of broiler flock's welfare status using camera-based technology. *Biosystems Engineering*, 173, 103–114.
- Ferrari, S., M. Silva, V. Exadaktylos, D. Berckmans, M. Guarino. 2013. The sound makes the difference: the utility of real time sound analysis for health monitoring in pigs. *Livestock Housing: Modern management to ensure optimal health and welfare of farm animals*. Edited by: Aland, A.; Banhazi, T., Pages: 407–417.
- Friedman, M. 1937. The use of ranks to avoid the assumption of normality implicit in the analysis of variance. *Journal of the American Statistical Association*. 32 (200): 675–701.
- Hovsepian K., M. al Ábsi, E. Ertin, T. Kamarck M. Nakajima, S. Kumar. 2015. Towards a gold standard for continuous stress assessment in the mobile environment. *Proc ACM Int Conf Ubiquitous Comput*, 493–504.
- Ismayilova, G., L. Sonoda, M. Fels, R. Rizzi, M. Oczak, S. Viazzi, E. Vranken, J. Hartung, D. Berckmans, M. Guarino. 2013. Acoustic-reward learning as a method to reduce the incidence of aggressive and abnormal behaviours among newly mixed piglets. *Animal Production Science*, art.nr. AN13202.
- Kashiha, M., A. Pluk, C. Bahr, E. Vranken, D. Berckmans. 2013. Development of an early warning system for a broiler house using computer vision. *Biosystems Engineering*, 116 (1), 36–45.
- Kashiha, M., C. Bahr, S. Ott, C. Moons, T. Niewold, F. Ödberg, D. Berckmans. 2014. Automatic weight estimation of individual pigs using image analysis. *Computers and Electronics in Agriculture*, 107, 38–44.
- Oczak, M., S. Viazzi, G. Ismayilova, L. Sonoda, N. Roulston, M. Fels, C. Bahr, J. Hartung, M. Guarino, D. Berckmans, E. Vranken. 2014. Classification of aggressive behaviour in pigs by activity index and multilayer feed forward neural network. *Biosystems Engineering*, 119, 89–97.
- Porges, S.W. 1995 Cardiac vagal tone: a physiological index of stress. *Neuroscience and BioBehavioral Reviews*, 19 (2), 225–233. Elsevier Ltd, USA.
- Shapiro, S. S., M.B. Wilk. 1965. An analysis of variance test for normality (complete samples). *Biometrika*. 52 (3–4): 591–611.
- Siegel, S. 1956. *Non-Parametric Statistics for the Behavioral Sciences*. New York: McGraw-Hill. pp. 75–83.
- Van Hertem, T., S. Viazzi, M. Steensels, E. Maltz, A. Antler, V. Alchanatis, A. Schlageter Tello, K. Lokhorst, C. Bites Romanini, C. Bahr, D. Berckmans, I. Halachmi. 2014. Automatic lameness detection based on consecutive 3D-video recordings. *Biosystems Engineering*, 119, 108–116.
- Van Hertem, T., T. Norton, D. Berckmans, E. Vranken. 2018. Predicting broiler gait scores from activity monitoring and flock data. *Biosystems Engineering*, 173, 93–102.
- Viazzi, S., G. Ismayilova, M. Oczak, L. Sonoda, M. Fels, M. Guraino, E. Vranken, J. Hartung, C. Bahr, D. Berckmans. 2014. Image feature extraction for classification of aggressive interactions among pigs. *Computers and Electronics in Agriculture*, 104, 57–62.



**Theme VI:**  
**Animal Production Systems and**  
**Equipment**



# Poultry Farming Information Management System Based on Cloud Database

Tiemin Zhang<sup>a,b,\*</sup>, Haikun Zheng<sup>a</sup>

<sup>a</sup> College of Engineering, South China Agricultural University, Guangzhou, Guangdong 510642, P. R. China

<sup>b</sup> National Engineering Research Center for Breeding Swine Industry, Guangzhou, Guangdong 510642, P.R. China

\* Corresponding author. Email: [tm-zhang@163.com](mailto:tm-zhang@163.com)

## Abstract

Aiming at breaking down the bottleneck problems of different scales of poultry farms, low profitability of poultry farming, and information management backward in China, an efficient information management system for poultry farming was designed. This system consists of (1) environmental parameter monitoring model, (2) production and traceability model, (3) disease diagnosis and warning model, in combination with the development and production mode and management mode of large-scale and intensive poultry farming. The environmental parameter monitoring module integrates the measurement of ammonia, sulfur dioxide, temperature, humidity and other parameters in each area of a poultry farm. The parameter distribution map of the farm was constructed and data visualization of the farm area was realized through Internet transmission. The production and traceability module includes real-time monitoring of poultry production information such as laying eggs and weight gain, as well as traceability information such as chickens, feed, vaccines, finished product output quarantine, transportation and sales. Disease diagnosis and warning module is based on the analysis of the characteristics of poultry through audio and video signals, combined with expert system to achieve the diagnosis and warning of poultry diseases. Each module operates independently and cooperates with each other to form a set of information management system for poultry breeding with wide functional coverage, high service efficiency, safety and convenience.

**Keywords:** Real-time monitoring system, information management system, cloud database, poultry farm

## 1. Introduction

Modern poultry farming companies need a complete management system to assist in managing their daily production activities. The system should cover and integrate personnel office management, purchase-sales-inventory management, environmental monitoring and control in poultry houses and monitoring of individual poultry information. At the same time, it also needs to include traceability management of products, diagnosis and early warning of poultry diseases to meet the need for future development.

More and more information and intelligent technologies are applied in the field of poultry farming. Yu Ligeng et al. (2018) developed a network-based data acquisition system using LabVIEW software for environmental monitoring in poultry management, which describes the construction of data acquisition system hardware and the process of data acquisition. The method also provides a reference for us to build an environmental monitoring module. British Irvine explored the British broiler meat value chain (Irvine, 2015) and provided a method for constructing the traceability module in the poultry breeding management system, through its in-depth analysis of the value chain. Research on applying wireless sensing systems along with mobile networking and cloud platform to some agricultural systems in crops (So-In et al., 2014) has provided us with new ideas to develop a similar information system for poultry farming. Although wireless sensing and cloud platform techniques are well advanced, there is no complete system that covers all of the functions to meet needs for poultry farming management. The technical difficulties include the unified construction of the system, the reasonable division of functional modules, the good mutual cooperation between modules, the interaction of software

and hardware of the system.

This paper reports a conceptual design of a poultry farming information management system with cloud database as the core hub, through the connection of the underlying hardware facilities in the poultry house and the upper management system and the cloud database to manage the daily office work and production management tasks of poultry breeding enterprises. In addition, this cloud-based management system also pays more attention to the storage and management of data information by separating the database system from the software system. The ultimate goal of the poultry farming information management system is to expand development of the poultry industry management system with big data analysis capability.

## 2. Materials and Methods

Figure 1 shows the overall structure of the system. The system is divided into three layers, which are the upper management system, the intermediate data service layer (a.k.a. the middle layer), and the underlying layer (a.k.a. the bottom layer, including hardware in the poultry house). The upper layer is a software management system that provides a good visual interface. The management system is divided into an OA automatic office module, a production management module, an expert system, and a traceability module. As for the middle layer, the cloud database is used to store the data and information generated by the upper layer and the bottom layer, and at the same time, construct a reasonable network environment to solve mutual communication problems by configuring the underlying server. At the bottom layer, in poultry house(s), environmental sensors, Wi-Fi receiving and transmitting devices, and single-chip microcomputers can be configured to timely acquire and transmit environmental information and poultry individual information (including poultry weight information, feed intake data information, drinking water data information, poultry egg quality information and information about), ventilation fans, evaporative cooling pads, heaters and other equipment placed in the poultry house to regulate environmental parameters such as temperature and humidity in the house.

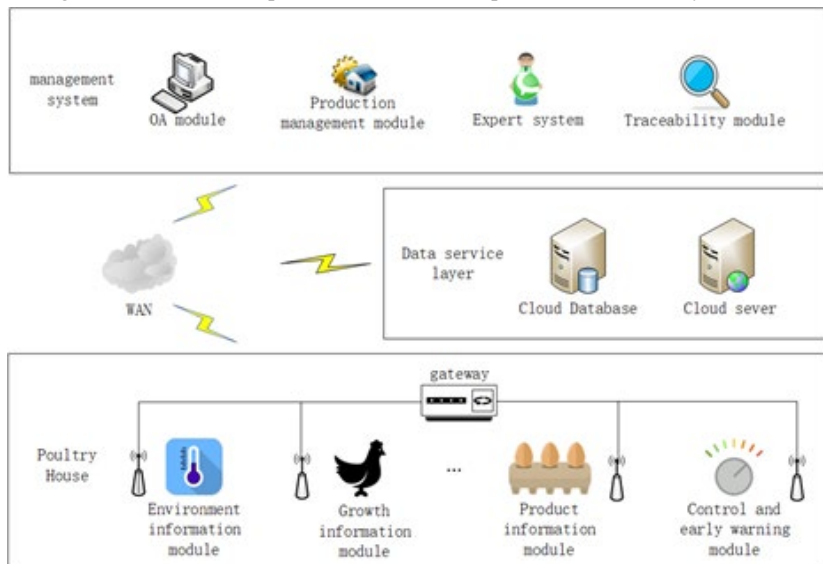


Figure 1. Overall structure of the poultry farming information management system.

### 2.1. System network construction and transmission method

Environmental parameter information sensor (including temperature and humidity sensor, ammonia sensor, carbon dioxide sensor, hydrogen sulfide sensor, light intensity sensor, etc.), feed

intake data monitoring module, drinking water data monitoring module, video monitoring system, fans, evaporative cooling pads, heaters, feeding and manure cleaning facilities in the poultry house together form the local area network system in the house. This section mainly reports the information transmission methods, local transmission strategies, and configuration of network nodes in poultry houses.

Data transmission between the poultry house and the house environmental control system is primarily provided by a suitable wired communication system, such as a fieldbus. There are some disadvantages (e.g. configure too many network endpoints, device address assignment rules and other issue) in using a full wireless system. Therefore, the local area network in the house uses a wireless/wireline hybrid construction (Mirabella and Brischetto, 2011). As shown in Table 1, among the three commonly used wireless transmission modes (i.e., Bluetooth, Wi-Fi and ZigBee), the Wi-Fi technology has the longest transmission distance and the fastest transmission speed (Challoo et al., 2012), therefore, Wi-Fi technology was selected as the wireless transmission method in the poultry house selects.

Table 1. Comparison of three commonly wireless transmission methods.

Transmission modes	Frequency band	Transmission distance	Power dissipation	Transmission rate
Bluetooth	2.4 GHz	2–30 m	20 mA	1 Mbps
Wi-Fi	2.4 GHz	100–300 m	10–50 mA	11–54 Mbps
ZigBee	2.4 GHz	50–300 m	5 mA	100 Kbps

Since there are many data transmission devices placed in the poultry house, it is necessary to set a routing node in the poultry house, to forward the network data package to the cloud database. Figure 2 shows the local transmission strategy of the routing node, taking into account the network factors such that the system data security is improved.

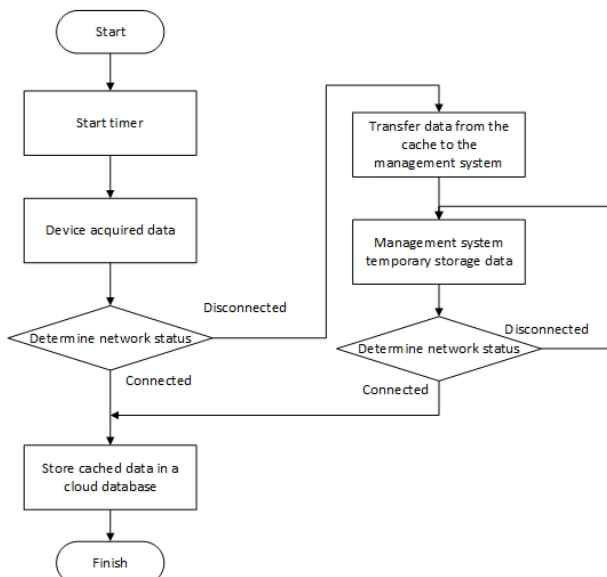


Figure 2. Flow chart of the local transmission strategy.

## 2.2. Cloud database

Alibaba Cloud Database RDS service was used in the system as it has a good visual operation

interface and numerous auxiliary analysis tools. It can generate database-related files such as E-R diagrams and data dictionary with one click, and it can also generate test data to ensure the test work during database development. The database uses a relational database, and the database version is MySQL5.7. As the core hub of poultry farming information management system, cloud database should carry out requirements analysis, concept design, logical structure design, construction E-R model, design table structure and primary-foreign key relationships in the process of design and construction. The intranet address of the system can be accessed by Alibaba Cloud Server, which has the advantages of fast reading speed and convenient setup. The external network address can be accessed by Internet users with access rights, and the database can be read and written. In the design stage, the selected database memory is 1024MB, 1 core CPU, the storage capacity is 20GB, and the maximum number of connections is 2000. It is confirmed in the actual development test that this configuration can meet the development needs.

### 2.3. Upper management system

The management system uses the C++ language as the main development tool, the latest Qt5 framework as an open source support library, and the Qt Creator as an IDE (Integrated Development Environment) for compilation and development. Figure 3 shows the functional framework of the poultry farming management system. The whole system is divided into four functional modules. The production management module mainly realizes the monitoring of environmental parameters in the poultry house, the monitoring of the growth information of individual poultry, and the management of the production operations in the poultry house. The office management module mainly fulfills the business tasks such as personnel management, financial management, and invoicing. The expert system module combines artificial intelligent technology such as data mining and machine learning to (1) realize egg shape index analysis; (2) provide feeding standards, breeding recommendations, mortality analysis and other functions, and (3) realize poultry disease diagnosis and early warning system based on audio and image analysis of poultry (Zhuang et al., 2018; Huang et al., 2019; Tiemin and Huang, 2019; Zhuang and Zhang, 2019). Modules are functionally independent, with data sharing capability.

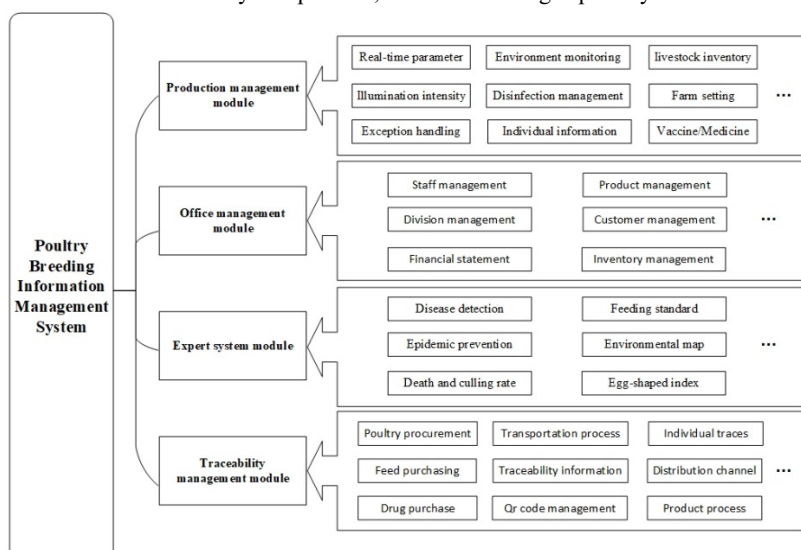


Figure 3. Functional framework of the poultry farming information management system.

### 3. Results and Discussion

#### 3.1. Management system implementation

The process of constructing the poultry farming information management system could be modularized, constructed and tested one by one. First, a comprehensive platform for the management system can be built, and the functional modules for subsequent development can, then, be assembled. Figure 4 illustrates the home page of the production management function module.

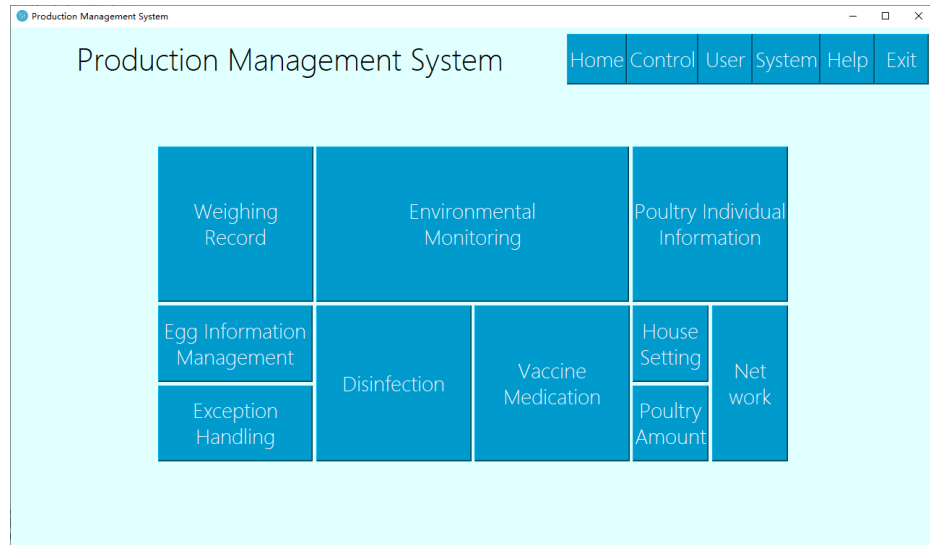


Figure 4. Production Management System Home.

The production management module collects real-time monitoring data of environmental parameters and individual hen production information. The data in the cloud database may be displayed in real time in the management system, as shown in Figure 5 and Figure 6. The first part of Figure 5 shows the coordinates ( $x, y$  position) where the environment parameters data are collected, and the second part is the measured environment parameter data at the specific location. Figure 6 shows the data information displayed in the form of a line chart. More specifically, at the (a) part in the figure, one can select the type of graphic and switch the specific environmental parameter type, at the (b) part in the figure, one can query and display the data according to the precise conditions, and at the (c) part in the figure, one can switch between the data table and the graphical display status.

#### 3.2. Construction of poultry breeding management system

Designing a comprehensive and practical poultry farming information management system, requires research on three aspects: (1) hardware design and networking of the underlying device, (2) database design and communication related issues, and (3) upper client software design.

LANs and servers should be deployed in poultry houses, and the use of wireless sensor networks (WSN) leads to low-cost and low-power deployments, making them the dominant choice (Garcia-Sanchez et al., 2011). The sensor is communicated as a child node in the local area network, and the data is connected to the external network through the server to upload the data to the cloud database for storage and query. The data format, transmission protocol, packet loss rate during transmission, and transmission strategy when network failure occurs should be further studied. Environmental monitoring in poultry houses is the top priority to address animal welfare. The system constructed in this study can be effectively managed from monitoring, transmission

and storage, visual display and control processes to seek the requirements for animal welfare.

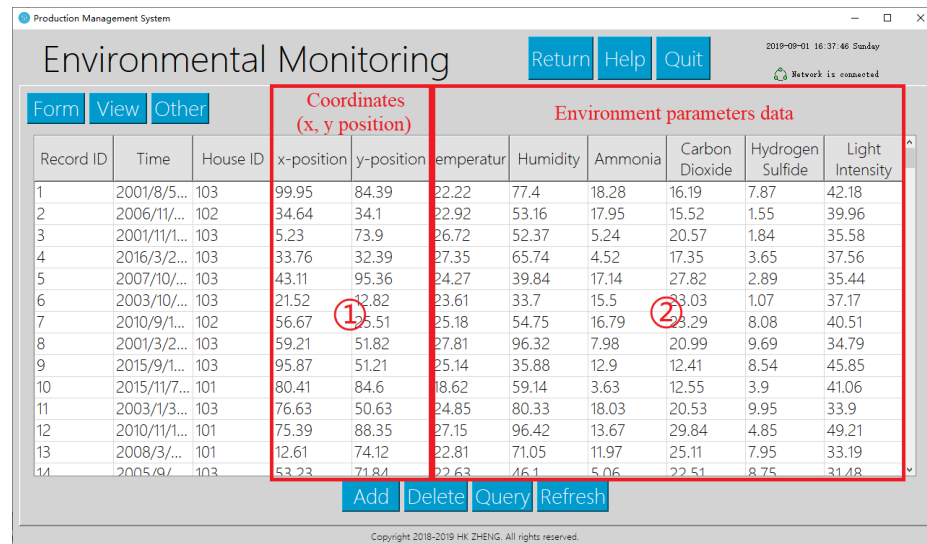


Figure 5. Environmental parameter display (Tabular presentation).



Figure 6. Environmental parameter display (Graphic display).

This study also includes the traceability of the poultry farming management system. The traceability system is a record-keeping system designed to track the flow of product or product attributes through the production process or the supply chain (Sallabi et al., 2011). This paper proposes a method of accurate traceability: through an accurate traceability of relevant information such as feed suppliers, accompanying manifests, distributors, and individual growth records stored in the management system database, more traceable traceability results can be obtained.

This paper reports the research work that was just started. How to effectively manage the massive information generated in the system is the primary goal of the future development. Through good monitoring and proper storage of data, data mining technology can be used to diagnose poultry disease and provide early warning opportunities. Moreover, using cloud database as the core hub in this study could also help with optimization of breeding environment and breeding methods.

#### 4. Conclusions

In order to meet the efficient management and the welfare of animal breeding of different scale poultry farm, this paper establishes a poultry farming information management system based on cloud database, which real-time monitoring of environmental information, poultry behavior information, and dietary information in poultry houses are integrated into the system. If successful, the system may meet the business needs of poultry industry in environmental monitoring of poultry houses, monitoring of individual growth information, disease monitoring and early warning, traceability and daily enterprise office management, and at the same time, the data information generated during the production process has been well managed, and the poultry breeding process is informationized and intelligent.

#### Acknowledgements

This work was supported by National key research and development plan [grant No. 2018YFD0500705] and Guangdong Province Special Fund for Modern Agricultural Industry Common Key Technology R&D Innovation Team [grant No. 2019KJ129], China.

#### References

- Challoo, R., A. Oladeinde, N. Yilmazer, S. Ozcelik, L. Challoo, 2012. An Overview and Assessment of Wireless Technologies and Co- existence of ZigBee, Bluetooth and Wi-Fi Devices. Procedia Computer Science. 12, 386–391. <http://dx.doi.org/10.1016/j.procs.2012.09.091>.
- Garcia-Sanchez, A.-J., F. Garcia-Sanchez, J. Garcia-Haro, 2011. Wireless sensor network deployment for integrating video-surveillance and data-monitoring in precision agriculture over distributed crops. Computers and Electronics in Agriculture. 75 (2), 288–303. <http://doi.org/10.1016/j.compag.2010.12.005>.
- Huang, J., W. Wang, T. Zhang, 2019. Method for detecting avian influenza disease of chickens based on sound analysis. Biosystems Engineering. 180, 16–24. <http://doi.org/10.1016/j.biosystemseng.2019.01.015>.
- Irvine, R.M., 2015. A conceptual study of value chain analysis as a tool for assessing a veterinary surveillance system for poultry in Great Britain. Agricultural Systems. 135, 143–158. <http://dx.doi.org/10.1016/j.agsy.2014.12.007>.
- Mirabella, O., M. Brischetto, 2011. A Hybrid Wired/Wireless Networking Infrastructure for Greenhouse Management. Ieee Transactions on Instrumentation and Measurement. 60 (2), 398–407. <http://dx.doi.org/10.1109/tim.2010.2084250>.
- Sallabi, F., M. Fadel, A. Hussein, A. Jaffar, H. El Khatib, 2011. Design and implementation of an electronic mobile poultry production documentation system. Computers and Electronics in Agriculture. 76 (1), 28–37. <http://dx.doi.org/10.1016/j.compag.2010.12.016>.
- So-In, C., S. Poolsanguan, K. Rujirakul, 2014. A hybrid mobile environmental and population density management system for smart poultry farms. Computers and Electronics in Agriculture. 109, 287–301. <http://dx.doi.org/10.1016/j.compag.2014.10.004>.
- Tiemin, Z., J. Huang, 2019. Detection of chicken infected with avian influenza based on audio features and fuzzy neural network. Transactions of the Chinese Society of Agricultural Engineering. 35 (02), 168–174.
- Yu, L., G. Teng, G.L. Riskowski, X. Xu, W. Gu, 2018. Uncertainty analysis of a web-based data acquisition system for poultry management with sensor networks. Engenharia Agricola. 38 (6), 857–863. <http://dx.doi.org/10.1590/1809-4430-Eng.Agric.v38n6p857-863/2018>.
- Zhuang, X., M. Bi, J. Guo, S. Wu, T. Zhang, 2018. Development of an early warning algorithm to detect sick broilers. Computers and Electronics in Agriculture. 144, 102–113. <http://dx.doi.org/10.1016/j.compag.2017.11.032>.
- Zhuang, X., T. Zhang, 2019. Detection of sick broilers by digital image processing and deep learning. Biosystems Engineering. 179, 106–116. <http://dx.doi.org/10.1016/j.biosystemseng.2019.01.003>.

## Effects of Different Claw Shortening Devices on Claw Condition, Fear, Stress and Feather Coverage of Layer Breeders

Haipeng Shi<sup>a,b</sup>, Baoming Li<sup>a,b,c</sup>, Qin Tong<sup>a,b,c</sup>, Weichao Zheng<sup>a,b,c,\*</sup>

<sup>a</sup> College of Water Resources and Civil Engineering, China Agricultural University,  
Beijing 100083, P.R. China

<sup>b</sup> Key Laboratory of Agricultural Engineering in Structure and Environment,  
Ministry of Agriculture and Rural Affairs, Beijing 100083, P.R. China

<sup>c</sup> Beijing Engineering Research Center on Animal Healthy Environment, Beijing 100083, P.R. China

\* Corresponding author. Email: [weichaozheng@cau.edu.cn](mailto:weichaozheng@cau.edu.cn)

### Abstract

Natural mating colony cage systems for layer breeders have been widely adopted by many commercial farms in China. However, the environment of such system is still relatively barren, enrichment devices such as claw abrasives may be required for improvement. Hens living in wire cages lack the opportunity to abrade their claws, resulting in uncontrolled claw growth. The objective of this study was to investigate the effects of claw abrasive devices (CADs) on claw length and sharpness, foot health, feather coverage, and physiological stress and mortality of the layer breeders. Three different CADs were investigated: abrasive strips (T1), metal plates with holes (T2), and rubber mats with grooves (T3); cages without CADs acted as controls (T4). Twelve replicates were used for each treatment with a total of 48 identical cages as the experimental units. Results showed that CADs had significant effects on claw length and sharpness of both hens and roosters. Birds in the T1 group had the shortest claw length and bluntest claw sharpness at 22, 32, 42 and 52 wk of age ( $P < 0.05$ ). The T1, T2 and T3 had higher scores for claw condition and significantly better overall plumage condition on the back and rump than T4 ( $P < 0.05$ ). No significant differences were found between treatments in concentration of triiodothyronine, thyroxine or 5-HT, except a significantly higher concentration of corticosterone in T4 as compared to T1, T2 and T3 ( $P < 0.05$ ). Overall mortality and mortality from cannibalism were both significantly higher in T4 than in T1, T2 and T3 ( $P < 0.05$ ). In conclusion, hens with access to CADs during the laying period had shorter and blunter claws, less damaged plumage, a lower plasma corticosterone secretion and mortality rate and were less fearful.

**Keywords:** Claw, colony cage, layer breeder, fear, stress, claw abrasive devices (CADs)

### 1. Introduction

Due to increasing consumer concern for animal welfare and growing labor costs, natural mating colony cage systems for parent-stock (PS) layer breeders have been widely adopted by many commercial farms in China. In these systems, more activity space is provided and the hens can express their natural mating behavior. However, compared with furnished-colony cages or aviary system for commercial laying hens, the environment of the natural mating colony cage systems is still relatively barren, Hens living in wire cages lack the opportunity to abrade their claws, resulting in uncontrolled claw growth (Tauson, 1986). In some case, the middle claw can grow from 18 mm to 30 mm by the end of cage-based laying (Glatz, 2004), enrichment devices such as nest boxes, perches and claw abrasives can be provided to improve the living environment in these systems (Habig and Distl, 2013).

When they become long and sharp, the claws can cause skin abrasions or scratches on their flock mates, particularly during periods of disturbance (Ruszler and Quisenberry, 1979). Hens may try to escape from the cage because of these disturbances, resulting in serious injuries to other hens using their claws. Consequently, pain from injury may cause stress or hysteria (Honaker and Ruszler, 2004). In addition, PS hens in natural mating colony cages are confined together with roosters. If the roosters' claws are long and sharp, they may damage the hens' backs, causing injuries, scratches, and damage to feathers during the frequent mating behaviors (Moyle et al.,

2010). There is a risk of severe feather pecking and cannibalism, especially if there is hemorrhage, broken skin and fresh wounds. Severe injury can even result in death or euthanasia (Savory, 1995). Longer claws may also cause an accident if they become caught in the cage (Honaker and Ruszler, 2004), possibly trapping the hen, which can lead to death (Glatz, 2002).

In practice, claw removal is commonly used to prevent greater growth of claws. Declawing has been reported to increase egg production (Ruszler and Quisenberry, 1979), improve feather coverage condition and effectively reduce mortality and hysteria (Compton et al., 1981). However, because of public concern towards animal welfare, declawing becomes a controversial management practice. Compton et al. (1981) reported that claw removal decreased the support of the foot on the cage wire, leading to poor foot condition. Neuromas have been reported in the toes of domestic fowl after declawing, and tissue and bone damage resulting from claw removal can potentially contribute to long term chronic pain (Gentle and Hunter, 1988). In some European countries, declawing has been prohibited. Another low-cost and non-invasive method to keep the claws of hens short and blunt is to provide claw abrasive devices (CADs) in cages. Commonly-used CADs include abrasive strips, abrasive paint, metal plates with filings, glue and sand (Glatz, 2002). However, results of previous studies about the effects of CADs on feather condition and mortality from prolapse and cannibalism were not consistent. Limited studies have been conducted on the use of CADs in natural mating colony cages for layer breeders.

The objective of this study was to determine the effect of 3 types of CADs (abrasive strips, metal plates with holes and rubber mats with grooves) on claw length and sharpness, feather pecking and feather coverage condition, foot health condition, fear and physiological stress and mortality from cannibalism for layer breeders in natural mating colony cages.

## 2. Materials and Methods

### 2.1. Birds, housing and care

The experiment was performed in a commercial PS layer breeder house (Huayu Poultry Breeding Co. Ltd., Handan, Hebei province, China), which can accommodate approximately 28,000 birds. Chicks (beak-trimmed Hy-Line Browns) were cage-reared in a different house following standard management practice and then transferred into natural mating colony cages in the experimental house at 16 wk. The house was 104 m × 12 m × 6 m (length × width × height), with 4 rows of 4-tier double-sided natural mating colony cages (304 cages in all) along the length of the house. Each cage was 4.80 m × 1.20 m × 0.71 m (L × W × H) and held 10 roosters and 90 laying hens together, with a floor area of approximately 576 cm<sup>2</sup> per bird. Feed was automatically distributed 4 times a day at 07:00, 11:00, 15:00 and 19:00 to ensure that birds had permanent ad libitum access to feed. Eggs were collected on conveyor belts and manure was removed from the house once a day using a belt system. The pullets were given 8 h of light at 16 and 17 wk per day. Light duration was then increased by 2 h at 18 wk, followed by 30-min increments per week until 16 h of light was given per day at 30 wk. At this stage, the light was switched on at 04:30 h and off at 20:30 h (16L:8D). The light intensity was about 5 lx at the height of the birds in the colony-cages. The average air temperature in the house was maintained between 16 °C and 23 °C during the experiment. All birds were subjected to the same standard management regime throughout the experiment.

This experiment involved 48 identical cages of the fourth tier in the house. They were divided into 4 different treatments (T1 to T4), which were compared in a random design. Three cages per treatment were distributed in the first, middle and last section of each row, giving a total number of 12 replicates for each treatment. The arrangements of the CADs can be seen in Figure 1. As shown in Table 1, the treatment cages were each provided with 16 CADs 10 cm W × 50 cm L, which were: abrasive strips (T1), a long rubber mat with grooves (T2) and metal plates with 3 mm diameter holes (T3). The T4, which was not equipped with any abrasives, acted as the control. The egg baffle was fixed on the rear of the feed trough, and the angle between the baffle and the bottom net was 60°. Before fixing the abrasives to the metal sheet egg baffle, it was scrubbed with

ethyl alcohol and allowed to dry (Figure 2)

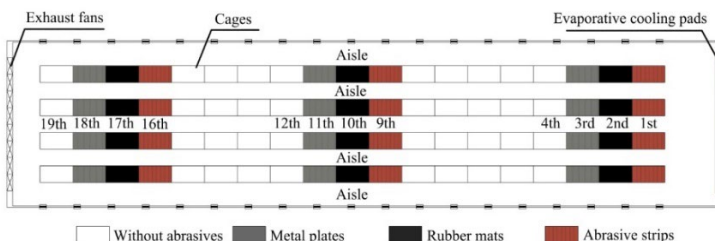


Figure 1 Schematic diagram of CADs arrangements of the fourth-tier cages

Table 1. Experimental treatments and measurement samplings.

Item	T1	T2	T3	T4
CADs <sup>1</sup>	AS <sup>2</sup>	RM <sup>3</sup>	MP <sup>4</sup>	No <sup>5</sup>
Measurement samplings				
Claw length and sharpness	12 hens and 6 roosters cage <sup>-1</sup> , at 16, 22, 32, 42 and 52 wk			
Plumage condition		12 hens cage <sup>-1</sup> , at 52 wk		
Blood parameters		3 hens cage <sup>-1</sup> , at 53 wk		

<sup>1</sup>CADs = claw abrasive devices; <sup>2</sup>AS = abrasive strip, <sup>3</sup>RM = rubber mat, <sup>4</sup>MP = mental plate;

<sup>5</sup>No = without nests or CADs



Figure 2. Schematic diagram of the cage and position of the CADs.

## 2.2. Claw length and sharpness

In each cage, the length and sharpness of the middle claws of 12 marked hens and 6 roosters were measured using photographs. At the age of 16, 22, 32, 42 and 52 wk, images of the claws were acquired through a camera fixed to a bracket. The toe portion was cropped out from the original photograph to a 10 cm × 10 cm sized picture by Photoshop CS6 (Adobe, USA). Then, the cropped image was imported into SketchUp 2014 (GoogleLLC, USA), which was used to measure the length and sharpness of the toes. The actual length and sharpness were transferred from the measurement in the cropped image by the ratio of image size to real length.

## 2.3. Feather coverage condition

The feather coverage condition of the 12 marked hens in each experimental cage was assessed at the age of 52 wk. The whole body of the bird was divided into 11 regions: head, upper neck, back, rump, tail, belly, breast, under-neck, legs, wings: primary feathers and wings: coverts (Bilcik and Keeling, 1999). To inspect feather condition, hens were taken individually from the cages and all 11 areas were carefully examined for damaged, broken and missing feathers. Feather damage of each part of the body was assessed using a 3-point scale: score 3: no or slight wear, (nearly) complete feathering (only single feathers lacking); score 2: moderate wear, i.e. damaged feathers (worn, deformed) or one or more featherless areas < 5 cm in diameter at the largest extent; score 1: at least one featherless area ≥ 5 cm in diameter at the largest extent (Welfare Quality, 2009).

## 2.4. Blood parameters and mortality

Blood samples were collected 1 week after the fear tests at the age of 53 wk. Three hens from

each cage (144 birds in total) were randomly selected between 13:00 and 18:00. The time between catching and sampling was recorded to ensure each sample were obtained within 2 min. Blood collection was cyclically conducted from T1 to T4 (12 cycles in total). Blood was drawn from the wing vein and collected into 2-mL EDTA tubes and then immediately stored on ice. Basal plasma concentrations of corticosterone, thyroxine (T4), triiodothyronine (T3) and 5-hydroxytryptamine (5-HT) were measured. During the experiment, the numbers of dead hens in all treatment groups were recorded, and each dead bird was assessed to determine if death was due to cannibalism.

## 2.5. Statistical analysis

All statistical analyses were performed using linear mixed models parameterized with SPSS (IBM SPSS Statistics 22.0, Armonk, USA). The data were analyzed with the fixed effects of claw abrasive devices, weeks of age, two-way interaction and the random effect of cage. For the traits except claw length and sharpness, the effect of age and its interaction with claw abrasive device was excluded. Effects in the statistical model were tested simultaneously and the effects were removed from the original model when they were not significant. When the effect was statistically different ( $P < 0.05$ ), further analysis was needed. Duncan's Multiple Range (LSD) test was applied for post-hoc group comparisons.

## 3. Results

### 3.1. Claw length and sharpness

Figure 3 and Figure 4 show the results and analysis of variation of claw length and sharpness in hens and roosters for the 4 groups. There was a significant effect of CADs on both claw length and sharpness: Average length reductions of 11.71 mm, 4.29 mm and 5.53 mm; and sharpness reductions of 1.52 mm<sup>-1</sup>, 0.74 mm<sup>-1</sup> and 0.92 mm<sup>-1</sup> were achieved by using abrasive strips, rubber mats with grooves and metal plates with holes, respectively. The birds using the abrasive strip (T1) had the shortest claw length and bluntest claw sharpness at all 4 ages ( $P < 0.05$ ). There was no significant difference in claw length of birds between T2 and T3. Claw lengths of birds in groups T2 and T3 were significantly shorter ( $P < 0.05$ ) than T4, except for roosters in T2 and hens in T2 and T3 at the age of 22 wk. Claw sharpness of birds in groups T2 and T3 were lower than that in T4 ( $P < 0.05$ ). There was no significant difference in claw sharpness for roosters between T2 and T3, but significant differences were found for hens between T2 and T3 at the age of 22, 42 and 52 wk. It was noticed that there was a gradual increase in claw length and sharpness with age in T2 and T3, while claw length and sharpness in T1 decreased with age until 52 wk, where the value was lower than in T2 and T3.

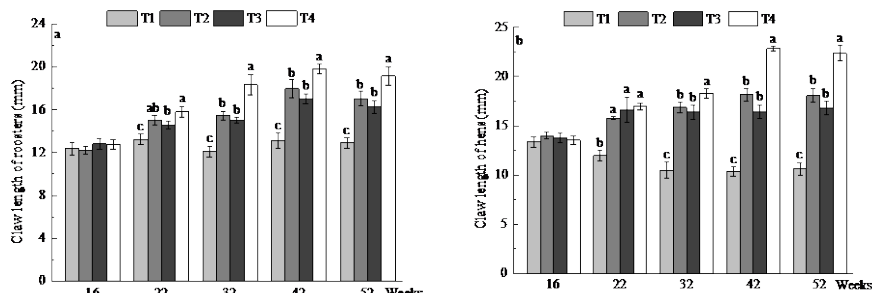


Figure 3. Claw length of hens (left) and roosters (right) at 16, 22, 32, 42 and 52 wk for the treatment groups and control. Values shown are means  $\pm$  SE. Within the same age group, no common superscript letter denotes a significant difference ( $P < 0.05$ ).

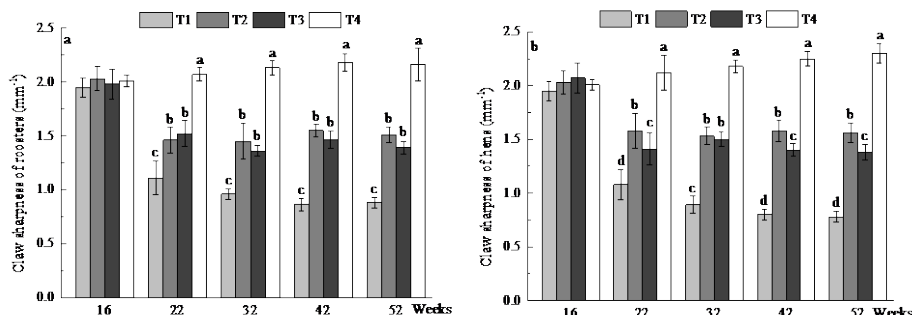


Figure 4. Claw sharpness of hens (left) and roosters (right) at 16, 22, 32, 42 and 52 wk for the treatment groups and control. Values shown are means  $\pm$  SE. Within the same age group, no common superscript letter denotes a significant difference ( $P < 0.05$ ).

### 3.2. Feather coverage condition

As shown in Table 2, no significant differences were found in feather coverage scores in the head, neck, coverts, legs, breast and under neck among the 4 groups, although hens in T1, T2 and T3 had a significantly better plumage condition on the back and rump than hens in T4 ( $P < 0.05$ ). For plumage coverage condition, the tails of hens in T1 and T3, the belly of hens in T2 and wing-primary of hens in T1 were better than hens in T4. In general, birds given CADs had significantly higher overall feather coverage condition than hens with no abrasives devices ( $P < 0.05$ ).

Table 2. Feather scores of 11 body parts of hens at 52 wk of age for the treatment groups and control<sup>1</sup>.

Body part	Feather scores (3-point scale)				LSD <sup>2</sup>
	T1	T2	T3	T4	
Head	2.83 $\pm$ 0.11	2.67 $\pm$ 0.14	2.75 $\pm$ 0.13	2.75 $\pm$ 0.13	NS <sup>3</sup>
Neck	2.83 $\pm$ 0.11	2.75 $\pm$ 0.13	2.67 $\pm$ 0.19	2.92 $\pm$ 0.21	NS
Back	2.67 $\pm$ 0.14 <sup>a</sup>	2.39 $\pm$ 0.18 <sup>a</sup>	2.42 $\pm$ 0.19 <sup>a</sup>	2.05 $\pm$ 0.22 <sup>b</sup>	1.31
Rump	2.42 $\pm$ 0.19 <sup>a</sup>	2.08 $\pm$ 0.23 <sup>b</sup>	2.17 $\pm$ 0.17 <sup>ab</sup>	1.67 $\pm$ 0.19 <sup>c</sup>	1.30
Tail	2.92 $\pm$ 0.08 <sup>a</sup>	2.75 $\pm$ 0.18 <sup>ab</sup>	2.83 $\pm$ 0.11 <sup>a</sup>	2.33 $\pm$ 0.17 <sup>b</sup>	1.37
Belly	2.75 $\pm$ 0.18 <sup>ab</sup>	2.92 $\pm$ 0.19 <sup>a</sup>	2.83 $\pm$ 0.11 <sup>ab</sup>	2.58 $\pm$ 0.22 <sup>b</sup>	1.40
Coverts	2.92 $\pm$ 0.11	2.75 $\pm$ 0.08	2.83 $\pm$ 0.14	2.67 $\pm$ 0.23	NS
Primary	2.92 $\pm$ 0.08 <sup>a</sup>	2.67 $\pm$ 0.17 <sup>ab</sup>	2.83 $\pm$ 0.11 <sup>ab</sup>	2.58 $\pm$ 0.08 <sup>b</sup>	1.36
Legs	2.83 $\pm$ 0.11	2.92 $\pm$ 0.29	2.75 $\pm$ 0.13	2.50 $\pm$ 0.11	NS
Breast	2.35 $\pm$ 0.13	2.33 $\pm$ 0.19	2.42 $\pm$ 0.19	2.42 $\pm$ 0.14	NS
Under neck	2.25 $\pm$ 0.45	2.08 $\pm$ 0.29	1.92 $\pm$ 0.08	2.17 $\pm$ 0.11	NS
Total score	2.72 $\pm$ 0.06 <sup>a</sup>	2.55 $\pm$ 0.07 <sup>a</sup>	2.57 $\pm$ 0.09 <sup>a</sup>	2.11 $\pm$ 0.11 <sup>b</sup>	1.34

<sup>1</sup>Values shown are means  $\pm$  SE; <sup>2</sup>LSD: least significant difference; <sup>3</sup>NS: not significant in analysis of variance; T1, T2 and T3: groups given abrasive strips, long rubber mats with grooves and metal plates with 3 mm diameter holes, respectively. T4 was not equipped any abrasives as the control; <sup>a, b, c</sup> Means within a column with no common superscript letter are significantly different ( $P < 0.05$ )

### 3.3. Blood parameters and mortality

As shown in Table 3, the only significant difference in blood parameters between groups was the significantly higher concentration of corticosterone in T4 than in T1, T2 and T3 ( $P < 0.05$ ). Mortality from cannibalism was significantly higher in T4 than in T1, T2 and T3 ( $P < 0.05$ ).

Overall mortality tended to be lower in birds with CADs than birds without access to these devices.

Table 3. Blood parameters at 53 wk of age and mortality from 22 wk to 52 wk<sup>1</sup>.

Test variable	Treatments				LSD <sup>2</sup>
	T1	T2	T3	T4	
<b>Blood parameters (ng ml<sup>-1</sup>)</b>					
Triiodothyronine	0.58±0.01	0.52±0.05	0.53±0.03	0.52±0.07	NS <sup>3</sup>
Thyroxine	14.19±1.19	15.50±1.54	13.90±0.82	16.62±2.10	NS
CORT	4.32±0.32 <sup>b</sup>	4.59±0.43 <sup>b</sup>	4.15±0.30 <sup>b</sup>	6.76±0.42 <sup>a</sup>	2.18
5-HT	29.82±4.37	26.31±5.27	30.40±4.41	26.87±5.99	NS
<b>Mortality (%)</b>					
Overall mortality	8.24 <sup>b</sup>	10.59 <sup>ab</sup>	9.41 <sup>b</sup>	14.12 <sup>a</sup>	2.23
Cannibalism	4.35 <sup>b</sup>	4.71 <sup>b</sup>	3.53 <sup>b</sup>	7.06 <sup>a</sup>	1.90

<sup>1</sup>Values shown are means ± SE, except mortality which is expressed as %; <sup>2</sup>LSD: least significant difference; <sup>3</sup>NS: not significant in analysis of variance; T1, T2 and T3: groups given abrasive strips, long rubber mats with grooves and metal plates with 3 mm diameter holes, respectively. T4 was not equipped any abrasives as the control; <sup>a, b, c</sup> Means within a column with no common superscript letter are significantly different ( $P < 0.05$ ).

#### 4. Discussion

##### 4.1. Foot condition, claw length and sharpness

As shown in Figure 3 and Figure 4, there was a clear effect of CADs on claw length and sharpness. Although claw length and sharpness were reduced by all three CADs, the abrasive strips adopted in the study were by far the most effective. The 11.71 mm length reduction obtained in this experiment were much greater than the 7.8 mm obtained by Glatz (2004) who used two 8 mm abrasive strips. This is probably due to the larger effective area of the abrasive strips provided in this experiment. In other non-cage systems, hens spend a great deal of their time foraging, including searching and scratching of the litter or soil seeking for food such as insects, seeds, grain or vegetative material, and this behavior can help to keep the claws short and blunt (Glatz, 2002). In colony cage systems, hens continue to demonstrate this high motivation to forage, even when they are provided with feed ad libitum (Pokharel et al., 2017). In this study, the hens were highly motivated to perform their foraging behavior by using their claws to scrape to against the CADs when they were fed. Two reasons may explain the significant differences in claw length and sharpness among the groups provided with CADs. First, the hens might use the abrasive strips fairly intensively through scratching with their claws on the opposite rear part of the feed trough. It was reported that the frequency of scratching on the feed trough with abrasive strips showed greater variation than for other abrasive materials (Tauson, 1986). The abrasive strips might be more attractive to birds and influence the frequency of scratches on the deflector. Secondly, the difference could be attributed to the abrasive efficiency of the materials' physical properties: the strip was more abrasive than the rubber mat or metal plate.

##### 4.2. Feather coverage condition

We noted that the neck, under neck and breast of the birds were in contact with the feed trough when they were being feed. In addition, extra wear on the head and wings resulting from contact with the cage was noted. In the present experiment, no significant differences were found among the treatment groups in feather coverage of the head, neck, coverts, breast or under the neck. In contrast, the cages without CADs had a significantly higher proportion of hens with feather damage on the back, rump and tail. The overall body coverage condition of hens with CADs tended to be higher, consistent with Roll et al. (2008) who found that laying hens with CADs had quantitatively better plumage quality. It is also in agreement with some results from Compton et al. (1981 b), who reported that total body plumage condition tended to be better in hens with

abrasives.

Several possible reasons could account for why CADs improved the feather condition of hens in this study. The PS hens in natural mating colony cages were confined together with roosters, and during copulation the roosters' long and sharp claws may contribute to poor back and rump feather cover (Jones and Prescott, 2000). Conversely, reduced claw length and sharpness would have minimized the influence of claws, as well as alleviating skin abrasions and scratches on their flock mates during periods of disturbance. Studies have shown that severe feather pecking is considered a major reason for poor plumage condition in hens (Bilcik and Keeling, 1999). Thus, it could be speculated that birds with the shortest and bluntest claws were less fear-stressed and engaged in reduced stereotyped pecking, leading to better feather cover. According to behavioral observations, the CADs appeared to be attractive to and sustain the interest of the hens: they pecked and scratched at the abrasives during the experiment. The hens consistently spent a longer time near the CADs and therefore transferred attention and pecking from conspecifics to the CADs. This might also account for the effect of CADs on feather condition.

#### 4.3. Blood parameters and mortality

Adrenal cortical and thyroid hormones are widely used as physiological indicators of stress in fowl (Gibson et al., 1986). In this study there were no significant differences in concentrations of thyroxine (T4), triiodothyronine (T3) and 5-HT between the groups given CADs. However, the plasma corticosterone concentrations of hens without access to abrasives were significantly higher than hens in cage with abrasives. This result expressed a consistent trend towards greater plasma corticosterone secretion in fearful hens, who showed long TI durations, a long avoidance distance and fear of the novel object in this study. A raised plasma corticosterone concentration has previously been associated with thirst, hunger, heat, fear, stress or a barren environment in laying hens (Franciosini et al., 2010). Fraise and Cockrem (2006) found that corticosterone responses and fearfulness were consistent with larger corticosterone responses to potentially threatening stimuli, and indicated a greater fearfulness. Results from Japanese quail, selected for low and high corticosterone responses to confinement, also support a correlation between corticosterone responses and fearfulness (Jones et al., 1994). The level of fearfulness increases with plasma concentrations of corticosterone during a corticosterone response when hens suffer fear stress (Cockrem, 2007). In summary, plasma corticosterone concentrations are positively correlated with the reactions of fear tests. In this experiment, hens without abrasives lived in a barren, unvaried and high pressure environment, which minimizes the opportunities for exploration behaviors and compromises birds' welfare by increasing fearfulness, depression and cognitive impairment. However, the degree of fear was not reflected accurately in the concentration of thyroxine, triiodothyronine and 5-HT, which may be because the situation is not straightforward in practice. The only accurate conclusion appeared to be that there are too many other uncontrolled factors exerting an effect to allow these variables to be used as simple and practical estimates of welfare.

Overall mortality and mortality from cannibalism tended to be lower in cages with CADs, which was in agreement with the results of previous studies that abrasive strips could reduce mortality of hens (Goodling et al., 1984; Ruszler and Quisenberry, 1979). However, conflicting results were observed by Tauson (1986), who reported that mortality is not affected by the use of abrasive strips; and Glatz (2004), who showed that cannibalism and mortality increased when abrasives were used. Honaker and Ruszler (2004) have also reported that declawing turkeys had a higher mortality compared to intact turkeys (1.87% vs 0.97%). The contradiction between different studies may be due to a complex interaction with a number of other environmental variables. In this study, it was hypothesized that, for PS layer breeders in cages without abrasives, copulation behavior may result in poor back and rump feather coverage and that hens may suffer from injuries or scratches. In addition, the longer and sharper claws of hens might also lead to skin abrasions or scratches on their flock mates particularly during periods of disturbance. There

is a risk of severe feather pecking and cannibalism, especially if there was hemorrhage, broken skin and fresh wounds.

### 5. Conclusions

In summary, the results of this study indicated that CADs used in colony cages for layer breeders could effectively reduce claw length and sharpness. Hens with access to CADs during the laying period had shorter and blunter claws, less damaged plumage, were less fearful and susceptible to TI, NO and AD tests and had a lower plasma corticosterone secretion and mortality rate. Such information contributes to our understanding of the behaviors and stress sensitivity of PS laying breeders. From the point of economic cost, the durability and ease of installation of abrasive strips makes them suitable as CADs in the natural mating colony cage for layers.

### Acknowledgements

The study was supported by the National Key R&D Program of China (2018YFD0500700) and the China Agricultural Research System (CARS-40). We acknowledge the manager and staff of Hebei Huayu Poultry Breeding Co. Ltd., Handan, Hebei, China. The help and support of colleagues at the department of Agricultural Bioenvironmental and Energy Engineering during the project was also appreciated.

### References

- Bilcik, B., L.J. Keeling. 1999. Changes in feather condition in relation to feather pecking and aggressive behaviour in laying hens. *British Poultry Science*. 40 (4), 444–451.
- Cockrem, J.F. 2007. Stress, corticosterone responses and avian personalities. *Journal of Ornithology*. 148 (2 supplement), 169–178.
- Compton, M.M., H.P.V. Krey, P.L. Ruszler, F.C. Gwazdauskas. 1981. The effects of claw removal and cage design on the production performance, gonadal steroids, and stress response in caged laying hens. *Poultry Science*. 60 (9), 2127–2135.
- Fraisse, F., J.F. Cockrem. 2006. Corticosterone and the measurement of stress and fear in cage housed laying chickens. *British Poultry Science*. 47 (2), 110–119.
- Franciosini, M.P., C. Canali, P.C. Projetti, O. Tarhuni. 2010. Plasma corticosterone levels in laying hens from three different housing systems: preliminary results. *Italian Journal of Animal Science* 4:276–278.
- Gentle, M.J., L.H. Hunter. 1988. Neural consequences of partial toe amputation in chickens. *Research in Veterinary Science Vet.* 45 (3), 374–376.
- Gibson, S.W., B.O. Hughes, S. Harvey, P. Dun. 1986. Plasma concentrations of corticosterone and thyroid hormones in laying fowls from different housing systems. *British Poultry Science*. 27 (4), 621–628.
- Glatz, P.C. 2002. Claw Abrasives in Layer Cages - A Review. *International Journal of Poultry Science*. 1 (1), 1–5.
- Glatz, P.C. 2004. Effect of claw abrasives in cages on claw condition, feather cover and mortality of laying hens. *Asian Australasian Journal of Animal Science*. 17 (10), 1465–1471.
- Goodling, A.C., D.G. Satterlee, G.C. Cerniglia, L.A. Jacobsberry. 1984. Influence of toe clipping and stocking density on laying hen performance. *Poultry Science*. 63 (9), 1722–1731.
- Habig, C., O. Distl. 2013. Evaluation of bone strength, keel bone status, plumage condition and egg quality of two layer lines kept in small group housing systems. *British Poultry Science*. 54 (4), 413–424.
- Honaker, C.F., P.L. Ruszler. 2004. The effect of claw and beak reduction on growth parameters and fearfulness of two Leghorn strains. *Poultry Science*. 83 (6), 873–881.
- Jones, E.K.M., N.B. Prescott. 2000. Visual cues used in the choice of mate by fowl and their potential importance for the breeder industry. *World's Poultry Science Journal*. 56 (2), 127–138.
- Jones, R.B., A.D. Mills, J.M. Faure, J.B. Williams. 1994. Restraint, fear, and distress in Japanese quail genetically selected for long or short tonic immobility reactions. *Physiology and Behavior*. 56 (3), 529–534.
- Moyle, J.R., D.E. Yoho, R.S. Harper, R.K. Bramwell. 2010. Mating behavior in commercial broiler breeders: female effects. *The Journal of Applied Poultry Research*. 19 (1), 24–29.
- Pokharel, B.B., I. Boecker, I.Y. Kwon, L. Jeyachanthiran, P. McBride, A. Harlander-Matauscheck. 2017. How does the presence of excreta affect the behavior of laying hens on scratch pads?. *Poultry Science*. 97 (3), 743–748.
- Roll, V.F.B., R.C. Briz, G.A.M. Levrino, E.G. Xavier. 2008. Effect of claw shortening devices in laying hens housed in furnished cage. *Ciencia Animal Brasileira*, 9 (4), 896–901.

- Ruszler, P.L., J.H. Quisenberry. 1979. The effect of declawing two flock sizes of 23-week-old pullets on hysteria and certain production traits. *Poultry Science*. 58 (4), 778–784.
- Savory, C.J. 1995. Feather pecking and cannibalism. *World's Poultry Science Journal*. 51 (2), 215–219.

## Effects of Stocking Density and Toy Provision on Production Performance, Behaviour and Physiology of Growing Pigs

Yongzhen Li <sup>a,b</sup>, Chaoyuan Wang <sup>a,b,\*</sup>, Shiwei Huang <sup>a,b</sup>, Zuohua Liu <sup>c</sup>, Hao Wang <sup>c</sup>

<sup>a</sup> Department of Agricultural Structure and Biological Engineering, China Agricultural University, Beijing 100083, P.R. China

<sup>b</sup> Key Laboratory of Agricultural Engineering in Structure and Environment, Ministry of Agriculture and Rural Affairs, Beijing 100083, P.R. China

<sup>c</sup> Chongqing Academy of Animal Science, Chongqing 402460, P.R. China

\* Corresponding author. Email: [gotowchy@cau.edu.cn](mailto:gotowchy@cau.edu.cn)

### Abstract

An experiment with  $2 \times 3$  factorial (with/without toys  $\times$  three levels of stocking density) arrangement was conducted to evaluate the effects of stocking density and toy provision on production performance, behaviour and physiology of growing pigs from the 7<sup>th</sup> to 13<sup>th</sup> week of age, in order to determine the proper floor area for scaled pig production in China. Two hundred and sixteen pigs were randomly allocated to pens with the stocking densities of 0.5, 0.7 and 0.9 m<sup>2</sup> pig<sup>-1</sup>, and the group size in each pen was fixed at 18. The average daily gain (ADG) and feed conversion ratio (FCR) decreased significantly with decreased space allowance. Pigs housed in low space allowance spent more time on fighting and feeding, meanwhile less on lying and resting. As increasing of the space allowance per pig, the body surface temperature of pigs was significantly decreased. Toy provision inside the pens effectively reduced water consumption of pigs with high stocking density, while no statistical impact was observed on production performance, body surface temperature, and concentration of saliva cortisol. It is concluded that decreased stocking density is beneficial to the production performance and health of growing pigs. Toy provision can significantly reduce the abnormal behaviour of pigs in barren environment, which is conducive to reducing space requirement of growing pigs at commercial level. The stocking densities ranged of 0.7–0.9 m<sup>2</sup> pig<sup>-1</sup> with toy provision are suggested for intensive growing pig production.

**Key words:** Stocking density, environmental enrichment, performance, behaviour, physiology, growing pigs

### 1. Introduction

With increasing attention from public in past decades, legislations on animal welfare have been made and required to be implemented at commercial farming level worldwide. It has been stimulating the development of welfare friendly production systems with the purpose to replace the conventional ones for large-scale pig farming, for EU countries in particular. In such welfare friendly systems, group size of pigs and its space allowance are gradually expanding to meet commercial production requirement, and the welfare of pigs is generally improved by increasing shared spaces, environmental enrichment, etc.

Stocking density is an important technological index in modern livestock housing system, which is directly related to welfare level as well as the production cost, performance and health level of the livestock. Previous studies have demonstrated that restricted space allowance contribute to lower weight gain and feed conversion ratio and increased mortality (Edmonds et al., 1998; Oh et al., 2010), and the stocking density also affects aggressive, abnormal behavior and immune system of pigs (Hemsworth et al., 2013; Vermeer et al., 2014). But information of optimal stocking density at different growth stages of the welfare friendly production system is still very limited. Meanwhile, some countries require pig producers to enrich the environment of the pens, among which toy provision is a typical solution (European Council Directive 2001), and the effects of environmental enrichment on the performance and health of pigs have been widely explored. However, limited research has been conducted to evaluate the influence of

environmental enrichment on space allowance requirement of the pigs.

China is the largest pork producer and consumer in the world (Yi et al., 2016), and a series of standards, including stocking density codes on group housed pigs, have been made in the progress of intensification of pig farming (Construction for intensive pig farms, 2008). Compared with the detailed space allowance requirements based on the body weights in different growth stages of western countries, the recommended code on stocking density of pigs in China is more general, and the values are typically differed. In the national code of China, the space allowance of 0.8–1.2 m<sup>2</sup> pig<sup>-1</sup> is suggested for the pigs from growing to finishing stage in traditional group housing systems, while optimization work is highly needed under the condition of welfare farming development.

The objectives of the study were to reveal the interacting effects of stocking density and environmental enrichment on productivity, health and physiology of growing pigs in China, and try to find its proper space allowance with toy provision.

## 2. Materials and Methods

### 2.1. Animals, housing and management

The study was conducted at a growing-finishing pig house of Chongqing Academy of Animal Science, China, from August 8 to September 18, 2018. Indoor temperature during the trial was between 22 °C and 28 °C, and relative humidity (RH) was within 60% to 95%.

A 2 × 3 factorial (with/without toys × three levels of stocking density) arrangement was used with 2 replicates per treatment. A total of 216 crossbred pigs (Landrace × Yorkshire × Duroc, with initial weight of 23.5±3.7 kg at approximately 70 days of age) were housed in a growing-finishing pig house with partly slatted floor (45% slatted floor and 55% solid concrete floor). Based on trade standards of China, the pigs were allocated to 12 pens with 18 pigs each, at three levels of stocking density of 0.5, 0.7, 0.9 m<sup>2</sup> pig<sup>-1</sup> according to initial body weights and gender (1:1) of the pigs. The densities for the three treatments were realized by modifying the pens to the areas of 9.0, 12.6 and 16.2 m<sup>2</sup>, respectively. Four toys consisted of stellate rubber and iron chain (Hongzhixing Company, Wuhan City, China) were suspended inside each of the pen. Each pen was equipped with two plastic feeders and four bowl shaped drinkers to allow the pigs *ad libitum* access to food and water. Evaporative cooling pads and air-exhaust fans were installed to ventilate the house and control room temperature during the experiment. A mechanical scrapper system was installed inside the manure pits underneath the slatted floor to remove the manure out of the barn, and solid floor of the tested pens was manually cleaned at 07:00 and 16:00 h daily as well.

### 2.2. Production performance

Pigs of each pen were weighed in a group on a weekly basis, and the data was used to calculate the average daily gain (ADG) at a week interval. Food intakes were recorded daily to determine the average daily feed intake (ADFI) and feed/gain (F/G). Daily water consumption was recorded by an automatic flowmeter equipped inside each pen.

### 2.3. Behaviour

Behaviours of pigs were recorded during the 1<sup>st</sup>, 2<sup>nd</sup>, 7<sup>th</sup>, 35<sup>th</sup> day after grouping using a digital video system with a resolution ratio of 1280×960 (Dahua Technology, Zhejiang, China). In each of the pen, three marked pigs were selected based on the weights, and the time budget on lying, negative social behaviour (includes fighting, attacking and escaping), eating, drinking, and toy playing behaviours was manually recorded (the percentage of total observation time for pig's behaviours was calculated in the study). Behaviours of pigs were continuously observed for 10 minutes in every half an hour in daytime (06:00–20:00 h) and for 5 minutes in every hour in nighttime (00:00–06:00, 20:00–24:00). The detailed description of the behaviour was shown in Table 1.

Table 1. Description of behaviour of marked pigs.

Behaviour	Description
Lying	Lateral or ventral lying on the floor over 3s;
Fighting	Pigs violently bite or hit with head each other over 3s;
Attacking	Pig violently bites or hits others, while the one being attacked escapes;
Escaping	Pig is attacked by others and runs away;
Toy playing	Pig chews or sniffs toys suspended inside pens over 3s;
Feeding	Pig stands in front of feeder with head lowered in feed hopper over 3s;
Drinking	Pig stands in front of drinker with snout in water bowl over 3s.

## 2.4. Physiology

### 2.4.1. Body surface temperature (BST)

Previous studies have shown that pig eyes are promising location in terms of practicability for infrared camera (IRC) and infrared thermometer (IRT) measurement of body temperature (Schmidt et al., 2013). Thus, in this paper the BST of pigs was evaluated by measuring eye temperature using thermal infrared imagery (220s, Fotric, Germany). Six healthy pigs with the gender ratio of 1:1 per pen were randomly selected, and their eye temperatures were measured at 08:00–09:00, 11:00–12:00, 14:00–15:00 and 17:00–18:00 h on every Thursday during the test.

### 2.4.2. Concentration of salivary cortisol

Mixed saliva samples were collected by the cotton ropes fastened on the fence of pens between 09:00–10:00 a.m. of every Sunday during the trial. During the collection, the cotton ropes were chewed by pigs for about 5–10 min until the rope getting wet enough, and then the saliva samples were collected (with about 2 ml saliva each) and stored provisionally at -20 °C. Then the samples were transported to Nanjing Jiancheng Bioengineering Institute, China for the measurement of salivary cortisol concentration using radioimmunoassay method.

## 2.5. Statistical analysis

The data were analyzed and related charts were made in SPSS 22.0 (IBM, USA) and Excel 2016. The effects of stocking density, toy provision and their interaction as fixed effect were tested with analysis of variance and Duncan. Significance was declared at  $P<0.05$ .

## 3. Results and Discussion

### 3.1. Production performance

The production performance indices were shown in Table 2, including ADFI, ADG, F:G and average daily water consumption. Overall ADFI was not differed among different treatments; however, the ADG and F:G were significantly affected by stocking density in groups with toy provisions. The groups with the space allowance of 0.9 m<sup>2</sup> pig<sup>-1</sup> gained 6.5% and 9.0% more weight than that in 0.7 and 0.5 m<sup>2</sup> pig<sup>-1</sup> ( $P<0.01$ ) with toys. The F:G was statistically higher in high stocking density, and a similar trend was observed in groups without toy provision. Average daily water consumption in small pens without toys, related to “water playing” behaviour of pigs, was much higher than the other two groups ( $P<0.01$ ), while there was no significant difference in toy groups, suggesting that pigs performed more abnormal behaviours in the barren and crowded environment. Generally, the results indicated that the weight gain, food conversion was increased and water consumption decreased significantly with the increasing of space allowance, which is consistent with the results of previous studies (Kim et al., 2016; Zhang et al., 2013).

Regarding the three levels of stocking density, no statistically differences on ADFI, ADG and F:G of growing pigs were found among the groups with and without toy provisions. However, compared to the groups without toy, the ADGs of toy provisions in 0.5 and 0.7 m<sup>2</sup> pig<sup>-1</sup> were 4.3% and 1.6% bigger, while no considerable effect was observed in 0.9 m<sup>2</sup> pig<sup>-1</sup> group, which suggested that toy provision was conducive to promoting production performance of growing pigs, and its effect was enhanced with the decreasing of space allowance. A similar finding was found by Xi

et al. (2007), showing that the ADG of the growing-finishing pigs housed inside toy provision pens was 10.84% higher than the groups without toys. Furthermore, effect of toy provision on production performance of pigs might be also affected by the number, and type of the toys. Water consumption of pigs greatly decreased with toy provision in crowded environment.

Table 2. Effect of stocking density on production performance of the growing pigs with/without toy provisions.

Toy provision	Stocking density ( $\text{m}^2 \text{ pig}^{-1}$ )	ADFI (kg $\text{pig}^{-1} \text{ d}^{-1}$ )	ADG (kg $\text{pig}^{-1} \text{ d}^{-1}$ )	F:G	Water consumption (kg $\text{pig}^{-1} \text{ d}^{-1}$ )
Yes	0.5	1.780±0.389	0.733±0.119 <sup>Bb</sup>	2.71±1.36 <sup>a</sup>	13.9±4.4
	0.7	1.737±0.362	0.750±0.112 <sup>ABb</sup>	2.49±0.67 <sup>ab</sup>	14.9±5.1
	0.9	1.823±0.400	0.799±0.070 <sup>Aa</sup>	2.39±0.68 <sup>b</sup>	15.2±7.8
	0.5	1.716±0.337	0.703±0.083 <sup>Bb</sup>	2.58±0.87	19.6±7.4 <sup>Aa</sup>
	0.7	1.774±0.383	0.738±0.100 <sup>ABb</sup>	2.50±0.69	13.4±5.5 <sup>Bb</sup>
	0.9	1.791±0.380	0.791±0.110 <sup>Aa</sup>	2.41±0.75	15.2±5.4 <sup>Bb</sup>

<sup>a</sup> Different letters indicate significant difference (A, B, C presents  $P<0.01$ ; a, b, c presents  $P<0.05$ ) in the same column.

### 3.2. Behaviour

#### 3.2.1. Toy playing

Figure 1 shows the percentage of the time budget in toy playing in the 1<sup>st</sup>, 2<sup>nd</sup>, 7<sup>th</sup> and 35<sup>th</sup> day after grouping. Pigs spent more time playing toys with the decreasing of pen size at the first 7 days after grouping. Afterwards, toy playing time of the pigs in 0.5  $\text{m}^2 \text{ pig}^{-1}$  was decreasing, while under the stocking density of 0.7 and 0.9  $\text{m}^2 \text{ pig}^{-1}$ , the duration showed a trend of quadratic relationship (decreased at 7<sup>th</sup> days and increased at the 35<sup>th</sup> day after grouping). It suggested that toy provision in bigger space allowance had stronger “freshness” and attraction to the pigs, but the effect weakened gradually for the groups with less space area as time went on. With the increasing of pen size, the space occupancy of toys decreased with a certain number of toys and the chance of pigs to contact with toys might be reduced, which led to the decreasing of toy playing time in the beginning of grouping compared to the pigs in higher stocking density, but the attraction of toys to the pigs lasted longer.

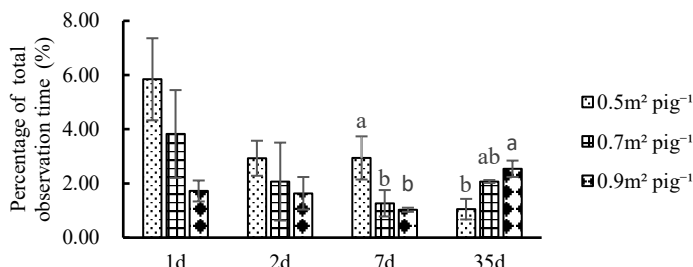


Figure 1. Percentage of total observation time for toy playing behaviour of pigs after grouping (Different letters means significant difference between stocking density groups).

#### 3.2.2. Negative social behaviour

In this research, the negative social behaviour of pigs mainly includes fighting, attacking and escaping. As shown in Figure 2, in the first 48 hr after grouping, more negative social behaviour of the pigs in 0.5  $\text{m}^2 \text{ pig}^{-1}$  groups without toy provision was performed, and the trend changed in

the 7<sup>th</sup> and 35<sup>th</sup> day after grouping. The negative social behaviour frequency was significantly reduced for pigs in groups with toy provision and 0.5 m<sup>2</sup> pig<sup>-1</sup> group without toys in the 7<sup>th</sup> day, and no significant difference between stocking density treatments in the 35<sup>th</sup> day was found. Generally, toy provision could significantly reduce the time budget of the negative social behaviour for pigs in the 1<sup>st</sup>, 2<sup>nd</sup>, 7<sup>th</sup> and 35<sup>th</sup> days after grouping among most groups, especially for the pigs with higher stocking density.

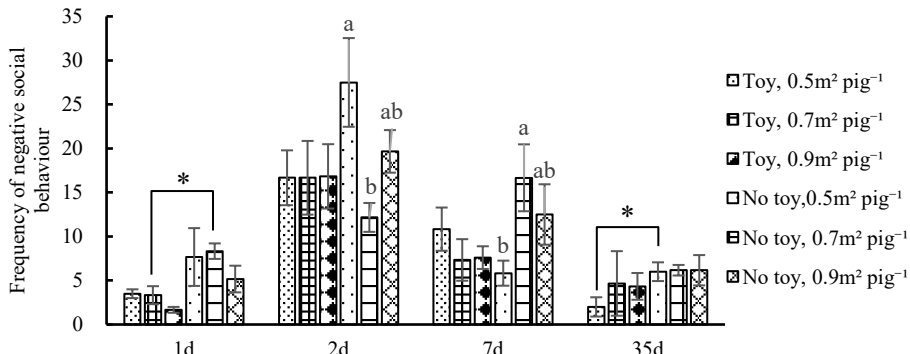


Figure 2. Frequency of negative social behaviour of the pigs after grouping (Different letters means significant difference between stocking density groups; the symbol of “\*” means significant difference between groups with or without toy provision).

### 3.2.3. Lying

Figure 3 presents the percentage of lying behaviour of pigs at the four days after grouping. The time budget in lying of pigs was relatively shorter in the first two days after grouping, which greatly increased at the 7<sup>th</sup> day and then decreased at the 35<sup>th</sup> day for all treatments. Among the three stocking densities, pigs of the 0.9 m<sup>2</sup> pig<sup>-1</sup> groups spent more time lying, and the difference was significant in the first two days ( $P<0.05$ ) for the groups without toy provision. Results showed that toy provision decreased the lying duration of the pigs in the first two days after grouping because pigs performed more exploration behaviour to the novel environment. Meanwhile, the enriched environment increased the duration of lying behaviour when the group stabilized, which could be easily found through the behaviour in the 7<sup>th</sup> and 35<sup>th</sup> days.

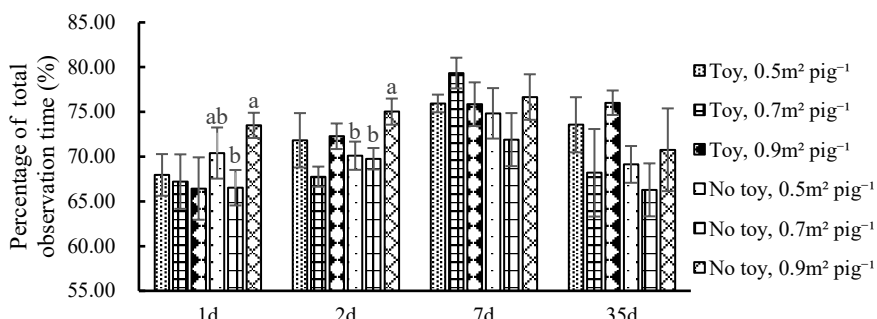


Figure 3. Percentage of total observation time for lying behaviour of pigs after grouping (Different letters means significant difference between stocking density groups).

### 3.2.4. Feeding

Feeding behaviour of pigs in the study, referred to feeder occupation behaviour, was plotted in Figure 4. Regarding the feeding duration, there was no significant variation for the first seven

days after grouping. While the duration significantly increased for all the groups at the 35<sup>th</sup> day, which could be attributed to the growth stage change of the pigs. Pigs spent more time eating the feed with the decreasing of pen sizes, especially for the groups without toy provision, and the behaviour was clearly illustrated in the 2<sup>nd</sup>, 7<sup>th</sup> and 35<sup>th</sup> of the days. During the experiment, pigs performed less feeding behaviour with toy provision, and the effect was enhanced in the highest stocking density of 0.5 m<sup>2</sup> pig<sup>-1</sup>, while no statistical difference was observed.

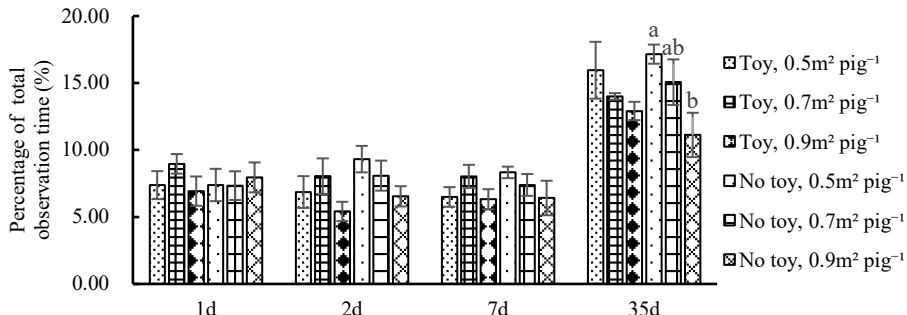


Figure 4. Percentage of total observation time for feeding behaviour of pigs after grouping (Different letters means significant difference between stocking density groups).

In summary, pigs performed more negative social behaviour at early stage after grouping and more feeding at late stage, and had less time of lying and resting in higher stocking densities in this study. The finding is generally consistent with most previous studies, showing that the pigs performed less exploring and moving behaviour in crowded environment (Beattie et al., 1996), and the time spent in drinking and fighting were significantly higher, while the resting was lower (Fu et al., 2016). As a way of environmental enrichment, previous studies have shown that pigs housed in pens with toy provision perform less aggressive and more exploration behaviour (Beattie et al., 1996), while in barren environment, the pigs prefer to explore the fixed facilities in pens, such as the feeders and drinkers, illustrating more abnormal behavior (Beattie et al., 2000). Similar feeding behaviour was found in our study.

### 3.3. Body surface temperature (BST)

The normal BST for growing and finishing pigs is around 38.5 °C based on the rectal temperature, while the eye temperature is generally lower. Figure 5 presents the weekly change of BST of pigs in different groups. There was no significant difference in BST among the groups in first four weeks, but the BST of the pigs in 0.5 m<sup>2</sup> pig<sup>-1</sup> was significantly higher, compared to the pigs in 0.7 and 0.9 m<sup>2</sup> pig<sup>-1</sup> from the 5<sup>th</sup> week ( $P<0.01$ ), which might be because of the increasing of weight and size of pigs, and the decreasing of living space in small pen size. Previous studies have shown that high BST of pigs may indicate inflammatory response (Sidhu et al., 2003), which suggested that the immune response of growing pigs could be affected by stocking density. No significant difference in BST between the treatments with and without toy provision was found.

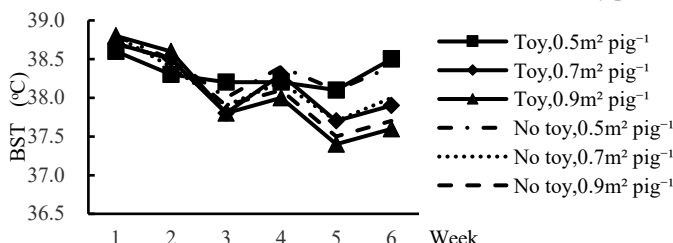


Figure 5. The weekly change of BST of the pigs.

### 3.4. Concentration of salivary cortisol

Cortisol is a glucocorticoid steroid hormone, which is typically released in response to stress (Kim et al., 2016). The weekly change of salivary cortisol concentration of pigs is presented in Figure 6. There was no regular trend for the change of concentration of salivary cortisol. No significant difference was observed among different treatments neither. The concentration of salivary cortisol tended to increase from the 4<sup>th</sup> week for different treatments, especially for group of  $0.5 \text{ m}^2 \text{ pig}^{-1}$  without toys, which could be explained by the crowded and barren environment in pens at the later stage. The result in our study varies from some previous studies, suggesting that the cortisol concentration of pigs is increased with the increasing of stocking density (Cornale et al., 2015). The cortisol concentration of pigs with toy provision was lower than the counterparts without toys in the first week after grouping and no clear difference was observed between toy and blank groups in other time.

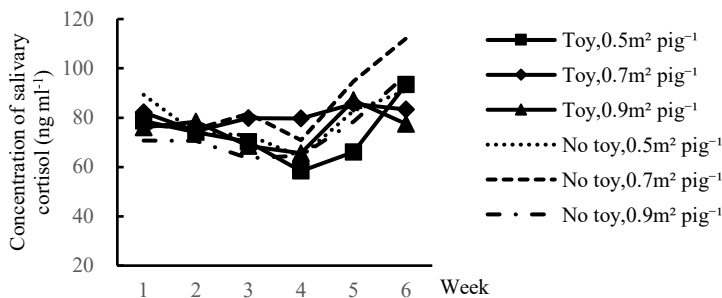


Figure 6. The weekly change of concentration of salivary cortisol of the pigs.

### 3.5. Discussion on proper stocking density for growing pigs

By studying the effect of stocking density on production performance and physiology of pigs at different stages of growth, Kim et al (2016) suggested the optimal stocking density for growing pigs (25–65kg) was  $0.44\text{--}0.64 \text{ m}^2 \text{ pig}^{-1}$ . Jang et al (2017) presented that the minimal space allowance of growing pigs was  $0.8 \text{ m}^2 \text{ pig}^{-1}$ . Previous studies show that the proper stocking density for pigs varies among different group size, management, environment control and so on. In our study, results indicate that the weight gain, behaviour and BST of growing pigs housed in high stocking densities ranged from  $0.5\text{--}0.7 \text{ m}^2 \text{ pig}^{-1}$  are negatively affected. For such stocking densities, although the pork yield per unit floor area could be higher, it is necessary to provide toys inside pens to reduce aggressive and abnormal behaviours of pigs, which is conducive to increase weight gain of growing pigs. At lower stocking densities of  $0.7\text{--}0.9 \text{ m}^2 \text{ pig}^{-1}$ , the weight gain and feed conversion of the pigs are significantly increased, meanwhile the abnormal behavior is reduced and the health of the pigs is improved. For these treatments, toy provision is suggested to improve the welfare and health of growing pigs. The minimum space allowance for growing pigs (30–50kg) required by EU is no less than  $0.4 \text{ m}^2 \text{ pig}^{-1}$  (European Council Directive 2008), and in China the range of  $0.6\text{--}0.9 \text{ m}^2 \text{ pig}^{-1}$  is advised for growing pigs (NYT1568–2007). The finding on stocking densities in the study supports the relevant standards.

## 4. Conclusions

In general, stocking density has a significant impact on the production performance, behaviour and physiology of growing pigs. Toy provision was found to have a significant effect on improvement of the behaviour and physiology levels of growing pigs, which is also conducive to promoting weight gain. High stocking densities ranged from  $0.5\text{--}0.7 \text{ m}^2 \text{ pig}^{-1}$  negatively affect the weight gain, welfare and health of growing pigs, and it is necessary to provide toys inside pens to improve production efficiency. Growing pigs have more positive performances with larger space allowances of  $0.7\text{--}0.9 \text{ m}^2 \text{ pig}^{-1}$ , and toy provision is suggested to improve welfare of pigs in such

ranges. Space allowance bigger than  $0.9\text{ m}^2\text{ pig}^{-1}$  might be even better for the production performance and health of the growing pigs, while the production efficiency could be limited under the same market condition. Effective toy provision is helpful to reduce the space requirement for growing pigs, especially for the groups with high stocking densities.

### References

- Beattie V.E., N. Walker, I.A. Sneddon, 1996. An investigation of the effect of environmental enrichment and space allowance on the behaviour and production of growing pigs. *Applied Animal Behaviour Science*, 48(3–4), 151–158.
- Beattie V.E., N.E O'Connell, B.W. Moss, 2000. Influence of environmental enrichment on the behaviour, performance and meat quality of domestic pigs. *Livestock Production Science*, 65(1), 71–79.
- Cornale P., E. Macchi, S. Miretti, M. Renna, C. Lussiana, G. Perona, et al. 2015. Effects of stocking density and environmental enrichment on behavior and fecal corticosteroid levels of pigs under commercial farm conditions. *Journal of Veterinary Behavior Clinical Applications & Research*, 10(6), 569–576.
- Edmonds M.S., B.E. Arentson, G.A. Mente, 1998. Effect of protein levels and space allocations on performance of growing-finishing pigs. *Journal of Animal Science*. 76, 814–821.
- European Commission. Council Directive 2001/93/EC of 9 November 2001, amending Directive 91/630/EEC laying down minimum standards for the protection of pigs. Brussels: EC, 2001
- Fu L.L., H. Li, T. Liang, B. Zhou, et al. 2016. Stocking density affects welfare indicators of growing pigs of different group sizes after regrouping. *Applied Animal Behaviour Science*. 174: 42–50.
- Hemsworth P.H., M. Rice, J. Nash, K. Giri, K.L. Butler, A.J. Tilbrook, et al. 2013. Effects of group size and floor space allowance on grouped sows: aggression, stress, skin injuries, and reproductive performance. *Journal of Animal Science*, 91(10), 4953–4964.
- Jang J.C., X.H. Jin, J.S. Hong, Y.Y. Kim, 2017. Effects of different space allowances on growth performance, blood profile and pork quality in a grow-to-finish production system. *Asian Australasian Journal of Animal Sciences*, 30(12).
- Kim K.H., K.S. Kim, J.E. Kim, D.W. Kim, Y.H. Kim, 2016. The effect of optimal space allowance on growth performance and physiological responses of pigs at different stages of growth. *Animal*, 11(3), 1–8.
- Oh H.K., H.B. Choi, W.S. Ju, C.S. Chung, Y.Y. Kim, 2010. Effects of space allocation on growth performance and immune system in weaning pigs. *Livestock Science*, 132(1–3), 0–118.
- Schmidt M., K.H. Lahrmann, C. Ammon, et al. 2013. Assessment of body temperature in sows by two infrared thermography methods at various body surface locations. *Journal of Swine Health and Production*. 21(4):203–209.
- Sidhu P., F.S. Aliaabadi, M. Andrews, P. Lees, 2003. Tissue chamber model of acute inflammation in farm animal species. *Research in Veterinary Science*, 74(1), 0–77.
- Vermeer H.M., D.K.H. Greef, H.W.J. Houwers, 2014. Space allowance and pen size affect welfare indicators and performance of growing pigs under comfort class conditions. *Livestock Science*, 159(1), 79–86.
- Xi L., Z.X. Shi, B.M. Li, L.D. Zhang, 2007. Effects of environmental enrichment on performance and carcass traits of finishing pigs. *Transactions of the Chinese Society of Agricultural Engineering*. 23(8):187–192.
- Yi L.I., L.I. Qian, J. Wang, X.L. Zhang, 2016. Evaluation of pork meat freshness using surface desorption atmospheric pressure chemical ionization mass spectrometry. *Journal of Chinese Mass Spectrometry Society*. 37(3):273–281.
- Zhang Z.F., J. Li, J.C. Park, I.H. Kim, 2013. Effect of vitamin levels and different stocking densities on performance, nutrient digestibility, and blood characteristics of growing pigs. *Asian Australasian Journal of Animal Sciences*, 26(2).

# Optimal Indoor Climate by Partial Recirculation of Air in a Fattening Pig House

André J.A. Aarnink <sup>a,\*</sup>, In-Bok Lee <sup>b</sup>

<sup>a</sup> Wageningen University and Research, De Elst 1, 6708 WD Wageningen, The Netherlands

<sup>b</sup> Seoul National University, San56-1, Sillim-dong, Gwanak-gu Seoul, Republic of Korea

\* Corresponding author. Email: [andre.aarnink@wur.nl](mailto:andre.aarnink@wur.nl)

## Abstract

In pig houses a lot of air is ventilated in summer, and in winter often very little. Ventilation rate is mainly controlled by the indoor temperature. The disadvantage of such a climate control system is that the concentrations of undesirable gases in the house vary with the ventilation rate. As a result, in the winter indoor concentrations of ammonia, dust and pathogens are very high. This has worsened in recent years by rising energy prices. The aim of this cooperative project is to develop an integral, practical climate control system with an emphasis on energy use, stable indoor climate and low emissions to the environment. It was hypothesized that this objective can be realized to a large extent by partially recirculation of exhaust air after cleaning and conditioning. Some fresh air is required to supply oxygen and remove carbon dioxide and other harmful gases. An existing heat and mass balance model for livestock houses has been extended to calculate the consequences of (partial) air recirculation on the energy and mass balances of a fattening pig house. To this model, various new components have been added, including an air scrubber, a groundwater heat exchanger and an air-to-air heat exchanger. Different scenarios have been calculated with the model. From these calculations it is concluded that with partial recirculation of air in a fattening pig house a stable indoor climate can be obtained, with a constant temperature of the incoming air and a slight variation in ventilation flow rate.

**Keywords:** Climate control, recirculation of air, air conditioning, air cleaning

## 1. Introduction

In pig houses a lot of air is ventilated in the summer, and in the winter the opposite is happening with mostly very little ventilation. The ventilation rate is mainly controlled by the indoor temperature. The disadvantage of such a system is that the concentrations of undesirable gases in the house vary with the ventilation rate. As a result, in the winter period the concentrations of ammonia, dust and pathogens can reach high levels. This has been worsened in recent years by rising energy prices, which means that many pig farmers have a tendency to ventilate somewhat less in the winter to save on heating costs.

The high ventilation rates during the summer season can be reduced if enough heat can be removed, e.g. by cooling the incoming air. Heat dissipation should be prevented in winter. If during the winter season the heat in the exhaust air can be recovered and reused, a lot of energy can be saved. The aim of this cooperative project is to develop an integral, practical climate control system with an emphasis on energy use, stable indoor climate and low emissions to the environment. It was hypothesized that this objective can be realized to a large extent by partially recirculation of exhaust air after cleaning and conditioning. Some fresh air is required to supply oxygen and remove carbon dioxide and other harmful gases. As a result, a stable climate can be maintained that promotes the health and production results of the animals. In addition, the incoming and/or outgoing air can be optimally treated, which minimizes the spread of pathogens and emissions of ammonia, odor, and dust.

The objective of this study was to determine the effect of partial recirculation of air on indoor temperature, humidity and gaseous concentrations for different scenarios. These scenarios were studied by model simulations.

So far, little research has been done on the recirculation of air in pig houses. In the Netherlands, some research was carried out at the Pig experimental research station in Raalte in

the 1990s. In this system, the air was also largely recirculated after cleaning and conditioning (Mouwen and Plagge, 1995). Their report concluded that this system offers perspectives, mainly because of the very low emissions to the environment.

The focus in this phase of this cooperative project between the Netherlands and the Republic of Korea is on exploring the feasibility and development of a technical design. In the present study different scenarios for recirculation of air have been investigated by model simulations.

## 2. Materials and Methods

### 2.1. Modelling

Figure 1 gives a schematic overview of the modeled and calculated design. Outgoing air goes to the air scrubber, where the air is largely cleaned from ammonia (95% reduction) and particulate matter (70% reduction). A part of the odor components is also washed out of the air. After the air scrubber, a part of the air is exchanged with fresh outside air. Then the mixed air (recirculation and fresh air) goes to the first heat exchanger. There the air is conditioned (cooled) with groundwater to a temperature of approx. 12 °C. In a second heat exchanger, the air is slightly heated to reduce the relative humidity from saturated to approx. 90%. It is also possible to include a heat pump in the system that can store the extracted heat from the first heat exchanger in water with a temperature of approx. 50 °C. This water could for example be used for heating the rooms for piglets and the farrowing rooms on a farm with fattening pigs and sows.

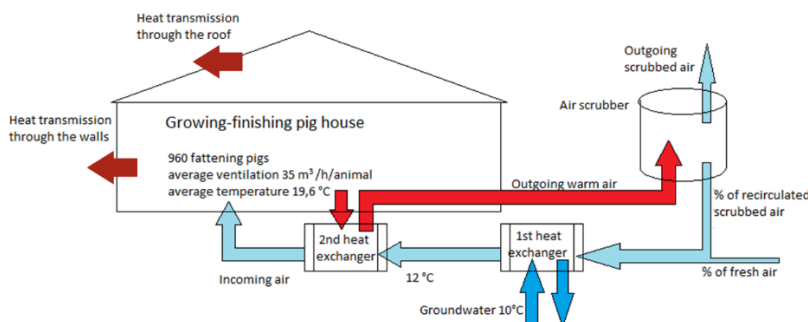


Figure 1. Schematic view of air and energy flows in a fattening pig house with partial air recirculation. This design was the basis for the model calculations.

From the design in Figure 1 a calculation model was made to calculate the mass and energy flows of the air in the system. The steady state model was made with the software package Matlab (version R2018B, MathWorks, 2018). Use was made of an already existing model for regular pig housing (Van Ouwerkerk, 1999). A schematic view of the model is given in Figure 2. The components in Figure 1 have been added to this existing model (air scrubber, 1<sup>st</sup> and 2<sup>nd</sup> heat exchanger). For the outdoor climate, use was made of the so-called degree hour table. This table shows how many hours (outside) temperatures occur during the year. The temperatures varied from -14 to 29 °C, with steps of 1°C (Breuer et al., 1991). This table also includes the average relative humidity, the solar radiation and the wind speed, which are associated with these temperatures.

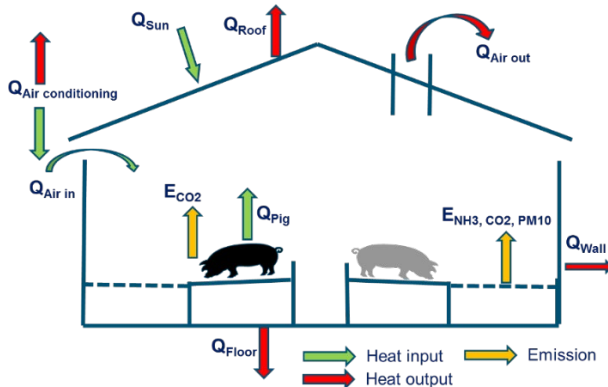


Figure 2. Schematic view of the Anipro model (adapted from Van Ouwerkerk, 1999) for calculating indoor climate (T/RH) and air quality (NH<sub>3</sub>, CO<sub>2</sub>, dust concentrations) of pig houses.

## 2.2. Characteristics of house and animals

The modeled barn had 8 sections with partially slatted floor for 120 animals (8 pens of 15 pigs per pen) (Figure 3). Every two weeks a section is emptied and new piglets are imposed. The building is 50 m long and 22 m wide. The departments are 12.5 m wide and 10 m long. The central corridor is 2 m wide. The ridge of the stable was 5.94 m high and the side walls were 2.3 m high. Each section had two windows with a surface area of approximately 0.63 m<sup>2</sup>.

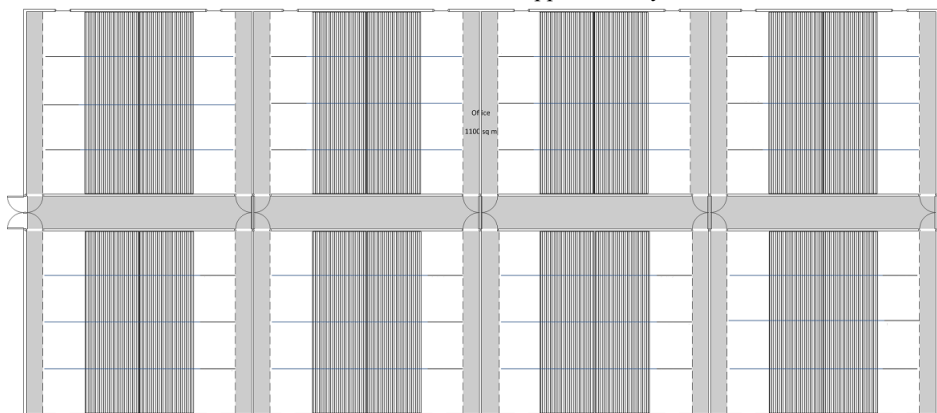


Figure 3. Lay-out of the modeled house for 960 pigs: 8 sections with 120 animals.

Table 1 shows the starting points for the modeling of the house with recirculation with regard to animal weight in the various weeks after the start of the fattening period, the desired minimum and maximum temperatures, the minimum and maximum ventilation rates and the growth of the animals. These starting points were also used for the reference house without recirculation, except that the minimum and maximum ventilation rates were different. The reference house is based on a traditional house, with an ammonia production of 3.46 kg y<sup>-1</sup> per fattening pig (Mosquera et al., 2011) with an air scrubber that reduces ammonia emissions by 95% and PM<sub>10</sub> emissions by 70%. The house with air recirculation is based on a low-emission house (1.40 kg y<sup>-1</sup> per fattening place, namely a pen with a convex floor equipped with an IC-V system). For PM<sub>10</sub> production inside the house, all scenarios are based on the value in the Rav list of 153 g y<sup>-1</sup> per fattening pig place (Infomil, 2019).

Table 1. Starting points for the model calculations with regard to the number of animals, animal weight, minimum and maximum desired temperatures and ventilation rates (with air recirculation) and growth rate.

Week	No. pigs	Weight (kg)	Min. T (°C)	Max. T (°C)	Min. vent. (m <sup>3</sup> h <sup>-1</sup> )	Max. vent. (m <sup>3</sup> h <sup>-1</sup> )	Daily gain (g d <sup>-1</sup> )
1	120	26.7	21.0	23.0	8.0	28.0	471
2	120	30.2	20.5	22.5	12.7	30.0	529
3	120	34.0	20.0	22.0	16.3	32.0	571
4	120	38.2	19.5	21.5	20.0	34.0	629
5	120	42.7	19.0	21.0	21.7	36.0	657
6	120	47.5	18.5	20.5	23.3	38.0	714
7	120	52.6	18.0	20.0	25.0	40.0	743
8	120	58.0	17.9	19.9	27.1	42.9	786
9	120	63.6	17.7	19.7	29.3	45.7	814
10	120	69.4	17.6	19.6	31.4	48.6	843
11	120	75.4	17.4	19.4	33.6	51.4	886
12	120	81.7	17.3	19.3	35.7	54.3	914
13	120	88.2	17.1	19.1	37.9	57.1	943
14	120	94.7	17.0	19.0	40.0	60.0	914
15	120	101.1	17.0	19.0	40.0	60.0	900
16	120	107.3	17.0	19.0	40.0	60.0	871

### 2.3. Scenarios

In addition to a reference scenario (a conventional ventilated house: Scenario 'reference'), three promising alternative scenarios (technical designs) were calculated using the model. These three scenarios are defined as following:

- Scenario 'constant flow': average ventilation flow rate over the year is constant and amounts to 35 m<sup>3</sup> h<sup>-1</sup> per pig (code: SE1).
- Scenario 'variable flow rate': average ventilation flow rate is kept constant at 30 m<sup>3</sup> h<sup>-1</sup> per pig at outside temperatures below 5°C and at 40 m<sup>3</sup> h<sup>-1</sup> per pig at outside temperatures above 5°C (code: SE2).
- Scenario 'without 2<sup>nd</sup> heat exchanger': same as scenario 1, except that the second heat exchanger is not installed (code: No he2 = 'without 2<sup>nd</sup> heat exchanger').

For the 'constant flow' and 'no 2nd heat exchanger' scenarios, a constant average flow rate was assumed, based on the average of the minimum and maximum ventilation rates, as shown in Table 1. This means that the maximum ventilation rate in the house during warm periods will be a bit higher and during cold periods a bit lower than 35 m<sup>3</sup> h<sup>-1</sup>. The same applies to scenario 'variable flow' with average values in winter of 30 m<sup>3</sup> h<sup>-1</sup> and in summer 40 m<sup>3</sup> h<sup>-1</sup>.

For the different scenarios model calculations have been made to determine the following:

- How much air can be recirculated and how much air must be refreshed under the following conditions:
  - The temperature remains between the desired minimum and maximum temperature as shown in Table 1.
  - Concentration of CO<sub>2</sub> in the barn should not exceed 0.8 volume percent.
  - Concentration of ammonia in the house should not exceed 15 ppm.
- The consequences of the foregoing for the concentrations of CO<sub>2</sub>, NH<sub>3</sub> and PM<sub>10</sub> in the house.
- The consequences of the foregoing for the temperature and air humidity in the house.

### 3. Results and Discussion

Many results were obtained with the model calculations. This report focuses on the effects of the different scenarios on the indoor temperature and relative humidity. More specifically, section 3.1 shows the results of the air conditions for the different recirculation scenarios and the reference at the house level and section 3.2 at section level.

#### 3.1. Air conditions at house level

Figure 4 gives an overview of the average temperatures at various locations in the system for the scenarios with recirculation of air. In SE1, 81% of the air can be recirculated and 19% of the air is refreshed. At a flow rate of  $35 \text{ m}^3 \text{ h}^{-1}$ , this means a refreshment of  $6.65 \text{ m}^3 \text{ h}^{-1}$  of outside air per pig. The outgoing air from the sections has an average temperature of  $19.6^\circ\text{C}$  and an average air humidity of approx. 70%. In the air scrubber the air is cooled to  $16.0^\circ\text{C}$  as a result of evaporative cooling and the air is saturated with moisture to an air humidity of almost 100%. In the first heat exchanger, the air is additionally cooled to a temperature of  $12.0^\circ\text{C}$  using groundwater. A lot of moisture will condense in this heat exchanger. This moisture can, for example, be reused in the air scrubber. In the second heat exchanger, the air is heated with approx.  $1^\circ\text{C}$  with heat from the outgoing air to bring the air humidity below 90%. For SE2 the average air conditions are comparable with Scenario 'constant flow'. However, since the absolute amount of fresh air is the same over the year, the percentage of fresh air varies with the ventilation volume (on average  $30 \text{ m}^3 \text{ h}^{-1}$  in winter and  $40 \text{ m}^3 \text{ h}^{-1}$  in summer). Scenario No he2 is also similar to previous scenarios with the difference that the incoming air in the barn has a humidity of 100% with a temperature of  $12.0^\circ\text{C}$ .

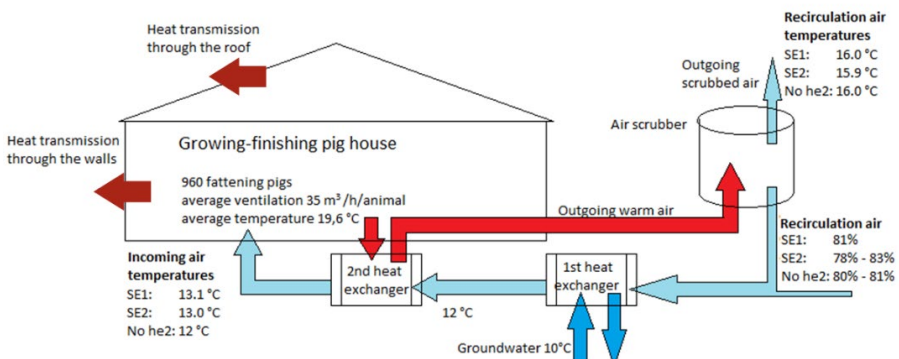


Figure 4. Schematic view of the air and energy flows in a fattening pig house with air recirculation. The figure shows the average temperatures as calculated with the calculation model. SE1 = 'constant flow'; SE2 = 'variable flow'; No he2 = 'without 2<sup>nd</sup> heat exchanger'.

Figure 5 shows the condition of the incoming air at different outdoor temperatures. The temperature of the incoming air is virtually unaffected by the (temperature) conditions of the outside air. Only at very low outside temperatures the temperature of the incoming air will drop slightly (approx.  $1^\circ\text{C}$ ) below the set point. The percentage of fresh air is also virtually independent of the outdoor conditions of the air. This percentage is mainly dependent on the precondition set for the maximum CO<sub>2</sub> concentration.

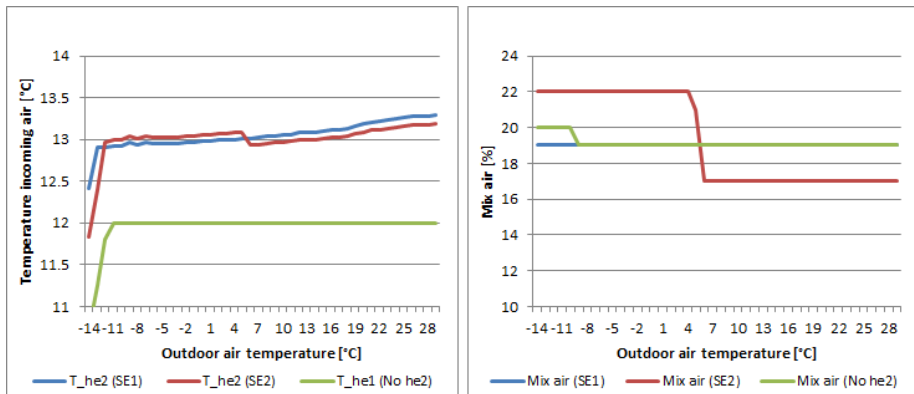


Figure 5. Conditions of the incoming air at various outdoor air temperatures for the different scenarios (SE1 = 'constant flow', SE2 = 'variable flow', No he2 = 'without 2<sup>nd</sup> heat exchanger'); left figure: temperature of incoming air of the sections; right figure: percentage of fresh outside air in the incoming air of the sections.

### 3.2 Air conditions at section level

The incoming air is distributed over the different sections. In each section, animals are at a different production stage, ranging from 1 to 16 weeks after start. These sections therefore require different air conditions (see Table 1). In the following section the consequences of air recirculation on temperature and relative humidity in the various sections are shown. For simplification only calculations have been made for departments with fattening pigs at 1, 7 and 16 weeks after start.

Figure 6 shows the air conditions inside the house (T and RH) in departments with slaughter pigs 1, 7 and 15 weeks after the start of the fattening period. The left figures show the situation for Scenario 'constant flow' and the right figures for Scenario 'reference'. No additional heating was used in both scenarios. From these figures it is clear that as a result of recirculation of air (Scenario 'constant flow') the house temperature and air humidity show much less variations than without recirculation (Scenario 'reference'). In the situation of recirculation of air no additional heating is required, except perhaps under extreme cold conditions with young fatteners. For animals at 7 and 15 weeks after start, the house temperature rises above the desired temperature at outside temperatures above 10°C. In the reference situation this happens at temperatures above about 14 °C. The advantage of the recirculation system, however, is that the house temperature is never more than 3 °C higher than the desired temperature, while this can be up to 14 °C higher for the reference house.

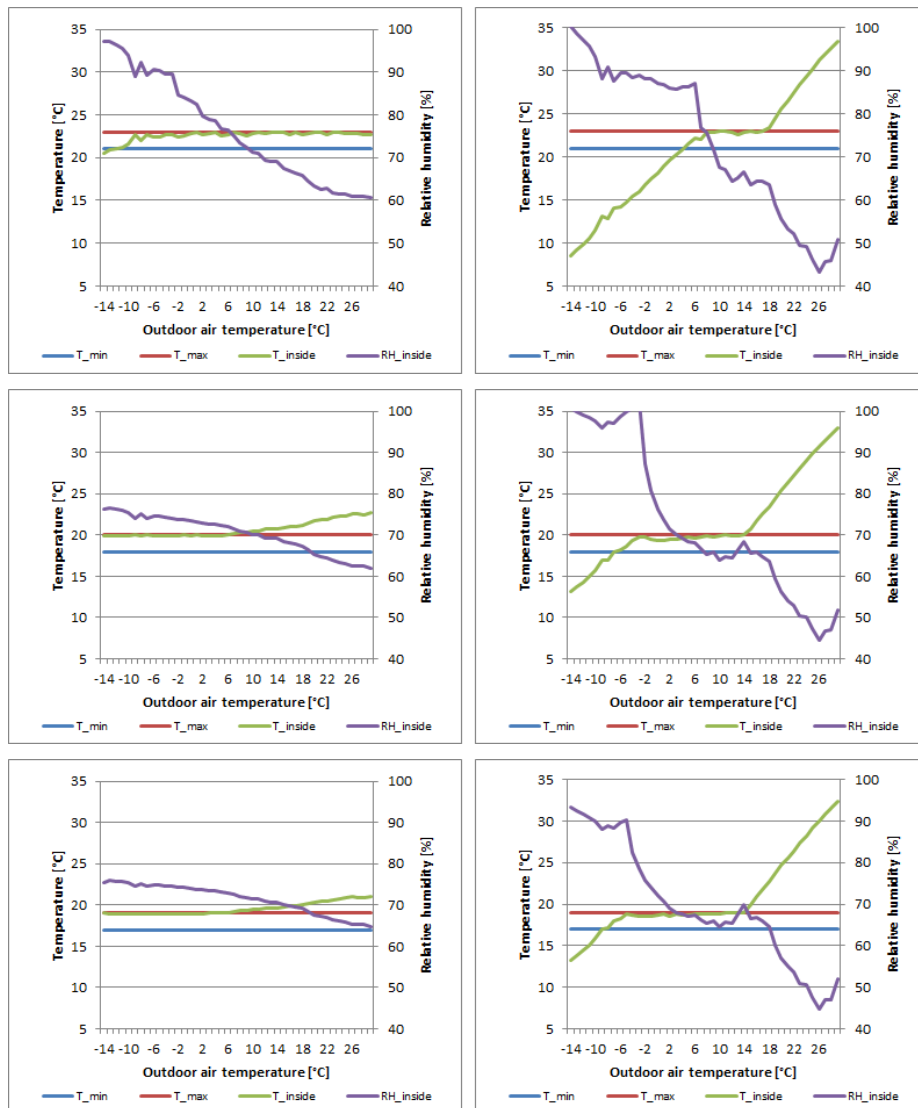


Figure 6. Air conditions in the fattening house (T and RH) in sections with fattening pigs at 1 week after start (top), 7 weeks after start (middle) and 15 weeks after start (bottom). The left figures show the situation for Scenario 'constant flow' and the right figures for Scenario 'reference'. No additional heating was used in both scenarios.

#### 4. Conclusions

From this preliminary study the following conclusions can be drawn:

- With partial recirculation of air in a fattening pig house a stable indoor climate can be obtained, with a constant temperature of the incoming air and a slight variation in ventilation flow rate.

- From the calculated scenarios, Scenario 'constant flow rate ( $35 \text{ m}^3 \text{ h}^{-1}$ )', Scenario 'variable flow' ( $30\text{--}40 \text{ m}^3 \text{ h}^{-1}$ ) and Scenario 'constant flow rate ( $35 \text{ m}^3 \text{ h}^{-1}$ ) without 2nd heat exchanger', it seems the last scenario is the best choice. A second heat exchanger to reduce the relative air humidity of the incoming air seems not necessary, and this reduces the costs of the system.
- The simulated system will be built at pilot scale to test the different components in the system and to validate the results from the simulations.

### References

- Breuer, J.J.G., A.M.v. Weele, A.H.C.v. Paassen, 1991. Referentiejaar voor de Nederlandse glastuinbouw. Klimaatbeheersing (4), p. 110–113.
- Infomil, 2019. Emission factors different animal categories. <https://www.infomil.nl/onderwerpen/landbouw/stalsystemen/emissiefactoren-per/>.
- Mosquera, J., J.M.G. Hol, A. Winkel, E. Lovink, N.W.M. Oginck, A.J.A. Aarnink, 2011. Fijnstofemissie uit stallen: vleesvarkens. Rapport 292, herziene versie. Livestock Research, Rapport 292, herziene versie, Lelystad. 37 p.
- Mouwen, I.A.A.C., J.G. Plagge, 1995. Studie naar klimatisering van de dekstal in relatie tot emissie en energie. Proefverslag nr. P. 1.125, Proefstation voor de Varkenshouderij, 39 pp.

## **Indexes**



## Author Name Index

<b>Author name</b>	<b>Page</b>
Aarnink, André J.A.....	381
Akter, Suraiya.....	232
Ammon, Christian .....	223
Amon, Barbara .....	223
Amon, Thomas .....	223
Andela, Yeb P.....	180
Anders, Ivonne .....	65, 72
Andre, Konrad .....	65, 72
Baumgartner, Johanne .....	65, 72
Berckmans, Daniel.....	337, 347
Black, Ramdi A .....	215
Bokma, Sjoerd .....	180
Branco, Tatiane.....	279
Bromfield, Corinne.....	39
Brown-Brandl, Tami M. ....	324
Cai, Zhen .....	107, 119
Cao, Ziyue .....	113
Cecilia, Conti.....	85
Chai, Lilong.....	3
Chen, Bin.....	127, 167, 188
Cheng, Bin.....	232
Cordova-Noboa, Alejandro H.....	232
Cuan, Kaixuan .....	301
Dai, Xiaorong .....	188, 264
Daniela, Lovarelli .....	85
Delaney, Lauren .....	39
Derks, Marjolein.....	180
Du, Qian .....	293
Federica, Borgonovo .....	85, 286
Gedikoglu, Haluk.....	235
Groot Koerkamp, Peter W. G. ....	180
Guido, Grilli .....	286
Heber, Albert .....	143
Heinicke, Julia .....	223
Hempel, Sabrina .....	223
Hennig-Pauka, Isabel.....	65, 72
Hocter, Jeb.....	151
Hoff, Steven J. ....	79
Hoffmann, Gundula .....	223
Hörtenhuber, Stefan J. ....	65, 72
Huan, Kangning.....	188
Huang, Junduan .....	301
Huang, Shiwei .....	373
Huang, Yangbo.....	317
Huang, Yong.....	242

Hui, Xue .....	19
Jacopo, Bacenetti .....	85
Janke, David .....	223
Jiang, Yifeng .....	264
Johnson, Anna K. ....	324
Joosen, Pieter .....	347
Kai, Peter .....	197
Knauder, Werner .....	65, 72
Knight, Reyna M. ....	151, 159
Kong, Xianwang .....	107, 119, 167
Krawczel, Peter D. ....	215
La, Amy .....	250
Lee, In-Bok .....	381
Lei, Changwei .....	11
Leonard, Suzanne .....	324
Li, Baoming .....	11, 100, 113, 134, 337, 364
Li, Guoming .....	293
Li, Jianrong .....	264
Li, Junying .....	57
Li, Xiaochuan .....	151
Li, Xiusong .....	127, 167, 188
Li, Xuechen .....	191
Li, Yan .....	57
Li, Yongzhen .....	373
Li, Zhichao .....	113
Li, Zonggang .....	11, 242
Lim, Teng-Teeh .....	39, 256
Liu, Dejia .....	127, 167
Liu, Dezhao .....	107, 119, 127, 167, 264
Liu, Longshen .....	309
Liu, Qiong .....	174
Liu, Tongshuai .....	19
Liu, Wei .....	57
Liu, Yingying .....	232
Liu, Zhidan .....	100
Liu, Zuohua .....	373
Lu, Jinfeng .....	329
Ma, Ruiyu .....	57
Man, Zun .....	107, 264
Marcella, Guarino .....	85
Marchant-Ford, Jeremy .....	347
Massey, Raymond .....	39, 235
Massey, Ryamond .....	256
Medeiros, de Oliveira .....	279
Mei, Xuehua .....	242
Melse, Roland W. ....	180
Mikovits, Christian .....	65, 72
Moura, Daniella Jorge de .....	279
Mua, Gang .....	191
Naas, Irenilza de Alencar .....	279
Ni, Ji-Qin .....	143

Nie, Luwei.....	337
Niebuhr, Knut.....	65, 72
Norton, Tomas.....	347
Oliveira, Jofran L.....	79
Ouyang, Zengli.....	242
Oviedo-Rondon, Edgar.....	232
Pan, Jinming .....	174, 273
Parsons, Rebecca .....	273
Payne, Craig .....	39
Peng, Zhong.....	329
Pinto, Severino .....	223
Piringer, Martin .....	65, 72
Ramirez, Brett C.....	79, 273, 324
Ren, Yanfei.....	191
Riccardo, Pascuzzo.....	286
Richardson, Brad .....	3
Robson, Stanley.....	279
Rong, Li.....	49, 92, 127, 167
Schauberger, Günther .....	65, 72, 127
Schönhart, Martin .....	65, 72
Shen, Mingxia.....	309
Shi, Haipeng .....	364
Shi, Zhengxiang.....	113
Shi, Zhifang .....	19
Siemens, Theresa Müschner .....	223
Stinn, John P.....	324
Street, Garrett M.....	317
Swanson, Janice C.....	207
Tabler, Tom .....	26
Tai, Meng .....	309
Tang, Jianan.....	242
Tian, Jialin .....	191
Tong, Qin.....	113, 134, 364
Tong, Xinjie.....	143
Valentina, Ferrante .....	85, 286
van 't Ooster, Bert .....	180
Verstegen, Jeroen A. A.....	180
Wan, Yi .....	57
Wang, Ailun .....	188
Wang, Chaoyuan .....	337, 373
Wang, Hao.....	373
Wang, Hongning.....	11
Wang, Jintao .....	309
Wang, Kailao.....	273
Wang, Kaiying .....	188
Wang, Leiping .....	188, 264
Wang, Tao .....	174
Wang, Xiaocui.....	113
Wang, Xiaoshuai .....	188
Wang, Yu.....	79
Wang-Li, Lingjuan .....	232

Wei, Yongxiang.....	11, 134
West, Derek .....	232
Wu, Chuandong.....	127
Wu, Jiegang.....	188
Xi, Lei.....	19
Xin, Hongwei .....	3, 79, 273, 324
Xin, Yicong .....	107, 119, 127, 167
Xing, Haohan.....	100
Xu, Yan .....	293
Xu, Yi.....	309
Xue, Hongxiang.....	309
Yang, Liangcheng.....	119
Yang, Xiao.....	317
Yang, Zhihua .....	188
Yi, Qianying .....	223
Yin, Yibin.....	273
Ying, Shihao.....	107, 119, 167
Yu, Yue .....	174
Zeng, Jinxin.....	11
Zhan, Kai.....	57
Zhang, Guochen .....	191
Zhang, Guoqiang .....	92, 197
Zhang, Hanbing .....	191
Zhang, Jian .....	191
Zhang, Qiang .....	250
Zhang, Tiemin .....	301, 329, 357
Zhang, Yifan.....	242
Zhang, Yuanhui .....	100
Zhao, Lingying .....	143, 151, 159
Zhao, Yang .....	3, 293, 317
Zheng, Haikun .....	357
Zheng, Weichao.....	11, 19, 100, 113, 134, 242, 364
Zhong, Zhentao.....	174
Zhu, Maixun .....	242
Zollitsch, Werner.....	65, 72
Zulovich, Joe .....	39, 256

## Author Affiliation Index

Author Affiliation	Page
Aarhus University, Denmark .....	49, 92, 127, 167, 197
Beijing Engineering Research Center for Livestock and Poultry Healthy Environment, China.....	100, 113
Beijing Engineering Research Center on Animal Healthy Environment, China.....	134, 364
Big Herdsman Machinery Co. Ltd., China .....	127, 167, 188
BioRICS NV, Belgium.....	347
Catholic University of Leuven, Belgium .....	337, 347
Central Institute of Meteorology and Geodynamics, Austria.....	65, 72
China Agricultural University, China .....	11, 19, 113, 134, 242, 337, 364, 373
China University of Mining and Technology, China.....	151
Chinese Academy of Sciences, China .....	264
Chongqing Academy of Animal Science, China .....	242, 373
Dalian Ocean University, China .....	191
Department of Veterinary Medicine, Free University Berlin, Germany .....	223
Embrapa – Informatics in Agriculture, Brazil.....	279
Henan Engineering Research Center on Animal Healthy Environment and Intelligent Equipment, China.....	19
Henan University of Animal Husbandry and Economy, China .....	19
Illinois State University, USA .....	119
Institute of Animal Husbandry and Veterinary Medicine, China.....	57
Iowa Select Farms, USA.....	324
Iowa State University, USA .....	3, 79, 324
Key Lab. Agri. Eng. Struct. & Env., China .....	11, 100, 113, 134, 337, 364, 373
Key Lab. Bio-Resource & Eco-Environ., Ministry of Education, China.....	11
Konya Food and Agriculture University, Turkey .....	235
Leibniz Institute for Agricultural Engineering and Bioeconomy, Germany .....	223
Michigan State University, USA .....	207
Mississippi State University, USA .....	3, 26, 293, 317
Nanjing Agricultural University, China.....	232, 309
National Engineering Research Center for Breeding Swine Industry, China.....	301, 357
New Hope Liuhe Co. Ltd., China .....	309
Ningbo Research Center for Urban Environment, Chinese Academy of Science, China .....	188
North Carolina State University, USA.....	232
Paulista University, Brazil .....	279
Purdue University, USA .....	143
R&D Center of Fisheries Equipment and Engineering, Liaoning, China .....	191
Seoul National University, Republic of Korea .....	381
Sichuan University, China.....	11
South China Agricultural University, China.....	301, 329, 357
State University of Campinas, Brazil.....	279
The Ohio State University, USA .....	143, 151, 159
The University of Tennessee, USA .....	79, 215
Università degli Studi di Milano, Italy.....	85, 286
University of Georgia, USA .....	3

University of Illinois at Urbana-Champaign, USA.....	100
University of Manitoba, Canada.....	250
University of Missouri, USA .....	39, 235, 256
University of Natural Resources and Life Sciences, Austria .....	65, 72
University of Nebraska-Lincoln, USA .....	324
University of Science & Technology Beijing, China.....	127
University of Tennessee Institute of Agriculture, USA .....	3
University of Tennessee, USA.....	273
University of Veterinary Medicine, Austria .....	65, 72, 127
University of Zielona Góra, Poland.....	223
UOC Neuroradiologia, USA.....	286
USDA ARS Crop Production Systems Research Unit, USA.....	317
USDA Livestock Behavior Research Unit, USA.....	347
Wageningen University and Research, The Netherlands.....	180, 381
Zhejiang A&F University, China.....	273
Zhejiang Huatong Meat Products Co. Ltd., China.....	127, 167
Zhejiang University, China.....	107, 119, 127, 167, 174, 188, 264, 273
Zhengkang (Yiwu) Pig Industry Co. Ltd., China.....	188



## **Animal Environment and Welfare**



Cover design by Ji-Qin Ni

Cover photographs by Lingjuan Wang-Li and Ji-Qin Ni